1907

AFFDL-TR-72-92

TECHNICAL LIBRARY
REFERENCE COPY

AD 743 408

proceedings of the eighth annual conference on manual control

university of michigan
ann arbor, michigan

17-19 may 1972

AD0743408

Approved for public release; distribution unlimited

Reproduced From
Best Available Copy

Reproduced by
NATIONAL TECHNICAL
INFORMATION SERVICE
U S Department of Commerce
Springfield VA 22151

FEB 5 1973

N O T I C E

THIS DOCUMENT HAS BEEN REPRODUCED FROM THE BEST COPY FURNISHED US BY THE SPONSORING AGENCY. ALTHOUGH IT IS RECOGNIZED THAT CERTAIN PORTIONS ARE ILLEGIBLE, IT IS BEING RELEASED IN THE INTEREST OF MAKING AVAILABLE AS MUCH INFORMATION AS POSSIBLE.

0416

AN26106
AD754908

UNCLASSIFIED
Security Classification

DOCUMENT CONTROL DATA - R & D

(Security classification of title, body of abstract and indexing annotation must be entered when the overall report is classified)

1. ORIGINATING ACTIVITY (Corporate author)	2a. REPORT SECURITY CLASSIFICATION
Air Force Institute of Technology Air Force Flight Dynamics Laboratory	Unclassified
	2b. GROUP

3. REPORT TITLE

Proceedings of the Eighth Annual Conference on Manual Control

4. DESCRIPTIVE NOTES (Type of report and inclusive dates)

17-19 May 1972

5. AUTHOR(S) (First name, middle initial, last name)

6. REPORT DATE	7a. TOTAL NO. OF PAGES	7b. NO. OF REFS
17-19 May 1972	646 649	None

8a. CONTRACT OR GRANT NO.	9a. ORIGINATOR'S REPORT NUMBER(S)
NSR-23-005-364 b. PROJECT NO.	AFFDL-TR-72-92
c.	9b. OTHER REPORT NO(S) (Any other numbers that may be assigned this report)
d.	

10. DISTRIBUTION STATEMENT

Approved for public release; distribution unlimited.

11. SUPPLEMENTARY NOTES	12. SPONSORING MILITARY ACTIVITY
	Air Force Flight Dynamics Laboratory Air Force Systems Command Wright-Patterson AFB, Ohio 45433

13. ABSTRACT

This volume presents recent developments in the field of manual control theory and applications. The papers give analytical methods as well as examples of the important interplay between man and machine, such as how man controls and stabilizes machine dynamics, and how machines extend man's capability. Included in the broad range of subjects are procedures to evaluate and identify display systems, controllers, manipulators, human operators, aircraft, and non-flying vehicles. Of particular interest is the continuing trend of applying control theory to problems in medicine and psychology, as well as to problems in vehicle control.

DD FORM 1 NOV 68 1473

UNCLASSIFIED
Security Classification

UNCLASSIFIED

Security Classification

14. KEY WORDS	LINK A		LINK B		LINK C	
	ROLE	WT	ROLE	WT	ROLE	WT
Manual Control						
Stability Control						
Human Operators						
Control Analysis						

ib

☆U.S.Government Printing Office: 1972 — 759-488/263

UNCLASSIFIED

Security Classification

AFFDL-TR-72-92

N0020723157

proceedings of the

eighth annual conference on manual control

PR

university of michigan
ann arbor, michigan

17-19 may 1972

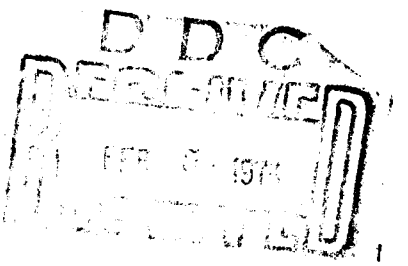

Approved for public release; distribution unlimited.

SPONSORED BY
UNIVERSITY OF MICHIGAN
NATIONAL AERONAUTICS AND SPACE ADMINISTRATION
AIR FORCE FLIGHT DYNAMICS LABORATORY

IC

PREFACE

On May 17, 18 and 19, 1972, the Eighth Annual Conference on Manual Control Systems was held at the University of Michigan. It brought together more than one hundred engineers and scientists interested in research and development of manual control systems, those systems in which the human operator plays a significant role in control and stabilization. As reflected in the volume of papers that follow, the discussions ranged from analytic approaches to system analysis and system identification to empirical studies of human operator performance in a variety of practical tasks. Although the predominate theme focuses on application to aircraft control and handling qualities, papers were also presented concerning human control of automobiles and supertankers. Both full papers and abstracts of shorter reports are included in this proceedings of the Conference.

The conduct of the Conference was supported under Contract NSR-23-005-364 with the National Aeronautics and Space Administration. I am grateful to the U. S. Air Force for publishing these proceedings; address requests to: AFFDL/FGC, Wright-Patterson Air Force Base, Ohio, 45433.

The reader of this volume may also be interested in earlier volumes in this series. They are referenced below.

First Annual NASA-University Conference on Manual Control, The University of Michigan, December 1964. (Proceedings not printed.)

Second Annual NASA-University Conference on Manual Control, MIT, Feb 28 to March 2, 1966, NASA SP-128.

Third Annual NASA-University Conference on Manual Control, University of Southern California, March 1 - 3, 1967, NASA SP-144.

Fourth Annual NASA-University Conference on Manual Control, The University of Michigan, March 21 - 23, 1968, NASA SP-192.

Fifth Annual NASA-University Conference on Manual Control, MIT, March 27 - 29, 1969, NASA SP-215.

Sixth Annual Conference on Manual Control, Wright-Patterson AFB, April 7 - 9, 1970.

Seventh Annual Conference on Manual Control, University of Southern California, June 2 - 4, 1971, NASA SP-281.

Richard W. Pew
The University of Michigan
July, 1972

ABSTRACT

This volume presents recent developments in the field of manual control theory and applications. The papers give analytical methods as well as examples of the important interplay between man and machine, such as how man controls and stabilizes machine dynamics, and how machines extend man's capability. Included in the broad range of subjects are procedures to evaluate and identify display systems, controllers, manipulators, human operators, aircraft, and non-flying vehicles. Of particular interest is the continuing trend of applying control theory to problems in medicine and psychology, as well as to problems in vehicle control.

CONTENTS

page

Preface ii

SESSION I. DEVELOPMENTS IN MANUAL CONTROL SYSTEM MODELING

1. Identification of the Human Operator Time Delay 3
W. R. Wells and J. R. Schiess
2. A Non-Linear Feedback Model for Tracking Studies 11
E. T. Pitkin
3. An Effective Technique for Extracting Pilot Model Parameter Values from Multi-Feedback, Single-Input Tracking Tasks 23
G. L. Teper
4. Operator Control of Crossover Model Parameters 35
Gary L. Rupp

SESSION II. NEW DEVELOPMENTS IN MANUAL CONTROL OUTPUT DEVICES

5. The Use of Advanced Pilot's Controllers in 'Fly-by-Wire' Vehicles . . . 49
M. Gordon-Smith
6. A Tactual Pilot Aid for the Approach-and-Landing Task 75
R. Gilson and R. E. Fenton
7. A Fingerstick with Binary Selectable Control Gain 81
G. Rothbauer, W. Krüger, and W. Kruse
8. A Lightspot Operated Typewriter for Quadriplegic Patients 89
M. Soede and H. G. Stassen
9. Photoelectric Head Movement Measurement as a Control Effector (Abstract) 101
B. Chouet and L. R. Young

SESSION III. AIRCRAFT DISPLAY CONCEPTS

10. Experimental Evaluation of a Display Parameter Using the Phase Margin Performance Measure 105
P. B. Sun
11. A Simulation to Evaluate PWI System Parameters in Visual Search 117
R. E. Curry, J. Dumeurger, E. H. Day, and J. W. Senders
12. Trends in Commercial Aircraft Crew Roles and Manual Control Research Applications 139
J. D. Warner

SESSION IV. VISUAL DISPLAY DEVELOPMENTS

13. Head-Up Display for the Visual Approach 159
J. M. Naish
14. Response Strategies with a Cross-Coupled Control System 175
P. D. McLeod
15. A Pilot Model for Tracking with Preview 191
L. D. Reid and N. Drewell

SESSION V. REMOTE MANIPULATION AND OTHER CONTROL STRATEGIES

16. The Mathematics of Coordinated Control of Prostheses and Manipulators . 207
D. E. Whitney
17. Active Force Feedback Rate Control of Manipulators 221
P. M. Lynch and D. E. Whitney
18. Interactive Aspects of Control by Man and Learning Machine 227
A. Freedy, G. Weltman, J. Lyman, and F. C. Hull
19. Mapping an Operator's Perception of a Parameter Space: II 231
R. J. Jagacinski

SESSION VI. RECENT DEVELOPMENTS IN CONTROL SYSTEM ANALYSIS PROCEDURES

20. Transfer Characteristics of Human Adaptive Response to Time-Varying Plant Dynamics 245
P. Delp and E. R. F. W. Crossman
21. Some Recent Experimental Results Pertaining to the Estimation of Power Spectra Using Finite Lengths of Data 273
R. F. Whitbeck and J. R. Knight
22. Principal Factors and Trade-Offs in the Rapidity of Convergence of Parameter Tracking Systems 291
S. J. Merhav
23. Adaptive Identification of Parameters in Models of Physiological Systems 299
R. Mekel

SESSION VII. ASSESSMENT OF THE DEGRADING EFFECTS OF ENVIRONMENTAL AND PHARMACOLOGICAL AGENTS ON HUMAN CONTROLLER

24. The Degradation of Tracking Performance as a Function of Environmental Stresses of Heat and Noise 309
G. M. Swisher and F. M. Maher
25. Vibration Effects on Manual Control Performance 319
R. W. Allen, H. R. Jex, and R. E. Magdaleno
26. Clinical Applications of Tracking 343
B. S. Repa, J. W. Albers, R. W. Pew, and W. W. Tourtellotte
27. Effects of d-Amphetamine on Quantitative Measures of Motor Performance (Abstract) 369
J. W. Albers, B. S. Repa, E. F. Domino, A. R. Potvin, and W. W. Tourtellotte

SESSION VIII. IMPROVING AND EVALUATING AIRCRAFT HANDLING QUALITIES

28. Preliminary Short Period Design Criteria through the Application of Pilot Modeling Technique 373
E. P. Salmon and D. F. Kesler
29. Pilot/Vehicle Control Optimization Using Averaged Operational Mode and Subsystem Relative Performance Index Sesitivities 387
G. G. Leininger, B. Lehtinen, and J. P. Riehl
30. The Use of Nonadjectival Rating Scales in Human Response Experiments (Abstract) 411
R. A. Hess and D. M. Layton
30.a The Sensuous SAS by Paper Pilot. 413
Teddy L. Hollis, Russell A. Hannen, James D. Dillow

SESSION IX. MANUAL CONTROL ANALYSIS OF AIRCRAFT: CONTROL AND HANDLING QUALITIES

31. An Analytical Study of Aircraft Lateral-Directional Handling Qualities Using Pilot Models (Abstract) 433
J. J. Adams
32. Prediction and Evaluation of Flying Qualities in Turbulence 435
E. D. Onstott

SESSION X. MANUAL CONTROL OF NON-FLYING VEHICLES

33. Simulation Investigation of Driver/Vehicle Performance in a Highway Gust Environment 449
D. H. Weir, R. K. Heffley, and R. F. Ringland
34. The Effects of Vehicle Dynamics on Asymptotic Stability in Car Following 471
G. O. Burnham and G. A. Bekey
35. Modelling the Helmsman of a Supertanker: Some Preliminary Experiments . 485
W. Veldhuyzen, A. van Lunteren, and H. G. Stassen

SESSION XI. EYE MOVEMENTS, EYE TRACKING, AND THE DISTRIBUTION OF ATTENTION

36. A Model for the Step-Like Combined Eye-Head Movement 505
G. Vossius
37. A Single-Channel Model of Attention Sharing in a Dynamic Dual-Task Environment 509
R. C. Cliff

SESSION XII. THEORY AND APPLICATION OF THE "CRITICAL TRACKING TASK"

38. Development of the Dual-Axis and Cross-Coupled Critical Tasks 529
H. R. Jex, W. F. Jewell, and R. W. Allen
39. Evaluation of Human Operator Aural and Visual Delays with the Critical Tracking Task 553
E. T. Pitkin and E. W. Vinje
40. Human Operator Remnant in a Subcritical Task 565
J. N. M. de Jong and A. van Lunteren
41. The Effect of Intermittent Error Displays on the Operator Critical Compensatory Tracking Performance 589
R. J. Bethke, G. M. Swisher, and M. J. Cook

SESSION XIII. NON-VISUAL MODES OF INFORMATION DISPLAY

42. Tracking with Kinaesthetic and Auditory Feedback 613
L. Buck
43. Flight Simulator Evaluation of Audio Displays for IFR Hover Control . . 625
E. W. Vinje
44. Pilot Describing Function Measurements for Combined Visual and Linear Acceleration Cues 651
R. F. Ringland and R. L. Stapleford

SESSION I

Developments In Manual Control System Modeling

IDENTIFICATION OF THE HUMAN OPERATOR TIME DELAY

WILLIAM R. WELLS
UNIVERSITY OF CINCINNATI
AND
JAMES R. SCHIESS
NASA LANGLEY RESEARCH CENTER

ABSTRACT

A limited amount of analysis has been performed on the identification of the hereditary system representing the human operator. The present paper is intended to explore the feasibility of the use of a Kalman type filter to the identification of unknown parameters in such a system. The pilot delay is kept in its pure form as opposed to the Pade approximation generally used for these systems. Some preliminary results of the application of nonlinear estimators to a simpler hereditary system are discussed.

INTRODUCTION

Various attempts have been made to apply linear estimation theory to determine the optimal set of parameters in particular pilot models using pilot response data (for example, references 1-3). Generally, a Pade approximation is applied to the pilot delay whenever it is to be included in the determination. When kept in its pure form, the pilot time delay occurs in a highly nonlinear fashion causing the resulting estimation problem to be nonlinear.*

The question addressed in the present paper is whether or not a linearized version of the dynamics is sufficiently accurate for the time delay estimate and how the linear filter should be applied to the resulting linear hereditary system.

PROBLEM DESCRIPTION

A block diagram of the pilot-airplane model used to represent the compensatory tracking task is given in Figure 1. The dynamics of the controlled elements are of the acceleration type (K/s^2). The pilot transfer function is given by (reference 7)

---

* Recent work in the area of the state prediction of linear and nonlinear time delay systems has been presented in references 4-6. Although an exact solution for the optimal filter is presented in these studies many practical computational difficulties exist when applied to a specific problem.

Preceding page blank

$$y_p(s) = \frac{K_1(\tau_3 s+1)e^{-s\theta}}{(\tau_1 s+1)(\tau_2 s+1)} \tag{1}$$

where K_1, τ_1, τ_2, τ_3, and θ are the pilot static gain, low-frequency neuromuscular time constants and pilot time delay respectively.

The pilot remnant function used is a second-order noise filter which converts white noise input $w_p(t)$ to colored noise output $\eta(t)$. The transfer function of the filter is

$$R_p(s) = \frac{1}{s^2+\alpha_1 s+\alpha_2} \tag{2}$$

In the time domain, the pilot-aircraft dynamics are given by

$$\ddot{c}(t) = K\delta(t) \tag{3}$$

$$\tau_1\tau_2\,\ddot{u}(t)+(\tau_1+\tau_2)\dot{u}(t)+u(t) = K_1[\tau_3\dot{e}(t-\theta)+e(t-\theta)] \tag{4}$$

$$\ddot{\eta}(t)+\alpha_1\dot{\eta}(t)+\alpha_2\eta(t) = w_p(t) \tag{5}$$

In terms of state variables the equations can be expressed as

$$\dot{\underline{y}}(t) = \underline{f}\,[\underline{y}(t),\ \underline{y}(t-\theta),\ D(t),\ D(t-\theta),t] + \underline{w}(t) \tag{6}$$

The components y_1 and y_3 represent the plant and pilot output (less the remnant) respectively. y_2 is the rate of change of the plant output; y_4 is the linear sum of the undelayed pilot output and the distrubance; y_5 is the remnant and y_6 is the time rate of change of the remnant. The remaining components of $\underline{y}$ are y_7 through y_{13} which represent the parameters K_1, τ_1, τ_2, τ_3, θ, α_1, and α_2. For more details of the state equation see reference 7. The measurements are taken as the stick output and the plant output. These can be written as

$$\underline{m}(t) = H(t)\underline{y}(t)+\underline{v}(t) \tag{7}$$

The noise vectors $\underline{w}$ and $\underline{v}$ are assumed to be white.

For the linear analysis equation (6) is linearized about a nominal solution $\underline{y}^*(t)$ in which the model parameters are assigned constant "guess" values and for which the process noise is zero (reference 7). The resulting equations for the off-nominal performance $\underline{\alpha} = \underline{y} - \underline{y}^*$ and measurement $\underline{\beta}$ are

$$\dot{\underline{\alpha}}(t) = A(t)\underline{\alpha}(t)+B(t)\underline{\alpha}(t-\theta)+\underline{w}(t) \tag{8}$$

$$\underline{\beta}(t) = \underline{m}(t) - H(t)\underline{y}^*(t) \tag{9}$$

where

$$A(t) = \left.\frac{\partial \underline{f}}{\partial \underline{y}(t)}\right|_{y=y^*} \tag{10}$$

$$B(t) = \left.\frac{\partial \underline{f}}{\partial \underline{y}(t-\theta)}\right|_{\underline{y}=\underline{y}^*} \tag{11}$$

DISCRETE FILTER EQUATIONS

The discrete form of equation (8) is

$$\underline{\alpha}(k+1) = \phi(k+1,k)\ \underline{\alpha}(k) + \Omega(k)\ \underline{\alpha}(k-q) + w(k) \tag{12}$$

where to first order

$$\phi(k+1,k) = I+\Delta t A(k) \tag{13}$$

$$\Omega(k) = \Delta t B(k) \tag{14}$$

$$q = \theta/\Delta t \tag{15}$$

The corresponding form of the linear Kalman filter used is

$$\hat{\underline{\alpha}}(k+1|k+1) = \phi(k+1,k)\ \hat{\underline{\alpha}}(k|k) + \Omega(k)\ \hat{\underline{\alpha}}(k-q|k)$$
$$+ F(k+1)\ \{\beta(k+1) - H(k+1)\,[\phi(k+1,k)\ \hat{\underline{\alpha}}(k|k)$$
$$+ \Omega(k)\ \hat{\underline{\alpha}}(k-q|k)]\} \tag{16}$$

The function F(k+1) is the Kalman gain matrix (see reference 7).

Some results of typical estimations are given in Tables I and II for simulated and real data respectively. For the simulated data, the variance of the process noise was 23.8 volts^2/sec^4 and the disturbance was D(t) = 2 sin t. The variance of the noise added to the measurements were taken as 9.2×10^{-4} volts^2.

The real data used in the analysis was obtained from closed-loop compensatory tracking tasks conducted by Langley personnel with engineers and test pilots used as subjects. A discussion of these data is reported in reference 8. The variance of the process noise was obtained by a power spectral density analysis of a model of the remnant. The value used was 23.8 volts^2/sec^4. The variance of the measurement noise was estimated as 9.2×10^{-4} volts^2. Further details of the real data are discussed in reference 7.

In Table I are listed the results of the simulated estimation after 2 seconds of data reduction. In Case I all parameters were held fixed at their nominal value and only the first 6 components of the state vector were computed. It was found that a poor estimate of y_3 and y_5 was obtained individually but that the linear sum $y_3 + y_5$ was estimated very well. This was to be expected since one of the measurements was this sum. Also y_1 was estimated well for the same reason. The components y_2 and y_4 were identified only reasonably well. In Case II the components $y_1, \ldots, y_6$ and K_1 were computed with similar results. It was found that K_1 never varied far from its initial estimate; however, the variance history indicated that it would slowly approach its correct value. A plot of the residuals of the measurements for Case I is shown in Figure 2. These results indicate that the data has been fitted fairly well; however, the signal is not as random as we would desire. Several other cases were tried for the simulated results in which an attempt was made to compute the time delay. In general, the estimates diverged after a very short time.

Table II gives the results for the estimates based on actual data for three cases. In Case I the parameters were fixed at these nominal values and not estimated. In Case II, K_1 was estimated and in Case III, θ was estimated. It is seen that the estimates are not altered greatly by including K_1 as an unknown; however, if θ is estimated, the estimates change considerably. In fact, a very tight initial variance on θ was necessary (10^{-8}) to keep the estimates from diverging. The result is that Cases I and II are probably reasonable, but not the results of Case III. A time history of the measurement residual error for Case II is given in Figure 3.

CONCLUDING REMARKS

The results of a linear Kalman filter approach indicate that reasonable estimates of the state variables and some parameters are obtained. However, the nonlinear nature of the time delay prevents its determination with strictly linear theory. To answer

the question as to whether existing nonlinear estimators will result in a good estimate of the time delay, the authors are presently simulating the estimation of a simple second-order hereditary system. Preliminary results indicate that, for this lower order dimensional system, a second-order filter will provide a good estimate for both the state and parameters including the time delay. The results have not as yet been extended to the pilot-aircraft model presented in this paper.

REFERENCES

1. Wierenga, Rodney D.: An Evaluation of a Pilot Model Based on Kalman Filtering and Optimal Control. Fifth Annual NASA-University Conference on Manual Control, Massachusetts Institute of Technology, Cambridge, Mass., March 1969.

2. Reid, L.D.: An Investigation into Pursuit Tracking in the Presence of a Disturbance Signal. Fifth Annual NASA-University Conference on Manual Control, Massachusetts Institute of Technology, Cambridge, Mass., March 1969.

3. Adams, James J., and Bergeron, Hugh P.: Measurements of Human Transfer Function with Various Model Forms, NASA TND-2394, August 1964.

4. Koivo, A.J., and Stoller, R.L.: "On Least Squares Estimation in Nonlinear Dynamical Systems with Time Delay," Proceedings of the 9th Joint Automatic Control Conference of the American Automatic Control Council, University of Michigan, June 1968.

5. Stoller, R.L., and Koivo, A.J.: "Estimation in Nonlinear Systems with Transport Delay," Proceedings of the IEEE Symposium on Adaptive Processes, Decision and Control, December 1971.

6. Kwakernaak, H.: "Optimal Filtering in Linear Systems with Time Delays," IEEE Transaction on Automatic Control, Vol. AC-12, No. 2, April 1967.

7. Schiess, James, and Wells, William R., and Roland, Vince: "Estimation of Nonlinear Pilot Model Parameters Including Time Delays," Proceedings of the Second Symposium on Nonlinear Estimation Theory and its Applications, San Diego, California, September 1971.

8. Adams, James J., and Bergeron, Hugh P.: A Synthesis of Human Response in Closed-Loop Tracking Tasks, NASA TND-4842, October 1968.

TABLE 1. - SIMULATED DATA

Parameter	True (t=0)	True t=2	Perturbed initial conditions	Case I (t=2) All parameters	Case II (t=2) K_1 estimated
				K_1=1.00, $\tau_1=\tau_2$=0.10, $\tau_3=\theta$=0.10, $\alpha_1=\alpha_2$=0.10	τ_3=0.50, $\tau_1=\tau_2$=0.10, $\tau_3=\theta$=0.10, $\alpha_1=\alpha_2$=0.10
y_1	0	33.55	0.10	33.78	33.75
y_2	0	148.87	0.10	164.20	161.98
y_3+y_5	0	60.98	-0.09	61.01	61.01
y_4	0.10	83.16	0.01	88.78	96.81
K_1	1.0	1.0	1.10	---	1.098

TABLE 2. - REAL DATA

Parameter	Nominal	Case I (t=15) All parameters fixed	Case II (t=15) K_1 estimated	Case III (t=15) θ estimated
		K_1=1.0, τ_3=0.50 $\tau_1=\tau_2$=0.10 $\alpha_1=\alpha_2$=0.10	θ=0.10, τ_3=0.50 $\tau_1=\tau_2$=0.1 $\alpha_1=\alpha_2$=0.10	K_1=1.0, τ_3=0.50 $\tau_1=\tau_2$=0.10 $\alpha_1=\alpha_2$=0.10
y_1	-0.500	-3.247	-3.243	-2.559
y_2	6.248	-0.172	-0.551	1.374
y_3+y_5	-0.028	2.148	2.147	2.146
y_4	-0.488	-24.835	-24.983	-23.653
K_1	1.00	1.00	1.00	1.00
θ	0.10	0.10	0.10	0.116

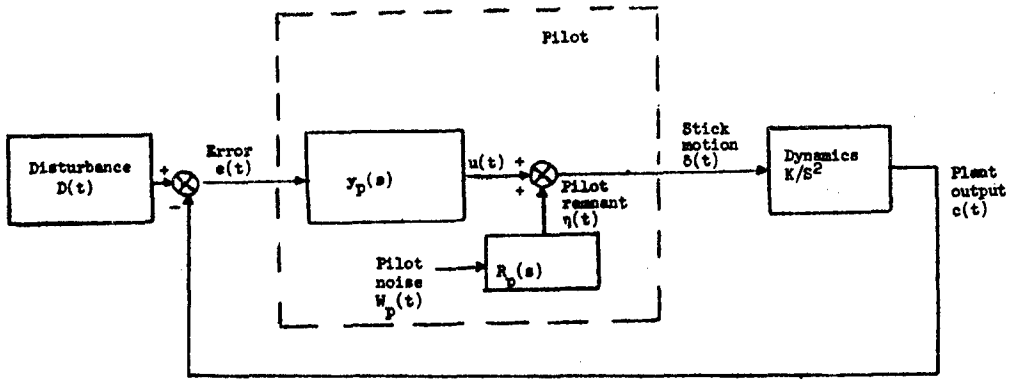

Figure 1.- Block diagram of pilot-dynamics.

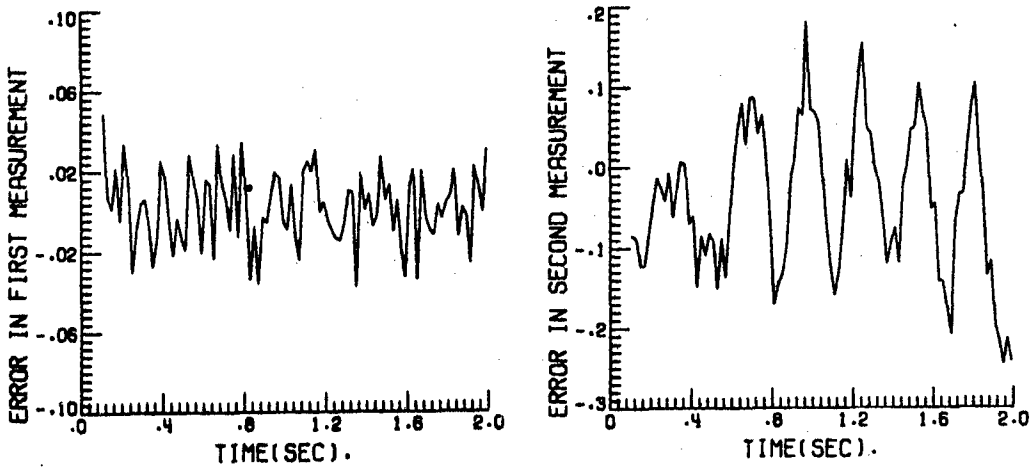

Figure 2.- Error in measurement - simulated data case 1.

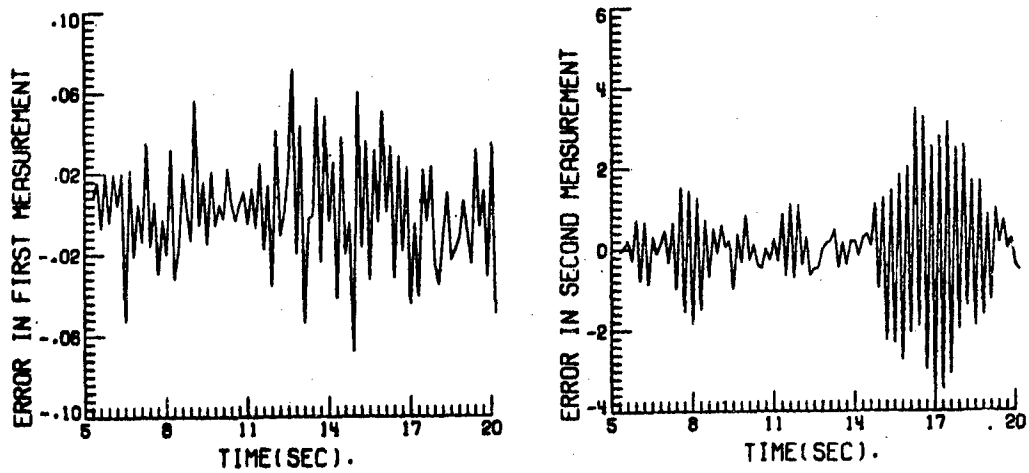

Figure 3.- Error in measurement - real data case 2.

A Non-Linear Feedback Model for Tracking Studies

Edward T. Pitkin*
University of Connecticut

ABSTRACT

A nonlinear feedback model of a human operator in a compensatory tracking loop is suggested. This model incorporates most of the standard features of conventional linear models including sample data models. In addition nonlinear feedback is employed to yield pulsing output with dynamics such as K/S^2. Time domain comparisons of model and human response to identical stimuli are presented.

INTRODUCTION

Much of the reported work on human tracking ability has been directed to analysis of an operator's response in a simple, single degree of freedom compensatory tracking loop. This is not surprising since the human operator has long been known to be "probabilistic, non-linear, and highly variable", (Ref. 1), so that even this elementary situation gives rise to interpretational difficulty. It is, however, somewhat surprising that the vast majority of research has also been confined to linear or quasi-linear models of the human operator. Most likely, this is due to the fact that control engineers can deal with linear models expressible in terms of transfer functions with much greater facility than non-linear models; that these models are fairly easily derived from experimental data with cross correlation techniques, and, furthermore, that in situations wherein the operator behaves in a quasi-linear fashion, the use of a linear model is a most appropriate engineering approximation. In other cases, where the operator behaves in a more non-linear fashion, it is to be anticipated that, in spite of their added difficulty, non-linear models might be used to better explain the human operator's behavior. It is with this latter case the present work is primarily concerned.

LINEAR MODELS

The majority of linear models that have been proposed may be characterized by a transfer function which can be expressed as a rational fraction of polynomials multiplied by a pure time delay. Tustin, (Ref. 2), first proposed a model of this form in 1947 which amounted to a conventional proportional-

---

*Professor of Mechanical and Aerospace Engineering

Preceding page blank

plus-integral controller multiplied by a pure time delay. Since then models of this type have been continuously generated and refined to the most recent nine-parameter model of McRuer et al., (Ref. 3), given in Eqn. [1] in which adaptable and fixed neuromuscular parameters are separated.

$$y_p(s) = K_p e^{-\tau_o s} \underbrace{\left[\frac{(\tau_L s+1)}{(\tau_I s+1)}\right]}_{\text{adaptable}} \underbrace{\left(\frac{\tau_K s+1}{\tau_K s+1}\left[\frac{\omega_n^2}{(\tau_{N_1} s+1)(s^2+2\xi\omega_n s+\omega_n^2)}\right]\right)}_{\text{neuromuscular}} \qquad (1)$$

Bekey, (Ref. 4), has proposed linear sample data models which complement the rational polynomial models. These models attempt to characterize human behavior in terms of the transfer functions of zero or first order sample-and-hold devices supplemented by some of the elements of the more conventional linear model discussed above. A typical transfer function for a zero order hold model is

$$y_p(s) = \frac{K_p e^{-\tau_o s}}{(\tau_I s+1)}\left[\frac{1-e^{-Ts}}{s}\right] \qquad (2)$$

When the gain and phase characteristics of these models are plotted on a Bode diagram, the results appear to be quite similar to those obtained from the rational polynomial models discussed above. The sample data models can be justified on the basis that there is considerable evidence that the human is not a continuous operator, but acts on discrete samples of information, produces discrete outputs and that he tends to extrapolate his response when input stimulus vanishes temporarily. Again, the sample data models have been quite successful in modeling human response in situations where the task is not too difficult and hence they may be considered as suitable alternatives to the rational polynomial models. For example, Bekey got very good simulation of human operator response when controlling a pure gain plant. Another factor that makes the sample data model interesting is that it incorporates an implicit pure time delay at low frequency due to the fact that the output of the sample-and-hold circuit follows the input function by roughly one-half a sampling period. If this implicit time delay is to replace the time delay used with the rational polynomial models, the sampling period must be of the order of .2 to .3 seconds, much longer than can easily be rationalized for input sampling. This might not, however, be too long for output "sampling", i.e., placing the sample-and-hold unit nearer to the output to give discrete step output.

The linear models described above will produce many of the main features

of the human operator response, particularly in tasks that are not too difficult; e.g., control of a pure gain or a single integral plant. As the task gets more difficult, however, these models are less accurate and the remnant, i.e., the portion of the operator's output which is not accounted for by the linear model, becomes an increasingly more important contributor (Ref. 5). In difficult tasks such as controlling a double integration, K/s^2, it is well known that the human operator resorts to a pulsing output behavior to develop enough lead to control. The linear models try to account for this through the adaptable lead-lag term which, though giving the necessary lead by properly adjusting parameters, do not, when simulated, usually give the very distinctive pulse-like behavior that is noted in the time history of the operator's output. Indeed, the difference between the model and the human operator outputs are so distinct that one can usually distinguish them at a glance. The need for improved modeling of this pulsing behavior has been noted by Jex and Allen, (Ref. 6). It might be expected that the pulses are, for the most part, showing up in remnant rather than as part of the linear model output. This suggests that more attention should now be directed to non-linear models.

NON-LINEAR MODELS

A relatively small fraction of the published literature on human operator models is concerned with non-linear aspects. One notable early exception is the work of Diamantides (Ref. 7), who in 1958 recognized the need for non-linear elements to obtain plausible time domain output. A block diagram of his model appears in Figure 1. His approach to pulsing behavior was to insert a step function which he called "anticipation bias" into the output each time the error crossed the zero point. Since this step precedes the output of the reaction time delay element at the summing junction, a lead pulse is generated. He also found the injection of a dither to be an appropriate model of the operator's tendency to continuously "feel out" system response. One other non-linear element will be noted; a threshold on the weighted error-plus-derivative signal. This was probably less important to the overall result than the non-linear bias element, but again demonstrates his recognition of the need for non-linear elements in the model. In his experiments Diamantides was able to trick experienced pilots into thinking that they were controlling the dynamics when the simulated model was actually doing the controlling. Also, his time domain traces of pilot and model output compared quite well.

More recently, Costello, (Ref. 8), noted that linear models lacked realism when called upon to track a step input. He therefore proposed a two-mode "surge" model in which normal control was accomplished by a conventional linear model while the transient at the beginning of a step was handled by switching to the surge. The surge consisted of a momentary double pulse (±) input after which control returned to the linear model. Costello's model and its switching line in the phase plane is shown in Figure 2. His results show significant improvement in the time history of response to the step input as

the surge model eliminates the high frequency ringing that is found to be present at the beginning of each pulse when the conventional linear model is used.

It appears then that non-linear models may offer considerable improvement in the characterization of human operator response. This is not to say that linear models should be abandoned, rather, they should be supplemented with non-linear elements where necessary. The ideal non-linear model should incorporate the major aspects of the linear models that have been developed and proved successful in application of models to design problems over the past twenty-five years. This implies that the describing function of a non-linear model should be both qualitatively and quantitatively comparable with describing functions that have been established for human operators. The non-linear effects should then, hopefully, decrease the difference between model and human operator input, i.e., a lesser amount of the output would then need to be attributed to a random remnant term.

NON-LINEAR FEEDBACK MODEL

The non-linear feedback model shown in Figure 3 is proposed along such lines. The first section of the model consists of conventional linear elements that have proven successful in the past. The error is processed to obtain an estimate of both its time derivative and integral and the results are summed to give a proportional plus integral plus derivative (PID) signal with adjustable or "adaptable" weighting factors. This section is then equivalent to the adaptable lead-lag section found in most linear models. The next element is a sample-and-hold unit. This element takes discrete samples of the PID signal and feeds them to the operator's output dynamics modeled here by a simple first-order lag. This could also be a damped second-order element with no significant change to the model. At this stage, the model appears to be much like Bekey's sample data model except for the fact that the sampler is not located at the input but rather at the output of the central processor. With the sampler in this location, the longer sampling periods required to correctly model the observed time delays may be more easily rationalized. The non-linear element in this model is in a feedback loop from the output back to the sampler input. A threshold unit is used in the feedback loop so that when the outputs are below a certain level, there is no feedback and the model acts as a conventional linear sample data model. Once the output rises above the threshold level, however, there is negative feedback of the output to the input of the sampler. If this signal is great enough, there will be a reversal of the signal to the sampler and the output will then exhibit a pulsing action. It can be seen that this model has the basic features that worked well in Costello's surge model - linear behavior for small signals and the pulsing behavior for large signals. However, this system differs in that the pulses are not always of the same amplitude and are triggered only by the level of the output of the central processor rather than by the input signal. This model behaves much like the

surge model when it encounters a step output, but furthermore, it will produce a continuing pulse-like action when dealing with difficult dynamics such as K/s^2 much like that actually observed in the output of human operators. The required lead is produced by the magnitude of the pulses and is governed both by the threshold level and the gains in the linear section.

In order to give some indication of how this model compares to reality, the time traces in Figures 4 to 6, obtained from analog simulation with this model, are presented. Figure 4 gives typical time traces of the input disturbance and the error signal for K/s^2 dynamics. The error signal was indistinguishable between human and model control of the system, i.e., as in Diamantides work, the operator could not tell from watching the error signal if he was or was not controlling the system. Simultaneous traces of human controller output and model output are presented in Figure 5 for a case when the human is actually controlling the system. A similar set of traces taken when the computer was actually controlling is given in Figure 6. Note that there is very little, if any, observable difference in the output characteristics between cases. Note also that in both cases the pulsing behavior is evident in both the model and the human operator output and that there is a nearly one-to-one correspondence between pulses which occur at a frequency of approximately two per second. The major difference that appears between the two outputs is that the human operator tends to flatten the tops of his pulses more than the model. It is expected that this small difference could be cleared up with some further refinement of the model.

In conclusion then, it appears that the addition of non-linear elements to conventional linear models can offer some improvement to human operator simulation. It is suggested then that pursuance of such models as adjuncts to the quasi-linear models now in vogue may be a very fruitful area of future research.

ACKNOWLEDGEMENT

The author wishes to express his appreciation to the University of Connecticut Research Foundation and to the Electrical Engineering Department of the University of Canterbury, Christchurch, New Zealand, for providing support and facilities to carry out this work.

REFERENCES

1. Gregg, L.T. "On Computer Simulation of Human Operator Performance". Simulation, Vol. 5, pp. 61-68, (1965).

2. Tustin, A. "The Nature of the Operator's Response in Manual Control and its Implications for Controller Design". J. IEE, Vol. 94, Pt. IIA, pp. 190-202, (1947).

3. McRuer, D.T., D. Graham, and E.S. Krendal. "Manual Control of Single Loop Systems". J. Franklin Institute, Vol. 283, pp. 1-29, (Jan. 1967), pp. 145-168, (Feb. 1967).

4. Bekey, G.A. "The Human Operator as an Optimal Controller and Information Processor". IEEE Trans. Human Factors in Electronics, HFE-3, pp. 43-51, (Sept. 1962).

5. Vinje, E.W. and E.T. Pitkin. "Human Operator Dynamics for Aural Compensatory Tracking". IEEE Trans. on Systems, Man and Cybernetics, (in press), 1972.

6. Jex, H.R. and R.W. Allen. "Research on a New Human Dynamics Response Test Battery". Proc. 6th Annual Conf. on Manual Control, p. 750, Wright Patterson AFB, (April 1970).

7. Diamantides, N.D. "A Pilot Analog for Airplane Pitch Control". Jour. Aeronautical Sci., Vol. 25, pp. 361-370, 394, (1958).

8. Costello, R.G. "The Surge Model of the Well-Trained Human Operator in Simple Manual Control". IEEE Trans. on Man-Machine Sys., Vol. MMS-9, pp. 2-9, (1968).

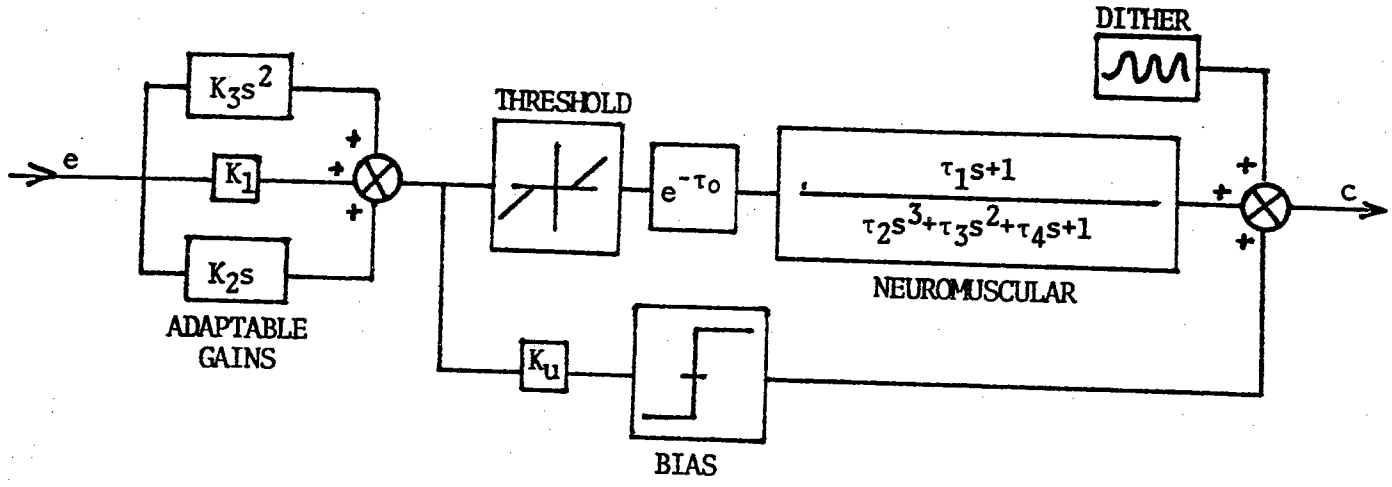

FIGURE 1 DIAMANTIDES' NON-LINEAR MODEL, CIRCA 1958

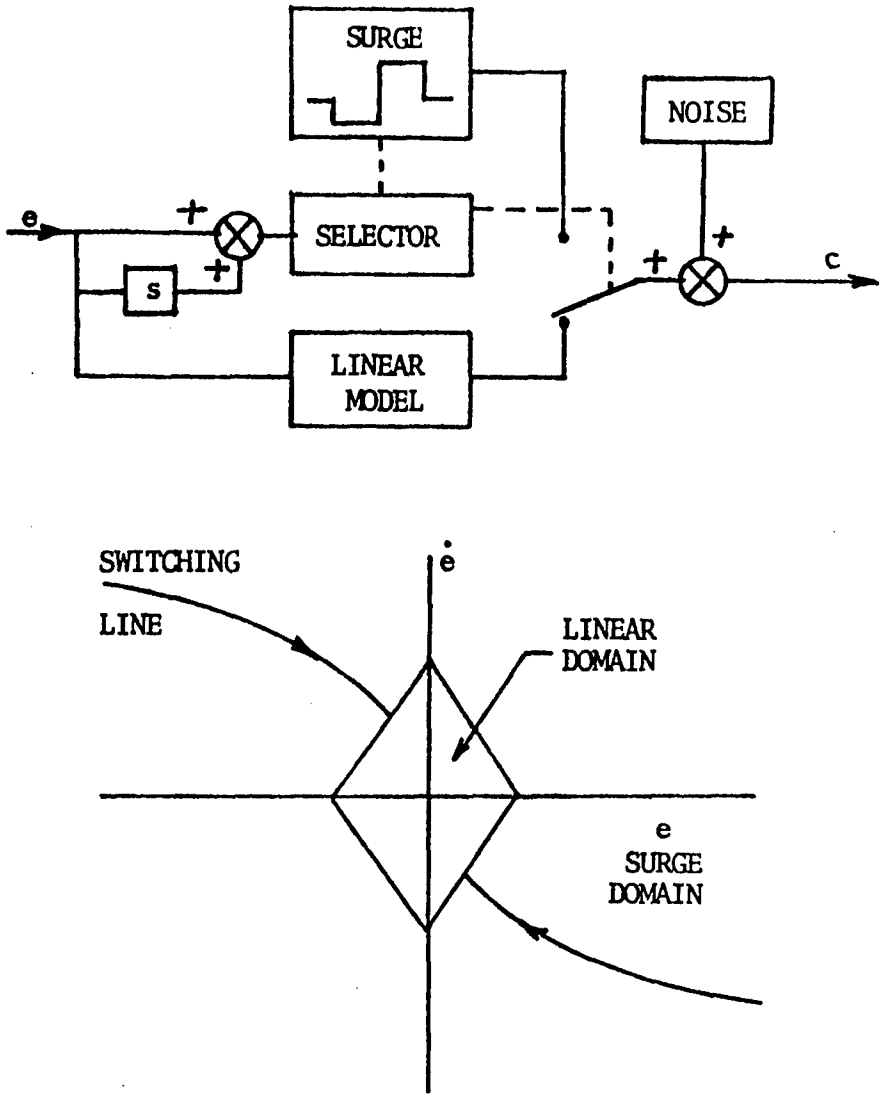

FIGURE 2 COSTELLO'S SURGE MODEL

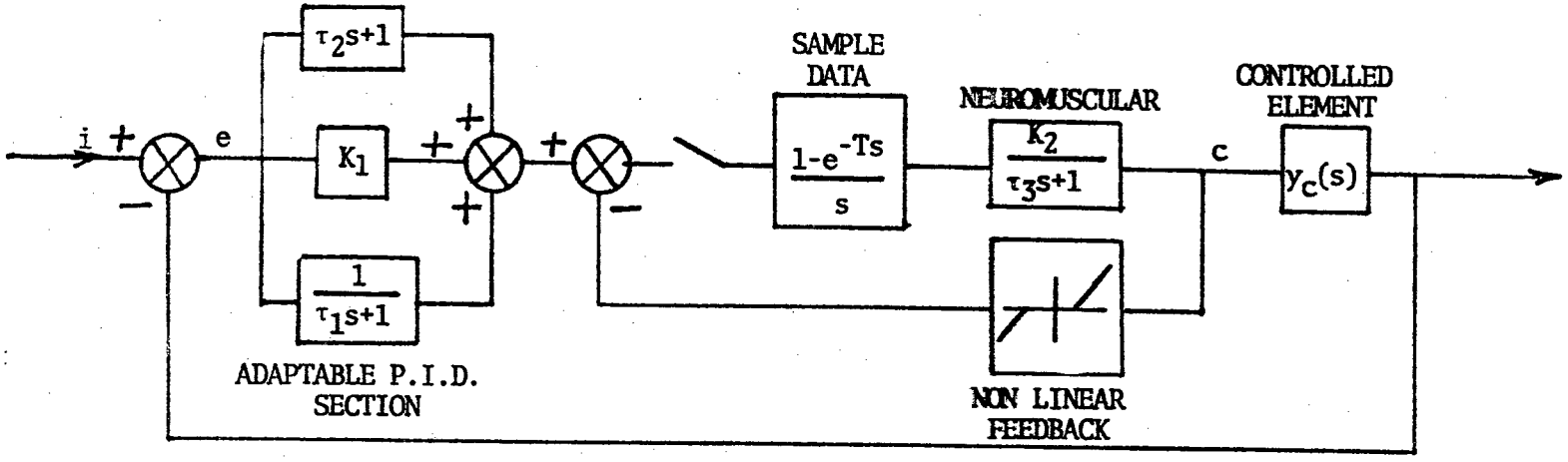

FIGURE 3 THE NON-LINEAR FEEDBACK MODEL IN A COMPENSATORY TRACKING LOOP

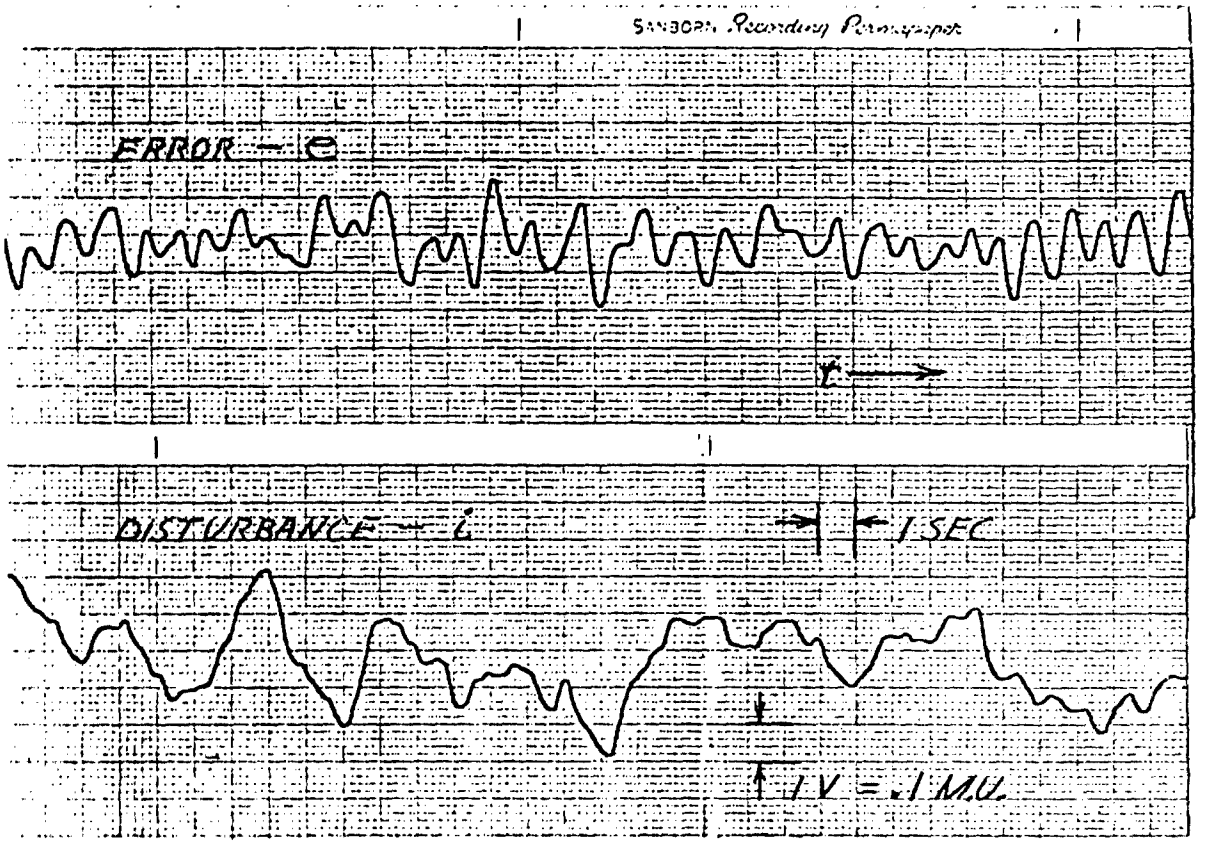

FIGURE 4. ERROR SIGNAL AND INPUT DISTURBANCE FOR SINGLE LOOP COMPENSATORY TRACKING OF $10/s^2$.

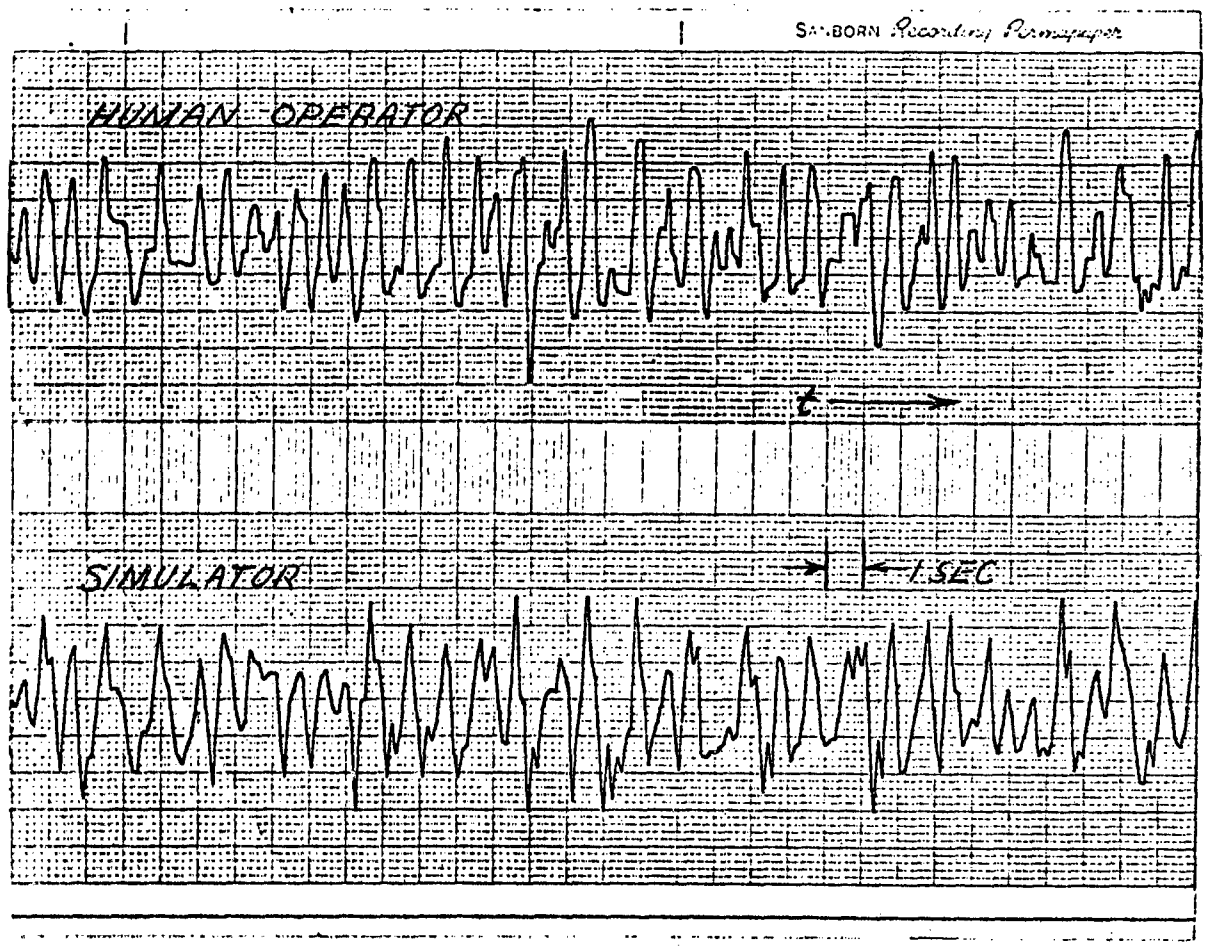

FIGURE 5. COMPARISON OF HUMAN OPERATOR AND ANALOG SIMULATED MODEL RESPONSE TO ERROR SIGNAL - HUMAN CONTROLLING.

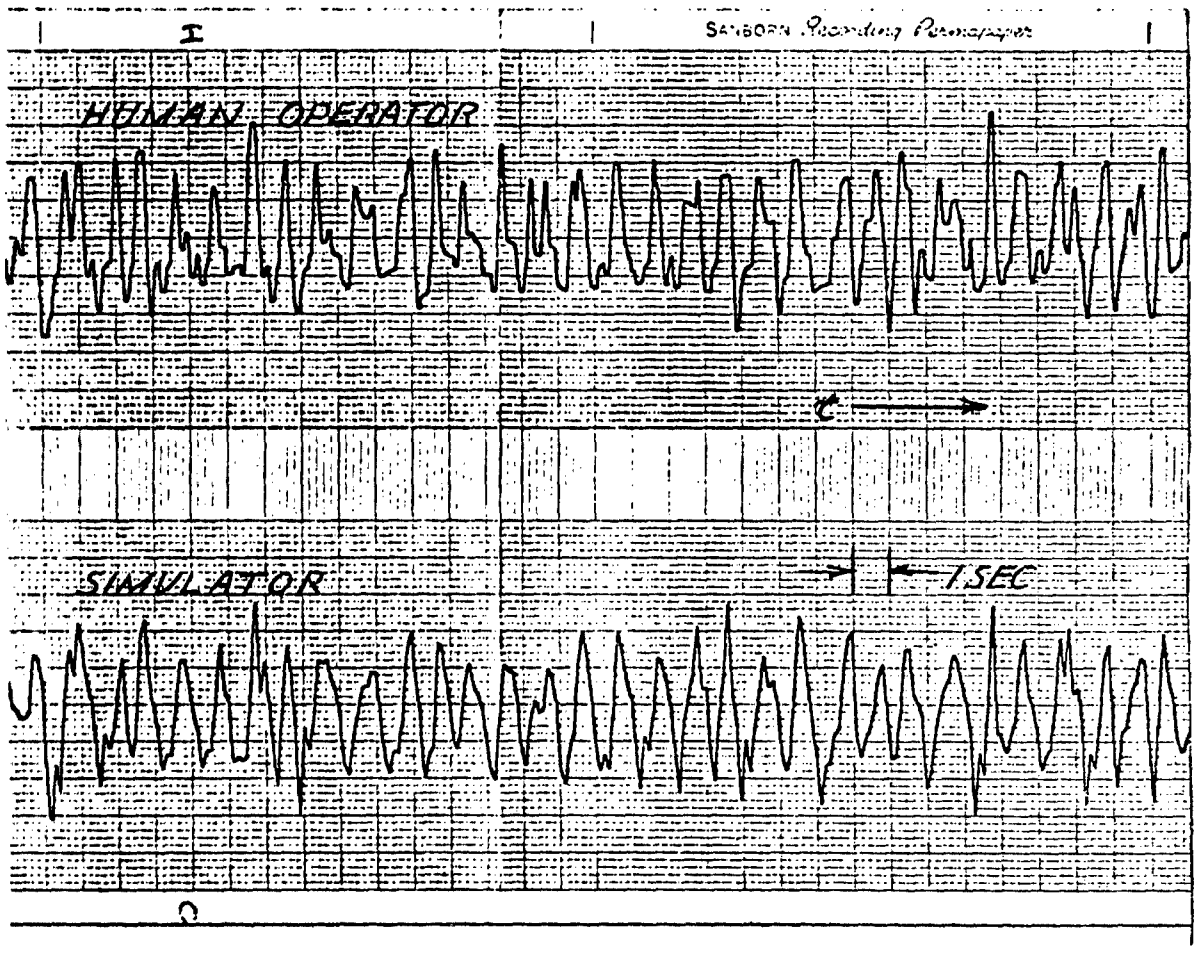

FIGURE 6. COMPARISON OF HUMAN OPERATOR AND ANALOG SIMULATED MODEL RESPONSE TO ERROR SIGNAL - MODEL CONTROLLING.

AN EFFECTIVE TECHNIQUE FOR EXTRACTING PILOT MODEL PARAMETER VALUES FROM MULTI-FEEDBACK, SINGLE-INPUT TRACKING TASKS

Gary L. Teper
Systems Technology, Inc., Hawthorne, California

ABSTRACT

Extensive quasi-linear describing function data exist for a human operator tracking a command in a single-loop (single controller, single input) task. Data for a multiloop task with a disturbance input, more typical of situations which occur in practice, are rare. A significant hurdle to obtaining a description of the human operator in a multiloop task has simply been the cost of reducing and interpreting the data. A reasonably efficient and effective technique which was recently developed and applied is described.

INTRODUCTION

Quasi-linear describing function models have a long history of usefully describing the human operator in a tracking task, and the appropriate measurement techniques are a well-developed art (e.g., see Ref. 1). Most previous measurements, however, have been made in command-input, single-loop (one feedback, one controller) situations. Although measurements have been made in multiloop tasks (e.g., Refs. 2 and 3), they are rare and have usually required extensive manipulation of the data. A recent program* required an efficient means of describing the human operator in a disturbance-input multi-feedback task. The technique to be described was developed and applied during this program and proved to be both effective and efficient.

To aid the description and look at some features in detail, the specific example of longitudinal control in a hovering vehicle will be used. The extension to other tasks including multiple-inputs and multiple-controllers is straightforward. Also, the description is in terms of a disturbance input consisting of a sum of randomly-phased sinusoids, as used during our program. The technique is not dependent on their use and could be applied with a filtered white noise disturbance.

---

*Accomplished in part under Contract F33615-71-C-1071 for the Air Force Flight Dynamics Laboratory.

HOVER CONTROL EXAMPLE

A pilot-vehicle system structure for maintaining position (x) using control stick (δ) alone is shown in Fig. 1. The vehicle has two degrees of freedom, longitudinal position (x) and pitch attitude (θ). The single system input is a horizontal gust disturbance (u_g). For the control structure shown in Fig. 1, an adequate description of the pilot requires both describing functions, Y_{p_θ} and Y_{p_x}, to account for that portion of the pilot's output, δ, which is correlated with the system input, u_g, and a remnant, η, which accounts for the rest of the pilot's output. The technique discussed here extracts the two describing functions.

DETERMINANCY

The describing functions cannot be measured directly in the single-input situation. Unless we make further assumptions, we can only obtain a single (complex, vector) equation in two unknowns, i.e.,

$$\delta(j\omega) = -Y_{p_\theta}(j\omega)[\theta(j\omega) + Y_{p_x}(j\omega) \cdot x(j\omega)] \qquad (1)$$

The equation relates the control stick output (δ) to the position (x) and attitude (θ) inputs. These can be determined by measurement of the describing function between any one response parameter and the input. For example, if the control stick (δ) to input (u_g) describing function is measured, all the vehicle response parameters can be determined via the known vehicle dynamics and gust input. Likewise, δ could be computed from the describing function measurement between any vehicle response parameter, say x, and the input.

To overcome the problem of indeterminancy we assumed fixed lumped-parameter pilot model forms. The general forms used during our program were:

$$Y_{p_\theta} = \frac{K_{p_\theta}[T_{L_\theta}(j\omega) + 1]e^{-j\omega\tau}}{[(j\omega/\omega_{NM})^2 + 2\zeta_{NM}(j\omega/\omega_{NM}) + 1]}, \text{ and}$$

$$Y_{p_x} = \frac{Y_{p_x}[T_{L_x}(j\omega) + 1]}{[T_{I_x}(j\omega) + 1]} \qquad (2)$$

With n input frequencies, the single non-redundant describing function provides 2n independent measures of the pilot characteristics. The factor of 2 is because the response at any one frequency has both an amplitude and phase (or, a real and an imaginary part). Thus, with the five input frequencies we used, our pilot models could have had up to ten independent parameters. As indicated above, a smaller number (up to 8) were used and a least squares fit of the data made. The fitting process is described later.

MEASUREMENT SENSITIVITY

A second problem is presented by the input dictated by the task. It also falls within the general area of system identification, which has received considerable attention. The necessity of exciting all the modes of the system and insuring that the measurements are sensitive to the parameters to be identified remains of cardinal importance. Skillful design of the input has also long been recognized as a means of satisfying these requirements. Unfortunately, this option was not available to us, as the complete nature of the input was prescribed by the task. The gust spectrum* at low altitude is of relatively low frequency, i.e., a bandwidth of about 0.3 rad/sec. This is aggravated further by the low-pass low-bandwidth gust-attenuation properties of the vehicle. Nonetheless, a relatively wideband description of the pilot was desired, say from 0.1 to 10 rad/sec.

Because the input signal power is very low at the higher frequencies of interest and could not, therefore, be properly tailored for measurement sensitivity, the alternative of designing the output measurement signal was taken. In the hovering pilot/vehicle system there are two† closed-loop modes of importance, the path mode, ω_p'' (approximately 0.8 rad/sec), and the attitude mode, ω_{sp}'' (approximately 3 rad/sec). These modes, in turn, are sensitive to the pilot's position and attitude describing functions,

*The sum of sinusoids used during our program approximated the frequency distribution of power of the gust spectrum.

†As it developed, a third mode of even higher frequency due to the combination of the pilot's neuromuscular system and the control stick turned out to be also of importance. The technique was capable of handling it also.

respectively. All the low frequency natural motion quantities of the system are dominated by either one or the other of these modes. The fact that none of the natural motion quantities have sufficiently wideband frequency content is clearly seen in the time histories from a typical simulation run shown in Fig. 2. The disturbance input (top trace of Fig. 2) has very little power at higher frequencies. The pilot's output, δ, is dominated by the higher frequencies. Continuing down Fig. 2 it can be seen that the signals, in sequence down the page, lose their high frequency power and gain in low frequency power. The longitudinal position (x) signal is completely dominated by lower frequencies.

To obtain an appropriate intermix of high and low frequency power a composite signal is contrived. This is shown in the bottom signal in Fig. 2 as the designed measurement signal, λ. As can be seen, it has a good portion of both low and high frequency power. The detailed nature of λ is described below.

As noted above, the describing function between any response parameter and the input would theoretically provide all the available information. Figure 2 clearly indicates why this is not so in practice. When measuring the describing function in one frequency region, power in other frequency regions are essentially noise. The signal-to-noise level in the control stick response at low frequency is extremely poor. Similarly, the signal in the position response at high frequency is non-existent for purposes of practical measurement. But, summing the position and stick motions, we can create a single measurement signal, λ, where $\lambda = x + C_\lambda \delta$, which is both prewhitened and presensitized. This is illustrated further in Fig. 3. For gust inputs, position is completely dominated by the path mode (ω''_p); information at short-period (attitude) frequencies in this signal would be 40 dB down even if the gust input spectra was flat out to this region. On the other hand, the control stick signal is dominated by the attitude mode (ω''_{sp}) with system numerator zeros essentially cancelling the path mode. As shown in Fig. 3, the measurement signal, λ, contains both modes in good proportion. The constant C_λ controls the relative amounts of the two signals. Its proper value is very much dependent on how the pilot closes the loops and therefore a function of the test condition variables. In practice, there

turned out to be a very simple solution to this potential problem. During the initial portion of each run the experimenter would observe the strip chart traces of the x, δ, and λ signals. Prior to the start of data recording, he would adjust C_λ until satisfied with the frequency content of λ. His visual observation of the time trace proved to be a sufficiently accurate indication of measurement power adequacy.

FITTING PROCEDURE

Given the measured closed-loop describing function, the next step is to extract the pilot model parameter values. A model matching program which minimizes the error between the measured and modeled properties was used. It was run on our digital timesharing facilities and allows the user to select from (or sequence) four parameter optimization or search routines — the Parallel Tangent Technique (Ref. 4), a modified Deflected Gradient (Davidon) Method (Ref. 5), Gauss' Least-Squares Method (Ref. 5), and a Random Search Routine (Ref. 6).

The manner in which the error between the model and measured describing functions was treated is as follows. The $\lambda/u_g(j\omega)]$" describing function at a single frequency, ω_i, has both magnitude and phase, i.e., it is a vector $q(j\omega_i)$. The closed-loop describing function of the <u>actual</u> pilot/vehicle system, $q_A(j\omega_i)$, can be measured ("data") and the corresponding transfer function for the <u>model</u> pilot/vehicle system, $q_M(j\omega_i)$, can be computed for assumed values of the pilot model parameters. The corresponding model versus data error is a vector. It is the squared magnitude of this error which is used in the "minimization cost function." This is given by:

$$\begin{aligned} \epsilon_i^2 &= |\overline{\epsilon}(\omega_i)|^2 \\ &= \left\{\mathrm{Re}[q_A(j\omega_i)] - \mathrm{Re}[q_M(\omega_i)]\right\}^2 \\ &\quad + \left\{\mathrm{Im}[q_A(j\omega_i)] - \mathrm{Im}[q_M(j\omega_i)]\right\}^2 \end{aligned} \qquad (3)$$

where $\mathrm{Re}[\ ]$ = real part of [ ]
$\mathrm{Im}[\ ]$ = imaginary part of [ ]

The "cost function" is the sum of these errors across all frequencies, i.e.,

$$CF = \sum_i \epsilon_i^2 \qquad (4)$$

An overview of the measurement technique is shown in Fig. 4

In operation, a single describing function is obtained during the simulation run, i.e., closed-loop λ/u_g. Variances of all the system responses are also measured. A pilot model form is assumed which, in combination with the known vehicle dynamic characteristics, provides an analytic pilot/vehicle system model. The model matching program then gives the "best fit" pilot model parameter values. These, in combination with the known disturbance, using standard programs, provide open-loop pilot and pilot/vehicle describing functions and system properties such as stability margins, crossover frequencies, closed-loop modes, etc. Finally, the variances of the model responses to the disturbance are computed. These are compared to the measured variances and, in combination with the other computed properties, provide an indication of the adequacy of the assumed pilot model forms.

EXAMPLE

An example of the information provided by the technique is shown in Fig. 5. A complete explanation of this figure is beyond the scope of this paper (see Ref. 7). The data for the run consisted of:

1. The measured closed-loop describing function, $\lambda/u_g(j\omega)]$", at the five input frequencies, shown in Fig. 5d, and

2. The total performance measures, i.e., the measured rms values shown in Fig. 5b.

The pilot model form used is shown in Fig. 5a.

The digital model matching program was used to obtain the pilot model parameter values given in Fig. 5c. In obtaining the best fit, all parameters were allowed to vary; it was an eight parameter fit to ten (real and imaginary parts at five frequencies) data points.

The derived model parameter values and the known vehicle characteristics were used to obtain the remaining information shown in Fig. 5. The closed-loop response of the model to the gust input is plotted (Fig. 5d) for a graphical indication of the adequacy of the fit. In several cases, the graphical comparison indicated that the search routine had reached a local minimum and further iterations were made. As is evident in Fig. 5d, the objective in designing the measurement signal, λ, was achieved; i.e., the significant modes of the closed-loop system are contained in the single signal. System surveys of the modeled inner- and outer-loops are shown in Figs. 5e and 5f.

The final items, Fig. 5b, are the rms responses of the model system to the gust input. Comparison of these responses with the measured data indicates that a significant portion of the total performance measures is due to inputs other than the gust, i.e., the pilot's remnant. Measurement of this component of the complete human operator description has been treated elsewhere, e.g., Ref. 8.

REFERENCES

1. McRuer, Duane, Dunstan Graham, Ezra Krendel, and William Reisener, Jr., Human Pilot Dynamics in Compensatory Systems — Theory, Models, and Experiments with Controlled Element and Forcing Function Variations, AFFDL-TR-65-15, July 1965.

2. Stapleford, Robert L., Samuel J. Craig, and Jean A. Tennant, Measurement of Pilot Describing Functions in Single-Controller Multiloop Tasks, NASA CR-1238, Jan. 1969.

3. Weir, David H., and Duane T. McRuer, Pilot Dynamics for Instrument Approach Tasks: Full Panel Multiloop and Flight Director Operations, NASA CR- , forthcoming.

4. Stapleford, R. L., D. T. McRuer, L. G. Hofmann, and G. L. Teper, A Practial Optimization Design Procedure for Stability Augmentation Systems, AFFDL-TR-70-11, Oct. 1970.

5. Wilde, Douglass J., and Charles S. Beightler, Foundations of Optimization, Englewood Cliffs, N. J., Prentice-Hall, 1967.

6. Johannsen, G., "A Method for the Development and Optimization of Controller-Models for Man-Machine Systems," Working Papers of the Advanced Study Institute on Displays and Controls, Berchtesgaden, March 15-26, 1971, pp. 5.3-19 to 5.3-35.

7. Teper, Gary L., An Assessment of the "Paper Pilot" — An Analytical Approach to the Specification and Evaluation of Flying Qualities, AFFDL-TR-71-174 (forthcoming).

8. Magdaleno, R. E., Serial Segments Method for Measuring Remnant, Systems Technology, Inc., Paper No. 106, Apr. 1971, paper presented at the 7th Annual NASA-Univ. Conf. on Manual Control, USC, 2-4 June 1971.

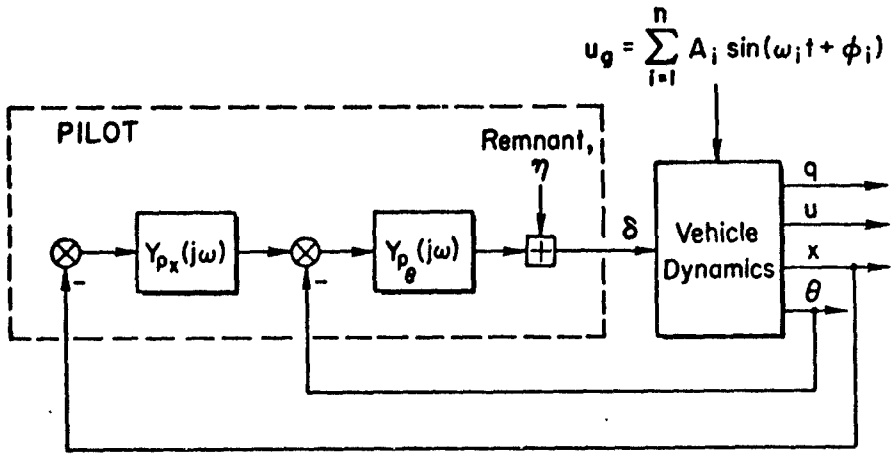

Figure 1. Pilot-Vehicle System for Longitudinal Hover Control

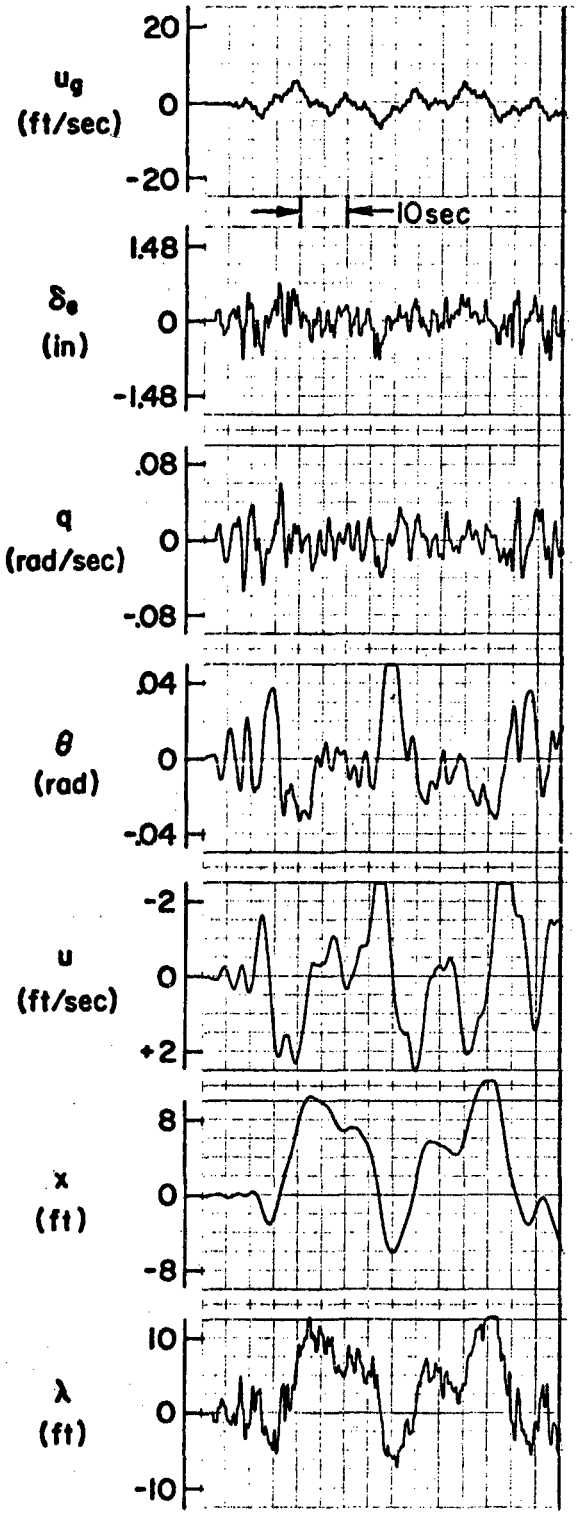

Figure 2. Typical Time Histories from Hover Simulation

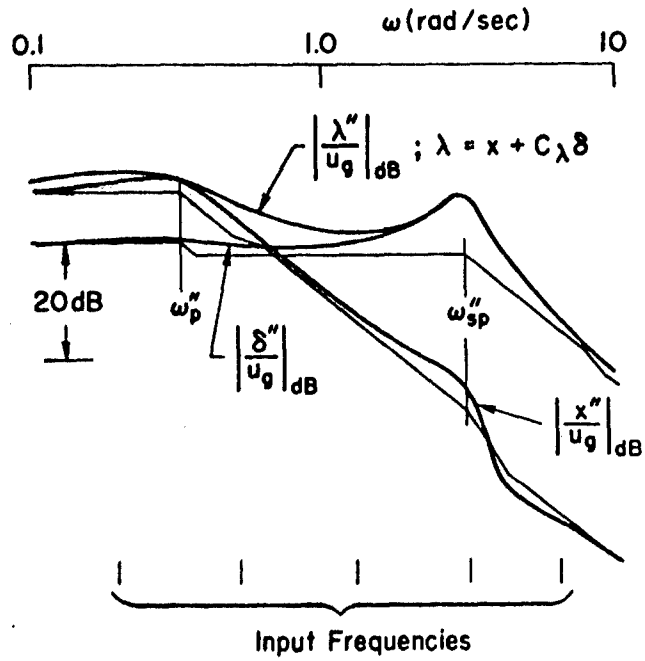

Figure 3. Typical Closed Loop Responses to u_g.

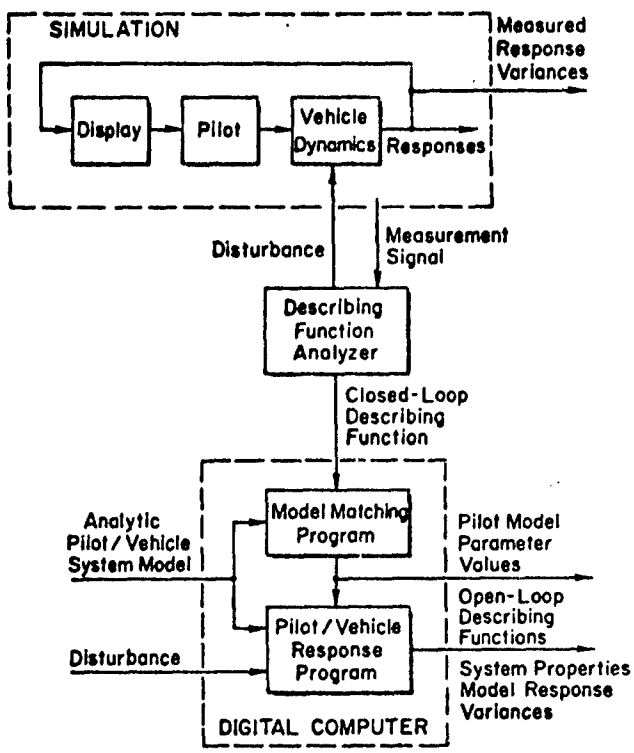

Figure 4. Block Diagram of Human Operator Dynamic Response Measurement Technique

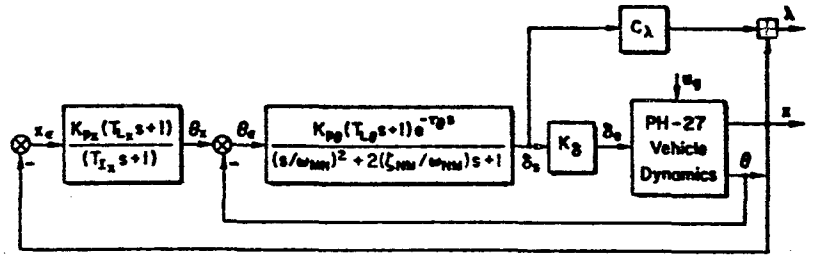

a) Pilot/Vehicle Model Precision Hover

	Model Response to u_g Input rms	Data Measured rms
X (ft)	.32814E 0	.41601E 0
U (ft/sec)	.13754E 0	.20636E 0
THETA (rad)	.33600E-2	.59598E-2
Q (rad/sec)	.30552E-2	.71777E-2
DE (in)	.56011E-1	.84462E-1
LAMDA (ft)	.31728E 0	.60307E 0

b) Performance Measures

Run 20-23, PH-27

K_δ = .80 ; C_λ = -5.67

σ_{u_g} = 2.55 ft/sec ; Pilot B

POR = 4

K_{p_x} = -.00921 rad/ser

T_{L_x} = 3.10 sec

T_{I_x} = .689 sec

K_{p_θ} = 23.5 in/rad

T_{L_θ} = .041 sec

τ_θ = .361 sec

ζ_{NM} = 0

ω_{NM} = 5.90 rad/sec

c) Pilot Model Parameter Values

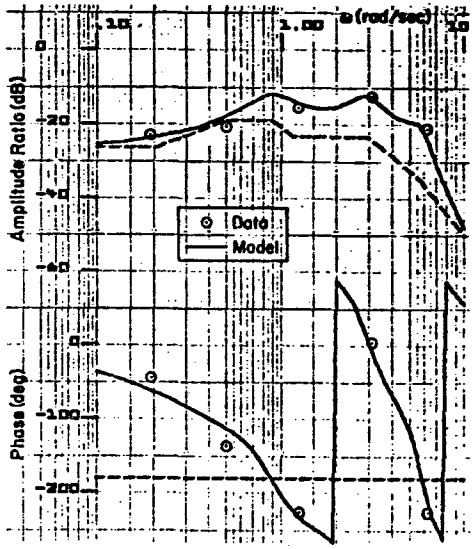

d) Closed-Loop Response to u_g Input, $\frac{\lambda}{u_g}(j\omega)$

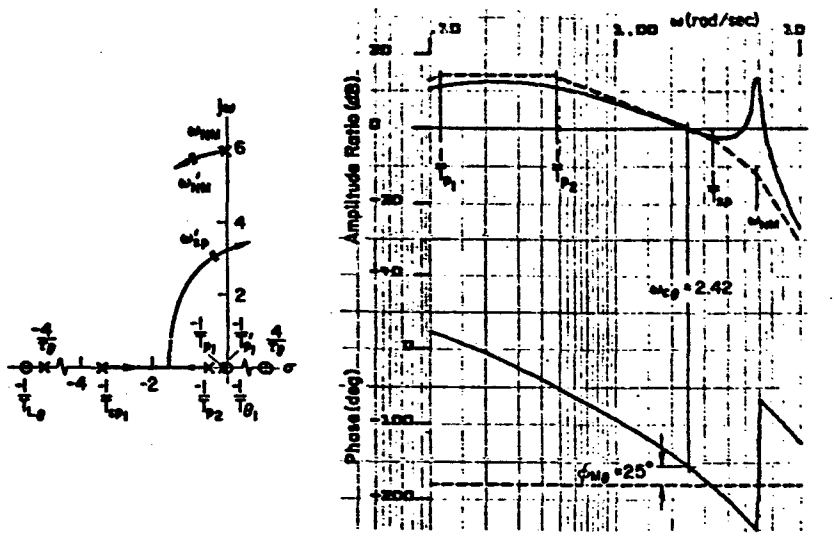

e) System Survey of Model Inner Loop, $\theta \rightarrow \delta_e$

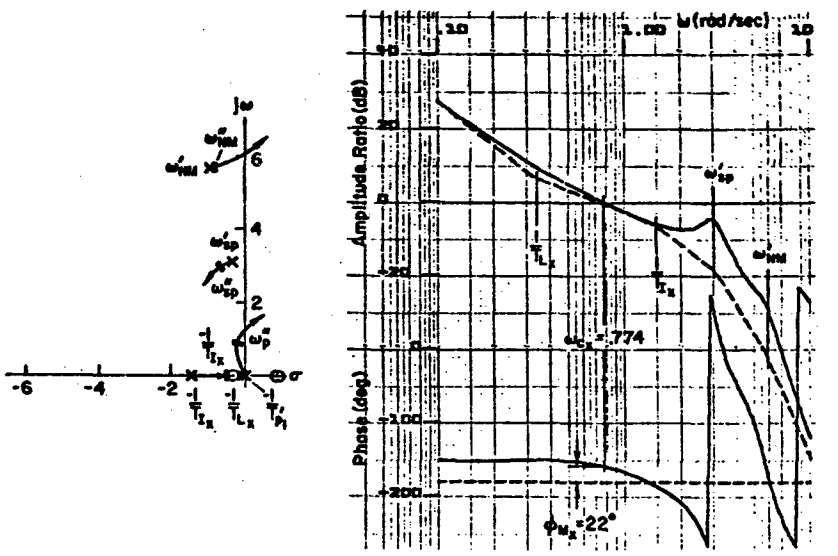

f) System Survey of Model Outer Loop, $x \rightarrow \theta_c$

Figure 5. Analysis of Data from Typical Run from the Hover Simulation

OPERATOR CONTROL OF CROSSOVER MODEL PARAMETERS

Gary L. Rupp
The University of Michigan

A parameter tracking system was utilized to provide on-line feedback of the crossover model parameters to operators performing a compensatory tracking task. Operators were required to control an integrator plant under conditions representing quite different styles of behavior in order to investigate the lability of the parameters. The usefulness of this kind of on-line feedback as a training device is also discussed.

From an engineering viewpoint the crossover model describes operator behavior very well in a rather wide variety of tracking tasks. (1) The operator tends to adjust his behavior such that the forward loop of the compensatory system can be closely approximated by the two parameters, gain and effective time delay, of the simple crossover model. This paper describes an attempt to determine the general meaningfulness of these parameters to the operator. In particular, if a parameter is meaningful then it ought to be labile, which in turn suggests that an operator should be able to voluntarily modify his gain and/or time delay. So one question to be explored is the issue of parameter lability. Secondly, if the parameter is labile, will the knowledge about that parameter contribute to improved tracking performance.

METHOD

The Display. A technique for providing an operator with on-line information about the status of his parameters can be derived from the parameter tracking version of the crossover model developed by Jackson (2).

Preceding page blank

Figure 1 depicts the basic configuration of the parameter tracking system. Both the compensatory system and the assumed model are excited by the same input disturbance. The two parameters of the crossover model are continuously updated, using gradient techniques, in order to provide a best match between the compensatory system output and the model output. These parameter updates can then be displayed to the operator while he is performing the tracking task.

The display selected to provide the operator with information about the crossover model is shown in Figure 2. The output of the parameter adjustment block of Figure 1 defines the current values of the parameters. The experimenter preselects a value of gain and/or time delay at which he wishes the system to be controlled. The operator then views information about the sign and magnitude of the deviation of his parameter values from the desired values. When both parameters are being controlled, the display becomes an ellipse whose diameters are proportional to the difference between desired and actual values of the model parameters. The horizontal diameter relates the magnitude of the gain difference. The vertical axis reflects the time delay deviation. The sign of the differences is displayed via a series of lights place around the periphery of the CRT. For example, if the +K light is on, the operator's gain is too high and must be lowered to the appropriate value.

The Experiment. Twenty subjects practiced tracking a two radian/sec. random imput signal for sixteen 90-second trials prior to the actual experiment. The imput signal had a Gaussian amplitude distribution

and was generated by appropriately filtering a pseudo-random pulse sequence with a third-order binomial filter. After each trial the integrated absolute error score (IAE) for that trial was displayed to the operator. Based upon their normalized integrated error score (NIAE), gain (K), and time delay (T) over the last 8 trials, fifteen Ss were matched into three groups of five Ss each.

The control group trained for five more days on the two radian/second input signal. Their task was to minimize their error score (IAE). As an aid they were provided with an on-line display consisting of a circle whose diameter was proportional to the average of their IAE for the preceding two seconds. After five days they transferred to a four radian/second tracking task for three more days.

The other two groups received the experimental treatment, ie. a display of crossover model parameters, gain and effective time delay. For the two rad./sec. (or slow) input forcing function both groups practiced under two conditions of gain and time delay. The HK condition required operators to control the compensatory system with a high gain and a low time delay. The values chosen were $K = 7.5$ sec.$^{-1}$ and $T = 0.175$ sec. In the LK condition, representing low gain and a low time delay tracking, $K = 4.5$ sec.$^{-1}$ and $T = 0.250$ sec. These two conditions on the crossover model parameters represent quite different styles of tracking behavior. Further, the LK condition will require an operator to sacrifice some error score in order to accomplish the task.

For the slow (two rad./sec.) input signal, one experimental group practiced five days under HK conditions and then transferred to the LK condition for three days. The other group began in the LK condition and on the sixth day transferred to the HK condition for an additional three days. After eight days both groups were transferred to the 4 rad./sec., or fast input signal for the final three days. They were asked to control the compensatory system with a high gain ($K = 6.0$ sec.$^{-1}$) and a low time delay ($T = 0.09$ sec.). The instructions suggested that these parameter values would be difficult to attain, but the parameter information should serve as a guide toward achieving low error scores.

Each day Ss performed 20 trials arranged in four blocks of five 90-second trials. A five second tone count (1/sec.) warned S prior to each trial. During the 45-sec. rest period following a trial, S viewed his IAE, gain, and time delay values for that trial. The control group only saw their IAE score. Parameter values were always initialized to the desired values so that the ellipse began as a point. The experimental groups were instructed to keep the ellipse a point and also to achieve as low an error score as possible.

The tracking error was displayed as a horizontally moving dot on a Hewlett-Packard Model 1300 CRT (.10 in/v sensitivity). The maximum peak-to-peak amplitude of the input was approximately 75v. The S was seated in a testing booth with his eyes about 28 in. from the display. The control stick was mounted on an arm rest, was grasped with the right hand, and required small pronating-supinating movements of the hand. A spring-restoring force of about .07 lb./deg. was produced by

a thin rubber sleeve that was not uniform in its response characteristics. The stick's moving friction was approximately .23 lb. and intetia about .05 lb.-ft^2. Its movement range was ± 22 deg. left-right with fore-aft movements mechanically blocked. Control stick sensitivity was 14.2 v/deg and the single integrator plant dynamics was 6/p. The tracking system was stimulated on an analog computer and used a first-order Pade approximation as the time delay in the crossover model.

RESULTS

In Figure 3,4 groups are labelled according to the condition in which they began the experiment. For example, the HK group practiced for 5 days under HK, 3 days under LK, and 3 days with the fast input. Also, days 6-8 for the control group are plotted on days 9-11 to permit comparison across groups for the fast input task. An average measure for all Ss on the day of matching is shown prior to day 1 on all graphs.

The power match is defined as

$$PM = 1 - \frac{\int_{45}^{90} (\text{matching error})^2 dt}{\int_{45}^{90} (\text{compensatory output})^2 dt}$$

and is a measure of the percentage of the compensatory system output accounted for by the crossover model. Power match is computed over the last half of a trial to allow for parameter convergence. In Figure 3 (top) the power match is shown averaged across subjects within groups for

each day of practice. Clearly the crossover model is a good match to S's system for both input bandwidths. For the slower 2 rps input signal the model accounts for about 98% of the operator output in the HK and control conditions. For the LK condition the model match is approximately 96%. With the faster 4 rps input bandwidth the power match is about 90% for all groups.

The error scores (IAE) are normalized with respect to the integrated absolute value of the input and plotted as a function of training in Figure 3 (bottom). Notice that operators in the LK condition were forced to sacrifice considerable error score to accomplish the low gain - high time delay tracking task. The fact that they also had lower power matches suggests that they probably sacrificed more error than necessary to perform the task. Secondly, operators tracking in the HK condition have error scores nearly identical to the control subjects. Also, the group making the LK-HK transition (day6) performs at about the same level of error under the HK condition as on the matching day and their rate of improvement parallels the other groups. Apparently practice in the LK condition, which represents suboptimal tracking error performance, did not aid nor hinder their ability to achieve low NIAE scores. Finally, both groups receiving the experimental treatment have slightly lower NIAE scores than the control Ss when transferred to the 4 rps input task. These differences may be significant but are certainly small and probably unimportant.

The variation of the model parameters with practice is shown in Figure 4. It is interesting to note that all Ss in both experimental groups were immediately successful in achieving the low gains for the 2 rps input bandwidth. The group making the LK-HK transfer had nearly the same gains and time delays on the day of transfer as on the day of matching. Apparently the training at low K's was similar to having no practice at all.

On the other hand, operators had more trouble getting high time delays after the HK practice. Only two Ss who transferred from the low T condition (HK) performed well at high time delays (another S was marginally successful) after three days of practice. Four of the five operators who began in the LK condition successfully managed the high time delays by day 2.

Both experimental groups receiving the HK condition achieved slightly lower gains with essentially the same effective time delays as the control group. In all, six Ss in the experimental treatment successfully controlled the system with high gains and low time delays. Four Ss never achieved high K's repeatedly and three Ss could not get low T's.

Both treatment groups exhibit slightly higher gains and somewhat lower time delays than the control group on the fast input tracking task. Between the experimental groups there are no gain differences but the HK group did have somewhat lower time delays.

DISCUSSION

The fact that it is very easy for operators in the slow input task to control a system at gains of 4.5 $sec.^{-1}$ suggests that performance at other gains below their normal tracking gain (as measured on the matching day) would also be easy. One would expect the gain parameter to be quite labile in this range. On the other hand, parameter feedback did not assist acquisition of gains above the free tracking value. Even though operators had an idea of what higher gains meant, they could not generate these gains without having a training period equal to that of control Ss. Presumably, operators could easily achieve all gains below the value to which they have been trained regardless of the training procedure.

It also appears to take somewhat more practice for operators to perform at time delays much different from their normal T. Operators in all groups require approximately equivalent training periods to achieve lowered T's. All operators could raise their time delay slightly above its free tracking value, but not all could achieve the specified T of 0.25 sec. The greater success in achieving higher time delays than lower ones could in part be explained by reasoning that the ease of maintaining the lower gains permitted more attention to be directed toward controlling T. Clearly there is some lability for the time delay parameter, but it is not as evident as for the gain parameter.

The similarity of error between the control and HK conditions suggests that operators do perform optimally according to an error minimization criteria. The feedback of parameter information only marginally improves

NIAE scores in the 4 rps task environment and so was not very useful as a procedure for training operators. Perhaps more complex tasks or different performance criteria would yield more important effects for this type of information feedback.

As might be expected, an examination of the S's control stick responses reveals that the many rapid movements of the HK condition become slower, almost square wave in nature for LK control. The following quote is an example of one S's perception of his control task; "If -T and +K lights are on: make the dot swing slowly back and forth across the center; do not necessarily attempt to stop the dot at the center. The oscillation should be about 1 inch on either side of the center and hand movements should be slow. Allowing the dot to swing to both sides of the center and not stopping it in the center raises T, while the slow hand movements and not jumping the dot back and forth lower K."

REFERENCES

1. McRuer, D.T., and Jex, H.R., A review of quasi-linear pilot models. IEEE Trans. on HFE. 1967, 231-239.

2. Jackson, G.A., A method for direct measurement of crossover model parameters. IEEE Trans. on MMS. 1969, 27-33.

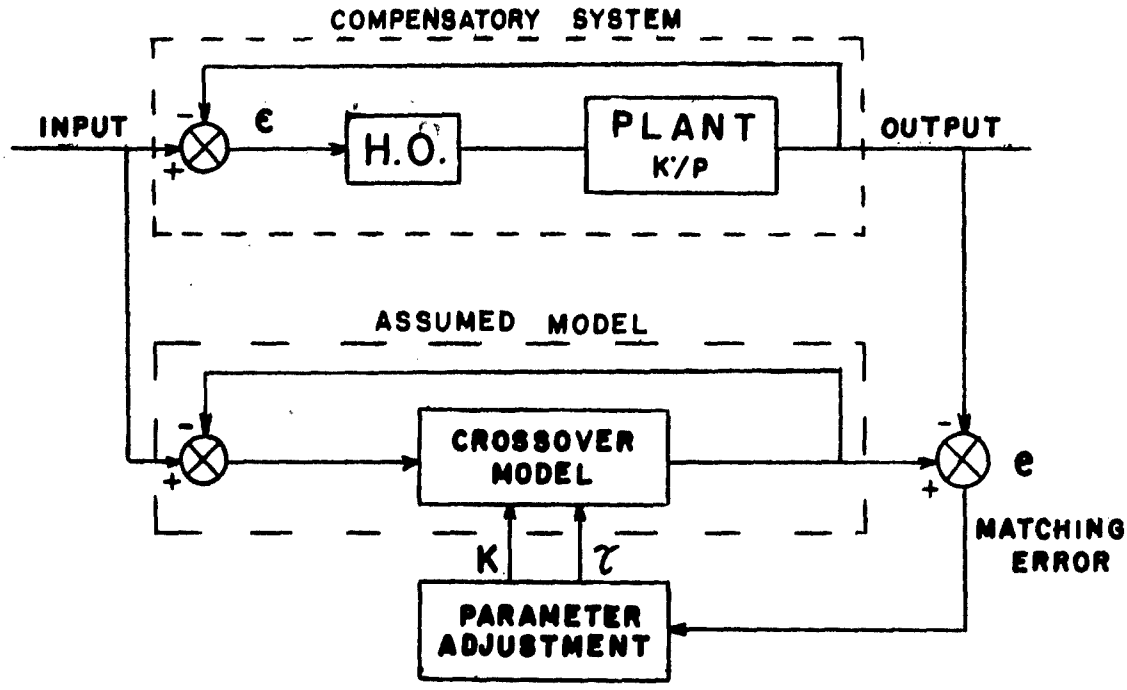

Figure 1. Block diagram of the tracking system. A random input signal drives both the compensatory system and the assumed model. Parameters are continuously adjusted by the method of output error.

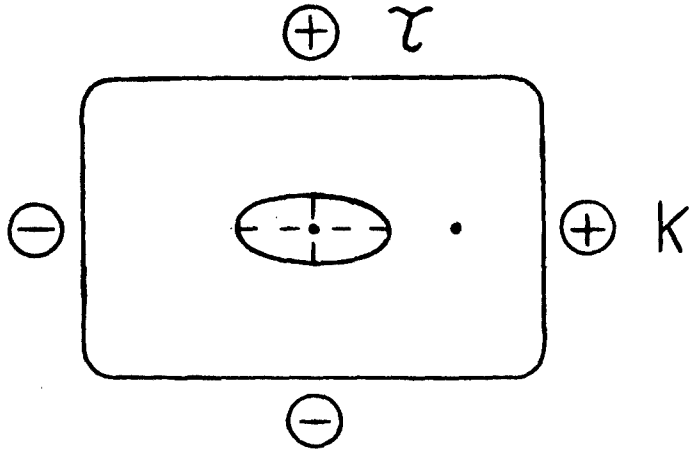

Figure 2. The display. The system of lights around the display screen indicate the sign, and the ellipse diameters relate the magnitude, of the difference between the S's parameters and the desired parameter values. The dot to the right of the ellipse is the error cursor.

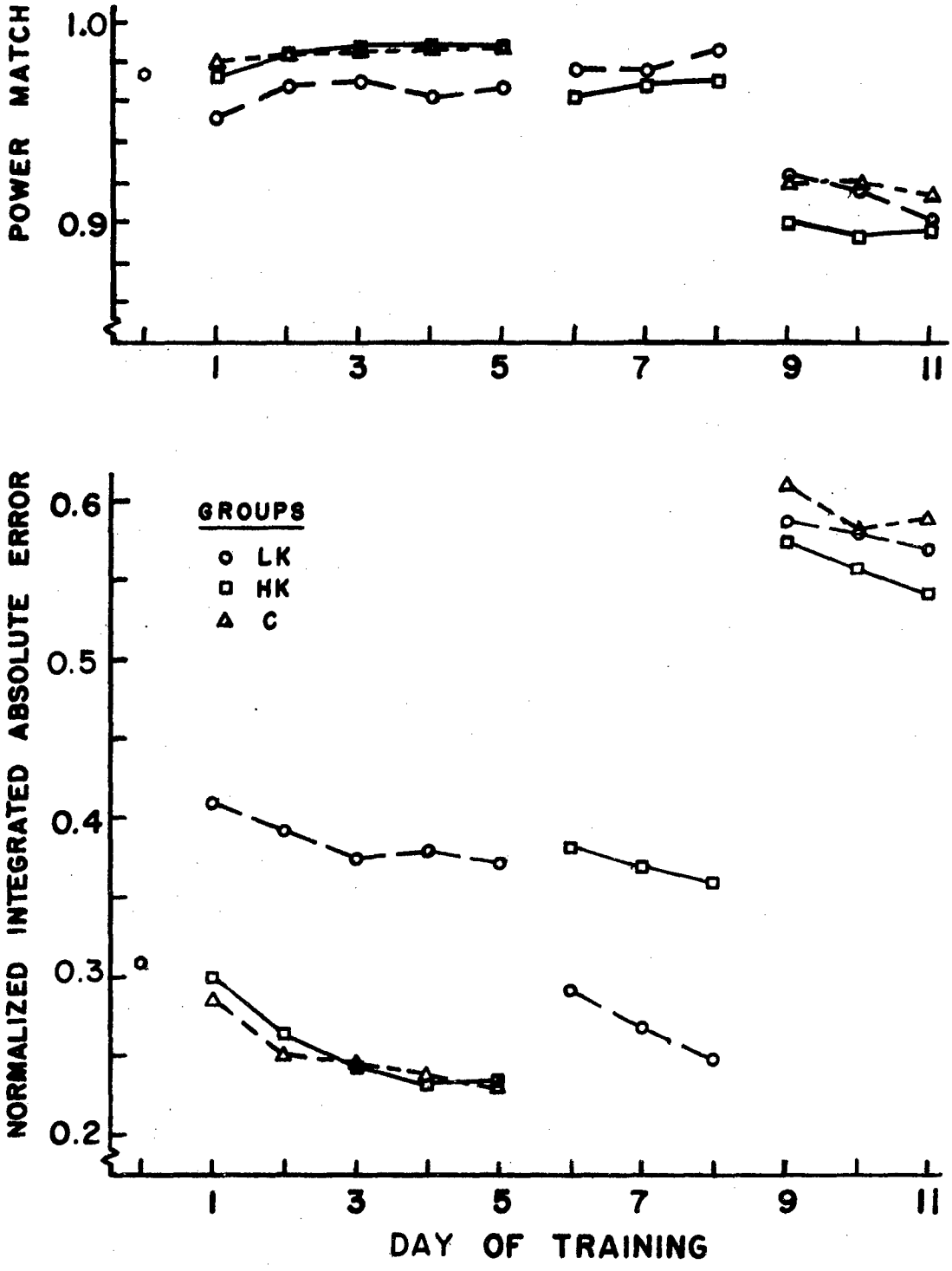

Figure 3. Measures of model match (top) and error score are shown for the three groups as a function of practice.

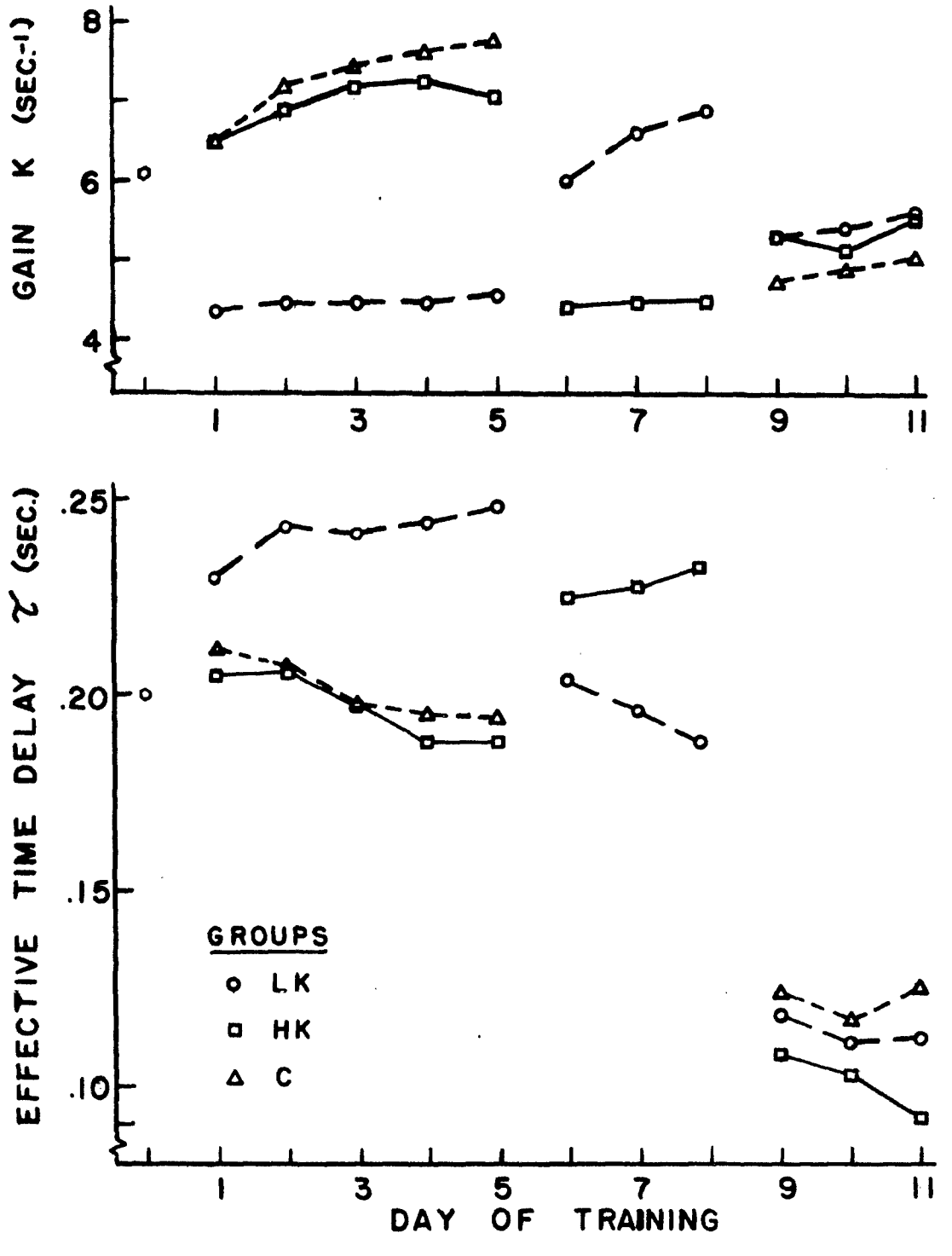

Figure 4. The two model parameters, gain and time delay, are displayed between groups as a function of day of training.

SESSION II

New Developments in Manual Control Output Devices

THE USE OF ADVANCED PILOT'S CONTROLLERS IN "FLY-BY-WIRE" VEHICLES[1]

Dr. M. Gordon-Smith
CAE Electronics Ltd., Montreal, Quebec, Canada.

ABSTRACT

As the state-of-the-art advances the future for "Fly-by-Wire" (FBW) flight control systems in both civil and military aerospace vehicles continues to brighten. FBW systems allow considerable freedom in the choice of the pilot's cockpit flight controls. The usual configuration proposed is that of a side-arm controller, but this does not necessarily represent the optimum. This paper reviews some of the factors that should be considered when determining the configuration of an advanced pilot's controller and makes brief mention of experience gained with a multi-axis side-arm controller in a helicopter.

I. INTRODUCTION

This paper stems from some recent work that was performed to determine the optimum configuration of an advanced pilot's controller for a helicopter. However, the discussion that follows is equally applicable to conventional fixed wing aircraft or space-craft, since in actual fact, these vehicles offer fewer problems than the helicopter, in many respects, when conducting trade-off studies of this nature.

II. BACKGROUND

A FBW flight control system is defined as one in which the mechanical linkages between the pilot's cockpit flight controls and the control surface actuators (or their equivalent) have been replaced by electrical signals. Figure 1 shows a sketch of the basic FBW system in which position transducers on the pilot's cockpit controls generate electrical signals that are operated on by the Command Augmentation System (CAS). These modified commands result in displacement of the usually electrohydraulic servo-actuators that position the aerodynamic control surfaces. The response of the vehicle is sensed by the Stability Augmentation System (SAS) that provides the necessary feedback signals to yield the desired stability characteristics. An important point to note is that the CAS and SAS may be modified independently of each other since their functions are quite different. In practice, one would first determine the parameters of the SAS to provide satisfactory stability throughout the flight envelope and then would adjust the parameters of the CAS to give acceptable vehicle response to pilot commands.

[1]The views and opinions expressed herein are not necessarily those of the U. S. or Canadian Governments.

Preceding page blank

One of the many projected advantages of a FBW system, over its mechanical counterpart, is that it results in considerable freedom to redesign the total cockpit environment such that, in combination with the ideal handling qualities that are theoretically possible through the appropriate choice of CSAS parameters, the optimum pilot/vehicle integration can be achieved.

The optimization of the pilot/vehicle command interface, i.e. the cockpit flight controls, is of critical importance in a FBW system, since the pilot's confidence in, and his acceptance of, the FBW concept will be governed to a large extent by the ease and harmony with which he can make command inputs to the vehicle so as to change its flight path.

When presented with this new freedom to apply their expertise in the relatively unconstrained atmosphere of the FBW flight control system, the first reaction of the cockpit layout designer and the human factors engineer is to propose that the conventional stick and rudder pedals (and collective, in the case of the helicopter) be replaced by a small multi-axis side-arm controller located in the armrest of the pilot's seat. The argument of the cockpit layout designer is that the control stick or yoke obscures essential display panel area, while that of the human factors engineer is that the characteristics of the side-arm controller can be more easily matched to the pilot and the single command input device allows greatly improved man/machine integration.

However, when viewed from the overall system standpoint, the matter is not nearly that simple. In fact, there are a large number of other equally important criteria to be considered before choosing the configuration of the pilot's controls. In many cases, the side-arm controller is clearly not the optimum configuration, and, no matter how attractive the concept may be theoretically, the transformation of this ideal into actual hardware to be used by pilots, on an operational daily basis, who are neither test pilots, astronauts, nor research engineers, creates problems that can often be insoluble.

The literature shows some activity in the area of the application of unconventional flight controls and side-arm controllers to operational vehicles over the last ten years or more, (References 1 to 5). However little success was achieved, mainly because the controllers were usually interfaced with mechanical linkages and, the combined problems of excessive sensitivity, and friction and backlash in the linkages, defeated their purpose. No unconventional flight controls reached the level of civil or military operational use as primary flight controllers. Side-arm controllers have appeared in other applications, such as the control of gun-turrets (Reference 6) and radar antenna, and in addition as flight controllers with limited authority for precision hovering manoeuvres of transport helicopters for cargo-

handling operations. The advent of genuine FBW flight control systems in the space vehicles (Reference 7) and in various military research and demonstration programs has resulted in renewed interest in what we shall call "Advanced Pilot's Controllers", (APC's). The literature on man/machine systems research contains many examples of specialized controllers or manipulators, however their use has been restricted to laboratory tracking experiments.

References 7 and 8 describe two interesting studies of the application of advanced pilot's controllers. But again they are restricted to the basic human engineering of the form and location of the APC or the in-flight evaluation of relatively unsophisticated hardware. The study that this paper will describe was performed in considerable detail as an attempt to evaluate as many aspects as possible of the APC with the purpose of making recommendations as to actual operational hardware to be built for a proposed production FBW vehicle.

III. GENERAL APPROACH

The following approach is suggested for a trade-off study of advanced pilot's controllers to determine the optimum configuration for a particular vehicle.

3.1 Ground Rules and Major Constraints

As a first step, the basic objectives of the vehicle and the conditions under which the controller must operate should be reviewed. In many cases, certain ground rules are laid down by the customer that result in major constraints on the controller design. These constraints should be clearly identified as early as possible in the design definition phase, such that time and effort are not wasted on obviously unsuitable configurations.

Among the possible constraints, a few of the more important are:

1. Redundancy Level. Most FBW systems require redundancy levels that allow the system to achieve "Operate/Fail/Operate/Fail/Operate" reliability. In other words, the system must be capable of withstanding two identical failures in any component. Under this constraint each axis of the controller must be equipped with multiply-redundant position transducers and also possibly control-force actuators. This results in large weight and bulk and greatly penalizes the multi-axis side-arm controllers.

2. CSAS Mode Changes. If the performance of the CSAS is allowed to degrade after failure such that both the control-response laws and the level of stability augmentation change, then the controller configuration and characteristics must take the worst case into account.

3. Fully Variable Force-Feel Characteristics. This constraint is a necessity if good pilot/vehicle integration is to be maintained over an extensive flight envelope. This applies in particular to VTOL vehicles and the space shuttle since they operate over much larger flight envelopes than fixed wing aircraft. In addition, since the pilot can no longer receive aerodynamically-generated force-feedback cues from the controls to warn him of the proximity of the envelope limits, the controls must be provided with actuators to develop the necessary forces.

4. Special Purpose Seats. If either ejection or "crash survivable" seats are specified for the vehicle, considerable difficulty will be experienced in integrating the controller into the seat structure. This is unfortunate, since in most modern cockpits the only available space for the control-force actuators, etc., would be underneath or behind the seat. This problem does not arise when a form of cockpit escape capsule is employed.

5. Cockpit Dimensions. Because of the drag penalties associated with fuselage frontal area and other basic structural requirements, the maximum dimensions of the cockpit are usually strictly limited. The most restricted dimension is that of the cockpit width and this is particularly true of the two-pilot cockpit with side-by-side seats and a center console.

3.2 Axis Integration

The number of command axes that can be integrated in a single controller device is directly related to the level of workload to which the pilot is subjected; the lower the workload the greater the number of axes that can be combined. Of course, for fixed wing aircraft the question is only whether or not to combine the yaw axis with the pitch and roll axes, but for the helicopter there is the possibility of integrating both the yaw and thrust axes into the controller.

The workload of interest is that of stabilizing the vehicle in the presence of outside disturbances and that of controlling its flight path so as to achieve the mission objectives. Other factors contribute to the pilot's workload and these can be grouped under the heading of general aircraft system management.

The major parameter that affects the pilot's workload is the bandwidth of command activity, and this is a function of:

1. The overall vehicle dynamics, including the influence of any augmentation systems. These determine the control-response laws and the sensitivity of the aircraft to outside disturbances.

2. The preciseness with which each axis of the vehicle must be controlled in order to achieve satisfactory performance.

It follows from the above that the higher the level of stabilization provided by the CSAS, the lower is the bandwidth of command activity and hence the lower is the pilot's workload. The various levels of stabilization range from the basic unaugmented aircraft, through attitude rate and attitude stabilization, to aircraft linear velocity stabilization. For the hovering helicopter it is also convenient to have aircraft position stabilization as well. The corresponding levels of controller axis integration range from the conventional controls to the four axis side-arm controller.

So little data is available on the use of multi-axis controllers in an operational environment that the engineer can make only what amounts to an educated guess, based on multi-axis tracking experimental results, as to the number of axes that should be integrated into a single device for his application. It may well be necessary to investigate more than one configuration and subject them to simulator and in-flight evaluations.

3.3 Controller Force-Displacement Characteristics

Having defined the candidate configurations for the controller, the next step is to determine how to implement the desired force-displacement characteristics for each axis. The optimum force-displacement characteristics are, of course, functions of the responses of the Control Augmentation System. If the ground rules specify variable force-feel characteristics and envelope limiting cues, then each axis must be equipped with some form of redundant control-force actuator. In addition, the necessary computational capability must also be provided. The control forces, usually viscous damping and spring forces, may be varied as functions of any number of aircraft variables, the most common being airspeed. Figure 2 gives a functional block diagram of a control-force system using a reversible actuator.

When the vehicle operates in a very limited flight regime, e.g. a spacecraft in orbit, then a simple mechanical control-force system can be used with suitable constant spring and damping rates. This greatly reduces the mechanical complexity of multi-axis controllers in this application.

A fundamental principle of the control-force system is that the pilot should be able to overcome any of the control forces. Thus the pilot has some measure of protection against hard-over failures in the force-feel system. The reliability and redundancy requirements of the system should be given some detailed study since, if a failure results in a force hard-over, the pilot may well lose his grasp on the controller and by the time he has regained it from some far corner of the cockpit the aircraft could well be in an unrecoverable attitude. In the event that the control-force system is allowed to fail completely and become passively inoperative, with the actuator bypassed in some manner, then one has to consider the incorporation of mechanical means of

developing adequate control forces such that the pilot can still continue his mission. However, if the level of stability augmentation is sufficient, this may not be strictly necessary. Furthermore, if the CSAS has degraded modes of operation then the controller force-displacement characteristics should change to match the new CSAS mode.

3.4 Synchronization Between Pilot Stations

For the two-seat cockpit, some means must be provided to synchronize the position of all axes of the controller. In general, it should be possible for the command of the vehicle to be transferred to the second pilot at any point in the flight envelope and during any transient manoeuvre. The choice must be made between mechanical synchronization, whose complexity severely penalizes side-arm controllers of any form, and electrical synchronization using a position servo-loop and the control force actuator of the inactive controller.

The electrical synchronization approach requires some complexity in the electronics and careful attention to the logic functions in the switching arrangement and of course, redundancy should be employed.

In particular, the system should be such that the CSAS receives inputs only from the pilot station in command.

A disadvantage of the servo-loop synchronization is that, if the command pilot is suddenly incapacitated, the second pilot must perform a positive action (e.g. pressing a "command take-over button") before he can gain control of the vehicle. This delay may be of critical importance under certain conditions.

3.5 Environmental Conditions

The environmental conditions of most importance to the controller are those of the external acceleration field and vibration. If sustained high levels of acceleration are exptected, as during a spacecraft atmospheric re-entry, then the configuration of the controller should be chosen so that the pilot can operate it easily, to the extent that it will be required during that flight phase, and at the same time have the operating limb adequately supported against the acceleration-induced forces. This is, of course, one of the greatest advantages of the side-arm controller mounted on the seat arm-rest. Even if large sustained accelerations are not expected during the mission, common aircraft manoeuvres can result in imposed accelerations that are large enough for it to be essential that all axes of the controller be fully mass-balanced. This requirement imposes a severe weight penalty on all side-arm configurations, particularly the 3- and 4-axis controllers.

The vibration environment is usually most pronounced in helicopters. Considerable care should be taken in the mechanical design of any

controller configuration to prevent structural resonant frequencies close to aircraft natural frequencies and to ensure adequate fatigue life of all components.

3.6 Review of Controller Configurations

Figures 3 to 10 show views of some of the possible configurations for an advanced pilot's controller. The configurations are based on the helicopter but, with the Z-axis removed, are applicable to any other vehicle. The configurations range from "improved" forms of the conventional controls to the 4-axis side-arm controller. One configuration that is conspicuous by its absence is the "pencil stick", one of the favourite laboratory experimental manipulators. It is not included for the simple reason that the handgrip has to be of a size sufficient to contain the switches and their associated cabling that are required by the operational pilot.

The linkages that would be required for mechanical synchronization between pilot stations are not shown in the figures, and neither are the electronic units that would provide the control-force computation and logic functions. The motions of the hand grip(s) or pedals are indicated by arrows and the axes are identified as follows:

X - Longitudinal axis	-	pitch	(Longitudinal cyclic)
Y - Lateral axis	-	roll	(Lateral cyclic)
H - Directional axis	-	yaw	(Pedals)
Z - Vertical axis	-	thrust	(Collective)

3.6.1 Configuration 2 + 1 + 1 A

This configuration, Figure 3, combines the pedals, collective, and cyclic mechanisms into a single unit that can be mounted partially or completely below deck. With the appropriate airframe design the unit can be easily removed for maintenance. The grip and pedal positions can be made adjustable to fit the individual pilot. This design would allow mechanical synchronization if necessary.

3.6.2 Configuration 2 + 1 + 1 B

This configuration replaces the centre stick with a yoke protruding from the instrument panel, Figure 4. Again the pedals, collective and yoke are combined into a single unit. The mechanization of the collective could be a problem, however. The pedestal could form the support of the entire instrument panel, and mechanical synchronization of pilot stations need not be too great a problem with this configuration.

3.6.3 Configuration 2 + 1 + 1 C

In this controller, Figure 5, the centre stick is replaced by one beside the seat and the mechanisms for the pedals and collective are separated into individual units. Each unit can be easily removed for maintenance and mechanical synchronization is still feasible. The controller units are not connected with the seat in any way and thus do not restrict its movement. The "side-seat" stick for the longitudinal and lateral axes, when used with an arm-rest on the seat, could give almost as good harmony of operation and fine control of movement as the centre stick, except for the case when the stick is full forward and full right laterally. The side-seat stick will require some additional space to avoid fouling on the centre console in the dual side-by-side cockpit.

3.6.4 Configuration 2 + 1 + 1 D

Figure 6 shows the next stage in the progression, in which the side-seat cyclic of configuration 2 + 1 + 1 C is replaced by a 2-axis side-arm controller. In this case the side-arm controller mechanism can be attached to the seat structure. The pedals and collective remain as separate units. The side-arm controller adds some width to the seat and mechanical synchronization would be quite difficult. In addition, the side-arm controller would have to be adjustable relative to the seat to accommodate a wide range of pilots.

The X-axis motion may be linear or rotational, with the axis in any location ranging from the center of the grip to well below the hand. This would apply to the X-axis of any of the following side-arm configurations.

3.6.5 Configuration 2 + 2

Combining the pedals and collective into a second side-arm controller gives the configuration of Figure 7. Both mechanisms are integrated with the seat structure, yet should be adjustable relative to it. The increase in seat width is considerable and mechanical synchronization would be difficult. The similar motions for the longitudinal and vertical axes could result in control harmony problems.

3.6.6 Configuration 3 + 1 A

In the next configuration, Figure 8, the directional axis is combined with longitudinal and lateral to give a 3-axis side-seat controller with a separate collective. The units are not attached to the seat structure and are easily removed for maintenance.

3.6.7 Configuration 3 + 1 B

By replacing the side-seat stick with the 3-axis side-arm mechanism we get the configuration shown in Figure 9. The side-arm controller

may be integrated into the seat structure but, as before, it would have to be adjustable. The mechanization is made more complex than that of the 2-axis side-arm controller by the addition of the H-axis and mechanical synchronization would be nearly out of the question.

3.6.8 Configuration 4

Finally, we have the 4-axis side-arm controller for use primarily in helicopters, Figure 10. In this case the Z-axis operates about a pivot point some distance forward of the elbow, and the X-axis should certainly be a linear motion to reduce cross-coupling. The mechanism would be extremely complex, particularly when redundant transducers and control-force actuators are employed, and mechanical synchronization would be effectively impossible.

3.7 Trade-Off Criteria

Having rejected the obviously unsuitable configurations, based on the ground rules and constraints, the remaining candidate controllers can then be compared using the criteria that are defined and briefly discussed below. The list does not attempt to be exhaustive, but it does cover the three important interfaces between the advanced pilot's controller and -

a. The pilot

b. The flight control system (CSAS)

c. The cockpit layout and general airframe.

3.7.1 Pilot-Centred Criteria

Pilot Physical Workload: The physical effort required of the pilot to operate the controls during flight. Configurations that use only the pilot's hands result in lower workload than those using both hands and feet. However, the 4-axis controller places a very heavy demand on a single limb and thus would be downgraded.

Control-Response Harmony: The relationship between controller displacements and pilot-applied forces and the resulting motions of the aircraft and the pilot-experienced accelerations. The yoke of configuration 2 + 1 + 1 B may offer some advantage in roll manoeuvres, but care would have to be taken with the Z-axis of configuration 2 + 2 to avoid harmony problems when performing complex, multi-axis operations.

Cross-Coupling Tendency: The tendency for the pilot to make inadvertent commands into unwanted axes because of the controller configuration. The risk of cross-coupling increases as the axes are integrated, being the greatest for the 4-axis configuration.

It can be avoided to some extent in the side-arm controllers by using a linear motion for the X-axis rather than a rotational one. This reduces the orientation changes of the H-axis to those produced by the Y-axis alone. The most severe cross-coupling in the 4-axis controller tends to occur between the X and Z axes.

Pilot Training Time: The time required to convert a pilot with considerable experience on conventional controls to the advanced controller. This training time will tend to increase with an increase in axis integration. It is possible that the 2 + 2 configuration may require the longest training period because it involves two axes on the left hand, which, for a normally right-handed pilot, could prove difficult. Looking further ahead, it may well be the case that it would be easier to train a pilot "ab initio" on the advanced controllers, rather than to convert a conventional pilot, since there would be no unlearning of old techniques involved.

Ingress/Egress: The ease with which the pilot can get into and out of his seat under both normal and emergency conditions. For single seat and dual-tandem cockpits there are few problems with any configuration in the area of ingress and egress since it normally occurs from above. However, for the dual side-by-side cockpit, where entry to the cockpit is usually from a central aisle, the side-arm configurations greatly hamper free movement. Unless the considerable increase in mechanical complexity of allowing the side-arm controllers to fold is acceptable, the pilot would be forced to clamber over the arm rest, or additional space would have to be left between the controller and the center console. For the helicopter pilot, emergency egress from the dual side-by-side cockpit usually occurs through a side door, but for the right hand pilot this would again mean climbing over or around the side-arm controller. Of course, if space permitted, the seat could be moved back some distance to clear the center console or to gain access to the side exit.

Biomechanics: The matching of the controller characteristics in each axis of operation to the capabilities of the actuating limb. This involves mainly the force-displacement characteristics of the controller and the ability of the pilot to displace the controller with ease and comfort to its maximum travels in each axis, individually or simultaneously, and at up to the maximum expected rates of displacement. In addition, the pilot should be capable of making small and precise commands, single or multi-axis, at any point in the controller's displacement envelope. Any of the advanced controllers can be designed to meet the biomechanical specifications, with the possible exception of the side-seat configurations of 2 + 1 + 1 C and 3 + 1 A, where the displacement envelopes will be restricted in the full forward - full right areas. Also under this criterion one should review the human factors aspects of the grip and armrest design, switch placement, etc.

Either Handed Operation: The ability of the pilot to operate the controller with either hand, mainly so that he can use the normal hand for the operation of switches and controls on the centre or side panels. This criterion should be considered for the single seat and dual-tandem cockpits, since a side-arm controller is effectively dedicated to a single hand and all switches and controls for communications, navigation, weapons, etc. must be placed where they can be reached with ease by the other hand. However, if the vehicle can be flown "hands off" for periods of time, then some controls can be placed near the side-arm controller for operation by the dedicated hand. In general, one should consider that no important controls or switches may be placed on the same side of the cockpit as the side-arm controller. For the dual side-by-side cockpit the left hand pilot cannot effectively operate any controls on the center console when flying with a right-handed side-arm controller unless he can fly "hands-off".

Confidence Level in Pilot Acceptance: An estimation of the reaction of the pilot to the controller-CSAS-vehicle combination. This will include the handling qualities, the novelty of the control-response concepts and the controller configuration, and the pilot's confidence in the overall system. It is expected that the dual 2-axis and the 4-axis side-arm controllers will be less willingly accepted by the pilots than the "improved" conventional controls or the 3-axis controllers.

3.7.2 System Interface Criteria

Controller Operational Performance: The inherent performance of the chosen controller mechanization in the areas of friction, backlash, hysteresis, static accuracy, dynamic response, etc. In general, no particular configuration should have poorer operational performance than any of the others. However, if mechanical synchronization between the pilot stations is employed then severe problems due to friction and backlash could arise with the side-arm configurations because of their much lower mechanical advantage and the complexity of the linkages.

Integration with the CSAS: The difficulty of obtaining the desired vehicle handling qualities by adjusting the CSAS functions and parameters when using a controller configuration whose maximum displacements have been determined on biomechanical grounds. For the side-arm controller configurations with their relatively small displacements, severe problems may occur, particularly in the pitch axis, when trying to reconcile the conflicting requirements of maintaining the control sensitivity at reasonably low levels for normal flight conditions, while at the same time having adequate margin to control the vehicle at the extremes of the flight envelope. The difficulties can be reduced by choosing certain specific control-

response laws but these are often only applicable in restricted flight regimes. In general, the CSAS mechanization can be simplified somewhat by choosing a controller configuration that allows reasonable displacements.

Degraded CSAS Modes: The ability of the pilot to maintain adequate pilot-vehicle performance with a degraded CSAS mode due to failures. This criterion also covers the ability of the pilot to retain control of the vehicle during the transient from full CSAS operation to degraded operation. The difficulty arises not only because of the time required for the pilot to adapt to the new control-response laws and stabilization level but also because the controller configuration or force-displacement characteristics may be unsuitable for use with the degraded CSAS mode. This situation can arise if the decision is taken to optimize the controller for only the fully-operational CSAS because of other considerations (cost, complexity, etc.).

3.7.3 Cockpit Layout and General Airframe Criteria

Space Envelope in Cockpit: This includes not only the displacement envelope of the controller but also the size of the basic structure. Consideration should be given to the space required to allow controller position adjustment. Cockpit space will always be at a premium in any vehicle and some side-arm controller configurations may well turn out to be too bulky because of the severe restrictions on cockpit width. Experience shows that it is difficult to build a controller narrower than about 5 inches, which means that for a dual side-by-side cockpit at least 10 inches of additional width would be required to allow adequate space for the center console and ingress/egress. Even with the controller integrated into the seat structure some increase in width would be required. Unfortunately, no great increases in cockpit width can be expected to occur in the forseeable future simply because the pilot requires a certain minimum of visibility laterally out of the cockpit and yet at the same time must be able to operate controls mounted on the center panel. Thus side-arm and side-seat configurations will tend to be penalized more heavily under this criterion.

Visual and Physical Access to Front and Sides: The influence of the controller configuration on the ability of the pilot to see and operate all the instruments and displays on the panel in front of him and to the side. Visual access to the side includes both that of the center console and out-of-the-window. This latter is of considerable importance to the helicopter pilot who requires a clear view of the ground during hovering manoeuvres. For this criterion the side-seat and side-arm configurations show a clear advantage with regard to the prime display panel area directly in front of the pilot, particularly for the single seat and dual-tandem cockpits. But, of course, they do obstruct the side console areas and out-of-the-window visibility. To properly apply this criterion it is necessary to employ some form of weighting factor to the importance of the front or side areas.

Weight: All configurations using mechanical synchronization between pilot stations will be considerably heavier than the equivalent electrically synchronized configurations. It is difficult at this stage to estimate how the weight of the indiviual configurations would compare, since the mass-balance requirements result in relatively large weight increases for the 3 and 4-axis controllers that tend to offset the weight reductions due to their smaller size.

Space Envelope in the Airframe: The space required below the cockpit floor for mechanical linkages, or elsewhere in the aircraft for the redundant electronic control units associated with the controllers. While the mechanically synchronized controllers would require considerably more space below the cockpit deck, the other space requirements should be approximately the same for all configurations.

Power Requirements: This criterion is concerned with the electrical or hydraulic power requirements for the controllers and their electronic units. At this stage it would appear that the power required should be relatively independent of the configuration, with the exception that the power demands of the control-force actuators for the side-arm configurations should be lower than the others because of the lower force levels involved.

Airframe Structural Requirements: The effect of the controller configuration on the airframe structure, including the provision for linkage anchorage points, supporting structure, and the difficulty of integrating the controller mechanism with the seat structure. Controller configurations that can be mounted directly to the cockpit floor as self-contained units rate highly under this criterion. In order not to negate the whole purpose of the "crash-survivable" seat, side-arm controller configurations should be fully integrated with the seat structure. This could be a formidable problem, particularly if the arm rests are to fold to provide ingress/egress. For the upward-ejecting ejection seat, it is not strictly necessary that the controller be physically integrated with the structure. Mechanical synchronization between pilot stations will result in airframe structural requirements that are relatively independent of the controller configuration.

3.7.4 General Criteria

Flexibility and Growth: The ease with which the controller can be modified during development or have new functions added at later stages. In general, the multi-axis configurations will be less flexible because of their greater mechanical complexity and their relatively more severe dimensional restrictions.

Technical Risk: The confidence level in the ability of the controller configuration to meet all its specifications. In general, we should consider that the multi-axis controllers would represent a higher technical risk than the "improved" versions of the conventional controls.

Cost: This criterion includes both the non-recurring costs during development and the total lifetime maintenance costs. The development costs will increase with the mechanical and electronic complexity of the controller, thus the 3 and 4-axis side-arm controllers will tend to be considerably more expensive to develop than the "improved" conventional configurations. On the other hand, the maintenance costs of these configurations should be quite low because of the ease with which they can be removed from the aircraft and replaced, resulting in a minimum of aircraft downtime. Controllers that are integrated into the seat structure will tend to be slightly more expensive to maintain since the seat itself would also have to be removed from the aircraft, and the controller components would be less accessible, resulting in longer repair times.

Reliability and System Safety: The reliability criterion includes safety-of-flight, mission and maintenance reliability, true redundancy level, failure detection and isolation capability and sensitivity to failures in other systems. System safety includes all the hazards due to material failure, maintenance and crew error, the effects of lightning strikes and radiation, etc. At this stage, it does not appear that any particular controller configuration would offer an advantage under this criterion, but more detailed analyses, based on specific mechanizations of a configuration, could reveal differences.

Survivability: This can be defined in terms of the total projected area of the controller and its electronic unit relative to the total target area of the vehicle and the ease with which the controller could be protected. The more compact 3 and 4-axis configurations would rate more highly for this criterion.

Maintainability: The ease with which the controller or component parts of the controller can be removed from the aircraft and maintained on the bench. This depends to a great extent on the detail mechanical design of the particular configuration and again, at this stage, no great advantage can be attributed to any configuration, with the exception that integrated seat-controller configurations and the 4-axis controller would tend to be more difficult to maintain because of their generally increased complexity.

Environmental Factors: These include protection against temperature, acceleration, vibration, humidity, dust, etc. One should consider that all controller configurations could be totally sealed against the environment. However, protection against vibration and acceleration effects would require careful mechanical design, and the problems associated with that would be proportional to the compactness and complexity of the controller configurations.

3.8 Scoring Techniques and Weighting Factors

To perform the actual quantitative trade-off study it is convenient to use a form of matrix arrangement, where the rows represent criteria

and the columns represent configurations. Having selected the candidate controller configurations, one would then review each criterion and allot a score for each individual configuration. The scores can be based either on a ranking technique, in which case the highest, or lowest, scoring configuration is the best, or they may be allotted on the basis that each configuration offers an advantage or disadvantage relative to some controller configuration that does not appear in the trade-off table. In this second technique one would use a range of positive and negative numbers to represent the magnitude of the advantage or disadvantage, and the best configuration would then be that with the algebraically largest score.

For a number of criteria no data at all, let alone reliable data exist at this point in time. Therefore, the scores can be allotted only on the basis of considered opinion and basic aircraft experience. Fortunately, the relatively large total number of criteria will tend to reduce the influence of these rather uncertain scores on the final outcome.

Since all the criteria are not of equal importance it is necessary to apply some form of multiplicative weighting function before summing the individual scores to arrive at the final values. The nature of the weighting function will depend to a great extent on the mission objectives of the vehicle in which the controller is to be used, and on the various priorities allotted by the customer or the design engineer. It would be advisable to investigate a range of weighting factors so as to identify any undue sensitivity of the results to the specific weighting function. One can have considerable confidence in the final outcome if it is found that the optimum configuration is the winner by a wide margin that is relatively independent of the weighting function.

IV. TAGS FOUR-AXIS SIDE-ARM CONTROLLER

The purpose of this section is to give a very brief description of the 4-axis side-arm controller that has been developed for the Tactical Aircraft Guidance System (TAGS). The object of this program, which is jointly funded by the U.S. Army and the Canadian government, is to demonstrate a FBW flight control system in a tandem-rotor transport helicopter. The flight evaluation of the system is still in progress and thus no final conclusions can be drawn.

4.1 Description of Controller

It should be stressed that the configuration of the controller did not come as a result of a trade-off study similar to the one described in this paper. The ground rules effectively determined the controller configuration from the beginning of the program. The

ground rules were:

- Controller was to be a single-handed device.
- Controller was to command aircraft linear velocity and heading rate.
- Controller was to maximize the pilot/vehicle integration and the alleviation of pilot workload.

Some of the other constraints on the design were:

- Weight to be less than 50 lbs.
- "TAGS pilot" would use left hand seat.
- No modifications would be allowed to the cockpit layout or seat.
- Electrical outputs to the flight control system were to be triplex.
- The control-forces did not have to be variable.

It was decided that a 4-axis side-arm controller offered the best solution, and a two year development program, in which a number of engineering developmental models were built and tested, on both fixed and moving base simulators, produced the configuration shown in Figure 11. The purpose of the developmental models was to determine the most suitable configuration for the four axes and to investigate various types of mechanism.

The maximum dimensions of the controller are approximately 7 inches wide x 27 inches long x 25 inches high, and it weighs 75 lbs. All axes are fully mass-balanced so as to be independent of attitude changes and aircraft acceleration and this contributes slightly more than 40% of the total weight.

Figure 12 shows the axis pivot locations and type of motion. The H-axis controls turn rate in hover (less than 40 knots) and bank angle in cruise (above 80 knots). The Y-axis controls lateral ground velocity in hover and a constant heading sideslip in cruise. The Z-axis commands vertical velocity while the X-axis commands longitudinal ground speed in hover and airmass referenced velocity in cruise.

The maximum travels in each axis are:

X-axis	+4.4, -1.1 inches
Y-axis	$\pm 30^{o}$

Z-axis	$\pm 30^{o}$
H-axis	$\pm 35^{o}$

The X-axis is equipped with a motorized trim drive that allows the pilot to insert very small velocity commands or constant rates of acceleration and deceleration. Mechanical detents define the zero command position of each axis and all axes can be locked in any position by either magnetic brakes or clutches that are operated by switches on the hand grip. To ensure flight worthiness the controller has been subjected to a wide range of environmental tests, of which the vibration requirement was particularly severe.

During the development program it was determined that, for a number of reasons, the best force-feel characteristic for this controller configuration was heavy viscous damping. Some springs were added to the H and Y-axes to investigate their effectiveness. The functions and parameters of the CAS portion of the flight control system were adjusted to suit these rather unique force-displacement characteristics to give reasonable handling qualities. During the flight and simulator evaluations, both the viscous damping rates and CAS parameters are being modified to further optimize the handling qualities.

With force-displacement characteristics of heavy viscous damping and an aircraft linear velocity flight control system, the following general relationships result (for the longitudinal and lateral axes).

Controller displacement	$\propto$	Aircraft velocity
Controller rate of displacement	$\propto$	Aircraft acceleration
Therefore, Controller applied force	$\propto$	Aircraft attitude

Thus the program is pioneering not only a particular flight control concept but also a 4-axis controller with rather unusual force-displacement characteristics. It is not surprising then that some pilot learning and adaptation problems have been experienced.

4.2 Present Status

In-flight and moving-base piloted simulation evaluations are in progress. Unfortunately, the time devoted to the side-arm controller and the optimization of the handling qualities has been limited due to problems in the flight control system.

The basic results are as follows, bearing in mind that the pilot sample is extremely small (2) and the training time on the controller

has been very short.

- Single-axis manoeuvres and 3-axis co-ordinated manoeuvres in the horizontal plane are very simple to perform. The pilots have accepted the concept of heavy viscous damping and are particularly pleased with the H-Y axis co-ordination.

- Manoeuvres involving the Z-axis are proving to be more difficult. It appears to be a co-ordination problem but the true source is not clear. Considerable work is required in this area.

V. SUMMARY AND CONCLUSIONS

This paper has discussed the type of trade-off study that would be required to identify the optimum configuration for an advanced pilot's controller to be used in a vehicle equipped with a FBW flight control system. Some of the possible candidate configurations have been described and a number of the specific trade-off criteria have been discussed. Some comments have also been made on the experience that has been gained with a multi-axis side-arm controller in a helicopter.

The lack of data is a serious handicap in a trade-off study of this nature. It is particularly difficult to make any meaningful extrapolations from the experimental data gathered in the laboratory to the real-life operational situation. The safest approach would probably be to build and test prototypes of both the optimum configuration and the second choice, unless the margin between them was extremely wide.

Considerable work remains to be done in the area of variable control-force characteristics that would be suitable for vehicles that operate over a wide range of flight regimes, e.g. the space-shuttle and the high-speed VTOL vehicle. A totally unexplored subject is the type of control force cues that should be used for envelope limiting.

A point that cannot be too strongly emphasized is that the advanced pilot's controller should not be designed in isolation from the rest of the system. Because of the intimate relationship that exists between the controller configuration and the flight control system, cockpit layout and airframe, it is essential that very close co-operation be maintained between all groups throughout the design and development stages. This close integration of the design effort will result in much improved pilot/vehicle integration in the final hardware.

REFERENCES

1. Brissenden, R.F. — "Some Ground Measurements of the Forces Applied by Pilots to a Side-Located Aircraft Controller" NACA-TN-4171 Nov. 1957.

2. Russell, W.R.
Alford, W.L. — "Flight Investigations of a Centrally Located Rigid Force Control Stick Used with Electronic Control Systems in a Fighter Airplane." NASA TN D-102 Sept. 1959.

3. Andrews, W.H.
Holleman, E.C. — "Experience with a Three-Axis Side-Located Controller During a Static and Centrifuge Simulation of the Piloted Launch of a Manned Multistage Vehicle." NASA TN D-546, Nov. 1960

4. Howell, G.C. — "Flight Experience of a Rate Demand Control Using Electric Signalling in the Avro 707C Aircraft." AGARD Report No. 536, May 1966.

5. Jaquet, B.M.
Riley, D.R. — "An Evaluation of Gemini Hand Controllers and Instruments for Docking." NASA TM X-1066, March 1965.

6. Briggs, P.
Hofmann, L.G. — "The Application of Human Operator Describing Function Theory to the Prediction of Tracking Performance in the Cheyenne Swiveling Gunner's Station." Proceedings of the Sixth Annual Conference on Manual Control, April 1970.

7. Rhoads, D.W. — "In-Flight Evaluation of Four Cockpit Controller Configurations in a Variable Stability Airplane." AFFDL TR-70-95, Sept. 1970.

8. Hall, H.J., Jr.
Way, T.C.
Belyea, I.L. — "Design and Evaluation of Primary Hand Controllers for Fighter Aircraft." AFFDL TR-71-16, July 1971.

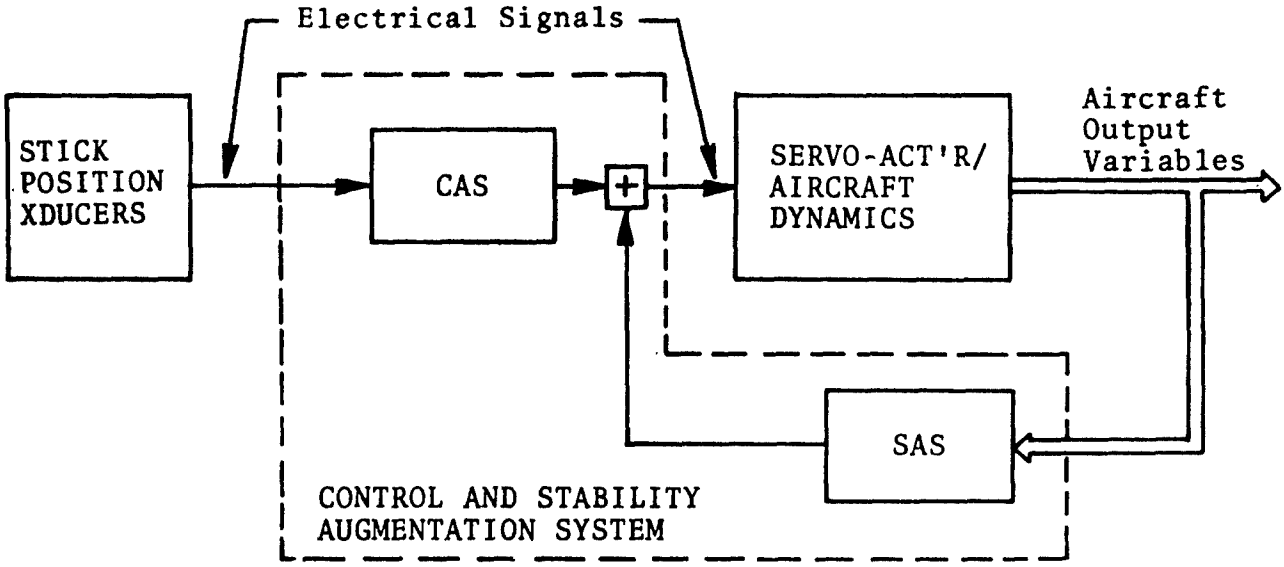

Figure 1. FUNCTIONAL BLOCK DIAGRAM OF FBW SYSTEM

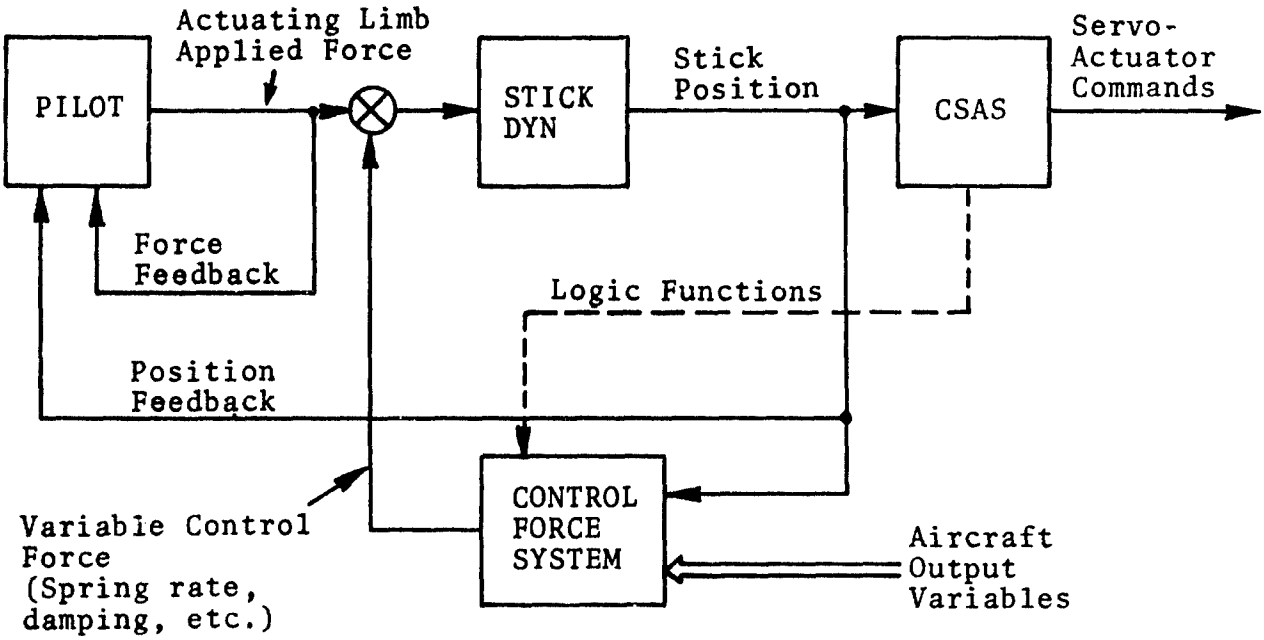

Figure 2. FUNCTIONAL BLOCK DIAGRAM OF VARIABLE CONTROL FORCE SYSTEM

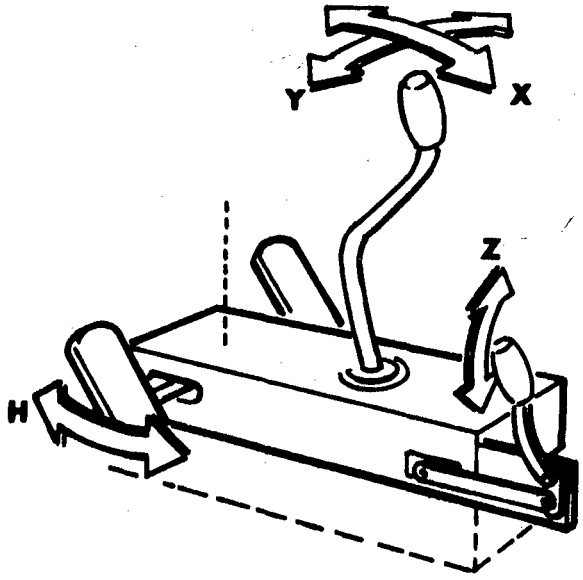

Figure 3. CONFIGURATION 2 + 1 + 1 A

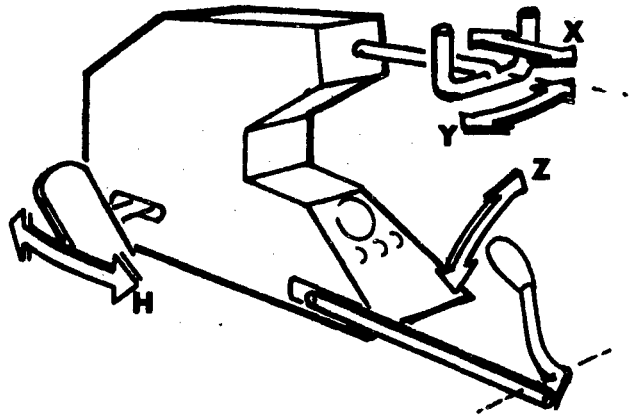

Figure 4. CONFIGURATION 2 + 1 + 1 B

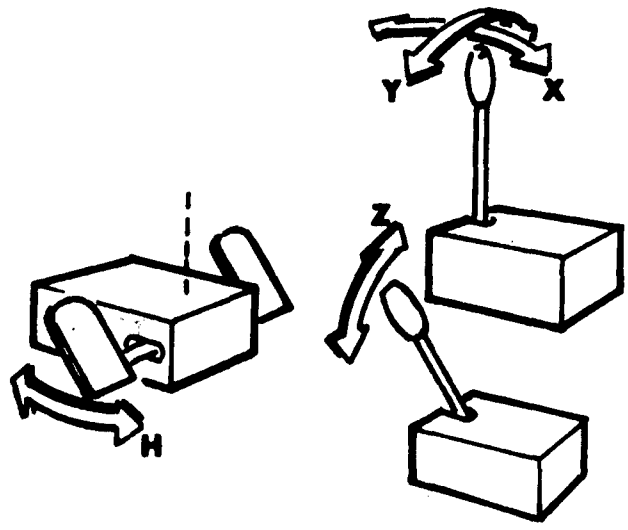

Figure 5. CONFIGURATION 2 + 1 + 1 C

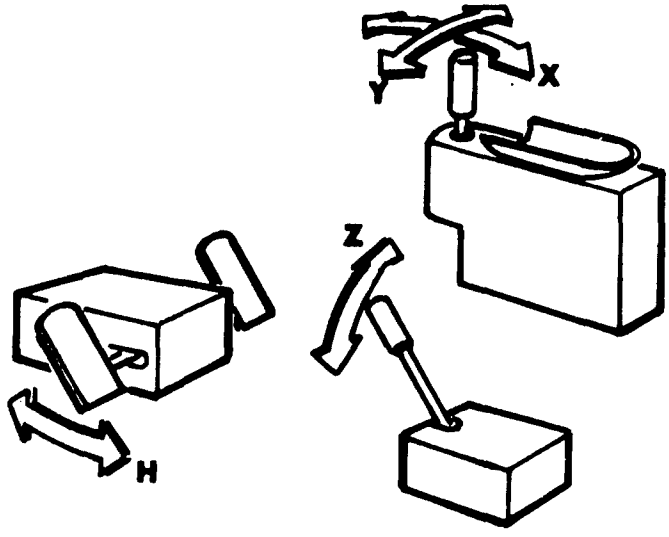

Figure 6. CONFIGURATION 2 + 1 + 1 D

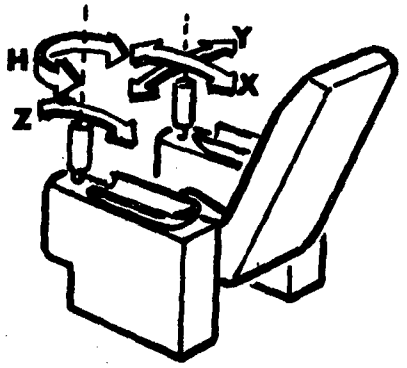

Figure 7. CONFIGURATION 2 + 2

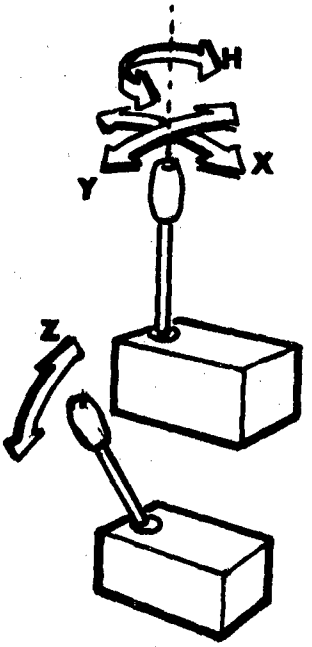

Figure 8. CONFIGURATION 3 + 1 A

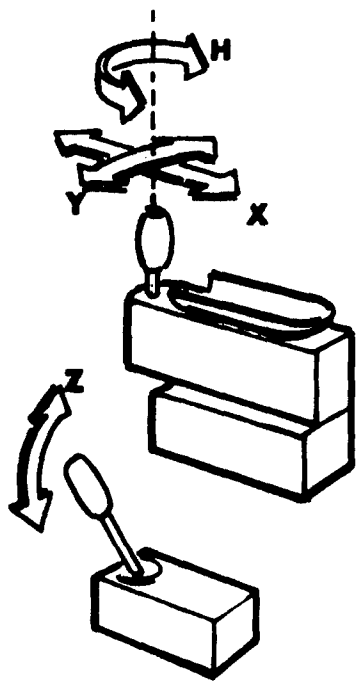

Figure 9. CONFIGURATION 3 + 1 B

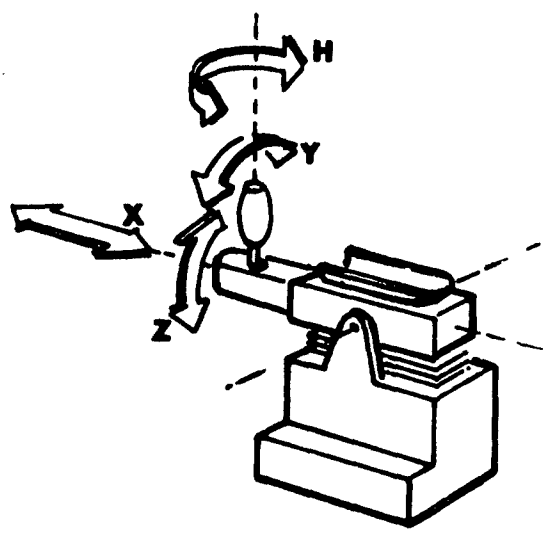

Figure 10. CONFIGURATION 4

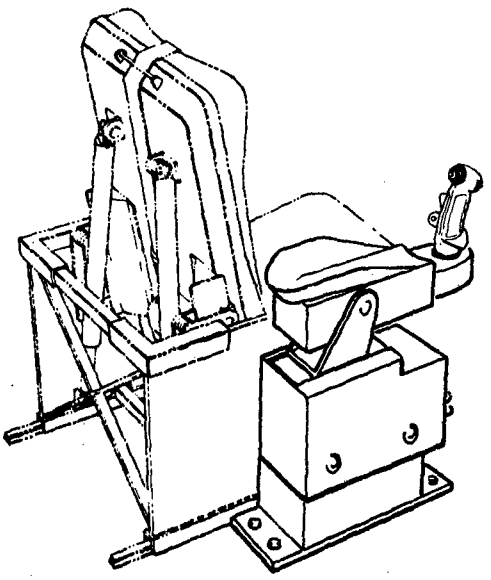

Figure 11. GENERAL VIEW OF TAGS 4-AXIS SIDE-ARM CONTROLLER

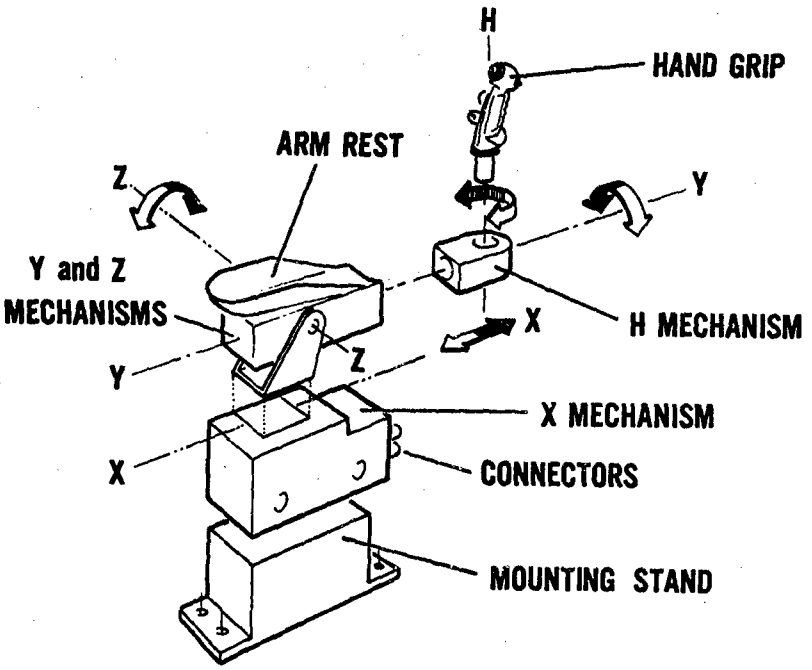

Figure 12. MODES OF OPERATION AND LOCATIONS OF AXES OF 4-AXIS CONTROLLER

A TACTUAL PILOT AID FOR THE APPROACH-AND-LANDING TASK

Richard Gilson and Robert E. Fenton
Dept. of Aviation Dept. of Electrical Engineering
The Ohio State University
2015 Neil Avenue
Columbus, Ohio 43210

ABSTRACT

A pilot aid -- a kinesthetic-tactile compensatory display -- for assisting novice pilots to maintain the desired airspeed during aircraft approach and landing has been tested using a simulator. Here a subject was required to perform three tasks -- two visually and one tactually -- in order to approximate the demands on his attention during approach and landing.

The simulator is described and the results obtained -- especially those pertaining to the efficacy of a tactile display for the suggested use -- are presented.

INTRODUCTION

The manual control of an aircraft during the approach and landing is a difficult task even under the best of conditions as is vividly illustrated in aircraft accident statistics. Approximately one half of all aircraft accidents take place during this phase of operation despite the fact that approach and landing usually constitutes only a brief part of total flight time.[1]

The difficulty of an accurate landing lies primarily in the necessity for precise and simultaneous control of two factors -- flight path and airspeed. Under most circumstances flight path information is derived from visual cues outside the aircraft while airspeed must be monitored on a cockpit display. Thus visual attention is divided during the approach to landing -- especially for novice pilots who lack the experience to use subtle pitch, inertial and aural cues for airspeed. It is hypothesized that if this division could be at least partially eliminated during the beginning stages of flight instruction, a learner's task would be simplified, his performance would be improved, and the number of accidents during the learning phase should be decreased. The following was an attempt to examine the first two parts of this hypothesis by using tactual rather than visual display of airspeed information.

Preceding page blank

SIMULATOR DESCRIPTION

A preliminary experiment was conducted using the moving-base automobile simulator which is shown in Fig. 1. A driver's immediate environment was simulated via a cockpit with an enclosed driver's seat, an instrument panel and a vehicle control device. A television monitor, simulating the windshield of the driven car, was mounted on the cockpit and provided a driver with a view of a lead car on a randomly curving road. The cockpit was mounted on a steel structure so that it could be both tilted fore-and-aft and rolled from side-to-side to simulate the kinesthetic and vestibular stimuli normally associated with driving (A more complete description of this simulator is contained in Reference 2).

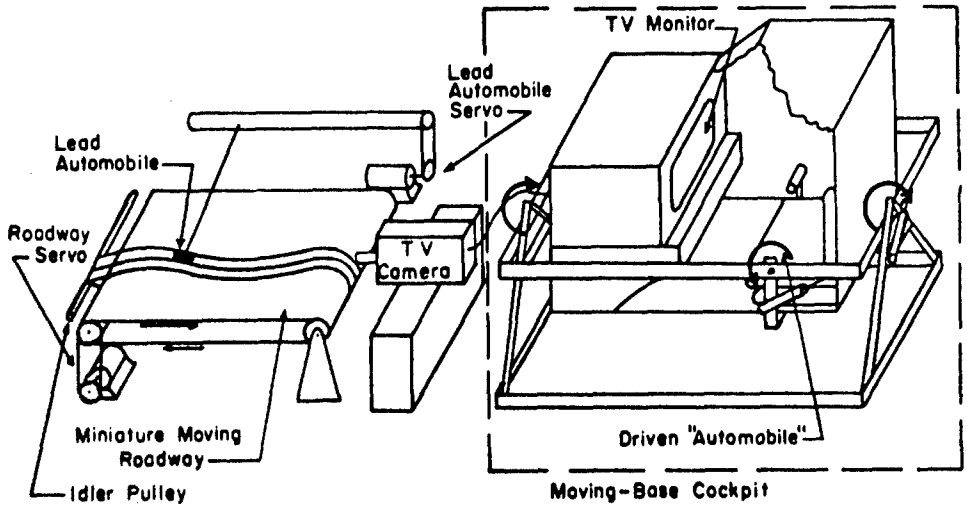

Fig. 1--A moving-base car-following automobile simulator.

Since this apparatus obviously precluded any realistic aircraft simulation, analogies to inflight tasks were assumed. Three cues used in a normal landing approach are those of alignment with the runway, perceived height to the point of touchdown, and kinesthetic and vestibular cues usually associated with airspeed changes. The first two were approximated by the steering and headway cues in the simulator which involve both lineup and depth perception. The third was approximated by relating speed changes to changes in the cab pitch.

The manual controls were similar to those found in military aircraft. A two degree-of-freedom control stick with a side-to-side motion for steering and a back-and-forth motion for adjusting the pitch and speed was located next to a subject's right side. Here pitch up resulted in a slower speed and pitch down in a higher one. A single degree-of-freedom control in the left hand was analogous to a throttle. By moving this control forward, headway was reduced and by moving it aft headway was increased.

Airspeed values in direct proportion to the cab pitch were presented either visually via an "airspeed indicator" or tactually via a

display built into the head of the two degree-of-freedom control stick.[3] With no error in pitch, and thus none in speed, a "finger" would be flush with the control stick head. When an error was present, the finger would either protrude from the front or rear surface of the head depending upon the polarity of the error. When protruding, a subject would move the control stick forward which would decrease the pitch angle to its desired value and nullify the speed error. The finger would then be in its flush position.

The cab was enclosed to prevent the subject from directly observing pitch. Therefore speed control was based either on the visual display in the absence of tactual information or on the tactual display in the absence of visual information.

EXPERIMENTAL DESCRIPTION

A complex control problem was generated by using three random forcing functions to vary the headway, the road curvature, and the cockpit pitch angle. The subject's task was thus:

a) To maintain a fixed headway with respect to the lead car:
b) To steer so as to maintain his position within the roadway: and
c) To maintain a constant pitch angle and hence a constant speed.

Performance was assessed on the basis of the absolute integrated error for pitch, the maximum value of pitch deviation, and the amount of time a pre-selected headway deviation threshold was exceeded. The first two measures are directly related to efficacy of the display type while the latter is a measure of the loading task simulating flight-path guidance.

Eight male flight students participated in the experiment with each receiving four separate four-minute runs. The first two, one visual and one tactual, were for practice and the second two were for data collection. Appropriate counterbalancing procedures were taken to minimize learning effects.

EXPERIMENTAL RESULTS

The experimental results obtained from the 3rd and 4th runs by each subject are shown in Figs. 2-4. First, note from Fig. 2 that an average reduction of 36.4% in integrated absolute speed error was obtained when the tactual display was used. Further, note from Fig. 3 that a 19.8% reduction in the extreme values of speed deviation also resulted.

A consideration of the subject's headway tracking performance (see Fig. 4) shows that when the tactual display was used the headway was, on the average, held within selected limits 41 seconds longer than with the visual display. This would indicate, not surprisingly, that there is better evaluation of depth cues with the tactual display simply because visual attention is uninterrupted without the necessity of constantly referring to the visual display.

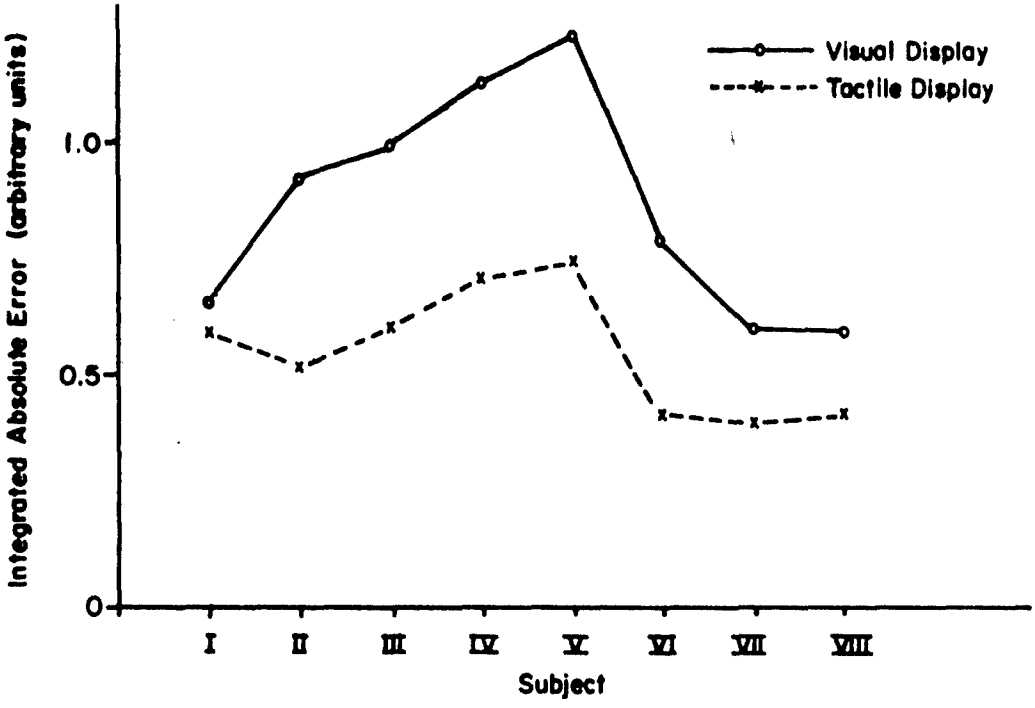

Fig. 2--Integrated absolute speed error for both tactual and visual displays.

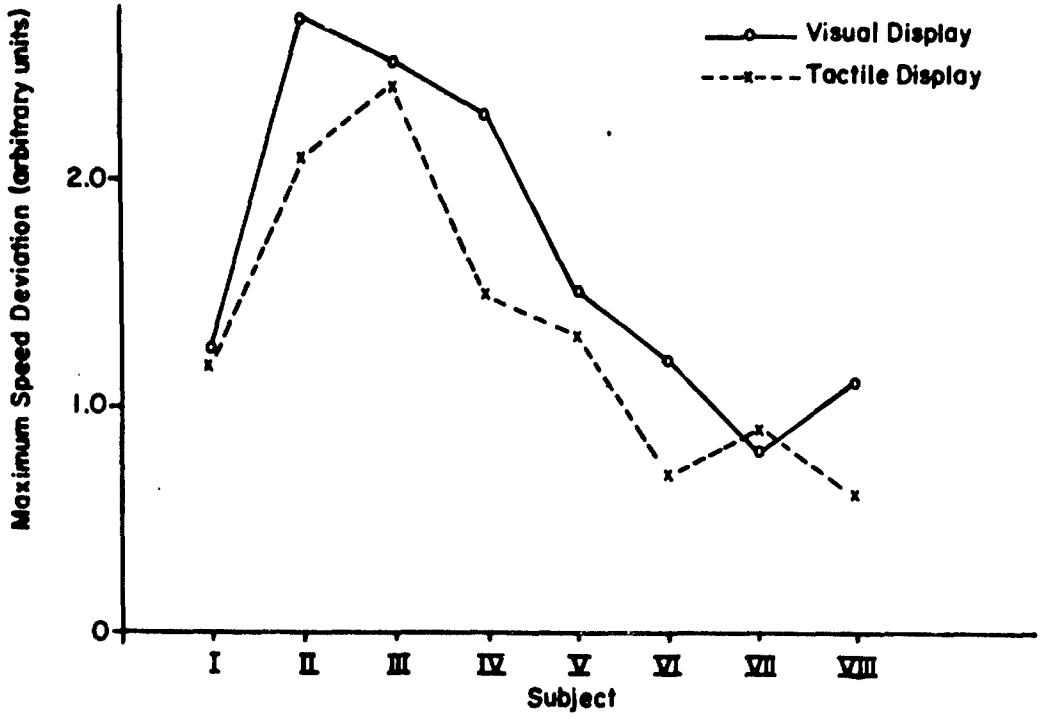

Fig. 3--Maximum speed error for both tactual and visual displays.

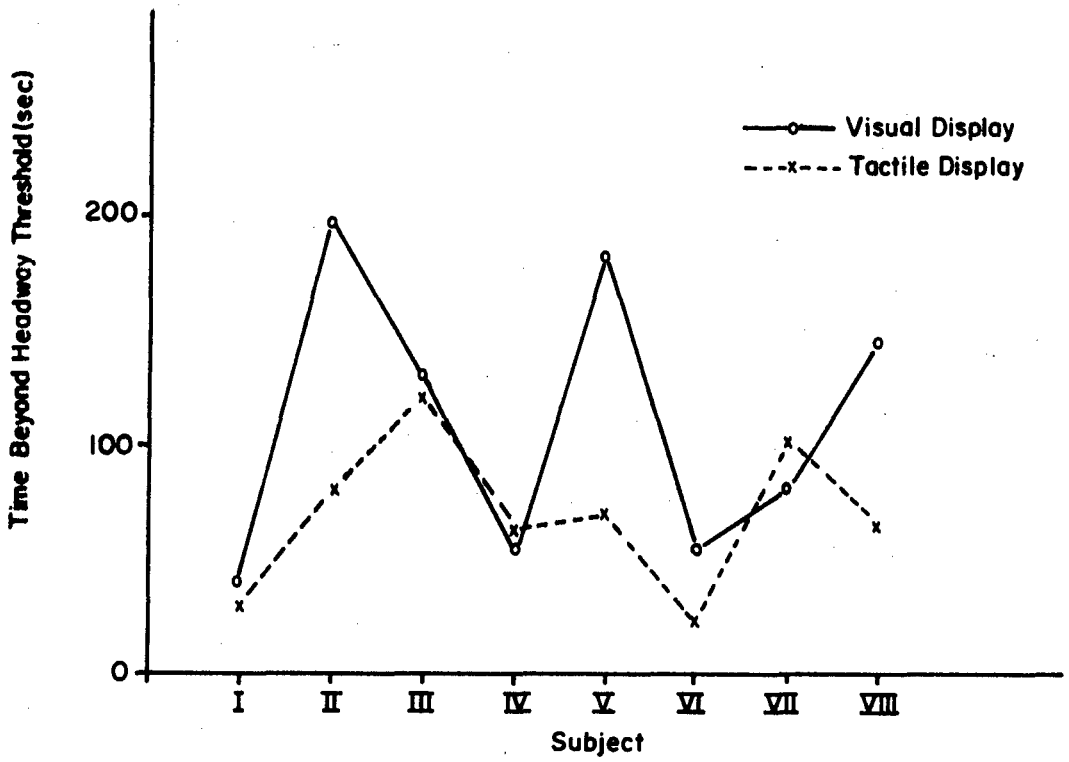

Fig. 4--Time during which subjects exceeded a preset headway threshold in a four-minute period.

CONCLUSIONS

These results would suggest a general improvement in inflight speed control and thus pitch control by the use of a tactual display. There should be little argument that more accurate airspeed control should result in a lower risk and that better depth or distance control should result in more accurate landing. Also, the chances of speed and pitch extremes, such as might result in aerodynamic stall, would appear to be reduced.

There may be other inflight benefits of a tactual display of airspeed (or more accurately angle of attack information) that cannot be assessed with this simulator alone. For instance, a tactual display mounted on the yoke of an aircraft leads to a fairly natural stimulus-response action of pushing or pulling on the yoke. Confusion to the novice pilot often comes when he sees either a low or high airspeed indication and he is confused as to whether to compensate with pitch attitude with the stick or throttle changes. Secondly, an improved rate of learning may be realized through the continual reinforcement of the nature of the relationship between aircraft attitude and airspeed. The stronger reinforcement with the tactual display would be the result of the simultaneous availability of airspeed information while aircraft attitude is being observed.

Even further improvement with the tactual display may be realized in the actual inflight situation by the supplementary information gained from perceiving the nose attitude of the aircraft which is how experienced pilots normally regulate airspeed. One might also expect a gain in safety because a pilot with visual attention constantly outside the cockpit would be more continuously aware of other traffic.

The encouraging results reported here, plus the above-mentioned factors, suggest that the testing of an inflight prototype would be a fruitful endeavor.

ACKNOWLEDGMENTS

Dr. Marlin O. Thurston first suggested that the tactual display described here could be applied to our experiments with tactual aids to the approach-and-landing task. Mr. Ronald Ventola was responsible for all simulator modifications and the collection of all test data. It is a pleasure to acknowledge these contributions without which this work would not have been performed.

REFERENCES

1. National Transportation Safety Board, Annual Review of U. S. General Aviation Accidents Occurring in Calendar Year 1968.

2. Ott, J. H., et al., "A Moving-Base, Car-Following Automobile Simulator," IEEE Trans. Veh. Tech., Vol. VT-19, No. 4, November 1970, pp. 238-245.

3. Fenton, R. E., Montano, W. B., "An Intervehicular Spacing Display for Improved Car-Following Performance," IEEE Trans. MMS, Vol. MMS-9, No. 2, June 1968, pp. 29-35.

A fingerstick with binary selectable control gain

Rothbauer, G.; Krüger, W. & Kruse, W.
Forschungsinstitut für Anthropotechnik
Meckenheim/Bonn, BRD

1. Introduction
2. Selectability between two levels of control gain
3. Experimental study
4. Experimental results and discussion

Abstract

An experiment was conducted to test advantages associated with leaving a binary choice of control gain to be used in a target designation task completely up to the operator. A fingerstick containing a pressure sensitive transistor for selection between two levels of control gain was used. A comparison of the operator performance with and without selectable control gain indicates : 1) No significant differences in designation time, but, 2) a significant increase in designation accuracy when control gain is set by the subject.

1. Introduction

In the design of a man machine control system arises the question about the optimum of control gain. The locus of control gain in a simplified man-machine system (MMS) is shown by the amplifier in Figure 1. Control gain is determined by the amplification or reduction of the signal output of the control. In this context, control gain must be clearly separated from display gain, where the latter means the amplification of the signals between input and output of the display.

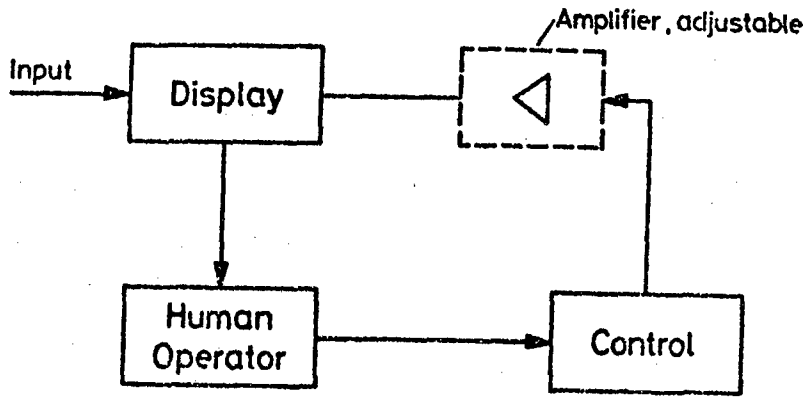

Figure 1 : Flow diagram of a MMS and locus of control gain

Normally the control gain will be established with respect to the special system and the task to be performed. In doing so one has to keep in mind several factors which can be influenced by the control gain.

1. When you have a control with limited deflection, e.g. a fingerstick, it is evident that the controlled area in a 0-order system increases directly with the magnitude of control gain. This fact is shown in Figure 2, representing a simple tracking apparatus. With a relative low level of control gain, the inner circle with R_1 can be controlled, with a higher level the outer circle with R_2 can be reached.

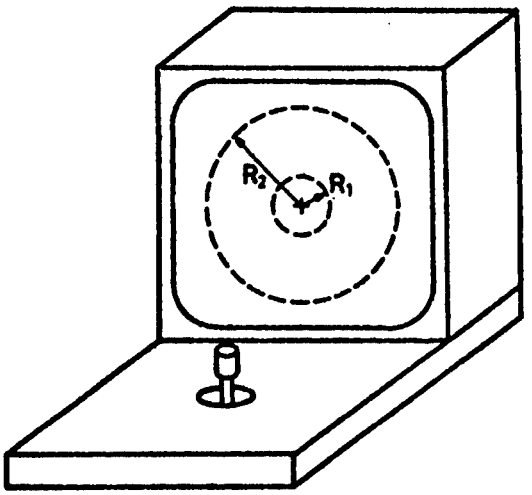

Figure 2 : Controllable areas at different levels of control gain

2. The higher the control gain, the coarser will be the movement of the cursor, because at high gain trembling and other nonlinearities of the hand-control movement-unit take greater effect.

3. Control gain also influences adjustment time in positional step tracking (HAMMERTON, 1962). Increasing the gain results in smaller necessary movement amplitudes of the control and, thereby, in shorter travel time (JENKINS & CONNOR, 1949). On the other hand, the fine adjustment of the cursor is rendered more difficult with high gain because any slight movement of the control produces large excursions of the cursor. Thus, the time for fine adjustment gets longer with increasing control gain.

   Consequently, the total time required in completing a target designation task is to some degree dependent on the special requirements of the task. If only coarse approach to the target is necessary, the time will be short with high gain, but long if accuracy of adjustment is needed.

   As a result of these considerations the following alternatives can be stated: Take high control gain and you will get a large controlled area and short time for coarse approach to the target. But you will have poor accuracy of adjustment.

   With low control gain, you will have a good accuracy and short time of fine adjustment, but you have to take the penalty of a small controllable area and long travel times.

Normally, the gain will be adjusted to some intermediate value with respect to adjustment time (GIBBS, 1962), controllable area and accuracy of adjustment.

One manual control, which has been developed over the last few years, violates the above mentioned rules in one respect. The rolling ball can control a theoretically unlimited area, independent of the level of gain. In spite of this merit, there remain two disadvantages. At reasonable control gain with respect to accuracy, the rolling ball takes relative long travel times (SCHMUCKER 1969). And one should never forget, that a rolling ball is rather expensive.

The question arose, is there any stick control, having the advantages of the rolling ball without its disadvantages ?

2. Selectability between two levels of control gain

A decision was made to explore the possibility of constructing a fingerstick by which some of the merits of the rolling ball could be realized while excluding several of its disadvantages. Thus, a fingerstick was developed which contained a feature for directly setting one of two possible control gains at any time and under the complete option of the operator. The procedures associated with using this special control in a target designation task is clarified by inspection of Figure 3, which shows the task situation on an analog display.

In the beginning of the task, the cursor is in the middle of the display (I). The dotted circle limits the area which can be controlled with low control gain. To get the cursor in the vicinity of the far distant target, the operator must switch to high control gain. By means of this, he displaces the low gain controllable area. When the target is in this hatched area (II), the operator can switch back to low gain for fine adjustment.

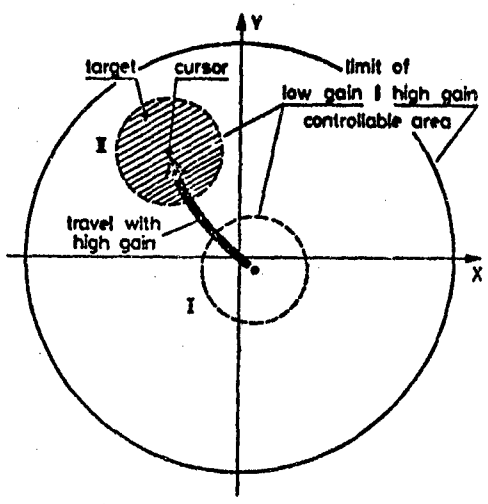

Figure 3 : Controllable areas on the display at selectable control gain

The concept of binary selectable control gain should now be examined principally for its usefulness in a practical situation. The work of the air traffic controller of the near future shall serve as an example. The air traffic controller will soon have the task of target designation by means of a rolling ball in cooperation with a digital computer. With the control he will locate and mark every airplane appearing on the radar screen with a code number. He then will transfer the momentary space coordinates and the corresponding code number to the computer. In short, the work of the air traffic controller will consist of designating accurately a suddenly appearing point on the screen as fast as possible.

At the first glance, the application of a fingerstick with binary selectable control gain seems reasonable for the above task, taking high gain for wide travel and low gain for fine adjustment. But there might be a difficulty, namely the necessity to change suddenly the sensory motor coordination.

Figure 4 shows the movement of the control and the cursor during an adjustment process in one dimension. The target jumps far from the middle of the display. The operator deflects the control with high gain, so that the movement of Δ affects the relative large movement δ_h of the cursor. At the overshoot the operator changes to low control gain for fine adjustment. After the moment of switch over, rather wide movements of the control have only little effect on the movements of the cursor. The same movement of Δ now affects only the little deviation δ_l of cursor position. This requires an abrupt change in the sensory motor coordination of the operator. In a simular situation, YOUNG et. al. (1964) found an adaptation time of about 1-2 seconds for sudden unpredictable decrease of control gain. Because of this sudden change in sensory motor coordination one has to expect a prolongation of adjustment time and relative high work load.

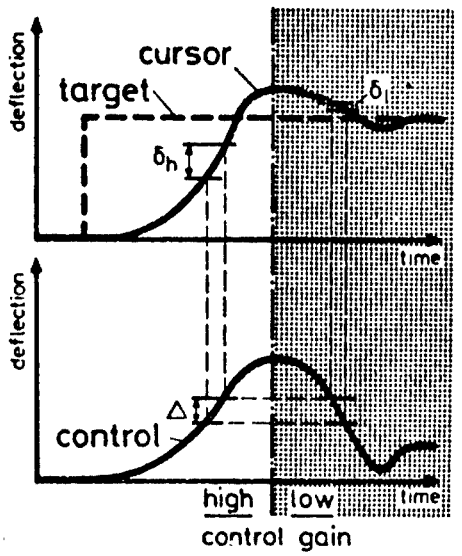

Figure 4 : Movement relationship with selectable control gain

A second disadvantage may result from the necessity for a decision. When the operator has located the cursor within the vicinity of the target, he has to decide at which moment to switch over from high to low gain. This may involve additional workload and an increase in adjustment time in keeping with the transition from simple to choice reaction time.

The question arises, whether the human operator is able to adapt easily and quickly to a self-initiated abrupt decrease in control gain which is well known in its effect. This ability of man is necessary whenever an improvement of performance by use of binary selectable control gain is to be expected.

3. Experimental study

An experiment was conducted to investigate the effects of two operator-selectable control gains on target designation performance in relation to performance when gain is preset at a fixed constant level. Twelve Ss (one female and 11 male) performed a task representative of those with which future air traffic controllers will have to deal.

All Ss worked under the fixed as well as the variable control gain situation for an average of 45 designations per experimental condition. Thus, a total of 1060 data points were generated. The apparatus used (Figure 5) consisted of a fingerstick, a data entry key, and a X-Y-Display measuring 30 cm on the diagonal. Viewed from the normal viewing distance of 31 cm the visual angle subtended at the display was 52°.

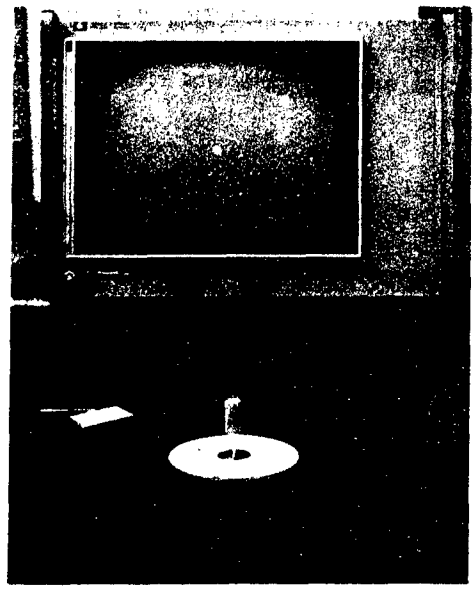

Figure 5 : The experimental setup

The fingerstick used was developed in-house and has the following characteristics :

1. Hight above surface		- 52 mm
2. Maximum deflection		- 16° in all directions
3. Movement arc (at stick top)		- 28 mm
4. Centration spring resistance		- 0.3 pond/mm (below human threshold)
5. Friction		- negligible
6. Grip :	diameter	- 7 mm
	hight	- 40 mm

A pressure sensitive transistor was contained in the top surface of the fingerstick. By means of this transistor, control gain could be binary selected. By pressing slightly on it, control gain switched from low to high at a ratio of 1 : 4. The high gain was set such that the edge of the display was reached with full deflection of the fingerstick. This condition was, of course, used whenever the Ss had no choice of control gain.

The S's task was the following :
In the initial condition, the target was in the center of the display. For any trial the target was driven to its random position on the display by sampling two independent sine-functions of different frequencies for each axis. Thus the probability function of target location was an arc sine in the X/Y-coordinates and the target therefore tended to jump to the outer regions of the screen. After the target jump, S had to superimpose the cursor and target as quickly and accurately as possible. When the S was satistied with the alignement, he pressed the data entry key for automatic recording of the response. To prevent simple target runthrough responses, Ss had to lock onto the target until it jumped back to initial position after .5 sec. Intertrial interval time was randomly varied such that $0 < t < 2.5$ sec.

4. Experimental results and discussion

Adjustment time and error were used as dependent variables to answer the questions posed above.

Figure 6 shows the frequency distributions of adjustment time under the two experimental conditions. In this figure (as well as in Figure 7) the characteristic distribution of the intrasubject variability is of interest ; therefore, a linear transformation was computed in order to supress confounding due to intersubject variability.

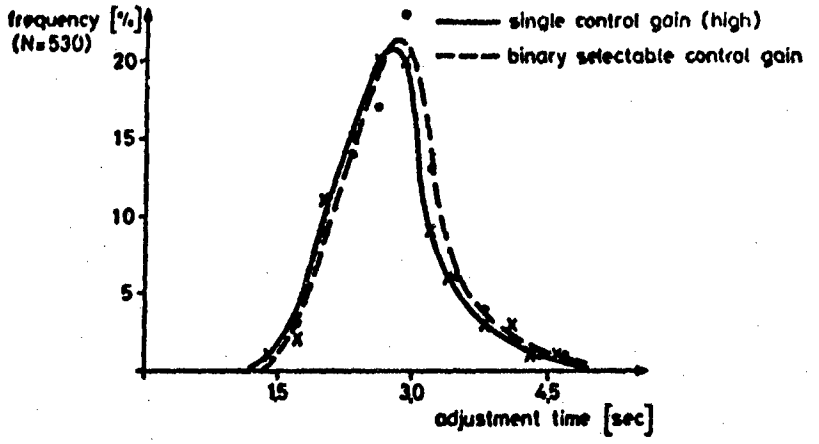

Figure 6 : Frequency distribution of adjustment time

The modal values of the two distributions of adjustment time are practically equivalent. With binary selectable control gain, however, a few more values fell outside the range of this figure. An examination of mean differences by the Wilcoxon Test indicates, that there was no significant prolongation of adjustment time resulting from selectability of control gain.

Figure 7 shows the frequency distributions of the second dependent variable for description of performance, namely of the adjustment error.

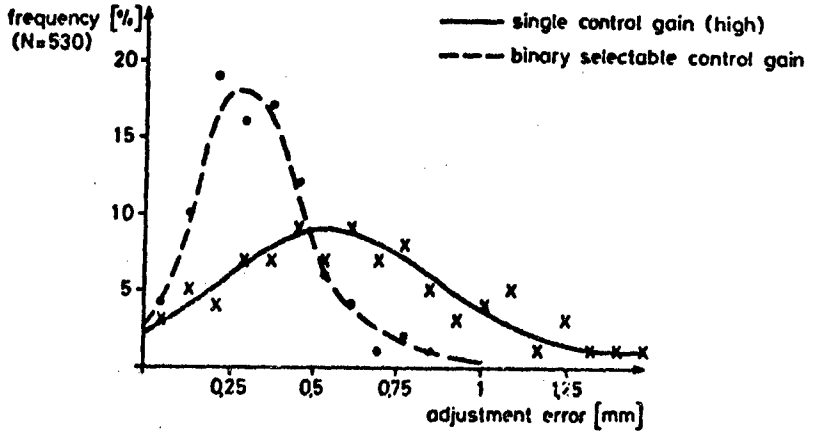

Figure 7 : Frequency distribution of adjustment error

The adjustment error with binary selectable control gain shows a frequency distribution which is to be expected of a one-side limited variable, i.e. a distribution steeper at the left side.

The frequency distribution of adjustment error with the conventional single gain control has a flatter form. A significantly higher mean and variance was found. The interindividual variance is also significantly greater with single control gain than with binary selectable gain.

A questionaire, administered following the experimental session, showed that Ss did not object to having the selectable control gain and they felt no more burdened than with single control gain.

The results show definitely, that the human operator is able to switch over very quickly from one control gain to a different one with respect to sensory motor coordination. He obviously succeeds in this, because he initiates the change in control gain himself, as opposed to the investigation of YOUNG et.al. (1964). This fact is very important, for he then has no difficulties in recognizing the change and he can therefore preadapt to (or expect) the changing system dynamics. With some practice - the Ss reached their individual mean in adjustment time after circa 40 training trials - the task with binary selectable control gain was performed almost automatically.

Although the introduction of several levels of control gain available for selection seems favorable from a technical point of view, it is unreasonable from a psychological standpoint. The operator then would have to switch over among several system dynamics, which would demand a high degree of concentration and could favour false movements shortly after a change in control gain.

Using the concept of binary selectable control gain seems beneficial for a person-centered definition of primary (coarse) and secondary (fine) adjustment in target designation. Furthermore binary selectable control gain should also be investigated with a rolling ball. By means of this concept, it might be possible to decrease the travel time without increasing the adjustment error with the ball.

In summary, it was shown that the precision and reliability of target designation performance can be increased by means of binary selectable control gain without markedly affecting operator workload.

Bibliography

1. GIBBS, C.B. "Controller design". Ergonomics 5, 1962, 385-402

2. HAMMERTON, M. "An investigation into the optimal gain of a velocity control system" Ergonomics 5, 1962, 539-543

3. JENKINS, W.L. & CONNOR, M.B. "Some design factors in making settings on a linear scale" J. Appl. Psychol. 33,1949, 395-409

4. SCHMUCKER, P. "Ergonomische Untersuchungen über den Einfluß verschiedener Parameter auf die Ortungsleistung des Radarbeobachters bei Aufgaben der Luftraumüberwachung" Institut für Ergonomie der Technischen Hochschule München, November 1969

5. YOUNG, L.R. GREEN, D.M. ELKIND, J.I. & KELLY, J.A. "Adaptive dynamic response characteristics of the human operator in simple manual control". IEEE Trans. on Human Factors in Electronics, vol. HFE - 5, No. 1, Sept. 1964

A LIGHTSPOT OPERATED TYPEWRITER FOR QUADRIPLEGIC PATIENTS.

by

M. Soede,

Laboratory of Ergonomic Psychology,
Organization for Health Research TNO,
The Netherlands,

and

H.G. Stassen,

Man-Machine Systems Group,
Laboratory for Measurement and Control,
Department of Mechanical Engineering,
Delft University of Technology,
The Netherlands.

0. Abstract

The man-machine aspects of the outline of a control panel unit for a typewriter for quadriplegic patients is discussed. The typewriter is operated by moving a light source fixed to the head of the patient, so that a lightspot can be projected on the control panel. The control panel consists of a matrix of characters, each of which is equipped with a light sensitive element. It is shown how (1) the character arrangement, (2) the geometry of lightspot and panel and (3) the way of generating a typecommand was optimized.
Some remarks about the first clinical test are made.

1. Introduction

Communication between human beings is essential for human life, and is probably even more important for severely bodily handicapped patients than for healthy persons, due to the fact that this type of patient is more or less thrown on intellectual activities. Therefore, various types of communication apparatus, which in one way or another can be controlled by the head of the patient, have been developed [1;2]. Some of them are commercially available.

The apparatus described here is based on the Patient Initiated Light Operated Telecontrol, the PILOT; a system which can be operated by relative small head motions of the patient[2]. In order to generate a control signal, a lightsource has been fixed to the patient's head, so that he is able to move a lightspot over a control panel provided with a matrix of characters. Each of these characters is equipped with a light sensitive element. By indicating one of the characters with the lightspot, and by generating simultaneously a type command to a typewriter, the patient is able to type the character selected. Although the PILOT-system supplies a certain want, the results are not satisfactory. This can be argued by the reason that, besides the fact that the technical design itself is not very sophisticated, too little attention has been paid to the man-machine interaction, that is, the adaptation of the control panel to the patient's capabilities.

The operating phylosophy of the newly developed communication system, the Lightspot Operated Typewriter or LOT, resulted in the following requirements:

- The physical load of the patient should be as low as possible, that is the displacements of the lightspot over the control panel have to be minimized.
- The mental load of the patient while operating the LOT should be as low as possible. This demands a simple operating procedure to provide easy positioning of the lightspot across the control panel. Furthermore, it favours a system which does not require two simultaneous actions of the patient, viz. where positioning of the lightspot and generation of a type command have to be performed. Finally, it should be mentioned that the operating of the system must not lead to any malfunctioning of other remaining functions of the patient.
- Undesirable movements of the head, such as spastic oscillations and tremors, must not lead to a malfunctioning of the LOT.
- High accelerations of the head should be avoided, since intensive motion cues can overstimulate the vestibular organ and thus may lead to motion sickness.

From the point of view of man-machine interaction these requirements can be translated into the optimization of the control panel of the LOT, that is:

- Optimize the character arrangement on the control panel.
- Optimize the geometry of the control panel.
- Optimize the generation of a type command.

2. The Lightspot Operated Typewriter.

The LOT consists of (1) a pair of spectacles with a light source and optics, (2) a control panel with a matrix of characters, each of which is provided with a light detector, (3) an interface between the control panel and the typewriter, and (4)

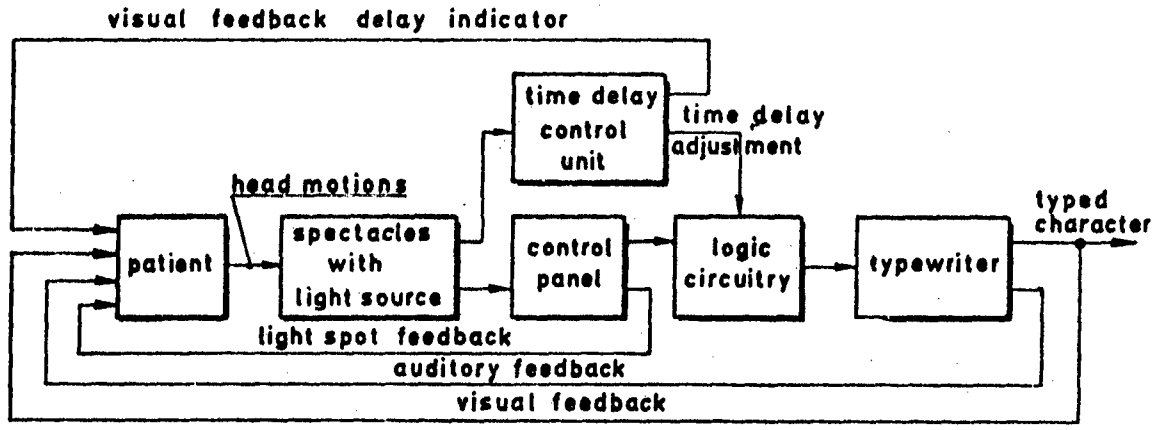

Fig. 1: Blockdiagram of the LOT-system.

an electrically driven typewriter. A blockdiagram of the system is presented by Fig. 1; Fig. 2 shows a picture of a patient operating the LOT.

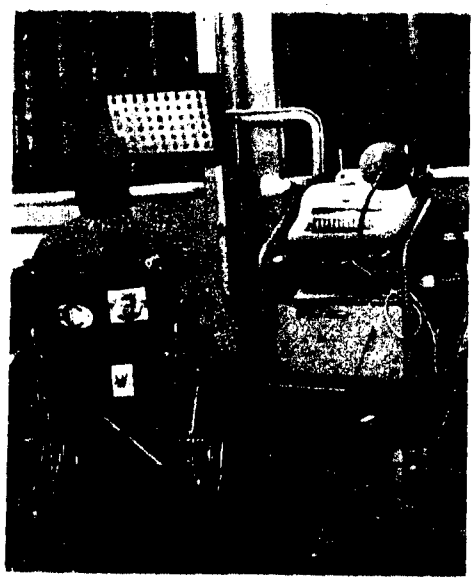

Fig. 2: A photograph of the LOT.

The patient who lies in bed or who sits in a wheelchair has been provided with a pair of spectacles, on which an optical system has been fitted, so that the patient is able to move a lightspot across the control panel in order to illuminate the lightdetector. Illumination of a lightdetector for a time longer than a certain preselected time delay will cause automatically the typing of a character, while the illumination of this lightdetector for a shorter time than the preselected time delay will have no effect, that is no character will be typed out. In this way it is possible to move randomly across the control panel, dependent on the velocity and on the diameter of the lightspot, without typing any character. The preselected time delay is at any moment adjustable by the patient himself.

From the blockdiagram in Fig. 1 it follows that the feedback of information from the LOT-system is mainly provided at three different levels, viz.:

- The visual feedback of the lightspot on the control panel.
- The auditory feedback of the activation of a certain key of the typewriter.
- The visual feedback of the text typed out, which the patient may or may not choose to monitor.

A complete description of the technical realisation of the system is intended for publication elsewhere[3].

3. The optimization of the control panel.

As mentioned before the optimization problem of the control panel can be divided into three different parts. The optimal solution for the character arrangement as well as the geometry of the control panel are about the same for a broad class of patients; they are determined by the characteristics of the language used and the neuro-physiological properties of the headmuscles. The generation of the typecommand, i.e. the preselected time delay, however, is dependent on the individual conditions of the patient.

3.1 Optimization of the character arrangement.

To minimize the physical load on the patient it is necessary to arrange the characters in such a way that for a given geometry of the control panel during typing the distance traveled by the lightspot is minimal. This distance can be computed from the bigramfrequencies of the characters of the language used; for the Dutch language these data are tabulated by the Mathematical Centre at Amsterdam[4]. In calculating this optimal arrangement, however, it should be realised that the number of possible combinations is 35!, hence a suboptimal

strategy to select the best arrangement has been accomplished. The strategy applied was the following. Consider the three most frequent characters of the Dutch language, viz. the e, space and n, and place them in the center of a rectangular matrix in a optimal way with reference to their bigramfrequencies (See Fig. 3a). Hereafter the next six most frequent

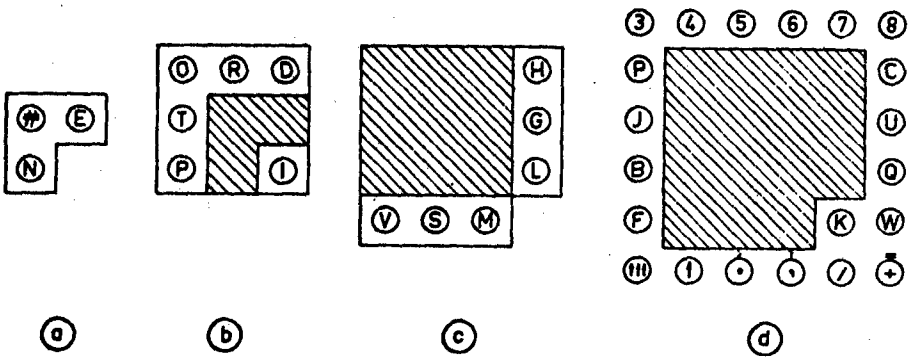

Fig. 3: The way of optimizing the character arrangement.

characters, viz. the a, t, r, d, o and i are chosen and placed around the first three as indicated in Fig. 3b. Out of the 6! possibilities the best arrangement has been derived. The same procedure has been repeated for the next six characters, viz. the s, l, g, h, v and m (see Fig. 3c; noting that already 9 characters have been placed). The 15 characters considered in this way take into account already 75.3% of the total number of character combinations; therefore the remaining characters were placed,without any calculation,in a logical way (see Fig. 3d and 4).
The procedure described above has been repeated for different ratios of height and width of the matrix element; the best results were obtained for equal heights and widths. Due to the particular fact that for bed-ridden patients the rotation of the head spans a larger angle than for a nod-movement, the control panel is more extended in breadth than in height.
As a result of the calculations it can be shown that the distance traveled in normal typing, based only on the 26 letters of the alphabet and the space, is about 1.83 times the separation between the characters of the matrix. In comparison with a keyboard of a normal typewriter, there was a notable gain of efficiency, since the traveled distance for such a keyboard is at least 2.9 times the separation between characters. Finally, it should be mentioned that color codings were used

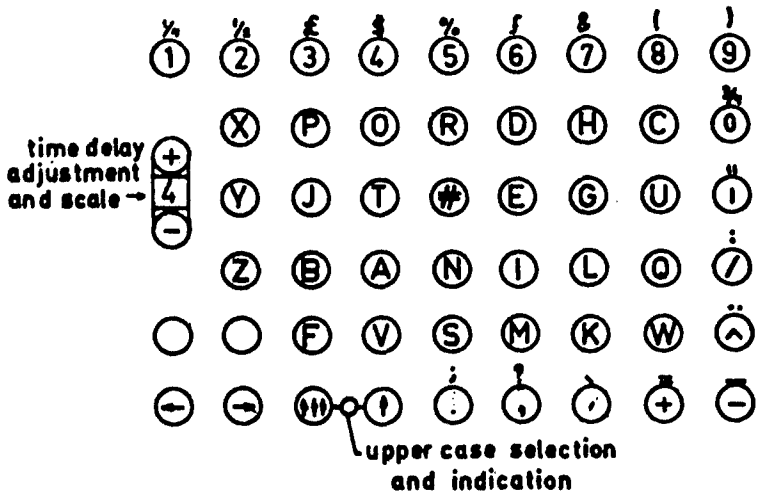

Fig. 4: The control panel layout.

to designate the type of characters. The following colors were chosen: letters yellow, digits blue, punctuation marks green, and operating functions (such as upper case etc.) red.

3.2 Optimization of the geometry of control panel and lightspot.

For a good functioning of a system the separation or pitch t between two characters has to be larger than the sum of the diameters of the lightspot D and the lightdetector d, that is the difference $s = t - D - d$ must be positive to guarantee that the patient is able to position the lightspot on the control panel without touching one of the lightdetectors (see Fig. 5). Therefore the movements of the lightspot caused by spontaneous headmovements were recorded for ten subjects. From these recordings a standard deviation σ of 0.98 mm for horizontal motions and of 1.15 mm for vertical motions was derived. By assuming that the motions will fit a Gaussian distribution, it follows then that a difference $s = 6\sigma \approx 6$ mm is sufficient with regard to spontaneous oscillations. Furthermore, it should be noted that due to this spontaneous oscillation it is self-evident that the lightspot diameter D must be at least as large as $d + s = 10$ mm.

The values of the diameter D and the separation t are strongly related to each other. On the one hand, for a fixed time delay T, an increase in the diameter D, and thus in the separation t, will result in an increase in operating time. On the other hand, increasing D probably simplifies the control of the lightspot movements across the control panel, which in turn may result in a decrease in operating time.

One remark should be made here: The muscles to control

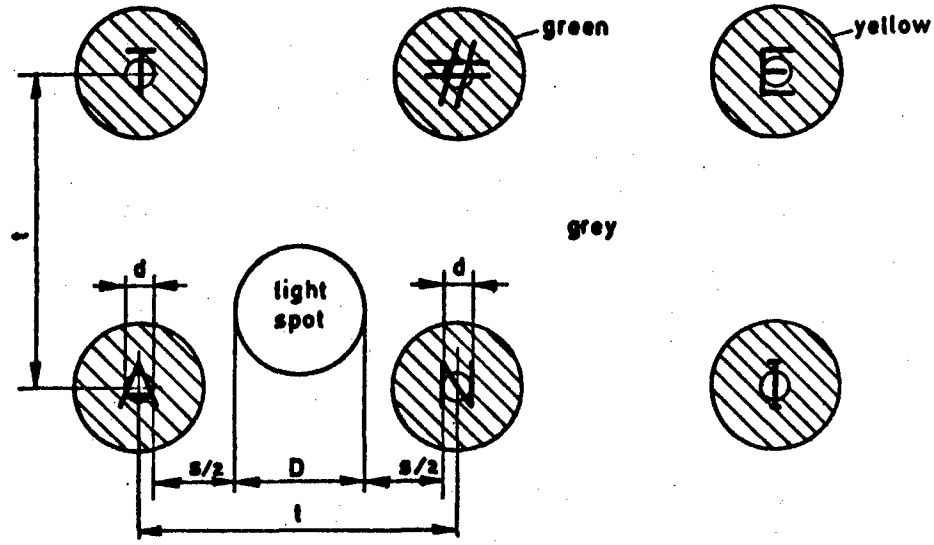

Fig. 5: The geometry of lightspot and control panel.

head motions are mainly controlled by the perception organs, in particular by the eyes and the vestibular organs. The control of the lightspot over the control panel adds to this function a second task. The resulting control of the head muscles therefore has to meet two probably conflicting goals, namely the visual searching activity to locate the character to be typed out and the control of the lightspot position. In what sense the search activity will be unnecessary after some experience and learning of the lay out of the control panel is unknown (see Fig. 6).

For the determination of the optimal value of the diameter D experiments on head motions similar to those executed to study arm motions were carried out.[5]. Three subjects and two patients had to position the lightspot from one point to another, while the following important variables which can influence the lightspot positioning were studied:

- The diameter D of the lightspot: D=6; 9; 12; 17 and 21 mm.
- The horizontal and vertical motions.
- The distance L between starting point and end point: L=45; 115 and 245 mm.

Some characteristic recordings are presented in Fig. 7; the figure shows that the responses can be categorized into three

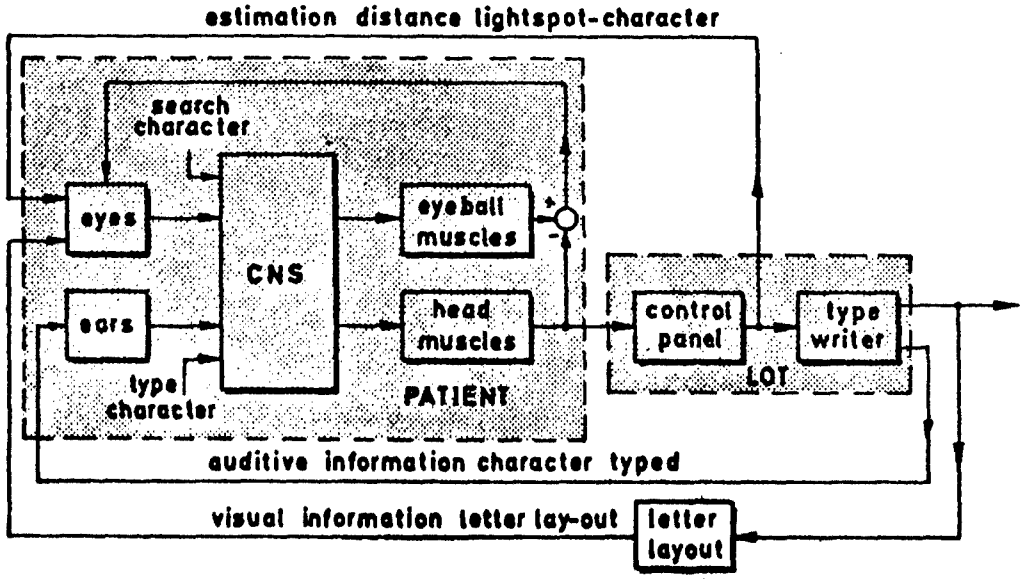

Fig. 6: Patient-LOT-system interaction.

time segments: the onset-time, the bang-bang time and the proportional time. According to the armmotion studies earlier mentioned in this paper the results showed that the onset time and the bang-bang time are almost independent on the diameter D. However, the proportional time is strongly dependent on the diameter D. Below a certain minimum value of D (see Fig. 8), there is a strong increase in the proportional time, hence a value of D = 18 mm (which is more than the required 10 mm) is a good choice.

Finally we consider the overshoot during the positioning of the lightspot. Fig. 9 shows the mean value μ_r and the standard deviation σ_r of the relative lightspot overshoot r, that is the overshoot devided by the lightspot diameter D. The Fig. 9 indicates that the relative overshoot r is decreasing with increasing lightspot diameter; for a lightspot diameter of D= 18 mm the mean value μ_r of the relative overshoot is about 1.0, and the standard deviation σ_r is about 0.6. Now, although the distribution of the relative overshoot is far away from a Normal one, the recordings showed that within a range of $0<s<\mu_r+2\sigma_r$ at least 95% of the overshoots have been covered. Therefore, for the separation t between two characters a value of 45 mm has been chosen. Note that this value is in any way larger than s + D + d = 28 mm.

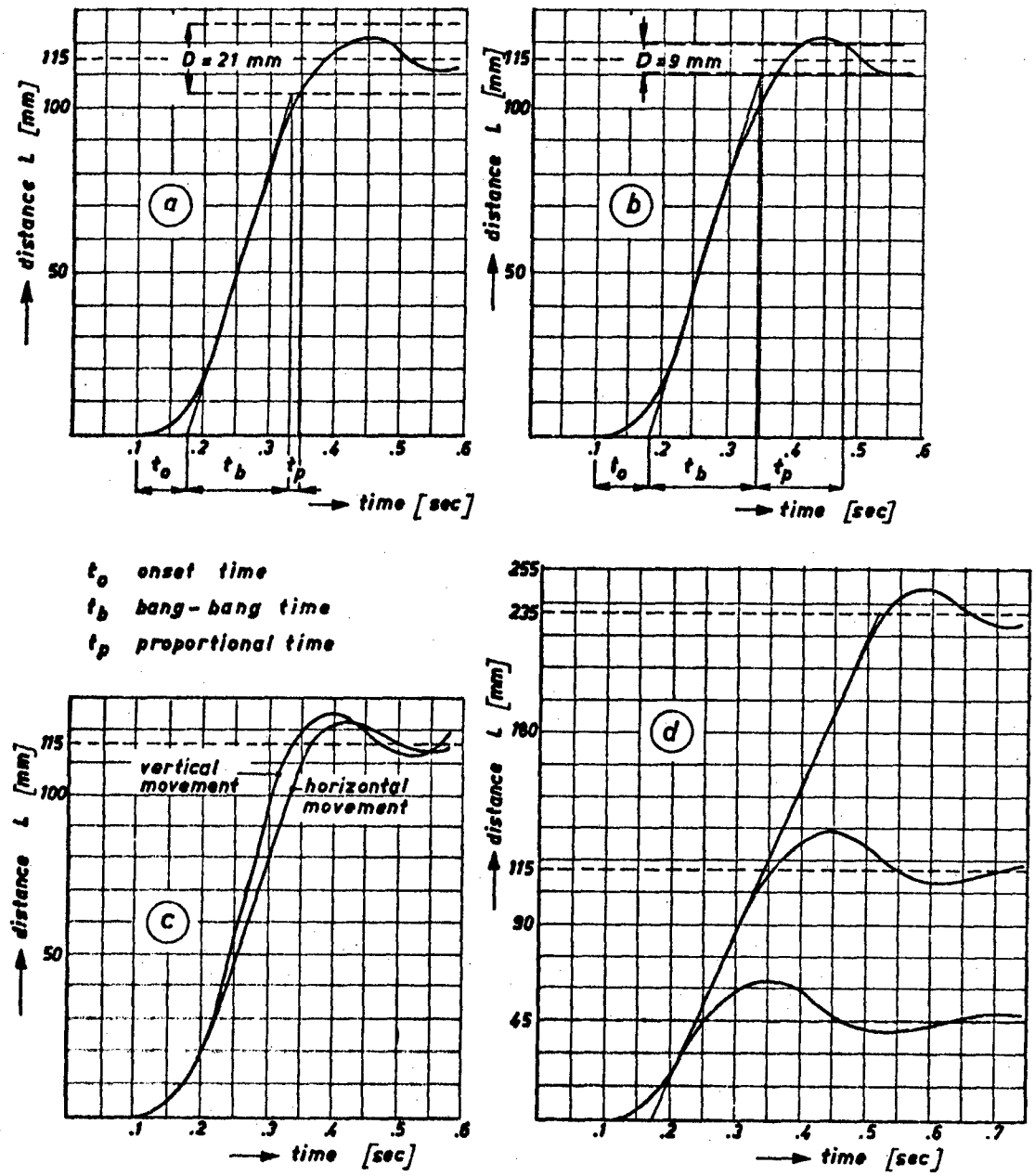

Fig. 7: Typical characteristics of lightspot motions.

a,b The influence of the targetsize D on the proportional time.
c The influence of the direction of movement.
d The influence of the distance L.

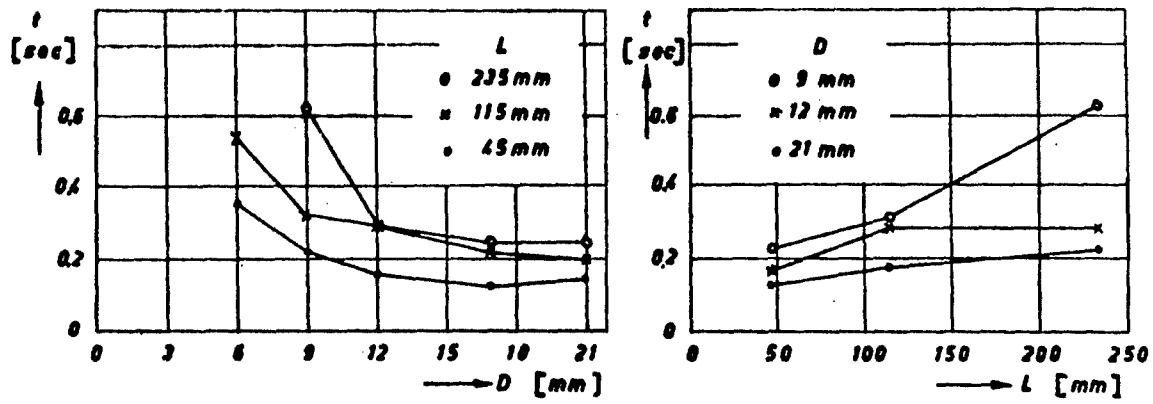

The proportional time as a function of the lightspot diameter D and the distance L.

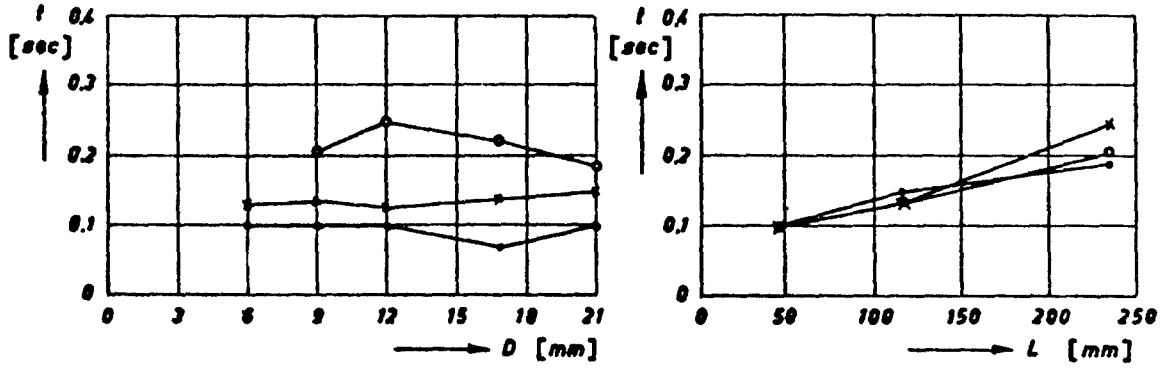

Fig. 8: The bang-bang time as a function of the lightspot diameter D and the distance L.

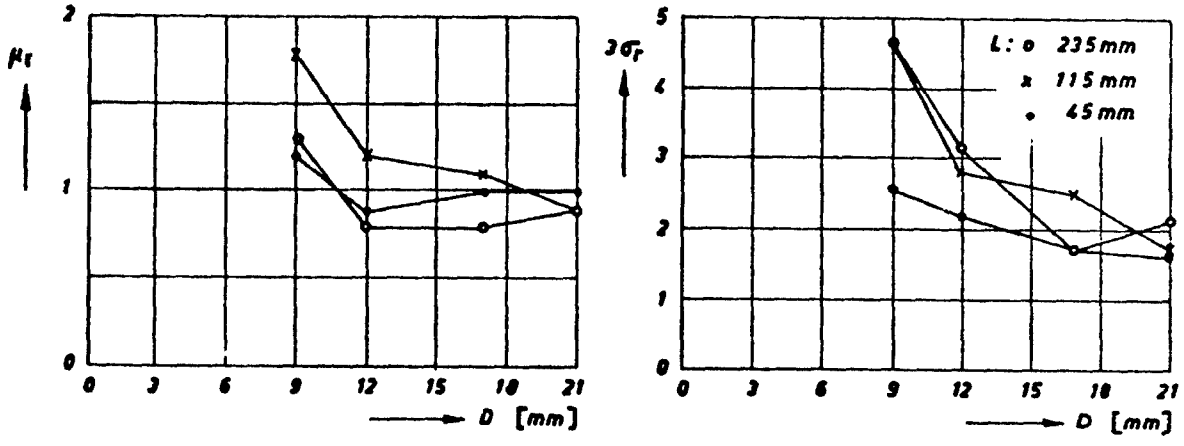

Fig. 9: The mean value μ_r and the standard deviation σ_r of the relative overshoot as a function of the lightspot diameter D and the distance L.

Summarizing the final results, it follows that the geometry of the control panel became:

- lightdetector diameter d = 4 mm.
- lightspot diameter D = 18 mm.
- separation between two characters t = 45 mm.

3.3 Optimization of the preselected time delay

The optimization of the preselected time delay is not possible for a group of patients as a whole. It is even doubtful if this is meaningful for one patient. The physical and mental condition of the patients vary from hour to hour and from patient to patient. For this reason an adaptive method has been chosen, i.e. the patient is able to change the preselected time delay by simple illumination of two lightdetectors with the lightspot. In this way he is able at any time to adapt the typing speed to his own capabilities. The preselected time delay can be varied with steps of 10 msec. in a range of 50 to 500 msec.

4 Concluding remarks

The LOT-system has been in use in one of the Rehabilitation Centers in the Netherlands for about a year; the first results are fairly encouraging. The two patients who are now able to handle the LOT-system are approaching a typing speed of about 80 characters per minute after a three months training period. However, besides this encouraging result, of even more importance is that both the patients found, due to the appreciation they feel for this job, a new goal in their lives; this fact very much favoured the mental condition of the patients.

One of the main problems in the clinical evaluation of the new-developed LOT-system was the development of a training program, so that patients who are motivated to learn to handle the apparatus can work for a typing certificate. To avoid disappointments with the patients, the training program was first tried out with three healthy subjects. The program is based on the following goals:

- To learn to control perfectly the vertical and horizontal head motions.
- To learn to locate the characters and symbols.
- To learn to move across the control panel from one character to the other in the shortest way.
- To learn to type words, sentences and letters, etc.

At the moment a second prototype is under construction. Particular attention will be paid to the reliability of the system, furthermore a character display to reproduce the last sentence typed on the typewriter is being added to the control panel.

Moreover, a possibility of applying the system as an input device for a digital computer is being considered.

5 Acknowledgements

The authors gratefully acknowledge the contribution of Miss W.J. Luitse, occupational therapist at the Rehabilitation Center "De Hoogstraat" at Leersum, the Netherlands, for the development of the training program and for the very enthusiastic way in which she assisted the subjects and patients in the training period.

6 References

1. Jenkin , R.: "Possum: A New Communication Aid", Special Education Vol. LVI No. 1, 1967, pp. 9-11.
2. Collins, D.W.: "New Developments", Rehabilitation 63, 1967, pp. 19-26.
3. Soede, M; Stassen, H.G.: "A Lightspot Operated Typewriter for Severly Disabled Patients", Technical Note, To be presented in Med. and Biol. Engng., 1972.
4. Berckel, J.A.Th.M. van; et al: "Formal Properties of Newspaper Dutch", Mathematical Centre Tracts No. 12. Math. Centrum, Amsterdam, 1965, p. 119.
5. Aldrich, J.W.; Lyman, J.; Stassen, H.G.: "A Formal Model for Arm Motion during Target Approach", 5th Annual NASA-University Conf. on Manual Control, MIT, 1969, pp. 581-608.

PHOTOELECTRIC HEAD MOVEMENT MEASUREMENT AS A CONTROL EFFECTOR

by

Bernard Chouet and Laurence R. Young

ABSTRACT

The possibility of using head motion as a natural way of stabilizing and controlling one's attitude in a zero-g situation has been investigated. An electro-optical system was built for dtection of such motions. The system consists of a set of eight silicon photodetectors mounted on the inner surface of a space helmet, and two light emitting diodes attached to the astronaut's helmet liner texture. Light emission is in the near infrared region within a narrow spectrum centered at a wavelength of 0.93 . Limits of rotation are $\pm$30° in both pitch and roll (helmet limits) and $\pm$80° in yaw (head limits). Each axis is decoupled using an on-line PDP-8 computer. Feasibility of the ACS is demonstrated in compensatory tracking tasks using a pseudo-random input of bandwidth 0.155 Hz on each axis and K/S dynamics. The subject showed excellent performance over a tenfold range of gain. No significant differences appear between the three axes.

SESSION III

Aircraft Display Concepts

Preceding page blank

EXPERIMENTAL EVALUATION OF A DISPLAY PARAMETER USING THE PHASE MARGIN PERFORMANCE MEASURE*

Pershing B. Sun

Instrumentation and Control Laboratory
Department of Aerospace and Mechanical Sciences
Princeton University

ABSTRACT

A trade-off study between stability augmentation and velocity vector gain is made in a simulated precision hovering task. The study is implemented by using the Phase Margin Performance Measure Technique. The advantages of this approach are that the error level corresponding to the actual task requirement can be specified independently and a high level workload situation is created automatically. Test results obtained from a fixed-base simulator experiments are presented and discussed. The effect of the instrumentation noise on the choice of velocity vector gain is also explored.

INTRODUCTION

A multi-colored integrated display for the trajectory control of helicopters and VTOL aircrafts was developed at Princeton University (Ref. 1). The basic format of the integrated display in the station keeping mode is shown in Fig. 1. One of the distinctive features of this display is the explicit presentation of the error velocity vectors in both the horizontal and vertical display areas. The importance of the velocity vector cannot be overemphasized. It provides quickening information in the position control task, and also serves as an additional source of correlation between the aircraft attitude (or acceleration) and its position. However, a display that is unduly sensitive to the velocity vector becomes distracting and leads to excessive control by the pilot. Thus, in order to quantitatively determine the merit of the velocity vector magnitude to other control system parameters is highly desirable.

After considering various alternatives, an experimental approach called the Phase Margin Performance Measure was chosen to facilitate such a trade-off study. A detailed description of this approach is presented in Ref. 2. The basic goal of the Phase Margin Performance Measure is to provide a means by which the maximum additional amount of phase shift that the pilot can handle can be measured as a function of the specified disturbance level, system output level, and feedback design (e.g. display) under high workload conditions. For

*The work reported in this paper was supported in part by the U. S. Army Electronic Command under Contract No. DA 28-043 AMC-02412(E).

Preceding page blank

the case of display parameter evaluation in a hovering task, the scheme is illustrated in Fig. 2. The velocity vector gain is the independent variable; the system disturbance characteristic and output level are fixed; and the dependent variable is the difficulty of the vehicle dynamics.

The longitudinal vehicle dynamics of a helicopter at hover is approximated by two integrators and two variable first order filters in series. The contributions of the drag damping X_u and velocity stability M_u to the system dynamics is neglected. However, artificial attitude stabilization M_θ is taken into consideration. The characteristic equation of the vehicle dynamics is simply

$$s^2 (s^2 - M_\theta^{\cdot} s - M_\theta) = 0$$

$$\text{or} \quad s^2 (s+K_1)(s+K_2) = 0$$

$$\text{where} \quad -M_\theta^{\cdot} = K_1 + K_2$$

$$-M_\theta = K_1 K_2$$

The coefficients K_1 and K_2 are the variable filter parameter values. It was found that the optimal value of the control gain should be increased as feedback augmentation increases in order to maintain control effectiveness in the precision hovering task, (Ref. 3,4). This effect is simulated by augmenting the control gain by $\sqrt{1 + K^2}$ in each filter.

During the test run, the filter parameters are adjusted automatically as a function of the difference between the prescribed error level and the actual output of the position error of the vehicle. If the position error is less than the prescribed level the parameter value decreases producing more phase shift between the pilot input and the vehicle output and vice versa. The equilibrium parameter value is reached when the average position error level matches the prescribed level in steady state operation. The amount of phase shift which the pilot has to handle is proportional to the degree of difficulty in vehicle dynamics. In other words, the filter parameter values relate directly to the inner loop stability feedback augmentations of the vehicle.

EXPERIMENTAL CONSIDERATIONS

The input disturbance simulating the aerodynamic moment produced by gust is made up of eight sine waves with amplitude ratios approximated by a first order filter having the corner frequency of 1 rad./sec. The frequency spacing is the same as that used in Ref. 5.

In order for an adaptive scheme to properly create a high workload situation, the prescribed error should be set at a level larger than that which the pilot considers as a tolerable error

margin (Ref. 6). At the same time, however, the prescribed level must be realistic for the task under investigation (Ref. 7). On the basis of these considerations and information obtained from preliminary experimental runs, the prescribed levels of .5 and 1.0 meters were used.

The following automatic adjustment rule was chosen for this investigation:

$$\dot{K} = A \log (|x|/e_c)$$

where $\dot{K}$ = parameter adjustment rate

A = adaptive loop gain

$|x|$ = absolute value of position error

e_c = prescribed error level

An adaptive loop gain of .1 was found to enable the variable parameter to converge smoothly to its equilibrium value at a reasonable rate. The display sensitivity of the position error was .5 cm/m, while the display range was approximately ±7 cm. The velocity vector gain was defined as the ratio of display magnitudes between the position error and velocity error; e.g. for a vector gain of 5 the velocity display sensitivity would be 2.5 cm/m/sec.

The duration of each test run was 200 seconds: the adjustment scheme took approximately 60 seconds to establish the equilibrium parameter value, thus leaving 140 seconds for steady state tracking. A sample of the test record is shown in Fig. 3. The increase in control output corresponding to higher workload as the variable parameter reaches its equilibrium value can readily be observed.

The following variables were measured: errors in position, velocity, and acceleration; the parameter and its filtered (20 second time constant) values; and the control inputs.

Four subjects were employed in the experiment. All subjects were licensed pilots with adequate simulator experience. An average training time of 3 hours was necessary for the subjects to establish proficiency in the tracking task. Four test runs per subject were conducted in each test cell.

RESULTS AND DISCUSSION

The average filter parameter value, over four subjects, is plotted as a function of vector gain in Fig. 4. The parameter value decreases markedly from 0 vector gain (no velocity vector display) to a vector gain of 1.7. However, there is no noticeable change in parameter value from the vector gain of 1.7 to 9.0. The trade-off between the display of velocity vector and automatic feedback augmentations is readily illustrated by the fact that

lower parameter values correspond to smaller amounts of stability augmentation. The insensitivity of the parameter value to changes in vector gain is somewhat surprising and suggests that in the absence of measurement noise, high vector gain can be tolerated by the pilot. The velocity vector is used by the pilot primarily as a quickened position indicator, and its magnitude, because of the adaptibility of the operator, does not have a significant effect on the closed loop performance. The effect of measurement noise on performance at high vector gain is discussed in the latter part of this paper.

In order to obtain more detailed information about the effect of vector gain on pilot behavior, the pilot transfer function was calculated. The Fourier transform of the position error and control input of the last 100 seconds of each test run were calculated by a digital Fast Fourier Transform program. The pilot transfer function was obtained by taking the ratio of the Fourier coefficients of the position error and the control input at the disturbance input frequencies (Ref. 8). The accuracy of the calculation is checked by using a lead-lag pilot transfer function as shown in Fig. 5.

Samples of pilot transfer functions for vector gain 0, 5, and 9 are shown in Fig. 6. A pilot time delay of .3 sec was used in all three cases to fit the phase angle data. For the case of zero vector gain, a 2.5 sec lead was generated by the pilot with a gain of .5. As the vector gain is increased to 5, the pilot lead time reduces to 1.6 sec since a 5 second lead is provided by the velocity vector. At the vector gain of 9, a lag of .7 sec appears in addition to a lead of 2.5 sec. This indicates that filtering of the velocity vector is employed by the pilot. The amount of phase shift produced by the variable filters is calculated at the closed loop frequency. The closed loop frequency and its corresponding phase margin are obtained from the Bode plot of the open loop pilot-vehicle transfer function such as that shown in Fig. 7.

The average phase shift and closed loop phase margin computed for two subjects are plotted against vector gain in Fig. 8. The amount of phase shift increases substantially between the vector gain of 0 and 3. It remains approximately constant between vector gain of 3 and 5, and then increases and decreases for subject B and C respectively at the vector gain of 9. The phase margin is essentially constant with the vector gains of 0, 3 and 5 for both subjects. At the gain of 9, the phase margin decreases for subject B and increases for subject C. A trade-off between the phase shift and phase margin is indicated by the opposite trends exhibited by these two quantities between the vector gain of 5 and 9.

Since the phase margin is a measure of the closed loop system stability and the phase shift is related directly to the stability augmentations of the controlled vehicle, the sum of these two quantities should be considered as a suitable measure of the relative

merits of various display vector gains. The total phase angle is plotted against vector gain in Fig. 8. It shows an increase of about 40 degrees in phase angle between the vector gains of 0 and 3. No additional increase of the phase angle is observed as the vector gain is increased to 9.

The average relative remnant coefficient is presented in Fig. 9 as a function of the vector gain. It is calculated from the ratio of the control power at the input frequencies and the total control power (Ref. 8). The average remnant coefficient increases slightly with vector gains up to 5 and then remains unchanged.

In the above results and discussion, measurement noise was not considered in the simulated task; therefore there is no real penalty in displaying the velocity vector at high gains. In order to investigate the effect of measurement noise on the choice of vector gains, a preliminary test series was carried out in which measurement noise corresponding to approximately .1 m/sec was added to the velocity vector. The influence of the added noise on the system performance at high vector gains is marked as shown in Fig. 10.

CONCLUSION

The application of the Phase Margin Performance Measure to the evaluation of display vector gains was conducted in a fixed-base simulated hovering task. The trade-off between the stability augmentation and the display of the velocity vector was observed. In the absence of instrumentation noise the closed loop performance, represented by the filter parameter values and their associated phase shifts, remains essentailly the same as the vector gain is increased from 1.7 to 9.0. When measurement noise is added to the velocity, the performance degenerates at high vector gains.

References

1. Dukes, T. A., "An Integrated Display for Trajectory Control of Helicopters and VTOL Aircraft", Proceedings of the 6th Annual Conference on Manual Control, 7-9 April, 1970, pp. 133-145.

2. Sun, P. B., and Dukes, T. A., "A Performance Measure for Manual Control Systems", Proceedings of the 7th Annual Conference on Manual Control, 2-4 June, 1971.

3. Seckel, E., Stability and Control of Airplanes and Helicopters, Academic Press, 1964.

4. Miller, D. P., and Vinje, E. W., "Fixed-Base Flight Simulator Studies of VTOL Aircraft Handling Qualities in Hovering and Low-Speed Flight", AFFDL-TR-67-152, Jan. 1968.

5. McRuer, D., Graham, D., Krendel, E., and Reisener, W. Jr., "Human Pilot Dynamics in Conpensatory Systems", AFFDL-TR-65-15, July 1965.

6. Kelley, C. R., "The Measurement of Tracking Proficiency", Human Factors, Vol. 11, No. 1, Feb. 1969, pp. 43-64.

7. Harper, H. P., Sardonowsky, W., and Scharpf, R., "Development of VTOL Flying and Hovering Qualities Requirements Based on Mission-Task Performance", Journal of American Helicopter Society, Vol. 15, No. 3, July 1970, pp. 57-65.

8. Taylor, L. W. Jr., "Discussion of Spectral Human-Response Analysis", Proceedings of the 2nd Annual Conference on Manual Control, NASA SP-128, Feb. 28-Mar. 2, 1966. pp. 403-412.

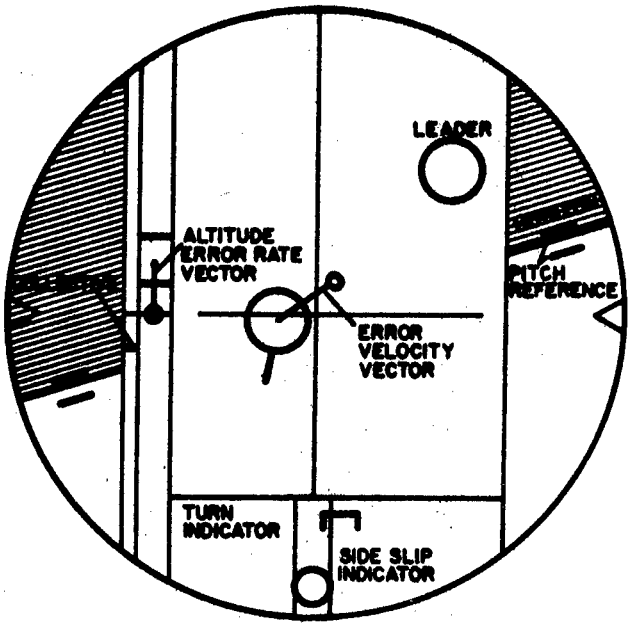

Figure 1. Integrated Display, Station Keeping Mode (Ref. 1)

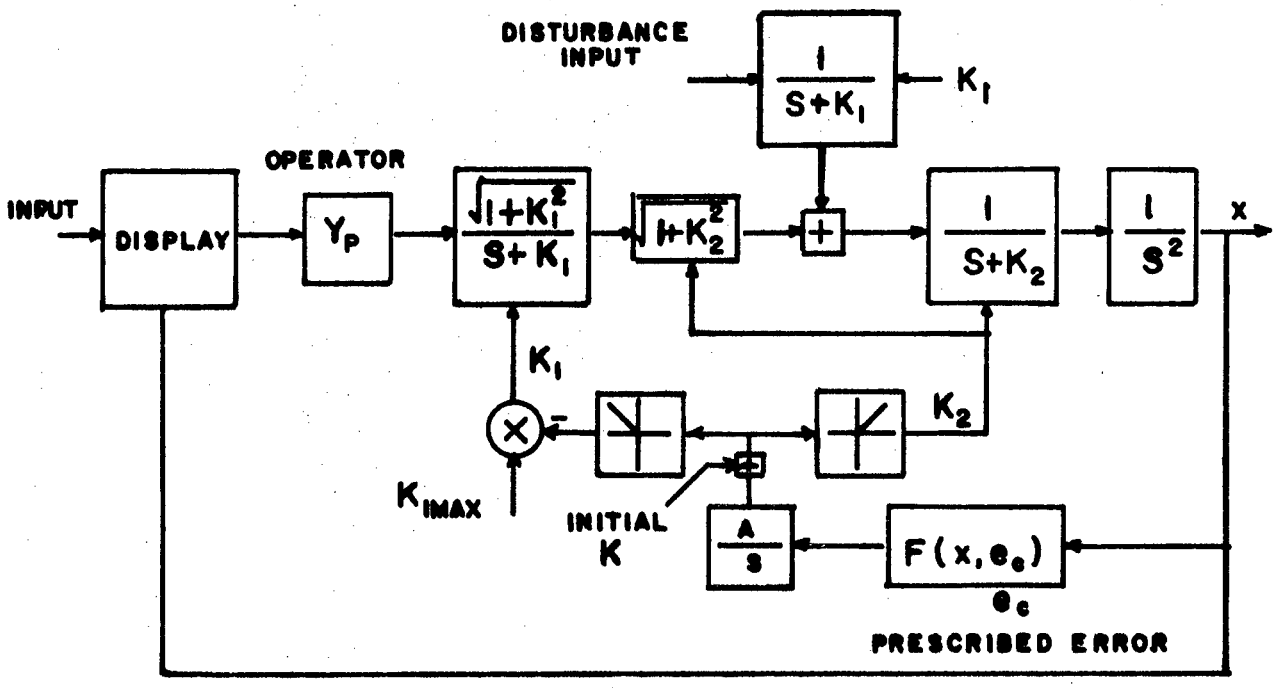

Figure 2. Block diagram of the Control Loop and the Adjustment Loop (Ref. 2)

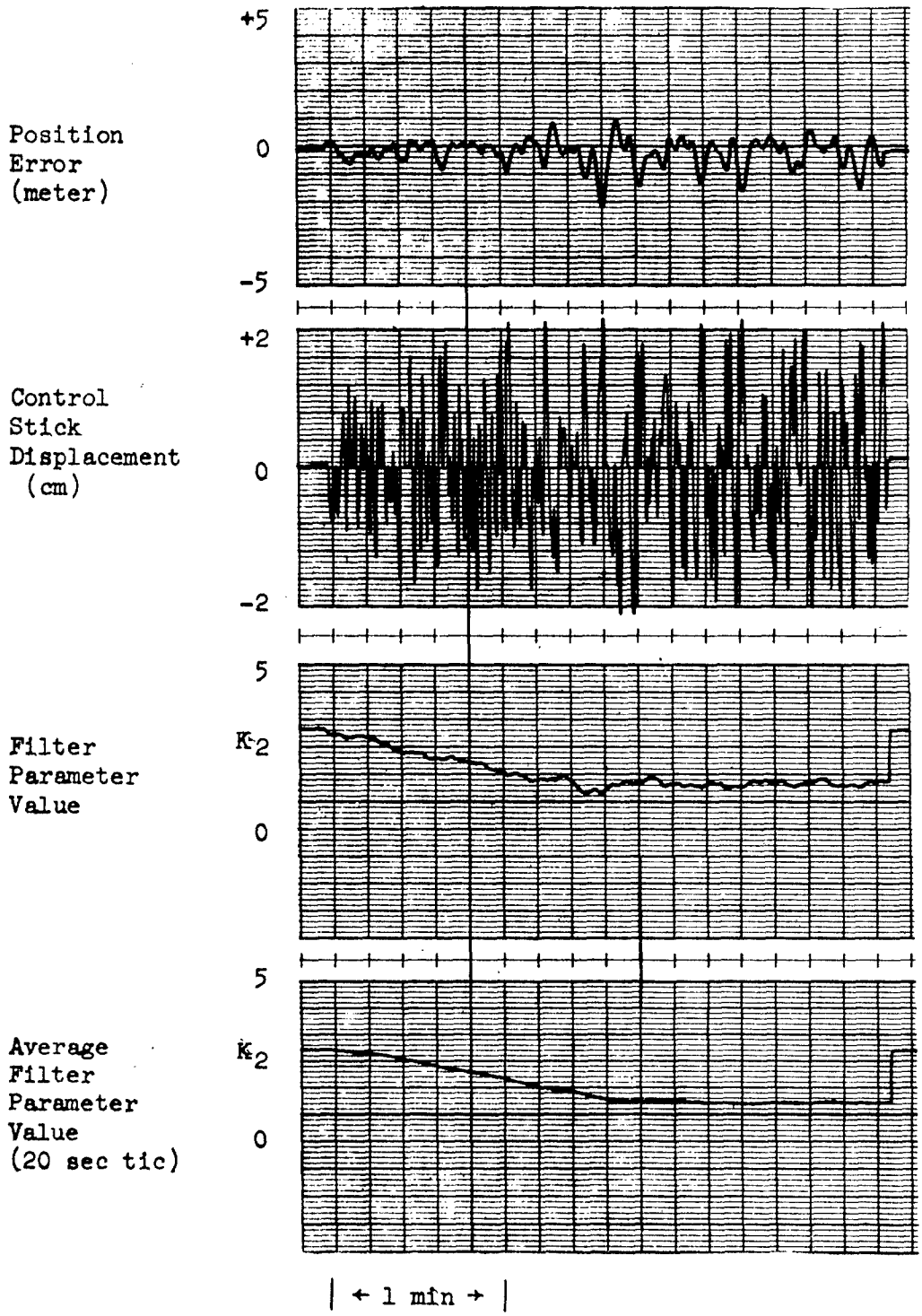

Figure 3 Sample of the Test Record

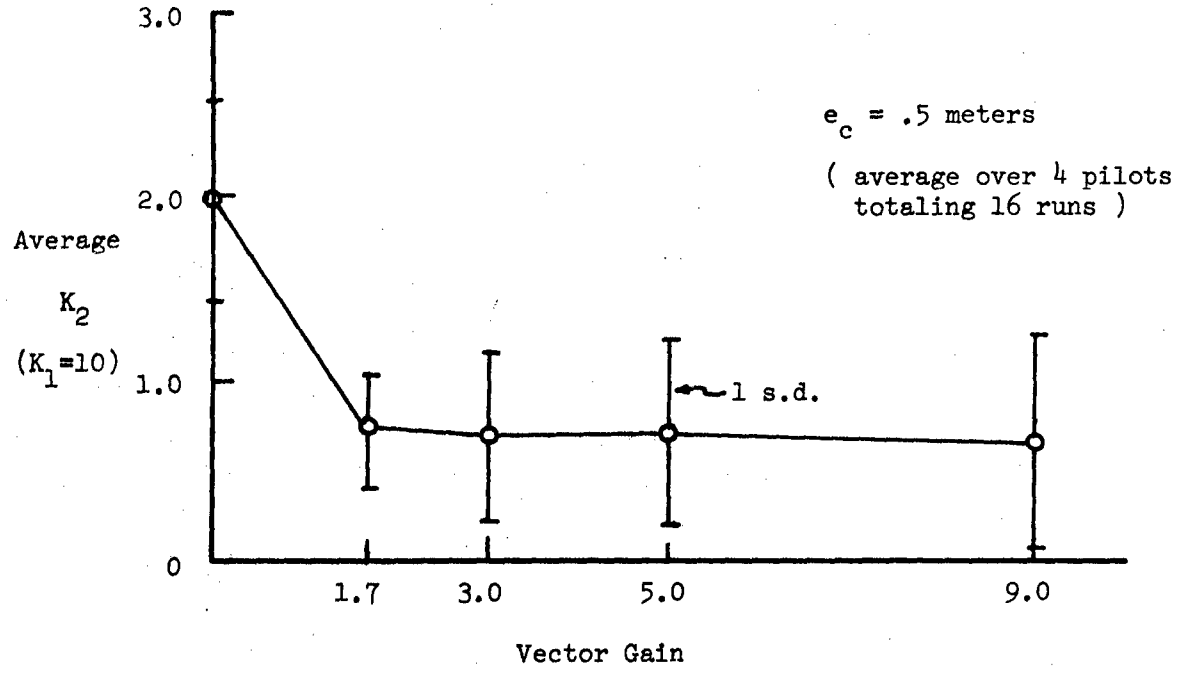

Figure 4. Average Filter Parameter Value Versus Vector Gain

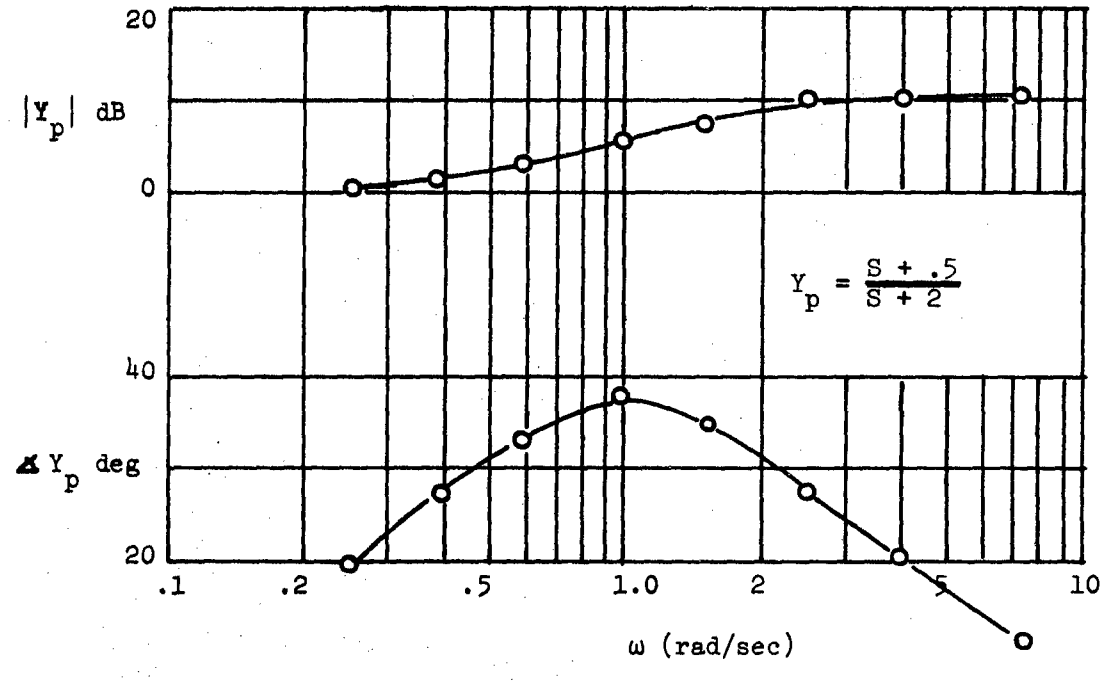

Figure 5 Accuracy check on Pilot Transfer Function Calculation

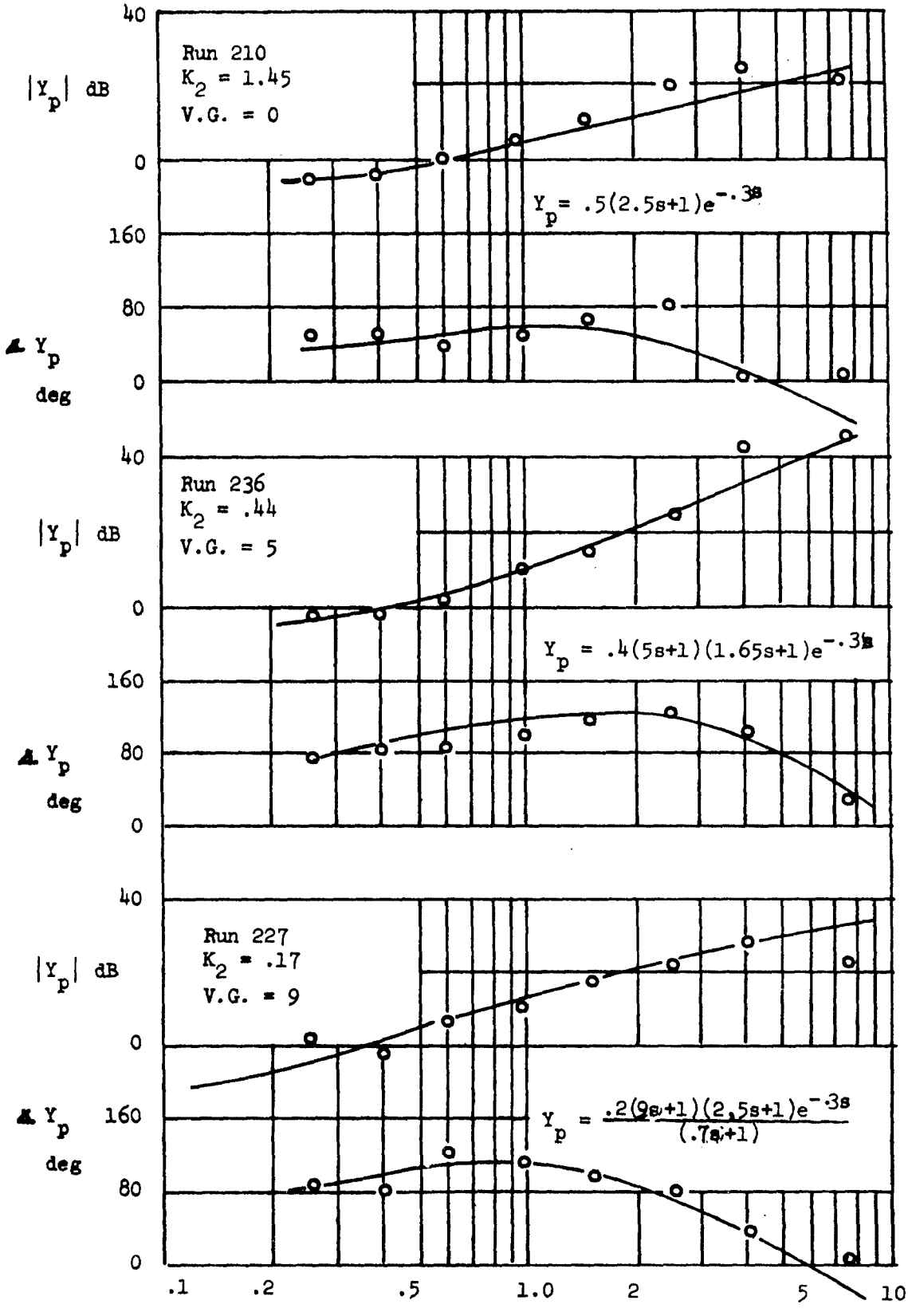

Figure 6 Pilot Transfer Function Vs Vector Gain

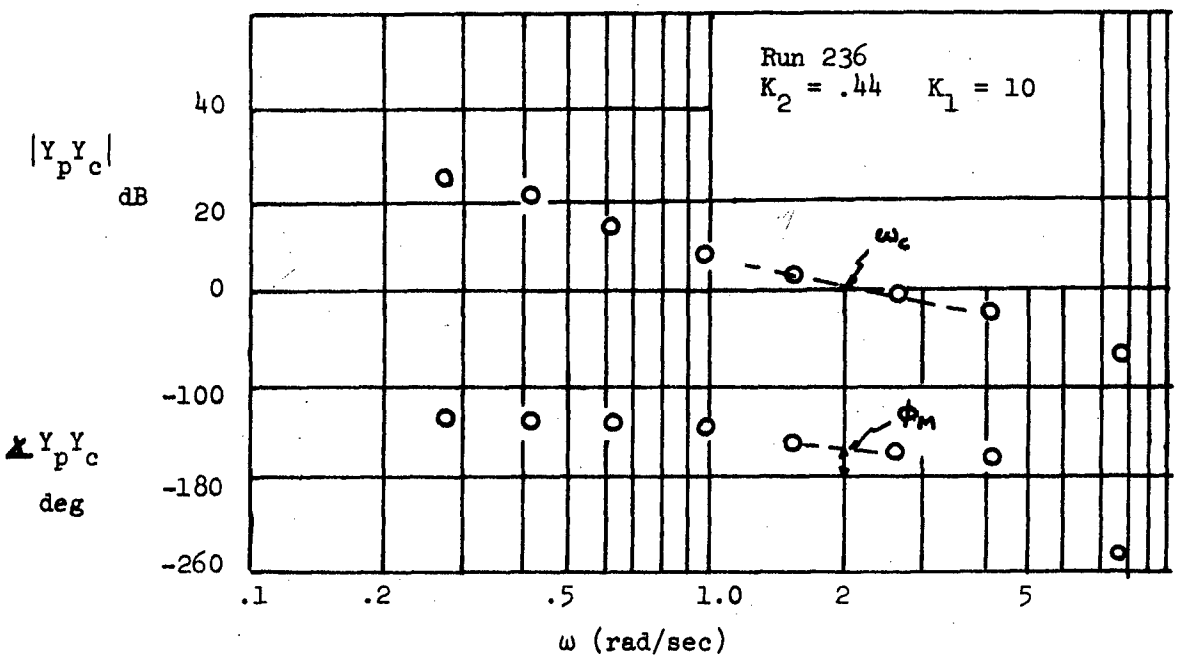

Figure 7 Closed loop Frequency and Phase Margin Calculations

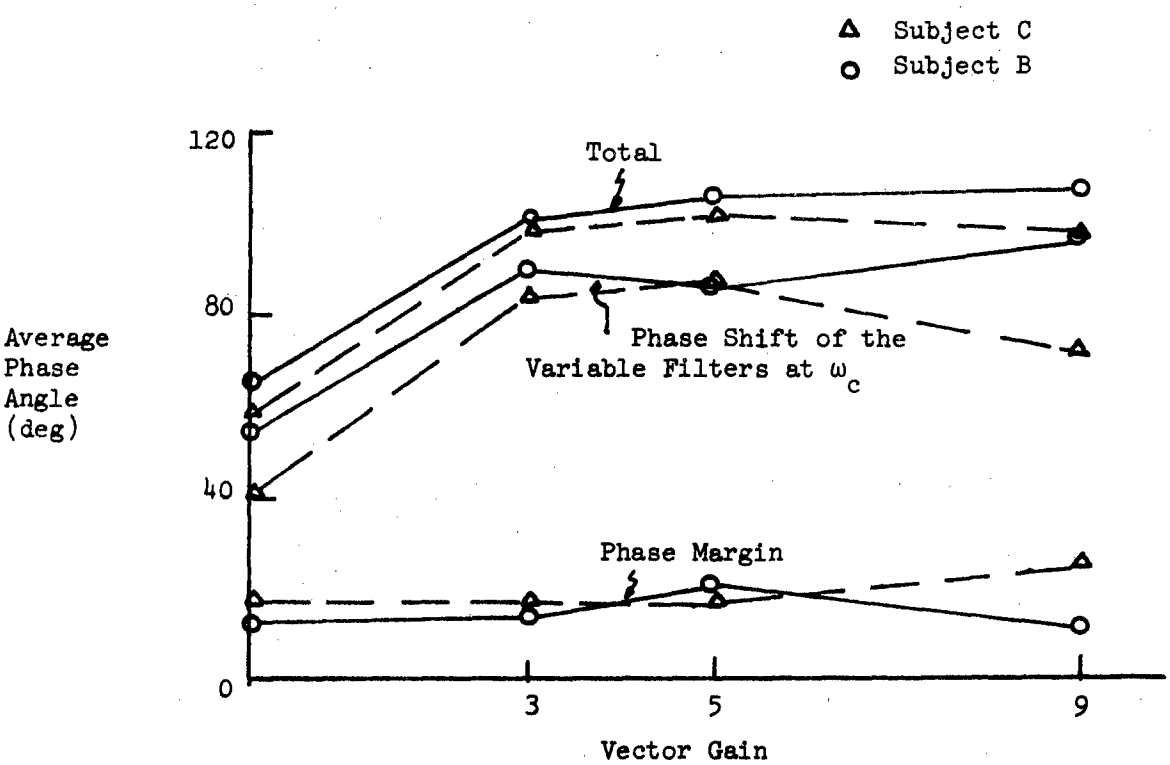

Figure 8 Phase Shift and Phase Margin Vs Vector Gain

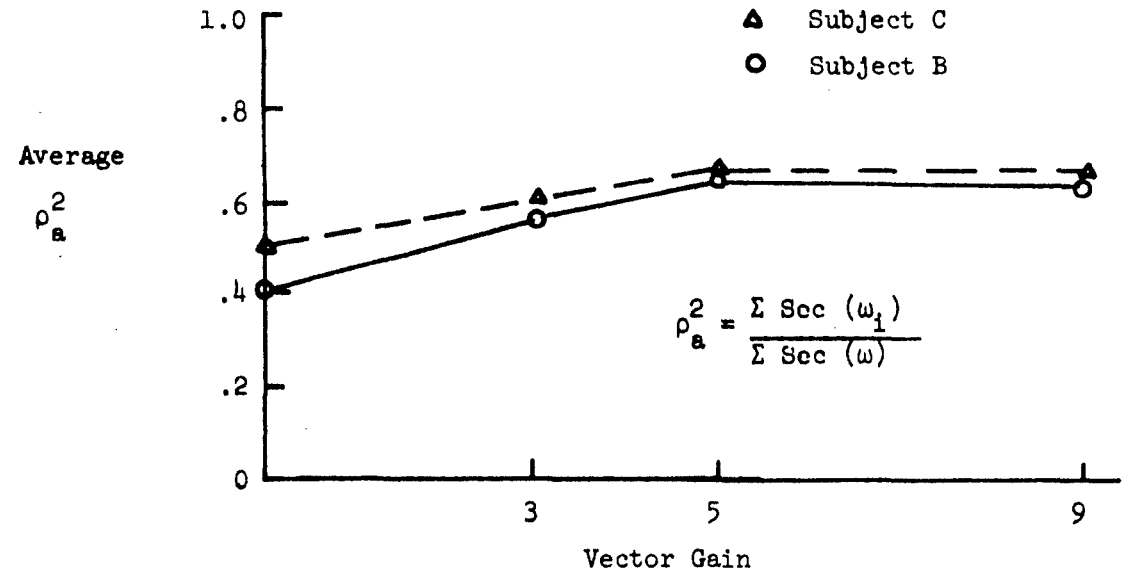

Figure 9 Average Relative Remnant Coefficient Versus Vector Gain

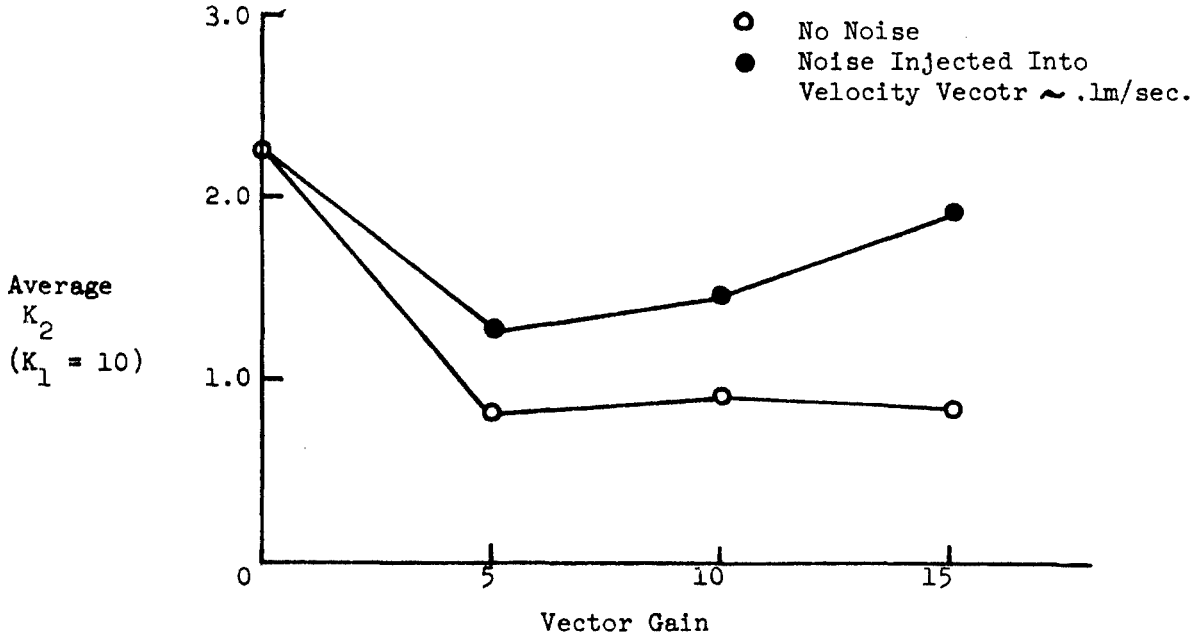

Figure 10 Effect of Measurement Noise on System Performance

A SIMULATION TO EVALUATE PWI SYSTEM PARAMETERS IN VISUAL SEARCH

by

Renwick E. Curry
Man-Vehicle Laboratory
Department of Aeronautics and Astronautics
Massachusetts Institute of Technology
Cambridge, Massachusetts

Jacques Dumeurger*
JLM International
Brookline, Massachusetts

Ernest H. Day*
Lincoln Laboratories
Massachusetts Institute of Technology
Lincoln, Massachusetts

John W. Senders
Senders Associates
Waltham, Massachusetts

I. INTRODUCTION

Background

The number of aircraft operations has been increasing at an accelerating rate over the past years and a fourfold increase is predicted by the 1990's. The Air Traffic Control Advisory Committee, or the so-called Alexander Committee, has suggested a plan for the organized and logical development toward a ground-based air traffic control system to relieve the congestion and maintain the safety levels in the face of the increase in the number of aircraft and operations.

One aspect of the safety question is that of midair collision. The risk of midair collisions can be reduced in the face of increased traffic density by restricting the airspace in which different classes of aircraft operate and by maintaining more accurate surveillance and control. A complementary approach is to equip each aircraft with an onboard system which determines

*Formerly Research Assistants in the Man-Vehicle Laboratory, Department of Aeronautics and Astronautics, Massachusetts Institute of Technology, Cambridge, Massachusetts

the threat of collision without the aid of ground-based equipment. It is in this latter category that such anti-collision systems as PWI and CAS systems fall.

The distinction between CAS (Collision Avoidance Systems) and PWI (Proximity Warning Indicator, or Pilot Warning Indicator) is usually made on the basis of the allocation of the anti-collision functions between the man and the machine. These functions are generally regarded to be:

1. Target detection
2. Threat evaluation
3. Selection of evasive maneuver
4. Maneuver execution.

Collision avoidance systems are usually defined to be those systems in which the first three functions are performed by the hardware and the execution of the evasive maneuver is done by the pilot. The most well-known CAS system at the current time is the time/frequency system being evaluated by the Air Transport Association (ATA). A PWI system is distinguished by the fact that the threat evaluation and evasive maneuver selection, as well as the maneuver execution are performed by the pilot. In order to evaluate the threat, the pilot must be able to detect the other aircraft visually or by some other means. Thus in this class of systems, there is a target detection by the PWI system and (usually) a visual acquisition by the pilot. Thus the pilot plays a very important role in the effective operation of the PWI system. This paper addresses itself to the first of those pilot functions, i.e., the visual detection of targets, through a simulation of pertinent variables in the air-to-air detection problem.

II. VISUAL SEARCH

Important Parameters in Visual Search

For the past several decades, many experiments have been carried out to determine the important variables in describing the human's ability to visually detect targets. As a result of these experiments, the following variables have been found to be of primary importance in visual detection:

Background (adapting) Illumination Level
Target Contrast Ratio
Target Size
Target Motion
Backgound Complexity
Observer's Scan Pattern
Position of the Target Image on the Retina.

Target shape, color, and rate of change of size/contrast ratio have been found to be of secondary importance. The rate of change of size and contrast ratio can be of primary importance, but not in the air-to-air detection of targets against a uniform background.

Perhaps the most commonly cited data are the so-called "Tiffany" data recorded by Blackwell (1946). Blackwell presented a set of visual detection threshold curves which are used as the basis of many preliminary calculations. One way in which these data are presented is shown in Figure 1. These curves show how, at a constant background illumination level, the size and contrast ratio should vary in order that the probability of detection remain at 50%. These data were recorded from experienced observers, and the observation time is extremely long. Even though these are recognized as being "optimistic" thresholds, they are useful as a common data base.

One of Blackwell's most important findings is that the probability of detecting a target depends only on the contrast ratio of the target relative to the threshold contrast. His data indicate that the cumulative probability distribution function is nearly Gaussian, and suggests that if one doubles the contrast ratio relative to threshold the probability of detection goes from 50% to 90%, halving the contrast ratio reduces the probability to 10%. This is an extremely important result and has been used to derive models of target detection.

A Model for Visual Search

A model which has been shown to describe the statistical behavior of detection in many circumstances is the "Visual Lobe" model first proposed by Koopman and discussed by Lomar (1960) and Hammill (1969). It is assumed that the search process consists of a sequence of "glimpses" in which the eye is momentarily stationary and during which there is a possibility of detecting the target. Furthermore, it is assumed that the probability of detection is independent from one glimpse to the next.(In practice, eye movement experiments have shown that the duration of the glimpses is approximately one-third of a second.) Under these assumptions, it can be shown that the cumulative probability distribution of the detection time is given by

$$P(t_D \leq t) = 1 - \exp\left[-\int_0^t g(u)\,du\right] \qquad (1)$$

where t_D is the detection time, t is the argument of the distribution function, and the function g(u) is the probability per unit time of detecting the target. This glimpse detection function depends on background complexity, the area to be searched, and contrast ratio above threshold (C/C_T). Under static stimulus conditions, the glimpse probability per unit time is equal to a constant and the cumulative distribution of Equation 1 becomes the familiar exponential form.

Philosophy of Generating the Target Stimulus

We have taken the approach in our simulation of reproducing those target characteristics which are most important in the detection process: background illumination, target size, contrast target motion, and background complexity. We have simplified matters by assuming that the real aircraft would appear against a uniform background, and this would be true in a majority of air-to-air encounters which result in a near miss. The angular target motion will be reproduced , and this will be discussed more fully under the description of the simulator. As for the three remaining variables (background illumination, size, contrast ratio), we find through the discussion of Blackwell's detection data and the detection model of Koopman, that the single most important parameter is the contrast ratio relative to threshold contrast (C/C_T). The target size and background illumination are effective only as they determine the threshold contrast C_T. Furthermore, we know that the shape of the target and the color of the target, as well as the sign of the contrast ratio at the background level of our simulation have only a secondary effect on the visibility characteristics of the target. Thus, it is with some confidence that we can use a circle of light against a uniform background to reproduce the important visibility characteristics of an approaching aircraft, namely, target motion and contrast ratio relative to threshold.

Visibility Characteristics of an Approaching Aircraft

In this section we discuss the calculation of the contrast ratio relative to threshold contrast for an approaching aircraft. The basic approach is to determine the angular size and contrast ratio of an approaching aircraft as a function of range, and then plot these two variables (with range as a parameter of the curve) on the same curve as the visibility threshold.

For the angular size of the aircraft, we use a small angle approximation:

$$\alpha = \frac{S}{R} \qquad (2)$$

where α is the angular size of the aircraft, R is the range of the approaching aircraft, and S is its size. To take account of atmospheric scattering effects, we used the exponential model to describe the contrast ratio at range R.

$$C(R) = C(0)e^{-3.9\frac{R}{M_r}} \qquad (3)$$

where C(R) is the apparent contrast ratio at range R, C(0) is the inherent contrast (contrast at zero range), R is the range in miles, and M_r is the meteorological visibility in miles. Equation 4 can be expressed in terms of angular size by substituting Equation 2 and leads to:

$$C(\alpha) = C(\infty)e^{-2.53\frac{S}{M_r}\frac{1}{\alpha}} \qquad (4)$$

where α is expressed in arc minutes, M_r in miles, and S in feet. This equation results in a single curve on the log size-log contrast coordinates and describe the contrast ratio of the target as it approaches the observer. The sketch of this curve and the thresold curves as determined by Blackwell for the background illumination against which the airplane will appear are shown in Figure 2 for two meteorological visibilities. The horizontal separation between these two curves is the all-important visibility characteristic -- log contrast above threshold. This variable can now be plotted as a function of range and results in a curve shown in Figure 3. The origin of the ordinate depends on the inherent contrast, and can be shifted upward or downward by changing the zero-range contrast ratio. The dotted lines shown in the figure are the actual values of log C/C_T achieved in the simulator and reflect the physical constraints on the ability to vary size and contrast ratio.

III. SIMULATOR DESCRIPTION

The cockpit in which subjects were situated was a Link GAT-1 single place General Aviation trainer. The GAT-1 has three angular degrees of freedom (pitch, roll, yaw). The dynamic characteristics of the trainer are not precisely representative of real aircraft because it is designed to be flown as an

instrument trainer with the pilot always "under the hood" and not flying with visual reference. But, it is felt that this was a realistic flying task even in the VFR mode. The instantaneous altitude, air speed, and three attitude angles of the trainer were measured and sent to the computer via trunk lines.

The target image consisted of a circular spot of light generated by a modified slide projector. The iris and polarizing filters were placed in the focal plane of the projection lens to control the target size and contrast ratio, and were under control of a local feedback servo system. The angular size of the target was variable from 3 arc minutes to 85 arc minutes although only the range from 80 to 10 was used in practice. The polarizing filters were able to control the target brightness over a range of 1.7 log units (brightness ratio of 50:1).

The targets were projected onto a screen composed of four-feet by six-feet plywood sections arranged to approximate a thirteen-foot radius sphere. The angular coverage provided by the screen is $\pm$110 degrees in azimuth and $\pm$50 degrees in elevation. The background illumination was provided by a circular florescent tube at the center of the sphere and three tubes on the floor of the simulator. The average background luminence was 1.3 ft-L above the painted horizon. At this background level, and with appropriate positioning of the floor lamps, the contrast differences due to the sharp corners between adjacent panels was eliminated.

The target's position on the screen was controlled by reflecting the beam of light from a mirror whose angular position was controlled by azimuth and elevation servo systems which followed commands from the computer.

The display/computer interface was constructed to give flexibility in designing and actuating PWI display configurations. The PWI display logic was controlled by a digital communcations system consisting of a thirty-two bit shift register fed by a data line and clock line. Each shift register bit is used to control a triac which acts as a switch between a display element,e.g. light or audio speaker, and the power supply to the element. This system permits independent control of thirty-two display elements.

The projection system, GAT-1, are shown in Figure 4 which a view taken from behind the trainer looking toward the screen. Suspended from above are the circular florescent light and the target position servos. Also visible on the side of the structure are the heat sinks for the servo amplifiers.

The experiments performed in the simulator were controlled and sequenced by a hybrid computer consisting of a PDP-8 digital computer with 4K words of memory, and a GPS 290T analog computer. In addition to sequencing and data logging functions, the software was responsible for computing the motion of the target and the angular position of the target in trainer-fixed coordinates. All targets were assumed to be in straight line motion, and from the voltages corresponding to trainer altitude, velocity, and yaw angle, the navigation of the target relative to the trainer was performed in real time regardless of the trainer attitude and altitude changes. This information was used to calculate commands to the target positioning servo system. Based on the calculated range of the target, the size and contrast ratio were also commanded to be the log C/C_T for an approaching aircraft.

Besides calculating the navigation computations relative to the trainer and calculating the commands to the target servo system, the computer program also determines the position of the target in aircraft-fixed coordinates based on the three measured angles of trainer rotation. This is an important feature since many of the proposed PWI systems have sensors mounted directly on the aircraft. Logic in the program further activates or inhibits the PWI display depending on the azimuth, elevation, and range of the target.

IV. SIMULATION EXPERIMENTS

Two sets of experiments were performed in the simulator. The first set of experiments consisted of determining visual thresholds in order to verify the experimental apparatus. This was performed by slowly sweeping the target contrast ratio while having the subject control the sign of the rate of change of target size with a two-position switch. It was hypothesized that the contrast thresholds measured by this technique would be higher than Blackwell's because of the various "field factors" (Bailey, 1970). These include the fact that our subjects were less

experienced at target detection than Blackwell's, and the fact that the thresholds were measured in a different manner.

The threshold curve measured in the simulator had the same shape as Blackwell's threshold curve at 1 ft-L, and were shifted to the right by approximately 1 log unit in contrast, thus verifying the hypothesis.

The next set of experiments consisted of simulated flights in the GAT-1 to investigate the effects on the detection process of pilot workload and target frequency, meteorological visibility, PWI display resolution, and target bearing.

Displays - Four displays were used in the simulation to evaluate the effects of azimuth resolution on target detection. Three of the displays had resolution elements of 15°, 30°, and 45°; the fourth display was an audio warning only, and since the azimuth coverage of the simulated PWI system was $\pm$90°, the resolution of this audio alone display was 180°.

Targets - The absolute target motion used in the simulation was straight level flight at a speed of 200 miles per hour. The target initial conditions were chosen so that with the trainer flying straight ahead, the target would pass within 700 feet in a horizontal plane and 260 feet higher in altitude. Forty targets were presented in each one-hour simulated flight. The initial bearings of these targets were evenly divided between angles of approximately 5°, 20°, 40°, and 70°, and between right and left of trainer course. In addition, the visibility conditions were evenly divided between 3 and 10 miles meteorological visibility.

Workload - There were two levels of workload during the simulated flights: high workload during climb and descent phases, and low workload during cruise. The tasks contributing to the two workload levels are flight path control with and without turbulence, VOR tracking, communications, and average target frequency. The task and criterion levels required of the pilots are shown in Table 1.

TABLE 1. COMPARISON OF WORKLOAD LEVELS

TASK	WORKLOAD LEVEL	
	High (ascent/descent)	Low (cruise)
Flight Path Control	Maintain 500' $\pm$100fpm	Maintain altitude $\pm$200'
Turbulence	Max. Rough Air	None
VOR Tracking	.2Hz Track Within 1 Dot	.02 Hz $\pm$ Track Within 1 Dot
Communications	Report All Traffic, Report Each 500' Altitude	Report All Traffic
Average Target Frequency	1 per minute	1 per 2 minutes

Subjects - Four subjects were used in the experiment, and they had a varying degree of experience. Subject 1 had 1800 hours total time, 1600 hours in jet fighter aircraft, and 200 in general aviation aircraft. Subject 2 had 900 hours with commercial, instructor, instrument, and multi-instrument ratings. Subject 3 had 250 hours and a commercial rating and subject 4 had 100 hours in general aviation aircraft, and was a radar observer on Naval fighter aircraft.

Experimental Plan - A factorial design was set up to evaluate the sixteen different treatment conditions: four displays, two workload levels, and two meteorological visibilities. The displays were administered in a Latin Square design balanced for order effects. The workload levels were high in the initial and final (climb and descent) phases of flight, and were low during the cruise phase. Half way through the simulated flight the meteorological visibility changed from its initial value (either high or low) to the alternate value. In this way, an equal number of targets were encountered under each of the experimental conditions.

Modification of the Experimental Plan - After six of the total of sixteen flights had been run, preliminary analysis was made of the results of the trials to that point. It was found that the inherent contrast of the target and the PWI detection range combined in such a way to give the following results. The targets were presented at an initial range of five miles. By examination of the log C/C_T curve shown in Figure 3, we see that for a meteorological visibility of ten miles and an inherent contrast ratio of 86.5 the target, when it appears at a five mile range, is above threshold. Although log C/C_T increases slowly for the high visibility, the subjects were able to detect the target before the 2.5 mile detection range of the PWI system. For the low meteorological visibility, the target came through threshold at a range which was very close to the PWI detection range. Since log C/C_T was increasing rapidly at this point, the target very quickly became easy to detect and one had the effect of targets "popping out" of the haze. The target was reported so quickly after the PWI alarm that there were very few performance differences among the four displays being evaluated.

At this point in the process of the experiment, it was decided to change the experimental conditions because of the unfavorable combination of inherent contrast ratio of the target and the PWI detection range. For the remainder of the targets, a neutral density filter was inserted in the projection system to lower the inherent contrast ratio from 86.5 to 16.3; furthermore, the detection range of the PWI was increased to four miles with the result that the average detection time (after the PWI alarm was activated) was eleven seconds for the high visibility targets and thirty-four seconds for the low visibility targets. Thus the latter set of data enabled us to test for differences between displays, and the former gave information on the visual detection of high contrast targets without displays.

V. DATA ANALYSIS AND DISCUSSION OF RESULTS

Introduction

The change in the experimental conditions partway through the Latin Square resulted in an unbalanced experimental design with the target detections falling into four groups: Target Detection Without Display, High Target Contrast; Target Detection With a Display, High Target Contrast; Target Detection With a Display, Low Target Contrast, High and Low Visibility. There were 117 target detections without a display, and all but 2 of them occurred under high meteorological visibility simulations. These two were discarded and the subsequent 115 points were analyzed as one group. The second group of targets (detections with a display, high target contrast) were confounded between subjects and displays and these data were not analyzed further. The third and fourth group of data consisted of a total of 385 data points.

The major drawback to the resulting unbalanced design was that not all interactions could be evaluated due to the confounding of their components of variance. The balancing of the order of the display treatments is still felt to distribute any residual effects since the Latin Square was followed for the entire set of trials. The other major factor,

learning, was included as a covariant in the subsequent analysis of variance through the subject's trial number.

In the analyses, we treat the following factors as independent variables and estimated their effects:

Displays (15°, 30°, 45°, 180°)
Visibility (3 miles, 10 miles)
Workload Level (high/low)
Subjects (four)
Target Azimuth (6°, 21°, 41°, 71°)
Subject's Trial Number (1-4)

As the three dependent variables of the simulation we chose:

Detection Time
Detection Range
Log C/C_T at Detection

We chose detection time and detection range because of their obvious importance in the collision situation. Although the detection model outlined previously suggests that there is an effect of exposure time with constant contrast above threshold, we chose to use log C/C_T as a measure of effectiveness of the various displays hoping that it might remain constant across meteorological visibilities conditions. This should be more nearly constant than either the detection time or the detection range because detection time depends strongly on the target azimuth (due to the relative velocity effect), and detection range depends on the meteorological visibility.

Target Detection Without a Display

The 115 target detections made without the aid of a PWI display were examined in the analysis of variance for detection time, detection range, and log C/C_T at detection. The results of these analyses are summarized in Table 2. For the four independent variables (workload, subjects, trial number, target azimuth), only the target azimuth is significant ($p<.05$) and this is the case for all three dependent variables.

Comparison of PWI Displays

At the low target contrast ratio and large PWI detection range, no target was visible until after the PWI alarm had sounded. As mentioned previously, this gave 385 data points divided evenly between high and low (10 and 3 miles) visibility, it approximates an extremely difficult target to detect.

The analysis of variance is summarized in Tables 3 and 4 for the dependent variables of detection time, detection range, and log C/C_T at detection for the two visibility conditions. The low meteorological visibility shows significant differences in the displays, subjects, azimuth, and trial number, the latter suggesting that learning is still an important factor in the experiments. Surprisingly enough, in spite of the attempts to load down the pilot, workload level did not contribute significantly. Note that all three dependent variables are significant at the same level ($p<.01$).

In the analysis of variance for high meteorological visibility (Table 4) we again get significant differences in displays, subjects, and, for detection time alone, a significant difference in target azimuth. The inconsistency between indicators of detection range and contrast ratio compared to detection time is explainable by the fact that the relative velocity of the target is much lower at high azimuths, and it takes a longer time to reach the same range as a target coming from a small azimuth. As with low meteorlogical visibility, workload level was not a significant factor, and in addition, all three dependent variables indicate that learning (as subject trial number is interpreted) was not important in the detection of the high meteorological visibility targets.

To examine the effects of sector size and meteorological visibility, we divided the targets into eight groups (four displays X two visibilities) and adjusted the group mean on the basis of subject and trial number effects using the UCLA computer program BMDX82. The results of these computations are shown in Figure 6 in which we have plotted detection performance (time, range, log C/C_T) as a function of display sector size. Each mean value is bracketed by the standard deviation of the process.

As expected, the difference between visibilities has a strong effect on detection range, and as a result, a strong effect on detection time. The performance with the audio-alarm (180° sector size) is not as good as with a smaller sector size. The difference between the 180° and 45° (the best of all the displays) is four seconds at low visibilities and these target approach speeds, and six seconds at the higher visibility. The corresponding differences in detection range a these approach speeds are approximately .6 and .3 miles for high and low visibility, respectively.

Figure 6 also shows that the log C/C_T measure of performance is not strongly affected by the change in meteorological visibility. The data for the high and low visibility conditions were pooled and a subsequent analysis of variance indicated that the change in visibility condition did not contribute significantly to the variance of the data.

Discussion of the Results

Display Sector Size - The t-tests indicate a significant difference between 180° sector size and the other three panel mounted displays of 15°, 30°, and 45°. Furthermore, as found in the simulation at NAFEC, and as predicted by some detection studies in a more abstract environment (Smith, 1970), there is an optimum sector size larger than 0°. Examination of Figure 6 shows that in view of the error variance in these data there appears to be little practical difference among the sector displays tested, but the difference between the 180° displays and the others may be of some practical importance in view of the kinematics of the collision geometry and PWI systems considerations.

Meteorological Visibility - Although the displays and subjects were significantly differently at both visibilities, these differences seem to be accentuated for the high visibility condition. This can be attributed to the fact that the rate of change of contrast is larger for the low visibility condition, and when the target comes into view, it becomes very visible quite rapidly. (One subject said he saw the "light turn on" when in fact it had been on all the time). This appears to explain why the variances under the low visibility conditions are smaller, but since the target becomes very visible quite quickly under low visibility conditions, there is less dependence on display and subject differences and this is reflected in the analysis of variance data. The high visibility targets, on the other hand, come through threshold much more slowly and thus are more difficult to detect and are therefore more sensitive to subject and display differences. The differences in target azimuth become significant at low visibility levels, and an explaination for this using the Koopman detection model is given by Curry, et al (1972). The effect seems to be a consequence of differences in the rate of change of contrast with time and with range.

Target Contrast Ratio - For those targets detected with the high target contrast ratio and under high visibility conditions without the aid of a PWI display, the trial number and subject

effects were not significant. This is apparently due to the fact that the targets were above threshold for the entire time that they were displayed and that the subjects adopted approximately the same type of scanning strategy. There were slight differences in target azimuth ($p<.05$), but these differences appear to be similar to those observed with the low target contrast ratio.

Workload - One of the more surprising results of the experiment was that the target detection performance during high workload phases (turbulent air, high frequency needle tracking, constant rate of climb, reporting of altitudes, and higher target frequencies) was not significantly different than during a low workload (cruise) phase. Two important factors in determining the performance during the high workload conditions are the type of workload that is imposed and the priorities assigned by the subject to the target detection task and his cockpit duties.

It was the opinion of all subjects that the workload during the climb and descent phase of flight was extremely high, higher than they would expect in a real flight. These tasks, which consisted primarily of monitoring altitude and responding the VOR needle, were the type which allowed the pilot to shift his scan from panel instruments to the windscreen for several seconds at a time without incurring severe penalties. In other words, the pilots recognized that they could let the VOR needle stray for a few seconds or miss their altitude by one of two hundred feet without jeopardizing their safety. An example of a task that would no doubt lead to a difference in target detection is one which requires a lengthy cognitive function, such as an arithmetic task or copying an ATC clearance, and furthermore a task in which the penalty for a mistake is high.

The question of penalties is a very important issue and in effect determines the assignment of priorities by the pilot between his cockpit duties and target detection duties. Not only will the priority assignment differ from subject to subject, but it is likely to be different in ground-based simulations and in the inflight situation because of additional stresses. Priority assignments will be further affected by the pilot's past experience with the PWI system, e.g., his understanding of the detection range and probabilities of false alarms and missed alarms.

In summary, it appears that the additional workload level imposed on the pilots did not degrade detection performance because first, it did not interfere with the task of searching and secondly, the penalty structure was such that detection duties had higher priority than cockpit duties. These results point out that the extrapolation of ground-based simulation results to the inflight situation are extremely tenuous because the pilot's assignment of priorities between PWI and cockpit functions will be mediated by the stress of being in flight and the pilot's past experience with the PWI system, and the penalty structure imposed by the immediate situation.

VI. SUMMARY AND CONCLUSIONS

An examination in the literature on visual target detection shows that the target parameters having primary influence are background complexity and illumination level, target size, motion, and contrast ratio. For targets against a uniform background, experimental data and mathematical models of the detection process indicate that there is one parameter of primary importance, the contrast ratio of the target relative to threshold (C/C_T).

A simulator was constructed for PWI detection studies, and was built around a Link GAT-1 trainer. This simulator has a capability of controlling C/C_T as would occur for a real aircraft. The motion of the target responds to trainer motion to add further realism to the detection process.

Four subjects were used in simulated flights to evaluate the effects of PWI display sector size, meteorological visibility, pilot workload, and target azimuth. There was little significant difference between sector sizes of 15°, 30° and 45°, although 45° provided the best performance. The 180° sector size (audio warning only) display was significantly worse in a statistical sense, but the practical significance remains to be evaluated through more general systems analyses.

The displays and subject differences were accentuated with high visibility, presumably due to the fact that the target remains at threshold for a longer period of time and is therefore more difficult to see. Log C/C_T was a good indicator of detection performance, since in these experiments, it was independent of meteorological visibilities when data for all

target azimuths were pooled. Detection time was most strongly influenced by the relative velocity of the targets, and this in turn was a function of the target azimuths. The detection range was most strongly influenced by meteorological visibility.

Detection performance without the PWI display occurred at a larger log C/C_T then when any of the displays had been activated. The implication here is that a pilot searching in the "warned" state even with 180° azimuth, performs better than the pilot in the unwarned state as measured by the log C/C_T criterion.

There is no significant difference between target detection in the high and low workload levels supplied in this simulation, even though the subjects felt that the high workload level was more than they would normally expect to carry in a normal flight. One explaination for this result is that the type of workload was such that it could be left for periods of time to search for targets without adversely effecting performance on these cockpit duties. The other reason seems to be that the pilots were placing a high priority on the search function relative to their cockpit duties in this ground-based simulation. Although one can determine the relative priorities assigned to these tasks in ground-based simulations, it is felt that the extrapolation of these data to the inflight situation is tenuous because these priorities will be mediated by the additional stresses of actual flight and the pilot acceptance and confidence in the display which depends on his operating experience with the PWI system over long periods of time.

REFERENCES

Bailey, H.H. Target detection through visual recognition: a quantitative model. Memorandum RM-6158/1-PR, USAF Project Rand, February 1970.

Blackwell, H.R. and Comfort, L. Contrast thresholds of the human eye. Journal of the Optical Society of America, 36:11, November 1946.

Curry, R.E., Dumeurger, J., Day, E.H., and Senders, J.W. PWI simulation experiments. Final Report, Contract DOT-TSC-132, Man-Vehicle Laboratory, Department of Aeronautics and Astronautics, M.I.T., May 1972.

Hammill, H.B. Modifications to visual detection model. Cornell Aeronautical Laboratory of Cornell University, November 1969.

Lamar, E.S. Search problems. Appears in "Visual Search Techniques", NAS-NRC Publication 712, 1960.

Smith, T.B. Determination of the optimum resolution element for a pilot warning indicator. S.M. Thesis, Department of Aeronautics and Astronautics, MIT, 1970. Man-Vehicle Lab Report MVT-70-4.

Source	Detection Time	Detection Range	log C/C_T
Workload	--	--	--
Subjects	--	--	--
Azimuth	$p<.05$	$p<.05$	$p<.05$
Trial No.	--	--	--

TABLE 2. Summary of Analysis of Variance, Detection Without Alarm

Source	Detection Time	Detection Range	log C/C_T
Display	$p<.01$	$p<.01$	$p<.01$
Workload	--	--	--
Subjects	$p<.01$	$p<.01$	$p<.01$
Azimuth	$p<.01$	$p<.01$	$p<.01$
Trial No.	$p<.01$	$p<.01$	$p<.01$

TABLE 3. Summary of Analysis of Variance, Low Meteorological Visibility

Source	Detection Time	Detection Range	log C/C_T
Display	$p<.01$	$p<.01$	$p<.01$
Workload	--	--	--
Subjects	$p<.01$	$p<.01$	$p<.01$
Azimuth	$p<.01$	--	--
Trial No.	--	--	--

TABLE 4. Summary of Analysis of Variance, High Meteorological Visibility

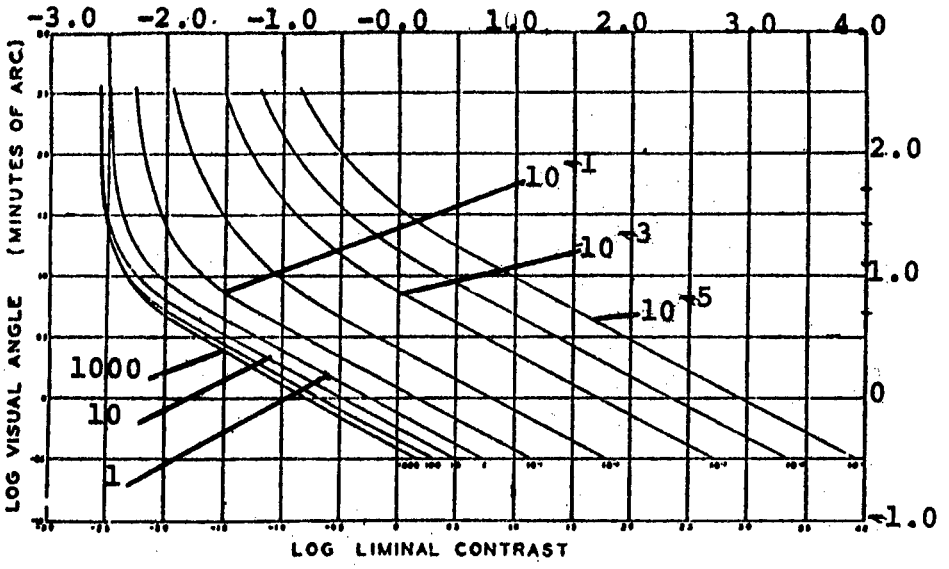

FIGURE 1. Visual Threshold Curves (Background in ft-L) (Blackwell, 1946)

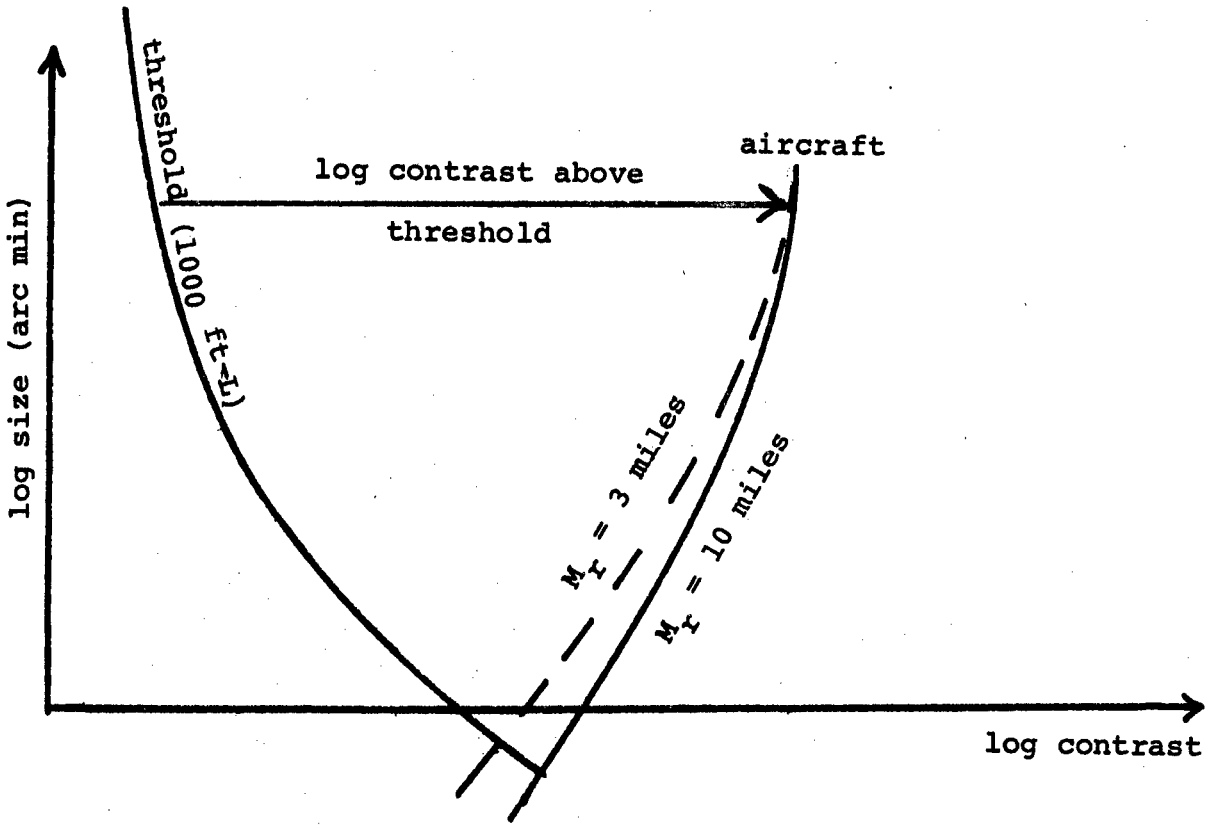

FIGURE 2. Sketch of Visual Threshold and Aircraft Contrast

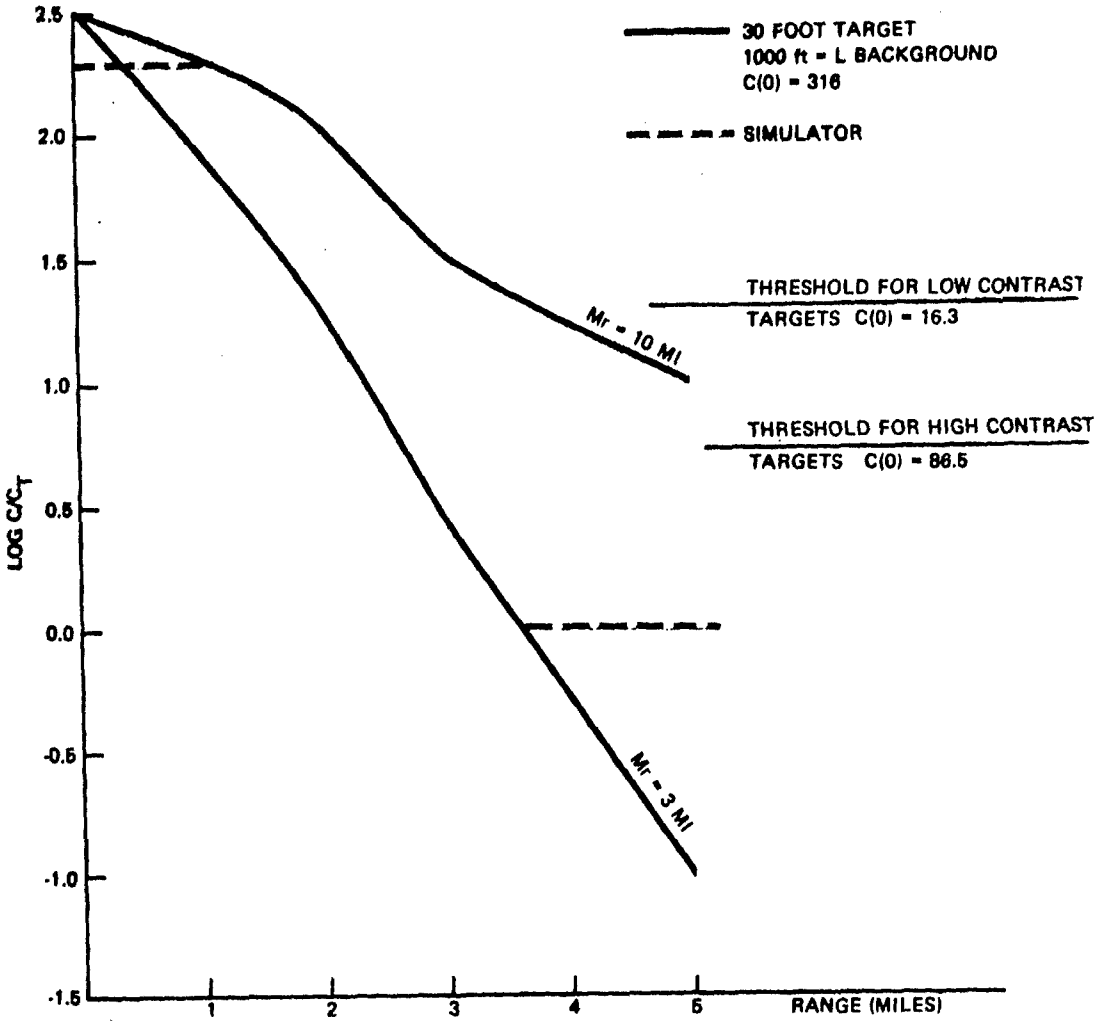

FIGURE 3. Log Contrast vs. Range

FIGURE 5. GAT-1 Panel with PWI Display and Tracking (VØR) Needle

FIGURE 4. View of GAT-1, Screen and Projection System

This page is reproduced at the back of the report by a different reproduction method to provide better detail.

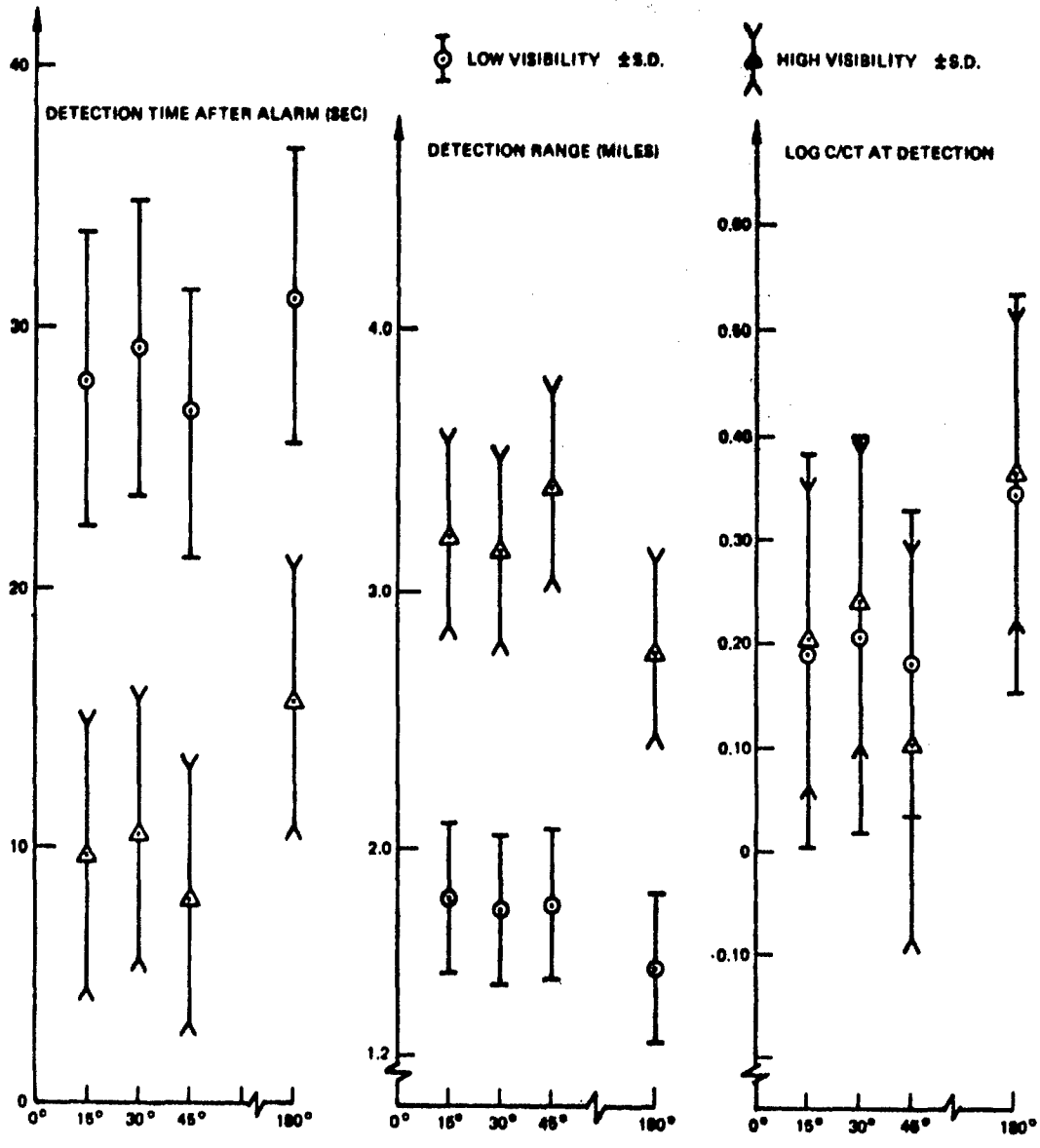

FIGURE 6. Detection Performance vs. Display Resolution

TRENDS IN COMMERCIAL AIRCRAFT CREW ROLES AND MANUAL CONTROL RESEARCH APPLICATIONS

John DeShon Warner
The Boeing Company
Seattle, Washington

Crew roles in commercial aircraft will undergo a change from current practice when new operational requirements anticipated as a result of the need to extend noise abatement procedures, develop improved traffic management procedures to reduce congestion and operate in lower minima begin to be implemented. This has stimulated development of new types of automatic aids and new cockpit display and control systems. As the crew becomes more involved in navigation and guidance decisions, and less involved in inner loop control processes, there is a resultant change in the application of manual control research knowledge.

INTRODUCTION

Operational requirements for commercial aircraft in the 1980's and beyond will be significantly changed from the present, with some notable implications on crew roles. There will be more stringent demands on the complexity and accuracy of operations, which dictates an increased use of automatic aids (Reference 1). The crew will, in most situations, be systems managers as opposed to short term controllers (Reference 2).

The dominant factors in commercial air transportation in the future will be high density traffic, reliable all-weather scheduling, and minimum community noise. Precision three- and four-dimensional navigation and guidance, involving both improved ATC procedures and greater aircraft system capability will be fundamental to high density operations. Automatic landing systems, with special monitoring and control techniques for crew management, will be the basis for landings in Category IIIa conditions, with eventual rollout and taxi guidance systems for Category IIIb and IIIc. Curved approaches and departures, coupled with optimum performance climbs and steep angle descents, will reduce aircraft noise and displace it from the noise sensitive community.

The capability to perform these operations in the next generation of commercial aircraft will be provided by integrated navigation, guidance and control systems. Airborne digital computers will form the heart of these systems, and computer-generated electronic displays will provide the principal interface with the crew (Reference 3).

Significant advances have been made in recent years in the application of new display techniques to commercial aircraft. The changing role of the crew is perhaps best illustrated through an examination of the types of information that these displays will present, which is the subject of part of this paper. The new displays differ from those in current use primarily in that they: (1) are highly integrated, (2) are pictorial in format, (3) are time-shared and (4) contain predictive information (Reference 4). They have reached a reasonably advanced state of development as a result of extensive research through simulator tests

and some flight tests (References 5 and 6). Their use in future aircraft seems certain if the operations described above are to be realized.

The new crew role is also predicated upon advanced control techniques. Full time stability augmentation will be provided to compensate for unacceptable handling qualities; normal manual control will be through "control-wheel-steering" modes of the flight control system; and powered controls will permit tailoring the force-feel characteristics as desired. With these aids, the manual control tasks will be more in the navigation and guidance processes than in the "inner-loop" attitude control processes. Just how this affects the crew role is discussed later in the paper.

Manual control research has helped point the way for many of the changes in crew roles, and in display and control system design, no matter how rapidly or slowly these changes come about. It is not unfair to ask if the results of manual control research are in fact applied in today's commercial aircraft development. Singleton (Reference 7) categorized three types of approaches to display design: (1) intuitive, drawing entirely upon pilot experience, (2) a systematic combination of operator requirement studies and available solutions, and (3) an approach based on known principles of human behavior and perception. Past practice has been primarily in the first category. The present development of advanced displays is more heavily weighted in the second category with influences from the first and third. There is a fairly common attitude that handling qualities, display design, etc., are totally subjective with little opportunity for science. Dispelling this attitude is possibly one of the larger challenges to those who are trying to implement display and control system changes on a rational basis.

Much work remains if we are to properly design the airborne systems for the best use of the human crew. This work can be accelerated, and false directions can be avoided by the knowledgeable application of manual control and decision-making theories now being advanced.

The application of manual control research to the new commercial aircraft problems is discussed at the end of this paper. But a word of caution is in order, lest the intent is misinterpreted: obvious application should not be a criteria for the

evaluation of the worth of research activity. We cannot afford to be that short sighted, especially in view of the increased rate of application of current research due to the need for continued improved operational capability for commercial aircraft.

THE CHANGING CREW ROLE

If all crew tasks associated with navigation, guidance and control functions are listed, it can be found that they can be organized into interrelated hierarchical levels (Reference 8). At the lowest level is the task of moving controls to cause displacement of ailerons, elevators, fuel valves, etc. This activity is a consequence of goals set by the crew on what should be the attitude angles, thrust and configuration. This in turn is preceded by establishment of desired velocity vector changes, which are a consequence of desired positions as a function of time. For the sake of brevity, these hierarchical levels can be referred to (in ascending order) as actuation, attitude control, velocity vector control (guidance), and position control (guidance and navigation).

We have known for some time, largely as a consequence of research on manual control processes, that the information processing, speed and precision required to perform the lower level tasks well are at the limits of human operator capability. Automatic systems can perform the actuation and attitude control tasks far superior to the human operator. The only reason they haven't taken over today in commercial aircraft is because of unsatisfactory reliability of such systems (Reference 1). This however is rapidly changing, with the result that the crew will be able to give up these tasks with confidence and concentrate on the higher level decision tasks associated with the navigation and guidance functions.

Figure 1 illustrates the various positions in the total control loop that the forthcoming commercial aircraft pilot will find himself. Nearly all operations will occur with the configurations of Figures 1(a) and 1(b).

In Figure 1(a), crew tasks are primarily of a monitoring nature, since presumably the system would continue through a total operation without specific action by the crew other than occasional mode selection and data entry. Area navigation system control, in which the crew monitors and modifies a stored flight plan through an alphanumeric keyboard will be a principal task.

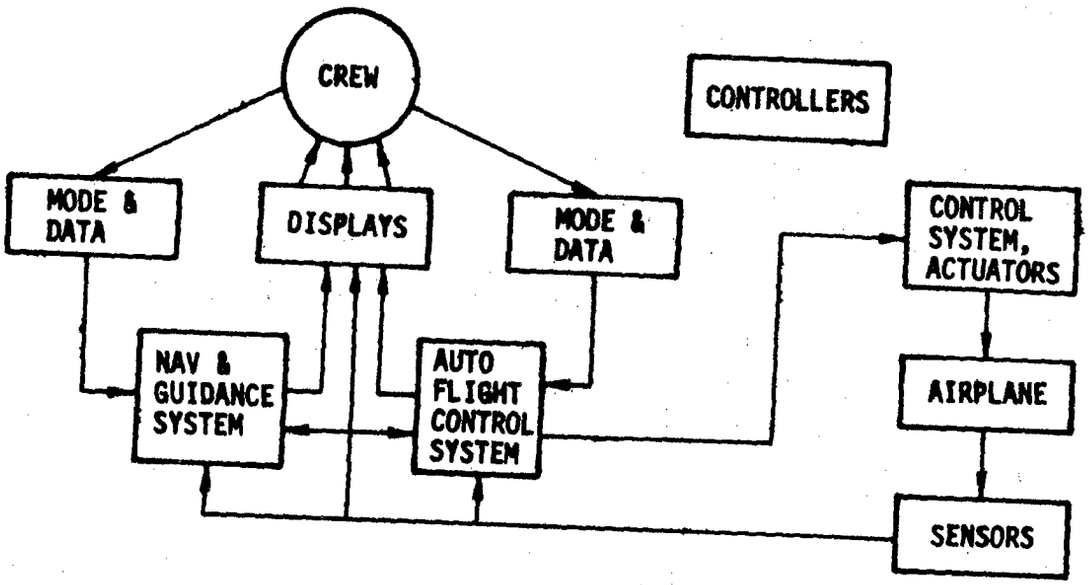

(a) Fully Automatic Control

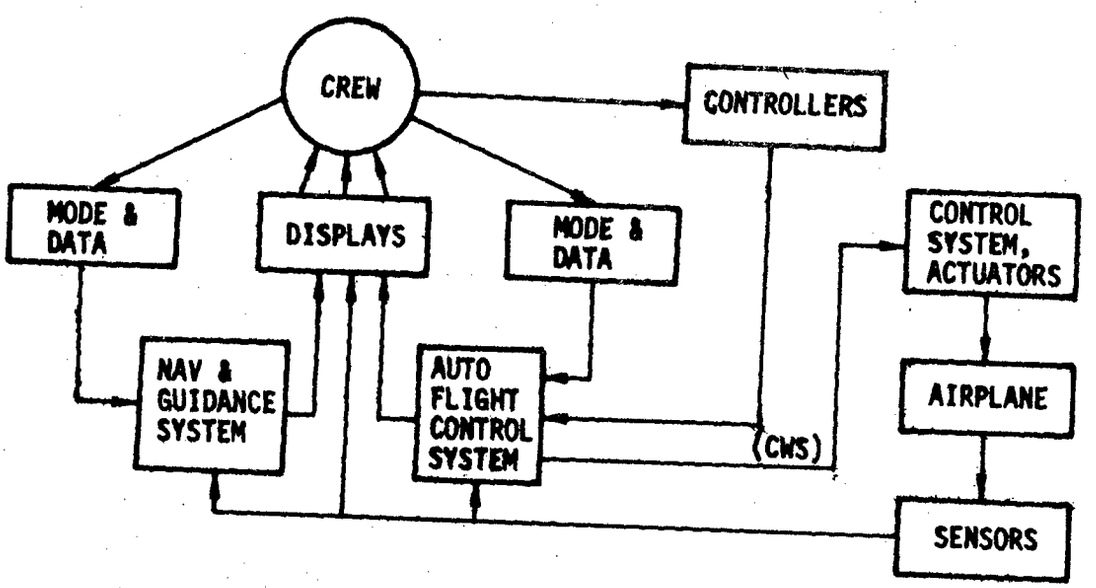

(b) Semi-Automatic Control

Figure 1. Configurations of Crew/Airborne Systems

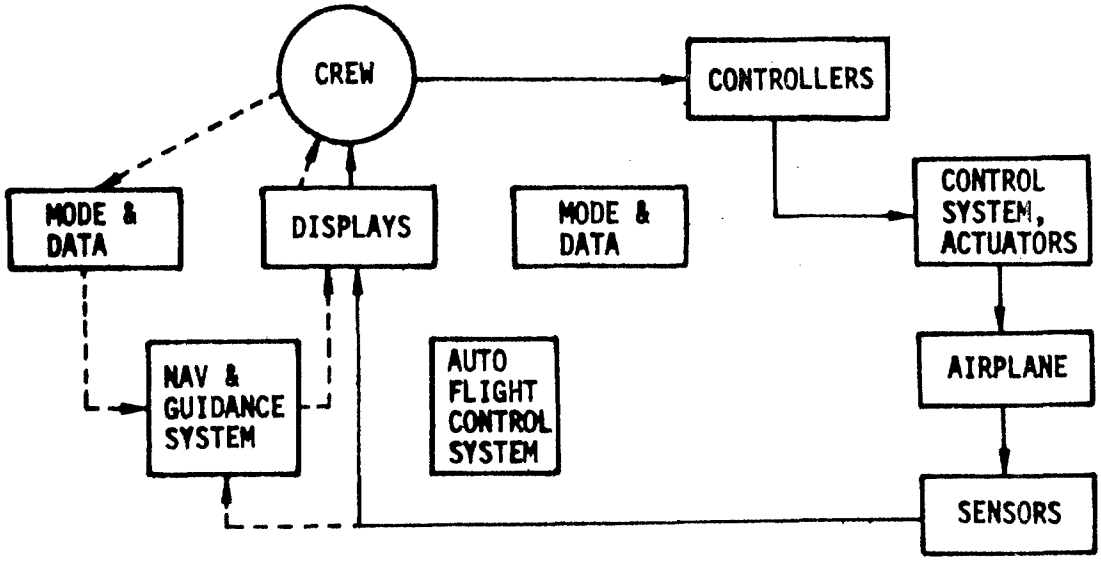

(c) Manual Backup Control

Figure 1. Configurations of Crew/Airborne Systems (Cont'd)

The active crew participation tasks in Figure 1(b), but with full operation of the on-board systems, is apt to become a common configuration for several very good reasons. First, manual control capability in this configuration will be very similar to the totally automatic configuration, with acceptable workload levels. This is because automatic aiding will be concentrated in the display presentations and in the apparent modification of controlled element dynamics to a very reasonable form. Second, it has been found that good performance in a failure mode, which creates a backup configuration like that of Figure 1(c), requires the pilot to be involved in the control process prior to the failure (Reference 9).

For the foreseeable future the crew will continue to perform backup control tasks in the event of automatic system failures. There is some question however for many of the aircraft being considered that the crew will ever have to contend with total failures which put them at the lowest level of actuation tasks. Powered controls and stability augmentation systems are being designed so that probability of failure can be classified as extremely remote.

In addition to the above tasks which involve the control of the aircraft state vector and the policies of that control, the crew will have subsystem monitoring and

control tasks, and communication tasks to add to their workload. However, systems are being developed to ease this burden. Automatic checklist systems will reduce the "housekeeping" chores to a minimum, and data link systems will make communications considerably less demanding than today.

DEVELOPMENTS IN DISPLAY AND CONTROL SYSTEMS

A change in crew role is dependent upon changes in the tasks, in the controlled element characteristics, and in the interface between man and machine. These changes have been in process over the last several years largely due to the increased interest in advances such as automatic landings and area navigation, and because of the special problems of complex aircraft such as the SST. Current aircraft systems are generally designed as separate, independent devices. To continue developing systems in this manner, as the dependence upon them increases, is not only inefficient but would probably not produce the desired results.

The next generation of aircraft will likely have totally integrated avionics systems, at least as far as the navigation, guidance and control functions are concerned. Digital computers will perform navigation functions by making position estimates based on optimal combinations of radio, air data and inertial sensor information. The same computers will execute guidance laws and perform data processing functions for special information presented on electronic cathode ray tube displays. Guidance errors will be fed to digital flight computers, or manual control inputs will be fed through these computers which in turn interface with the actuators for control surfaces.

There have been many individual advanced display developments in recent years, including head-up displays, map displays, special purpose monitoring displays, etc. A fully integrated display system development, considering all navigation, guidance and control tasks, has been underway as well. Figure 2 shows a simulator cab in which the integrated displays have been evaluated, along with a simulation of advanced guidance and control schemes. The two primary displays, the electronic attitude director indicator (EADI) on the top and the multifunction display (MFD), on the bottom present hierarchically related information in common formats, as recommended in Reference 8. Situation, predictive and command data for vertical

This page is reproduced at the back of the report by a different reproduction method to provide better detail.

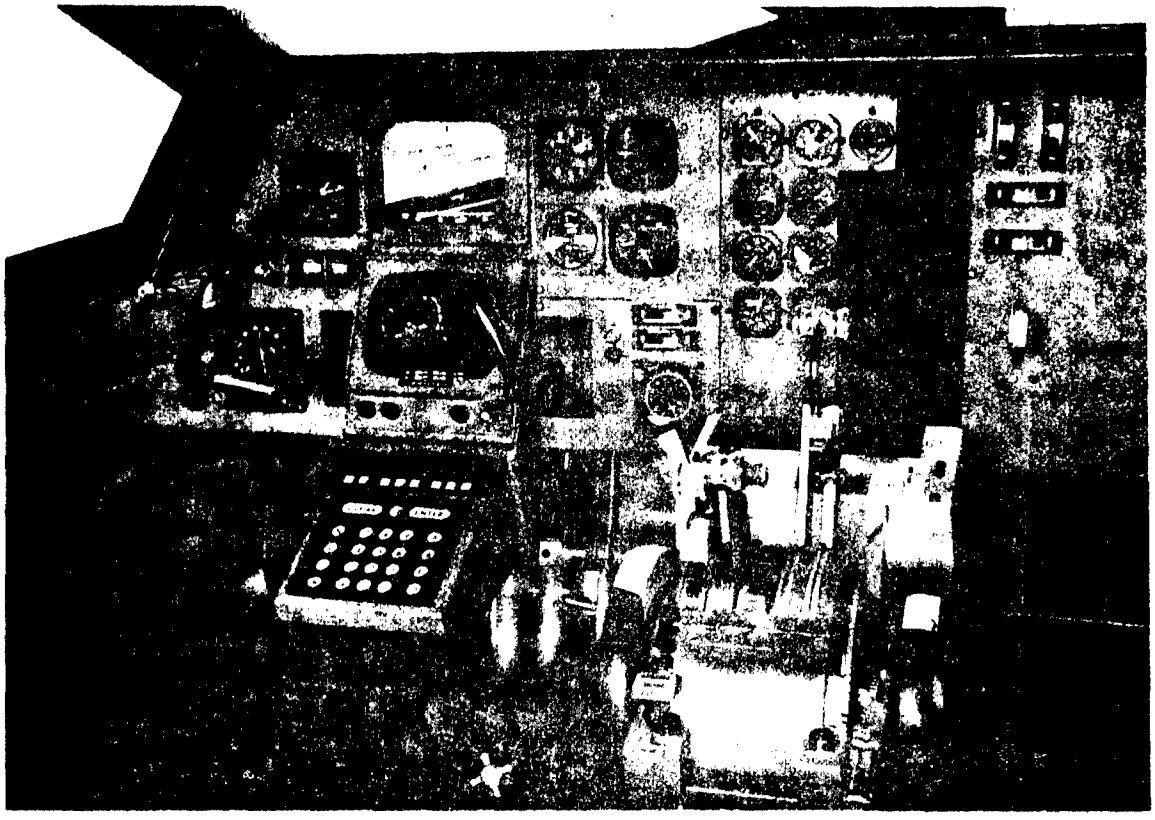

Figure 2. Integrated Display System in Simulator Cab

navigation, guidance and control is presented on the EADI, while the same type of data in the horizontal plane is presented on the MFD. Some horizontal information is also presented on the EADI to provide a tie between the two displays, and to be self-sufficient in certain higher workload situations such as approach and landing.

Both the EADI and MFD are computer-generated cathode ray tube displays. One version of the EADI is illustrated in Figure 3. An airplane symbol is fixed in the center of the screen as a reference for attitude data. The vertical scale moves with pitch attitude and rotates with roll attitude, like a conventional attitude indicator. In departure from conventional displays however is the velocity vector symbol which consists of the pair of rectangles. In Figure 3a, this symbol is showing a flight path angle of about -1 1/2 degrees. The gap between the two rectangles is the instantaneous velocity vector.

The four pointed star symbols represent waypoints* (the same as shown on the multi-function display) and portray the present bearing and elevation angle from the aircraft to the waypoint. Thus, whenever a waypoint is centered in the gap of the velocity vector symbol, the aircraft is moving directly towards the waypoint. The waypoint can thus be thought of as a command for the velocity vector symbol in a pursuit format. However, it is pure situation information. Also, the task usually is to approach a waypoint on a specific flight path angle (in the vertical plane) and on a specific track angle (in the horizontal plane). Thus the task is to control velocity vector orientation such that it and the waypoint are coincident at a specific angle on the linear scale. (The MFD format takes care of the horizontal task.)

The star with the superimposed X represents a waypoint very close to the aircraft, with the X telling the pilot that a transition is required to fly to the next waypoint.

The small rectangle to the left of the velocity vector symbol shows acceleration along the flightpath. When aligned with the velocity vector, the acceleration

*Waypoints are fixed, three-dimensional points in space which form the definition of a flight path.

This page is reproduced at the back of the report by a different reproduction method to provide better detail.

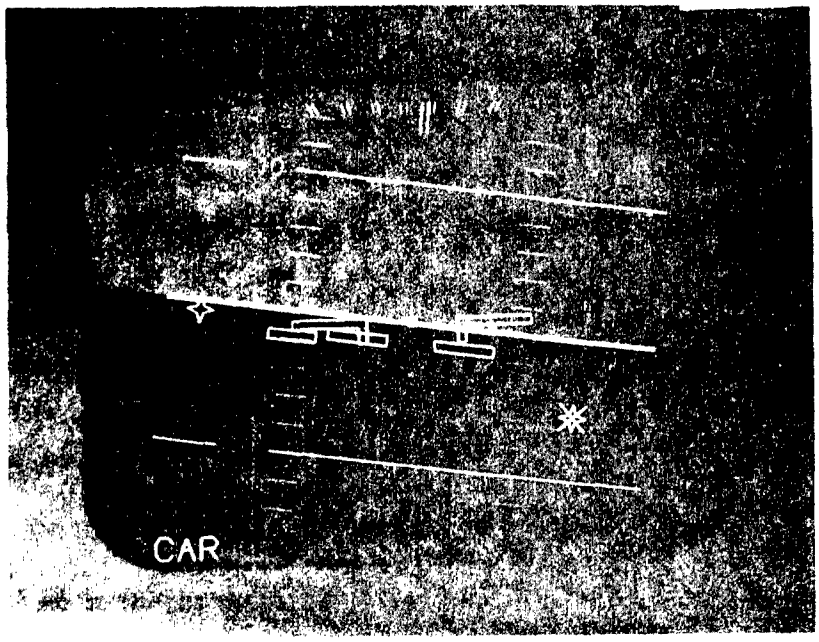

(a)

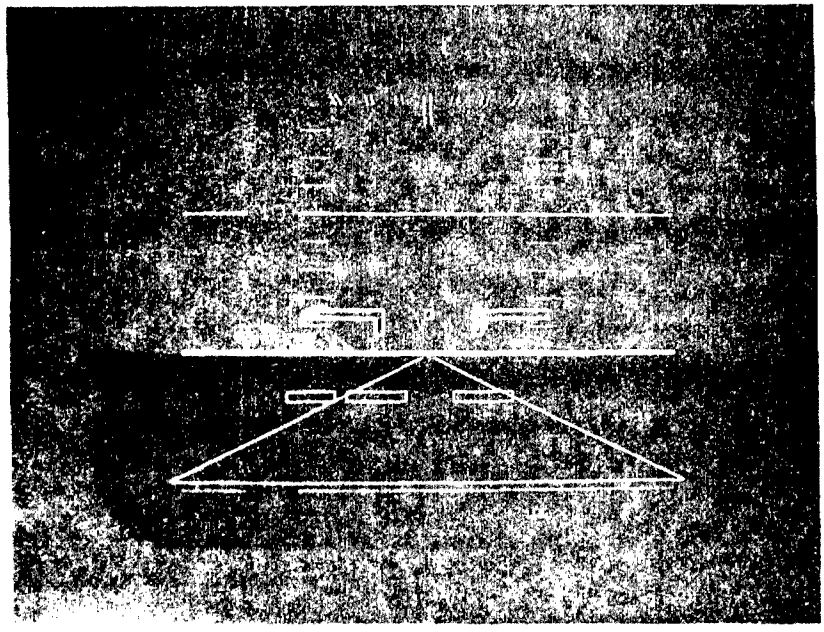

(b)

Figure 3. Electronic Attitude Indicator Formats

is zero. If below, the aircraft is decelerating. The symbol is scaled such that it indicates the thrust/drag difference in terms of steady state effect on flight path angle (Reference 3). It provides the pilot with a direct anticipation of thrust required for a desired change in flight path angle. This is a predictive quality that has been extensively evaluated through flight test with a high rate of pilot acceptance (Reference 5).

The EADI can also present a symbolic runway symbol (Figure 3b) or a direct image of the terrain ahead of the aircraft from a television camera fixed to the aircraft, or perhaps from a special radar sensor with the ability to form an image despite reduced visibility. The runway symbol with superimposed velocity vector tells the pilot the predicted touchdown point. Improvements are needed for this type of symbology however, as the perspective runway presentation has certain outstanding deficiencies (Reference 10).

Other display information can be presented on the flexible EADI; however the samples shown here illustrate the more novel features which affect the manual control tasks. The flight control system will operate in a flight path angle control-wheel-steering mode in the vertical channel. What this means is that, in essence, control inputs command a proportional rate change in actual flight path angle. Thus, in such a mode and with the EADI as described, the control loop from pilot to display has K/s dynamics, which is known to be a desired form for the apparent controlled element (Reference 11) and which will increase the processing capabilities of the pilot for other tasks (Reference 12).

The waypoint star, or runway symbol on the EADI, creating a pursuit task, moves in a highly predictable manner because of its pictorial or real-world format. Even though lead is required, simulator experience has shown that this manual control task is quite easy while providing the pilot with information promoting his understanding of the situation. The predictive information on the EADI, the predictability of the target and the knowledge of the situation derived from the display format allows the pilot to bring his higher level decision processes to bear directly on the guidance and control task.

The multifunction display format for horizontal navigation, guidance and control is illustrated in Figure 4. The airplane is represented by a triangle fixed in the

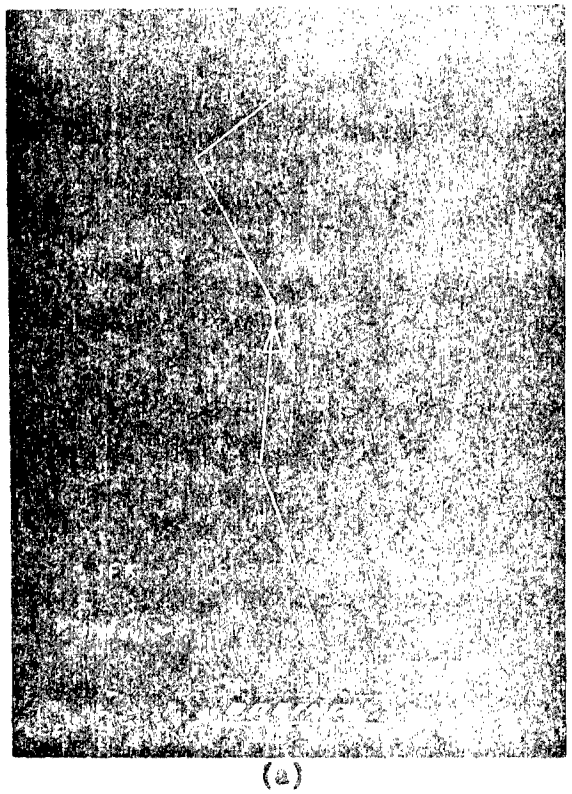

(a)

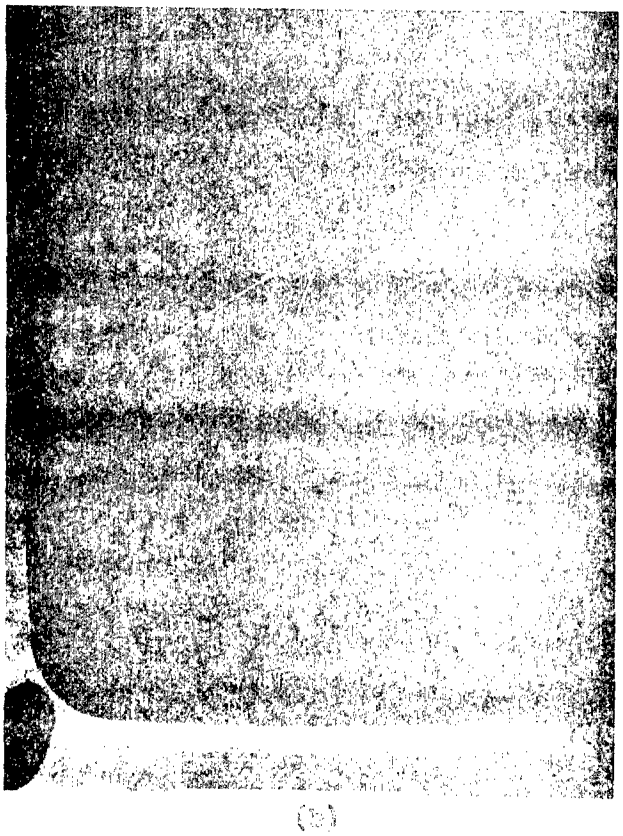

(b)

Figure 4. Horizontal Navigation [illegible] Function Display

This page is reproduced at the back of the report by a different reproduction method to provide better detail.

center of the screen. The desired route, displayed as straight or curved line segments between specific waypoints, translates and rotates relative to the airplane symbol. This is known as a track-up format, and is most useful in capture and tracking maneuvers. A north-up, fixed chart mode is also available for planning purposes, as are a variety of chart scales and other navigation data (Reference 6).

A key feature of the display is the predicted path symbol, illustrated in Figure 4b. This is a three-segment curve, showing predicted path relative to the desired path based on present ground speed and rate of change of track angle. Each segment of the symbol represents thirty seconds of prediction span, so that the end of the symbol away from the airplane triangle is the predicted aircraft position 90 seconds away. This symbol provides the necessary cue to capture a specific route line, as illustrated in Figure 4b. The symbology is straightforward, and because of its direct correlation with bank angle, is very easy to control. This is further enhanced with control-wheel steering modes in the lateral axis, in which a bank angle rate is commanded proportional to controller displacement.

This predictive symbology also permits easy "rendezvous" with a moving time slot, a necessity if precision four-dimensional flight path control is to become a reality. The sequence in Figure 5 illustrates how the symbology is used by the pilot to capture a moving time slot, indicated by a rectangle. The three small circles on the route ahead of the rectangle are its predicted position 30, 60 and 90 seconds away. The control policy is to match the gaps in the airplane predictor symbol to the small circles. As the maneuver is completed in Figures 5b and 5c, it can be seen that the aircraft will be behind the time slot since the control policy was not exactly satisfied. This is normally a complex maneuver; however the proper type of display information has reduced processing requirements by the pilot to a minimum. By use of the proper control-wheel-steering modes, the control process becomes very easy for the pilot, though there is no question that he is completely involved in the total process.

When monitoring and control tasks beyond four-dimensional flight path control functions become complex and demanding, a third multifunction display may be included. Figure 6 illustrates such a display in a possible location, portraying an altitude-speed schedule and aircraft situation and trend. This display could be time-shared with checklist information, airplane configuration information, and so on. The

This page is reproduced at the back of the report by a different reproduction method to provide better detail.

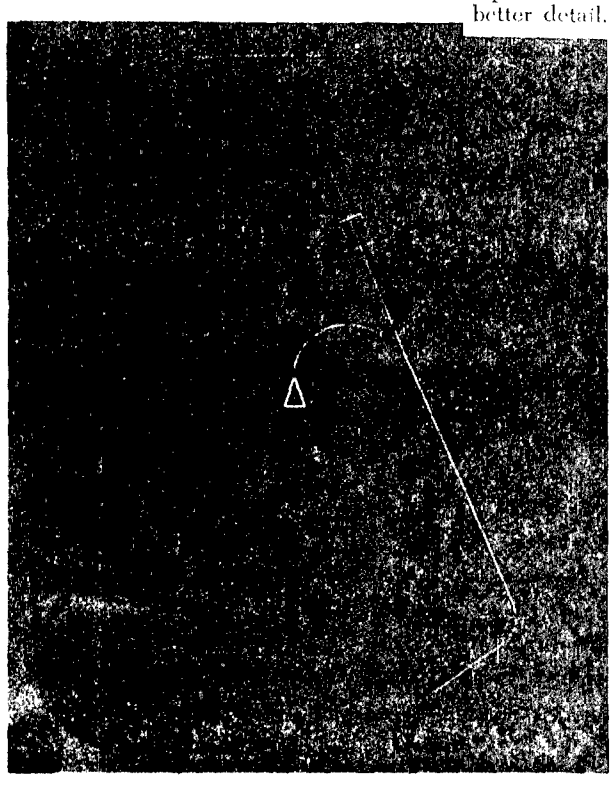

(a)

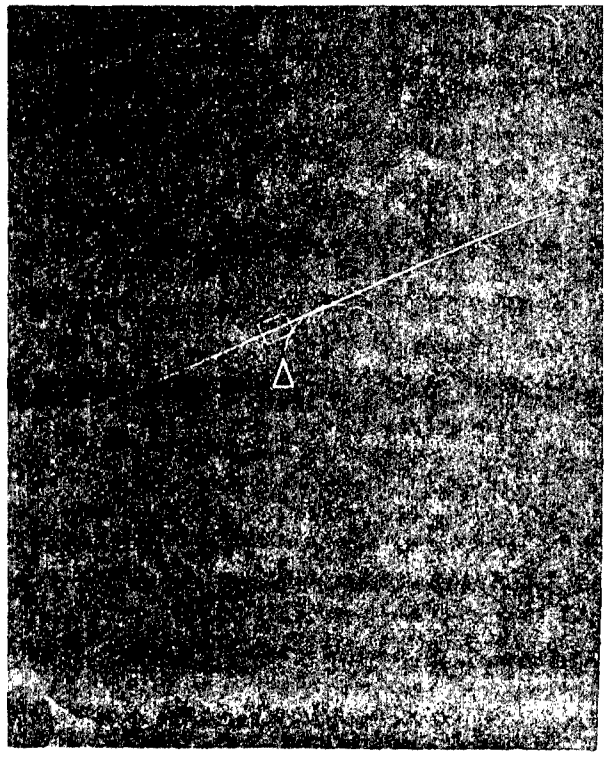

(b)

Figure 5. Moving Time-Slot Capture Using the Multifunction Display

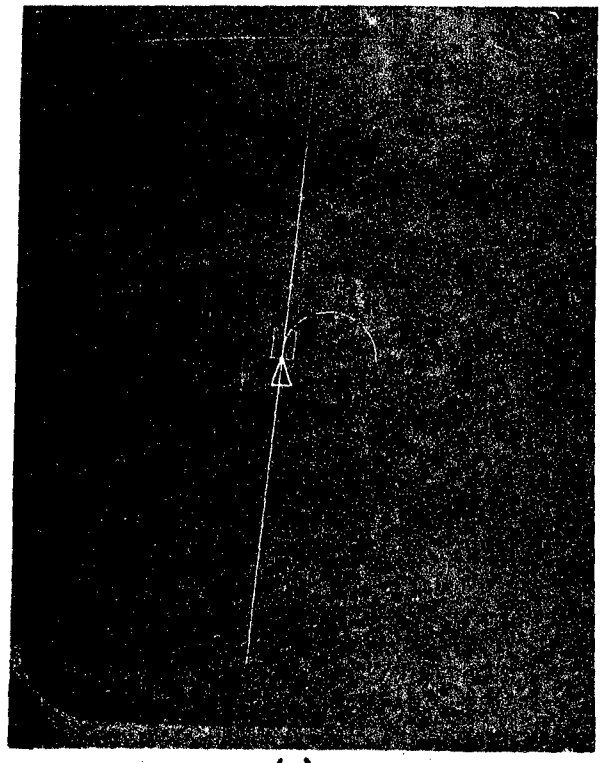

(c)

Figure 5. Moving Time-Slot Capture Using the Multifunction Display (Cont'd)

message is clear: electronic, computer-generated displays permit optimum forms of information presentation to the crew, making the most desired crew roles feasible.

This page is reproduced at the back of the report by a different reproduction method to provide better detail.

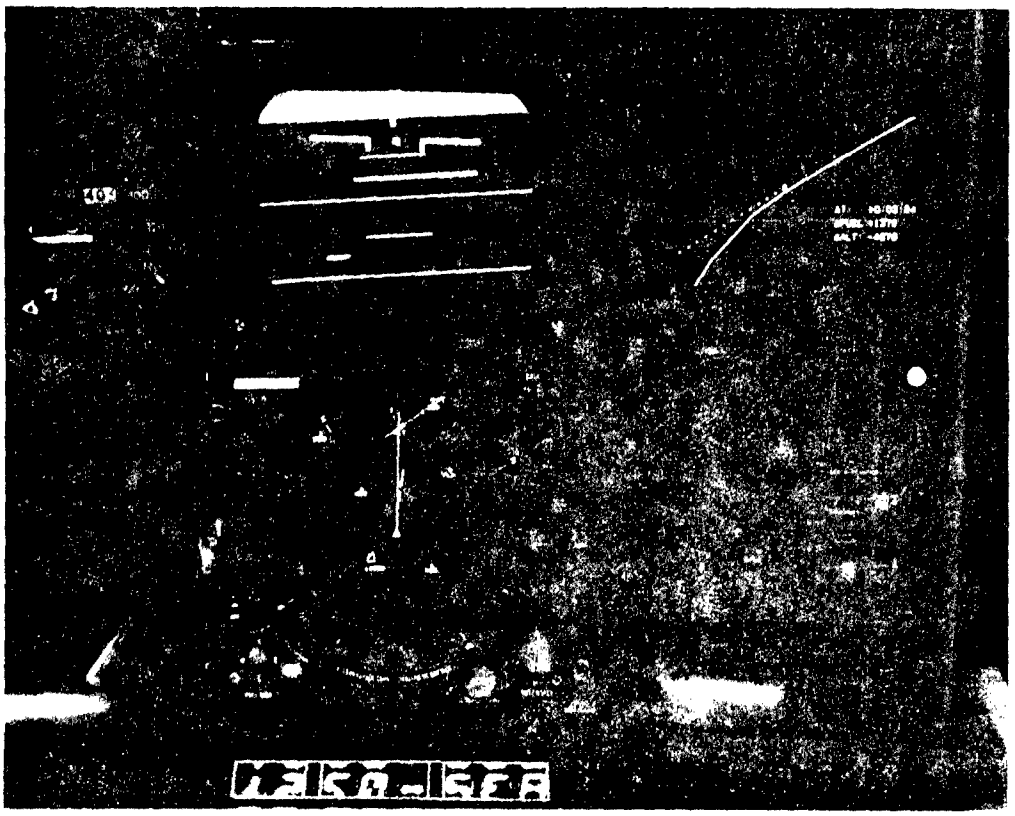

Figure 6. Simulator Cockpit with Second Multifunction Display

This page is reproduced at the back of the report by a different reproduction method to provide better detail.

APPLICATION OF MANUAL CONTROL RESEARCH

There are two general categories of research activities in the manual control field that are relevant to the development of commercial aircraft: applied research on display and control systems, using human factors criteria, and basic research on the understanding of the human operator as an element of the total system. In each category there are certain types of research that are applicable to the future roles of the crew and their interface equipment, as described previously in this paper. References 13 and 14 for example treat human performance with predictive displays, which is of interest in the development of display information as shown in Figures 4 and 5. It is usually straightforward to identify the applicability of this type of research because the tasks are well defined, and it is often directed towards a specific application.

It is more difficult to determine the applicability of research which analyzes the operator, since by its very character it is often more disassociated from the application. The importance of this research is too easily overlooked. But in face of increasing levels of automation, it is important to understand the relative capabilities of man and mechine in the higher order control processes. With little knowledge of human operator capabilities in this area, the defense of the man in the advanced roles is based largely on intuition. As a result, not only the design of systems, but the justification for a responsible crew role will be strongly affected by our scientific understanding of the human as a higher level controller and decision maker.

From the display formats described above, it can be seen that pursuit tracking tasks with predictable input signals are common. As a result, the usefulness of models based on compensatory tracking tasks with pseudo random input signals is quite limited.

The control tasks of interest almost always will involve multiple channel processing. Having understood for some time the advantage of integrated displays (Reference 15) it is not surprising to find the new displays featuring a high level of integration. The application of recent research on instrument scanning (References 16 and 17) is therefore limited to current aircraft situations. (Note however that current

aircraft cannot be practically retrofitted with the advanced integrated displays. Scanning problems are therefore going to be present for quite a long time to come.)

Because predictive elements are being incorporated into the new displays, it is important that we understand the predictive skills of the human operator. Certain preliminary human operator decision models may form the basis for this understanding, and permit determination of whether a display enhances control skills or predictive abilities (Reference 18). With preview being an important ingredient of predictive displays, the preview models of the human operator also should be closely watched by display designers (Reference 19).

There has been considerable recent work on optimal control models of the human operator. While the application of these models may be somewhat distant yet, several experiences with advanced displays have demonstrated the need for these models. In particular, it has been observed frequently that when subject pilots are given predictive and situation displays, they tend to use different control policies, betraying different concepts of the cost function to be minimized. This latitude is purposely designed for in the new displays, but predictability of pilot response has diminished as a result.

The philosophy behind the predictive display concept of course is to use the adaptive capabilities of the pilot. As a direct consequence there is a significant trend away from command-only symbology, such as flight directors. Flight directors have been an aid for sometime, but they do little to increase the pilot's understanding of the situation. While flight directors are in widespread current use, and may be used even with the advanced displays as an option or for backup, the application of compensatory tracking models to flight director design (Reference 11) is probably of most interest to present aircraft.

The backup role of the crew, though infrequent, is nevertheless of continued importance. Handling qualities studies are applicable here in designing stability augmentation systems, but normal control modes with control-wheel-steering will have, by definition, superb handling qualities. The change in controlled-element dynamics in case of a failure could be quite significant. The case for pressing for the development of a theory of manual adaptive control to treat this type of problem has already been well made (Reference 20).

Another problem for the backup control modes is the preparation of the crew to handle them. One question might be: What display features used in normal operation are also useful as training devices for backup control modes? If we understood the training effects due to information presentations, we might be better equipped to treat this problem.

The largest tasks for the crew are the system management decisions, bringing us finally to the need for decision models and high level control models. The decision processes alone have been analyzed to the extent of providing model guidelines (Reference 21), and other starts have been made on understanding monitoring and sampling behavior (References 22 and 23). An example monitoring and control problem to be found in commercial aircraft operations (including future operation of current aircraft) is the modification of waypoints in a flight plan through the area navigation computer. This modification is made to minimize a complex cost function, subject to complex constraints. The ability to do this depends on the pilot's knowledge of the relation between his adjustment inputs and the cost functions. Recent research, such as that of Reference 24, may help us understand this very complicated, higher order process.

CONCLUSION

Crew roles in commercial aircraft will be changing for better use of the crew in the presence of new operational requirements. Though significant results of manual control research are applicable to certain display and control problems pertinent to current types of pilot tasks, we need to acquire much more knowledge to treat the future crew role.

REFERENCES

1. Cook, W. H. and Clifford, D. R., "Evolution of Automatic Flight Control," AIAA Paper No. 68-208, February 1968.

2. Gannett, J. R., "Flight Management Concept," presented at the ALPA Air Safety Forum, Seattle, Washington, July 9-11, 1968.

3. Warner, J. D., "Advanced Controls and Displays for Future Commercial Aircraft Operations," AIAA Paper No. 70-938, July 1970.

4. Warner, J. D., "Advanced Display Systems for Commercial Aircraft," presented at the Human Factors Society 14th Annual Meeting, San Francisco, California, October 12-16, 1970.

5. Annin, G. D., "Electronic Attitude Director Indicator Development for the Supersonic Transport," presented at the ISA 16th National Aerospace Instrumentation Symposium, Seattle, Washington, May 11-13, 1970.

6. Warner, J. D. and Fadden, D. M., "Computer-Generated Map Displays," presented at the FAA Symposium on Area Navigation, Washington, D. C., January 24-25, 1972.

7. Singleton, W. T., "Display Design: Principles and Procedures," IEEE Transactions on Man-Machine Systems, Vol. MMS-10, No. 4, pp. 181-193, December 1969.

8. Roscoe, S. N., "Airborne Displays for Flight and Navigation," Human Factors, Vol. 10, No. 4, pp. 321-332, August 1968.

9. Weir, D. H. and Johnson, W. A., "Pilot's Response to Stability Augmentation System Failures," in Fourth Annual NASA-University Conference on Manual Control, NASA SP-192, March 1968.

10. Wempe, T. and Palmer, E., "Pilot Performance with a Simulated Pictorial Landing Display Including Different Conditions of Resolution and Update Rate," in proceedings of the Sixth Annual Conference on Manual Control, Air Force Flight Dynamics Laboratory, WPAFB, Ohio, April 1970.

11. McRuer, D. T., Weir, D. H., and Klein, R. H., "A Pilot-Vehicle Systems Approach to Longitudinal Flight Director Design," AIAA Paper No. 70-1001, August 1970.

12. Wempe, T. E. and Baty, D. L., "Human Information Processing Rates During Certain Multiaxis Tracking Tasks with a Concurrent Auditory Task," in Fourth Annual NASA-University Conference on Manual Control, NASA SP-192, March 1968.

13. Miller, D. C., "Human Performance in Time-Optimal State Regulation Tasks," in Fifth Annual NASA-University Conference on Manual Control, NASA SP-215, March 1969.

14. Warner, J. D., "A Fundamental Study of Predictive Display Systems," NASA CR-1274, February 1969.

15. Levison, W. H. and Elkind, J. I., "Studies of Multivariable Manual Control Systems: Two Axis Compensatory Systems with Compatible Integrated Display and Control," NASA CR-554, August 1966.

REFERENCES

16. Clement, W. F., Jex, H. R., and Graham, D., "Application of a Systems Analysis Theory for Manual Control Displays to Aircraft Instrument Landing," in Fourth Annual NASA-University Conference on Manual Control, NASA SP-192, March 1968.

17. Weir, D. H. and Klein, R. H., "Measurement and Analysis of Pilot Scanning Behavior During Simulated Instrument Approaches," in Proceedings of the Sixth Annual Conference on Manual Control, Air Force Flight Dynamics Laboratory, WPAFB, Ohio, April 1970.

18. Ferrell, W. R. and Cohen, H. S., "Prediction and Decisionmaking in Manual Control," in Fourth Annual NASA-University Conference on Manual Control, NASA SP-192, March 1968.

19. Sheridan, T. B., "Three Models of Preview Control," IEEE Transactions on Human Factors in Electronics, Vol. HFE-7, 1966.

20. Young, L. R., "On Adaptive Manual Control," IEEE Transactions on Man-Machine Systems, Vol. MMS-10, No. 4, December 1969, pp. 296-331.

21. Schrenk. L. P., "Aiding the Decision Maker--A Decision Process Model," IEEE Transactions on Man-Machine Systems, Vol. MMS-10, No. 4, December 1969, pp. 204-218.

22. Baron, S. and Kleinman, D. L., "The Human as an Optimal Controller and Information Processor," in Fourth Annual NASA-Univeristy Conference on Manual Control, NASA SP-192, March 1968.

23. Sheridan, T. B., "On How Often the Supervisor Should Sample," in Proceedings of the Sixth Annual Conference on Manual Control, Air Force Flight Dynamics Laboratory, WPAFB, Ohio, April 1970.

24. Pew, R. W. and Jagacinski, R. J., "Mapping an Operator's Perception of a Parameter Space," The University of Michigan,

SESSION IV

Visual Display Developments

HEAD-UP DISPLAY FOR THE VISUAL APPROACH

J. M. Naish

Douglas Aircraft Company

Long Beach, California

Abstract

Discussion of the information requirements for a superimposed display for the visual approach. Analysis of methods depending on the presentation of a fixed angle of depression, or the direction of the flight path. Consideration of the influence of wind, and effects of error and noise.

Introduction

It has previously been shown that the pilot's natural forward view yields little information determining the flight path in the vertical plane(1). An accurate approach can only be made with the help of auxiliary information, which is normally supplied by the flight instrument panel: for example, the altimeter may be used in conjunction with known ground positions to determine the glide slope. But the pilot then has to deal with two visual fields, separated in position and understood by different methods of interpretation, so he needs time to transfer attention from one to the other. In these circumstances, the information process is discontinuous.

The continuity problem is avoided when the auxiliary information is provided by a ground aid, which may show a change of shape, a change of color, or a change of pulse rate as the pilot moves above or below the glide slope. Another method of ensuring a continuous information process is to superimpose a "head-up" display on the forward view by means of a reflecting collimator, thus allowing display and forward view to be combined. In these methods, the pilot gains information, from the ground aid or the display, without having to relinquish contact with the forward view.

Preceding page blank

Since visual ground aids are not universal, there will be occasions when only an airborne method is admissible, and the present aim is thus to consider how the Head-Up Display (HUD) may be used for the visual approach. This system was previously developed for mainly instrument flight purposes, and could be used with ILS guidance for the all-weather approach. It has now to be adapted for the case when no guidance signal is available and information is generated within the resources of the airplane.

There are two basic methods for the head-up visual approach. The fixed depression, or selected flight path method consists in showing the ground position of an elevation line (or plane) passing through the eye position at a fixed angle of depression from the horizontal[2]. The velocity vector, or flight path method[3], consists in projecting the impact point of the line along which the airplane is considered to be moving. As will be shown, the methods differ in showing either present position with respect to a selected path, or future position with respect to the touchdown zone, and it is to be asked which of the two kinds of information is better for the visual approach. It should then be possible to select from the methods, or some combination of methods, to define the content of the display format.

At this stage, it becomes desirable to reconcile the new type of display format with organizational concepts developed in earlier work[4], and with more general perceptual ideas. It is, moreover, necessary to consider effects of error and noise insofar as they reduce the performance expected of either method. Finally, since the format is to be changed, and since the type of information presented has an effect on the field of view[4], it is necessary to consider the field required in the present application.

Head-Up Visual Approach Methods

(1) Fixed Depression (Selected Flight Path) Method. With the help of an inertial platform, it is usually possible to set up a plane which remains parallel with itself for any position or attitude of an aircraft. Such a plane can be used to show the position of the aircraft in relation to an ideal approach path. Thus, a plane passing through A, Figure 1, and depressed from the horizontal by a selected path angle, ζ, intersects the ground plane in a line through S, where both this line and the depressed plane are taken as being perpendicular to the plane of the diagram. If A is also the eye position of the pilot, the ground line through S, if rendered visible, would appear as a line ss' in the pilot's frontal plane, Figure 2. When the aircraft is at B, a similar plane intersects the ground in a line through L, which would be seen as 11' in the frontal plane. Then if T is the desired point of touchdown, and another ζ - plane is drawn through T, the lengths LT, TS are obviously proportional to the offsets of the aircraft from this plane, BB', AA'.

The ground intercept of a ζ-plane may be shown to the pilot simply by superimposing a horizontal line symbol in his frontal plane, as HUD allows, and deflecting it from the direction of the airplane axis by the angle $\theta + \zeta$, where θ is pitch attitude. Position with respect to the selected approach path is then observed as the angle between this line and the touchdown zone. Thus, the angle between 11' and tt' in Figure 2 represents displacement above the selected path, where tt' is the position of the line symbol for zero

displacement. Accuracy will perhaps be improved if a reference line is maintained at tt', but this means having to compute a stabilized ground position.

(2) Flight Path Method. When the flight path of the aircraft is known, it may be represented immediately in the pilot's frontal plane. All that is needed is to displace an appropriate symbol by the angle of attack, α, from the position of the aircraft axis. When no azimuth information is available, or if it is considered unnecessary to provide lateral guidance because the forward view provides ample information for this purpose, the symbol may be a line such as ff' in Figure 2, representing the point F at which the path AB intersects the ground plane. The pilot is thus shown where the flight path terminates.

Relation of Information to Control Task

At the simplest level, the task in the head-up visual approach is to reach the touchdown zone. Whether this task will be achieved is shown directly by the flight path method. The fixed depression method does not give this information directly, although it allows the destination to be inferred, as the position of the symbol, when the path displacement does not vary. The flight path method therefore provides more accessible information at the most elementary level. This conclusion is entered in Table I with other results obtained in the present section.

More realistically, it is requisite not only that the touchdown zone be reached, but that it be reached with the correct speed, especially if the longitudinal touchdown dispersion is to be small. As a means to this end, it may be convenient to reduce the number of variables with which the pilot must deal, as is possible by selecting a particular approach path. Or, a selected approach path may be needed for obstacle clearance or noise abatement reasons. Path displacement is then of prime interest, and may be used to estimate the speed change expected in reducing the displacement. The fixed depression method provides this information but the flight path method does not, except in the special case of constant zero displacement.

A consequent requirement is that deviations from the desired path be reduced gradually, to avoid oscillation of the flight path, so it is desirable to know crosstrack velocity in the vertical plane. The fixed depression method offers some help in this respect because crosstrack velocity can be inferred from changes in displacement from the ideal path, as shown by symbol movements in the frontal plane: for example, from ss' to ll' in Figure 2. The flight path method, however, gives no indication of crosstrack velocity because it shows only the end point of the flight path, which can be reached from several directions and, therefore, with an unknown normal component: for example, two paths meeting at F, Figure 1, may intersect the desired path through T at different angles. The fixed depression method should thus be more useful in achieving a desired path smoothly.

Extending the last argument, it may be supposed desirable to supply pitch attitude information as a means for controlling crosstrack velocity. In either method this is possible, simply by noting changes in the position of an aircraft reference symbol with respect to the *framework* of the visual

background. But, of course, this information cannot be so used in the flight path method because crosstrack velocity is unknown.

Another consequence of the selected path concept is the desirability of rapidly detecting an incipient departure from the path. Assuming an initial on-path condition, departure is shown in either method by the symbol moving away from the touchdown zone. In the flight path method, it moves at the onset of the condition causing a departure. In the fixed depression method, it moves only as a departure occurs. The flight path method is therefore better in showing the onset of a disturbance, though less useful in correcting it because the extent of the disturbance is not shown.

Finally, there is a different capability for showing the initial on-path condition which has been assumed. The flight path method cannot, of course, be used for this purpose because it does not show displacement: in the period before intersecting the approach path it only shows that the flight path is, say, horizontal. Thus, the path AF in Figure 3 appears as ff' in Figure 4. On the other hand, the fixed depression method shows directly when a starting position is reached, at the moment the symbol coincides with the touchdown zone, and path displacement becomes zero. Referring again to Figure 3, as the vehicle moves through A and B to the on-path position C, the symbol moves from aa' through bb' to cc'.

Perceptual Workload

It was found in developing HUD for instrument flight that a low workload is secured when the display is interpreted by rules similar to those applicable in the natural forward view[5]; that is, when display and forward view are conformable. A similar conformity should be advantageous when HUD is used for the visual approach because the user again interprets a display superimposed on the forward view. This relation between workload and conformity can also be derived from the following information model.

Information represented in some visual form can only be acquired when the nature of the representation is perceived. For example, symbols used in a display format may be perceived to convey meaning by a scale and pointer relationship, as when a movable index shows present height by its position in a range of possible heights. An essential part of this kind of acquisition is in placing a given perceptual event (the pointer in its present position) within a framework of possible events (the scale), and information can only be conveyed when this framework of interpretation is understood.

When there is no ambiguity about the framework of interpretation, (because only one frame is admissible, or because only one frame suggests itself, or because the frame is foreknown) the user may proceed directly to evaluate the relationship of the perceptual event within the framework. In other cases, since his attention cannot simultaneously be given to considering alternate frameworks[6], time is lost in arriving at the correct choice. Clearly, if a new event occurs before the right framework is established, information is lost or, at least, work is done in recalling the former event. According to this model, it will be generally advantageous to reduce the number of alternate frameworks with which the user is confronted; that is, to increase the degree of conformity.

In applying this conclusion to HUD in the visual flight mode, it has to be considered how the symbols providing assistance in the vertical control plane are related to the background against which they are seen. In the previous application to a flight director symbol, it was only necessary to secure conformity of direction (for example, "turn right to a given heading" was shown as a command displacement to the right in geographical axes); conformity of scale was not important because there is no absolute scale of command. Also, attitude information was shown at reduced scale because it was only used in a supporting role, to show the nature of the maneuver being commanded, and because it could in any event be interpreted in isolation, as a relation between scale and pointer within the display format. In the present application to visual flight, the situation is different because attitude information is of greater significance. Moreover, the symbol position, showing either flight path or fixed depression, has to be understood in relation to the external world, and has little or no meaning when isolated within the display format. It follows that the display symbols, for either of the methods of improving visual approach accuracy, are conformable, and thus conducive to low workload, when presented at one-to-one scale in the framework of the external visible world.

As regards relative workload level for the two methods, the flight path symbol is easier to understand at the lowest level of interpretation, because its meaning is shown directly, while the fixed depression symbol has to be interpreted as showing path difference. At a higher level, the flight path method provides little information, thus adding little to the total workload. The two methods therefore differ in workload, but they also differ in information content.

Error Effects

Each method is subject to errors arising in the display equipment, and errors due to the way the equipment is used. Equipment error results in the display symbol being driven to the wrong angular position, through inaccuracies of data sources, transmission, computation and calibration. Experience suggests that the total equipment error is unlikely to be less than 0.25 degree, and may well be twice as large. Personal error arises through limitation of the ability to discern symbol position in relation to a background object. Under optimum conditions, personal error is expected to be of the order of one symbol linewidth, nominally one milliradian or about 3 minutes of arc; more generally it may be twice as large.

In the fixed depression method, the effect of an equipment error, η, is simply to alter the angle of the selected flight path from ζ to $\zeta + \eta$, since this is determined entirely by the angle of depression, Figure 1. The airplane still arrives at the touchdown zone, but with a more difficult task of energy management because vertical speed now differs from the nominal value. The effect of a personal error, e, is to make the airplane arrive at a point offset from the touchdown zone by this angle. The effect is small, it decreases with range, and it is independent of η: at a distance of one mile it should amount to a path error of about 5 feet.

In the flight path method the effects are more complex, and there is an important relation between the two kinds of error, because equipment error causes a displacement of the symbol which eventually becomes discernible.

If the airplane is at A, Figure 5, and the flight path symbol is located at T, the actual flight path is AB, where $\angle TAB = \eta$. As the airplane moves along AB, the symbol diverges from T to the point T', where BT' is parallel to the original direction of the symbol, AT. The process continues until TT' subtends ϵ at B; that is, until AB also subtends ϵ at T. The flight path may then be rotated by the angle ϵ until the symbol again lies over T, and the airplane proceeds along BP', where $TBP' = \eta$. The same process is repeated each time a new segment of the flight path generates the angular subtense ϵ at T, and by the time the airplane reaches the ground, a total of N segments are formed such that $N\epsilon = \gamma$, where γ is the initial flight path angle. At any of the turning points, the pathlength to T can readily be found, since

$$TB = TA \left[\cos \epsilon - \sin \epsilon \cot (\eta + \epsilon)\right]$$

and each succeeding pathlength, TC, TD, T.....Q, is related to its predecessor in the same way. The final pathlength, TQ, is the ground intercept and this is

$$TQ = TA \left[\cos \epsilon - \sin \epsilon \cot (\eta + \epsilon)\right]^N \qquad .....(1)$$

where N is taken as an integer.

Variation of the ground intercept with η and ϵ is illustrated in Figure 6 for an approach from a height of 1000 feet on a 3-degree path, with ϵ held constant at 0.1 degree for the η-curve and with η = 1 degree for the ϵ-curve. It is seen that the intercept cannot be made small simply by reducing ϵ but has a minimum value which is not negligible, being about 950 feet in the chosen case. On the other hand, TQ can be made small by reducing η, although the approach to zero is slow at small values of η. These results, which obtain generally from equation (1) and also for negative values of η, show that errors have a significant effect on longitudinal dispersion in the flight path method. It is beneficial to make equipment error as small as possible but even when η = 0.5 degree the ground intercept is still not negligible, being about 80 feet.

Noise Effects

The methods used to adapt HUD for visual flight depend on airborne data sources and are thus prone to noise effects. This is especially true of the flight path method, where angle of attack is the essential information, and this is obtained by probing the airstream directly. Earlier investigation[3] showed the difficulty of smoothing the resulting signal without loss of significant information: either the signal was smoothed but out of date, or it was up-to-date but noisy. With the help of an inertial platform and advanced smoothing techniques, it may be possible to derive a more useful form of flight path signal from a combination of vertical and forward speeds. Preliminary results with this method are encouraging[7].

The fixed depression method is less prone to noise because it presents a direction fixed in relation to an essentially stable datum, namely, the artificial horizon. Moreover, this datum is provided by equipment which is generally available, such as the vertical gyro. There is ample experience

to show that adequately stable information can be obtained in this way for head-up presentation.

Influence of Crosswind

In a crosswind approach, the optical axis of the display is generally turned away from the runway direction because the HUD optical system moves with the airplane. This is of comparatively little consequence when the format is of the flight director type, involving no absolute direction, but it directly affects operation in the visual approach because both of the proposed head-up methods depend on showing a relation between runway and symbol. The format, it is true, can be slewed to compensate for drift, and thus bring runway and symbol into the same vertical plane, but only within the field of the optical system. The operating conditions in HUD visual flight are thus limited by the display field.

The type of system which can be installed without major changes in cockpit design has a fairly small field. Previous flight tests have shown that the format can then only be slewed about 8 degrees in either direction[4], and this is insufficient for general purposes. It may well be that about twice as much drift compensation is needed, in which case the display facility will have to be considerably enlarged.

Influence of Longitudinal Wind Component

The effect of a longitudinal wind component is to alter both direction and displacement of the flight path, and thus influence both methods of presentation. The information needed to determine the proper position of the flight path symbol may not always be available, however, in the airplane. If the symbol is driven by a signal derived from angle of attack, it does not show fully the effect of longitudinal wind. If the driving signal is derived from high quality inertial data, wind is included. On the other hand, the fixed depression method reflects longitudinal wind directly in its effect on path displacement. The facility provided by each method for detecting wind shear can therefore only be considered comparable if adequate information is available for computing flight path direction.

Summary

There are two basic methods of using HUD in the visual approach to provide much-needed information in the vertical control plane. A symbol depressed from the true horizon by a constant angle can be used to show displacement from a given flight path. A symbol displaced from aircraft datum by the angle of attack can be used to show termination of the current flight path.

Choice of method depends on the significance attached to the type of information presented. If the main consideration is to reach the touchdown zone, the flight path method provides adequate information directly, while equivalent information can only be obtained indirectly by the fixed depression method. If it is important to control displacement from a given path, only the fixed depression method can be used generally. In the special case when displacement is constant and zero, the flight path method is usable, and with the advantage of showing an incipient departure immediately. From this

analysis, it appears that the fixed depression method should be chosen when energy management is important, or when a specific profile is to be achieved.

Workload considerations give little guidance in the choice of method. By analogy with previous results and by means of a proposed information model, both methods are conducive to low workload when presented conformably, so as to allow a common interpretative scheme. In the present context, this means a one-to-one relation between display and outside world. On grounds of self-evidence, the flight path method is easier to interpret but this advantage is offset by a lower level of information content.

Both methods are subject to equipment and personal errors. The former is the greater by an order of magnitude, and has the effect of simply altering the path angle in the fixed depression method. In the other method, the two kinds of error interact and increase longitudinal touchdown dispersion, though this is not very sensitive to change in personal error. The influence of noise is more difficult to suppress in the flight path method because of a dependence, direct or indirect, on noisy source data. The fixed depression method is thus to be preferred on grounds of error and noise; it is also more easily used to show wind shear. Both methods require an enlarged display field because real-world symbols are used. These results are collected in Table II.

This work was performed under the sponsorship of the Independent Research and Development Program of the McDonnell Douglas Corporation.

References

1. Naish, J. M., "Control Information in Visual Flight," 7th Annual Conference on Manual Control, U.S.C.; Douglas Paper 5921, June 1971.

2. Johnson, D., Symposium on Displays, J. Roy. Aero. Soc., vol 69, October 1965, p. 673.

3. Naish, J. M. and Shiel, R., "Flight Trials of HUD in Meteor and Hunter Aircraft," Tech Rep 65254, Royal Aircraft Establishment, Farnborough, England, November 1965, pp. 41-42.

4. Naish, J. M., "Flight Tests of HUD in DC-9-20," MDC J-0878, Douglas Aircraft Company, Long Beach, California, September 1970.

5. Naish, J. M., "Combination of Information in Superimposed Visual Fields," Nature, vol 202, May 1964, pp. 641-646.

6. Broadbent, D. E., "Mechanical Model for Human Attention and Immediate Memory," Psychol Rev., vol 64, 1957, pp. 205-215.

7. Anon., "A-7D Flight Demonstrations at Le Bourget," Aviation Week, June 28, 1971, pp. 48-50.

INFORMATION PROVIDED BY HEAD-UP VISUAL FLIGHT METHODS

INFORMATION	FLIGHT PATH METHOD	FIXED DEPRESSION METHOD
FLIGHT PATH INTERSECTION WITH TOUCHDOWN ZONE	YES	NOT DIRECTLY
PATH DISPLACEMENT	NO (EXCEPT WHEN ZERO AND CONSTANT)	YES
VERTICAL CROSSTRACK VELOCITY	NO	YES (INFERRED)
PITCH ATTITUDE*	YES (BUT CANNOT BE USED TO REDUCE DISPLACEMENT)	YES
PATH DIVERGENCE	YES (IMMEDIATE)	YES (DELAYED)
STARTING POSITION	NO	YES

*WITH AIRCRAFT REFERENCE

Table 1. Information Provided by Head-Up Visual Flight Methods

OVERALL COMPARISON OF METHODS

INFORMATION (TABLE I)	PATH METHOD SHOWS IMPACT POINT DIRECTLY. DEPRESSION METHOD ALWAYS GIVES PROFILE AND START POSITION.
WORKLOAD	BOTH METHODS REQUIRE ONE-TO-ONE PRESENTATION. PATH METHOD IS SELF-EVIDENT BUT PROVIDES LESS INFORMATION.
ERRORS	FLIGHT PATH ANGLE IS AFFECTED BY EQUIPMENT ERROR IN BOTH METHODS. LONGITUDINAL TOUCHDOWN DISPERSION IS AFFECTED BY COMBINED ERRORS IN PATH METHOD.
NOISE	TENDS TO BE MORE EVIDENT IN PATH METHOD.
WIND	DISPLAY FIELD AFFECTED IN BOTH METHODS BY CROSSWIND. DEPRESSION METHOD ALWAYS SHOWS LONGITUDINAL WIND.

Table 2. Overall Comparison of Methods

FIXED DEPRESSION (ζ) AND FLIGHT PATH (γ) METHODS OF AIDING VISUAL APPROACH

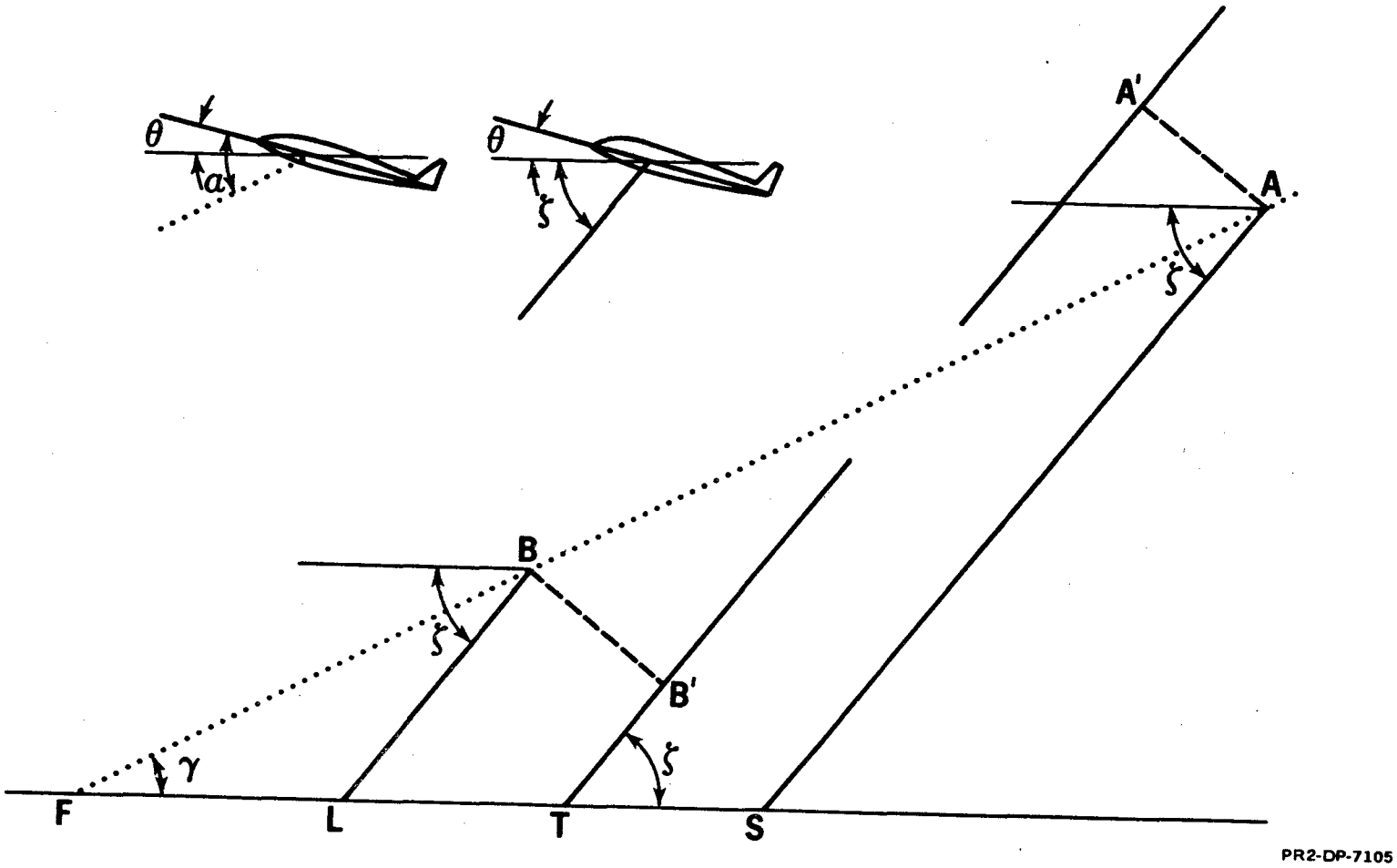

Figure 1. Fixed Depresssion (ζ) and Flight Path (γ) Methods of Aiding Visual Approach

FIXED DEPRESSION AND FLIGHT PATH SYMBOLS IN PILOT'S FRONTAL PLANE

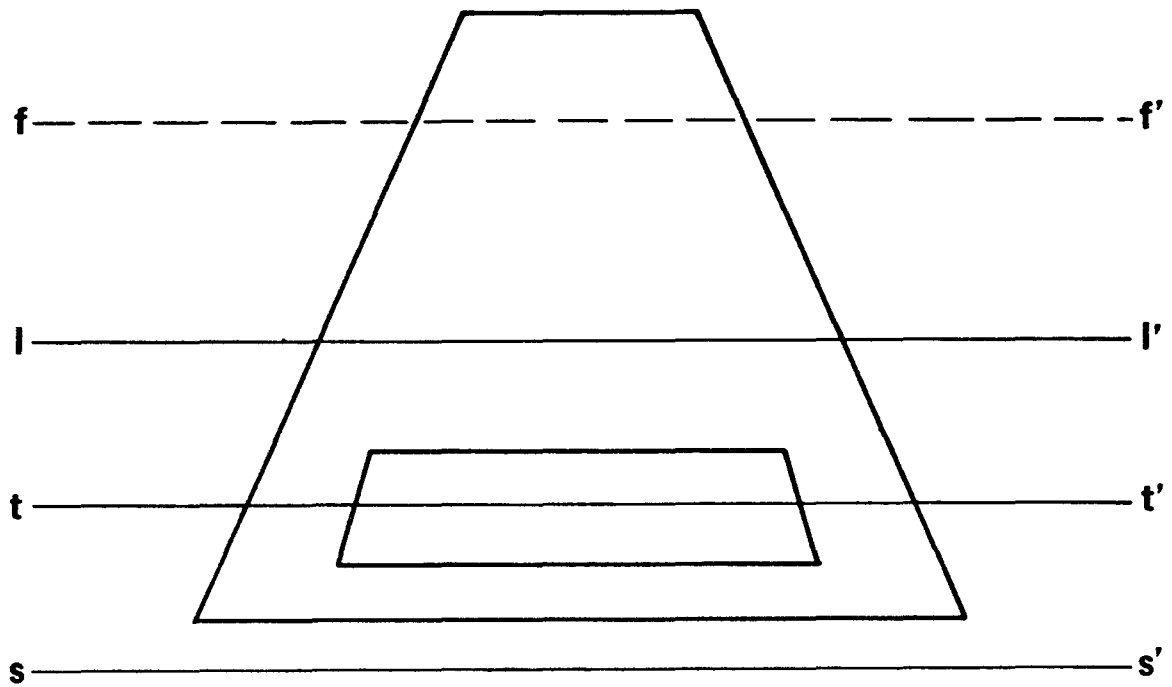

PR2-DP-7102

Figure 2. Fixed Depression and Flight Path Sympbols in Pilot's Frontal Plane

INTERSECTION OF FLIGHT PATH AND DESIRED APPROACH PATH

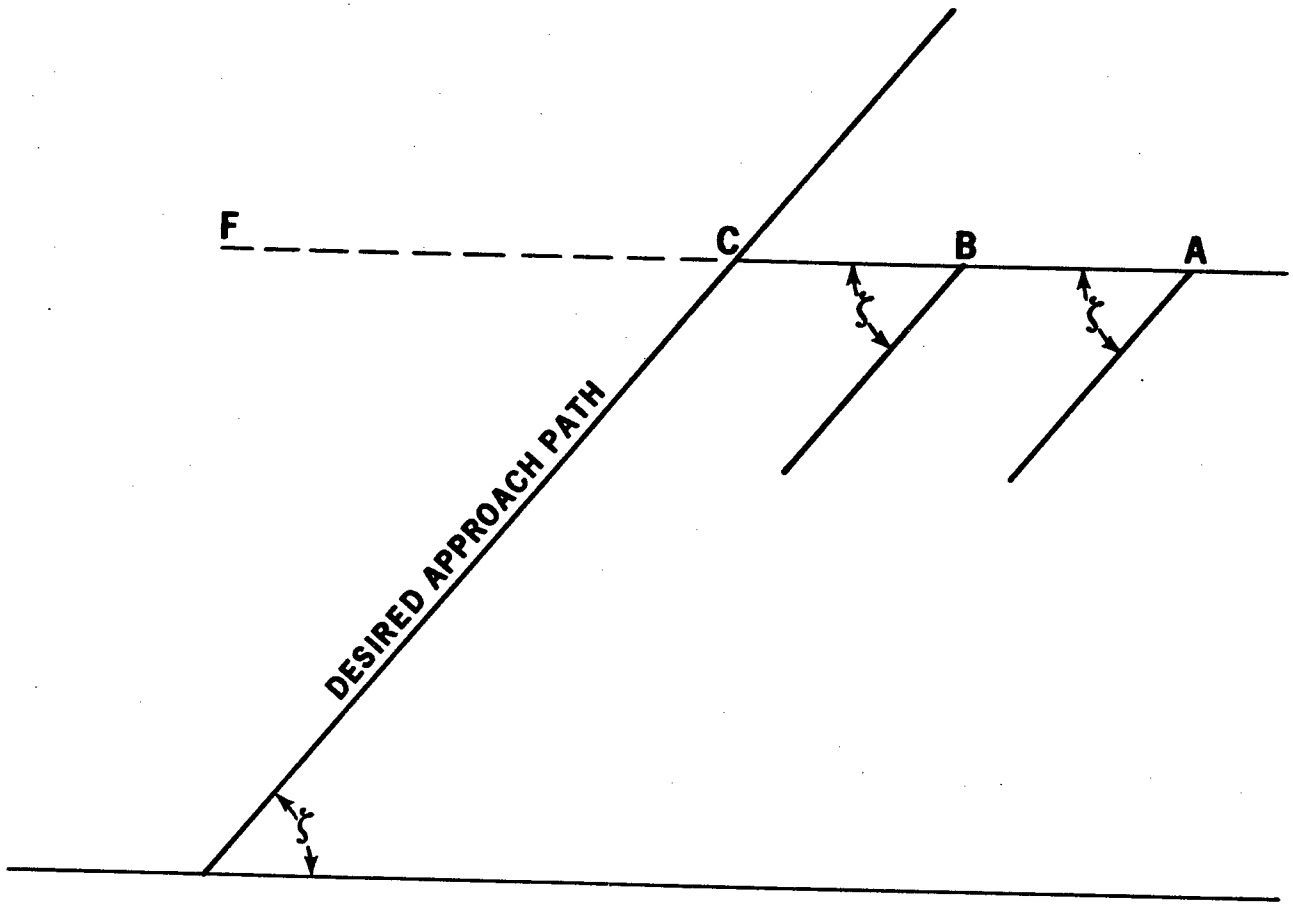

Figure 3. Intersection of Flight Path and Desired Approach Path

DEPRESSION AND PATH SYMBOLS AT START OF APPROACH

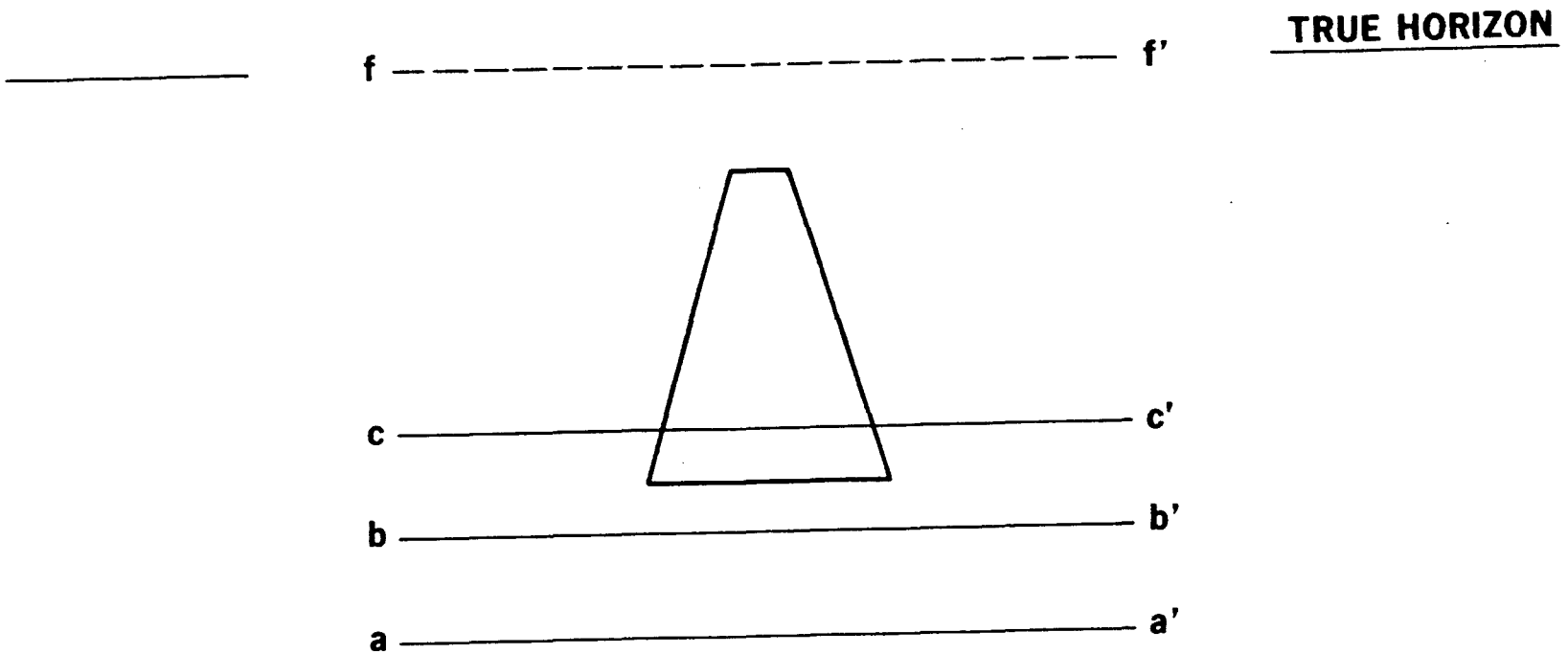

Figure 4. Depression and Path Symbols at Start of Approach

ERRORS IN FLIGHT PATH METHOD

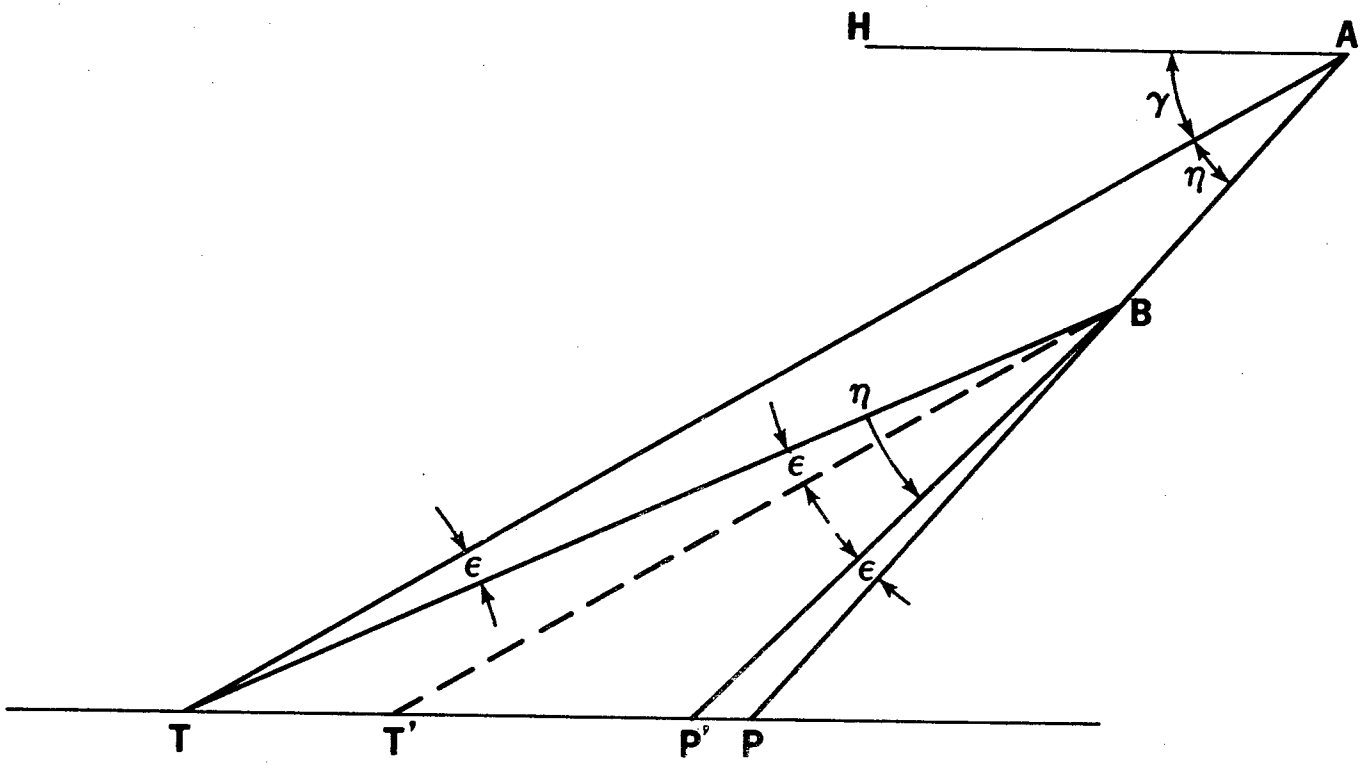

PR2-DP-7107

Figure 5. Errors in Flight Path Method

VARIATION OF GROUND INTERCEPT WITH ERRORS

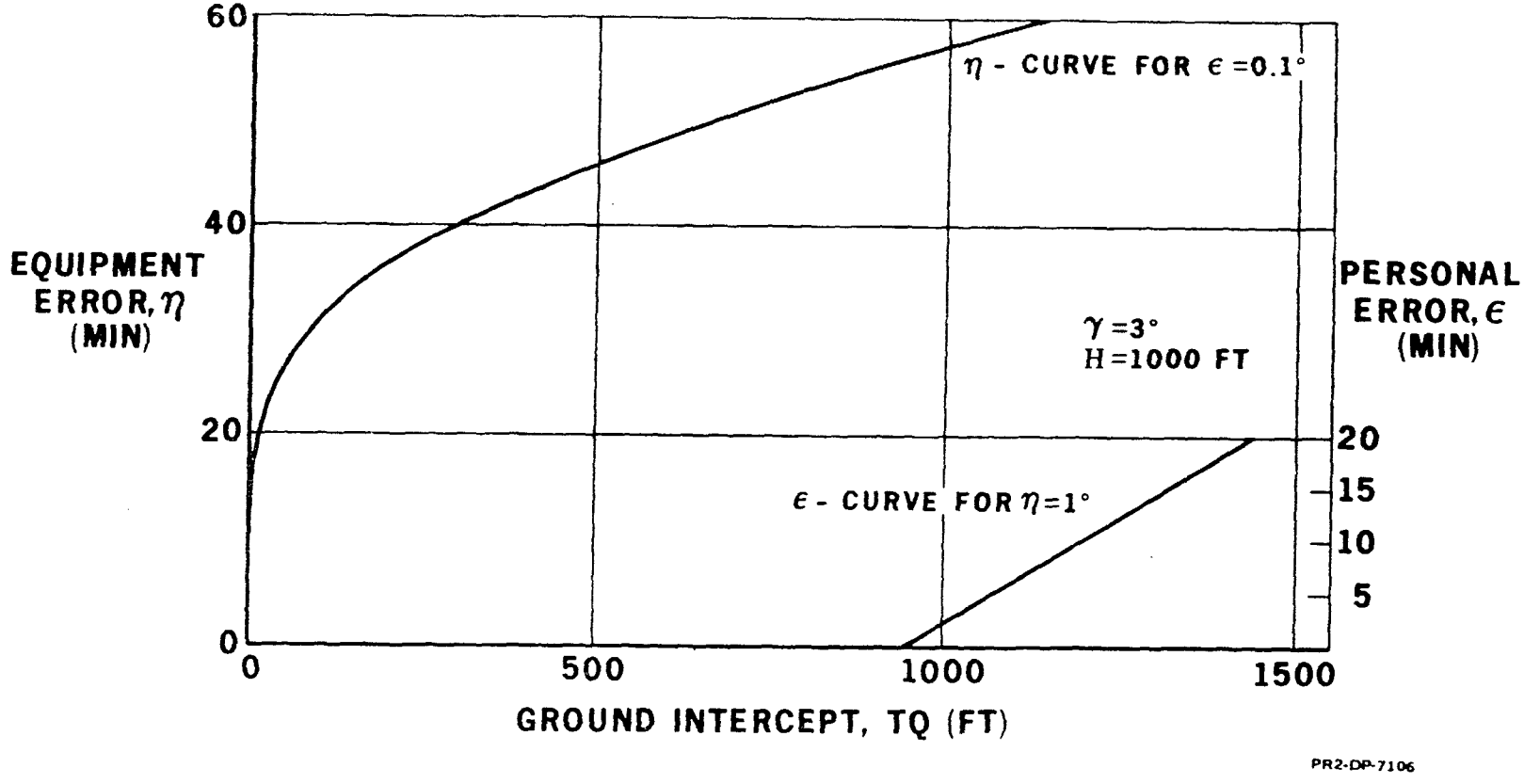

Figure 6. Variation of Ground Intercept with Errors

RESPONSE STRATEGIES WITH A CROSS-COUPLED CONTROL SYSTEM

PETER McLEOD
Medical Research Council, Applied Psychology Unit, Cambridge, England

ABSTRACT

A cross-coupled control system is one in which there is an angular disparity between the frames of reference of the control and the controlled object. Naval ratings performed a pursuit tracking task, with a lagged rate control, in which the cross-coupling (c-c) angle varied sinusoidally with time. Separate groups of six Ss tracked with different combinations of maximum c-c angle and sinusoidal frequency. For some groups the c-c angle was displayed visually. Performance was dependent on maximum c-c angle and independent of rate of change of c-c angle.

The results were predicted with error < 5% by a model which assumed that Ss adopted an heuristic response strategy which ignored the value of the c-c angle. The results would not be predicted by any model which assumed that S's individual responses are related to the input. A successful model would have to assume that only the sum of responses integrated over time was related to the desired result.

It might be reasonable to assume in a task of the sort typified by tracking, that as performance improves with time, the skilled man is learning the optimum set of movements to produce the result he requires. This assumption is implicit in any model of the man in the control loop which assumes that each individual control movement is related directly to the desired result.

This paper will describe a control task in which it is not true to say that the man tries to learn the optimal set of movements. He acquires an effective strategy for coping with the system while ignoring the possible optimal control movements. It seems likely that it is only in simple control tasks that individual responses bear a close relationship to the optimal response. In a difficult control task it is necessary for a model of the human operator to ignore individual control movements and look instead at the result of movements integrated over a period of time.

The task is tracking with a cross-coupled control. A cross-coupled control system is one where there is an angular disparity between the frames of reference of the control and the controlled object. Briggs and Waters (1958), Todosiev (1967), Bernotat (1970) and Smothergill, Martin and Pick (1971) have studied various conditions of cross-coupling (c-c) but always use a fixed c-c angle on any trial (that is, the angular disparity between control movement and controlled object movement is constant).

Briggs and Waters used a two dimensional compensatory tracking display with simulated aircraft control dynamics. They had separate groups with a fixed c-c angle between 0° and 68° in the horizontal dimension and no c-c in the vertical dimension. After forty, 30 sec trials, spread over three days, all groups tracked equally accurately. Bernotat used a compensatory display with a second order control. Ss tracked for successive 10 min periods with c-c angle increasing in 45° steps from 0° to 360°. He found performance at 0° and 180° to be equally good, with a slight decrement 45° away from those angles and a much greater decrement at 90° and 270°. Smothergill, Martin and Pick used a maze tracing task where visual feed-back was provided by a closed-circuit T.V. camera. They rotated the camera between trials in 15° steps between 0° and 180°. They found that time on target remained roughly constant up to 45° and then started to increase.

These studies are reasonably agreed that a fixed c-c angle of less than 45° has little effect on tracking performance. However these studies fail to show whether S alters the frame of reference of his responses to overcome the c-c or whether he uses some other response strategy.

EXPERIMENT I

This experiment examined the effect of a constantly varying c-c angle. Ss performed a continuous pursuit tracking task, controlling a spot on a CRT, with a lagged rate control. The angle between the frames of reference of the joy-stick and spot varied sinusoidally with time. The experiment was designed to compare the relative effects on performance of the maximum c-c angle and the rate of change of c-c angle.

METHOD

Apparatus

S faced a circular CRT display, 15 cms. in diameter. Between his knees was a vertical joy-stick 30 cms. long. The movement of the free end in any direction away from the centre-point was 12 cms. The plane of movement of the joy-stick was at right-angles to that of the CRT. The joy-stick was not self-centering. S controlled the velocity of a spot 1 mm in diameter on the CRT. Maximum velocity of the spot was 18 mm/sec. The joy-stick output was subject to an exponential lag with a time constant of 0.8 sec.

Subjects

Six groups of six naval ratings were used.

Task

S performed a continuous pursuit tracking task. The target, an annulus with internal diameter 2 mm and external diameter 4 mm, moved horizontally with a quasi random velocity; av. vel. = 2.7 mm/sec, max. vel. = 14 mm/sec, target movement extent 8.6 cms. The target course repeated every 185 secs during which time there were 11 direction reversals. S's spot started each trial 5 cms. above the centre of the target track.

Training

Before his first trial, S practised (with an uncross-coupled control) until he appeared to appreciate the relationship between movement of the spot and of the joy-stick. Each S then had four 30 sec trials a day for 10 days, with the trials separated by about 10 secs.

Scoring

The score taken was modulus error in the horizontal and vertical dimensions summated over the four trials. Scores were posted on the

door of the experimental room after each session.

A record was taken of the joy-stick movements of a control group, with no cross-coupling, and a group with ± 46° at 3 cpm. The stick movements were recorded on an Evershed and Vignoles two channel pen recorder, one channel showing movements from left to right and one showing movements away from and towards S.

Cross-coupling

All groups tracked for the first three days with an uncross-coupled control. This familiarised Ss with the task and gave a base-line of tracking ability which allowed better comparison of the performance of the groups with cross-coupled controls. On the fourth day all except the control group were told that the task could become harder and the spot more difficult to control. They were told that control was still possible and that their task remained as before, to keep the spot as near to the centre of the circle as possible. Each group then tracked for the remaining seven days with one of the following conditions of sinusoidally varying cross-coupling:

± 23° at 6 cpm; ± 46° at 3, 6 or 12 cpm; ± 69° at 2 cpm.

The cross-coupling was achieved by a mechanical oscillation of the box containing the joy-stick. S could not see this rotation, neither were any proprioceptive cues available about the c-c angle.

RESULTS

Figure 1 shows the effect of increasing the average rate of change of c-c angle, while leaving the maximum c-c angle constant. The median scores of the three groups with ± 46° at 3, 6 and 12 cpm are shown in a plot of error (volts) against time. An analysis of variance over days 4-10 shows a significant effect of days $F(6,90) = 29.85$, $p < .001$. There is no significant effect due to groups, $F(2, 15) = 1.10$, nor an interaction between groups and days, $F(12, 90) = 1.24$.

Figure 2 shows the effect of increasing the maximum c-c angle, while leaving the average rate of change constant. The median scores of the three groups with ± 23° at 6 cpm, ± 46° at 3 cpm and ± 69° at 2 cpm are shown in a plot of error (volts) against time. An analysis of variance over days 4-9 shows a significant effect of days, $F(5, 75) = 7.10$, $p < .001$, and a significant difference between the groups, $F(2, 15) = 6.24$, $p < .025$. There is no significant interaction between groups and days, $F(10, 75) = 1.84$.

Thus the results may be summarised as: (i) for a given average rate of change of c-c angle, performance deteriorates with increasing maximum cross-coupling angle; (ii) for a given maximum cross-coupling angle, performance is independent of the average rate of change of c-c angle.

The stick movement analyses are shown in Figure 3. The triangles refer to the group with cross-coupling, and the circles to the control group. The dotted lines show the error of the two groups (the R.H. axis) over days 4-8, the first five days of cross-coupling. The solid lines refer to the L.H. axis. The measure here is the distance the controller moves his stick, summated over the two dimensions measured, and averaged over the 30 sec of each run. A Mann-Whitney U Test on the individual stick movement data shows that the two groups do not differ significantly on day 4, but on days 6 and 8 the groups are reliably different ($p < .01$).

Figures 1, 2 and 3 about here

EXPERIMENT II

It might be thought that the experimental situation did not give S a reasonable chance to learn about the c-c angle. The conclusions drawn from the results might seem invalid in a situation where more information about the c-c was available to S than that arising from the unexpected movement of his spot. To check this possibility three new groups were run at $\pm$ 23° at 6 cpm and $\pm$ 46° at 3 and 12 cpm. All conditions except one were identical with the previous experiment. Throughout the experiment a line appeared across the whole width of the CRT screen at the level of the target track. The angular discrepancy between this line and the horizontal was equal to the c-c angle. Thus on days 1-3 the line remained horizontal, and on the remaining days it oscillated with one of the combinations of amplitude and frequency shown above, in phase with the c-c applied to the joy-stick output.

Before the first run on day 4 the information available from the line was explained to each S at some length and with various practice trials. He was told that a particular joy-stick movement would always result in the same movement of the spot relative to the line. Thus, for example, pulling the stick towards him would make the spot move at right-angles to the line, irrespective of the position of the line. On subsequent days Ss were asked to explain the purpose of the line to E to ensure that it was understood.

Figures 4, 5 and 6 show the performance of these three groups (triangles) compared with the three comparable groups without the displayed c-c angle (squares). An analysis of variance shows that in each case the groups do not differ significantly ($p > .05$) over days 4-10.

We may therefore conclude that the discussion which follows would apply to a system in which the c-c angle was or was not displayed.

Figures 4, 5 and 6 about here

DISCUSSION

There would appear to be two broad classes of strategy available to S in this experiment. Either he can try to compensate for the cross-coupling, adjusting his responses by the appropriate angle. Or he can make control movements until he finds one which produces the required stimulus event, i.e. the spot approaching the circle.

If he chooses the first strategy, each movement might be corrected by an amount approximating to the c-c angle observed on the previous movement. This movement would itself be incorrect by an amount proportional to the difference in cross-coupling angle at successive movement times. This difference would increase as the rate of change of c-c angle increased. The total error due to c-c would be a function of the sum of differences in c-c angle at successive sampling periods. The error would therefore increase with frequency for a fixed maximum c-c angle. Since this does not happen (See Figure 1) we may assume that S does not try to correct for the c-c angle.

If S uses the second class of strategy, we can produce a model to predict his performance, provided we know the population from which he draws his movements. The simplest assumption would be that S makes each stick movement as if there were no cross-coupling. With his next movement S corrects the error, again with a movement which ignores the cross-coupling of his control.

Figure 7 about here

S makes a stick movement which with no c-c would make the spot travel a distance D along the solid line towards the goal in one sampling period. Due to c-c the spot actually moves along the dotted line, producing an error e. (See Figure 7.)

$$\frac{e}{2} = D. \sin \frac{\theta}{2} \qquad (\theta = \text{c-c angle})$$

Total error due to c-c

$$\propto \sum_{\theta = 0}^{\theta = \theta \max} \sin \frac{\theta}{2}$$

$$\propto \int_{\theta = 0}^{\theta = \theta \max} \sin \frac{\theta}{2} \cdot d\theta$$

$$\propto \left[- \cos \frac{\theta}{2} \right]_{\theta = 0}^{\theta = \theta \max}$$

$$\propto \left[1 - \cos \frac{\theta \max}{2} \right]$$

Therefore error due to cross-coupling $\propto (1 - \cos \frac{\theta}{2}\,\text{max})$

This model predicts that the ratio of errors at maximum cross-coupling angles of 23°, 46° and 69° will be:

$$\frac{(1 - \cos \frac{46}{2}) - (1 - \cos \frac{23}{2})}{(1 - \cos \frac{69}{2}) - (1 - \cos \frac{46}{2})} = 0.616$$

The experimental value of this ratio can be found from Figure 2, by taking the mean value of $\frac{\text{Error (46°) - Error (23°)}}{\text{Error (69°) - Error (46°)}}$ over days 4-9. To allow for initial differences in skill between the three groups a constant is added to the scores on days 4-9, which would have given the three groups the same median error score averaged over days 2-3 (when they were all performing the same task).

It is reasonable to assume that the strategy will be developed over training, so the data from days 4-9 can be treated in two halves, with the ratio in the second half being predicted as 0.616. The average observed ratios for days 4-6 and 7-9 are 0.98 and 0.59.

The closeness of data and prediction suggests that the strategy adopted by the practised S in this experiment is that embodied in the model. Ss do not alter their responses by an angle corresponding to the c-c angle. Rather they make a series of movements, ignoring the cross-coupling of the system, which produces the required stimulus event.

If this were so, one could predict which of two types of aided display would help S most. One could display the c-c angle with cross-hairs on the screen (as in Experiment II). If S were altering the frame of reference of his responses to compensate for the c-c angle this display would be optimal. Or, alternatively, one could attach a line to the spot which would point in the direction in which the spot was going to move, given the current joy-stick demand and c-c angle. If S were following the strategy indicated by the model this display would be more useful. S would have to wait less time to see the consequences of his movements and make the appropriate corrections. These two display modes have been compared by Bernotat (1970). His Ss tracked for periods of 10 mins. with fixed c-c angles varying in 45° steps from 0-360°. Separate groups used an unaided display or one of the two aided displays. Both aided displays improved performance. But at all angles the vector display gave better performance than the display with cross-hairs. The improvement was most marked at 90° and 270°, where the decrement of the group with the unaided display was greatest.

Any model of S's behaviour which suggests that he learns to make the correct movements would presumably predict that as he became more practised, his movements would become more precise, and that the distance he moved his joy-stick would tend to decrease with time. The model put forward in this paper suggests that S is searching with successive imprecise movements for one which will produce the correct effect. The skilled S will learn to search more rapidly through a wider range of movements. The prediction would therefore be that as the performance improves, the extent of stick movement would increase. It is clear from Figure 3 that as the tracking skill with the cross-coupled control improves, so does the extent of the stick movement.

The response mode suggested by this experiment is an example of an heuristic response strategy. The goal of the spot moving towards the circle is achieved by a set of individual responses which are not all related to the desired result. Pew (1966) showed for a difficult control of a different sort that the strategy adopted was one where it was the result of responses integrated over a period of time rather than the individual responses which was related to the required result. It seems likely that any model of the man which assumes that individual movements are related to the desired result would only be an accurate description of the controller in comparatively easy tasks.

REFERENCES

BERNOTAT, R. Rotation of visual reference systems and its influence on control quality. IEEE Transactions on Man-Machine Systems, 1970, MMS-11, 2, 129-131.

BRIGGS, G. E. and WATERS, L. K. Training and transfer as a function of component interaction. Journal of Experimental Psychology, 1958, 56, 492-500.

PEW, R. W. Acquisition of hierarchical control over the temporal organization of a skill. Journal of Experimental Psychology, 1966, 71, 764-771.

SMOTHERGILL, D. W., MARTIN, R., PICK, H. L. Perceptual motor performance under rotation of the central field. Journal of Experimental Psychology, 1971, 87, 64-70.

TODOSIEV, E. P. Human Performance in a cross-coupled tracking system. IEEE Transactions on Human Factors in Electronics, 1967, HFE-8, 3, 210-217.

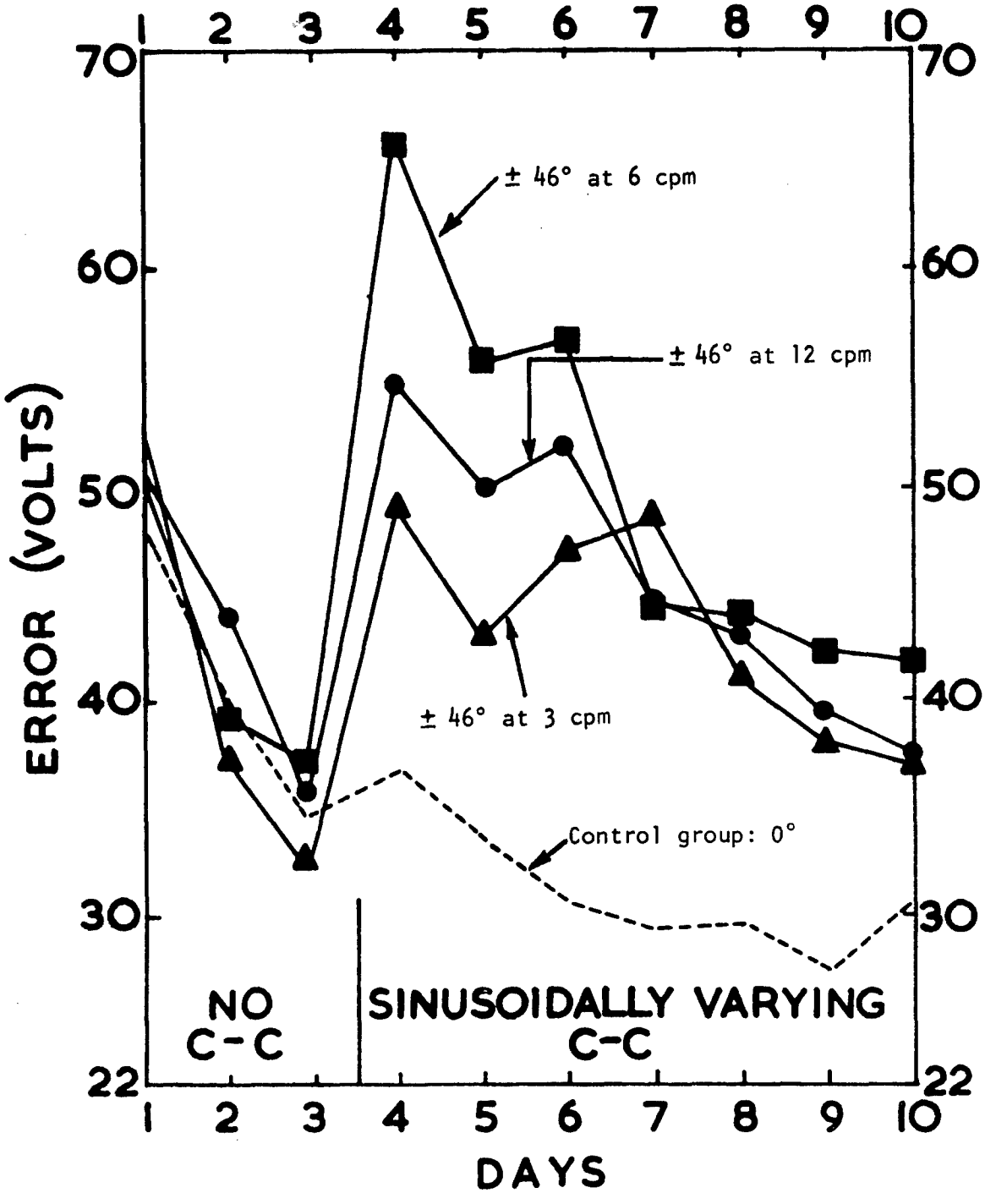
1 2 3 4 5 6 7 8 9 10
70
60
50
40
30
22
ERROR (VOLTS)
± 46° at 6 cpm
± 46° at 12 cpm
± 46° at 3 cpm
Control group: 0°
NO C-C
SINUSOIDALLY VARYING C-C
DAYS

Figure 1

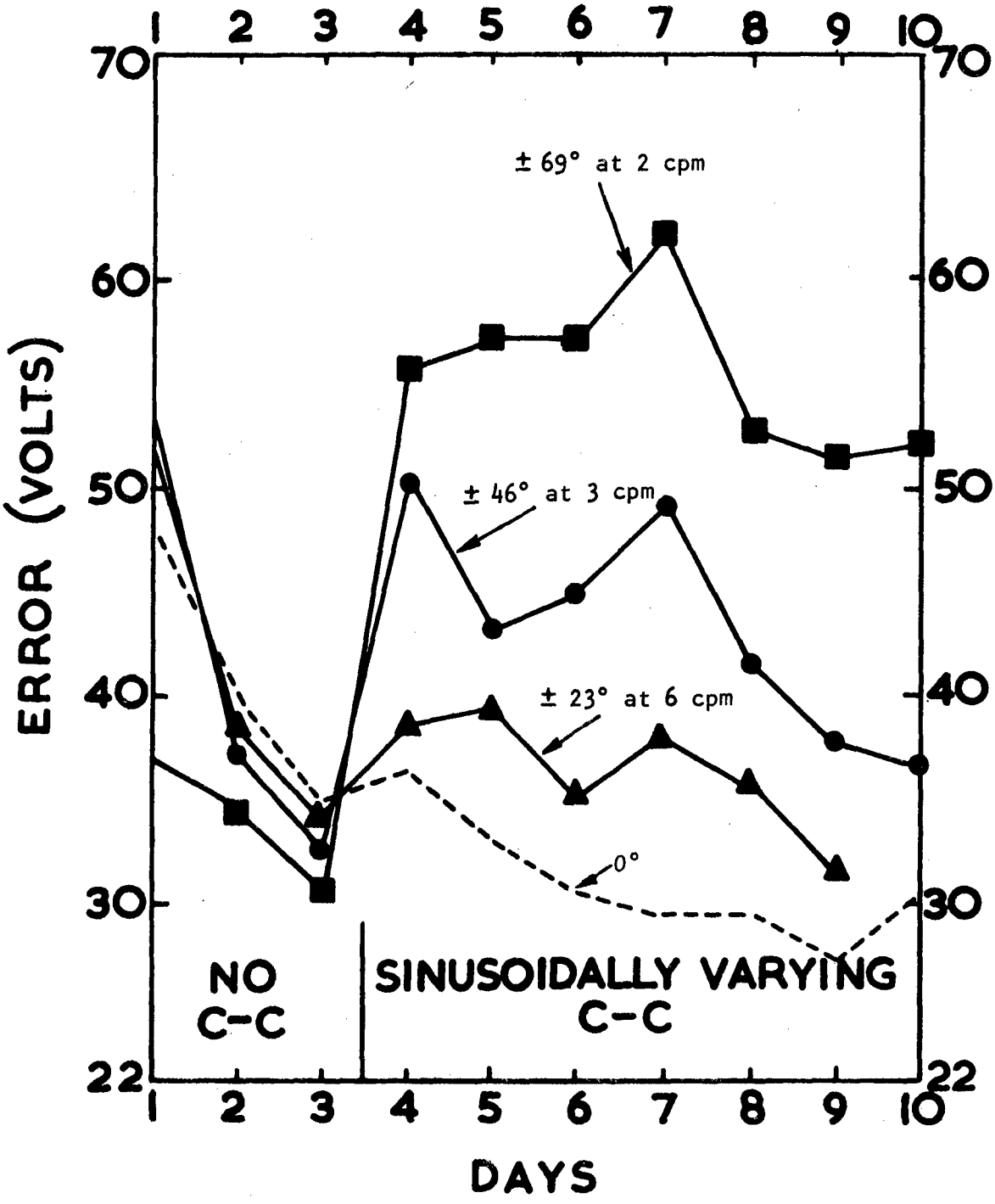
1 2 3 4 5 6 7 8 9 10
70
60
50
40
30
22
ERROR (VOLTS)
± 69° at 2 cpm
± 46° at 3 cpm
± 23° at 6 cpm
0°
NO C-C
SINUSOIDALLY VARYING C-C
DAYS

Figure 2

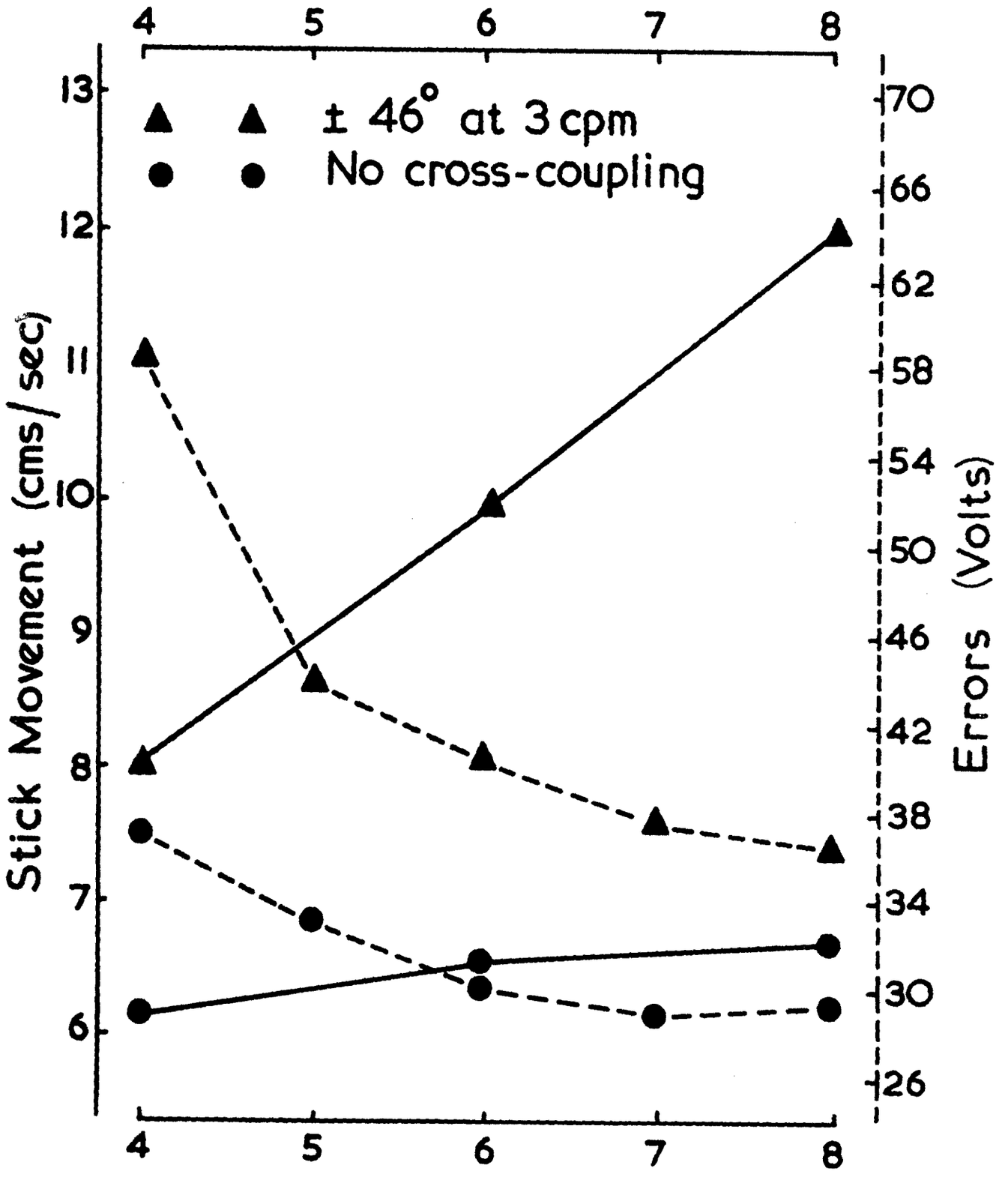
4
5
6
7
8
13
12
11
10
9
8
7
6
± 46° at 3 cpm
No cross-coupling
Stick Movement (cms/sec)
70
66
62
58
54
50
46
42
38
34
30
26
Errors (Volts)
Days

Figure 3

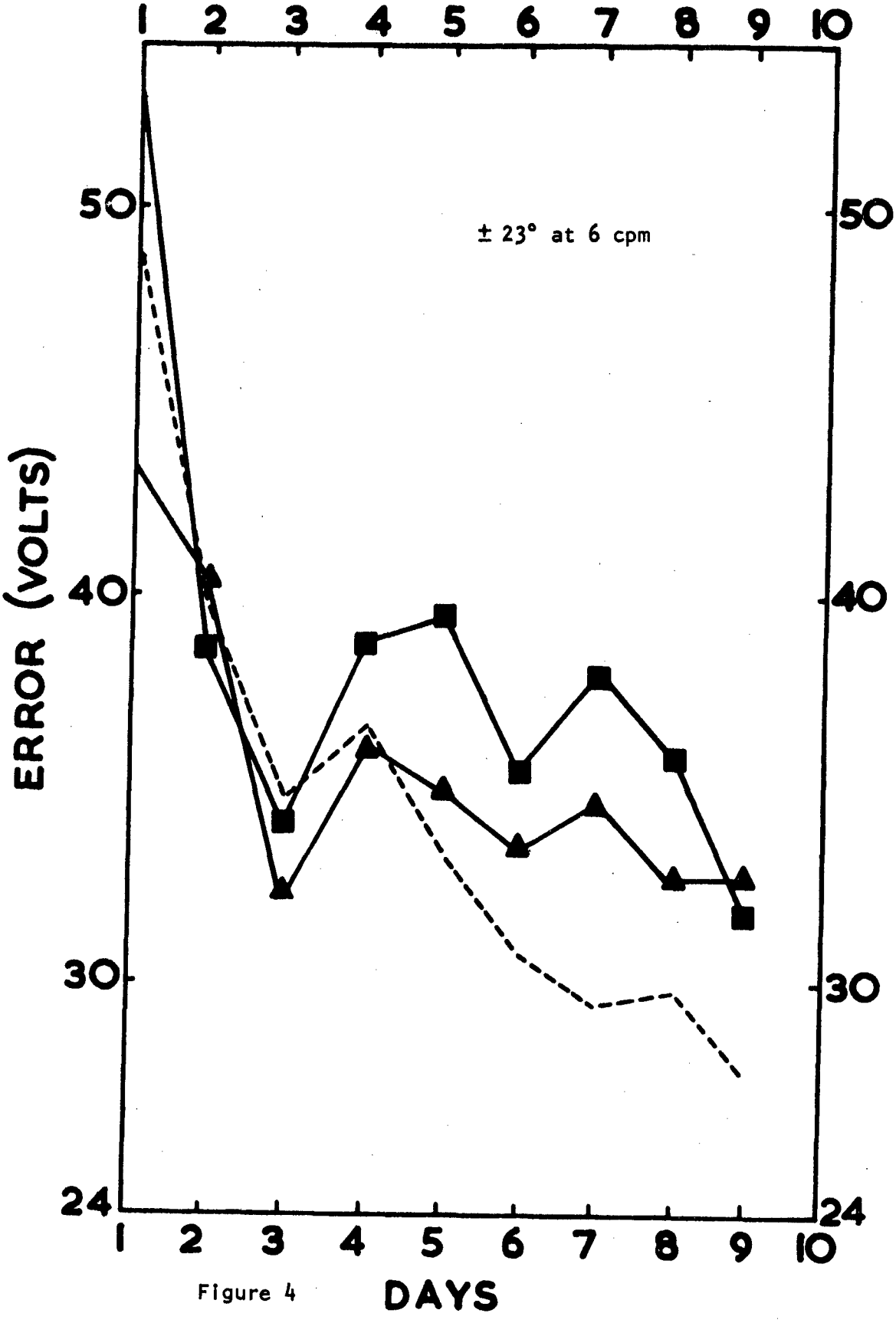

Figure 4

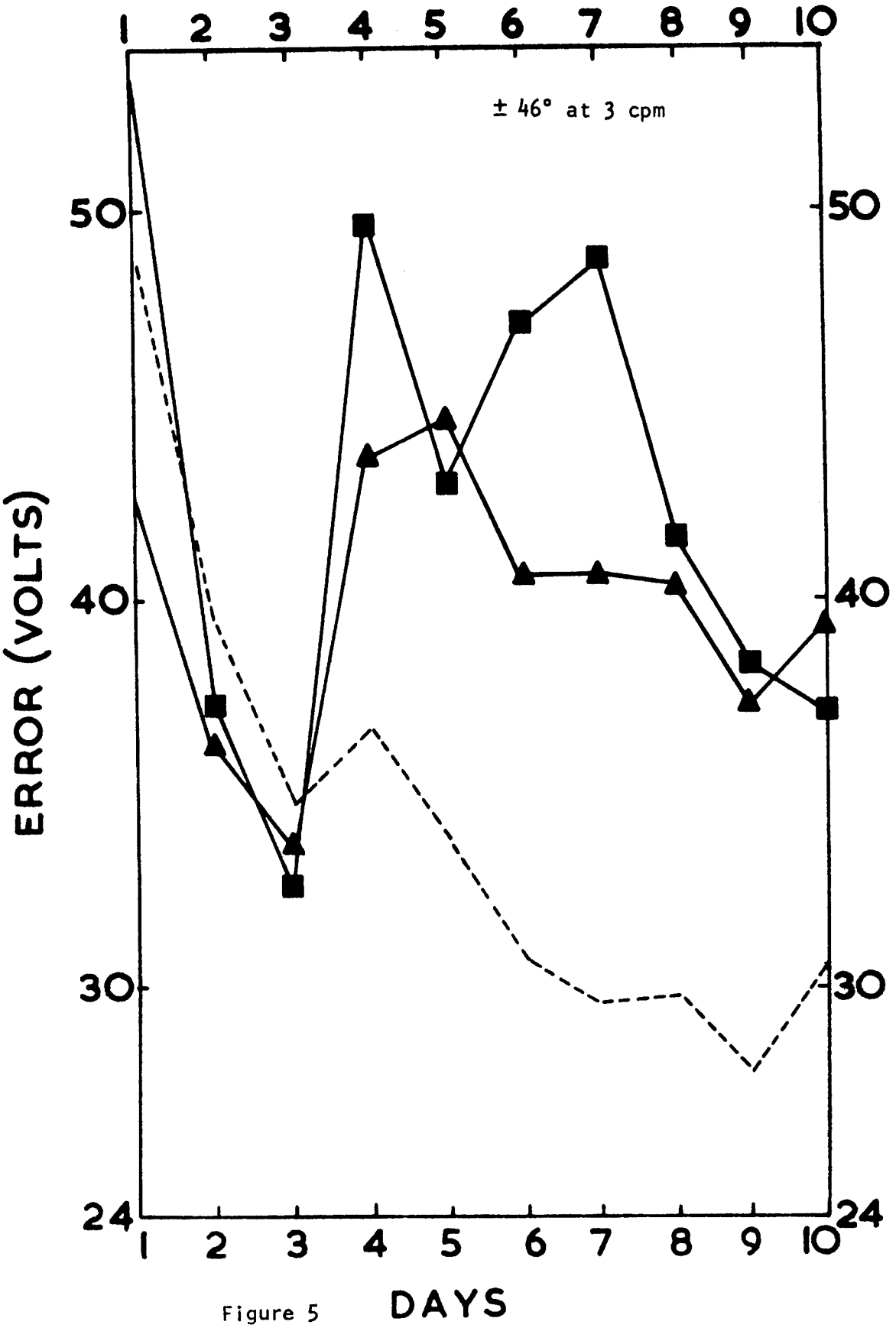

Figure 5

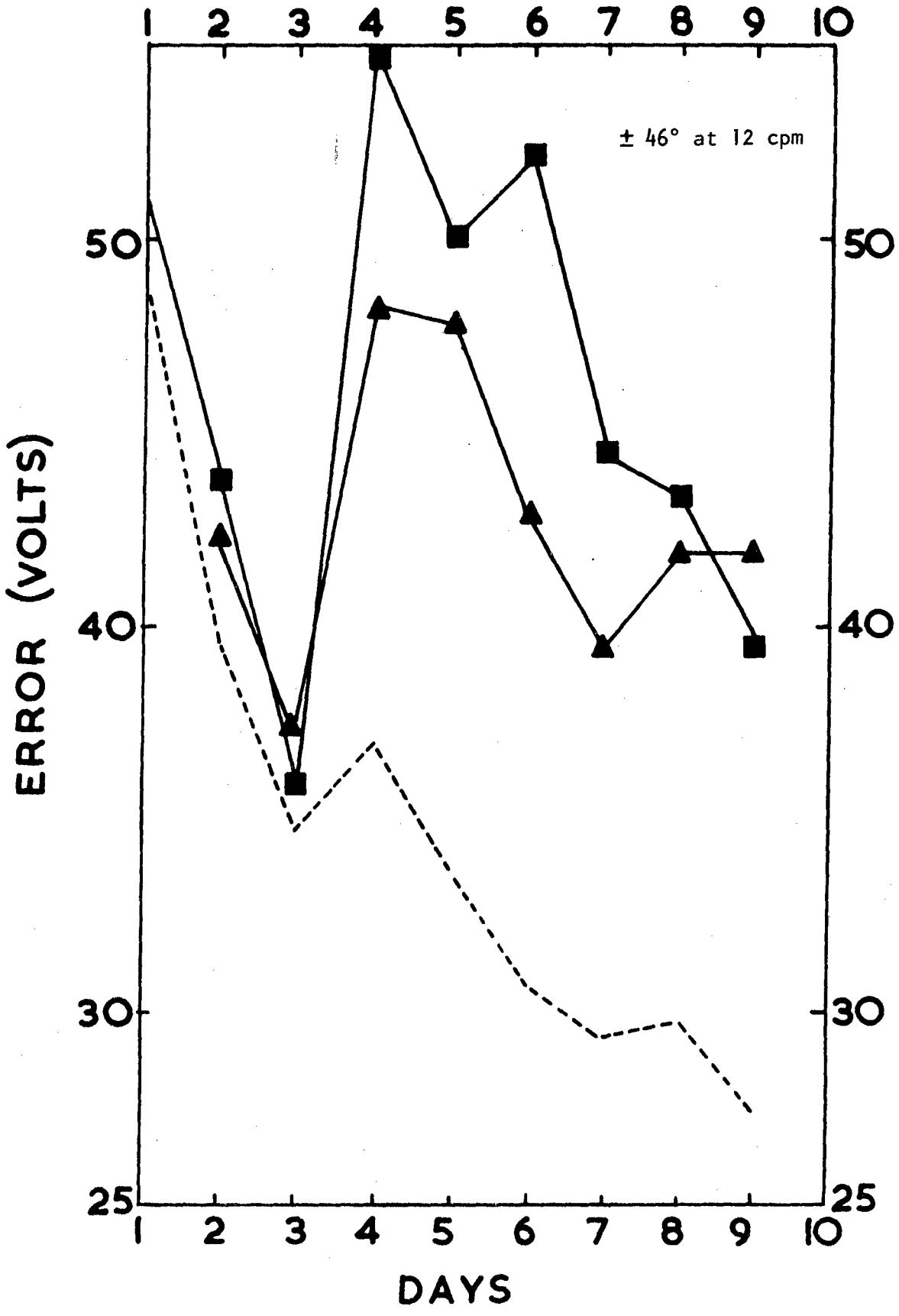

Figure 6

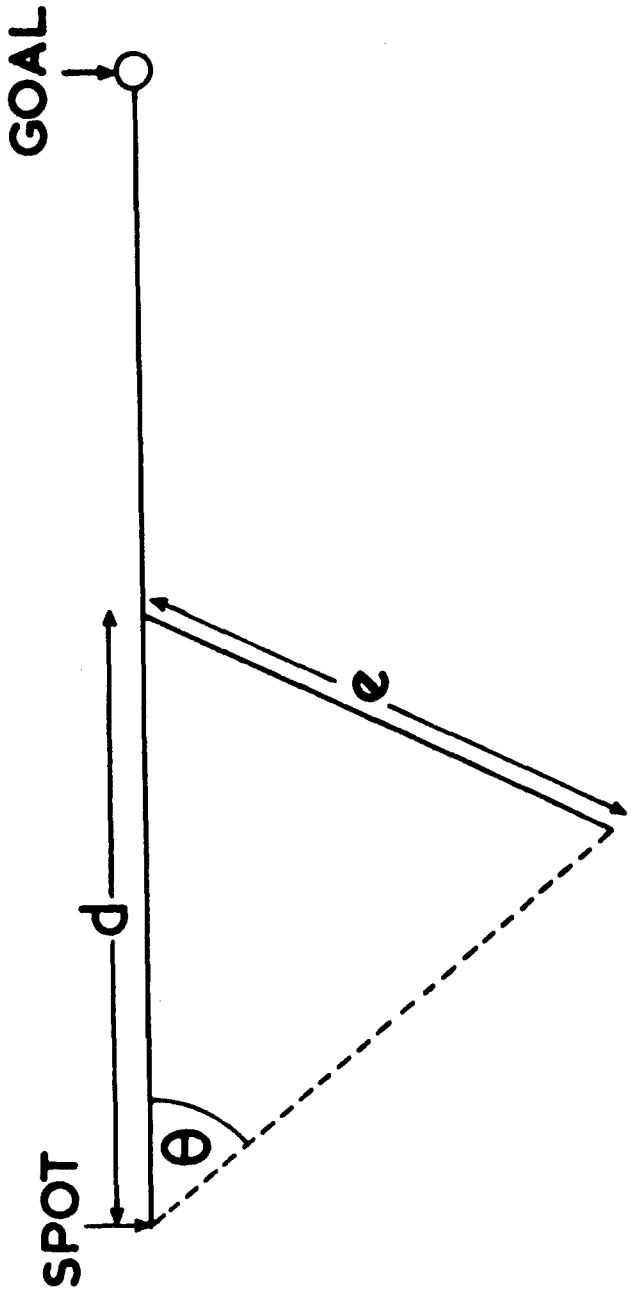

Figure 7

A PILOT MODEL FOR TRACKING WITH PREVIEW

By

L. D. Reid
N. H. Drewell

University of Toronto
Institute for Aerospace Studies

ABSTRACT

A set of describing functions was measured for subjects performing a rate control pursuit task with preview in an attempt to study the time delay and lead characteristics found in pilot models. The preview utilized ranged up to 0.8 sec., appearing as a tail to the right of the target symbol. It was found that the preview had dramatic effects on the form of the describing functions.

INTRODUCTION

The work outlined in this paper constitutes a preliminary investigation into the ability of human pilot describing functions to model the pilot when the future course of the target is displayed. A more complete description appears in Ref. 1. Several considerations prompted this research. First, there is an important class of tracking tasks that involve preview. For example low level missions requiring the pilot to follow the contours of the terrain can involve preview. A more down to earth case would be a drive along a winding road. Results pertinent to these situations would help to extend the range of application of pilot models. Second, it was of interest to determine whether the describing function form of pilot model could be applied to tasks involving an element of predetermination in the flight path. The preview task appeared to be a step in this direction. Third, the influence of preview on the time delay and lead terms in the pilot model were unknown. By employing a range of previews it was hoped that some light could be shed on the use of the lead term by the pilot in predicting the future course of the target.

THE TRACKING TASK

The task employed was the normal single degree of freedom tracking task with a random input and rate control vehicle dynamics. The unique feature was the display system. This allowed the display of from 0 to 2 sec. of input preview or postview. This system functions as follows. The random input signal is sampled at 50 samples per second and a running 2 sec. history in digital form is retained in a shift register with 8 bit precision. A selectable part of the history is displayed as the wavy line shown in Fig. 1. The point on this line above the tracking symbol (circle) is taken to be the present level of the input, all data to the right being preview and all that to the left postview. The line is actually a series of dots with the inter-dot space representing 0.02 sec. In the present experiment the dots were spaced every 0.10 in. and the vertical resolution was 0.017 in. The pattern moves across the screen (an 8 x 10 in. CRT) from right to left, with new hills and valleys

appearing from the right, moving past the tracking symbol (a 0.13 in. diameter circle) and disappearing off the screen to the left.

The subject's task was to keep the tracking symbol on the terrain line by moving a joystick in the fore and aft direction. The tracking symbol responds by climbing or descending at a fixed horizontal position on the display. This horizontal position can be set by the experimenter to give the desired amount of preview and postview. In this study only preview was used. The amount of preview can be altered by selecting the number of dots to be displayed.

Thus it is seen that the task is pursuit in nature, the case of 0 sec. preview being nothing more than a pursuit tracking task. Further details of the equipment are given below.

Vehicle Dynamics - Rate control, $^{c}/_{s}$. The open loop gain was set such that the target symbol climbed at 0.94 in./sec. for each degree of rearward stick deflection.

Joystick - Lightweight with a spring constant of 0.34 ounces per degree of deflection. Natural frequency 11.8 rad./sec. and damping ratio of 0.0067. Maximum deflection ± 17.5 degrees. Hand grip 18.5 in. above pivot point.

Input Signal - Filtered white noise. See Fig. 2 for the power spectrum where

$$\frac{\Phi ii(\omega)}{\Phi ii(o)} = \frac{1}{1.032^2}\left(\left(\frac{6}{j\omega+6}\right)^2 + 0.032\left(\frac{121}{-\omega^2+7.92j\omega+121}\right)^2\right)^2$$

DC level = 0.0, RMS level = 0.5 in.

Viewing Distance - Subject to display, average 20 in.

Recording Equipment - Digital tape recorder running at 25 samples per second per channel.

EXPERIMENTAL DESIGN

6 male graduate students served as subjects. As a group they completed 1200 3 min. runs during training and 420 during the main body of the experiment. Of these 240 were recorded and analyzed to produce describing functions. The main experimental variable was the amount of preview which took on the values 0, 0.1, 0.2, 0.4 and 0.8 sec. All subjects tracked with all previews in a randomized design.

CALCULATION OF PILOT DESCRIBING FUNCTIONS

The problem is to determine a model for a pilot performing a pursuit tracking task with a non-standard form of display. It is possible to speculate on a range of models depending upon one's impression of how the pilot utilizes the display. As a first approximation we have chosen the simplest approach by assuming that a compensatory linear pilot model relating o(t) to e(t) is sufficient. See Fig. 3a. This was based on the results of Ref. 2 where it

was found that for pursuit plus disturbance tasks with the present form of input a single linear pilot model tended to dominate. As can be seen from Fig. 3a any decrease in the open loop time delay as the result of the pilot monitoring the future target position will appear in this model along with the stick dynamics (which are negligible). It will be shown that this approximation was reasonable for the present tracking task.

The pilot describing functions were calculated using the power spectral density techniques outlined in Ref. 2 as

$$Y_p(\omega) = \frac{\Phi io(\omega)}{\Phi ie(\omega)}$$

The signals were sampled at 25 samples per second and record lengths of 150 sec. used. τ_{max} in the intermediate correlation functions was set at 9.96 sec. This gave an estimate of the describing functions at intervals of 0.631 radians per second starting at 0.315 radians per second.

In order to demonstrate the relationship between this simple model and a more complex form consider the structure of the model of Fig. 3b. Here it is assumed that the pilot views the input signal at a point τ_1 sec. upstream of the tracking point and responds to this signal, thus taking advantage of the preview. In addition he closes the loop to form e(t) in order to keep his open loop response from drifting away from the terrain line. If the linear model includes the assumption that the remnant n(t) is uncorrelated with i(t) then the following applies (Laplace transform notation).

$$\bar{o} = \bar{e}Y_A(s) + \bar{i}\, e^{\tau_1 s}Y_B(s) + \bar{n}$$

$$\bar{e} = \bar{i} - \bar{o}\, A(s)$$

$$\Phi_{io}(\omega) = \Phi_{ie}(\omega)\, Y_A(j\omega) + \Phi_{ii}(\omega)e^{j\omega\tau_1}Y_B(j\omega)$$

$$\Phi_{ie}(\omega) = \Phi_{ii}(\omega) - \Phi_{io}(\omega)\, A(j\omega)$$

which reduces to

$$\frac{\Phi_{io}(\omega)}{\Phi_{ie}(\omega)} = \frac{Y_A(j\omega)+e^{j\omega\tau_1}Y_B(j\omega)}{1-A(j\omega)e^{j\omega\tau_1}Y_B(j\omega)}$$

Thus our simple model $Y_p(j\omega)$ could in actual fact represent the combination of several terms of a more complex model.

TRACKING SCORES

Tracking scores were calculated as

$$\text{SCORE} = \frac{o\int^T e^2(t)dt}{o\int^T i^2(t)dt} \times 100\%.$$

As expected scores improved with increasing preview. See Fig. 4. Note that 0.4 sec. appears to be a critical preview beyond which little improvement

with increased preview occurs. This value of preview also appears to be a critical point in the describing function measurements.

CORRELATION COEFFICIENTS

When using $Y_p(\omega)$ as defined above it is customary to determine the goodness of fit for the linear model from

$$\rho^2(\omega) = \frac{|\Phi_{io}(\omega)|^2}{\Phi_{ii}(\omega)\Phi_{oo}(\omega)} = 1 - \frac{\Phi_{pp}(\omega)}{\Phi_{oo}(\omega)}$$

where

$$\bar{p} = \bar{n}\left(\frac{1}{1+A(s)Y_p(s)}\right)$$

and n(t) is the remnant shown in Fig. 3.

It is shown in Ref. 3 that a different fit parameter defined as

$$\rho_1{}^2(\omega) = 1 - \frac{\Phi_{nn}(\omega)}{\Phi_{oo}(\omega)}$$

is also a good fit parameter and in addition it gives a more pleasing result. See Fig. 5. The plots in this figure compare ρ^2 and $\rho_1{}^2$ for a compensatory task employing rate control and the input spectrum of the present project. The difference between the two seems to be the influence of the closed loop system response on ρ^2.

In this report ρ^2 will be employed to allow comparisons with past work.

RESULTS AND DISCUSSION

The data obtained in this study tend to break into two subsets, those for previews of 0, 0.1, and 0.2 sec. and those for 0.4 and 0.8 sec.

The results for the small preview cases are shown in Fig. 6. These plots are based on the mean and standard deviation obtained by combining 8 replications of the task by all 6 subjects. The results for 0 sec. preview have been compared with those for a similar task in Ref. 2 (with the open loop gain equalized) in Fig. 6. The close agreement is taken to indicate that the present group of subjects is typical of those used in the past for tracking studies. In addition, the fact that the plots of ρ^2 are equivalent indicates that the present use of a compensatory pilot model provides a fit to the human pilot that is at least as good as that obtained in the past for other tasks.

In general terms, the trends in the data as the preview is increased go far beyond a simple reduction in the open loop time delay term, although this effect is obviously present in the phase data. Quite surprising was

the observed shift to higher frequencies found in the resonant frequency attributed to the neuromuscular system. This can be noted from the amplitude plots where the resonant peak starts at about 18 rad/sec. for 0 sec. preview and is almost outside the measurement range by 0.2 sec. preview. In addition the low frequency amplitude characteristics are influenced by the preview, tending to flatten out as the preview approaches 0.2 sec. The correlation coefficient does not seem to be influenced to any extent by the amount of preview.

An 8 parameter pilot model of the form (Ref. 4)

$$Y_p(\omega) = Ke^{-j(\omega\tau+\frac{\alpha}{\omega})} \frac{(T_L j\omega+1)}{(T_I j\omega+1)} \frac{1}{(T_{N_1} j\omega+1)\left(\left(\frac{j\omega}{\omega_N}\right)^2 + \frac{2\zeta_N}{\omega_N} j\omega+1\right)}$$

was fitted to these plots by a computer program developed for the purpose. The results of this work are shown by the solid curves in Fig. 6 and the parameters in Table 1. One point of interest is the fact that for the 0 sec. preview case the program which started with an initial value of T_{N_1} = .09 sec. drove this term to zero to achieve the best fit.

The following general trends can be seen with increasing preview up to 0.2 sec.

(1) the subjects' DC gain term K increases.

(2) use is made of the preview feature of the display to reduce the time delay term, although the total potential reduction is perhaps not realized. (Note that the value of τ = 0.219 sec. at 0 sec. preview could be reduced in the model by insisting on the inclusion of the T_{N_1} term.)

(3) there is no apparent influence of preview on the lead term T_L. This may indicate that despite the advantages presented by the preview display, the subject wishes to achieve the maximum lead compensation possible even if it means the generation of T_L which requires some extra effort on his part.

(4) there is an associated increase in crossover frequency (ω_c) and reduction in phase margin Φ_m. See Table 1.

For large previews (0.4 and 0.8 sec.) the variability of the measured describing functions was much greater than for the small values of preview. In particular the inter-subject variability was too large to allow the data to be averaged. Fig. 7 illustrates typical measured describing functions for 0.4 sec. preview and Fig. 8 the same for 0.8 sec. preview. The majority of the describing functions measured for these large previews were similar in general form to those of subject 6, but showed larger fluctuations in amplitude and phase (as a function of frequency) and had much larger standard deviations. Note that the data shown for subject 3 represents only half of his tracking runs, the rest looking more like those for subject 6. The plots of the correlation coefficients indicate that the model fits for these preview values are generally as good as for the small previews.

The data represented by subject 6 is a reasonable extrapolation of the small preview data. The phase lag is further reduced at high frequencies, the neuromuscular resonance is beyond the measurement range and the amplitude plot is boosted at low frequencies. (We have not yet begun a detailed analysis and pilot model development for the large preview data.) Of note is the report by all subjects that for large previews they "followed the waves in" (from the right hand side of the screen to the tracking point). They generally focussed their attention about 1.5 to 2 in. (i.e. 0.3 to 0.4 sec. of preview, no measurements were taken) to the right of the tracking point. Any high frequency disturbances were followed visually to the tracking point in order that these rapid changes in input could be tracked accurately. High frequency in this case means any wave with apparent period less than twice the time interval of 0.3 to 0.4 sec., i.e. frequencies greater than about 8 rad./sec.

SUMMARY

1. The measured correlation coefficients indicate that a simple linear pilot model can be used to describe tasks with preview.

2. Preview had no influence on the lead term in the pilot model for previews of 0.1 and 0.2 sec.

3. In going from a preview of 0.2 sec. to 0.4 sec. it appears that a significant alteration in tracking technique takes place.

BIBLIOGRAPHY

1. Drewell, N. H. — "The Effect of Preview on Pilot Describing Functions in a Simple Tracking Task". To be published as UTIAS Tech. Note 176, 1972.

2. Reid, L. D. — "The Measurement of Human Pilot Dynamics in a Pursuit-Plus-Disturbance Tracking Task". UTIAS Report No. 138, April 1969.

3. Frostell, C. E. — "A Comparison of Pilot Describing Function Measurement Techniques". UTIAS Tech. Note No. 167, October 1971.

4. McRuer, D. Graham, D. Krendal, E. Reisener, W. Jr. — "Human Pilot Dynamics in Compensatory Systems". AFFDL-TR-65-15, 1965.

TABLE 1

Preview	K	τ	α	$1/T_L$	$1/T_I$	$1/T_{N_1}$	ω_N	ζ_N	ω_c	Φ_m °
0	0.44	0.22	0.08	0.23	2.09	-	18.33	0.08	3.3	75
0.1	0.81	0.10	0.0	0.24	1.41	19.34	20.67	0.08	4.6	60
0.2	1.04	0.02	0.0	0.22	4.70	2.45	21.56	0.12	6.5	40
0.4									11.5	75
0.8									11.5	105

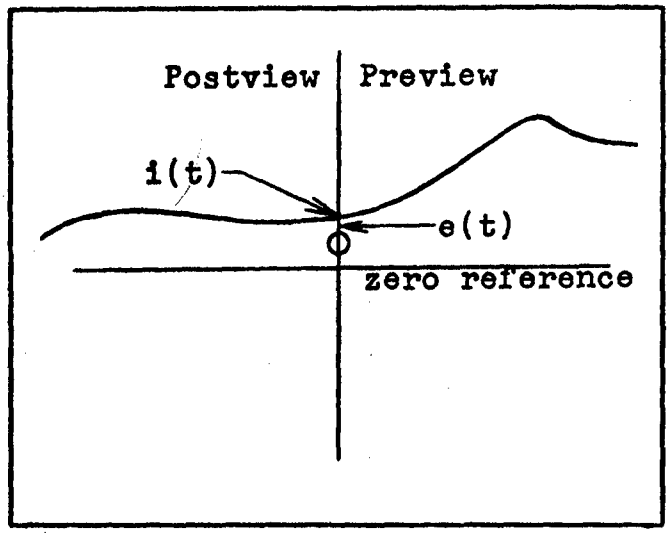

Schematic view of the preview display at time t.

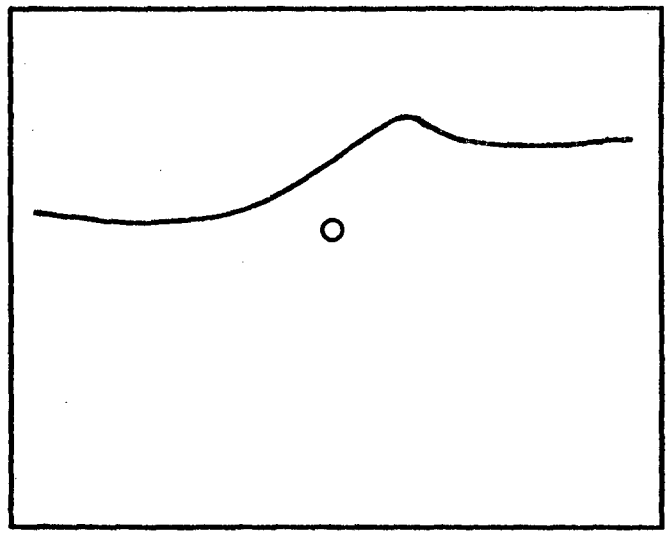

View at t+0.4 seconds

PREVIEW DISPLAY

FIGURE 1

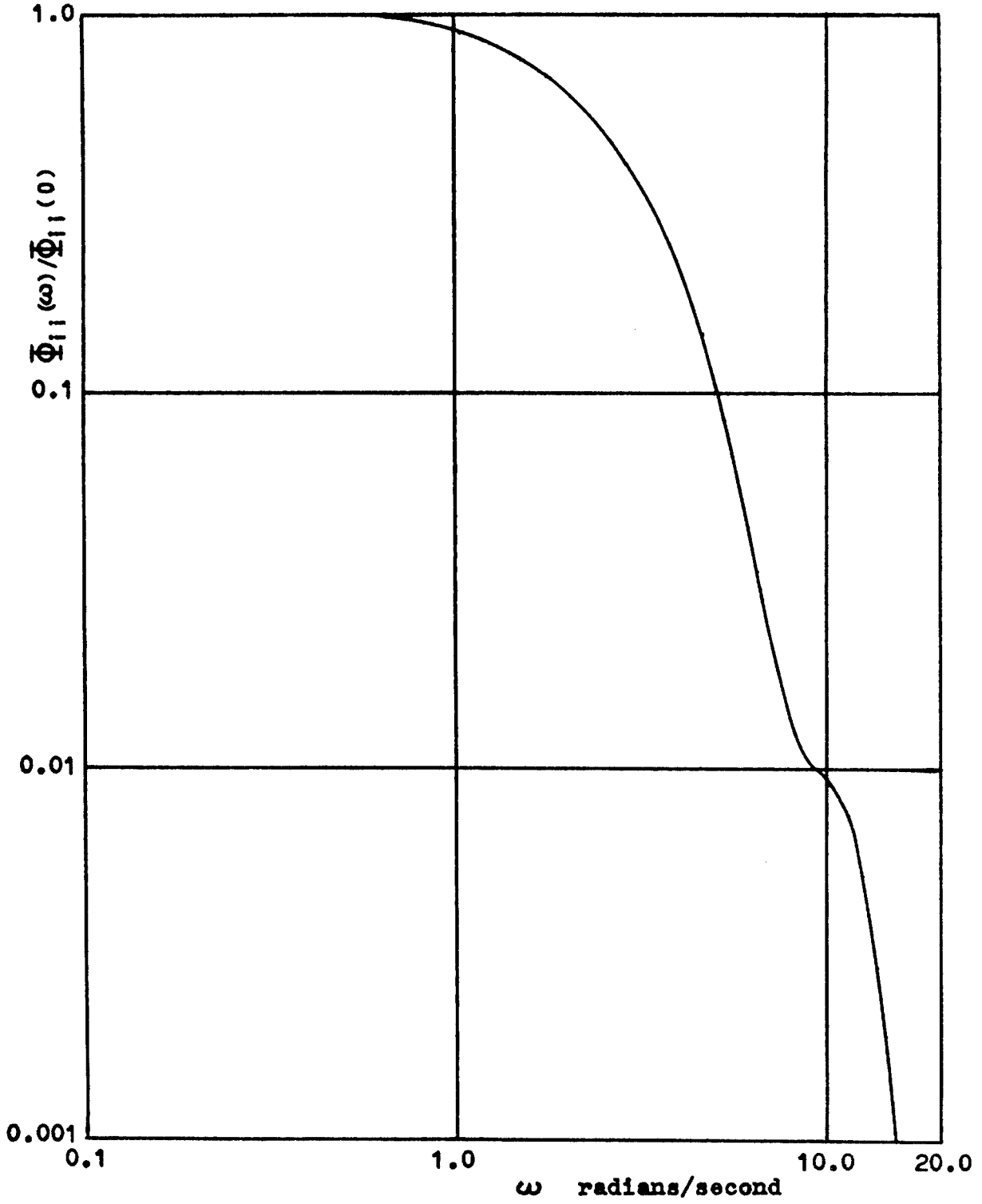

INPUT POWER SPECTRAL DENSITY

FIGURE 2

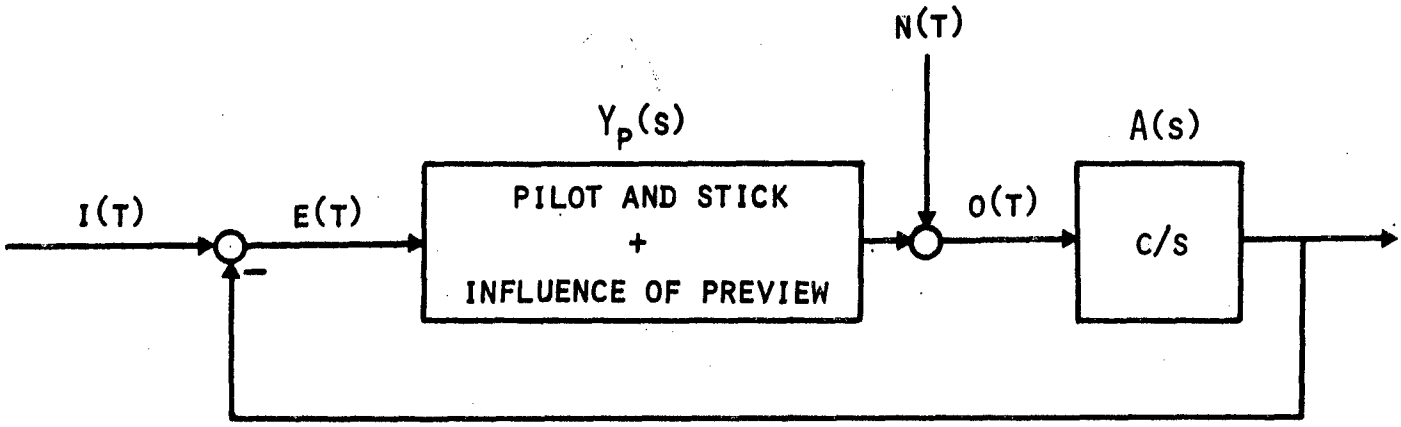

SIMPLE MODEL - PREVIEW TASK

FIGURE 3A

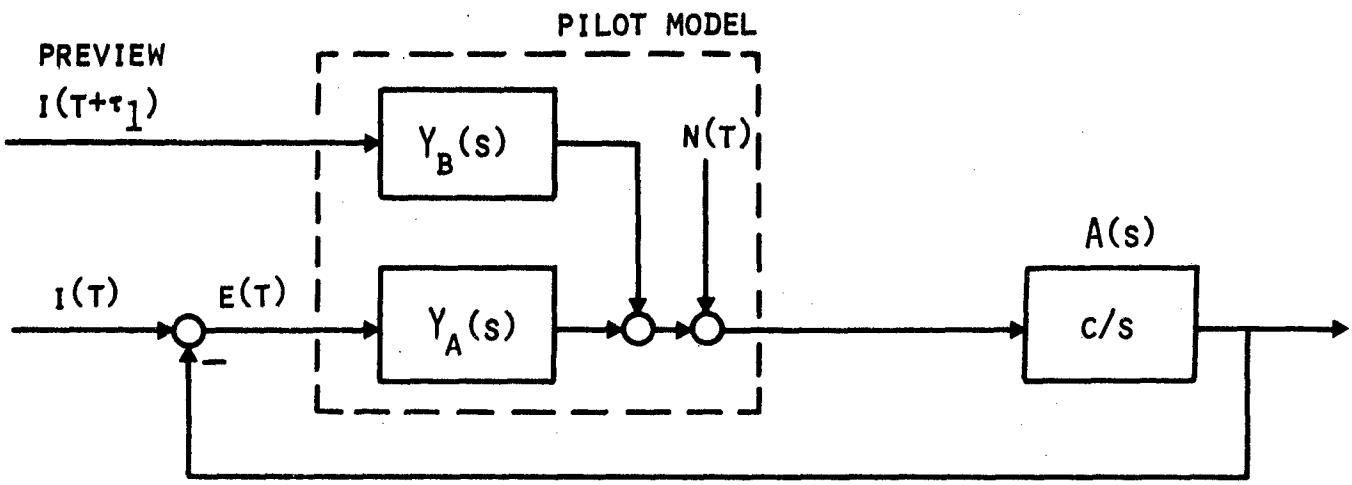

EXAMPLE OF COMPLEX MODEL-PREVIEW TASK

FIGURE 3B

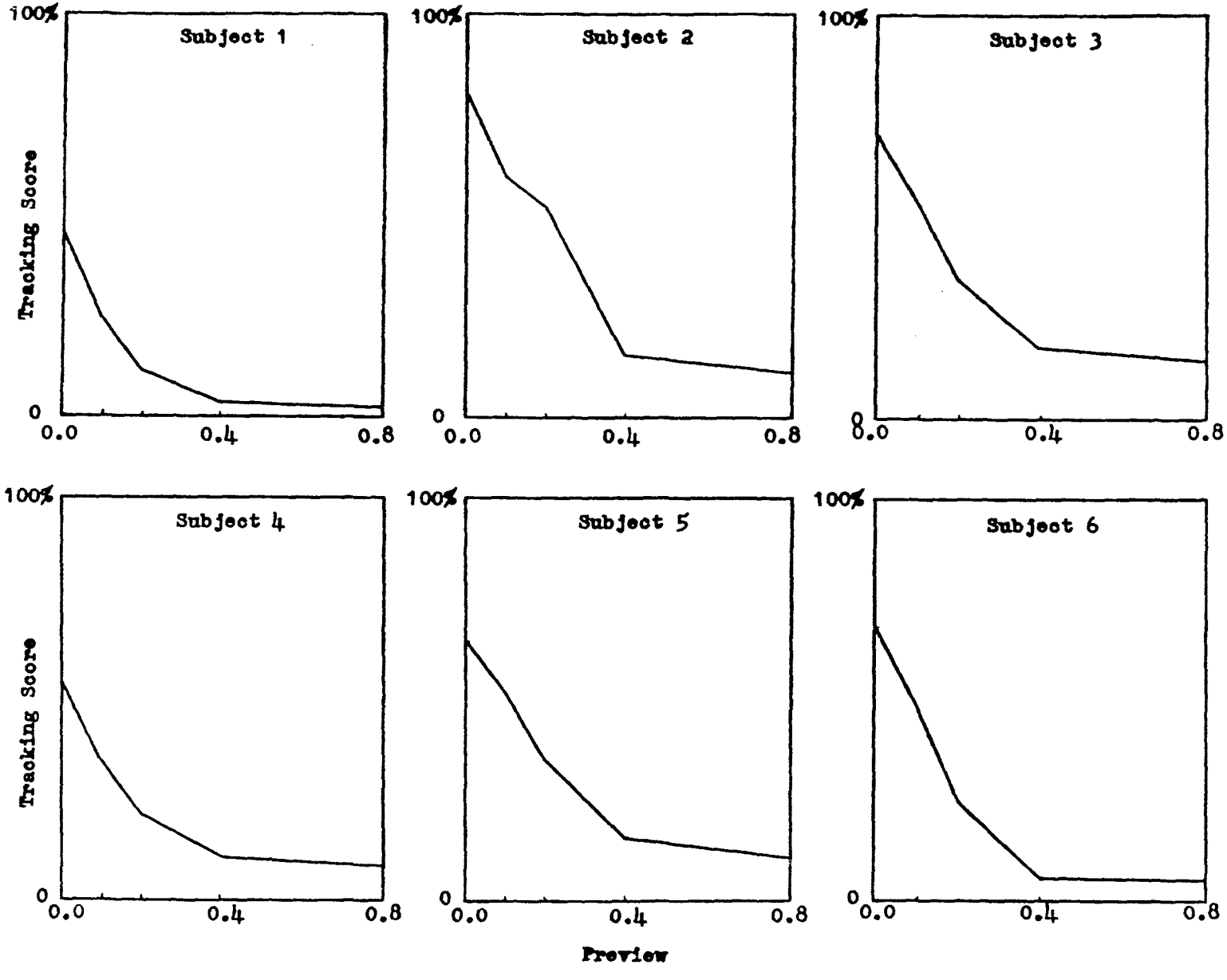

TRACKING SCORES

FIGURE 4

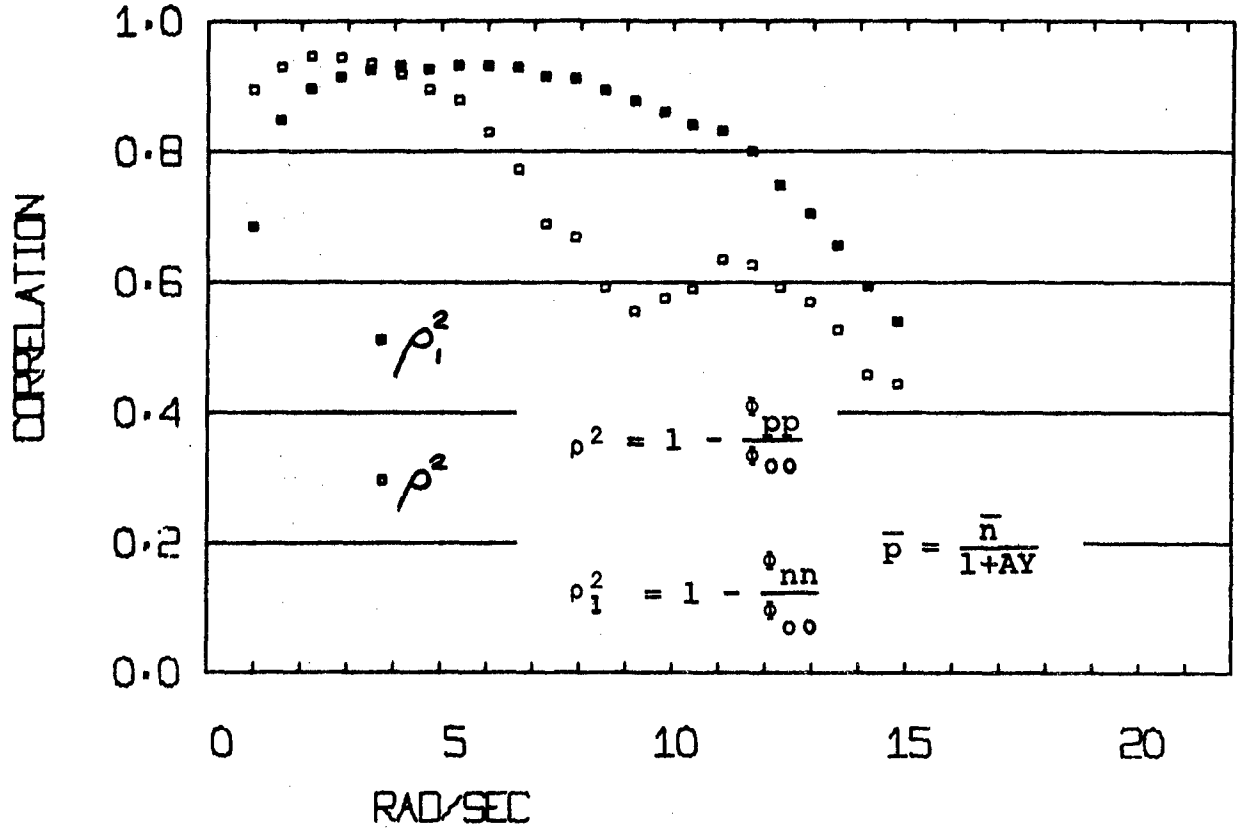

COMPARISON OF MODEL FIT PARAMETERS

FIGURE 5

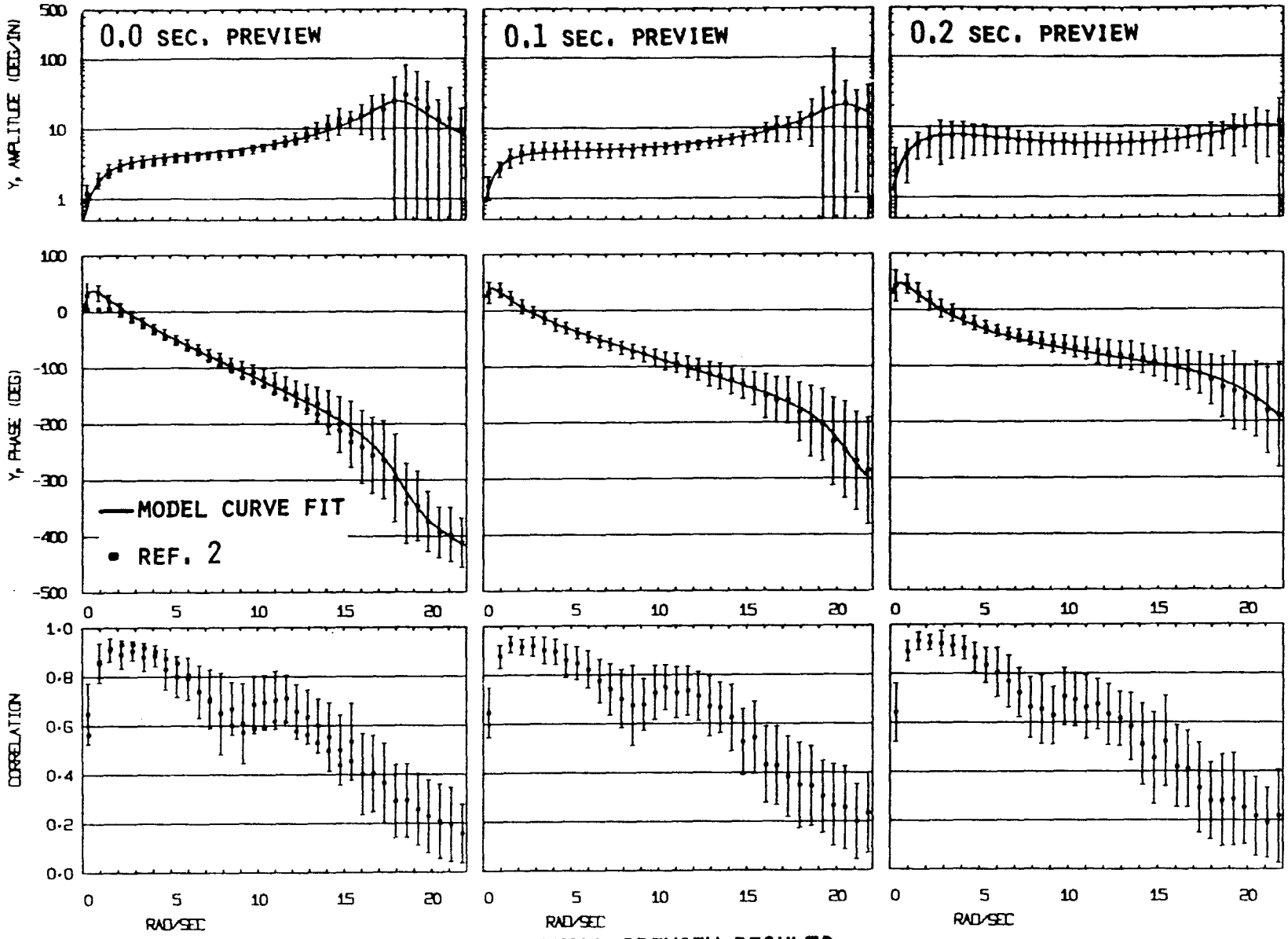

SMALL PREVIEW RESULTS

FIGURE 6

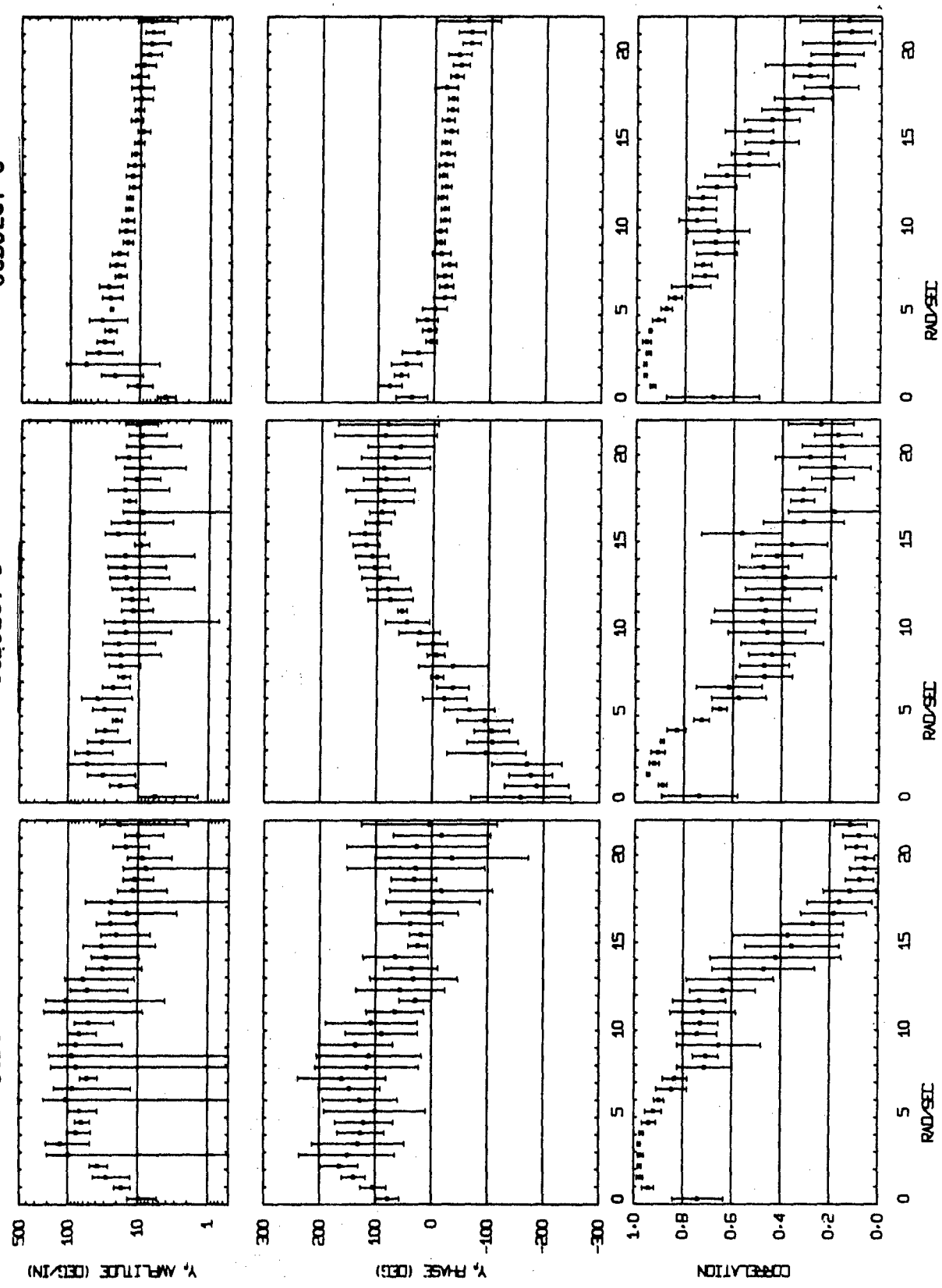

0.4 SEC. PREVIEW RESULTS

FIGURE 7

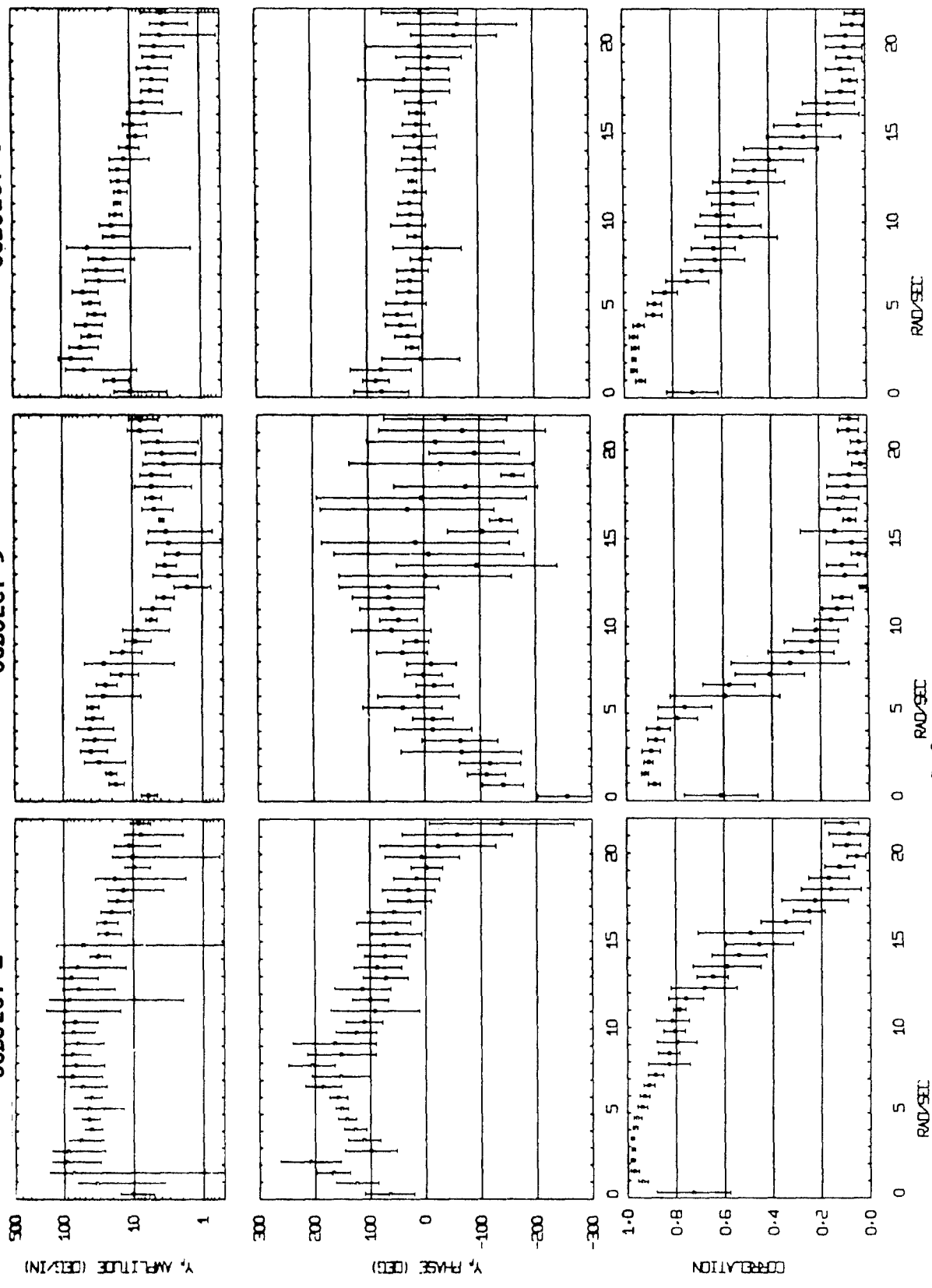
SUBJECT 1
SUBJECT 3
SUBJECT 6
Y, AMPLITUDE (DEG/IN)
Y, PHASE (DEG)
CORRELATION
RAD/SEC
0.8 SEC. PREVIEW RESULTS

FIGURE 8

SESSION V

Remote Manipulation and Other Control Strategies

THE MATHEMATICS OF COORDINATED CONTROL OF PROSTHESES AND MANIPULATORS

by Daniel E. Whitney

DuPont Associate Professor of Mechanical Engineering
Massachusetts Institute of Technology
Cambridge, Massachusetts 02139 USA

ABSTRACT

The problems of coordinated rate control and position control of multidegree of freedom arms are treated together in this paper. Previous work by the author is summarized and revised, and a coherent theory is presented which allows:

1) real time computer control
2) rate control commands expressed in a wide variety of external coordinate systems including hand-oriented coordinates, rectangular or spherical coordinates, or motion along special axes such as line of sight
3) any number of command axes to be activated simultaneously
4) solution of the position control problem by means consistent with the rate control problem, allowing desired final position to be specified in terms of meaningful external coordinates, and obviating the need for numerical search or solution of complicated equations to find the final joint angles
5) consistent treatment of redundant arms
6) attention to singularities
7) liaison to optimal control of dynamic models of arms

Work supported by NASA Contract SNPN-54 and
NASA Grant NGR-22-009-002.

Preceding page blank

Introduction

This report briefly summarizes the results of several years' work by the author and his colleagues on the development of coordinated motion control of computer-driven arms. The basic ideas are set out in reference [1], a first attempt at hardware realization is described in [2], and the latest and most successful realization is contained in [3], which also contains details of hardware and the contributions of many co-workers.

The objective of coordinated control is to allow the operator of a mechanical arm to command rates of the arm's hand along coordinate axes which are convenient, task-related, and visible to the operator. A useful set of coordinates, fixed to the hand itself, is shown in Figure 1. To accomplish such motions, several joints of the arm must move simultaneously at time-varying rates. This is extremely difficult to accomplish if conventional rate control (switches connected one-to-one to the joint motors) is used. Some means of coordinating the joint motions is needed, to resolve the useful command directions into the necessary joint motions. For this reason, the method described here is called resolved motion rate control. Previous work in this area by others is contained in [4] - [10].

The method allows commands to be exerted in a wide variety of coordinate systems in addition to that shown in Figure 1, using arms of any sufficient number of joints. Generally the minimum number of joints equals the number of command directions, but arms with extra joints can be accommodated. The commands in Figure 1 can be called for independently, or superposed in any proportions. For example, reach will occur without the hand's orientation in space changing, since reorientation is controlled by other commands.

Using the commands of Figure 1 as a base, we could mechanize spherical coordinates with arbitrary center, cartesian coordinates, motion along or about axes peculiar to some tool being grasped by the hand, and so on.

Computation of Resolved Rate for Hand-Oriented Commands

Figure 2 shows a manipulator hand with its attached coordinate frame plus $\underline{V}$, the velocity vector of that frame's origin, and $\underline{\Omega}$, the rotation rate vector about that origin. The frame ${}^1X$, ${}^1Y$, ${}^1Z$ represents the shoulder or base. The components of $\underline{V}$ along R, L and S give the reach velocity, lift velocity and sweep velocity respectively while $\underline{\Omega}$'s components give the rotation rates about these axes. A six element vector $\dot{\underline{S}}$ representing the command rates along hand axes may be written

$$\dot{\underline{S}} = \begin{bmatrix} \underline{V} \\ \hline \underline{\Omega} \end{bmatrix} \qquad (1)$$

Each component of $\dot{\underline{S}}$ may be expressed as a sum of coefficients times joint angle rates. Call the six joint angles $\underline{\Theta}$ and the six joint angle rates $\dot{\underline{\Theta}}$. Then $\dot{\underline{S}}$ and $\dot{\underline{\Theta}}$ are related by

$$\dot{\underline{S}} = \underset{\sim}{J}(\underline{\Theta}) \cdot \dot{\underline{\Theta}} \tag{2}$$

where each element in the six by six matrix $\underset{\sim}{J}(\underline{\Theta})$ depends on $\underline{\Theta}$ and is given by

$$\underset{\sim}{J}_{ij} = i^{th} \text{ component of } \dot{\underline{S}} \text{ per unit } \dot{\Theta}_j \text{ when all other } \dot{\Theta}_k = 0 \text{ for } j \neq k \tag{3a}$$

An equivalent expression for this is

$$\underset{\sim}{J}_{ij} = \text{partial derivative of the } i^{th} \text{ positional or angular coordinate of the hand with respect to the } j^{th} \text{ joint angle} \tag{3b}$$

Having obtained $\underset{\sim}{J}$, we may find the required $\dot{\underline{\Theta}}$ by inverting $\underset{\sim}{J}$ to obtain

$$\dot{\underline{\Theta}} = \underset{\sim}{J}^{-1} \dot{\underline{S}} \tag{4}$$

For example, if the user wants the hand to lift, (4) will generate the required $\dot{\underline{\Theta}}$. Since the commanded rotation rates are zero, the hand will not rotate while reaching but will keep a fixed orientation in space.

Calculation of J by Vector Cross Products

The vector cross product method [11] for computing J is indicated in Figure 3. A coordinate frame is assumed to be attached to each joint, the j^{th} frame at the j^{th} joint, $j = 1, \ldots, 6$, with the hand frame being the 7^{th} and frame 1 at the shoulder. O_j is the origin of frame j. In Figure 3, the j^{th} joint, the shoulder frame and the hand are shown, together with the unit vector $\underline{u}_j$ along the axis of $\dot{\Theta}_j$, the vector $\underline{b}_{j7}$ from O_j to O_7, and $\underline{V}_j$ and $\underline{\Omega}_j$ which result from $\dot{\Theta}_j$ if all other $\dot{\Theta}$'s are zero. Then

$$\underline{V}_j = \underline{u}_j \times \underline{b}_{j7} \cdot \dot{\Theta}_j \tag{5}$$

$$\underline{\Omega}_j = \underline{u}_j \cdot \dot{\Theta}_j \tag{6}$$

where all vectors are expressed in frame 1. Using vectors $\underline{V}_j$ and $\underline{\Omega}_j$ as is will allow us to obtain hand motion along or around frame 1 axes,

useful, for example, for generating lift along a fixed vertical axis. To obtain motion along or around frame 7 axes, we need to express $\underline{V}_j$ and $\underline{\Omega}_j$ in hand coordinates. This is done by multiplying by a 3 x 3 rotation matrix. The upper left 3 x 3 partition of $\underset{\sim}{AEQ}_7$* is called ${}^1\underset{\sim}{C}_7$ because it expresses frame 7 vectors in frame 1. Its transpose ${}^1\underset{\sim}{C}_7^T$ is ${}^7\underset{\sim}{C}_1$, which expresses frame 1 vectors in frame 7. Thus

$$ {}^1\underset{\sim}{C}_7^T \cdot \begin{bmatrix} \underline{V}_j \\ \underline{\Omega}_j \end{bmatrix} , \quad j = 1, \ldots, 6 \tag{7} $$

expresses $\underline{V}_j$ and $\underline{\Omega}_j$ in hand coordinates. Thus the ${}^7Y$ component of $\underline{V}_j$ is $\dot{\theta}_j$'s contribution to reach, and the ${}^7Y$ component of $\underline{\Omega}_j$ is $\dot{\theta}_j$'s contribution to twist. The column vector in (7), when divided by $\dot{\theta}_j$, gives the j^{th} column of $\underset{\sim}{J}$ according to (3). Thus

$$ \underset{\sim}{J} = {}^1\underset{\sim}{C}_7^T \left[\begin{array}{c|c|c|c} \underline{u}_1 \times \underline{b}_{17} & \underline{u}_2 \times \underline{b}_{27} & \text{etc.} & \underline{u}_6 \times \underline{b}_{67} \\ \hline \underline{u}_1 & \underline{u}_2 & & \underline{u}_6 \end{array}\right] \tag{8} $$

Although the Argonne E-2 has only turn joints, some manipulators have sliding joints. If the j^{th} joint is a slider then θ_j is fixed and s_j, the slide coordinate, is a variable. The j^{th} column of $\underset{\sim}{J}$ is then

$$ {}^1\underset{\sim}{C}_7^T \begin{bmatrix} \underline{V}_j \\ \underline{0} \end{bmatrix} / \dot{s}_j , \quad j = 1, \ldots, 6 \tag{9} $$

where $\underline{V}_j = \underline{u}_j \cdot \dot{s}_j$

and the lower 3 x 1 partition is zero. $\underline{u}_j$ is, as before, the unit vector along ${}^j\underline{Z}$, the slide direction as shown in Figure 3.

Other Coordinate Directions

As an example of other possible coordinate directions which can be mechanized, consider reach motion along a line of sight from an eye to the hand. Let the eye be at 0_8, the origin of frame 8. Then the desired reach motion is to be along the vector $\underline{b}_{87}$ and will be obtained if the

* $\underset{\sim}{AEQ}_7$ is a 4 x 4 transformation matrix which converts the position and orientation of frame 7 into the position and orientation of frame 1. See [3] for details.

second row of $\underset{\sim}{J}$ in (8) is replaced by

$$V'_j = (\underline{v}_j^T \hat{\underline{b}}_{87})/\dot{\theta}_j \qquad \text{for } j = 1, \ldots, 6 \qquad (10)$$

where conversion by ${}^1\underset{\sim}{C}_7^T$ is omitted, and

$\underline{v}_j = \underline{u}_j \times \underline{b}_{j7} \cdot \dot{\theta}_j$ as before

$\hat{\underline{b}}_{87}$ = unit vector along $\underline{b}_{87}$ expressed in frame 1 coordinates

$(\underline{a}^T\underline{b})$ = dot product of $\underline{a}$ and $\underline{b}$

Methods for Computing $\underset{\sim}{J}$

We have explored two methods for obtaining $\underset{\sim}{J}$ in real time. Each has some advantages. The first method used was numerical interpolation. For this, $\underset{\sim}{J}^{-1}$ was calculated at a number of joint angle values, corresponding to a center position, a positive extension and a negative extension for each joint, the other joints being centered when each joint was extended. This designated 13 points at which $\underset{\sim}{J}^{-1}$ was precalculated and stored. Values of $\underset{\sim}{J}^{-1}$ at arbitrary points were computed by interpolation with good accuracy. The value of this method lies in its use of read-only memory and fairly rapid computing time. Its disadvantage is that accuracy is preserved only within a region of θ values somewhat smaller than the arm's useful range.

The other procedure is to calculate $\underset{\sim}{J}$ using (8) in real time. This uses eraseable storage and takes slightly longer than the interpolation, but it allows almost unlimited motion of the hand. It is the method currently in use.

Extension to Position Control

For position to position control we assume that the hand is in some position and orientation such that $\underline{b}_{17}(\underline{\theta}_i)$ and ${}^1\underset{\sim}{C}_7(\underline{\theta}_i)$ are known, and that we desire the hand to move to a new position whose $\underline{b}_{17}(\underline{\theta}_f)$ and ${}^1\underset{\sim}{C}_7(\underline{\theta}_f)$ are given. $\underline{\theta}_f$ itself, the new joint angles, is not assumed to be known. Information in the form $\underline{b}_{17}(\underline{\theta}_f)$ and ${}^1\underset{\sim}{C}_7(\underline{\theta}_f)$ could come from a pointing system or other information source describing the location and grasp direction of some object we want grasped. Assuming that the hand is to move to the new position in a time interval T, we have

$$\underline{V} = {}^{1}\underset{\sim}{C}_{7}^{T}(\underline{\Theta})\,(\underline{b}_{17}(\underline{\Theta}_f) - \underline{b}_{17}(\underline{\Theta}_i))/T \tag{11}$$

= first three components of $\dot{\underline{S}}$ for use in eq. (4)

This says that $\underline{V}$ in hand coordinates sweep, reach, and lift is obtained from the initial vector difference in $\underline{b}_{17}$ (in shoulder coordinates) projected into current hand coordinates by ${}^{1}\underset{\sim}{C}_{7}^{T}(\underline{\Theta})$. The current $\underline{\Theta}$ must be obtained either by reading the joint angles or computing the integral

$$\underline{\Theta} = \underline{\Theta}_i + \int_0^t \dot{\underline{\Theta}}dt \tag{12}$$

The last three components of $\dot{\underline{S}}$ are obtained by finding an axis vector $\underline{\Omega}$ about which frame 7 should turn so as to change ${}^{1}\underset{\sim}{C}_{7}(\underline{\Theta}_i)$ into ${}^{1}C_{7}(\underline{\Theta}_f)$. A matrix C_{if} exists which will accomplish this rotation. These three matrices are related by

$${}^{1}\underset{\sim}{C}_{7}(\underline{\Theta}_f) = {}^{1}\underset{\sim}{C}_{7}(\underline{\Theta}_i)\underset{\sim}{C}_{if} \tag{13}$$

so that

$$\underset{\sim}{C}_{if} = {}^{1}\underset{\sim}{C}_{7}^{T}(\underline{\Theta}_i)\,{}^{1}\underset{\sim}{C}_{7}(\underline{\Theta}_f) \tag{14}$$

The desired rotation axis $\underline{\Omega}$ is the one vector in hand coordinates which is unchanged during this rotation. That is

$$\underset{\sim}{C}_{if}\underline{\Omega} = \underline{\Omega} \tag{15}$$

This means that $\underline{\Omega}$ is the eigenvector of $\underset{\sim}{C}_{if}$ with unit eigenvalue. The angle α through which frame 7 turns about axis $\underline{\Omega}$ may be obtained from examination of Figure 4. Here $\underline{\Omega}$ is the axis vector and is assumed to have been normalized to unit length. $\underline{X}$ and $\underline{X}'$ are the original and final unit vectors along the X axis of frame 7, described here for convenience in original frame 7 coordinates. α is measured in the plane normal to $\underline{\Omega}$. The X component of $\underline{\Omega}$ is Ω_x and by definition of $\underline{\Omega}$ this is the same as the $\underline{X}'$ component of $\underline{\Omega}$, $\Omega_{x'}$.

That is

$$\Omega_x = (\underline{\Omega}^T\underline{X}) = (\underline{\Omega}^T\underline{X}') = \Omega_{x'} = \text{first element of } \underline{\Omega} \tag{16}$$

The projection of $\underline{X}$ onto the plane normal to $\underline{\Omega}$ is $\underline{X} - \Omega_x\underline{\Omega}$ and the corresponding projection of $\underline{X}'$ is $\underline{X}' - \Omega_x\underline{\Omega}$. The dot product of unit vectors along these projections gives α:

$$\cos \alpha = \frac{(\underline{X} - \Omega_x \underline{\Omega})^T (\underline{X}' - \Omega_x \underline{\Omega})}{|\underline{X} - \Omega_x \underline{\Omega}| \cdot |\underline{X}' - \Omega_x \underline{\Omega}|} \tag{17}$$

$$= \frac{(\underline{X}^T \underline{X}') - \Omega_x^2}{1 - \Omega_x^2} \tag{18}$$

(In case $\underline{\Omega}$ lies along $\underline{X}$, this formula is inapplicable. Replace $\underline{X}$ with $\underline{Y}$ and $\underline{X}'$ with $\underline{Y}'$ in that case.)

Now that α is known, we need only scale $\underline{\Omega}$ by α/T and then take this as the rotational rate vector for frame 7. It is already expressed in frame 7, so its elements are directly the rates for tilt, turn, and twist, thus providing the last three elements of $\dot{\underline{S}}$. Barring numerical or servo errors, this $\dot{\underline{S}}$ will carry the hand to the new position and orientation. The calculation may be made closed loop (hence less error prone) by defining a new $\underline{\Theta}_1$ periodically along the trajectory, calculating a new $\underline{b}_{17}(\underline{\Theta}_1)$ and a new T for use in eq. (11), plus a new $\underset{\sim}{C}_{1f}$, $\underline{\Omega}$ and α.

This procedure is an improvement over numerical search methods [12] or direct analytical attacks on the geometric equations [13]. The former can have convergence difficulties while the latter are applicable only to certain types of arm configurations.

Dynamic Control of Arms

The previous sections have derived joint angle rate histories based on input commands and coordination constraints which are purely kinematic. In this section we discuss methods by which arms having inertia may be commanded to follow such trajectories. Previous work in this area is limited to a few papers, notably those of Kahn and Roth [14], which considers the minimum time control problem for a three-joint arm, and Monster [15], who studied stabilization and trajectory tracking problems in the Case Arm-Aid. The main roadblock to the study of dynamic control of arms is the sheer difficulty of obtaining the equations of motion. Progress made by Sturges [16] in computer-generation and, more important, computer-simplification of these equations has made possible the work described below. Computer equation generation requires great amounts of computer memory at present, so that arms with more than four joints have not yet been treated.

It is for this reason that a simple linearization method, applicable to arms with any number of joints, is valuable [17]. The equations of motion are obtained easily and quickly in numerical form by considering a linearization of Lagrange's equations. The result is the following

state variable representation:

$$\dot{\underline{s}} = \begin{bmatrix} \underset{\sim}{0} & \underset{\sim}{I} \\ -\underset{\sim}{\mathcal{M}}^{-1}\underset{\sim}{K} & -\underset{\sim}{\mathcal{M}}^{-1}\underset{\sim}{B} \end{bmatrix} \underline{s} + \begin{bmatrix} \underset{\sim}{0} \\ -\underset{\sim}{\mathcal{M}}^{-1} \end{bmatrix} \underline{\tau} \qquad (19)$$

where

$$\underline{s} = \begin{bmatrix} \underline{\delta\Theta} \\ \underline{\dot{\delta\Theta}} \end{bmatrix} \qquad (20)$$

is the 2N x 1 state vector containing angular and angular rate deviations from nominal. All the submatrices in (19) are N x N. $\underset{\sim}{\mathcal{M}}$ represents inertia, $\underset{\sim}{B}$ is a diagonal matrix of damping terms at each joint, $\underset{\sim}{K}$ is a diagonal matrix of spring constants across each joint, and $\underline{\tau}$ is an N vector of the torque sources. A simple and fast computer program returns numerical expressions of the matrices in (19).

Since (19) can easily be shown to be controllable, standard optimal regulator theory can be used to stabilize it about this nominal. Since this requires measurement of both $\underline{\delta\Theta}$ and $\underline{\dot{\delta\Theta}}$, it is useful to know that the system is observable using only measurements of $\underline{\delta\Theta}$.

A trajectory control scheme was developed by assuming that the above equations applied to the whole state rather than to deviations from nominal [18]. Optimal linear servo theory [19] was used to develop feedback gains and control functions. These were then applied to simulation equations representing all dynamic nonlinearities. A typical result is shown in Figures 5A and 5B, in which angles are in radians and torque in foot-pounds. Although the arm moves at a leisurely pace, the errors are quite small, as are the required torques.

Conclusions

We have presented a unified theory of kinematic rate and position control of computer-driven arms, providing coordination in a variety of coordinate systems. Progress in dynamic control is also described and it is concluded that standard techniques are capable of providing adequate performance when the speed of the arm is not excessive.

References

1. Whitney, D. E., "Resolved Motion Rate Control of Manipulators and Human Prostheses," IEEE Trans. on Man-Machine Systems, v. MMS-10, no. 2, June, 1969, pp. 47-53.

2. Lesser, E., and T. Turai, "Demonstration of Resolved Motion Rate Control," SM Thesis, MIT Mech. Eng. Dept., June, 1970.

3. "First Annual Report for the Development of Multi-Moded Remote Manipulator System," C. S. Draper Laboratory (Division of MIT) Report C-3790.

4. Johnson, E. G., and W. R. Corliss, "Teleoperators and Human Augmentation," NASA SP-5047.

5. Moe, M. L., and J. T. Schwartz, "A Coordinated, Proportional Motion Controller for an Upper-Extremity Orthotic Device," in Proc. of 3rd International Symposium on External Control of Human Extremities, Dubrovnic, August, 1969.

6. Greeb, F. J., "Equations of Motion for Control of an Upper Extremity Splint Structure," MS Thesis, Univ. of Denver, May, 1970.

7. Apple, H. P. and P. L. Lawrence, "A Seven Degree of Freedom Digital Incremental Electric Orthotic Arm," presented at the 8th Annual International Conference on Medical and Biological Engineering, Chicago, July, 1969.

8. Gavrilović, M. M., and M. R. Marić, "An Approach to the Organization of the Artificial Arm Control," in Proc. of 3rd International Symposium on External Control of Human Extremities, Dubrovnic, August, 1969.

9. Wirta, R. W., and D. R. Taylor, "Multiple-Axis Myoelectrically trolled Prosthetic Arm," Final Report, Krusen Center, Moss Rehabilitation Hospital, Philadelphia, Sept., 1970.

10. Simpson, D. C., "An Experimental Design for a Powered Arm Prosthesis," Health Bull., vol. 23, no. 4, Sept., 1965, pp. 75-78.

11. Klumpp, A., "Resolved Motion Rate Equations for a Mechanical Arm," unpublished MAT memo #32, in ref. 3 above, pp. 163-70.

12. Whitney, D. E., "Optimum Stepsize Control for Newton-Raphson Solution of Nonlinear Vector Equations," IEEE Trans. Auto. Control., v. Ac-14, no. 5, Oct., 1969, pp. 572-74.

13. Pieper, D. L. and B. Roth, "The Kinematics of Manipulators Under Computer Control," Proc. 2nd International Conference on the Theory of Machines and Mechanisms, Warsaw, Sept., 1969.

14. Kahn, M. E. and B. Roth, "The Near Minimum-Time Control of Open-Loop Articulated Kinematic Chains," Trans. ASME v. 93, series G, no. 3, Journal of Dynamic Systems, Measurement, and Control, Sept., 1971, pp. 164-172.

15. Monster, A. W., "On Some Control Problems in the Case Research Arm-Aid, MK-II," Engineering Design Center Report No. EDC 7-66-14, Case Western Reserve Univ., 1966.

16. Sturges, R. H., "Progress Report on Digital Simulation," unpublished memo no. MAT-20, C. S. Draper Laboratory (Division of MIT), August, 1971. (A review of this material appears in ref. (3).)

17. Lynch, P. M., "A Mathematical Model of Mechanical Manipulator Cynamics," SM Thesis, MIT Mech. Eng. Dept., June, 1970.

18. Townsend, A. L., "Linear Control Theory Applied to a Mechanical Manipulator," SM Thesis, MIT Mech. Eng. Dept., Jan., 1972.

19. Bryson, A. E., and Y. C. Ho, Applied Optimal Control, Blaisdell, 1969, Chapter 5.

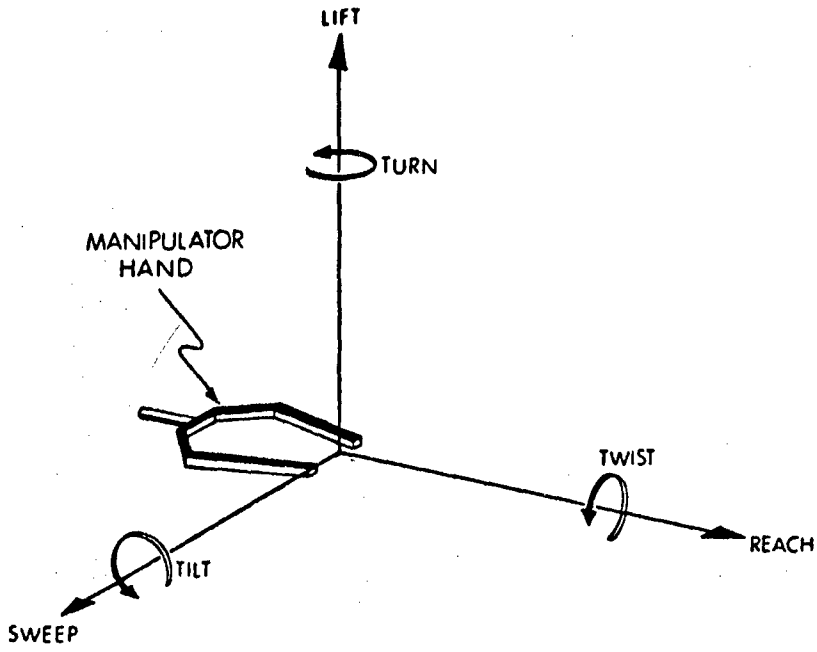

Figure 1 Hand with Hand-Oriented Coordinate System

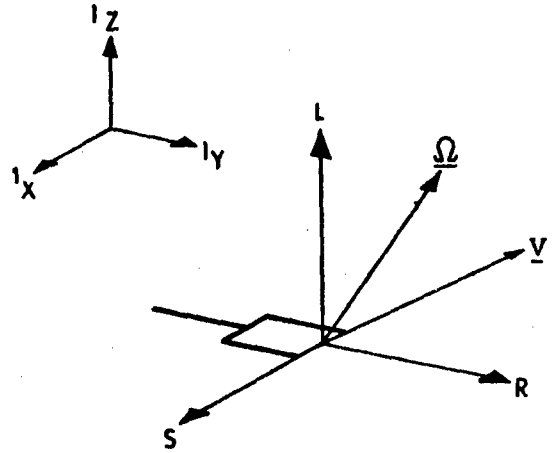

Figure 2 Hand Coordinates Related to $\underline{V}$ and $\underline{\Omega}$

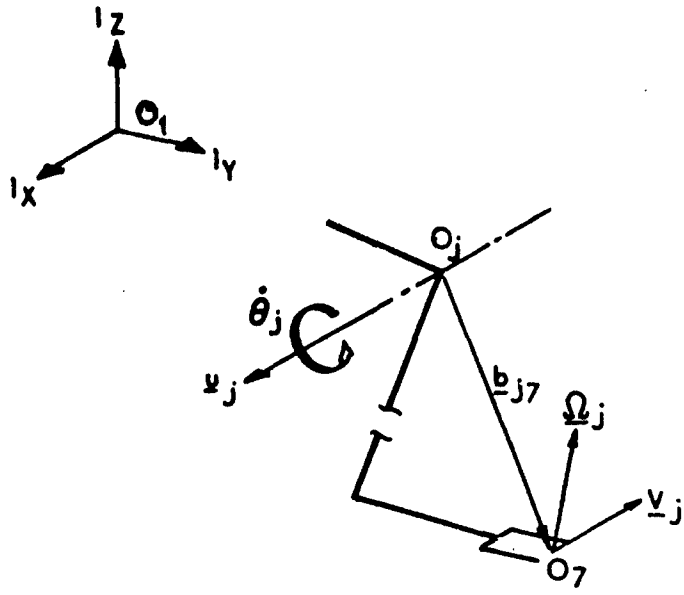

Figure 3 Illustration of Vector Cross-Product Method for Computing J

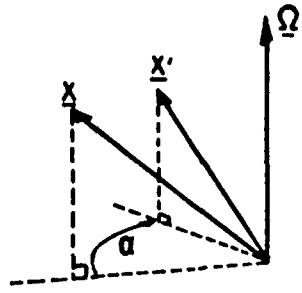

Figure 4 Definition of Angle α

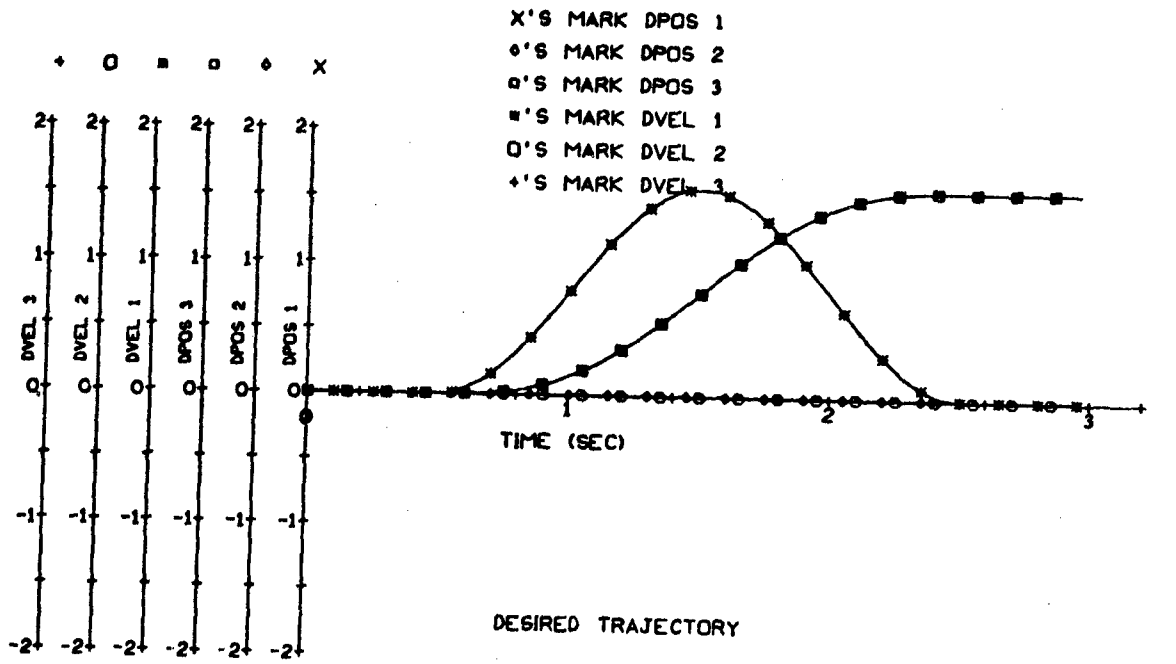

DESIRED TRAJECTORY

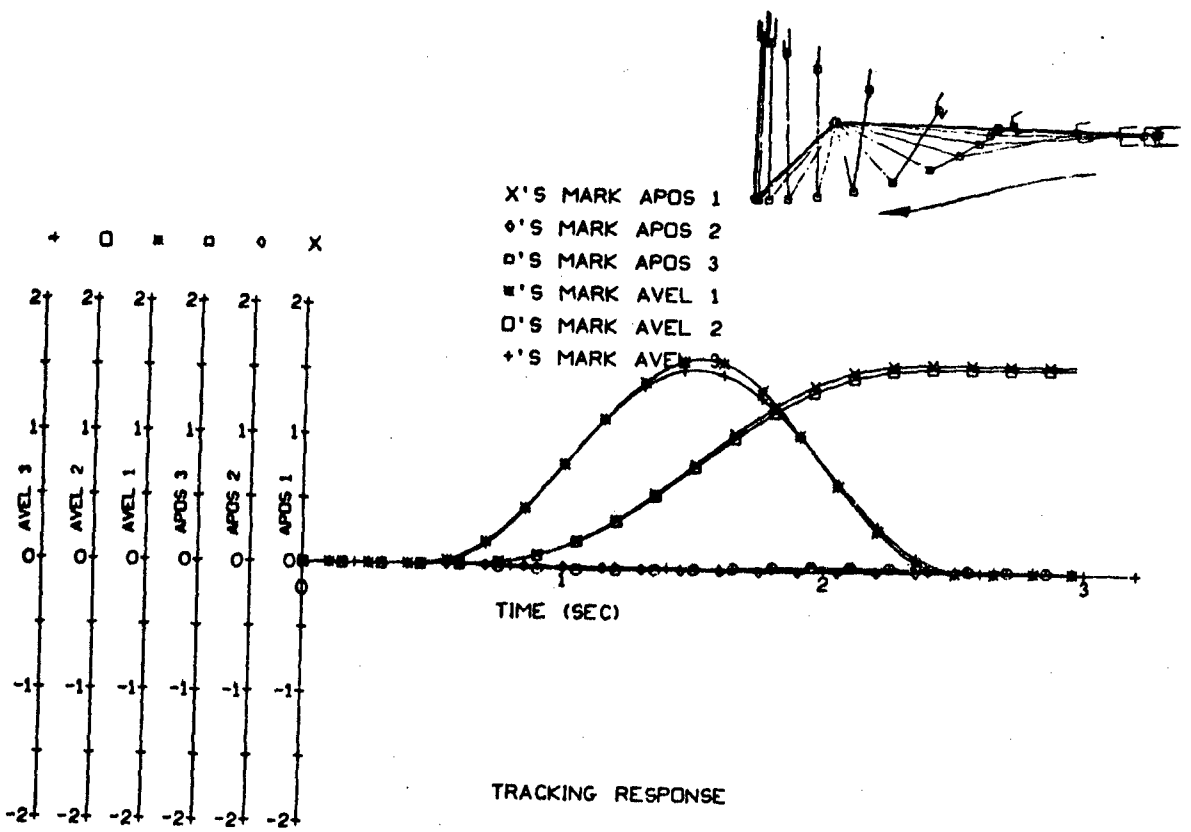

TRACKING RESPONSE

THREE LINK ARM TEST NO. 21 SHEET A

Figure 5A

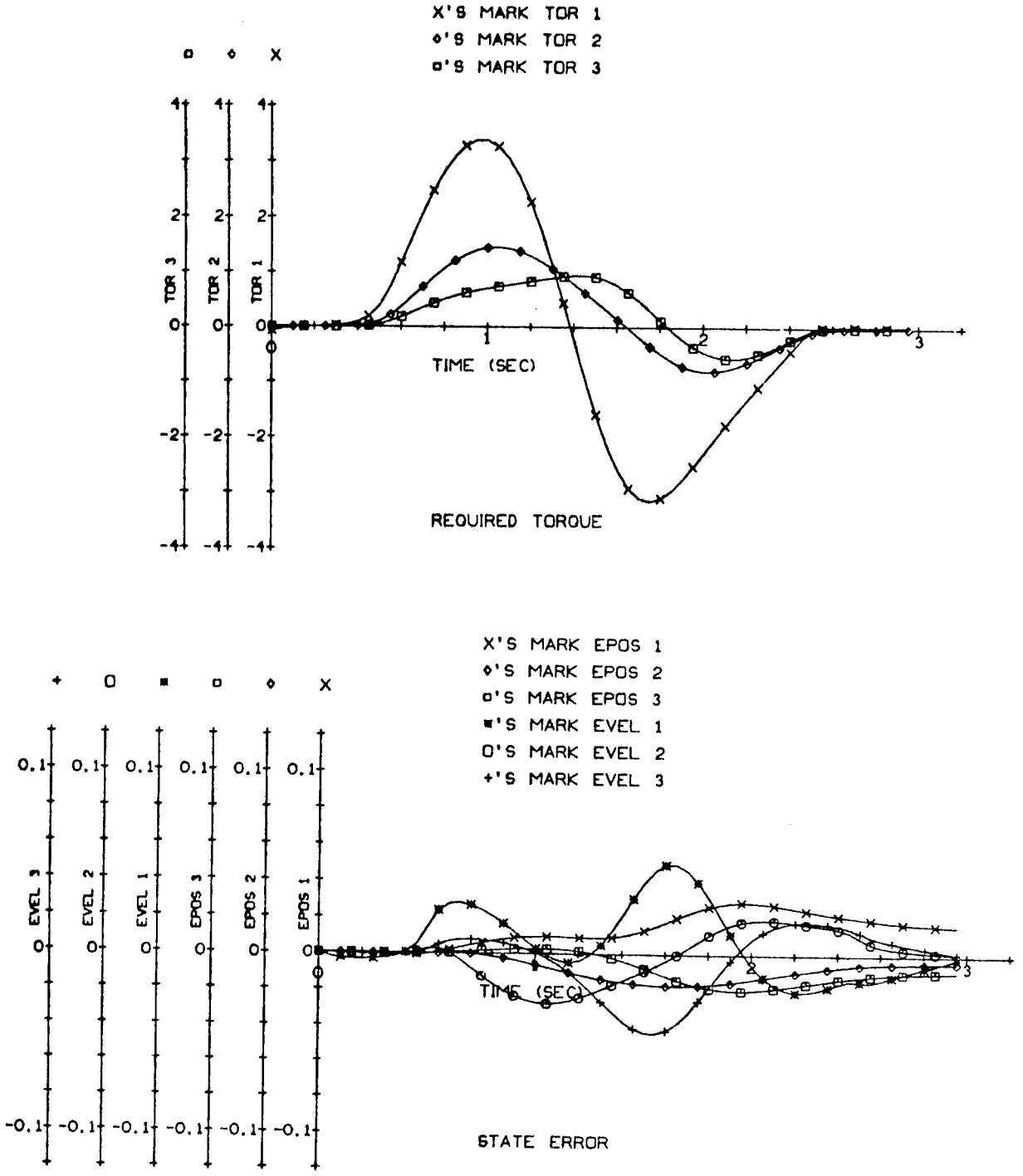

THREE LINK ARM TEST NO. 21 SHEET B

Figure 5B

ACTIVE FORCE FEEDBACK RATE CONTROL OF MANIPULATORS

by Paul Michael Lynch* and Daniel E. Whitney**

*Research Assistant, Department of Mechanical Engineering
**DuPont Associate Professor of Mechanical Engineering
Massachusetts Institute of Technology
Cambridge, Massachusetts 02139 USA

ABSTRACT

A one-dimensional model was developed for a rate control manipulator with force feedback. A control stick with force feedback capability was coupled with an analog computer simulating a manipulator. Subjects were asked to perform simple manipulation operations with the simulated manipulator using the control stick. Subjects' performance using rate control with force feedback was compared to their performance using other manipulation schemes. Certain refinements were made to the rate control with force feedback.

This research was supported in part by NSF contract SNPN54.

Introduction

The purpose of this research is to investigate the possibilities and limitations of rate control with force feedback to the operator's control stick. Conceivably, compact rate control devices could be used to guide manipulators over large domains with no loss of precision. Force feedback not only aids in the completion of manipulation tasks, but the force feedback may also provide information to the operator which may be obtained in no other way.

The plan of the research is to develop a model for force feedback rate control and to simulate this model on an analog computer. A subject with a control stick equipped with force feedback attempts to control the simulated manipulator on a display screen. His performance is measured and compared to his performance using other schemes of manipulation.

System Model

A one-dimensional model of rate control with force feedback was chosen. In this model, there is one dimension of control stick position and one dimension of manipulator position. The manipulator is modeled simply as shown in Figure 1. The manipulator consists of a mass m moved by a motor. A rate sensor detects the speed with which the motor moves the mass. Damping resists the motion of the manipulator. On the end of the mass is a massless bumper spring. If the manipulator encounters a barrier, this bumper spring is compressed between the mass and the barrier. It is the force which is transmitted through this bumper spring which is the basis for the force feedback to the operator's control stick. The bumper spring is compressed only when the manipulator encounters a barrier; forces required to accelerate the mass by the motor are not felt by the bumper spring.

Figure 2 shows a block diagram of the manipulator dynamics. The stick position is transformed by feed forward coefficient C into a commanded manipulator velocity $\dot{x}_c$. The difference between the commanded manipulator velocity $\dot{x}_c$ and the actual manipulator velocity $\dot{x}_a$ is transformed by the motor constant M into a force on the manipulator mass m. Other forces on the mass arise from the damping of the manipulator motion and forces arising from an encounter with a barrier.

From the force sum on the manipulator mass, its acceleration, velocity, and position are computed. The force through the bumper spring is multiplied by force feedback coefficient K_{fb} to produce the force applied to the control stick.

Note that if the manipulator is stopped at a barrier, then the force with which the bumper spring is compressed is proportional to the displacement of the control stick. Hence, once an encounter with a barrier is made, the control stick becomes a manipulator force control. No force can be maintained by the manipulator against the barrier if zero velocity (that is, zero force) is commanded with the control stick.

Experimental Plan

The plan of the experiment is to couple an analog computer simulating a manipulator with a control stick equipped with a force feedback capability. The manipulator appears as a dot on a display screen, and subjects are asked to perform simple manipulation operations by controlling the dot with the control stick. The analog computer makes changing manipulator designs easy, and also allows easy measurement of all variables. Examples of data that may be taken are operation completion time, final manipulator position error, maximum force felt by manipulator, or phase plane plots of the control stick motion or manipulator motion.

The control stick is simply a shaft mounted on and at right angles to the shaft of a torque motor. The position of the torque motor shaft, and consequently the position of the control stick, is measured by a potentiometer connected to the torque motor shaft. The torque motor is driven by a large operational amplifier controlled by the analog computer.

A cam is mounted on the torque motor shaft. This cam operates switches which are used to produce dead zones in the velocity commanded by the control stick. Hence, a small range of stick positions around zero position actually produces a zero command velocity. The dead zone is added to make it easier to command exactly zero manipulator velocity.

Experiments

The first series of experiments involved a simple manipulation operation. The subject was asked to move the manipulator from a starting position to a position next to a barrier. He was asked to perform the operation as quickly as possible, to bring the manipulator to rest as close as possible to the barrier without compressing the bumper spring, and to encounter the barrier with as little force as possible. Subjects performed with visual feedback and no force feedback, with force feedback and no visual feedback, and with both force feedback and visual feedback.

It was clear from the first experiments that rate control with force feedback was quite stable, depending upon the system parameters. A Routh criterion analysis which assumes simple dynamics for the control stick and human arm shows that unstable behavior could occur for large values of the feedforward or feedback coefficients, i.e., the coefficients between stick position and commanded velocity and between force through the bumper spring and feedback force produced on the control stick. In fact, unstable behavior was produced experimentally by raising these coefficients to large values. However, satisfactory manipulation was achieved with modest values of these coefficients, and therefore instability was not a problem in the experiments.

When the subjects were positioning the manipulator against the barrier without force feedback, their errors seemed to depend almost entirely on how accurately they could estimate the position of the dot. The relative positioning accuracy between visual feedback alone and force feedback alone seemed to depend on the relative sensitivity of the two feedback channels for a particular set of task and manipulator parameters. For example, the stiffer the bumper spring, or the greater the force feedback coefficient, the more sensitive the force feedback would be to the presence of the barrier, and the more accurately the subject could position the dot with only force feedback.

When subjects had force feedback available, they tended to find the edge of the barrier either by moving the manipulator very slowly and stopping when they felt a slight force, or by encountering the barrier to feel a force, then backing the manipulator off slowly until the manipulator stopped with no force feedback being felt. When the manipulator is just touching the barrier, there is no compression of the bumper spring; hence, there is no force feedback to the control stick. Finally, when the subject was attempting to back the manipulator off slowly from an encounter, certain ranges of manipulator dynamics made the manipulator tend to bounce off the barrier. If the subject was performing with no visual feedback, he had no way to tell how far off the barrier he had bounced.

Two means of improving positioning accuracy were considered. One method was to create a sharp change in the level of force feedback at the beginning of the bumper spring compression, either by adding a force derivative feedback term to the proportional force feedback or by introducing a simple step in force feedback at the beginning of spring compression. The second method was to adjust the manipulator dynamics so that the manipulator will not bounce off the barrier if the subject brings the control stick to zero after he has hit the barrier. This method would require that the subject have a means to know when he has commanded zero velocity. The second series of experiments concerned these possibilities for improving positioning accuracy.

The addition of the force derivative feedback had a serious fault in that the more slowly one encountered the barrier, the smaller the step produced in the force feedback. Hence, the force derivative feedback disappeared just when it was needed.

Large steps added to the force feedback at the beginning of spring compression were confusing to the operator and could lead to unstable behavior. The steps moved the subject's hand and the control stick and also stimulated reflex actions by the subject, all of which led to unsatisfactory performance. Small steps, however, gave the information needed without moving the subject's hand noticeably. Consequently, errors in positioning were markedly decreased by the addition of the small step to the force feedback.

The smallest positioning errors were achieved by adjustments made to manipulator dynamics to prevent bounce off. A microswitch detent arrangement was connected to the control stick so that the detent was located at zero command velocity. To position the manipulator, the subject would simply encounter the barrier, then bring the command speed to zero by moving the control stick into the detent and holding it there if necessary. The manipulator dynamics would bring the manipulator to rest exactly next to the barrier. This scheme does not depend on any method of feedback once the encounter is achieved. Hence, positioning errors were essentially zero for cases using force feedback with no visual feedback, visual feedback with no force feedback, visual and force feedback, and even with no feedback at all.

Conclusions and Further Research

With proper design, rate control with force feedback is a stable manipulation scheme. In addition, rate control with force feedback can be used to perform manipulation tasks without visual feedback--tasks that could not be performed at all in systems without force feedback.

Experiments are in progress which involve more complicated one-dimensional manipulation operations. Examples of these are to use the manipulator to push along a box with Coulomb friction, or to try to push such a box into a detent. Experiments are also being done in which subjects must complete their tasks under time limits or maximum force limits, or both. Finally, research will be done comparing rate control with force feedback to position control with force feedback.

FIGURE 1: MANIPULATOR MODEL

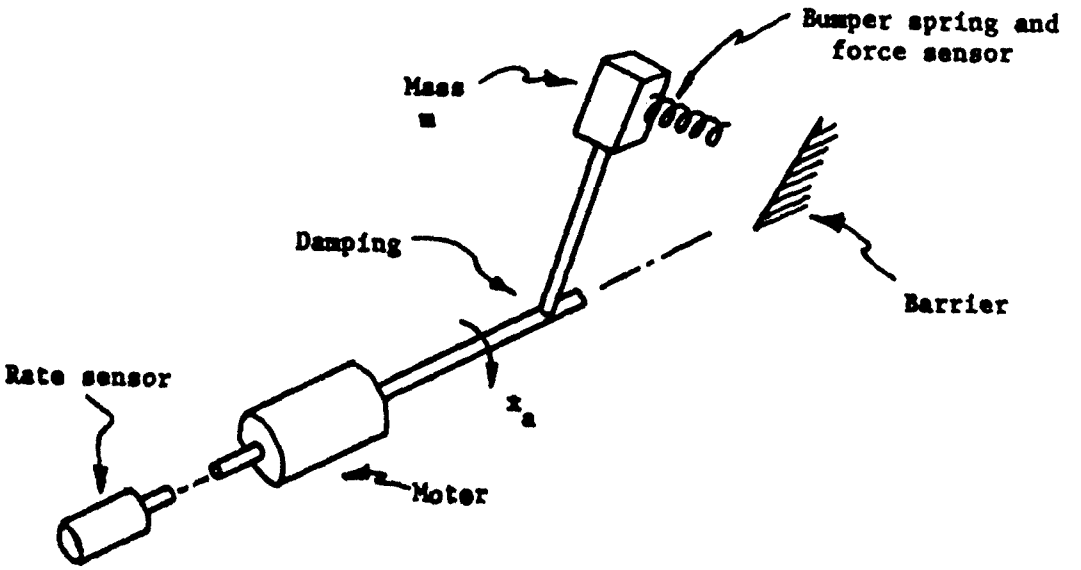

FIGURE 2: MANIPULATOR DYNAMICS BLOCK DIAGRAM

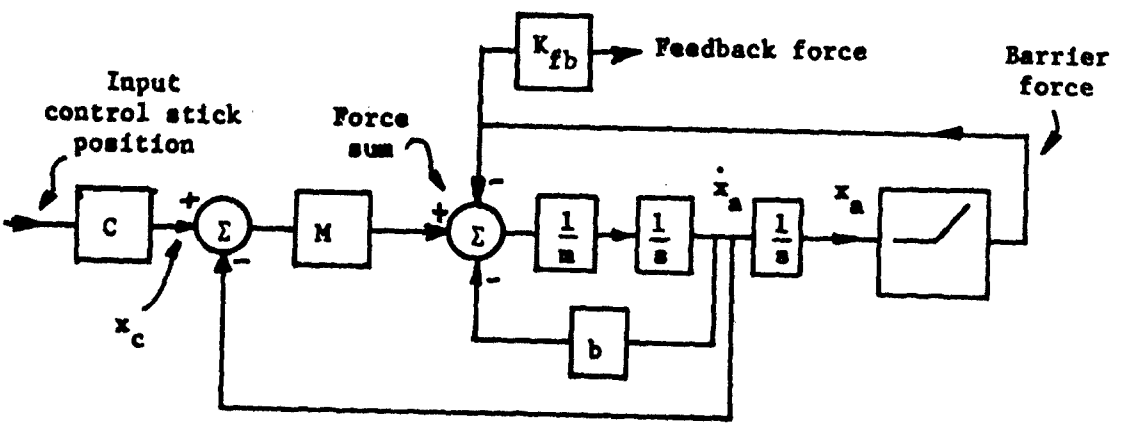

Interactive Aspects of Control by Man and Learning Machine

Amos Freedy
Gershon Weltman
John Lyman
Frederick C. Hull

Perceptronics, Inc. Encino, Calif. and UCLA

A new concept for improving performance in man-machine control systems by sharing control responsibility between the human operator and a "learning" automaton has been developed. The automaton is able to observe the operator's responses, learn the task at hand, and take appropriate control actions.

The automaton, termed as an Autonomous Control Subsystem (ACS), is based on a mathematical model of learning and decision making and is implemented on a digital computer. Its purpose is to relieve the operator of routine or exacting control requirements, reduce his information-handling load and permit him to concentrate on his most effective role as an initiator and supervisor.

Technical description of the ACS was provided in an earlier publication* (where the ACS was used to control a remote manipulator). This paper describes a study for establishing the "rules" which govern the interaction between the human operator and the adaptive aiding system. A series of studies examine the effect on system performance of such factors as: decision feedback amounts and mode, computer learning rate and machine decision criteria.

---

* Freedy, A. et al "A Computer-Based Learning System for Remote Manipulator Control", IEEE Trans. on Systems, Man and Cybernetics, Vol. SMC-1, No. 4, Oct. 1971, pp. 356-363.

Initial work with the ACS revealed that in addition to problems of purely technical interest, it introduces a novel and unfamiliar dimension to the man-machine relationship: this is the ability of the operator to derive optimum help from a system which generates its own behavioral patterns. This paper introduces specific observations and problems associated with such a system.

Factors of importance to this new relationship include how the operator approaches his shared task, as well as how closely the ACS is adjusted to fit the operator's capabilities. For example, the learning rate of the machine is adjustable -- the basic question is how closely this rate should match the normal operator's learning rate, and how it affects the operator's performance.

A related problem is the Feedback aspect of the system. Here the question is what type of feedback the operator must have from the learning system (in addition to the normal required feedback which is associated with operator control). There are a number of possibilities, among them is to provide a display which indicated to the operator the level of experience the learning system has acquired. Such information can be transformed into a certainty measure which will indicate to the operator what decision is to be made, and its level of certainty.

The study is based on a generalized control task simulation. A square task space is defined on a 10 X 10 oscilloscope screen. The task involves moving a spot cursor over the entire task domain through a simulated environment of obstacles. The task conceivably represents a number of real control situations. As the control process is configured training of the ACS to aid the operator occurs "on the job". The operator performs the task manually while he is being monitored. As operation continues the aiding system learns from the operator the control strategy and begins to take over control. The learning system is implemented on an Interdata Model-70 computer which is interfaced for on-line real-time operation.

This paper provides a discussion of the system parameters that are studied and a description of the experimental techniques used. The following system aspects are described:

(1) How are typical tasks relearned by the aiding system and the operator individually and in combination.

(2) How major system variables effects task learning.

(3) Can the operator evaluate accurately the help of the aiding system and can he devise optimum help from it.

(4) What human factors design features improve the transfer of information between the operator and the adaptive aiding mechanism.

Mapping an Operator's Perception of a Parameter Space: II

Richard Jagacinski

University of Michigan

Abstract[1,2]

Operators adjusted the parameters of one of two crossover models having independent inputs on the basis of pursuit displays of their respective input and output signals. The operators' task was to make discrete, real-time adjustments of either gain, k, and time delay, τ, or of gain, k, and closed-loop natural frequency, ω_n, of one of the models until its behavior matched the style of tracking behavior exhibited by the other fixed model. The average adjustment tendencies for each of the two sets of adjustment controls were plotted in a two-dimensional (τ,k) parameter space. The adjustment patterns in the (τ,k) space showed striking individual differences as well as overall similarities among subjects. There were also large differences between the adjustment patterns for the two sets of adjustment controls. However, this difference could not be taken as strong evidence against the existence of a basic underlying two-dimensional perceptual space, because a city-block metric rather than a Euclidean metric was used to define optimal performance.

Introduction

When one goes about analyzing the behavior of a dynamic system via formal mathematical techniques, there are certain parameters that emerge from the analysis as convenient descriptors of system behavior. For example, in describing compensatory tracking in terms of differential equations, the parameters of open-loop gain, k, and effective time delay, τ, in the McRuer Crossover Model are two such convenient descriptors. A whole family of different tracking behaviors ranging from very sluggish to very oscillatory can be simply described in terms of the corresponding values of gain and time delay. In other words, these two parameters provide a convenient way of relating or comparing different system behaviors.

If we accept the proposition that these two parameters make good sense from the analytic point of view of control theory, one can ask the question: are these two parameters also convenient descriptors at a phenomenal level? Given a dynamic visual display of two tracking systems, can a person perceive

---

[1]This research was supported by NASA under Contract NAS-23-005-364 while the author was also receiving support from a National Science Foundation Graduate Fellowship.

[2]The author wishes to thank Dr. Richard Pew for his guidance throughout the course of this research.

Preceding page blank

how their behaviors are related in terms of gain and time delay? Or, should the two degrees of freedom characterizing this family of tracking behaviors be partitioned in a different manner in order to facilitate description at the phenomenal level? For example, differences in closed-loop natural frequency might be more easily perceived than differences in open-loop time delay.

Method

In order to investigate this question, subjects were seated in front of a CRT display of the momentary input and output signals of two McRuer Crossover Models (Figure 1). The input to each system was displayed as a single dot moving horizontally. Each output was displayed as a pair of vertically aligned dots 3/4 - inch apart and centered about an imaginary horizontal line passing through the corresponding input dot. The two models had independent random inputs that consisted of band-limited pseudo-random noise produced by shift registers with second-order low pass filters on their outputs. The filters had cut-off frequencies of 2 rad/sec. One crossover model had values of gain and time delay that remained fixed at $k_1 = 4.2$ sec^{-1} and $\tau_1 = 0.12$ sec throughout the four weeks of experimentation. The other model was randomly set to different values of k and τ at the beginning of each experimental trial, and the subjects' task was to adjust two controls to make the values of k and τ in this model equal the values of k_1 and τ_1 of the fixed model. When this match was achieved, the two models would exhibit the same style of tracking behavior. The two system outputs would, of course, not be moving in unison, because the two system inputs were independent. However, the dynamic relationship between the input and output of the adjustable model would equal the dynamic relationship between the input and output of the fixed model.

Three college students served as subjects and received six sets of 78 trials each over a four-week period. In Sets 1, 4, and 5 the controls consisted of four pushbuttons which would increment or decrement k by 0.6 sec^{-1} and increment or decrement τ by 0.02 sec. Subjects could push only one pushbutton at a time and so were constrained to move along the rectangular grid shown in Figure 2, one move at a time. The 78 initial conditions pictured in Figure 2 were presented in each set, but the order of presentation was randomly varied from set to set.

In Sets 2, 3, and 6, the four pushbuttons incremented or decremented k by 0.6 sec^{-1}, and incremented or decremented ω_n, the closed-loop natural frequency of the tracking system. Since a first order Padé approximate was used to simulate the time delay in the two crossover models, $\omega_n^2 = \frac{2k}{\tau}$. Hence, loci of constant ω_n are straight lines going through the origin in (τ,k) space as shown in Figure 3. In order to achieve this fairly uniform spacing of the diagonal lines over the (τ,k) space, ω_n was actually incremented and decremented in equal steps of $1/\omega_n$. Pressing an appropriate pushbutton incremented or decremented $1/\omega_n$ by 0.011 sec. Subjects were thus constrained to move along

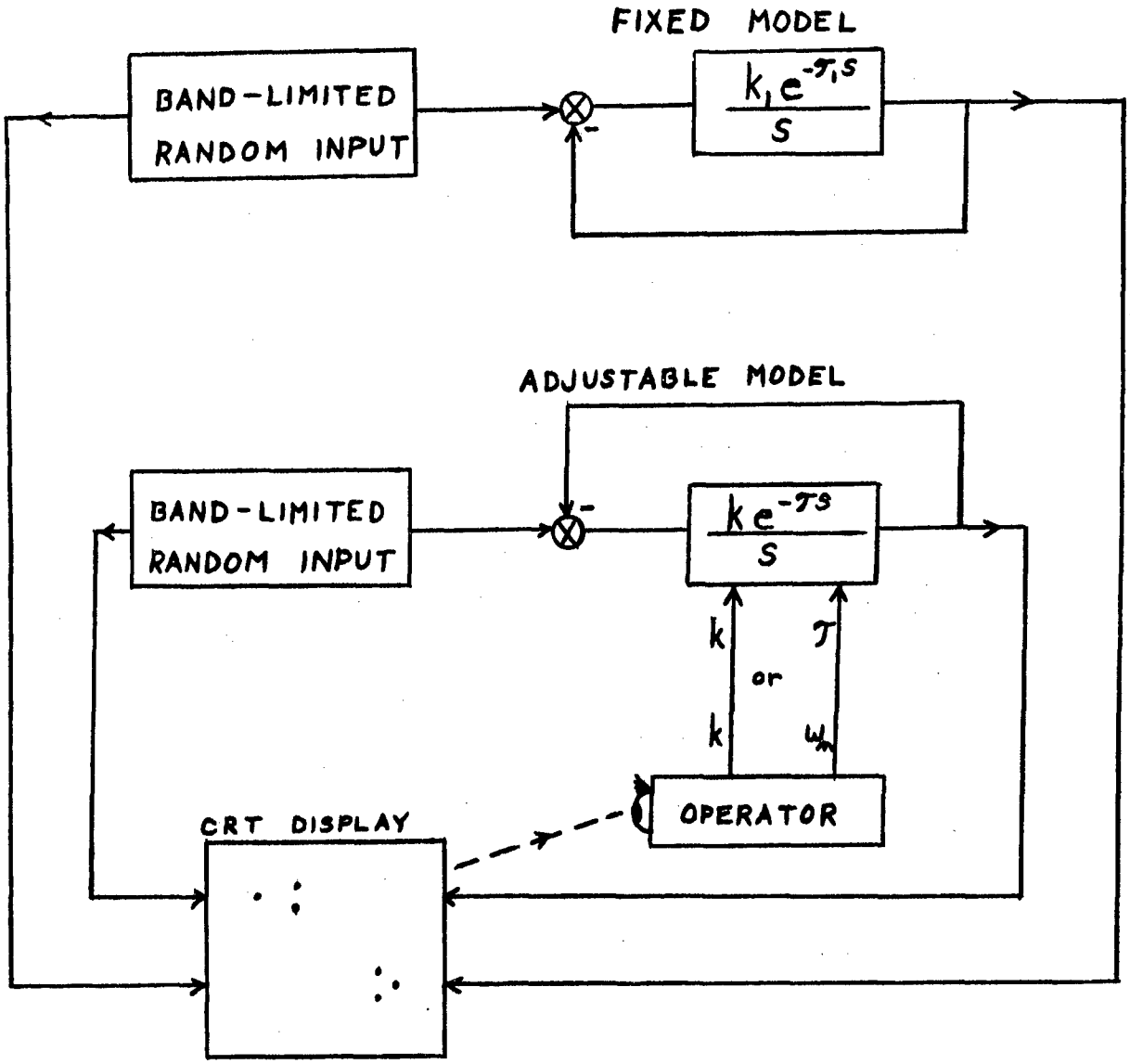

Figure 1 - Block diagram showing the human operator adjusting k and τ, or k and ω_n in order to match the values of k and τ of the adjustable model to the values k_1 and τ_1 of the fixed model.

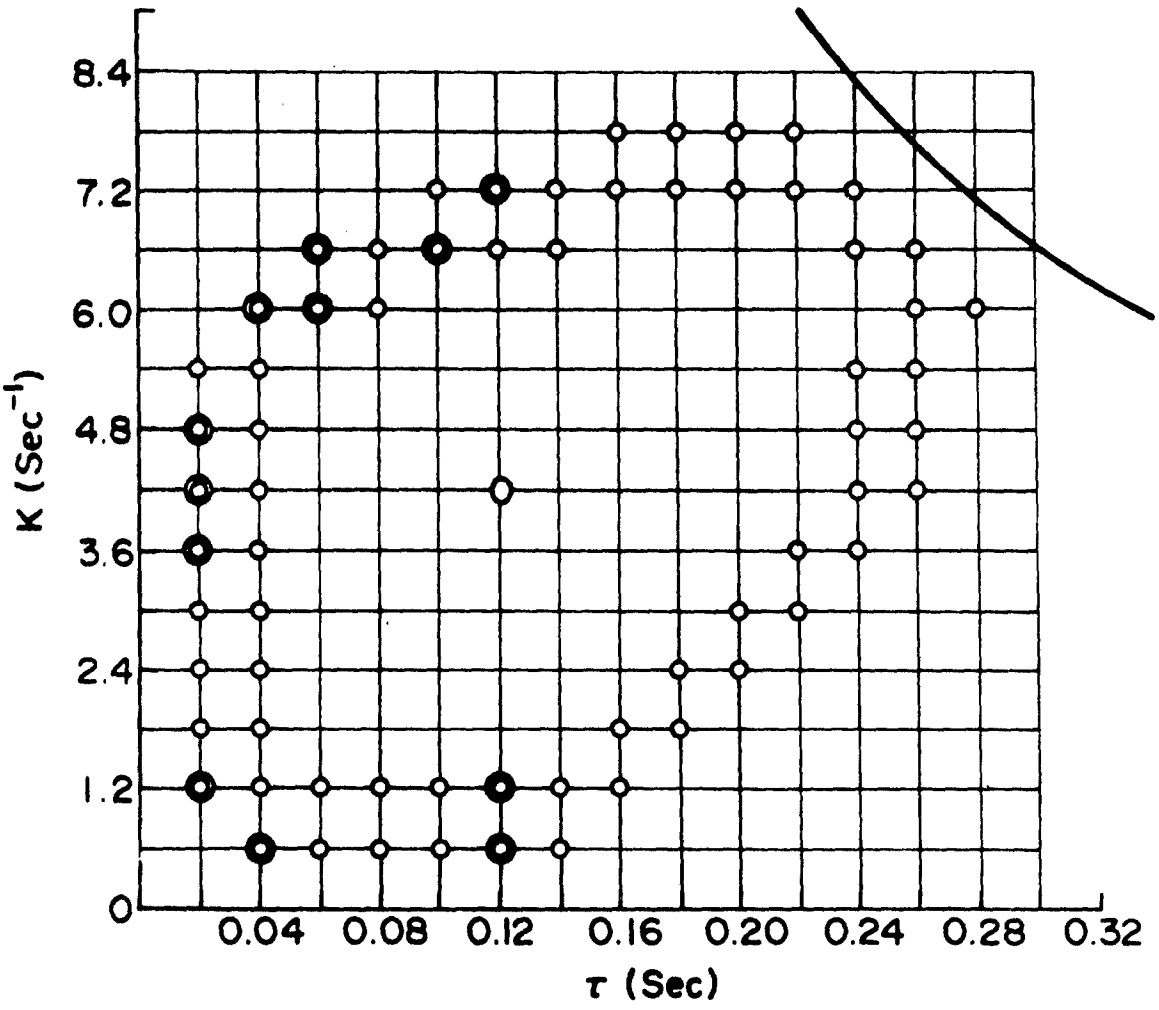

Figure 2 - Adjustment grid for the k,τ adjustment controls. The circles indicate the 78 initial conditions of the adjustable model. Two concentric circles indicate that two trials had the same initial condition.

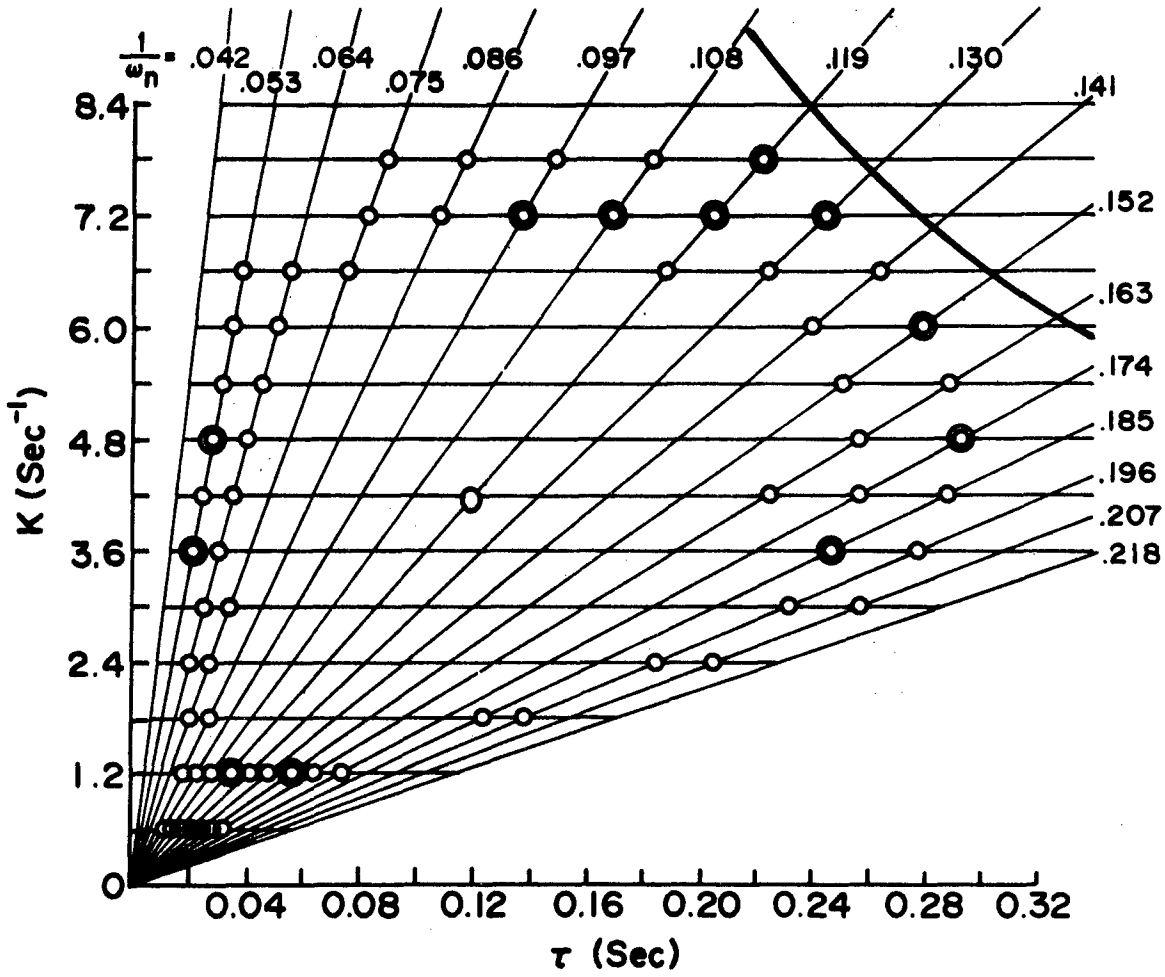

Figure 3 - Adjustment grid for the k, ω_n adjustment controls. The circles indicate the 78 initial conditions of the adjustable model. Two concentric circles indicate that two trials had the same initial condition. The values of $1/\omega_n$ are in seconds.

the grid shown in Figure 3, one move at a time. The 78 initial conditions pictured in Figure 3 were presented in each set, with the order of presentation randomly varied from set to set. The 78 initial conditions for the k,τ adjustment controls and for the k,ω_n controls were both chosen such that perfect performance would require a total of 139 actuations of each of the four pushbuttons.

Subjects were instructed to achieve a match between their adjustable tracking system and the fixed tracking system in as few moves as possible. There was a minimum waiting time of six seconds between moves in order to encourage the subjects to choose each move carefully. This six second period also permitted transients from the preceding parameter adjustment to die out before the next move was made. The termination of the six second waiting period was indicated to the subjects by the onset of a 700 hz tone. Trials were terminated by subjects' stating that they had achieved a match, by a three minute time limit, or by a subjects' reaching one of the boundaries of the grids shown in Figures 2 and 3. After each trial subjects were told how many adjustments they had made, how many more they would have needed to achieve a match, and what the minimal number of adjustments was for that trial.

Results

The data for each set of 78 trials was tabulated in the manner reported in Pew and Jagacinski (1971), and the reader is referred to that report for a graphic presentation of the data reduction process. At each point in the grids in (τ,k) space, the number of times a subject made each of the four possible adjustments was tabulated across the 78 trials of the set. These numbers were interpreted as vectors indicating the relative likelihood that the subject moved in each of the four possible directions, and were determined for each point in the (τ,k) space. The four vectors were then vectorially added and normalized to produce a summary vector indicating an average adjustment tendency at each point on the grid. Based on this array of summary vectors, average flow lines from the periphery of the (τ,k) space toward the target behavior were drawn in by eye as shown in Figure 4.

The data in Figure 4 are from two subjects: Brian on the left and Gary on the right. Brian did not have a background in control theory and was not told what the adjustment controls were. He merely knew that there were two factors controlling the tracking system and that he could increase and decrease the values of each of these factors. Gary, on the other hand, had a thorough background in control theory and was also told exactly what each of the adjustment controls were. The upper graphs represent the average of the 78 trials of Set 5 with k,τ adjustment controls. The lower graphs are the average of the 78 trials of Set 6 with k,ω_n adjustment controls.

Discussion

At the outset of this experiment there was some doubt as to whether subjects would be able to do the task at all. Of four subjects who began the

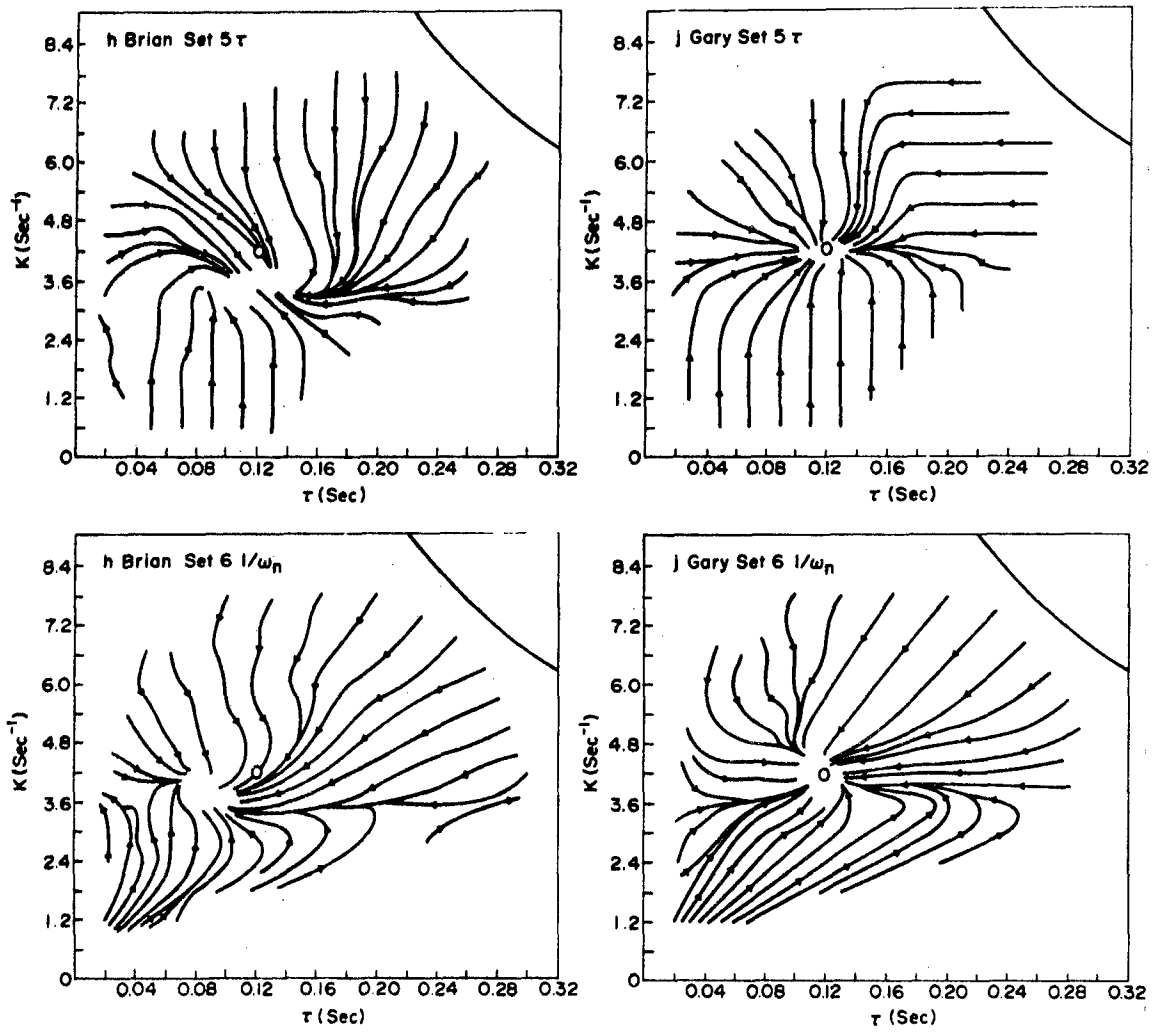

Figure 4 - Average adjustment tendencies for Brian (left) and Gary (right) with k,τ controls (top) and k,ω_n controls (bottom).

the experiment, one dropped out after two days, claiming that he simply did not know how to go about the task. Because the inputs to the two models were independent, the task was not simply a matter of making the two outputs move in unison as was the case in Pew and Jagacinski (1971). Rather, the subjects were required to match the dynamic relationship between input and output in the adjustable model to the corresponding dynamic relationship in the fixed model. The subjects' general success in converging toward the target behavior (Figure 4) is therefore evidence that they were able to characterize the dynamic relationship between input and output and were able to relate this characterization to the effects of the adjustment controls.

Looking at the fine detail of the convergence process, one notes striking individual differences between subjects. Brian was unable to converge from the low τ, low k region of the space with either set of controls, and was unable to converge from the low k, high τ region when using the k,ω_n controls. In contrast, Gary was able to achieve convergence from all regions of the (τ,k) space. Brian also exhibited what might be called a perceptual bias. When he thought he had achieved a match between the two models, the values of both k and τ tended to be too low. Gary, on the other hand, did not exhibit a bias. On the average, Brian ended up 2.5 moves from the target when using the k,τ controls, and 3.5 moves from the target when using the k,ω_n controls. Gary's comparable figures were 1.0 moves for the k,τ controls and 1.5 moves for the k,ω_n controls. The initial location at the beginning of a trial was an average of 7 moves from the target. Although both Gary and Brian came closer to the target when using the k,τ controls, a third subject not reported in detail here came closer with the k,ω_n controls. Therefore, no simple conclusion about the relative superiority of the two sets of controls can be drawn from these data.

Besides failing to stop directly on target, subjects also exhibited systematic inefficiencies in the paths they used to traverse the (τ,k) space. Since performance was measured by the number of steps taken to move through the grids, there was no unique optimal path between two points in the space if the two points differed on both their k and τ coordinates. For example, if at the beginning of a trial, the adjustable model was set with both the k and τ values too low, the subject could choose a number of different paths and still reach the target in the minimal number of moves. He might first increase τ as much as necessary and then increase k; he might increase k as much as necessary and then increase τ; or, he might alternate k and τ moves in any one of a number of ways. If, however, a path doubled back at any point, then it could not reach the target in the minimal number of moves. This doubling back phenomenon was the other type of inefficiency that subjects exhibited besides failing to stop directly on target. For example, starting from the low k, low τ region Brian had a tendency to increase k up to the target value and then decrease k when using the k,τ controls. With the k,ω_n controls, Gary had a slight tendency to decrease k and then increase it for starting points with τ too low and k about equal to the target value.

It is interesting to note that at first glance both subjects seem to have exhibited marked doubling back in the lower right-hand corner of the graphs for the k,ω_n controls. However, this doubling back is only in terms of the Euclidean metric that we tend to assume in looking at graphs. Actually, in terms of the city-block grid imposed by the k,ω_n controls (Figure 3), these paths do not represent a doubling-back. The subjects first increased k and then increased ω_n in approaching the target from this region. In the process of increasing k while holding ω_n constant, the discrepancy between the τ values of the adjustable model and the target increased, but of course, the discrepancy between ω_n values remained constant.

Unanswered Questions

The above mentioned phenomenon suggests an interesting experiment. Suppose that subjects were permitted to vary both adjustment controls simultaneously and that optimal performance was defined in terms of a Euclidean metric. A unique optimal path would then exist between any two points in the space. Given this situation, would subjects traverse the same paths through the (τ,k) space regardless of which adjustment controls they used? Such a result would be evidence for some basic underlying two-dimensional perceptual space. The results of the present experiment with a city-block metric seem to be evidence against such a notion. The controls do have a large effect on the paths through the space. However, the city-block metric does not really provide strong evidence against a basic underlying two-dimensional perceptual space, because optimal performance is simply not sufficiently constrained. Subjects may be aware of several paths between two points in the (τ,k) space but merely choose one of these. Therefore, the adjustment patterns in Figure 4 cannot be considered a strong test of the subjects' perceptual abilities.

On the other hand, if the results of the present experiment in the lower half of the (τ,k) space were replicated with a Euclidean metric to define optimal performance, then the paths in the lower right of the graphs for k,ω_n controls would indeed be inefficient. The paths in the lower right-hand portion of the graphs for the k,τ controls would also be inefficient in terms of a Euclidean metric. One would infer that the perceptual space is essentially one-dimensional in the region of low k. With both sets of controls, the subject would be forced to increase the k control first until he reached a region of the space where he could perceive differences in the other dimension. Only then could he begin to move horizontally in the space. Therefore, in the region of low k the set of controls would strongly influence the path taken toward the target, because the subjects would not be able to perceive horizontal movement through this region of the (τ,k) space. This inference could only be made, however, with the use of a Euclidean metric. Our results using a city-block metric must be considered merely suggestive.

Overview

In summary, this research is an attempt to develop a methodology for describing perceptual spaces. Namely, subjects are asked to "walk" through

the spaces as efficiently as they can, and their average paths are then graphically depicted. Hopefully, this methodology will be useful in characterizing not only perception of dynamic systems, but perception of other parametrically defined complex stimuli as well. Perception of multidimensional apparent motion, color perception, and auditory stimulation are all candidates for this type of analysis.

References

Nolan, G. R. Human response in matching the parameters of an operating dynamic system. Unpublished SM Thesis, Department of Mechanical Engineering. MIT, June, 1959.

Pew, R. W., and Jagacinski, R. J. Mapping an operator's perception of a parameter space. Proceedings of the 7th Annual Conference on Manual Control. In press, 1971.

SESSION VI

Recent Developments in Control System Analysis Procedures

Preceding page blank

TRANSFER CHARACTERISTICS OF HUMAN ADAPTIVE RESPONSE TO TIME-VARYING PLANT DYNAMICS

Peter Delp* and E.R.F.W. Crossman

Department of Industrial Engineering and Operations Research
University of California
Berkeley, California

ABSTRACT

Previous studies of human response to time-varying plant dynamics have generally employed stepwise parameter changes. However, real vehicles and other plant may suffer slow irregular changes. Frequency domain characterization of human adaptive response would assist in predicting system performance under these conditions.

The paper presents gain and phase estimates for human adaptive response, obtained in tracking a quasirandom forcing function with second-order plant and sinusoidal variation of natural frequency and damping ratio, results being analyzed by Gabor transformation. Estimated meta-bandwidth (i.e., adaptive response cutoff frequency) was on the order of 0.015 Hz, and there was a transport lag on the order of 2.8 seconds.

*Now with the Department of Industrial Engineering, University of Wisconsin, Madison, Wisconsin.

Preceding page blank

INTRODUCTION

It is generally agreed that the human operator responds adaptively to time variations in input spectra and plant dynamics, modifying his transfer characteristics to provide in some sense optimal system performance, within individual limitations of gain-bandwidth product, equalization capacity, linearity and internal noise level.

The value of this distinctively human adaptive response is somewhat limited in practice by the time required for its completion. Thus rapid or instantaneous changes in task parameters may produce transiently poor performance or temporary breakdown, which may or may not be acceptable to the designer and system manager. To predict and analyze these effects we need data on the dynamics of the adaptive process, which have not hitherto been available. The present paper reports methodology and results of a study of adaptive response dynamics employing sinusoidal time variations in natural frequency and damping factor of a second-order plant, controlled in compensatory mode by moderately skilled experimental operators, with a non-time-varying quasirandom forcing function. Performance feedback was provided, but this did not appear to materially affect operator performance.

It will be convenient at the outset to introduce a compact terminology for discussing time-varying parameter systems, and at the same time to set forth the perhaps rather obvious conceptual model underlying the experiments. Starting with a conventional closed-loop manual control system with a quasirandom forcing function (Figure 1), we consider time variations in forcing function input and plant dynamics as higher level or "meta" inputs, occurring in meta-time. The (meta-) time history of forcing function spectral parameters will be referred to as an "input meta-forcing function , while the time history of plant dynamic characteristics is termed a "plant meta-forcing function". Both of these meta-time histories can also be represented in the frequency domain and, if statistically stationary, can be characterized respectively as input and plant meta-forcing spectra.

Continuing in this vein, the human operator's adaptive response to input and plant meta-forcing may be termed his "meta-transfer characteristic". The main hypothesis underlying the present study was that this meta-transfer characteristic could be modeled as a linear lowpass filter with a measurable break frequency or frequencies constant for a given individual and task situation, though perhaps changing with (regular)forcing function frequency, practice, and the task environment. In the outcome we found that a first-order model yielded a good enough fit to the meta-forcing function response for many design purposes.

Previous studies of the human operator's response to what may now be termed plant meta-forcing have almost universally employed transient time functions such as stepwise changes in forward gain [1] order of control [2,3,4] or ramp function changes in pole location [5]. These authors have reported adaptation times on the order of five seconds, corresponding to a cutoff-frequency around 0.2 radians per second in the meta-transfer characteristics, but study of the transient adaptive response has not so far yielded a more complete characterization.

Hess [6] employed sinusoidal plant meta-forcing with a single sine wave forcing function input. Hence he obtained performance of a precognitive type, and his data do not serve to identify the more normal compensatory meta-transfer characteristic. We were unable to find any reported study revealing the operator's meta-transfer characteristic in enough detail to test our linear low pass filter hypothesis, and we therefore proceeded to experimental estimation.

METHODOLOGY

A review of methodology for characterization of time-varying systems indicated that previous investigators had been handicapped by lack of a robust procedure for estimation of time-varying spectra and nonstationary system response from experimental data. Our solution to this problem has been presented at an earlier Annual Manual [7] where we concluded that an optimum point estimation method for analyzing nonstationary data would employ Fourier transformation of experimental time series with Gaussian data weighting centered on a sequence of selected reference times. We termed this Gabor transformation after Denis Gabor who first pointed out the engineering significance of the Gaussian envelope for generation of elementary signals [8]. We have since reduced this method to standard practice, and its use rendered the present study feasible.

A brief outline of the underlying theory will be given here for completeness.

Given an arbitrary real time function x(t), we define its (complex) Gabor transform $G[x(t)]$ as follows:

$$G[x(t)] = \int_{-\infty}^{\infty} x(t) \exp\left[-\frac{1}{2}\left(\frac{t-t_r}{\sigma_t}\right)^2 - j\omega_r(t-t_r)\right] dt \qquad (1)$$

where ω_r, t_r are the reference frequency and reference time at which $G[x(t)]$ is to be evaluated.

σ_t is the standard deviation of the Gaussian time window applied to the data.

In practice it is not necessary to evaluate the infinite integral shown in (1), since the rapidly decreasing Gaussian weighting renders the definite integral in the range ±3 or $\pm 4\sigma_t$ a good approximation. In the present study the limits were $\pm 3\sigma_t$.

The Gabor transform $G[x]$ is a single complex number; to obtain a spectral meta-time history for nonstationary $x(t)$ we consider $G[x(t)]$ as a function of ω_r and t_r with constant σ_t, writing this $G[x,\omega_r,t_r]$, while to estimate the spectral response meta-time history $\hat{Y}(\omega_r,t_r)$ of a non-stationary two port system element with input $x_i(t)$ and output $x_o(t)$, we take the complex ratio of Gabor transforms

$$\hat{Y}(\omega_r,t_r) = \frac{G[x_o,\omega_r,t_r]}{G[x_i,\omega_r,t_r]} \qquad (2)$$

In the present study we formed estimates of the human operator response $\hat{H}(\omega_r,t_r)$ and plant response $\hat{Y}(\omega_r,t_r)$ respectively from the ratios of Gabor transforms of manual output $m(t)$ and displayed error $e(t)$,

$$\hat{H}(\omega_r,t_r) = \frac{G[m,\omega_r,t_r]}{G[e,\omega_r,t_r]} \ , \qquad (3)$$

and of plant response $c(t)$ and manual output $m(t)$,

$$\hat{Y}(\omega_r,t_r) = \frac{G[c,\omega_r,t_r]}{G[m,\omega_r,t_r]} \ . \qquad (4)$$

Thus all estimates formed were "open-loop".

The Gabor transform yields significantly better estimates than either the classical truncated Fourier transform (computed by FFT or otherwise) or the auto-cross-correlation method. First, estimates are symmetrically localized about a specific instant in meta-time; and second, the spectral window is symmetrical with no sidelobes (see Figures 2 and 3). Mathematically, it can be shown that for sinusoidal $x(t)$ with angular frequency ω, we obtain the following Gabor transform

$$G[x,\omega_r] = \sigma_t\sqrt{2\pi}\ \exp\left[\frac{1}{2}\,\sigma_t{}^2(\omega-\omega_r)^2\right] \qquad (5)$$

The spectral weighting (the spectral window or filter characteristic) is also a Gaussian function with mean value ω_r and standard deviation

(6)

$$\sigma_\omega = \frac{1}{\sigma_t} \quad .*$$

The time and frequency window widths are thus reciprocally related, which means that we can trade resolution in meta-time for spectral resolution, and vice versa, by adjusting a single parameter.

Gabor transform estimates could in principle be analog-computed, but present technology favors digital methods. We therefore evaluate (1) as a sum rather than an integral, taking the usual precautions to avoid aliasing. In normal application for human operator studies a set of values of ω_r and the time window width parameter σ_t are selected to match the forcing function. The Gabor transform is then computed for a sequence of reference times t_r, yielding a spectral and/or response meta-time history. Due to overlap of the Gaussian time windows, successive estimates covary to an extent dependent on σ_t and vanishing at about $4\sigma_t$ spacing (see Table 1). Hence time variations can be detected in the experimental record in periods on the order of $8\sigma_t$. Expressing this in the meta-frequency domain, the Gabor transform operates as a Gaussian lowpass filter with cutoff on the order of $\pi/4\sigma_t$ radians/second.

Employed in the manner outlined above, the Gabor transform provides spectral and response estimates reflecting conditions in the neighborhood of time t_r and frequency ω_r, with symmetrical and reciprocally-related weighting falling off rapidly and monotonically with departure from the selected time and frequency. These properties are ideal for off-line analysis of experimental time histories, and permit a very straightforward approach to time-varying spectra and response functions.

To contrast the effectiveness of Gabor and truncated Fourier transforms, Figure 4 shows time sequences of log-amplitude ratio and phase estimates obtained at several forcing frequencies with respectively $\sigma_t = 2.5$ sec and truncation at ±7.5 seconds, for a stepwise change in plant dynamics.

The Gabor procedure is seen to yield the expected Gaussian integral response, while Fourier transformation shows considerable "ringing".

The procedure is less useful for online system identification since x(t) must be known for negative t out to at least $-3\sigma_t$, which implies a $3\sigma_t$ delay in obtaining $G[x(t)]$. Spectral and response estimates may be formed more rapidly at a sacrifice in resolution by employing assymmetric exponential

---

*This relation was previously given as $\sigma_\omega = 1/(2\sigma_t)$ by Crossman and Delp [7] as an erroneous derivation from data and spectral window dispersions based on amplitude rather than power.

weighting. This method was employed by Sheridan [2] in his classical study of human operator time-variations.

For online analysis in our case the suitably filtered error e(t) and manual output m(t) were digitized at 4.75 samples/second, and Gabor transformed* with σ_t = 2.5 sec and $3\sigma_t$ cutoff, at reference times spaced 15 seconds apart, at a single reference frequency. As part of this computation the sum-squared error and output were also computed to provide the feedback performance metric for each ten second period.

Magnetic tape analog records were also acquired for offline analysis, performed as above for all forcing function frequencies with 1 to 5 second spacing. Records were digitized with 8-bit precision at 10 samples/second.

EXPERIMENTAL DESIGN

The experimental control task was conventional compensatory tracking with a horizontally displaced CRT display and a lightly spring-centered automobile steering wheel control (see Figure 5). Simulated plant dynamics (Figure 6) were provided by an analog computer with sinusoidal parameter variations implemented by a low-frequency oscillator and analog multipliers to provide meta-response forcing.

Among the many possible plants, second-order dynamics of the form

$$Y(j\omega) = \frac{K}{(j\omega)^2\left(\frac{1}{\omega_n(t)}\right)^2 + 2j\omega\left(\frac{\zeta(t)}{\omega_n(t)}\right) + 1} \qquad (7)$$

were selected. This relatively complex pattern of time-variation was selected to provoke major adaptive response in the subject while avoiding discontinuous change and loss of control. Figure 7 shows the response variation at each forcing function frequency as a function of the meta-forcing input p(t). The plant parameters, ω_n and ζ varied over a 0.3:1 range, each being proportional to a single meta-forcing time function p(t), thus

$$\begin{cases} \omega_n(t) = 12.65 \quad p(t) \quad \text{rad/sec.} \\ \zeta(t) = 0.237 \quad p(t) \end{cases} \qquad (8)$$

*Using a PDP-8 computer with FOCAL interpreter.

where $p(t) = 0.35 \cos(\Omega t) + 0.65$. Plant dynamic characteristics are shown as static functions of p in Figure 8.

Russell's [9] five-component* quasirandom forcing function was prerecorded on analog magnetic tape and employed throughout (see Table 2). This was preferred over the STI and other possible functions as having fewer more widely and uniformly spaced frequency components, permitting use of a wider frequency window, hence narrower time window and greater meta-time resolution. Unfortunately, however, operator coherency proved too low at the top frequency, 0.83 Hz, and attempts to analyze response to this component were abandoned after early trials. Results quoted here are therefore based on four components in the range 0.1 to 0.7 Hz. Performance feedback was coded into the vertical line on the CRT, whose lateral position indicated error magnitude. This was computed online as described above and updated every ten seconds.

The main independent variable was meta-response forcing frequency Ω. Five values in the range 0.01 to 0.12 Hz were employed (see Table 3a). Four male and one female non-pilot graduate student subjects underwent five five-minute training sessions each, with a stationary plant, the meta-forcing function p being set at five different constant values (see Table 3b). The experimental trials proper also lasted five minutes each. Both training and experimental conditions were assigned to subjects in a Latin square design (see Table 4), with minor modifications to accommodate individual problems.

As indicated by protocols, operators varied considerably in their subjective responses to the quite challenging experimental task; there was a marked learning effect through experimental runs with sinusoidal plant meta-forcing. In further studies of this type it would be preferable to employ extended familiarization periods and a quasirandom meta-forcing function. However, the present results are believed to be representative of operator response at an intermediate skill level with only moderate meta-precognition.

RESULTS

1. Constant Plant Dynamics

Overall average error power (Table 5) varied relatively little between subjects, but diminished markedly with the meta-forcing parameter p. Time average transfer characteristics were computed for each subject and value of p, the latter (Figures 9a,b) showing the usual negative slope with frequency. However, the meta-time histories on which these averages were based revealed considerable sample to sample variation; one subject's results shown in Figure 10 revealed what may be termed "dropouts" in gain, these occurring more often at high than at low forcing frequencies. Standard deviations of log-gain and phase estimates were computed for

*A fifth frequency component, 0.83 Hz was added to Russell's forcing function.

all subjects (Figure 11) showing variation with p. There was some indication of minimum variance around p = 0.65 at all forcing frequencies, but we have no explanation for this phenomena.

The results discussed above can be considered as operator response to plant meta-forcing inputs at zero frequency. Operators evidently show an adaptive response, succeeding, as shown in Table 5, in stabilizing their error power scores against variation of plant dynamics.

2. Time-Varying Plant Dynamics

Initial analysis showed that none of the operators responded significantly to plant meta-forcing at the top two meta-frequencies (0.08 and 0.12 Hz), at any input forcing function frequency; and further study was therefore restricted to the three lower meta-forcing frequencies (0.05, 0.02, and 0.01 Hz). This result immediately places the cutoff frequency of the postulated human meta-transfer characteristic well below a tenth of a cycle per second, for this type of plant and forcing function, an outcome which was somewhat unexpected in view of relatively fast "adaptation" observed with transient meta-forcing by Elkind [3] and others.

Operator response covaried with plant dynamics at the lower frequencies. To illustrate this a sample time history for Ω = 0.01 Hz, is shown in Figure 12 and again presented somewhat differently as a travelling Bode plot in Figure 13.

Relatively little can be learned by direct inspection of these meta-time histories, and we therefore resorted to meta-spectral analysis to estimate meta-transfer characteristics. The procedure adopted was to compute the Gabor transform of the spectral gain and phase meta-time histories for each combination of forcing and meta-forcing frequency thus obtaining what has been termed (after Zadeh [10]) a bi-frequency characterization of the human operator. After some trial-and-error, we decided to perform this analysis on the logarithmic (decibel) amplitude ratios, for principal reason that these are more nearly normally distributed than the amplitude ratios themselves. Meta-amplitude ratios (i.e., ratios of decibel amplitude ratio changes occurring with adaptation) do not have an inherent (unit gain) reference such as exists for the amplitude ratios themselves. Alternate choices of reference are the amplitude ratios of the operator estimated by model-fitting at zero meta-forcing frequency, which may be termed "self-referred" meta-amplitude ratios, $\Lambda_H(\omega_i,\Omega)$, and the instantaneous amplitude ratio of the plant being controlled at the same meta-time, $\Gamma(\omega_i,\Omega)$, termed "plant-referred" meta-amplitude ratios.

Bi-frequency meta-response amplitude, phase, and coherence estimates formed in the former (self-referred) way are presented for one subject in Table 6, and in the latter (plant-referred) manner for 2 subjects in Table 7. Corresponding three dimensional plots are presented in Figure 14a and b with gain and phase of the estimates shown relative to log Ω and log ω.

It will be noted that plant referred meta-amplitude ratios show a gain on the order of 30 db at low and a loss around 5 db at high forcing frequencies. This reflects in meta-frequency domain the phenomenon seen in the meta-time histories of the estimates, where operator gain varies more than plant gain at some forcing frequencies, less at others. The overall adaptive response thus appears to be almost independent of forcing frequency, but quite highly dependent on meta-forcing frequency. The operator's response does not reflect the highly frequency-dependent variations of this particular plant in meta-time. He (or she) appears to respond to variations in the averaged (spectrally smoothed) plant dynamics rather than to the detail variations at each frequency.

3. Modelling the Human Operator's Meta-Transfer Characteristic

While bi-frequency response estimates have been obtained for relatively few pertinent meta-forcing frequencies, and are far from precise, they do permit a tentative model to be constructed on the lines suggested in the introduction. As shown in Figure 15, self-referred adaptive amplitude ratios for Subject 100 conform quite well to a first-order model with a well-defined breakpoint and 20 db/decade slope while the phase estimates indicate fixed lag element in the model. Fitting a model of this kind to the gain estimates by conventional means we obtained a break-frequency at about 0.0135 Hz (time constant, T_A = 11.8 seconds). An excess phase lag of about 10° at this frequency indicates a computation or "transport" lag of about 2.8 seconds. The fitted meta-transfer model thus takes the form

$$\Lambda_H(\omega_i,\Omega) = K_A \frac{e^{-j\tau_A\Omega}}{jT_A\Omega + 1} \qquad (9)$$

where Ω = meta forcing frequency

$T_A = 1/\Omega_A$ = (meta bandwidth)$^{-1}$, time constant of adaptation

K_A = zero frequency adaptive gain ($\simeq$ 0 db)

We note that the right hand side of Equation 9 is independent of ω_i, expressing the fact that the adaptive response has essentially the same meta-dynamics at any forcing frequency.

A similar model is fit to the plant adaptation meta-transfer estimates, referred to "instantaneous" plant dynamics:

$$\Gamma(\omega_i,\Omega) = \frac{A(\omega_i)e^{-\tau_A j\Omega}}{T_A j\Omega + 1} \qquad (10)$$

where $T_A \simeq 11.8$ seconds ($\Omega_A = \frac{1}{T_A} \simeq .0135$ Hz)

$\tau_A \simeq 2.8$ seconds.

$A(\omega_i) \simeq$ zero meta-frequency, input frequency dependent gain constant.

As seen in Figure 14b, low meta-frequency amplitude ratio, $|\Gamma(\omega_i,\Omega)|_{(\Omega=.01\ Hz)}$, varies considerably across the input forcing function frequencies, ω. This is due to the meta-transfer estimate input power range: from negligible at $\omega = .105$ Hz to a variation at .679 Hz characterized by a strong third harmonic [see Figure 7]. Further analysis will be required to obtain a satisfactory model for this case.

CONCLUSIONS

While much more could be said concerning the detailed operator response to plant meta-forcing inputs, and while the recorded data show considerable intra-and inter-operator variability, our results support the view that the human adaptative response in tracking has relatively simple dynamic characteristics resembling those of a first-order filter. While without further data we cannot generalize to plants other than conventional fast-response, zero through second order dynamics, nor to tasks with other forcing functions, our results do appear to be in rough agreement with those obtained by the earlier investigators cited above using transient meta-forcing inputs (sudden plant changes). In all these cases the operator reportedly continued his pre-change response for at least a second or two, then required tens of seconds to a minute for final adjustment to the post-change conditions. Figure 16 shows the meta-time history predicted from our simple first-order model. More detailed reconciliation to these investigators' results is presented elsewhere [11].

Application

As an illustration of a real-life control task involving a time-varying plant we may take lateral (steering) control of an automobile. In this case the plant retains basically second-order characteristics, but parameters vary with forward speed, vehicle loading, highway surface friction, tire inflation, and other factors. A variety of plant meta-forcing inputs are therefore encountered, some predictable and others not. Forcing functions are derived from side-winds and surface irregularity, as well as command inputs due to traffic and highway geometry. Time variations in these present input meta-forcing. System performance criteria include limiting absolute error to values dependent on highway geometry and traffic characteristics.

The magnitude and speed of required driver adaptation may be estimated for particular cases. Thus according to Szostak [12], the natural frequency ω_n moves from 11.2 radians/ second for a full size sedan car travelling at 20 mph to 6.2 radians/ second at 60 mph, and about 5.5 radians/second at 80 mph. Since this transition may take perhaps 15 seconds upward, and 5 seconds downward, meta-transfer bandwidths on the order of 0.2 radians/second would be desirable. This is somewhat better than our data would ascribe to the average operator. However, meta-precognition may assist in this case.

Considering a rear tire blowout at 60 mph, ω_n drops by a factor of four, to 1.53 radians/second, perhaps in a period on the order of 2 seconds. Given the presence of some forcing-function, the operators adaptive meta-bandwidth would certainly predict large transient error in this case. Similar considerations apply to encountering ice or snow, and to mechanical failure in the steering system. We feel it would be worthwhile exploring such applications of our results in more detail than has been possible here.

REFERENCES

1. Young, L. R., Green, P. M., Elkind, J. I. and J. A. Kelly, "The Adaptive Dynamic Response Characteristics of the Human Operator in Simple Manual Control." NASA TN D-2255, April 1964.

2. Sheridan, T. B., "Time Variable Dynamics of Human Operator Systems." AFCRC-TN-60-169 (ASTIA AD-237045), March 1960.

3. Elkind, J. I. and D. C. Miller, "On the Process of Adaptation by The Human Controller." IFAC, Proceedings of the 3rd Congress, Vol. 1:2, 1966.

4. Weir, D. H. and A. V. Phatak, "Model of Human Operator Response to Step Transitions in Controlled Element Dynamics." NASA CR-671, January 1967.

5. Jex, H. R., McDonnell, J. D. and A. V. Phatak, "A 'Critical' Tracking Task for Manual Control Research." IEEE Trans., Vol HFE-7, No. 4, p. 138- , Dec. 1966.

6. Hess, R. A., "The Human Operator as an Element in a Control System with Time Varying Dynamics." AFFDL-FDCC-TM-65-34, June 1965.

7. Crossman, E.R.F.W. and Peter Delp, "Application of Gabor's Elementary-Signal Theorem to Estimation of Non-stationary Human Spectral Response." Fifth Annual NASA-University Conference on Manual Control. NASA SP-215, 1969.

8. Gabor, D., "Theory of Communication." IEE Journal (British), Pt. III, 1946.

9. Russell, Lindsay, "Characteristics of the Human as a Linear Servo-Element." M. S. Thesis, M.I.T., May 1951.

10. Zadeh, L. A., "Frequency Analysis of Variable Networks." Proceedings of the IRE, Vol. 38, No. 3, pp 291- , 1950.

11. Delp, H. P., "Adaptive Response of the Human Operator to Time-Varying Plant Dynamics". Ph.D. Dissertation, Department of Industrial Engineering, University of California, Berkeley, 1972.

12. Szostak, H., "Investigation of the Dynamic Steering Response of a 1965 Ford Sedan Test Vehicle." HFT Group Working Paper 67-8, University of California, Berkeley, 1967.

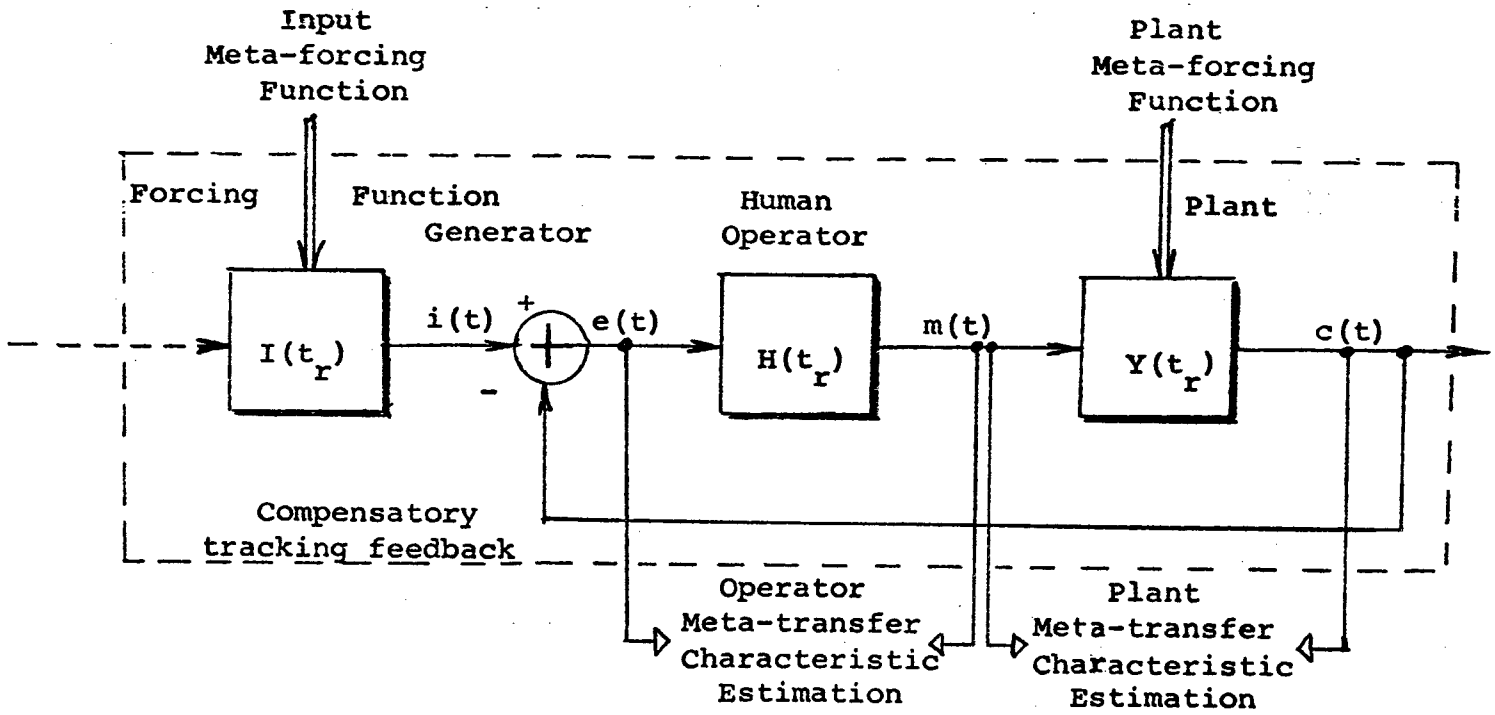

FIGURE 1 TIME-VARYING MANUAL CONTROL SCHEME

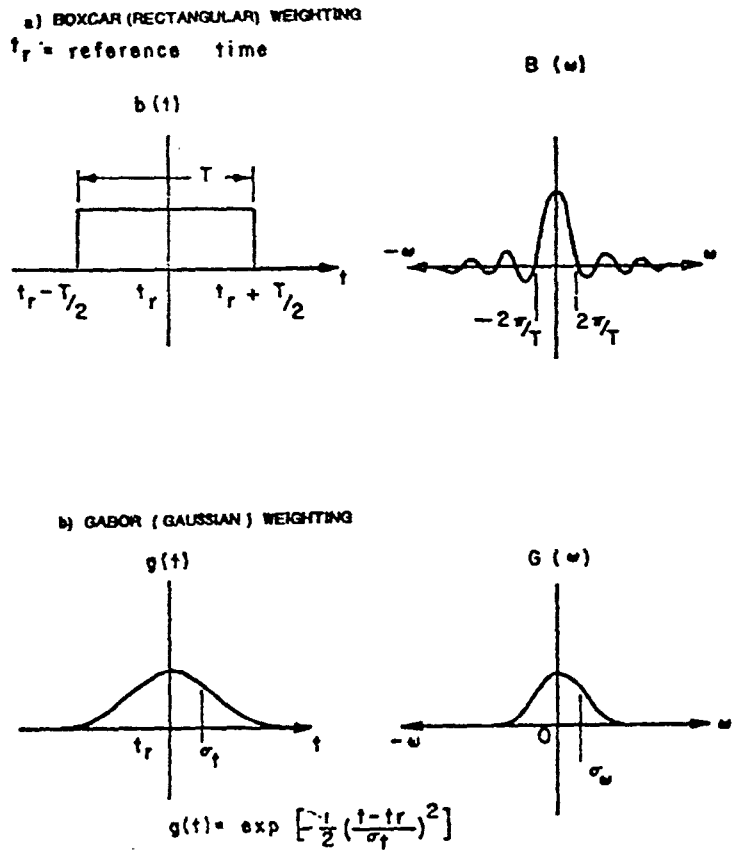

FIGURE 2 BOXCAR AND GAUSSIAN DATA WEIGHTINGS AND THEIR CORRESPONDING SPECTRAL WINDOWS.

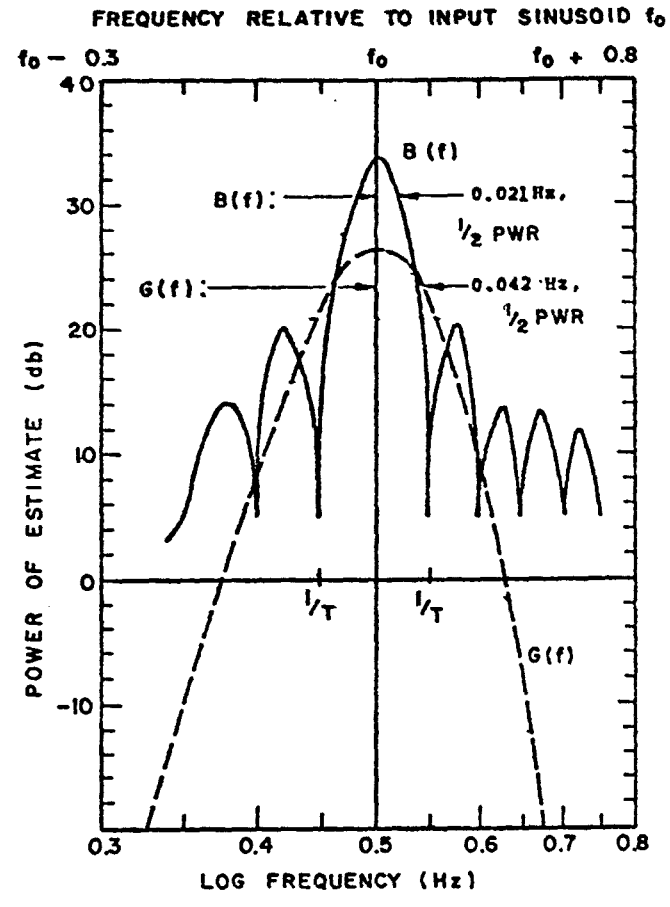

Boxcar, b(t): T = 20 secs., 1/T = 0.05 Hz

Gabor , g(t): σ_t = 3.2 secs, $\sigma_f = 1/2\pi\sigma_t$ = 0.05 Hz

FIGURE 3 COMPARISON OF GABOR AND BOXCAR SPECTRAL WINDOWS

TABLE 1 THE CORRELATION BETWEEN SUCCESSIVE FREQUENCY ESTIMATES FORMED BY GABOR TRANSFORMATION AT DIFFERENT REFERENCE TIMES

Interval Between Estimates (Seconds, fractions of σ_t)	Correlation Between Successive Estimates
0	1.00
0.5	0.94
1.0	0.78
1.5	0.57
2.0	0.37
2.5	0.21
3.0	0.11
3.5	0.05
4.0	0.02
4.5	0.01
5.0	∿ 0.00

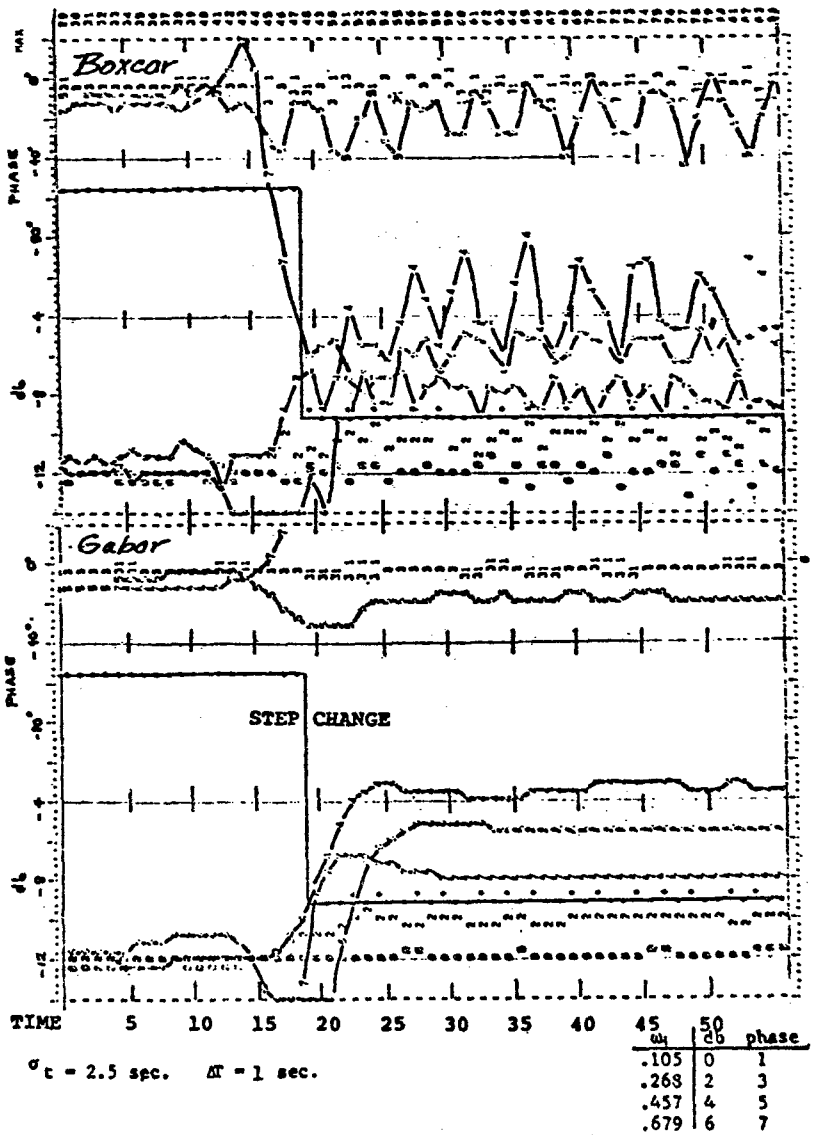

FIGURE 4 COMPARISON OF GABOR AND BOXCAR TRANSFORM: THE TIME RESOLUTION OF A STEP CHANGE IN THE SIMULATED PLANT DYNAMICS

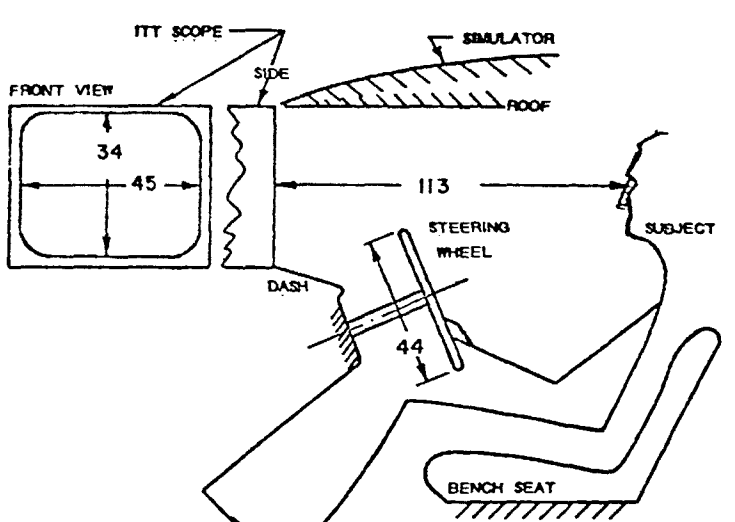

FIGURE 5 LAYOUT OF SIMULATOR EXPERIMENTAL SETTING

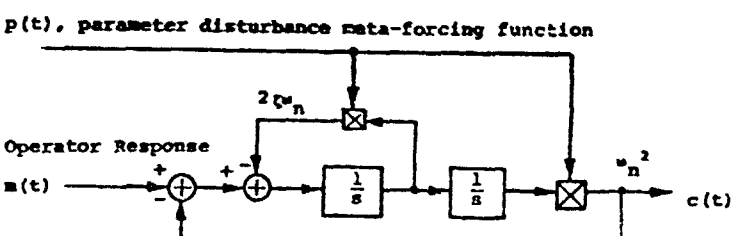

a). Implementation of Time-Varying Dynamic System

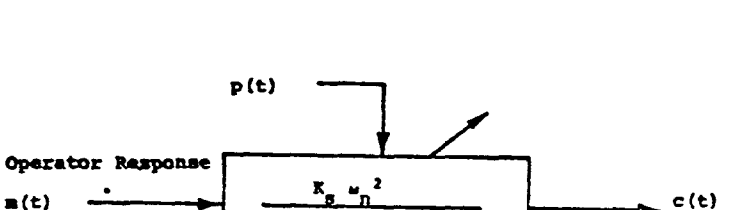

b) Equivalent Representation for Low Frequency Disturbance of Plant Parameters

FIGURE 6 BLOCK DIAGRAMS FOR TIME-VARYING PLANT

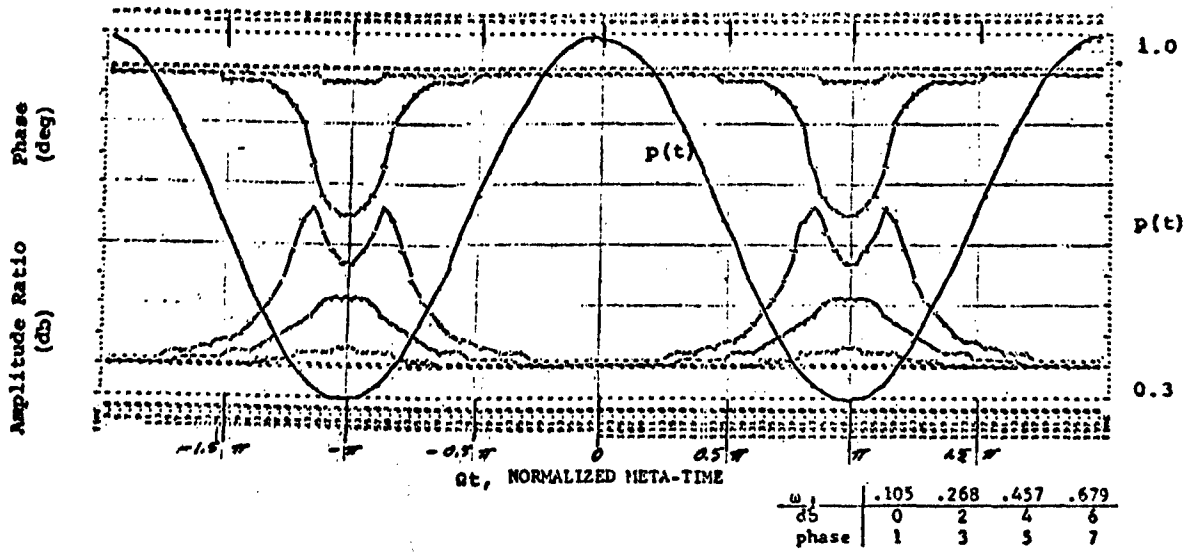

FIGURE 7 TIME HISTORY OF CALCULATED VARIATION OF THE PLANT TRANSFER FUNCTION $Y(j\omega,t)$ AT EACH INPUT FREQUENCY, ω_i.

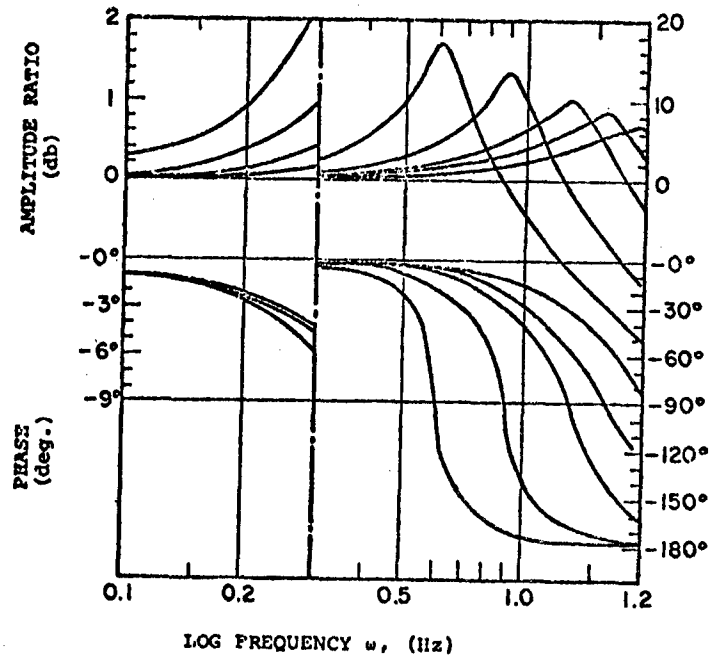

FIGURE 8 BODE PLOT OF SECOND ORDER PLANT TRANSFER CHARACTERISTIC AT VARIOUS PARAMETER SETTINGS.

TABLE 2. INPUT FORCING FUNCTION COMPONENT FREQUENCIES

	Frequency (Hz)	Frequency rad/sec	Separation Δf (Hz)	Nom. Amplitude	Filtered† Amplitude
ω_0	0.105	0.66	.210*	1	0.77
ω_1	0.268	1.68	.163	1	0.51
ω_2	0.457	2.87	.189	1	0.32
ω_3	0.679	4.27	.222	1	0.22
ω_4	0.83**	5.22	.251	0.1	0.02

† Filtered through a first order lag with break frequency of 1 rad/sec

* Separation, $\Delta f = 2(\frac{\omega_0}{2\pi})$

** Frequency ω_4 was extrapolated using equal log spacing. The other frequencies are from Russell (1951).

TABLE 3 PARAMETER DISTURBANCE FUNCTION

a) Time-Varying Plant Parameter Runs

RUN	$p(t) = .65 + .35 \cos(\Omega t)$ Meta-Forcing Function, Ω_k (Hz)	rad/sec	Period (Sec)
R60	.01	.063	100
R70	.02	.126	50
R80	.05	.315	20
R90	.08	.504	12.5
R00	.12	.756	8.3

b) Constant Plant Parameter Tasks

TASK	Meta-Forcing Function $p(t) = p_i$, constant	Second Order Plant Parameters ω_n (rps)	ζ, damping
T10	1.0	12.65	0.237
T20	0.80	10.13	0.190
T30	0.65	8.22	0.154
T40	0.45	5.70	0.107
T50	0.30	3.80	0.0711

TABLE 4 ORDER OF EXPERIMENTAL TRIALS

Training Tasks: Constant Parameter Plant

Plant Level P_i		Subject				
		S100	S200	S300	S400	S500
T10	1.0	2	4	2	1	5
T20	0.8	5	1	4	2	3
T30	0.65	3	5	1	3	4
T40	0.45	1	3	5	4	2
T50	0.3	4	2	3	5	1

Experimental Adaptive Runs: Time-Varying Plant

Parameter Forcing Frequency Ω (Hz)		Subject				
		S100	S200	S300	S400	S500
R60	.01	2	1,(6)*	4	5	3
R70	.02	3	4	1	2	5
R80	.05	1	5	3	4*	2,(6)*
R90	.08	4	2	5	3	1
R00	.12	5	3	2	1	4

*Repeated at end of experimental session

TABLE 5 RMS ERROR SCORES FOR CONSTANT PLANT TASKS AND TIME-VARYING PLANT RUNS

Subject	Constant Plant Tasks				
	S100	S200	S300	S400	S500
T10	29.4	29.5	26.2	27.0	31.2
T20	28.2	26.9	28.3	29.3	31.0
T30	30.9	30.5	31.6	30.1	31.2
T40	36.0	32.0	35.2	40.2	33.8
T50	36.2	36.6	42.7	52.8	36.6
	Time-Varying Plant Runs				
R60	32.4	35.5	34.9	35.1	33.5
R70	34.6	35.6	34.2	37.5	33.3
R80	34.2	39.3	35.2	35.4	34.6

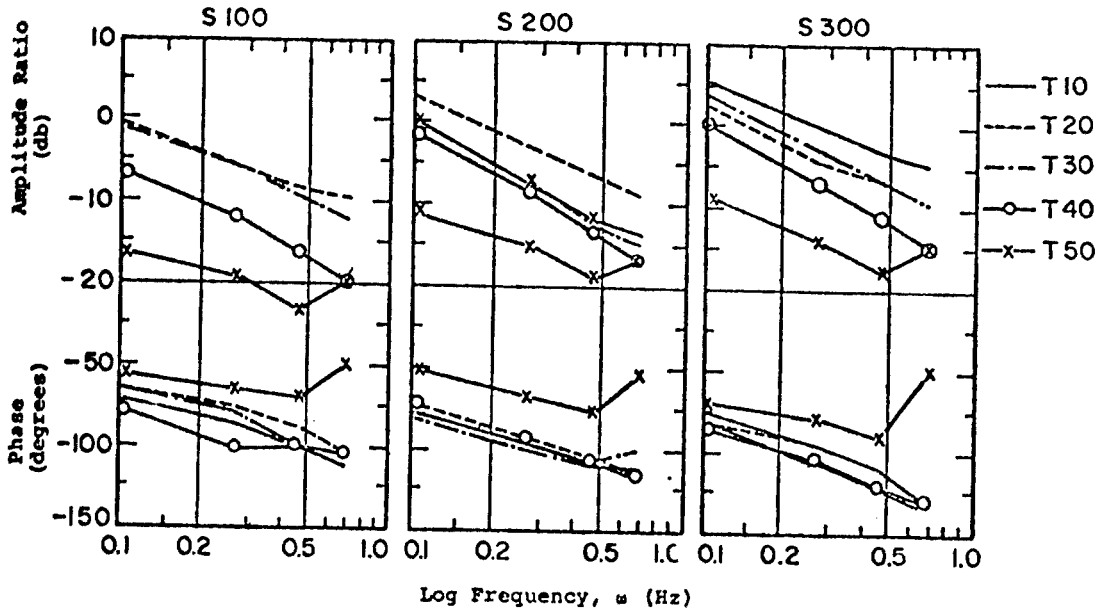

FIGURE 9a) BODE PLOTS OF SMOOTHED ESTIMATES $\bar{H}(j\omega,p_i)$, THE HUMAN OPERATOR TRANSFER CHARACTERISTIC FOR CONSTANT PLANT TASKS, (S100, S200, S300).

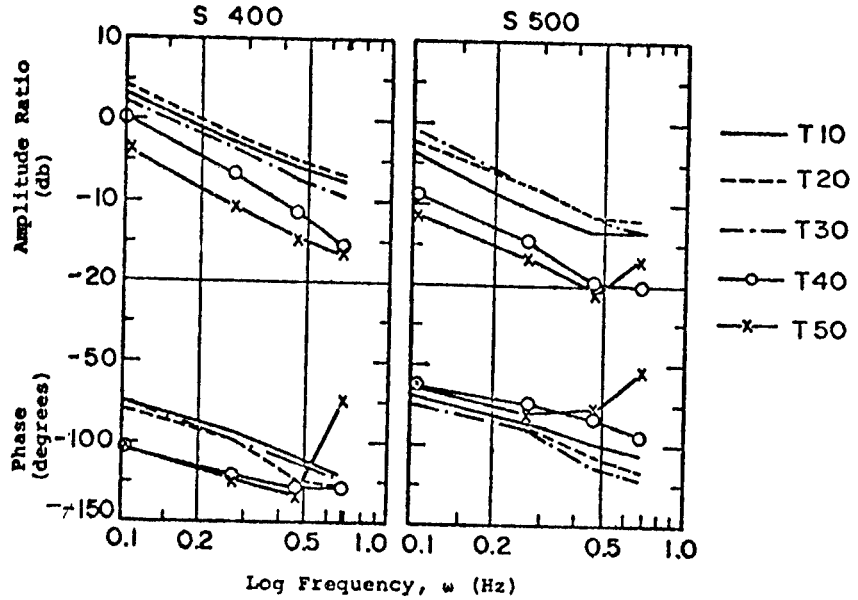

FIGURE 9b) BODE PLOTS OF SMOOTHED ESTIMATES $\bar{H}(j\omega,p_i)$, THE HUMAN OPERATOR TRANSFER CHARACTERISTIC FOR CONSTANT PLANT TASKS, (S400, S500).

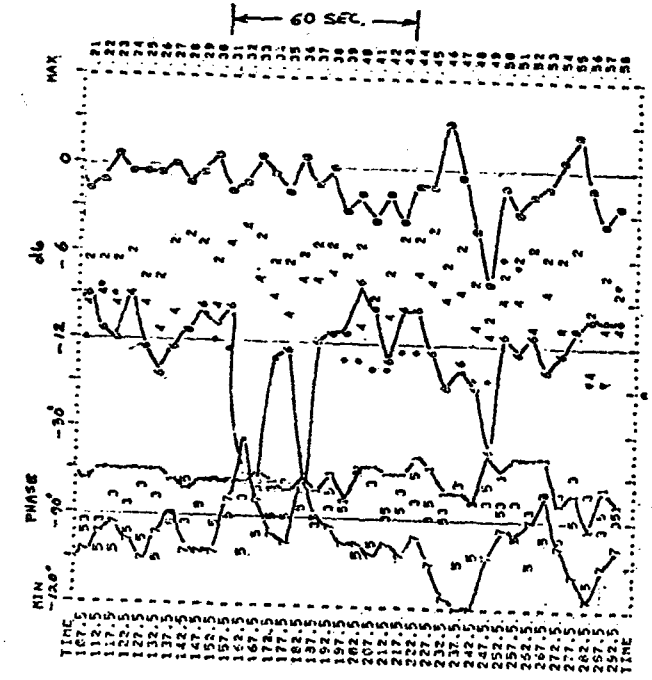

σ_t = 2.5 sec. ΔT = 5 sec.
TASK T30 (P_1 = 0.65)
SUBJECT: S100

ω_1	db	phase
.105	0	1
.268	2	3
.457	4	5
.679	6	7

FIGURE 10 TIME HISTORY OF VARIATION OF $\hat{H}(j\omega,k\Delta T)$, THE LOCALIZED HUMAN OPERATOR TRANSFER CHARACTERISTIC ESTIMATES FOR A CONSTANT PLANT TASK, (S100).

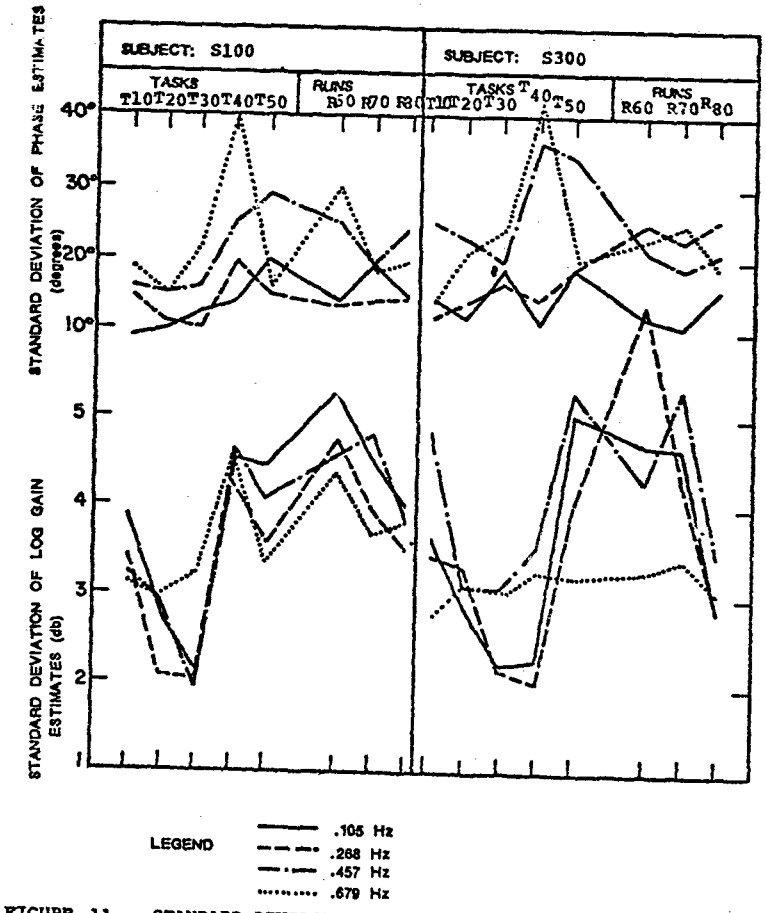

FIGURE 11 STANDARD DEVIATIONS OF TIME-VARYING HUMAN OPERATOR LOCALIZED TRANSFER CHARACTERISTIC ESTIMATES H(jω,t) FOR VARIOUS PLANT PARAMETER CONDITIONS.

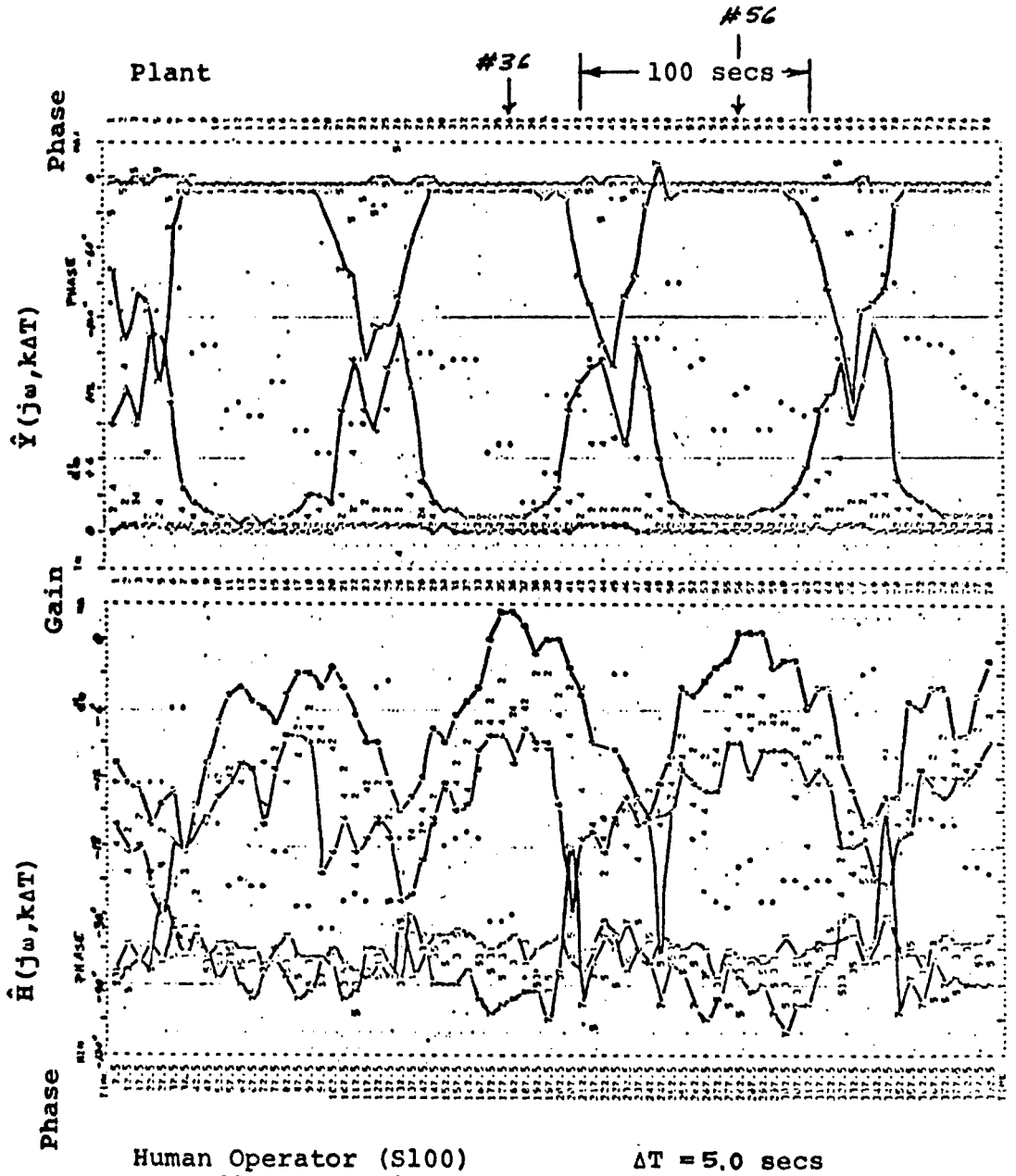

Human Operator (S100)
Run R60, Ω_k = .01 Hz

ΔT = 5.0 secs
σ_t = 2.5 secs

ω_i	.105	.268	.457	.679
db	0	2	4	6
Phase	1	3	5	7

FIGURE 12) TIME HISTORY OF SUCCESSIVE LOCALIZED ESTIMATES $\hat{H}(j\omega,k\Delta T)$ and $\hat{Y}(j\omega,k\Delta T)$, THE HUMAN OPERATOR AND PLANT TRANSFER CHARACTERISTICS FOR TIME-VARYING PLANT RUNS, (σ_t = 2.5 secs, Ω_k = .01 Hz).

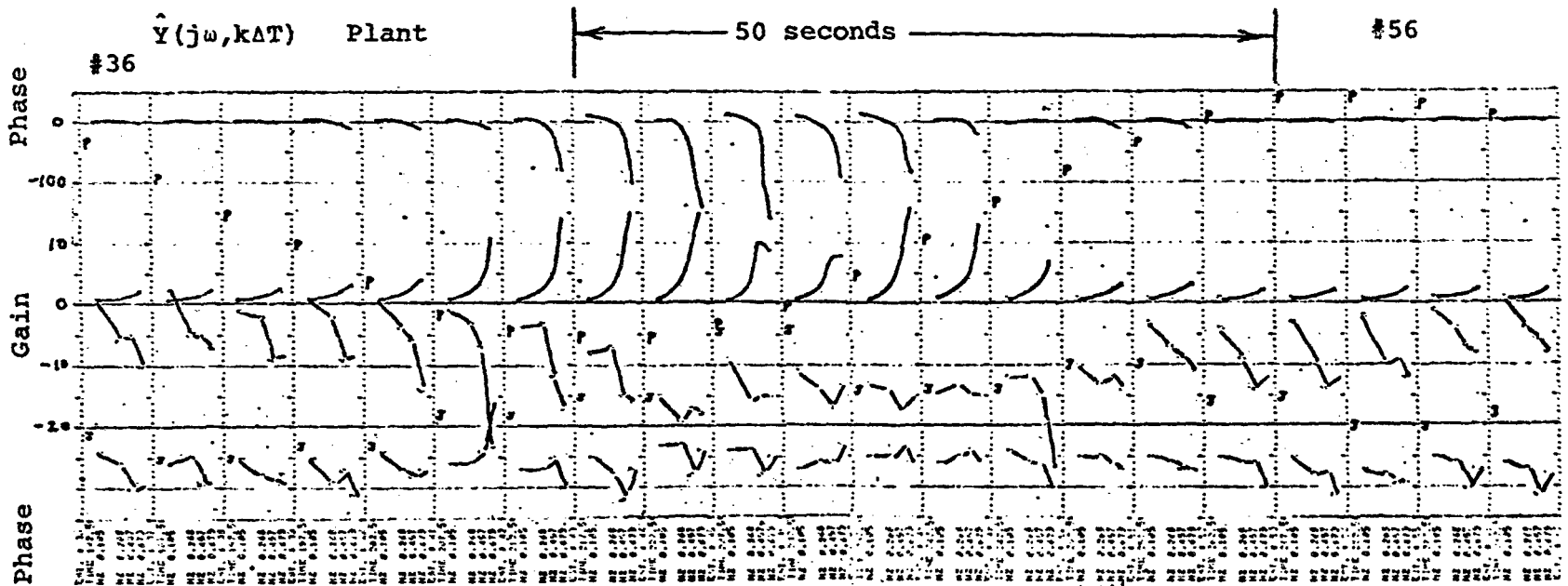

$\hat{H}(j\omega,k\Delta T)$ Human Operator, S100

R60, Ω_k = .01 Hz, (σ_t = 2.5 secs)

ω_i (Hz) { .105, .268, .457, .679

p = meta-forcing function

J = performance index

FIGURE 13) "TRAVELING BODE PLOTS" OF SUCCESSIVE LOCALIZED HUMAN OPERATOR AND TIME-VARYING PLANT SPECTRAL ESTIMATES, (R60, Ω_k = .01 Hz)

Reproduced from best available copy.

PLANT PARAMETER META-FORCING FUNCTION FREQUENCIES

INPUT FORCING FUNCTION FREQUENCIES

Ω_k (Hz), Run	ω_0 .105 Hz			ω_1 .268 Hz			ω_2 .457 Hz			ω_3 .679 Hz		
	Gain (db)	Phase (deg.)	Coh. ρ	Gain (db)	Phase (deg.)	Coh. ρ	Gain (db)	Phase (deg.)	Coh. ρ	Gain (db)	Phase (deg.)	Coh. ρ
.01 R60	0.7	-47	.974	-0.5	-51	.974	-1.4	-38	.978	-0.6	-32	.969
.02 R70	-7.8	-92	.814	-5.5	-97	.896	-4.5	-79	.883	-2.4	-77	.952
.05 R80	-9.7	-53	.938	-10.8	-79	.936	-8.3	-73	.927	-7.1	-102	.929

TABLE 6 BI-FREQUENCY ESTIMATES OF $\bar{\Lambda}_H(\omega_i, \Omega_k)$, THE HUMAN OPERATOR ADAPTIVE GAIN RESPONSE RELATIVE TO THE RESPONSE OF THE GAIN ADAPTATION MODEL FOR CONSTANT PLANT TASKS, (S100).

PLANT PARAMETER META-FORCING FUNCTION FREQUENCIES

INPUT FORCING FUNCTION FREQUENCIES

Subject	Ω_k (Hz), Run	ω_0 .105 Hz			ω_1 .268 Hz			ω_2 .457 Hz			ω_3 .679 Hz		
		Gain (db)	Phase (deg.)	Coh. ρ	Gain (db)	Phase (deg.)	Coh. ρ	Gain (db)	Phase (deg.)	Coh. ρ	Gain (db)	Phase (deg.)	Coh. ρ
S100	.01 R60	32.8	145	.967	15.9	135	.969	3.6	148	.980	-2.0	160	.874
	.02 R70	22.6	135	.607	12.5	97	.931	-0.2	99	.830	+0.8	151	.923
	.03 R80	22.3	187	.914	7.5	118	.927	-4.4	112	.830	-4.9	116	.963
S300	.01 R60	28.3	175	.926	11.1	186	.934	-2.1	129	.826	-6.6	211	.716
	.02 R70	32.6	148	.690	15.7	159	.953	2.2	178	.814	-4.4	177	.711
	.03 R80	22.6	153	.889	7.9	122	.867	-7.6	131	.523	-6.8	112	.895

TABLE 7 BI-FREQUENCY ESTIMATES OF $\bar{\Gamma}(\omega_i, \Omega_k)$, THE HUMAN OPERATOR ADAPTIVE RESPONSE RELATIVE TO THE TIME-VARYING PLANT TRANSFER CHARACTERISTIC, (S100 and S300).

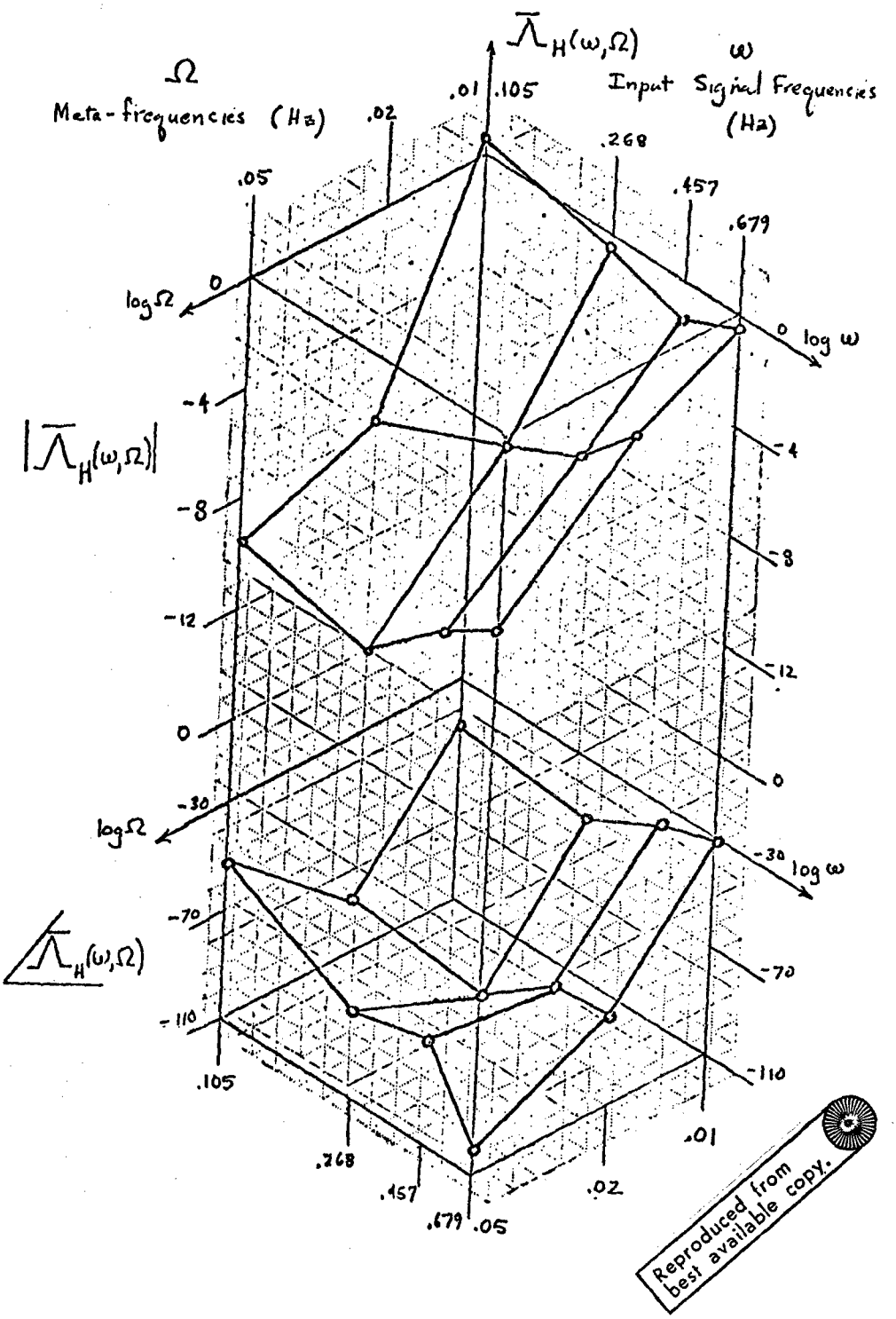

FIGURE 14a) PLOTTED BI-FREQUENCY ESTIMATES OF $\bar{\Lambda}_H(\omega_i, \Omega_k)$, THE HUMAN OPERATOR ADAPTIVE GAIN RESPONSE RELATIVE TO THE RESPONSE OF THE GAIN ADAPTATION MODEL FOR CONSTANT PLANT TASKS, (S100).

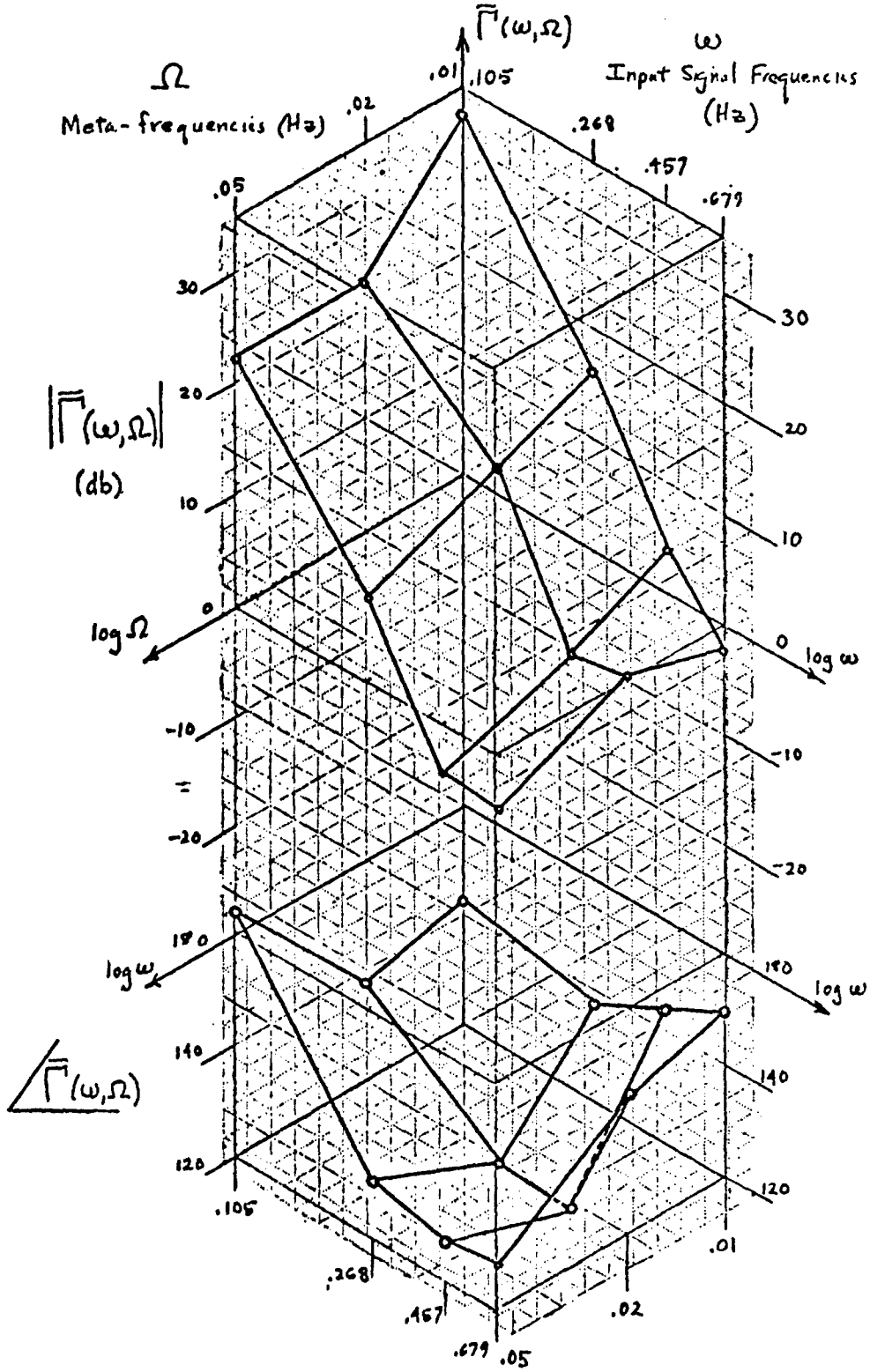

FIGURE 14b) PLOTTED BI-FREQUENCY ESTIMATES OF $\overline{\Gamma}(\omega_i,\Omega_k)$, THE HUMAN OPERATOR ADAPTIVE RESPONSE RELATIVE TO THE TIME VARYING PLANT TRANSFER CHARACTERISTIC (S100).

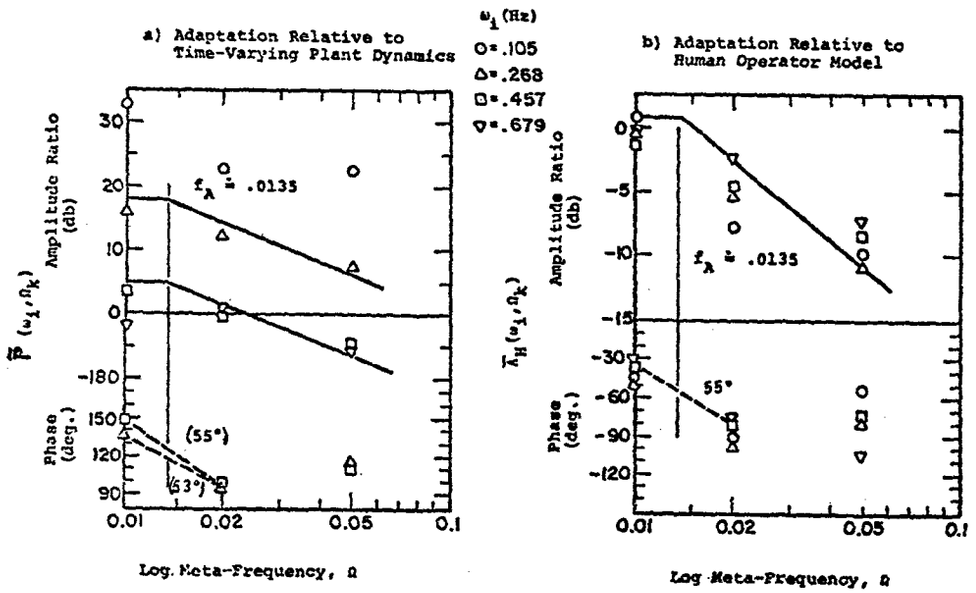

FIGURE 15 BODE PLOT OF FIRST ORDER FIT TO ADAPTIVE TRANSFER CHARACTERISTICS

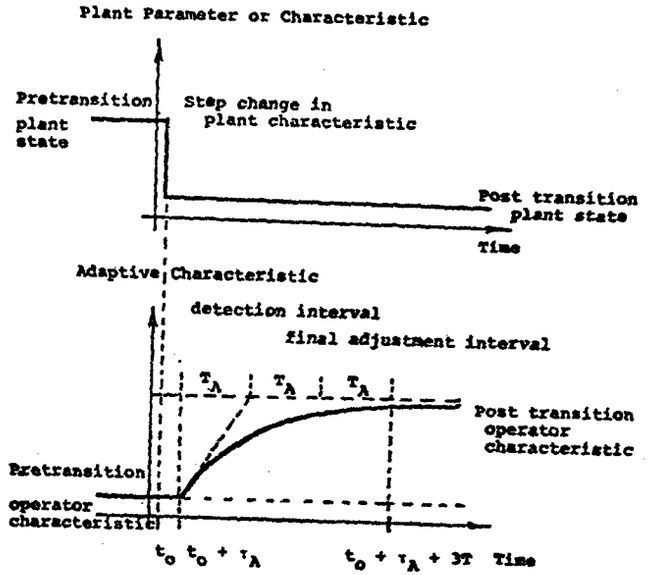

Transient Adaptation Derived From Frequency Response Model

$$A(\omega_i, \Omega) = \frac{K_A \, e^{-j\Omega\tau_A}}{T_A j\Omega + 1} \quad \text{where} \quad T_A = \frac{1}{\Omega_A}$$

Ω_A = meta-bandwidth

FIGURE 16 HYPOTHETICAL TRANSIENT ADAPTATION TO CHANGE IN PLANT DYNAMICS.

SOME RECENT EXPERIMENTAL RESULTS PERTAINING TO THE ESTIMATION OF POWER SPECTRA USING FINITE LENGTHS OF DATA

Richard F. Whitbeck and James R. Knight
Cornell Aeronautical Laboratory, Inc.
Buffalo, New York 14221

Abstract

Spectral estimation, using finite lengths of data, is an important tool for modeling the human. This paper presents experimental results which demonstrate a significant improvement in auto and cross spectral estimates when a particular combination of time-domain filtering and frequency-domain averaging is used.

1. Introduction

Under a National Aeronautics and Space Administraction contract (NAS-1-10514), a modeling approach, which utilizes a matrix of transfer functions to describe the human pilot in multiple-input, multiple-output control situations, was studied. The approach used was to extend a well-established scalar Wiener-Hopf minimization technique to the matrix case and then study, via a series of experiments, the data requirements when only finite record lengths are available. Although the ultimate objective was to run many variations on a two-controller roll tracking task in order to assess the effect, on the pilot model, of increasingly complex tasks, fundamental problems surfaced in the early stages of the study which ultimately restricted the effort to only one configuration. Identification of these problems and the manner in which they were solved are important results of this study.

The primary problem was the failure to obtain anticipated results in estimating test case dynamics, such as K/s^2 . We refined our computational algorithms to the point where acceptable estimates were obtained, although over a frequency range which was considerably narrower than one would anticipate on the basis of sampling theorem considerations. It was demonstrated that this restricted range was attributable to the presence of certain anomalies that are introduced by use of finite lengths of data. The purposes of this paper are: 1) to describe these anomalies; and 2) to present experimental evidence of the need for careful consideration of both filtering the raw data in the time domain and ensemble averaging the spectral estimate in the frequency domain. In addition, it is pointed out that computational procedures based upon the theoretical independence of two signals may be invalid when cross power spectra are computed using finite lengths of data.

Preceding page blank

2. Direct Computation of Power Spectra Using the Fast Fourier Transform

Several approaches are possible for the computation of power spectra. One may first use the time signals in the computation of the auto-correlation function, followed by a Fourier transform to arrive at an estimate of the power spectra. This is an attractive way to proceed in those cases where an estimate of the power spectra is desired at only a few discrete frequencies. An alternate approach, which is preferable when the power is being estimated at a very large number of frequencies, is to estimate the auto-or cross-spectra directly from the time signals themselves, using, for example, the equation

$$\hat{\phi}_{xy}(\omega) = \frac{1}{2T}\frac{1}{N}\sum_{i=1}^{N} X_i(-j\omega)\,Y_i(j\omega) \tag{1}$$

That is, one first computes the truncated transform of $x(t)$ and $y(t)$, using the equations

$$X_i(j\omega) = \int_{-T}^{T} x_i(t)\,e^{-j\omega t}\,dt\,, \tag{2}$$

$$Y_i(j\omega) = \int_{-T}^{T} y_i(t)\,e^{-j\omega t}\,dt\,. \tag{3}$$

Theoretically, this is done for a very large number of realizations of the random variables x and y and then an ensemble average (across frequency) is carried out in order to arrive at a smooth estimate. In the limit, the true cross power spectrum

$$\phi_{xy} = \lim_{T\to\infty}\frac{1}{2T}E\left\{X(-j\omega)\,Y(j\omega)\right\} \tag{4}$$

is attained as the number ensembled across and the length of each record approaches infinity. The advantage (a considerable one) in using Equation (1) to approximate Equation (4) is that the Fast Fourier Transform can be used to compute the (truncated) Fourier Transforms. That is, one proceeds directly from the time to the frequency domain without the intermediate stop in the correlation (τ) domain.

3. Time Windows and Their Relationship to Lag and Spectral Windows

Since the literature which discusses the "Lag" and "Spectral" windows is concerned with the relationships which exist between the correlation and frequency domains, and since our interest is with relationships which exist

between time and frequency, it will next be necessary to present a slight clarification of the relationships which exist between all three of these domains (i.e., t , τ and ω).

Basically, the process of working with finite lengths of data can be visualized as multiplying the infinite record length by a signal such as

$$f(t) = \begin{cases} 1 & -T < t < T \\ \\ 0 & |T| \geq T \end{cases} \tag{5}$$

This $f(t)$ is called a time window, and has a corresponding spectral window of the form $(\sin \omega T/\omega T)^2$. The basic relationships associated with the square time window are given in Equation (6), where $\hat{\phi}_{XY}$ is the estimate of the power spectra, R_{XY} is the true underlying correlation function and $\phi(\omega)$ is the true underlying power spectra.

$$\begin{aligned} \hat{\phi}_{XY} &= \frac{1}{2T} E\left\{ X(-s) \quad Y(s) \right\}\Big|_{s=j\omega} \\ &= \int_{-2T}^{2T} \left(1 - \frac{|\tau|}{2T}\right) R(\tau) e^{-j\omega\tau} d\tau = \frac{T}{\pi} \int_{-\infty}^{\infty} \phi(\omega_1) \left[\frac{\sin(\omega - \omega_1)T}{(\omega - \omega_1)T}\right]^2 d\omega_1 \end{aligned} \tag{6}$$

Equation (6) can be extended to a more general case, which will permit the use of temporal windows other than the usually used square one. This is most important, because the use of the Fast Fourier Transform (FFT) requires direct computation of the Fourier Transform of the signals. Thus we are not at liberty to work with the correlation function and filter the data in the τ domain -- we must know what the temporal windows look like in order to filter directly in the time domain.

Let

$$f(t) = \begin{cases} \text{even} & -T < t < T \\ \\ 0 & |t| \geq T \end{cases} \tag{7}$$

then Equation (6) becomes

$$\begin{aligned} \hat{\phi}_{XY} &= \frac{1}{2T} E\left\{ X_T(-s)\, Y_T(s) \right\} = \frac{1}{2T} \int_{-\infty}^{\infty} R(\tau) \left[\int_{-\infty}^{\infty} f(t) f(\tau - t)\, dt \right] e^{-j\omega\tau} d\tau \\ &= \frac{1}{4\pi T} \int_{-\infty}^{\infty} \phi(\omega_1)\, F^2(\omega - \omega_1)\, d\omega_1 \qquad \text{where} \quad F(\omega) = \mathcal{F}\left\{ f(t) \right\} \end{aligned} \tag{8}$$

Refer to Reference 2 for a derivation.

It is our experience that a comparison between "windows", using spectral estimates obtained from only one record length is almost meaningless. It is not until one filters the data in time and then ensembles across a number of estimates (in the frequency domain) that the true distinctions between the time filters becomes apparent.

The properties of three windows are listed in Table I. In this paper, results pertaining only to the first two time windows will be presented.

4. Scalar Experiments

The first scalar experiment was the pilot-in-the-loop roll tracking task shown in Figure 1.

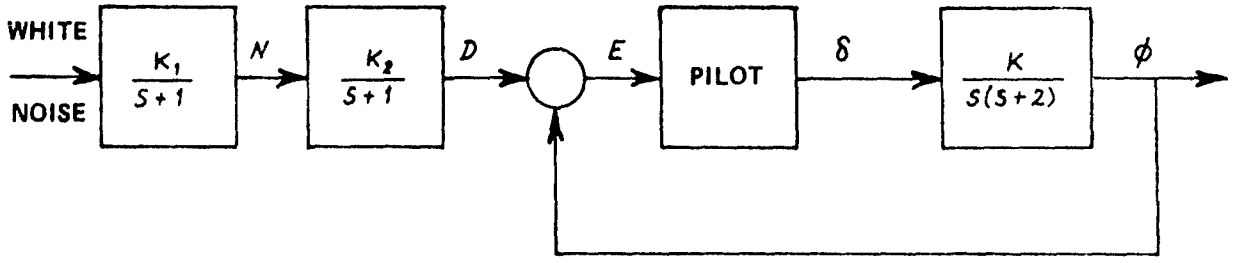

Figure 1 EXPERIMENT #1

Analog data was recorded and, simultaneously converted to digital form through the use of analog to digital recording equipment. The various power spectra were then computed.

The final sampling rate used was 125 S/S, given a sampling frequency of approximately 785 rad/sec and a folding frequency of about 392 rad/sec. In this experiment, the CAL fixed-base simulator was flown by an instrument rated pilot. The disturbance source was derived from a gaussian white noise source passed through two cascaded first-order filters.

The second scalar roll tracking task is depicted in Figure 2.

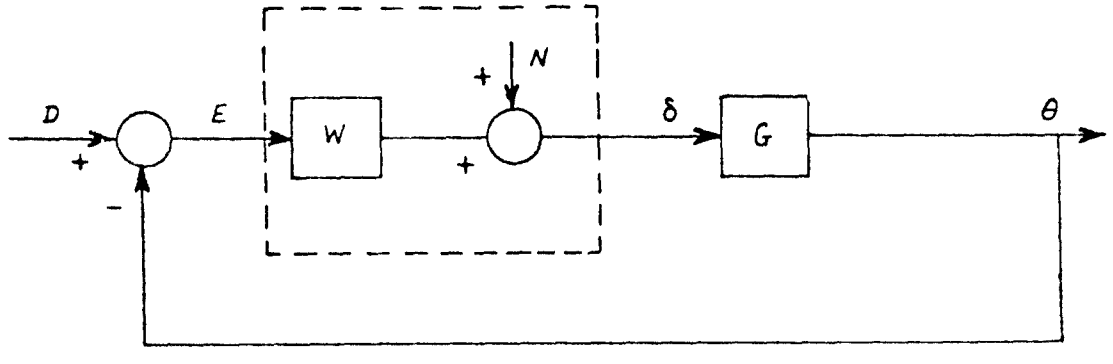

Figure 2 EXPERIMENT #2

TABLE I
CHARACTERISTICS OF SPECTRAL WINDOWS

TIME WINDOW	LAG (τ) WINDOW	SPECTRAL WINDOW	$\hat{\phi}_{xy}$
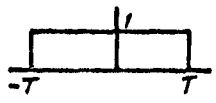	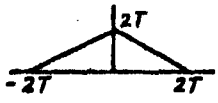	$\left(\frac{\sin \omega T}{\omega T}\right)^2$	$\frac{T}{\pi}\int_{-\infty}^{\infty}\phi(\omega_1)\left[\frac{\sin(\omega-\omega_1)T}{(\omega-\omega_1)T}\right]^2 d\omega_1$
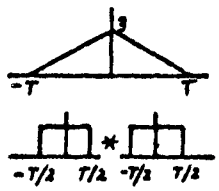	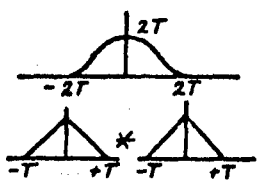	$\left(\frac{\sin\left(\frac{\omega T}{2}\right)}{\frac{\omega T}{2}}\right)^4$	$\frac{T}{4\pi}\int_{-\infty}^{\infty}\phi(\omega_1)\left[\frac{\sin\frac{(\omega-\omega_1)T}{2}}{\left(\frac{\omega-\omega_1}{2}\right)T}\right]^4 d\omega_1$
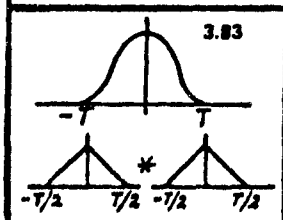	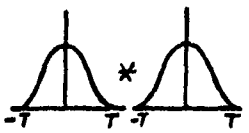	$\left(\frac{\sin\left(\frac{\omega T}{4}\right)}{\frac{\omega T}{4}}\right)^8$	$\approx\int_{-\infty}^{\infty}\phi(\omega_1)\left[\frac{\sin\frac{(\omega-\omega_1)T}{4}}{\left(\frac{\omega-\omega_1}{4}\right)T}\right]^8 d\omega_1$

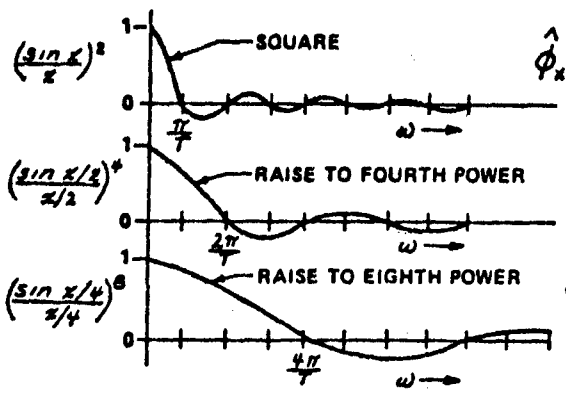

$$\hat{\phi}_{xy} = \frac{1}{2T} E\left\{X(-s)\, Y(s)\right\} = \frac{1}{4\pi T}\int_{-\infty}^{\infty}\phi(\omega_1)\, F^2(\omega-\omega_1)\, d\omega_1$$

$$= \frac{1}{2T}\int_{-\infty}^{\infty} R(\tau)\left[\int_{-\infty}^{\infty} f(t)\, f(\tau-t)\, dt\right] e^{-j\omega\tau}\, d\tau$$

WHERE

$$f(t) = \begin{cases} \text{EVEN} & -T < t < T \\ 0 & |t| \geq T \end{cases}$$

$$\mathcal{F}\left\{f(t)\right\} = F(\omega)$$

This experiment is an analog simulation of the "Subject M" run described in Table III of Reference 1, the case where Disturbance (Volts^2) = 5.61.

The disturbance input in Figure 2 is obtained by feeding white noise through the transfer function $K/(s+1)^2$ while the noise (remnant) is obtained by feeding white noise through the transfer function $K/(s+10)^2$. In the analog simulation, the signals D, E, N, δ and θ were recorded.

The main task in this experiment is to estimate the given W of Figure 2, given that the noise source N cannot be measured (i.e., N is internal pilot noise). In addition, it was felt that estimates of K/s^2 should also be made since the dynamic range of the input power spectra was quite large (on the order of 60 db on a power basis, 120 on a voltage basis).

5. Computation Procedure

The data was collected in digital format via the CAL digital recording facility (COREC), which consists of a data acquisition unit and a tape transport.

The data acquisition unit accepts analog or digital inputs and produce digital outputs suitable for recording on the digital tape transports. The analog inputs are sampled sequentially and converted to digital signals by a high speed A/D converter.

Various combinations of tape speeds and packing densities determine the rates at which the transports can accept data from the data acquisition units. These rates, combined with the number of variables determine the permissible sampling rates for each variable. For 5 variables plus a digital count channel, the choices of sampling rates close to 100 samples/second are 58 S/S, 125 S/S and 350 S/S. The rate of 125 S/S was selected.

The steps in the data handling procedure are:

(1) Record data on digital tape using COREC hardware.

(2) Use blocking program (part of COREC software) to break records into lengths that can be handled by normal computer I/O subroutines (32,760 bytes is the maximum physical record for normal tapes on IBM 370 computers, our data records were around 203,000 bytes).

(3) Convert the data to normal floating point numbers while checking for errors in the input data (missed bytes because of bad spots on tape or hardware problems). This step uses the general purpose COREC program.

(4) Special program to arrange data into arrays by variable, for efficient I/O.

(5) Multiply each piece of record, of length $2T$ seconds, by the desired time window.

(6) Use Fast Fourier Transform.

(7) Sum real and imaginary parts of each spectral estimate with values for these variables and frequency from previous records (ensemble average).

6. Overview of Computational Efforts

At this point, it is appropriate to review the computational efforts on these experiments in order to make it quite clear that the spectral estimates presented in this paper represent the net effort of following several alternate options. First, the matter of data rate was explored. In each experiment, we observed a "roll up" and "break up" phenomenon (to be defined shortly) which was first attributed to folded power (the sampling rate was initially 20 S/S). However, increasing the sampling rate to 125 S/S did not improve matters.

Next, averaging "around" a frequency point was tried. That is, the hypothesis that frequency estimates in the immediate neighborhood of a given frequency were (in some sense) "close" estimates of what was occurring at the given frequency, gave impetus to the idea of averaging adjacent points in the frequency domain. This procedure was also unsuccessful in improving the estimates.

Next, the correlation (lag) method was tried, even though the computations were considerably more costly to carry out. The results were essentially identical with the estimates obtained directly in the frequency domain.

Increasing record length from 20 sec. to 60 sec. to two minutes did enlarge the range of frequencies over which the estimates were better, however, it did not eliminate the basic phenomenon observed ("roll up" and "break up") at the end points of the estimates.

Next, the number of estimates ensembled across was carried to a very high number (≈ 134) but even this did not eliminate the "roll up" in the spectral estimates.

To investigate the possibility that the problem was noise, generated by the analog-to-digital recording process, the second experiment was run in an all digital manner (using a state space approach) on the IBM 370 digital computer. However, the problem still persisted.

These long series of experiments convinced us that the experimental anomalies were not due to noise, that ensemble averaging did not eliminate them and neither did filtering alone seem to have a great effect.

Finally a combination of ensemble averaging (in the frequency domain) and filtering (in the time domain) was tried which produced a significant improvement in the estimates of the power spectra. Moreover, even with this improvement, the deviation from the true values of the system dynamics at high and low frequencies was significant. This forced us to conclude that the observed anomalies were truly the consequence of a computational algorithm operating on finite pieces of data. With this hypothesis, it was possible, using several analytical examples, to conclusively demonstrate the presence of three anomalies in the spectral estimates (Reference 2). We identify these as:

(1) "Roll Up" at high frequency

(2) "Break Up" at high frequency

(3) "Roll Down" at low frequency

7. Roll Up, Break Up and Roll Down

These terms are best understood with the aid of Figure 3 (K/s^2 dynamics from Experiment #2). "Roll Up" is defined to be an increase in the power magnitude for $\omega > 50$ rad/sec, "Break Up" is the term ascribed to the large divergence (oscillations) in both the phase and magnitude plot for $\omega > 50$ rad/sec, while "Roll Down" is the term used to describe a magnitude plot which has decreased to about -2 db at $\omega = .048$ rad/sec when it should read around +22 db.

The theoretical analysis given in Reference 2 demonstrates conclusively that all three of these phenomena are fundamentally tied to the finite length of the data available. That is, even when the signals are well above the digital noise level, the sampling rate is extremely high, and a very large number of fixed length records are available, we will still observe the roll up, break up and roll down anomalies in the spectral estimates.

For future reference, the K/s^2 dynamics were estimated using a triangular time data window and by ensemble averaging across, in the frequency domain, 100 estimates.

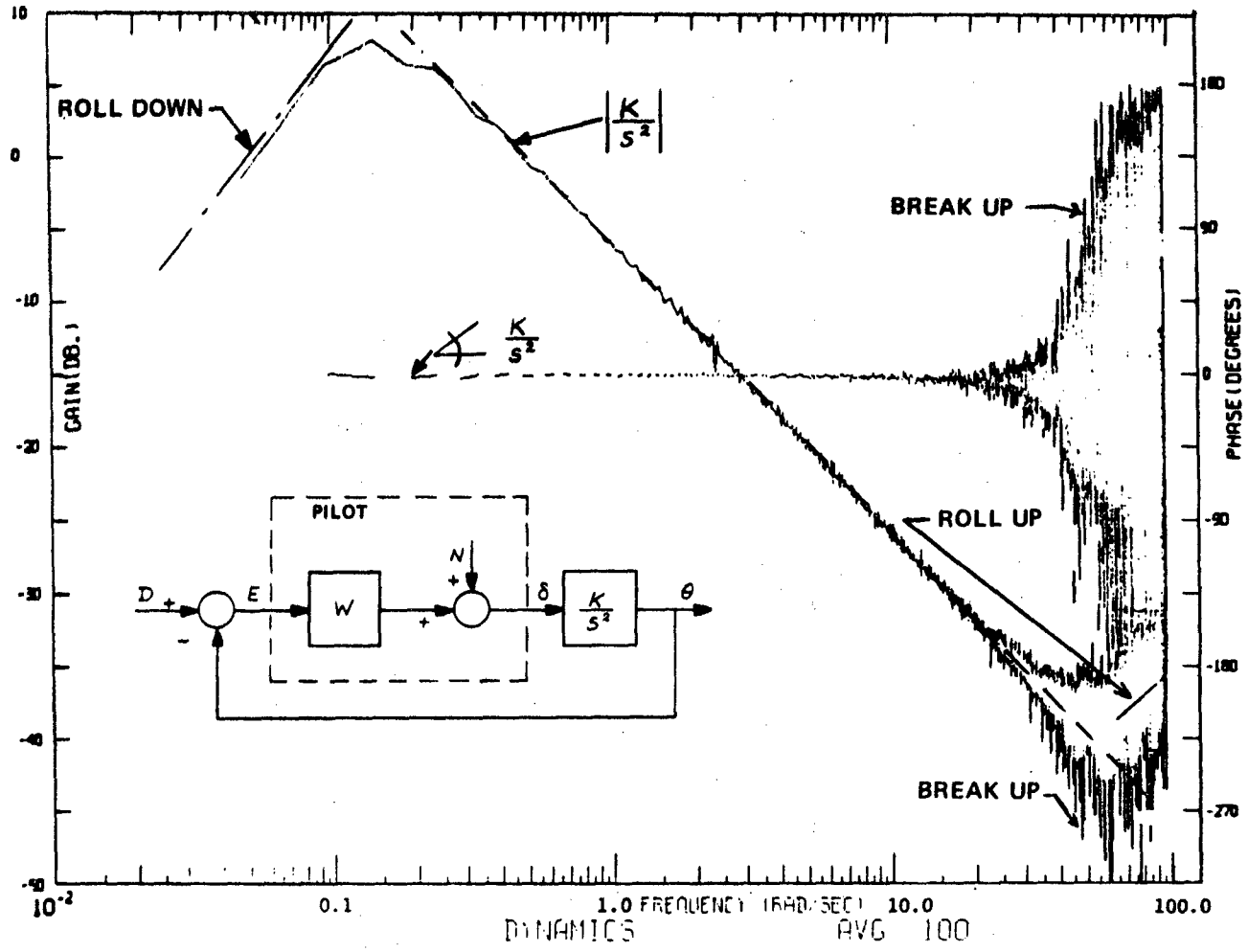

FIGURE 3. EFFECT OF ANOMALIES ON THE ESTIMATION OF $K/S2$

8. Effect of Data Window

Two spectral estimates of the dynamics $(K/s(s+2))$ are given in Figure 4. The sampling rate was 125 S/S, giving a folding frequency of approximately 390 rad/sec (only data out to 100 rad/sec was plotted). The cases shown are for an ensemble average across 28 estimates of the various auto and cross spectral densities used in the computation of the transfer functions. The time window used in 4a was the "square" window of Table I. Observe that "break up" (and roll up) occur at about 20 rad/sec, more than a decade away from the folding frequency. It was this plot which first convinced us that the break up was truly built into the algorithm used for computing the estimates and further, that some combination of direct filtering on the temporal data, as well as ensemble averaging, were required to reduce the bias in the high frequency region (it should be noted that in previous runs of this experiment (and Experiment 2), filtering appeared to be ineffective in reducing the variances in the spectral estimates). Thus our idea was to

employ the triangular data window of Table 1 in the hope of decreasing the bias while at the same time depending on ensemble averaging to keep the variance at an acceptance level. The results of this approach are shown in Figure 4b, where it is seen that a significant improvement has been achieved. Specifically, the frequency at which break up starts has been moved out on the order of two octaves and, more importantly, the dynamic range has been extended by approximately 10 db (in power) (For ease of presentation, the 4a plot has been biased upward by approximately 7db.)

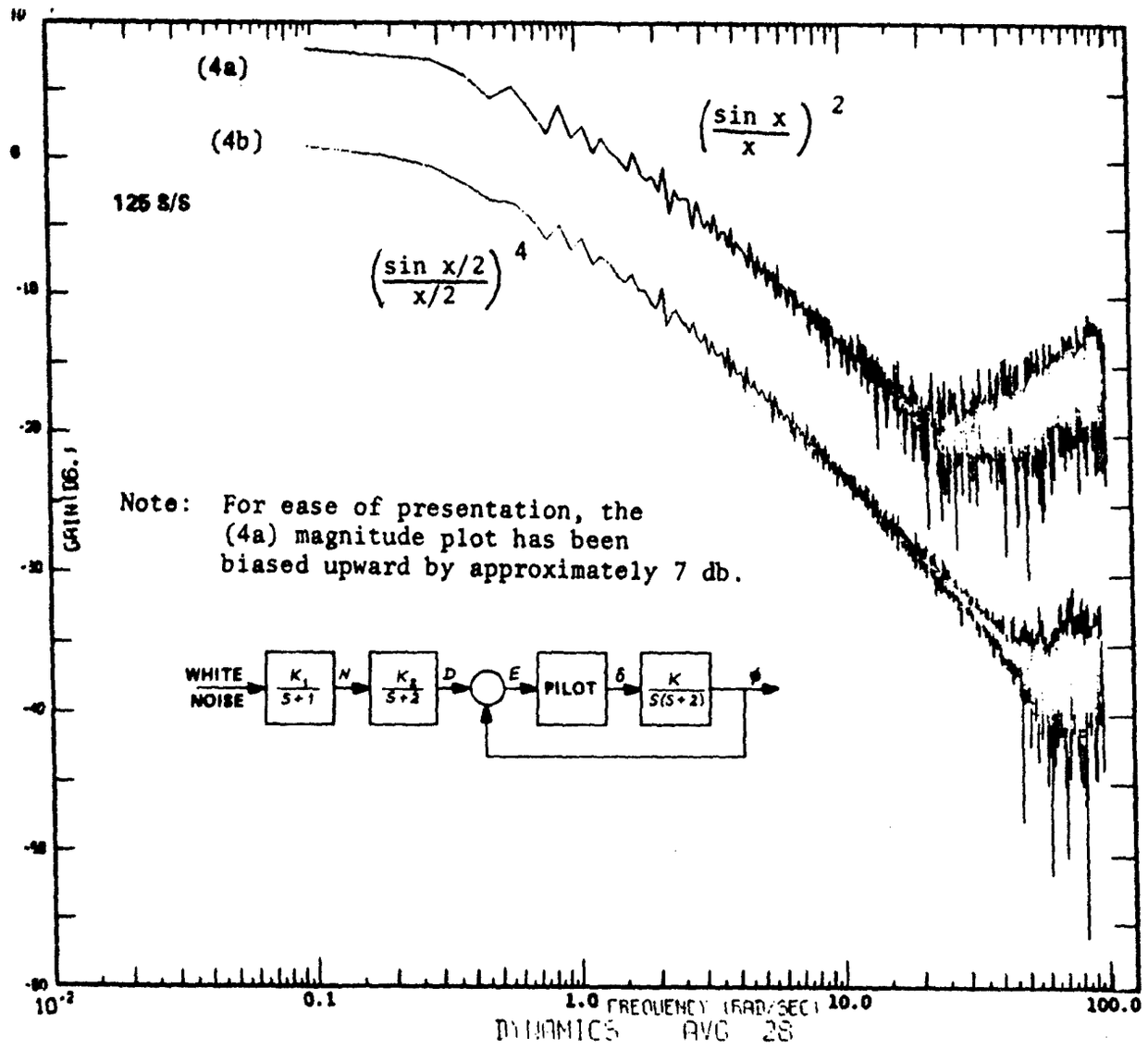

FIGURE 4. SINGLE CONTROLLER ROLL TRACKING EXPERIMENT, ENSEMBLE AVERAGING WITH (A) SQUARE TIME WINDOW (B) TRIANGULAR TIME WINDOW

These results show that the triangular time "window" is effective in reducing distortion. However, it must not be presumed that filtering is the entire story. In order to demonstrate that ensemble averaging is also required, a plot of the $(K/s(s+2))$ dynamics, without ensemble averaging, is shown in Figure 5. Additional experimental evidence will be presented in the next section.

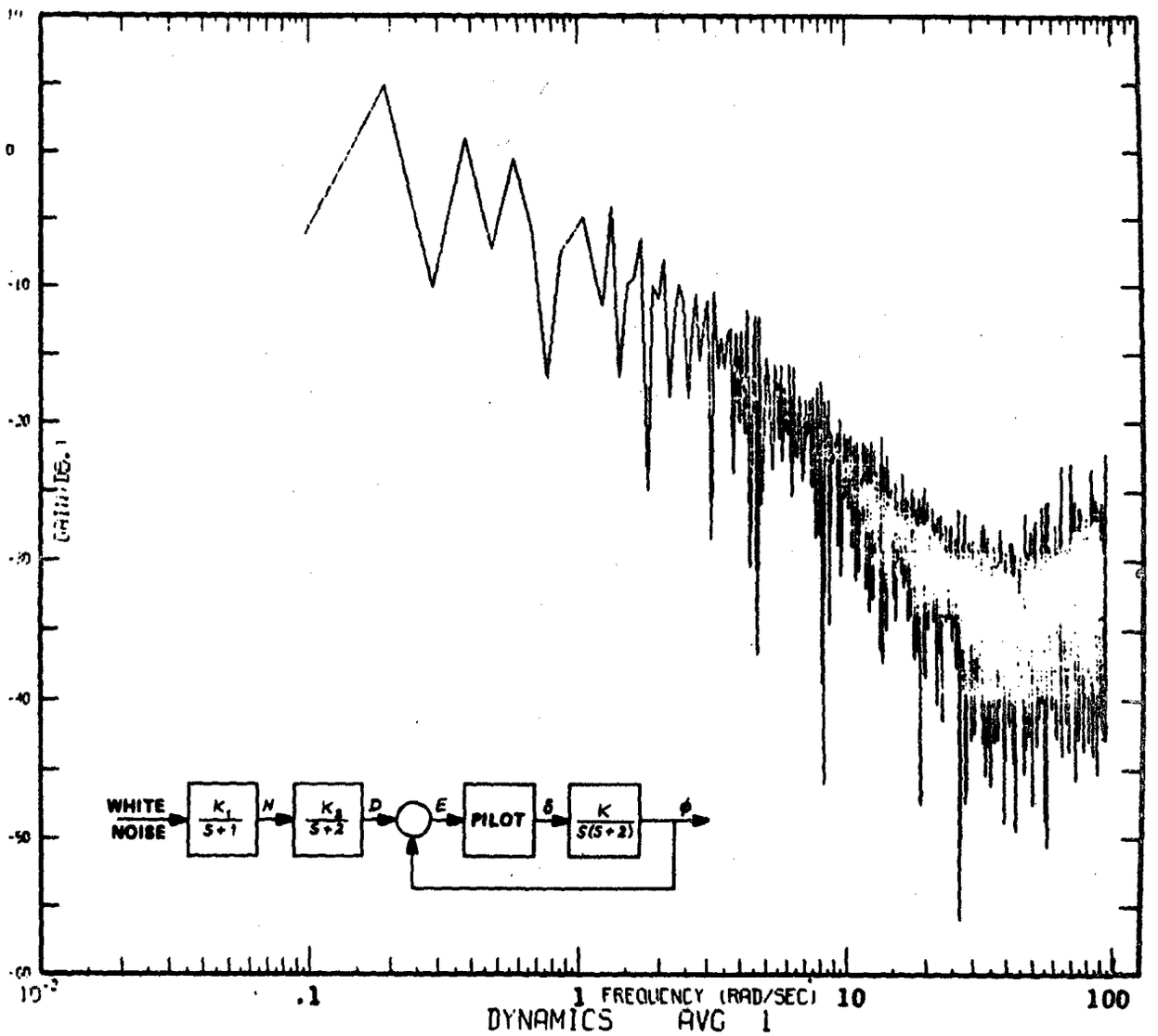

FIGURE 5. SINGLE CONTROLLER ROLL TRACKING EXPERIMENT, TRIANGULAR TIME WINDOW WITH NO ENSEMBLE AVERAGING

9. The Need for Ensemble Averaging

The improvement in the quality of the estimates of the $\frac{K}{S^2}$ dynamics of experiment 2, as the number of estimates averaged across increases, is shown in Figures 6 and 7. They are for ensembles of 1, 5, 10 and 50. (The average across 100 has been already shown in Figure 3).

The improvement between the ensemble of one and that of five is significant. Indeed, one would conclude that the results for an ensemble of 10, at least for this scalar experiment (dynamic range of 60 db), give as much information as the average of 50 results. Of course, the ensemble across 100 is extremely good, at least for the limited frequency range for which the aforementioned anomalies do not distort the estimate (see Figure 3). It is estimated that one could extrapolate usable results out to approximately 60 rad/sec before the break up and roll up completely confuse the picture - thus a useful range on the order of only $.2 < \omega < 60$ rad/sec is achieved even though the upper bound, using the sampling theorem, would be one half of the sampling frequency or about 390 rad/sec. In the two controller roll tracking experiment (Reference 2), which is not discussed in this paper, we encountered dynamic ranges on the order of 120 db (power basis) when the full scale six degree of freedom aircraft equations of motion were used. The useful (that is, believable) frequency range was reduced down to as low as 7 rad/sec even though the folding frequency was still on the order of 390 rad/sec. In Reference 2, it is shown, using an analytical analysis, that estimates based on the ratio of a cross to auto spectra can vary dramatically depending on how fast the input spectra is "rolling off" in frequency.

10. Cross Power Between Two Independent Signals

Before concluding with the second experiment, an important result, associated with the finite length of data will be commented on. The intent of the Subject "M" experiment was to identify the W transfer function of Figure 2 in the presence of the unmeasurable noise N. It is hypothesized that the remnant (N) is uncorrelated with the disturbance input D. This says, for the ideal situation of infinite record length that the exact equation for estimating W,

$$W = \frac{\phi_{D\delta} - \phi_{DN}}{\phi_{D\varepsilon}} \tag{9}$$

can be reduced to

$$W = \frac{\phi_{DS}}{\phi_{D\varepsilon}} \tag{10}$$

because $\phi_{DN} \equiv 0$.

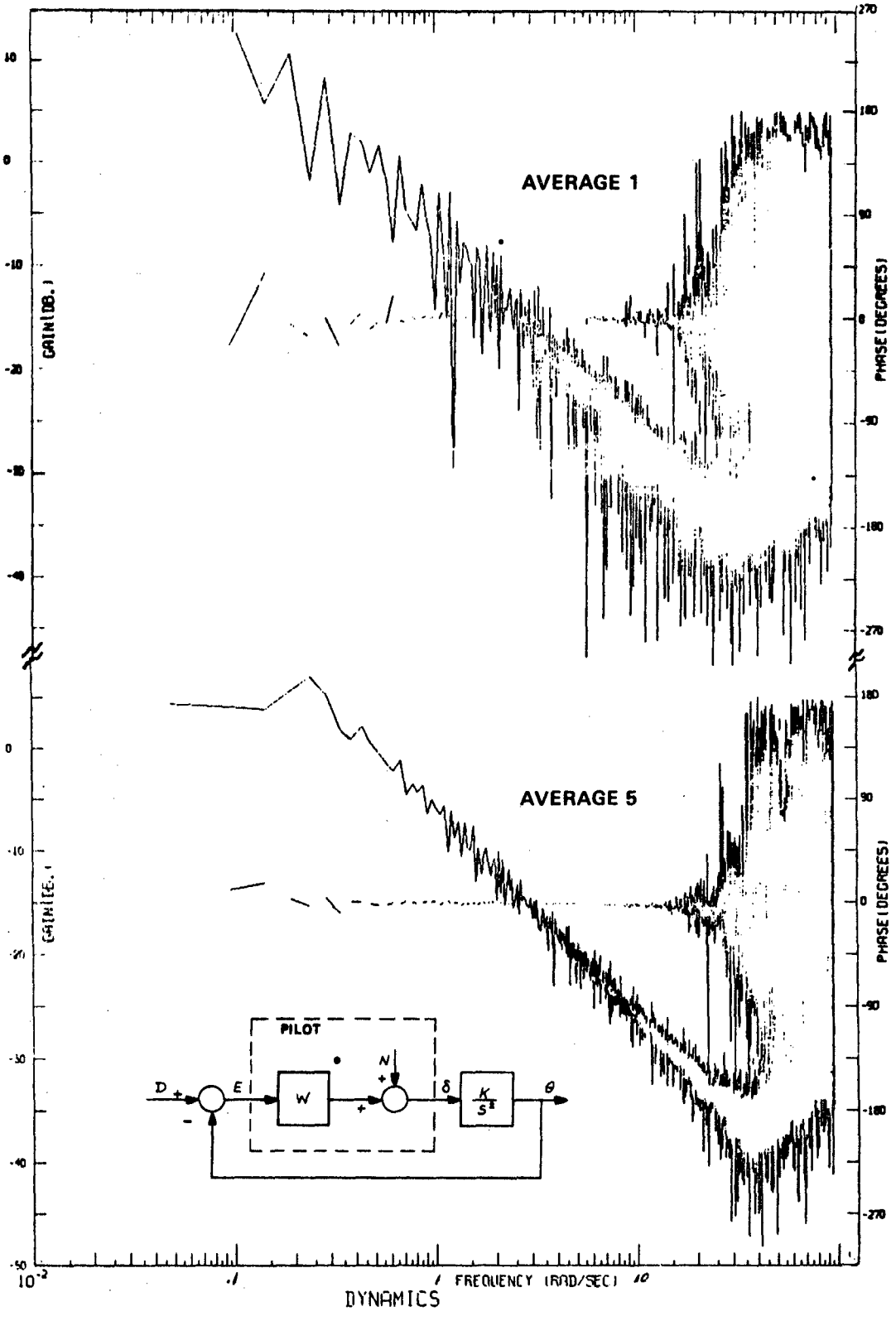

FIGURE 6. ESTIMATION OF $K/s2$, USING A TRIANGULAR DATA WINDOW, FOR AVERAGES OF 1 AND 5

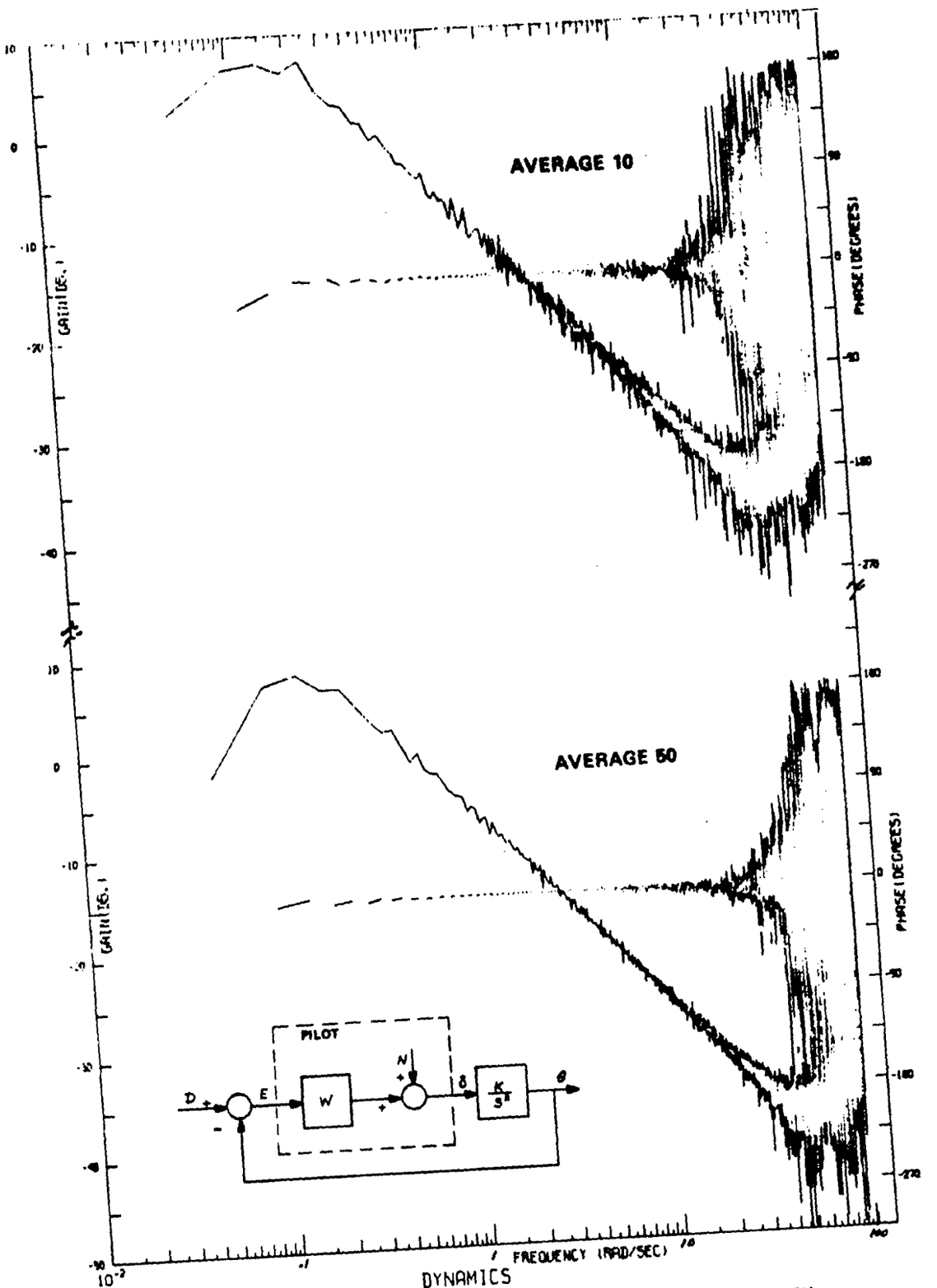

FIGURE 7. ESTIMATION OF K/s^2, USING A TRIANGULAR DATA WINDOW, FOR AVERAGES OF 10 AND 50

While this is true for an infinite set of records, each of finite length, it is a fact of life that the estimate of ϕ_{DN} will have, for a finite number of record data lengths, appreciable power. In Reference 2 it is shown that the magnitude of the estimate of cross power between two independent signals (call them X and Y), when no ensemble averaging is employed is,

$$|\hat{\phi}_{XY}| \cdot \sqrt{|\hat{\phi}_{XX}| \cdot |\hat{\phi}_{YY}|} \tag{11}$$

Furthermore, the employment of ensemble averaging diminishes this estimate of the cross power only by $1/\sqrt{n}$, n being the number of estimates ensembled across.

To illustrate this point, results from experiment #2 are given in Figure 8. In Figure 8, the pilot is estimated in two ways. In the first, it is assumed that N is measurable (i.e., $\phi_{DN} \neq 0$) while the second presumes that N is not physically assessable. The difference in the estimates are appreciable and are, of course, due to the fact that ϕ_{DN} is unequal to zero for finite data lengths (refer to reference 2 for the justification that the noise sources D and N used in this experiment were indeed independent). In the estimate for W in which N is assumed measurable, the straight line approximation for the magnitude plot has been drawn in. Figure 9 is the same as Figure 8 except that the phase plots are also included. (Note the tendency of the $\tan^{-1}$ routine to jump 180°).

11. Summary of Theoretical Conclusions and Experimental Observations

To summarize the theoretical analysis as well as the experimental observations:

(1) When working with finite lengths of data, the roll up, break up and roll down phenomena are to be expected.

(2) These anomalies will force a significant decrease in the frequency band over which believable estimates can be achieved. That is, the danger of looking at a spectral estimate which really portrays the characteristics of the filtering algorithm is very real.

(3) In general, one may anticipate distortion at a given frequency when the spectral window, which corresponds to a time domain filtering algorithm, is falling off more slowly than the true underlying spectral density.

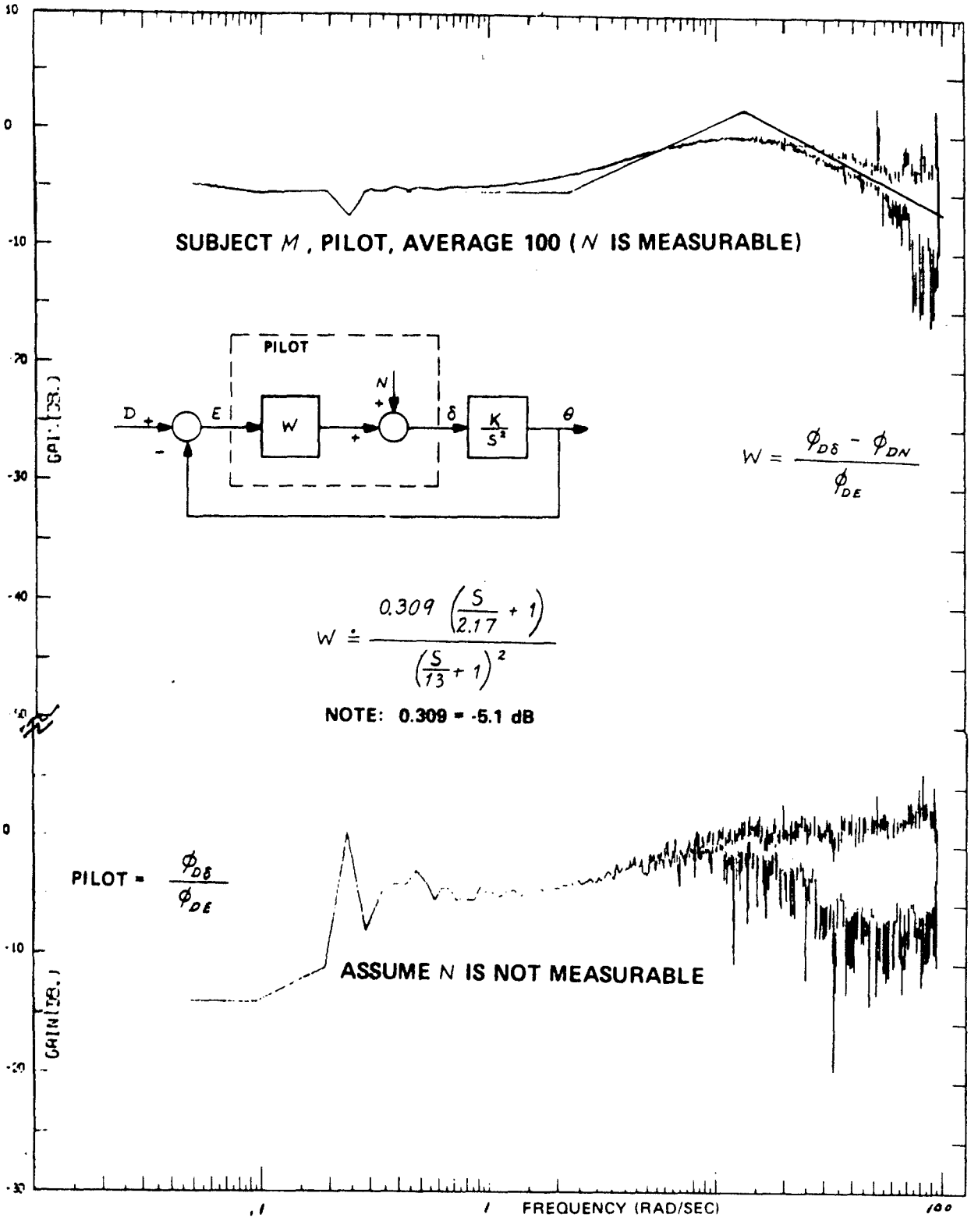

FIGURE 8. ESTIMATION OF W IN THE SUBJECT "M" EXPERIMENT

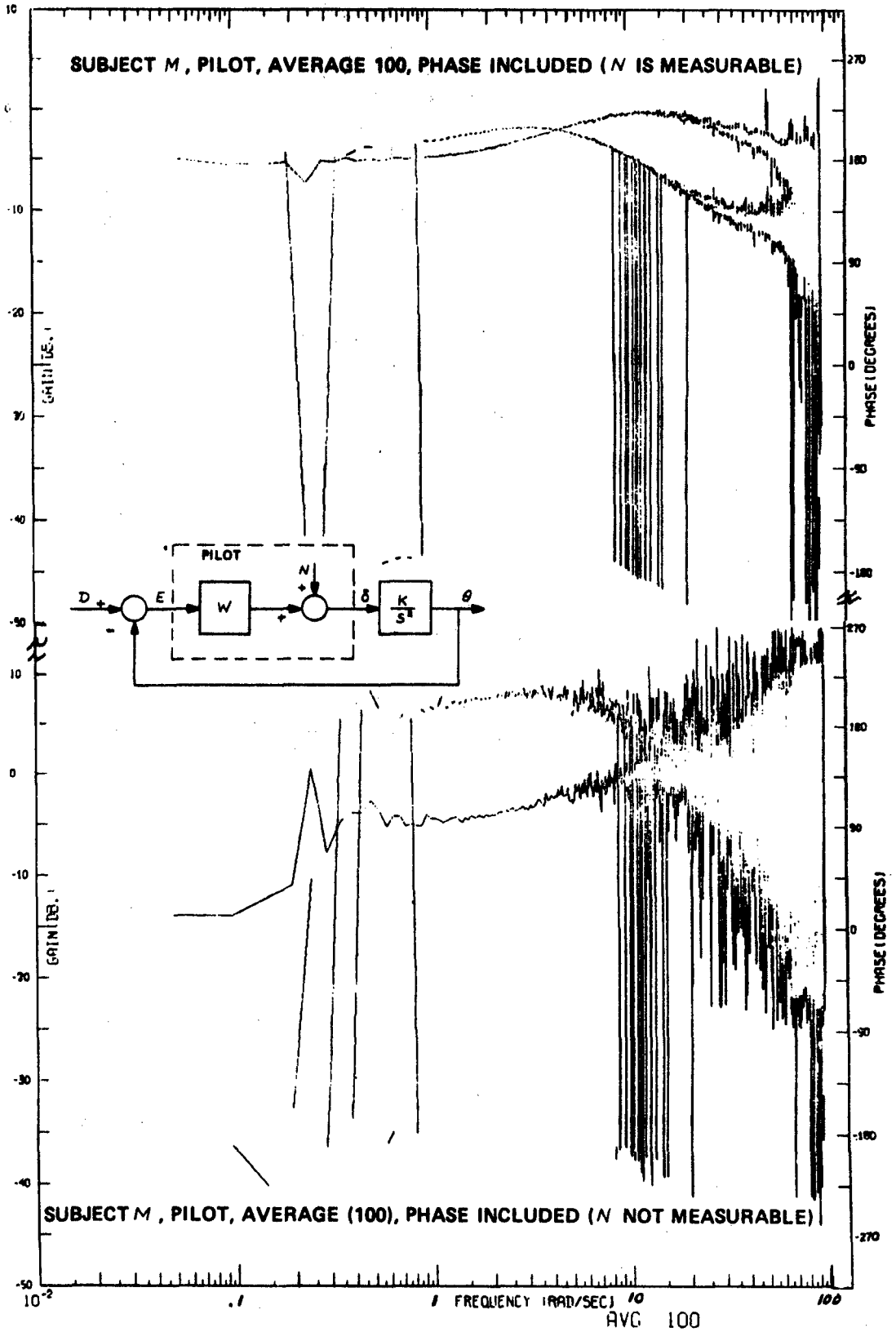

FIGURE 9. ESTIMATION OF W IN THE SUBJECT "M" EXPERIMENT, PHASE INCLUDED

(4) When we used ensemble averaging with no overt filtering (i.e., the square time window), the estimate obtained averaging over as many as 134 estimates was unsatisfactory. For example, in Experiment 2, had we not known the underlying dynamics were K/s^2, it is doubtful that we would approximate the estimate as K/s^2.

(5) The triangular filtering algorithm in time, which corresponds to a $((\sin x/\omega)/(x/\omega))^8$ spectral window, produced results which were an order of magnitude better when used in conjunction with ensemble averaging.

(6) Regardless of what time domain filtering algorithm is invoked, the estimate of the cross power between two independent random variables goes down only as $1/\sqrt{n}$, n being the number ensembled across.

Other useful results, too detailed for this presentation are given in Reference 2.

12. References

1. Adams, J. J. and Bergeron, H. P., A Synthesis of Human Response in Closed-Loop Tracking Tasks, NASA Technical Note, NASA TND-4842, October 1968.

2. Whitbeck, R. F. and Knight, J. R., A Study of Pilot Modeling in Multicontroller Tasks, CAL Report No. IH-3037-J-1, to be published.

PRINCIPAL FACTORS AND TRADE-OFFS IN THE RAPIDITY OF CONVERGENCE OF PARAMETER TRACKING SYSTEMS.

(Expanded Abstract)

by

S.J. MERHAV
Department of Aeronautical Engineering,
Technion - Israel Institute of Technology,
Haifa, Israel.

1. General

Common to all types of parameter tracking systems is the notion of a model M which minimizes its distance in function space to a linear system S. The two-norm

$$||\underline{y} - \underline{z}||_2 = \left[\int_a^b \langle \underline{y}(\tau) - \underline{z}(\tau), \underline{y}(\tau) - \underline{z}(\tau)\rangle d\tau\right]^{1/2} = d_2(\underline{y},\underline{z}) \qquad (1)$$

defines this distance. $\underline{y}(\tau)$ is a system-related output vector and $\underline{z}(\tau)$ a model related output vector. In most problems of interest this distance is one-dimensional so that:

$$d_2(y,z) = \{\int_a^b [y(\tau) - z(\tau)]^2 d\tau\}^{1/2} \qquad (2)$$

2. Steady-State Solution:

$z(\tau)$ which minimizes $d_2(y,z)$ provides the best description of S in the form of a parameter vector $\{\beta_1 \ldots \beta_m\}$ contained in $z(\tau)$. The component values are obtained from:

$$\frac{\partial d_2(y,z)}{\partial \beta_j} = \int_a^b e(\tau)\sigma_j(\tau)d\tau = 0; \quad j=1\ldots m \qquad (3)$$

where $e(\tau) = y(\tau) - z(\tau)$ and $\partial z(\tau)/\partial \beta_j = \sigma_j(\tau)$ are error and sensitivity respectively and are orthogonal on [a,b]. If S is excited by a stationary random signal, d_2 in (2) is itself a random variable. Therefore the expectation $E[d_2]$ over the sample space of d_2 will be minimized. This leads to

$$E[e(\tau)\sigma_j(\tau)] = 0; \quad j = 1\ldots m \qquad (4)$$

which is a form of the principle of orthogonality in estimation theory.[1] In general (4) yields m nonlinear equations in β_j. Their solution

may be difficult and uniqueness is not guaranteed.

Let $\{w_1 \ldots w_m\}$ (a linearly independent set) be a finite function basis which does not contain $\beta_1 \ldots \beta_m$. We construct

$$z(\tau) = \sum_{i=1}^{m} \beta_i w_i(\tau) \tag{5}$$

and we say that $\beta_1 \ldots \beta_m$ are the coordinates of $z(\tau)$ with respect to the basis $\{w_1 \ldots w_m\}$. From (4) we have:

$$E\{[y(\tau) - \sum_{i=1}^{m} \beta_i w_i(\tau)][-w_j(\tau)]\} = 0, \quad j = 1 \ldots m \tag{6}$$

This leads to

$$\underline{A}\,\underline{\beta} = \underline{u} \tag{7}$$

$\underline{A}$ is a mxm symmetrical covariance matrix with elements $E[w_i w_j]$ and $\underline{u}$ is a m-vector with elements $E[y\, w_j]$. $\underline{A}$ is nonsigular and $\underline{\beta}$ has the unique solution

$$\beta_{opt} = \underline{A}^{-1}\,\underline{u} \tag{8}$$

- If $\text{Min}\{E[d_2]\} = 0$ we have a zero distance model.
- If $\lim_{m\to\infty} \text{Min}\{E[d_2]\} = 0$, $\{w_1 \ldots w_m\}$ is complete
- Thus, a complete set can constitute a zero distance model when $m \to \infty$.
- $E[d_2] = 0$ implies $d_2 = 0$ which implies $e(\tau) \equiv 0$.
- If only the class of S is known, its phenomenological characteristics, such as impulse or frequency response can be exactly identified at the expense of an infinite dimensional model.

If the structure of S is known, that is,

$$y(\tau) = \sum_{i=1}^{n} \alpha_i v_i(\tau) \tag{9}$$

we say that $y(\tau)$ is n-dimensional with respect to the basis $\{v_1 \ldots v_n\}$, and M can be constructed on the same basis so that

$$z(\tau) = \sum_{i=1}^{n} \beta_i v_i(\tau) \tag{10}$$

Since $\{v_1 \ldots v_n\}$ is linearly independent the error $e(\tau) = \sum_{i=1}^{n} (\alpha_i - \beta_i) v_i(\tau)$ is zero if, and only if, $\beta_i = \alpha_i$ for all $i=1 \ldots n$. Thus, if the structure of S is known, $\underline{\beta}$ can be exactly determined on a finite known basis.

3. Dynamic Performance:

The implementation of the parameter tracking system is based on the steepest descent relation:

$$\frac{\partial}{\partial \beta_j} E[d_2] = - \frac{1}{k_j} \frac{d\beta_j}{dt} \; , \tag{11}$$

$k_j, (j = 1 \ldots m)$ are positive constants. This leads to:

$$\dot{\underline{\beta}} = - \underline{K}\, \underline{A}\, \underline{\beta} + \underline{K}\, \underline{u} \tag{12}$$

where $\underline{A}$ and $\underline{\beta}$ are as in (7) and $\underline{K}$ is a diagonal gain matrix.

Assuming for the present a stationary input and constant system parameters, one has:

1. In the expansion of $E[d_2]$, $E[z^2(\tau)] > 0$, thus $E\{[\sum_{i=1}^{m} \beta_i w_i(\tau)]^2\} > 0$, so that the inner product

$$\langle \underline{\beta}, \underline{A}\, \underline{\beta} \rangle > 0 \tag{13}$$

and $\underline{A}$, which is symmetrical, is also positive definite.

2. Since $\underline{K}$ is positive-definite, the product $\underline{K}\, \underline{A}$ is also positive definite.

3. All the eigenvalues of $- \underline{K}\, \underline{A}$ have negative real parts and the system (12) is asymptotically stable.

4. If all elements in $\underline{K}$ are equal $- \underline{K}\, \underline{A}$ retains its symmetry and all its eigenvalues are negative and real.

5. All the eigenvalues are proportional to k_j and to the signal level which determines the elements $E[w_i w_j]$ in $\underline{A}$.

The transition matrix related to (12) is:

$$\Phi(t, t_o) = \Phi(t - t_o) = e^{-\underline{K}\, \underline{A}(t - t_o)} \tag{14}$$

and the solution is:

$$\underline{\beta}(t) = \Phi(t - t_o)\underline{\beta}_o + \int_{t_o}^{t} \Phi(t - \tau)\ \underline{K}\,\underline{u}(\tau)d\tau \qquad (15)$$

$\underline{\beta}_o = \underline{\beta}(t_o)$. Assuming $\underline{\beta}_o = 0$, $t_o = 0$, and $\underline{K}\,\underline{u}$ being considered constant, the "start-up" transient is:

$$\underline{\beta}(t) = \left[\int_{o}^{t} \Phi(t - \tau)d\tau\right]\underline{K}\,\underline{u} \qquad (15)$$

From $\Phi(t) = e^{-\underline{K}\,\underline{A}t} = Pe^{-\Lambda t}P^{-1}$, (15) can be expressed by

$$\beta_i(t) = \sum_{k=1}^{m} b_{ik} - \sum_{k=1}^{m} b_{ik}\, e^{-\lambda_k t} \qquad (16)$$

Thus, since the system is stable, $\underline{K}\,\underline{A}$, and therefore $\lambda_1 \ldots \lambda_m$ can, in principle be made arbitrary large so that the "start-up" transient defined as an ensemble average can be quite short.

4. Types of Parameter Tracking Systems [2]

Type I: System parameters $\{\alpha_1 \ldots \alpha_n\}$ are contained in $y(\tau)$ only. Here $\underline{A}$ is independent of $\{\alpha_1 \ldots \alpha_n\}$ and, for a stationary input, remains constant. Variations in $\{\alpha_1 \ldots \alpha_n\}$, manifest themselves in $\underline{u} = u(t)$ which takes the form of a time-varying forcing vector function. This type of system lends itself to standard methods of linear system analysis by using Laplace Transform techniques:

$$[SI + \underline{K}\,\underline{A}]\ \underline{\beta}(s) = \underline{K}\,\underline{u}(s) \qquad (17)$$

$$\underline{\beta}(s) = [SI + \underline{K}\,\underline{A}]^{-1}\ \underline{K}\,\underline{u}\ (s) \qquad (18)$$

The dynamic error $\Delta\underline{\beta}(s)$ is readily obtained from (18).

Parameter tracking system based on parallel filters or canonical models configured in parallel with S belong to this type.

Type II: System parameters are contained in $z(\tau)$ only. Hence $\{\alpha_1 \ldots \alpha_n\}$ is contained in $\underline{A}$, and if $\{\alpha_1 \ldots \alpha_n\}$ vary in time, $\underline{A}$ becomes time-varying, while $\underline{u}$ remains constant. Standard methods do not apply. If $\Phi(t)$ can be determined $\underline{\beta}(t)$ can be found from (15).

Parameter tracking systems known as "series compensation systems" in which S is placed in series with an inverse model belong to this class.

Type III. System parameters $\{\alpha_1 \ldots \alpha_n\}$ are contained both in $y(\tau)$ and $z(\tau)$. In this case, both $\underline{A}$ and $\underline{u}$ become time varying so that:

$$\dot{\underline{\beta}} = -\underline{K}\,\underline{A}(t)\underline{\beta} + \underline{K}\,\underline{u}(t) \tag{19}$$

(19) can be solved if $\Phi(t)$ can be found. Since $\{\alpha_1 \ldots \alpha_n\}$ generally vary slowly much can be learned from (18) which can be considered an approximation for Type II and III as well.

Parameter tracking systems known as "equation error" systems belong to this type.

5. Implementation:

Eq. (4) is a condition for the ensemble average. In the actual implementation, a particular sample of the ensemble expressed in (6) must satisfy:

$$e(t)w_j(t) = -\frac{1}{k_j}\frac{d\beta_j}{dt} \tag{20}$$

The left hand side is the input to an integrator so that:

$$\beta_j(t) = \int_0^t e(\tau)w_j(\tau)d\tau \tag{21}$$

In the steady-state, as $t \to \infty$, $\beta_j(t)$ takes the form:

$$\beta_j(t) = \beta_{jopt} + \tilde{\beta}_j(t) \tag{22}$$

The first term is the average in accordance with (8). The second term is a zero mean random component due to $e(t) \neq 0$. It vanishes only in a zero distance system where $e(t) \equiv 0$.

Let $e_o(t) = y(t) - \sum_{i=1}^{m} \beta_{iopt}\, w_i(t)$ be called the minimum distance error. Substituting $e_o(t)$ into (20) one obtains:

$$\dot{\tilde{\underline{\beta}}}(t) + \underline{K}\,\tilde{\underline{A}}(t)\tilde{\underline{\beta}}(t) = e_o(t)\,\underline{K}\,\underline{w}(t) \tag{23}$$

$\tilde{\underline{A}}(t)$ - time varying mxm matrix with elements $w_i(t)w_j(t)$.

$\underline{K}$ - Diagonal gain matrix $(k_1 \ldots k_m)$

$\tilde{\underline{\beta}}(t)$ - $\mathrm{Col}\{\tilde{\beta}_1(t) \ldots \tilde{\beta}_m(t)\}$

$w(t) - Col\{w_1(t)...w_m(t)\}$

6. Concluding Comments:

- No solution of (23) is attempted. Since the equation is linear, and $e_o(t)$ acts as a forcing function, the m.s. of any $\beta_j(t)$ is proportional to the m.s. of $e_o(t)$ so that

$$E[\beta_j^2(t)] = C_j E[e_o^2(t)] \qquad (24)$$

  $C_j (j = 1...m)$ is a constant.

- $E[\beta_j^2(t)]$ is practically indpendent of $\underline{K}$ if $\underline{K}$ is large. Thus, if $e_o(t)$ is small, the large $\underline{K}$ required for fast convergence can also be afforded by consideration of $\underline{\beta}(t)$.

- The closer the system is to a zero distance system ($e_o(t) = 0$), the larger a $\underline{K}$ can be afforded and the faster a dynamic response of the parameter tracker is obtained.

- In a zero distance system the parameter vestor $\underline{\beta}_{opt}$ is a deterministic set of numbers whereas in general, for $e_o(t) \neq 0$, $\underline{\beta}_{opt}$ is an average determined by (8).

- In a non-zero distance system the dynamic response tends to be slower due to limitations on $\underline{K}$ and more time is needed to evaluate the average from (23).

- All the parameter trackers which are constructed on a linear function basis are asymptotically stable.

- More sophisticated measures for minimization instead of $d_2(y,z)$, which include error derivatives, lead to increased values of the elements in $\underline{A}$. This improves the dynamic performance but does not alter the basic properties of the system.

- Uncorrelated noise does not affect (4) and $\underline{\beta}_{opt}$ in (8) but will increase $\underline{\beta}(t)$. Correlated noise will also modify $\underline{\beta}_{opt}$.

References

1. Nahi, N.E., " Estimation Theory and Applications", John Wiley & Sons, 1969, Chapter 4.

2. Åström, K.J. and Eykhoff, P., " System Identification - A Survey" Automatica, Vol. 7, pp.123-162, 1971.

ADAPTIVE IDENTIFICATION OF PARAMETERS IN MODELS OF PHYSIOLOGICAL SYSTEMS*

Ralph Mekel

The City College
of
The City University of New York

ABSTRACT

This paper presents a nonlinear adaptive identification technique which is utilized to identify and control a physiological system's model parameters. The technique is based upon a model-reference system configuration and a Liapunov function formulated for this purpose. The identification loops are synthesized directly from the time derivative of the Liapunov function. A digital computer simulation allows the identification process to interact with the experimentation in a mutually beneficial way.

I INTRODUCTION

Numerous studies concerned with the identification of parameters in mathematical models of physiological systems have appeared in the literature (see ref. 1-8). Most of the techniques employed in these studies are linear and limited to linear system configurations. Experimental evidence has shown that physiological systems are basically nonlinear. Therefore, the utilization of nonlinear techniques becomes essential when one desires to formulate mathematical models of physiological systems.

The purpose of this study is to examine the utility of a nonlinear identification technique which enables one to formulate mathematical models of physiological systems. The technique is based upon a model-reference system configuration as shown in Fig. 1 and a Liapunov function formulated for this purpose. The reference system is the actual physiological system. The model system is constructed initially as an approximate mathematical representation of the reference system and is derived from consideration of the physiological processes evident in the actual physiological system. The Liapunov function is formulated to possess variable characteristics to take into account the identification dynamics. A digital computer program is used to allow the interaction between the identification dynamics and the Liapunov function.

II STATEMENT OF PROBLEM AND SYSTEM REPRESENTATION

Consider the model-reference system configuration depicted in Fig. 1. The reference system represents the actual physiological system. It is assumed that the stimulus-response data are available from experimentation. Let the stimulus be denoted by r and the response by z. Let us assume that the reference system may be described by the vector differential equation

$$\dot{\underline{z}} = A\underline{z} + H\underline{r} \qquad (1)$$

*This research is partially supported by NASA, Langley Research Center Grant NGR-33-013-053

Preceding page blank

where $\dot{\underline{z}} = d\underline{z}/dt$ and the square matrices A and H are unknown. The problem is to identify these matrices, thereby obtaining a mathematical description of the reference system. In order to achieve this goal one may choose a tentative model system having the same mathematical form. Let this model system be described by the vector differential equation

$$\dot{\underline{x}} = B\underline{x} + C\underline{r} \tag{2}$$

where r is the same stimulus (input) as above, x denotes the model's response and $\dot{\underline{x}} = d\underline{x}/dt$. The square matrices B and C are also unknown except that one may assign initial values to these matrices. The restriction on the initial values is that they must be inside the stability region of the tentative model system.

It is obvious that initially the response of the reference system will not be the same as the response of the tentative model. The difference between the model's response and the reference system's response is the model-reference system error. Let this error be denoted by vector $\underline{e}$ and defined as

$$\underline{e} = \underline{x} - \underline{z} \tag{3}$$

Then

$$\dot{\underline{e}} = \dot{\underline{x}} - \dot{\underline{z}} \tag{4}$$

where the dot denotes differentiation with respect to time. Substitution of Eqs. (1) & (2) into Eq. (4) yields, after some algebraic manipulations, the vector error differential equation for the model-reference system configuration

$$\dot{\underline{e}} = B\underline{e} + \underline{bu}^T\underline{z} + \underline{dw}^T\underline{r} \tag{5}$$

where

$$\underline{bu}^T = (B - A) \tag{6}$$

$$\underline{dw}^T = (C - H) \tag{7}$$

Note that superscript T denotes the transpose. The form of Eq. (5) is derived using a phase variable representation of the tentative model system. The choice for this type of model representation was governed by the desire to obtain a controllable realization of the model system. Note also that Eqs. (6) & (7) contain the identification dynamics for the model system's parameters. It should be pointed out that other realizations of the model system would lead to modified forms of Eq. (5).

III FORMULATION OF THE MATHEMATICAL MODEL

Equation (5) may be viewed as consisting of three perturbational vectors, namely $\underline{e}$, $\underline{u}$ and $\underline{w}$. An appropriate Liapunov function should be positive definite in the error as well as the parameter perturbations. Therefore, one may choose a Liapunov function of the form

$$V = \underline{e}^T M\underline{e} + \underline{u}^T N\underline{u} + \underline{w}^T Q\underline{w} \tag{8}$$

where matrices M, N and Q are symmetric square matrices. Differentiating

Eq. (8) with respect to time and then substituting Eq. (5) and its transpose, one obtains the time derivative of the Liapunov function

$$\dot{V} = -\underline{e}^T D \underline{e} + 2\left[\underline{\dot{u}}^T N + \tfrac{1}{2}\underline{u}^T \dot{N} + \underline{z}^T(\underline{b}^T M \underline{e})\right]\underline{u} + 2\left[\underline{\dot{w}}^T Q + \tfrac{1}{2}\underline{w}^T \dot{Q} + \underline{r}^T(\underline{d}^T M \underline{e})\right]\underline{w} \qquad (9)$$

where

$$D = (B^T M + MB + \dot{M}) \qquad (10)$$

Liapuncv's criterion for stability calls for $V > 0$ and $\dot{V} \leq 0$. One way to comply with Liapunov's criterion for stability and have control over the identification dynamics is to constrain the elements of the D matrix, denoted by d_{ii} and d_{ij}, to satisfy the conditions

$$d_{ii} > 0 \qquad (11)$$

and

$$d_{ij} + d_{ji} = 0 \qquad (12)$$

where i and j denote row and column respectively and let

$$\underline{\dot{u}}^T N = -\tfrac{1}{2}\underline{u}^T \dot{N} - \underline{z}^T(\underline{b}^T M \underline{e}) \qquad (13)$$

$$\underline{\dot{w}}^T Q = -\tfrac{1}{2}\underline{w}^T \dot{Q} - \underline{r}^T(\underline{d}^T M \underline{e}) \qquad (14)$$

The conditions given by Eqs. (11)&(12) enable one to evaluate the elements of D and M matrices (see ref. 10). At this point one must perform a test to insure the positive definitness of these matrices. Matrices N and Q must also satisfy the conditions $N > 0$, $Q > 0$ and are kept as free design parameters in order to influence the convergence rate of the identification mechanism. Equations (13) & (14) constitute the basic equations from which the identification loops are synthesized.

It should be noted that the resulting $\dot{V}$ is negative semidefinite because it depends only upon the model-reference system error and does not depend on the vectors $\underline{u}$ and $\underline{w}$. This suggests that one should expect some slight oscillations in the model parameters at the end of the identification interval, even if the model-reference system error $\underline{e}$ is zero.

In order to construct the identification loops one must formulate a relationship among Eqs. (6), (7), (13) & (14). Assuming that the changes in the reference system are much slower than the identification time required for the model's parameters, one may think of matrices A and H as being time-invariant during the identification interval. Therefore, differentiating Eqs. (6) & (7) with respect to time yields

$$\dot{B} = \underline{b}\underline{\dot{u}}^T \qquad (15)$$

and

$$\dot{C} = \underline{d}\underline{\dot{w}}^T \qquad (16)$$

since $\underline{b}$ and $\underline{d}$ are constant vectors. (See Eqs. (6) & (7)). Rearranging Eqs. (13) & (14), then substituting the rearranged equations into Eqs. (15) & (16), one obtains after integration

$$B = B_o - \int_o^t \left[\tfrac{1}{2} \underline{b} \underline{u}^T \dot{N} N^{-1} + \underline{b} \underline{z}^T N^{-1} (\underline{b}^T M \underline{e}) \right] dt \tag{17}$$

$$C = C_o - \int_o^t \left[\tfrac{1}{2} \underline{d} \underline{w}^T \dot{Q} Q^{-1} + \underline{d} \underline{r}^T Q^{-1} (\underline{d}^T M \underline{e}) \right] dt \tag{18}$$

Substitution of Eqs. (17) & (18) into Eq. (2) yields the mathematical model

$$\dot{\underline{x}} = \left\{ B_o - \int_o^t \left[\tfrac{1}{2} \underline{b} \underline{u}^T \dot{N} N^{-1} + \underline{b} \underline{z}^T N^{-1} (\underline{b}^T M \underline{e}) \right] dt \right\} \underline{x} +$$

$$+ \left\{ C_o - \int_o^t \left[\tfrac{1}{2} \underline{d} \underline{w}^T \dot{Q} Q^{-1} + \underline{d} \underline{r}^T Q^{-1} (\underline{d}^T M \underline{e}) \right] dt \right\} \underline{r} \tag{19}$$

where B_o and C_o are the initially assumed matrices for the mathematical model. The mathematical model's identification loops are given by Eqs. (17) & (18). The integrals in Eq. (19) represent the nonlinear identification dynamics for matrices B and C. As mentioned before, matrices N and Q must satisfy the conditions $N > 0$, $Q > 0$ and are kept as free design parameters in order to influence the convergence rate of the identification mechanism.

Since Eqs. (17), (18) and (10) are nonlinear and interrelated, the difficulties arising in their computations may be alleviated by using a digital computer. For this purpose one may form the following set of iterative equations

$$(B_k^T M_k + M_k B_k + \dot{M}_k) = D_k \tag{20}$$

$$B_k = B_o - \int_o^{t_k} \left[\tfrac{1}{2} \underline{b} \underline{u}^T \dot{N} N^{-1} + \underline{b} \underline{z}^T N^{-1} (\underline{b}^T M_{k-1} \underline{e}) \right] dt \tag{21}$$

and

$$C_k = C_o - \int_o^{t_k} \left[\tfrac{1}{2} \underline{d} \underline{w}^T \dot{Q} Q^{-1} + \underline{d} \underline{r}^T Q^{-1} (\underline{d}^T M_{k-1} \underline{e}) \right] dt \tag{22}$$

and solve them iteratively by a digital computer. Note that index $k = 0, 1, 2 \ldots\ldots m$, where m denotes the end of the identification interval.

The model is considered identified (representing the reference system) when $\underline{e} = 0$. Due to the semidefinite $\dot{V}$, the model's parameters oscillate about some nominal values. Therefore, with this identification technique one may consider these nominal values as being the identified parameters for matrices A and H. Experimentation has shown that with the proper choice of N and Q matrices, one achieves a very rapid identification of parameters. By extending slightly the computer computation time one may obtain a quite accurate value of the nominal parameter values.

In order to eliminate these oscillations the presented identification technique is presently being improved. This requires the forcing of $\dot{V}$ to

be negative definite. To force $\dot{V}$ to be negative definite one has to let the coefficients of $\underline{u}$ and $\underline{y}$ in Eq. (9) (braketed expressions) be some, negative odd function of $\underline{u}$ and $\underline{y}$ respectively. This modification of $\dot{V}$ will produce modified identification loops. In terms of Liapunov's stability theory this means that the model-reference system will be asymptotically stable which, in turn, implies that not only $\underline{e} \rightarrow 0$ at the end of the identification interval but also $\underline{u} \rightarrow 0$ and $\underline{y} \rightarrow 0$. In this modified approach one should get perfect identification of the model parameters. This approach is presently being studied.

IV CONCLUSIONS

A nonlinear identification technique has been presented for realizing mathematical models of certain physiological systems. The present study has its advantages and disadvantages as indicated throughout the paper. Improvements in this technique are being studied.

A very useful feature of this study is the development of a digital computer program which is easily implemented and modified concurrent with experimentation. In this way, the identification process interacts with the experimental data in a mutually beneficial way. The use of the digital computer permits one also to effectively apply the Liapunov's function in the identification process.

Note also the state observers in the model-reference system configuration. These state observers construct state variable information that are difficult to measure and are necessary for the realization of the identification loops. For the design of such state observers see ref. 11.

V REFERENCES

1. R. A. Hannen, M. Kabrisky, C. R. Replogle, V. I. Hartzler and P. A. Roccaforte, "Experimental Determination of a Portion of the Human Vestibular System Response Through Measurement of Eyeball Counterroll" IEEE Trans. Bio-Medical Engineering, vol. BME-13, pp. 65-70, April 1966
2. C. S. Burrus, T. W. Parks and T. B. Watt, Jr., "A Digital Parameter-Identification Technique Applied to Biological Signals," IEEE Trans. Bio-Medical Engineering, vol. BME-18, pp. 35-37, Jan. 1971
3. R. H. Jones, D. H. Crowell, J. K. Nakagawa and L. E. Kapuniai, "An Adaptive Method for Testing for Change in Digitized Cardiotachometer Data" IEEE Trans. Bio-Medical Engineering, vol. BME-18, pp. 360-365, Sept. 1971
4. R. M. Jones, J. G. Webster and U. T. Keesey, "An Active Feedback System for Stabilizing Visual Images," IEEE Trans. Bio-Medical Engineering, vol. BME-19, pp. 29-33, Jan. 1972
5. V. K. Jain and S. K. Guha, "A Control System for Long-Term Ventilation of the Lungs," IEEE Trans. Bio-Medical Engineering, vol. BME-19, pp. 47-53, Jan. 1972
6. N. Sugie, "A Model of Predictive Control in Visual Target Tracking" IEEE Trans. Systems, Man and Cybernetics, vol. SMC-1, pp. 2-7, Jan. 1971

7. J. M. Dutton and W. H. Starbuck, "Computer Simulation Models of Human Behavior: A History of an Intellectual Technology," IEEE Trans. Systems, Man and Cybernetics, vol. SMC-1, pp. 128-171 April, 1971
8. G. L. Gottlieb and G. C. Agarwal, "Control and Regulation of the Human Motor System" IEEE Trans. Systems, Man and Cybernetics, vol. SMC-1, pp. 379-383, Oct. 1971
9. G. N. Saridis and R. N. Lobbia, "Parameter Identification and Control of Linear Discrete-Time Systems," IEEE Trans. Automatic Control, vol. AC-17, pp. 52-60, Feb. 1972
10. R. Mekel and P. Peruo, Jr., "Design of Controllers for a Class of Nonlinear Control Systems," IEEE Trans. Automatic Control, vol. AC-17, pp. 206-213, April 1972
11. D. G. Luenberger, "An Introduction to Observers," IEEE Trans. Automatic Control, vol. AC-16, pp. 596-602, Dec. 1971

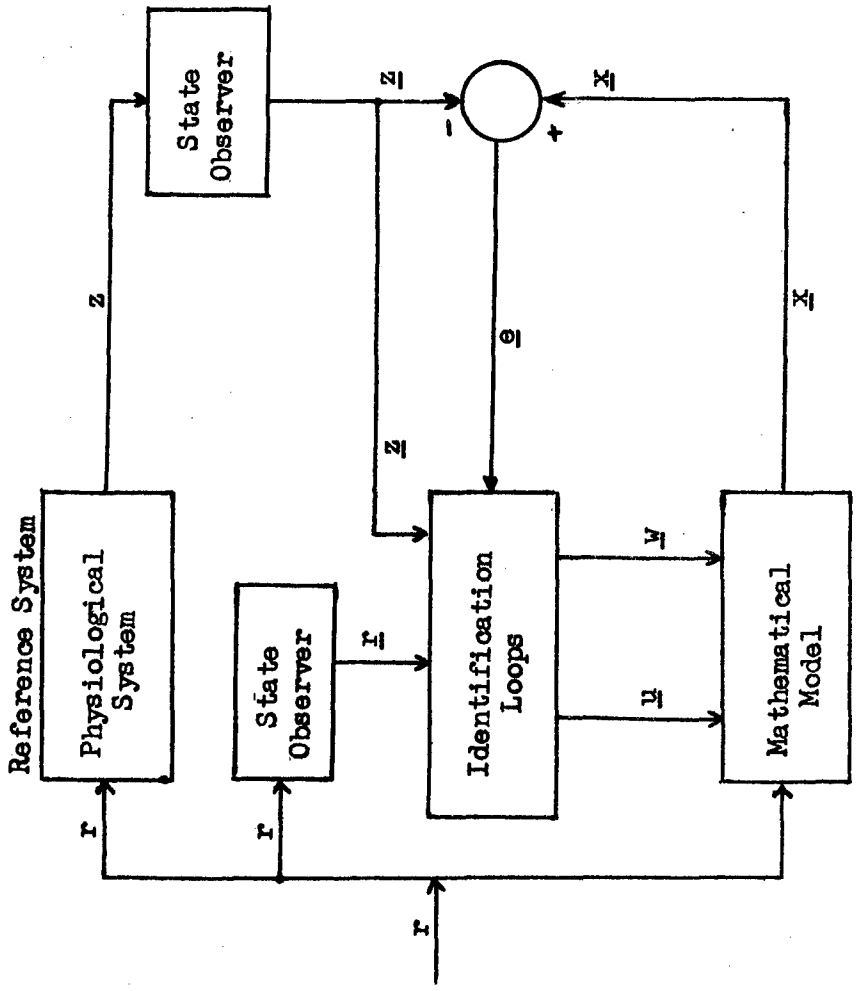

Fig. 1. Model-Reference System Configuration

SESSION VII

Assessment of the Degrading Effects of Environmental and Pharmacological Agents on Human Controller

Preceding page blank

THE DEGRADATION OF TRACKING PERFORMANCE AS A FUNCTION OF ENVIRONMENTAL STRESSES OF HEAT AND NOISE†

George M. Swisher
Wright State University
Dayton, Ohio

Frank A. Maher
Wright Patterson Air Force Base
Dayton, Ohio

ABSTRACT

The zero order autopaced Jex "critical task" was used as a primary task to measure the degradation of tracking performance while the human operator is subjected to one hour of 120°F heat, 95dbA noise and combined heat and noise. The performance measures used for the eight subjects were total tracking time, average absolute error, average operator output, critical divergence frequency, and rate switching time. The variances in performance under the experimental conditions support the conclusion that Jex's task is a viable tool for investigating the effects of environmental stress on operator performance.

INTRODUCTION

Background

The material presented here is part of a United States Air Force program to determine sensitive measures of performance under environmental stresses of heat, noise and vibration. This experiment is concerned with investigating the environmental stress sensitivity of critical tracking tasks using only heat and noise.

Preceding page blank

† This work was sponsored under #F33615-70-C-1598 for The Aerospace Medical Research Laboratory, Wright Patterson Air Force Base.

The tracking task used was the no input zero order autopaced Jex (1) critical task. A full description of the task is included in the method section. The critical instability scores were shown by Jex and Allen (2) to be excellent indicators of the closed loop man machine bandwidth and of the effective time delay while tracking. For skilled subjects these scores were also shown to have very low variability among subjects and among trials although only five trials are reported in (2). Jex's task has been used as a secondary task by Jex (3), and has been used as an independent variable in a study to establish that eye pupil size of a subject performing the Jex task increased with an increase in λ[Westbrook et. al. (4)]. However, no published work has been noted applying this task in environmental stress conditions to date.

METHOD

Subjects

Eight male college students were employed as subjects. All subjects reported 20/20 (un) corrected vision and freedom from auditory and psychomotor deficiencies. Subject age ranged form 19 to 31 years of age.

Apparatus

Figure #1 shows the analog mechanization of the no input Jex task and the performance measuring circuits using three EAI TR-20 10 volt analog computers in a slaved configuration. The scope used for the compensatory display was a Hewlitt Packard 122A set at a 0.366 $\frac{cm}{volt}$ sensitivity. The control stick used was a United States Air Force Type Number C-1 Formation Stick with $\pm$ 1 0. volt output. The force calibration of the stick resulted in a 4.16 volts/Newton stick sensitivity.

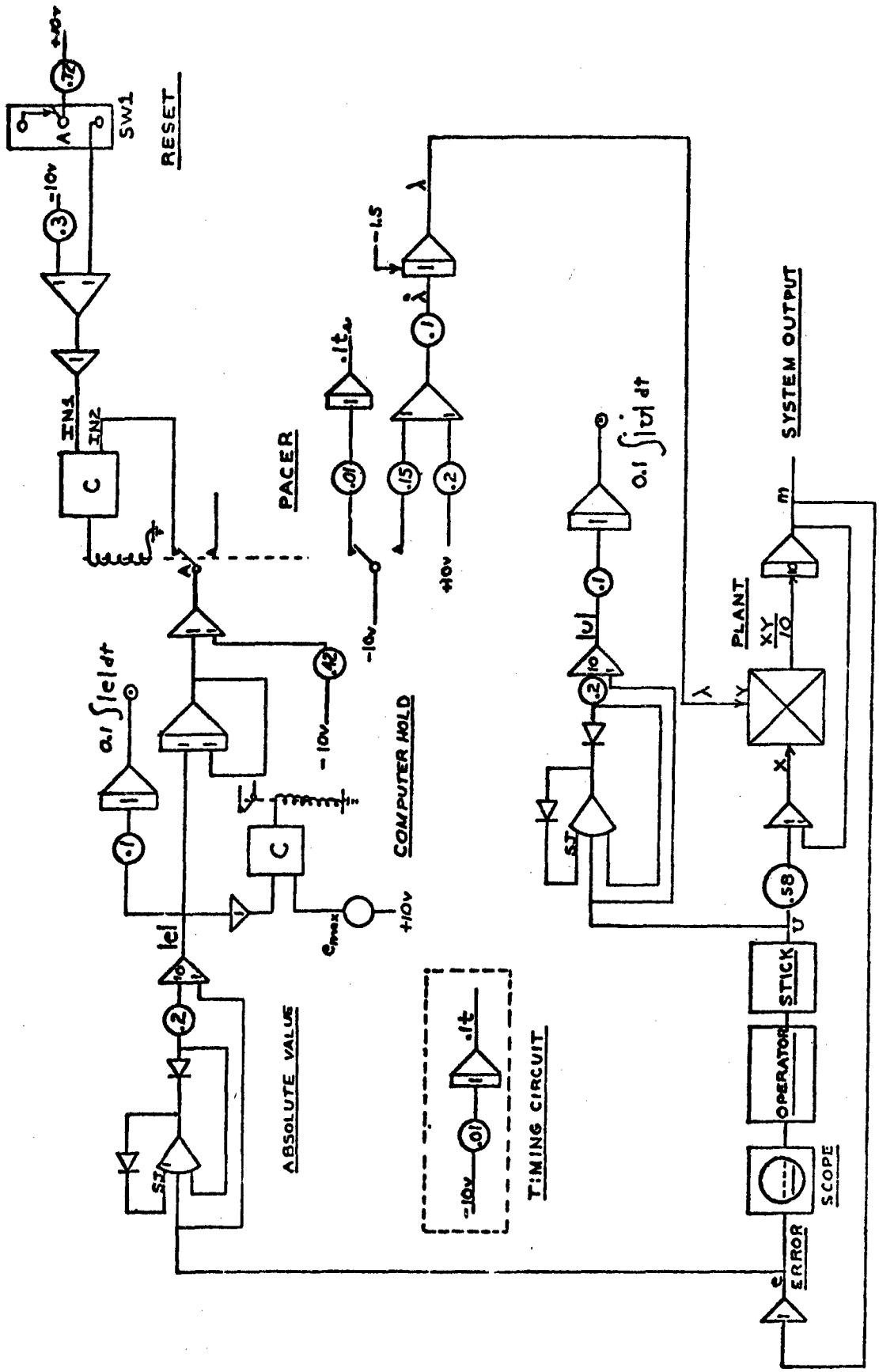

Figure 1 Analog mechanization of the Jex Task.

The C-1 Formation stick was made compatible to the control stick used by Jex by cascading the C-1 stick with a 0.58 potentiometer with the resulting stick system having a sensitivity of 2.4 volts/Newton.

The tracking performance measures recorded for each tracking run were T (total run time), λ_c (critical divergent frequency), integrated absolute error, integrated absolute operator output, and t_s (time of rate shift on auto-paced task). These voltages were read on a Cubic Instrument System 250.

The subjects were tested in two 4' x 4' x 8' insulated test chambers. One chamber was used exclusively for pretest conditions. A recirculating fan was used to maintain a uniform temperature distribution throughout the heated chamber. Two 6000 watt heaters brought the temperature up to the 120° F level; one heater was then required to maintain the temperature at 120° F. A temperature control systems was designed using a thermistor as the sensing element and the TR-20 analog computer as the logic element to control the heater on switching. The temperature was maintained at 120° $\pm$ 2° F.

A General Radio Co. Type 1390-A Noise Generator was used to generate the 95 db (A weighted) broad band noise. For simplicity the noise was tape recorded on a Sony TC-630 40 watt stereo tape recorder. The dual stereo speakers were placed on the floor of the chamber to the left and to right of the subject. The sound power level was measured with a Brüel and Kjaer Type 2203 Impulse & Precision Sound Level Meter. A traverse about the subject's head showed no more than $\pm$ 1db deviation within a 2 foot sphere centered at the subject's head.

Training

Each subject was briefed concerning the experiment and his task prior to training. After demonstrating the tracking task to the subject, he trained on the slow rate of $\dot{\lambda} = 0.05$ until he reached his asymptotic level of performance. (The actual task was then presented for practice until the subject again reached an asymptotic level of performance as denoted by λ_c.)

Testing

A repeated Latin-Square design, was used to assign the order of presentation for the stress conditions. Each subject was tested under a single test condition during each test session. The training and four test sessions were each completed on separate days. Two hour sessions, on five consecutive days were required to complete the testing on each of the eight subjects. Every test session consisted of four sets of trials: The first set was completed in the ambient chamber. The three-test sets were given in the stress chamber. Each set involved 48 tracking trials, and each set was separated by a rest period. Each set required 15-20 minutes with the period of time within the stress environment averaging one hour, depending on the length of individual tracking times.

RESULTS

The descriptive statistics were computed using the 07D Computer program while the analyses of variance were computed using the 07D and 02V programs. Both programs are part of the UCLA Biomedical Package which are in permanent file on the CDC 6600 of the Computer Science Center at Wright Patterson Air Force Base, Dayton, Ohio.

Total time T, was measured from the onset of a tracking trial until the subject lost control and the system went into the hold position.

Group performance, as defined by the total time score, is displayed in Table I. Significant differences ($P<.01$) in performance were indicated as a function of environmental stress. Total time was longest under the control condition and shortest for the heat stress condition.

TABLE I Total Time For Tracking, T (Seconds)

Condition	Mean	Standard Deviation	N
Ambient	24.482	8.690	144
Heat	19.648	9.496	144
Noise	20.568	8.768	144
Heat & Noise	20.171	7.967	144

Switching time, t_s, represented the time from the onset of a trial until the instantaneous absolute system error reached the level at which the instability rate switched from high to low rate. Group performance, as defined by the switching time score, is displayed in Table II. No significant differences were found as a function of workload stress.

TABLE II Switching Time, t_s (Seconds)

Condition	Mean	Standard Deviation	N
Ambient	11.556	5.706	144
Heat	12.881	4.877	144
Noise	12.697	4.579	144
Heat & Noise	11.923	3.968	144

The critical divergence frequency λ_c, is defined as that divergence frequency when the subject loses control. The group performance is displayed in Table III. Significant differences ($P<.01$) in λ_c were indicated as a function of environmental stress. The λ_c was greatest under the

control condition and least under the combined stressor.

TABLE III Critical Divergence Frequency, λ_c $\left(\frac{\text{radians}}{\text{second}}\right)$

Condition	Mean	Standard Deviation	N
Ambient	4.301	0.801	144
Heat	4.270	0.854	144
Noise	4.232	0.772	144
Heat & Noise	4.122	0.726	144

The average absolute error is a measure of how accurately the human operator can track. It is defined by:

$$e \triangleq \frac{1}{T} \int_0^T |\text{System error}|\,dt$$

where T is the total time as defined previously. Group performance as defined by e is displayed in Table IV. There was no significant difference in e for environmental stress.

TABLE IV Average Absolute Error (Volts)

Condition	Mean	Standard Deviation	N
Ambient	1.224	0.381	144
Heat	1.168	0.376	144
Noise	1.165	0.380	144
Heat & Noise	1.218	0.350	144

The average absolute stick voltage is a measure of how hard the human operator must work during tracking. It is defined by:

$$U \triangleq \frac{1}{T} \int_0^T |\text{Stick Voltage}|\,dt$$

Group performance as defined by U is displayed in Table V. Significant differences in U were indicated as a function of environmental stress ($P<.01$). U was largest for the combined stressor and smallest for the heat stress.

TABLE V Average Absolute Stick Output (Volts)

Condition	Mean	Standard Deviation	N
Ambient	1.226	0.382	144
Heat	1.189	0.450	144
Noise	1.206	0.476	144
Heat & Noise	1.295	0.432	144

CONCLUSIONS

The performance measures of total time, T, and the critical divergence frequency, λ_c, indicate that performance is better under ambient than under environmental stress. Average absolute stick voltage indicated performance was best under heat stress. The variances in performance under the various experimental conditions, especially the significant ($P<.01$) differences recorded for total time, T, and λ_c support the conclusion that Jex's critical task is a viable instrument for investigating the effects of environmental stress on operator performance. The commonly used average absolute error, however, appeared to be insensitive to the effects produced by the relatively short (one hour) stress durations.

REFERENCES

1) Jex H.R., McDonnell, J.D., and Phatek, A.V. "A Critical Tracking Task for Manual Control Research" IEEE Trans. HFE-7 (4) December 1966, 138-154.

2) Jex H.R. and Allen, R.W., "Research on a New Human Dynamic Response Test Battery." 6th Annual Conference on Manual Control, April 1970.

3) Jex, H.R., Two Applications of a Critical Instability Task to Secondary Work Load Research, Hawthorne California: Systems Technology Inc. TR#155-1 February 1967.

4) Westbrook, C.B., Anderson, R.O., and Pietrazek, P.E., Handling Qualities and Pilot Work Load, WPAFB Flight Dynamics Laboratory TRFDCC TM 66-5 September 1966.

VIBRATION EFFECTS ON MANUAL CONTROL PERFORMANCE*

R. Wade Allen, Henry R. Jex, and Raymond E. Magdaleno
Systems Technology, Inc., Hawthorne, California

SUMMARY

A variety of dynamic response and performance measurements are presented for compensatory manual control tasks performed under both vertical and lateral sinusoidal vibration. Special, on-line measurement techniques allowed the partitioning of error and control response variances into portions correlated with the tracking task and vibration inputs, and an uncorrelated or remnant portion. Vibration effects on visual-motor dynamic response were generally small, whereas significant effects occurred in error remnant and "vibration-induced feedthrough" to the control response. Dramatic increases in remnant were obtained under low frequency lateral vibration with a low-spring-gradient displacement stick, while an isometric control showed little effect.

INTRODUCTION

Degradation of human performance in vibration environments is a continuing problem in the man-machine systems area. Current operational problems include:

- Controlling large elastic aircraft through strong convective turbulence and maneuvering fighters under transonic buffet conditions.
- Piloting and manual fire control operations in out-of-balance rotor craft.
- Control of high-speed vehicles over rough terrain or waves.

The design and development of these systems would be considerably aided if the effects of the biodynamic environment on the pilot/vehicle control system could be quantitatively assessed. This is currently not possible, however, because of the inadequacy of applicable dynamic models and data, particularly in regard to the performance of complex manual control tasks.

A great deal of effort has been expended over the years on measuring the effects of vibration on man, and the body of this research is summarized

*The research reported in this paper was sponsored by the Aerospace Medical Research Laboratory, Aerospace Medical Division, Air Force Systems Command, Wright-Patterson Air Force Base, Ohio, under Contract No. F33615-71-C-1487. The voluntary informed consent of the subjects used in this research was obtained as required by Air Force Regulation 80-33.

Preceding page blank

in Refs. 1-10. Human tolerance and subjective comfort levels of vibration have been fairly well quantified (Refs. 5, 11-17), and models for the biomechanical response of the body (transmissibility) to vertical motion inputs (vibration and shock) are available (e.g., Ref. 5). Biodynamic response to lateral and longitudinal vibration is less well understood, however, and knowledge of psychomotor performance effects is mainly empirical, although some attempts have been made to coalesce and extrapolate the present data base (Refs. 8-10).

The lack of quantification of performance effects is mainly due to the absence, until fairly recently, of a validated theoretical basis and efficient measurement techniques for the elusive and complex properties of human operator control performance. This situation has changed, however, for two reasons:

- There now exists an excellent, albeit piecemeal, set of reasonably well validated human operator system models which could be assembled into a suitably comprehensive "grand model" (Refs. 18, 19, and 20). Such a model is urgently needed to guide the measurements and data analysis for vibration effects on manual control performance.
- Test techniques and equipment have been recently developed for measuring both dynamic response behavior and performance in manual control systems (Refs. 21 and 22). This approach offers efficient and sensitive means to reveal vibration effects at safe levels of vibration and within economical experimental designs.

Earlier discussion of our point-of-view, approach, and typical problems is given in Ref. 20. The research reported here represents the first results of an Air Force program designed to apply these recent manual control measurement techniques to the vibration problem. Details of our work are given in Ref. 30.

APPROACH

The measurement and modeling approach taken in this research is illustrated in Fig. 1. We are concerned with a compensatory manual-control system including a standard tracking or command input and an undesirable vibration input. Because of the separate (and presumed uncorrelated) tracking and vibration inputs, the human operator is described by two quasi-linear processes:

- Y_p, the traditional visual motor response function that operates on the system error signal.

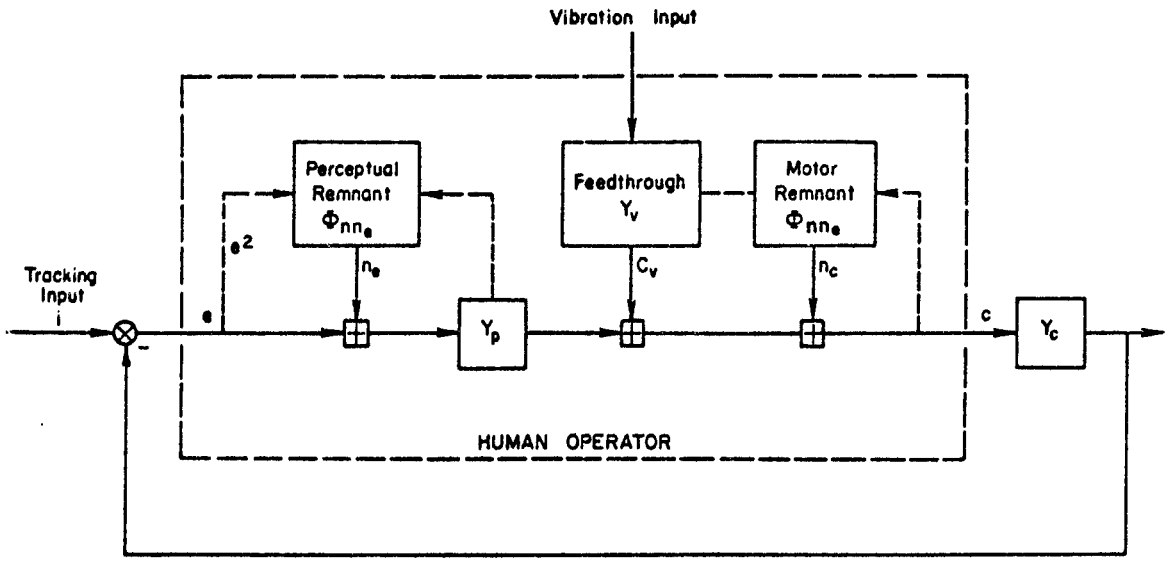

Figure 1. Measurement Model Structure

- Y_v, a vibration feedthrough process that causes control activity correlated with the vibration environment.

Two remnant processes are also ascribed to the human operator: Φ_{nn_e}, the now routinely accepted perceptual (visual) noise process (Refs. 23 and 24), and Φ_{nn_c}, an output (motor) noise process which the present research indicates to be significant under certain biodynamic circumstances.

It is desirable to measure each of the elements of human operator behavior shown in Fig. 1 if we are to understand the complex and often confounding effects caused by a stress such as vibration. Some of the possible biodynamic environment effects are as follows:

- Visual Motor Dynamics (Y_p). Both voluntary and involuntary effects may occur here. For controlled elements requiring lead generation vibration may interfere with the rate perception process, thereby reducing lead capabilities. Vibration may also mechanically interfere with the neuromuscular system, thus affecting the high frequency portion of the human operator's response (i.e., increasing high frequency phase lags). Finally, the operator may voluntarily control the amount of lead and gain he employs in order to mediate the effect of factors such as increased remnant and vibration feedthrough.
- Vibration Feedthrough Dynamics (Y_v). Vibration feedthrough will appear in the control response, and depending on frequency

content and magnitude as determined by Y_v and the environment, recirculate around the tracking loop and become a significant factor in the system error. Also, in an operational situation such as piloting, the induced high frequency control activity can cause adverse effects on a flight control system and/or excite high frequency structural modes, which would further aggravate the vibration environment.

- Perceptual Noise (Φ_{nn_e}). Differential motion between the display and eye (due to eye, head and torso resonance effects) can cause visual blurring which might increase remnant generation at this point.
- Motor Noise (Φ_{nn_c}). This source may be due to a variety of effects including vibration interference with the neuromuscular actuation process and proprioceptive feedbacks.

It should be noted that with only one control output from the man we can measure but one uncorrelated power source, so implicit techniques will be required in order to differentiate between perceptual and motor sources.

In order to gain some insight into the complex relationships between dynamic response and performance of the system in Fig. 1, let us now consider the relationships describing the spectral properties of the various signals. Assuming linearized dynamic processes to represent the perturbations about an operating condition, we can partition the error spectrum into components associated with the tracking input, vibration input and the visual and motor noise processes.

Total = Components from:

$$\Phi_{ee}(\omega) = \overbrace{\Phi_{ee_i}(\omega)}^{\text{Tracking Input}} + \overbrace{\Phi_{ee_v}(\omega)}^{\text{Vibration Input}} + \overbrace{\Phi_{ee_{n_e}}(\omega)}^{\text{Perceptual Noise}} + \overbrace{\Phi_{ee_{n_c}}(\omega)}^{\text{Motor (Output) Noise}}$$

$$\Phi_{ee} = \left|\frac{1}{1 + Y_pY_c}\right|^2 \Phi_{ii} + \left|\frac{Y_vY_c}{1 + Y_pY_c}\right|^2 \Phi_{vv} + \left|\frac{Y_pY_c}{1 + Y_pY_c}\right|^2 \Phi_{nn_e} + \left|\frac{Y_c}{1 + Y_pY_c}\right|^2 \Phi_{nn_c} \quad (1)^*$$

*All the spectra and transmittances are generally functions of the complex variable, $s = \sigma \pm j\omega$; and all measurements are functions of the frequency variable ($\pm j\omega$). The arguments (ω) and ($j\omega$) will be dropped for convenience.

Similarly, for the control output power spectrum:

$$\Phi_{cc} = \Phi_{cc_i} + \Phi_{cc_v} + \Phi_{cc_{n_e}} + \Phi_{cc_{n_c}}$$

$$= \left|\frac{Y_p}{1 + Y_pY_c}\right|^2 \Phi_{ii} + \left|\frac{Y_v}{1 + Y_pY_c}\right|^2 \Phi_{vv} + \left|\frac{Y_p}{1 + Y_pY_c}\right|^2 \Phi_{nn_e} + \left|\frac{1}{1 + Y_pY_c}\right|^2 \Phi_{nn_c} \quad (2)$$

We can see from these equations that the operator has some control over the vibration feedthrough term if he can influence the feedthrough dynamics, Y_v. If the vibration power is within the bandwidth of the tracking loop, then the operator must adjust the system closed-loop dynamics $[1/(1 + Y_pY_c)]$ in order to avoid undue amplification of the feedthrough, particularly at low vibration frequencies (< 2 Hz).

Equations 1 and 2 also show that the remnant processes have different effects on the error and control signal spectra. If the controlled element dynamics (Y_c) are similar to an integrator (as many "good" vehicles are), the dynamic functions multiplying the injected spectra in the error spectrum (Eq. 1) approach a finite value at low frequency, while the corresponding functions in the control output spectrum (Eq. 2) approach zero. Thus, the error spectrum and other error measures will usually contain more low frequency remnant than will the corresponding control quantities.

In this paper we present performance and visual motor response measurements (Y_p) obtained under various vibration conditions. Vibration feedthrough dynamics (Y_v) were measured and are presented in Ref. 26 which discusses the feedthrough process and models and their implication on manual control system performance.

EXPERIMENTAL SETUP

Two separate experiments were conducted with sinusoidal vibration in the vertical (G_z) and lateral (G_y) axes. The G_z experiment was scheduled as a preliminary study to verify equipment setup, measurement techniques, etc. Relatively quick success in the setup phase enabled a complete experiment to be accomplished on three subjects, albeit with a limited set of conditions and measurements. Having perfected the measurement technique at this stage and determined some of the general effects of vibration, we

then turned to lateral vibration for the formal experiment, with the complete set of desired measurements. Previous experiments (e.g., by Shoenberger, Ref. 27) have shown lateral effects to be more dramatic and complex than vertical cases, and the additional measurements utilized in this second experimental round were crucial in explaining the observed phenomena.

Physical Setup

In Fig. 2 a subject is shown performing the control task on the AMRL-BBV Lab's Western Gear shaker (Model 4010) located at Wright-Patterson Air Force Base, Ohio. A Tektronix Model 601 CRT, having a view area of 8 × 10 cm, was used as the visual display for the compensatory tracking task. The subject controlled the task with a joystick, as shown in Fig. 2. The aluminum seat shell and the control stick pivot and display were rigidly attached to the table such that there were no resonances or other distortions within the frequency range of interest in these studies.

The subject was seated on a standard F105 parachute container and insulation pad. This setup provided a stiff, yet comfortable, coupling between the seat and subject, without adding significant dynamic effects to the transmissibility measurements. A standard fighter aircraft shoulder strap and seat belt arrangement was also employed. The belts were adjusted to a comfortable tension, but the shoulders were not pinned to the back of the seat. The setup closely simulated the arrangement in a typical military aircraft.

In order to define the transmissibility and control feedthrough properties of the subjects, accelerometers were used to measure the motion of the seat, and the subject's shoulder, head and elbow. The accelerometers mounted on the subject were lightweight (< 1/8 oz) Endevco Model 2222B units. The shoulder accelerometer was securely taped to the bony point of the shoulder (acromian), and the elbow unit was strapped around the arm (against the proximal extremity of the ulna). The head accelerometer was affixed to the skull via a small, lightweight bite rod that was gripped in the teeth like a pipestem. Each subject had his own bite bar with an individualized dental impression formed from a thermosetting plastic.

This page is reproduced at the back of the report by a different reproduction method to provide better detail.

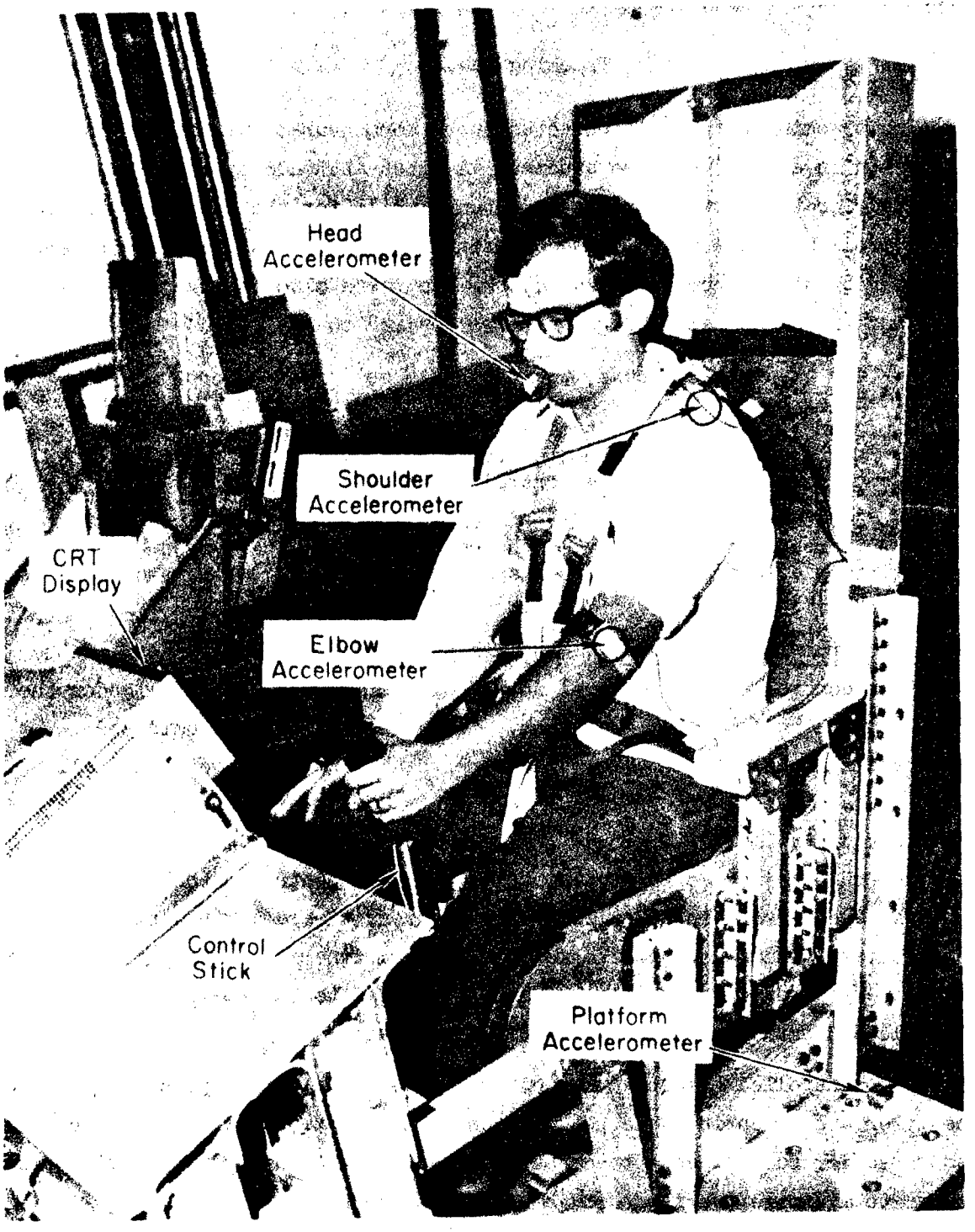

Figure 2. Instrumented Subject Performing Tracking Task Under Vibration

The above setup was similar for both the vertical (G_z) and lateral (G_y) studies. The only differences were in the orientation of the accelerometers, the display format, and the control stick axis, as appropriate to the specific control task (pitch or roll) discussed below.

Tracking Tasks

The tracking tasks were selected to be commensurate with the axis of vibration in each of the two studies. A pitch-attitude-type task was selected for the vertical vibration study, while for the lateral vibration study, roll attitude tracking was chosen. In addition to being pertinent to the vibrating aircraft scenario, the two tasks also involved different types of vibration feedthrough which we desired to investigate:

- For the vertical case, the stick vibrations were perpendicular to the pitch control motions, thereby minimizing direct vibration-induced control action. Only the secondary vibrational motions, transmitted by the operator's arm from his torso, appeared in the control response.
- For the lateral case, direct control responses are caused by inertial forces acting on the combined arm/stick mass due to platform motion as well as relative shoulder motions due to lateral torso transmissibility.

Pitch Control Task (G_z Study). In this task the fore-aft movement of the joystick controlled the vertical motion of a simulated horizon line on the CRT (conventional "inside-out" view). This line and the illuminated reference line were very bright and could easily be perceived under all conditions. Two different sets of control dynamics were employed. The simplest controlled element was a first-order instability (Ref. 21) which allowed the subject to act as a pure gain (i.e., control outputs proportional to displayed error) in addition to his inherent time delay and neuromuscular properties. The second controlled element had dynamics approximating the short period response of a large bomber (similar to the XB-70) and required some lead generation by the pilot ($T_L \doteq 0.5$ sec).

The controlled element dynamics and appropriate human operator response behavior are given in Table 1. The controlled element gains (K_c) were adjusted for subject acceptance but were set on the low side of optimum in order to minimize the feedthrough effect on the task.

TABLE 1

TRACKING TASK PARAMETERS

a. Controlled Element Dynamics

TASK		CONTROLLED ELEMENT DYNAMICS, $Y_c(s)$	APPROPRIATE HUMAN OPERATOR BEHAVIOR, $Y_p(s)$
Pitch Attitude Tracking (G_z Study)	First Order	$\frac{K_c}{s - 1}$	$K_p e^{-\tau e j\omega}$
	Short Period	$\frac{K_c(s + 1.42)}{s[s^2 + 2(.56)(1.71)s + 1.71^2]}$	$K_p(T_L s + 1)e^{-\tau e j\omega}$ $T_L \doteq 0.5$ sec
Roll Attitude Tracking (G_y Study)		$\frac{K_c}{s(s + 3)}$	$K_p(T_L s + 1)e^{-\tau e j\omega}$ $T_L \doteq 0.3$ sec

b. Tracking Command Input

FREQUENCY, ω_k		AMPLITUDE, A_k	
(Hz)	(rad sec)	Pitch Task (cm on CRT)	Roll Task (deg on CRT)
0.08	0.503	0.646	12.9
0.20	1.26	0.258	5.16
0.48	3.04	0.107	2.16
1.00	6.28	0.0516	1.04
1.67	10.5	0.0309	0.062
Displayed rms, σ_i		0.5 cm	10 deg

c. Control Stick Properties

STICK	FORCE GRADIENT (Newtons/meter)	NATURAL FREQUENCY (rad/sec)	DAMPING RATIO
Spring	164	23	0.3
Stiff	13,900	207	0.014

Two different control sticks were employed with widely different spring restraints in order to investigate the effects of arm/control stick coupling. The "spring" stick had a very light spring gradient with no damping other than ballbearing friction. The "stiff" stick was essentially an isometric (force stick) control. In this case arm motion at the hand was constrained to move with the platform motion, and actually provided another anchor point for the body in addition to the seat and feet. The control stick properties are listed in Table 1.

A sum of five non-simple-harmonic sinusoids with random initial phasing was used as the input forcing function for the tracking task. The frequencies were roughly logarithmically spaced to most efficiently cover the range of interest for visual-motor response measurements, and the amplitudes were set inversely proportional to frequency (Table 1) in order to yield adequate power in the error spectrum at each frequency.

Roll Control Task (G_y Study). In this task left and right movement of the joystick controlled the rotation of the luminous horizon line on the CRT display (conventional "inside-out" view). Based on the findings of the G_z study, the controlled element configuration did not appear to have a large interaction with vibration effects, so a single set of moderate-difficulty dynamics were selected for the lateral case. The controlled element form approximates the roll response of a stability-augmented aircraft. The controlled element gain was again set to an acceptable level on the less sensitive side of optimum in the opinion of the subjects. The controlled element properties are summarized in Table 1.

The "spring" and "stiff" control sticks employed in the vertical vibration study were again used here. The same input forcing function was used as well, except that the amplitude is now characterized in terms of the angular rotation of the horizon line as given in Table 1. The amplitude was set such that vertical displacements at each edge of the horizon line were comparable to the amplitude used in the G_z study.

Measurements

Our primary measurement scheme is illustrated in Fig. 3. A Describing Function Analyzer (DFA) provided a sum of five sinusoids forcing function

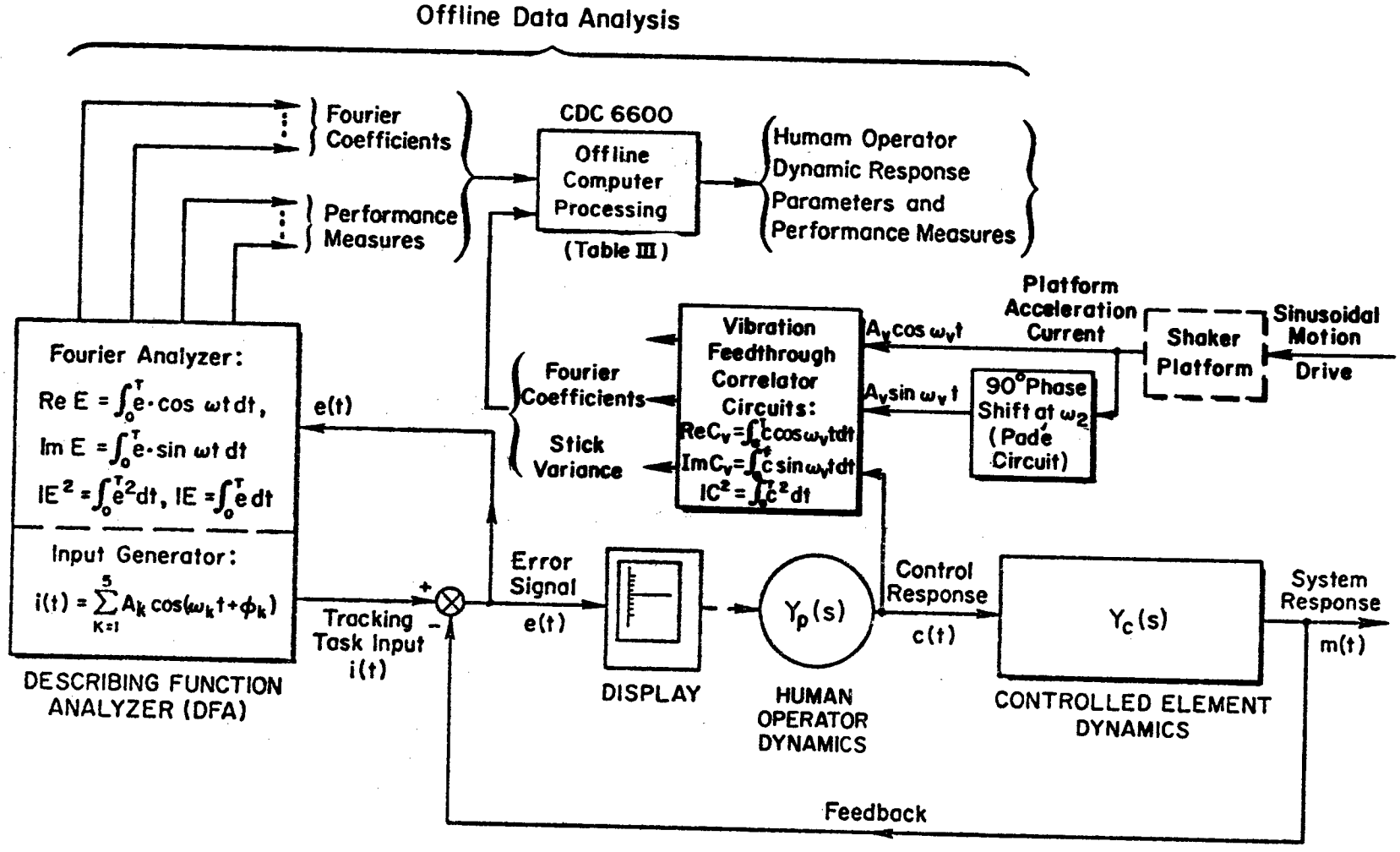

Figure 3. Tracking Tasks, Data Measurements and Analysis

to the tracking and Fourier analyzed the resulting error signal during the tracking runs. The resulting data was then processed off line to yield measures of the subject's visual-motor describing function (Y_p) and system open loop describing function, in addition to the total and input correlated portion of the error and control response variances. This technique has been described in detail elsewhere (Ref. 22a) and has proven to give reliable measurements in several applications (Refs. 21, 22, 24, 25).

The system open loop describing function data near the gain and phase crossover regions were reduced to a set of simple parameters which can efficiently summarize trends in dynamic response behavior under vibration. The parameters include:

- **Gain Crossover Frequency** (ω_c), which is proportional to the subject's visual-motor gain, and gives a measure of the bandwidth of the manual control loop.
- **Phase Margin** (φ_M), a system stability margin measured at ω_c which is generally large when the operator is attempting to minimize the performance effect of noise injected into the loop and small for accurate tracking of the command input.
- **Phase Crossover Frequency** (ω_u), a high frequency measure of phase lag properties with contributions from lead generation, neuromuscular and limb/manipulator dynamics.

Summary performance parameters obtained from the above measurement technique include:

- **Error Variance** (σ_e^2), the average mean square dynamic power in the error signal after removing dc offsets.
- **Error Coherence** (ρ_e^2), the fraction of the total error variance linearly correlated with the describing function measurements. The remaining power is due to noise sources internal to the human operator.

A technique similar to the DFA was also employed using analog circuits to measure the vibration feedthrough dynamics and vibration correlated control power during the G_y experiment. Since the vibration was sinusoidal, the control stick signal was multiplied by the platform accelerometer output (a_p) and integrated to obtain the in-phase vibration correlated component (real part Fourier coefficient). The accelerometer output was also phase shifted by 90 deg (using a Pade circuit set at the vibration frequency) and multiplied by the control response to obtain the quadrature (imaginary coefficient) vibration component of control response. Combining

data from the DFA and control feedthrough measurements we were then able to partition the variance in the error and control response signals, as indicated by Eqs. 1 and 2, into input and vibration correlated components and the remaining uncorrelated (noise) power:

$$\sigma_e^2 = \underbrace{\sigma_{e_i}^2}_{\text{Tracking Input Correlated}} + \underbrace{\sigma_{e_v}^2}_{\text{Vibration Feedthrough Correlated}} + \underbrace{\sigma_{e_n}^2}_{\text{Uncorrelated Noise (Remnant)}} \qquad (3)$$

$$\sigma_c^2 = \sigma_{c_i}^2 + \sigma_{c_v}^2 + \sigma_{c_n}^2 \qquad (4)$$

Thus the relative importance of these various factors on manual control performance could be assessed. Transmissibility measurements (response of various points of the subject's body relative to platform motion) were obtained from recordings of the four accelerometers shown in Fig. 2. Since the vibration wave forms were sinusoidal, it was fairly easy to read amplitudes, and relative phase shifts from the recordings.

In the first (G_z) study strip chart recordings were also used to identify the control feedthrough response due to vibration. In this situation the subjects were asked to stabilize the short period dynamics with no input forcing function to the control task, and it was easy to identify the control response component corresponding to the vibration frequency appearing in the accelerometer traces. In the second (G_y) study the vibration correlated control response was computed during each run, however, as described above; and these measurements were shown to agree with the components visually apparent in the strip chart recordings.

Vibration Conditions

All vibration conditions were run at a zero to peak amplitude of 0.4 g, a relatively substantial level that previous studies (e.g., Ref. 27) indicated would give definite effects, yet was within safety/tolerance bounds under BBV lab policy. For the G_z study the frequencies 2, 6, and 10 Hz were selected for the formal data sessions to be below, at, and above the vertical whole body resonant point respectively. Transmissibility and vibration correlated control response data via strip chart recordings were obtained

at several intervening frequencies as well. Previous studies (Refs. 27, 28) have shown lateral vibration effects to occur at low frequencies, so 5 frequencies for the G_y study were selected to range from 1.3 Hz (between the highest two tracking input sinusoids) to 10 Hz and were spaced approximately logarithmically for convenience in interpreting vibration feedthrough dynamics data. In both studies, static (zero vibration) conditions were also included.

Subjects, Training, and Procedures

The subjects were selected from the BBV hazardous duty panel and all but one had previous tracking experience under vibration. Three subjects were employed for the G_z experiment, and four were selected for the G_y tests. The subjects were given training under both static and vibration conditions, and analysis of the training data indicates the subjects reached reasonably asymptotic performance levels.

To minimize the effects of order of presentation, fatigue, etc., the vibration conditions in the G_z experiment were randomized between subjects. For the G_y study the order of presentation was counterbalanced between subjects, and in addition pre and post exposure static conditions were administered in an attempt to measure any potential fatigue and/or practice effects. Two 2 min (100 sec measurement period) were administered for each condition in the G_z experiment, while three 1 min (50 sec measurement period) trials were employed in the G_y study.

RESULTS AND DISCUSSION

Transmissibility and Vibration Correlated Control Response

The physical effects of the G_z and G_y vibration environments are compared in Fig. 4. Dramatic differences in subject motion effects are noted in the shoulder transmissibility data between G_z and G_y vibration. Under vertical motion the shoulder resonates significantly in the region of 5 Hz due to the well known dynamic properties of the torso (Refs. 5, 29). Shoulder motion was not appreciably attenuated at 10 Hz, and the subjects acknowledged visual blurring at this condition. Other transmissibility data, for head and elbow motion, are given in Ref. 30.

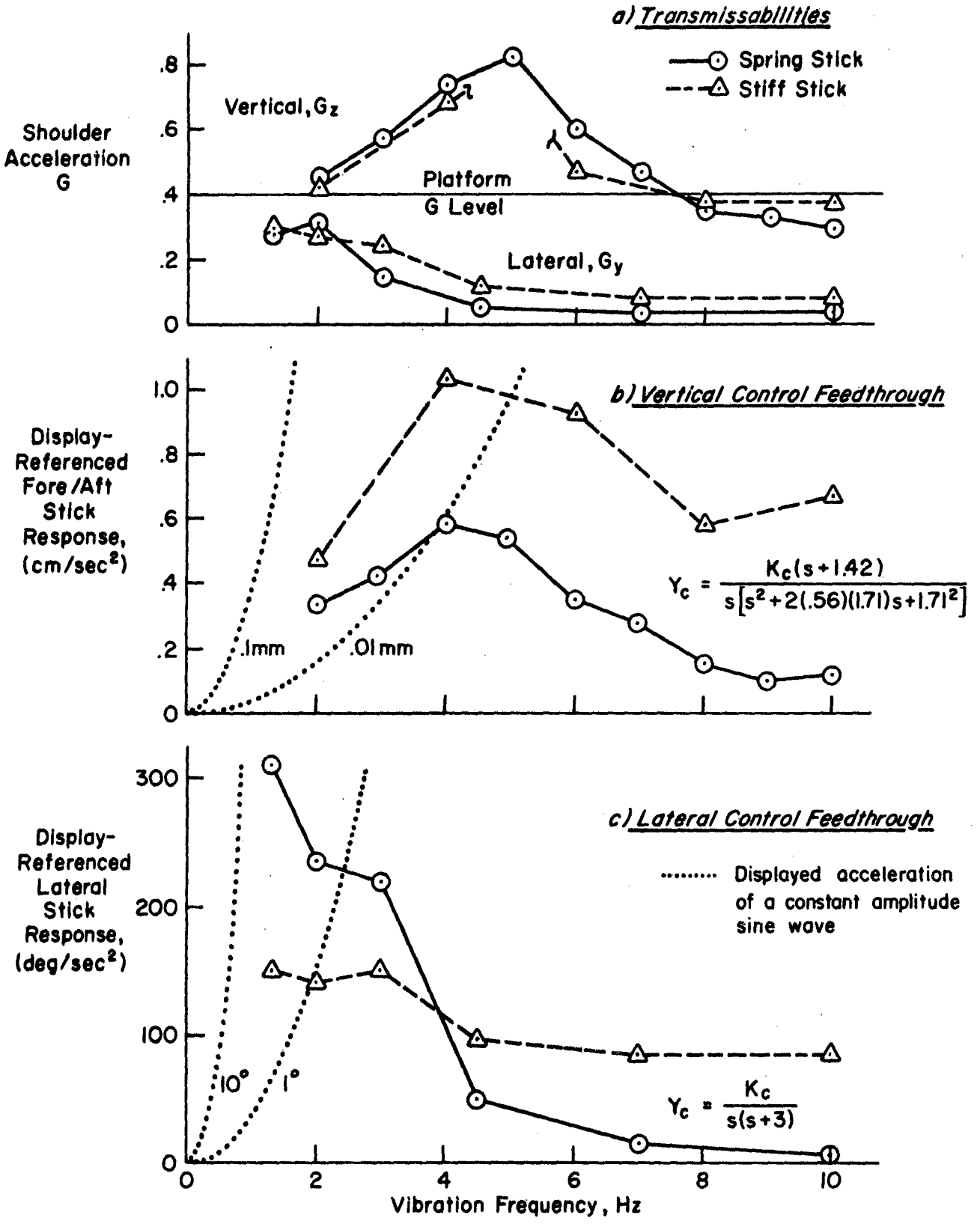

Figure 4. Comparison of Transmissibility and Vibration Control Feedthrough for G_z and G_y Vibration

For lateral vibration the shoulder motion is maximum at low frequency and attenuates at higher frequencies. By observation it was obvious that the subject's shoulder and head were essentially inertially stable at the higher vibration frequencies, and no incidence of visual blurring was reported. Under both G_Z and G_Y, the control stick characteristics seem to have some minor effects on shoulder response. The stiff stick appears to help attenuate the shoulder motion at lower frequencies, but at higher frequencies it helps to "drive" the shoulder, thereby producing less high frequency attenuation than with the spring stick.

The vibration control feedthrough data presented in Fig. 4 reflects the frequency response character of the shoulder responses, as well as rather significant effects due to stick characteristics. The outputs of the two control sticks have basically different physical dimensions (i.e., force for the stiff stick and displacement for the spring stick), so in order to compare them, stick motions are referenced to the display. This was accomplished by noting that the controlled element dynamics can be approximated by a double integration at higher frequencies ($f > 1$ Hz):

$$Y_c = \frac{m}{c} \doteq \frac{K_c}{s^2} \tag{5}$$

Since there is no command input (i) at these frequencies we can essentially assume that the second derivative of displayed error is proportional to the stick output signal,

$$\ddot{e} \doteq K_c c \tag{6}$$

and it is the scaled stick signal, $K_c c$, that is plotted in Fig. 4.

In order to show the practical significance of stick feedthrough in terms of displayed errors, the equivalent displayed acceleration of constant amplitude sine waves is also plotted in Fig. 4. It is apparent for the G_Z data that vertical displayed errors due to vibration control feedthrough are small and below visual thresholds. For lateral vibration control feedthrough was at a maximum at low frequencies, however, which resulted in suprathreshold rotational amplitudes of the horizon line.

We have developed simplified biodynamic models which (along with closed loop signal relationships) satisfactorily explain these control feedthrough results. The models and their implications for manual control performance in vibration environments are given in Ref. 30.

Vertical Vibration Effects on Performance and Dynamic Response

The results of the vertical vibration experiment are summarized in Fig. 5. Error performance consistently degraded under vibration, with the effect increasing with frequency. Error coherence decreased under vibration and was consistently lowest under the highest vibration frequency. The dynamic response results are less consistent than the performance effects. The phase crossover frequency (ω_u) effects show that the higher this parameter is in static tests of a given task/control stick configuration, the more it decreases under vibration. Thus vertical vibration apparently affects high frequency phase lags, and the effects increase with vibration

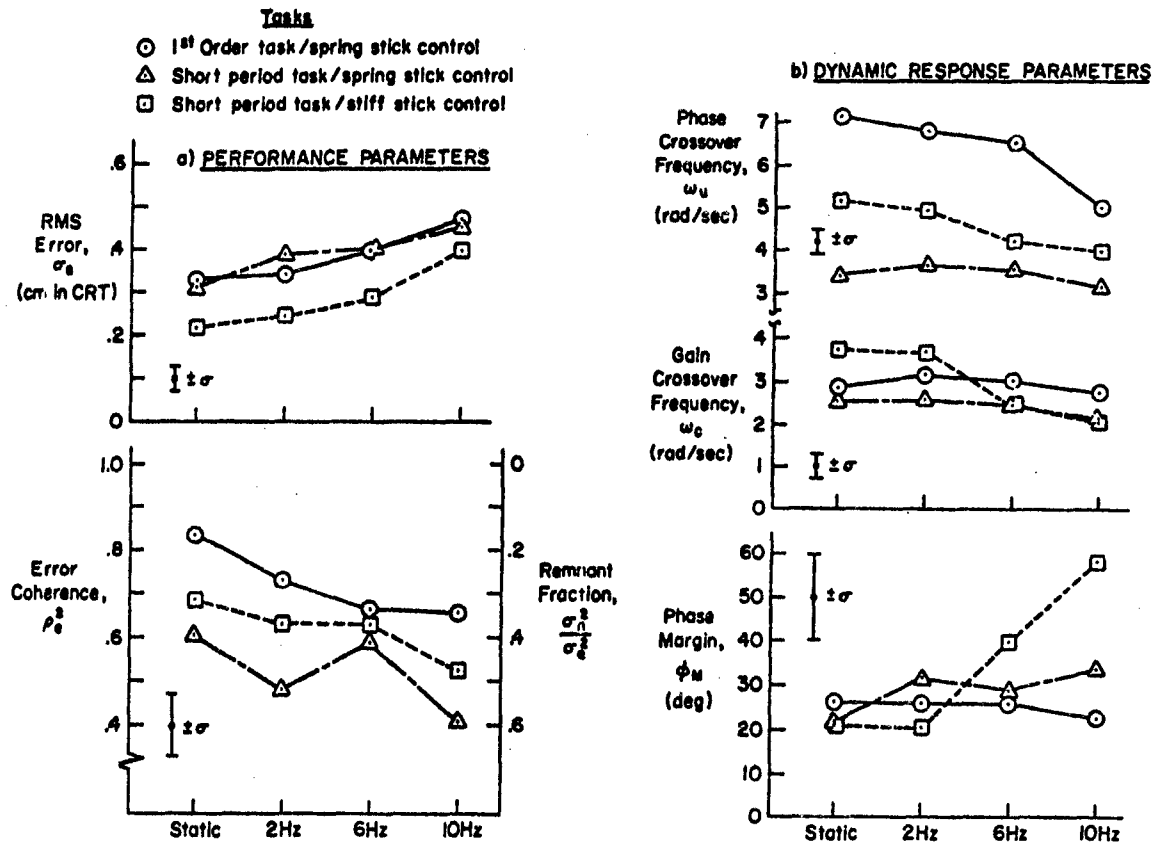

Figure 5. Performance and Dynamic Response Parameters Averaged Over 3 Subjects under ±0.4 G_z Sinusoidal Vibration

frequency. This suggests a direct effect of vibration on the perceptual or neuromuscular systems which determine the human operator's high frequency dynamic response properties. From some subject comments noting more sluggish movement tendencies at high vibration frequencies, we suspect that the neuromuscular system is vulnerable to vibration in the region of 10 Hz vibration.

Somewhat surprisingly, only the task with the stiff stick control showed a significant drop in gain (ω_c) under vibration, which resulted in a concomitant increase in stability margins (φ_M). With the spring stick the closed loop system dynamic response was relatively stable under vibration, considering the ω_c and φ_M results. Since the error performance degraded significantly under vibration with corresponding decreases in error coherence, it is concluded that remnant increased under high frequency vertical vibration.

Lateral Vibration Effects on Performance and Dynamic Response

The performance and dynamic response results from the lateral vibration experiment are summarized in Fig. 6. The performance results are considerably different from those obtained under vertical vibration. Stick characteristics had a profound influence on performance; performance with the stiff stick showed little sensitivity to vibration, while the spring stick allowed severe performance degradation under low frequency vibration which differs from the G_z results where the main effects occurred under high frequency conditions.

The error coherence results in Fig. 6a show that the spring stick errors under low frequency vibration were largely remnant (uncorrelated with either the tracking input or vibration feedthrough). The dynamic response results shown in Fig. 6b show little sensitivity to vibration (although there is a consistent increase in stability margins of $\Delta\varphi_M = 5^\circ$ to 10° under vibration). This implies that the large increase in closed loop remnant with the spring stick is due to induced increases in the remnant sources (thresholds, motor noise, etc.) rather than closed loop amplification of existing noise.

In order to obtain additional insight into the performance effects of lateral vibration, the control stick and error variances were partitioned into correlated and uncorrelated components, per Eqs. 3 and 4, and the results are given in Fig. 7*.

---

*Log scales are used on Fig. 7 to cover the wide range of values; thus components are not graphically additive, and the remnant fraction tends to be suppressed.

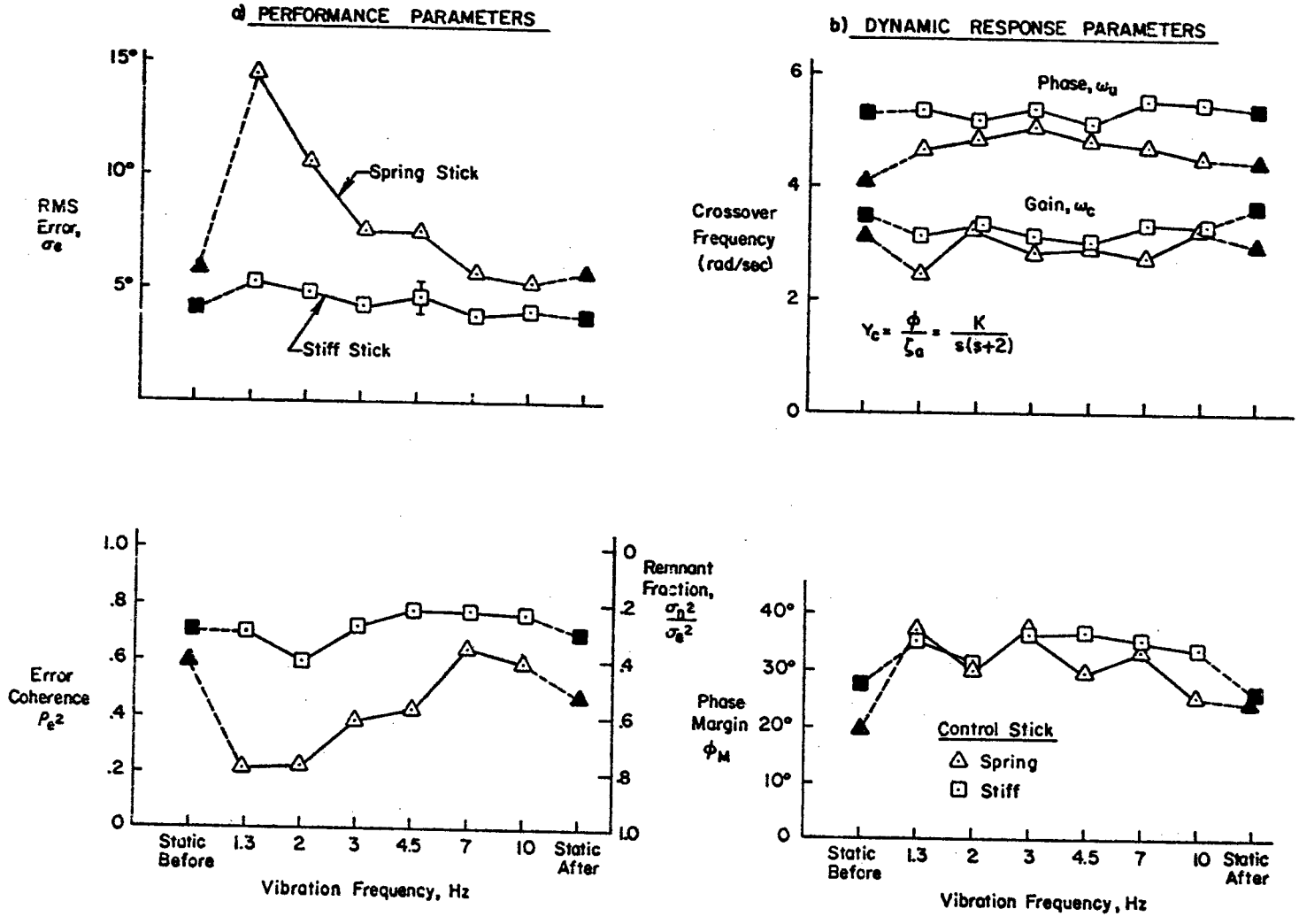

Figure 6. Performance and Dynamic Response Parameters Averaged over 4 Subjects for ±0.4 G_y Sinusoidal Vibration

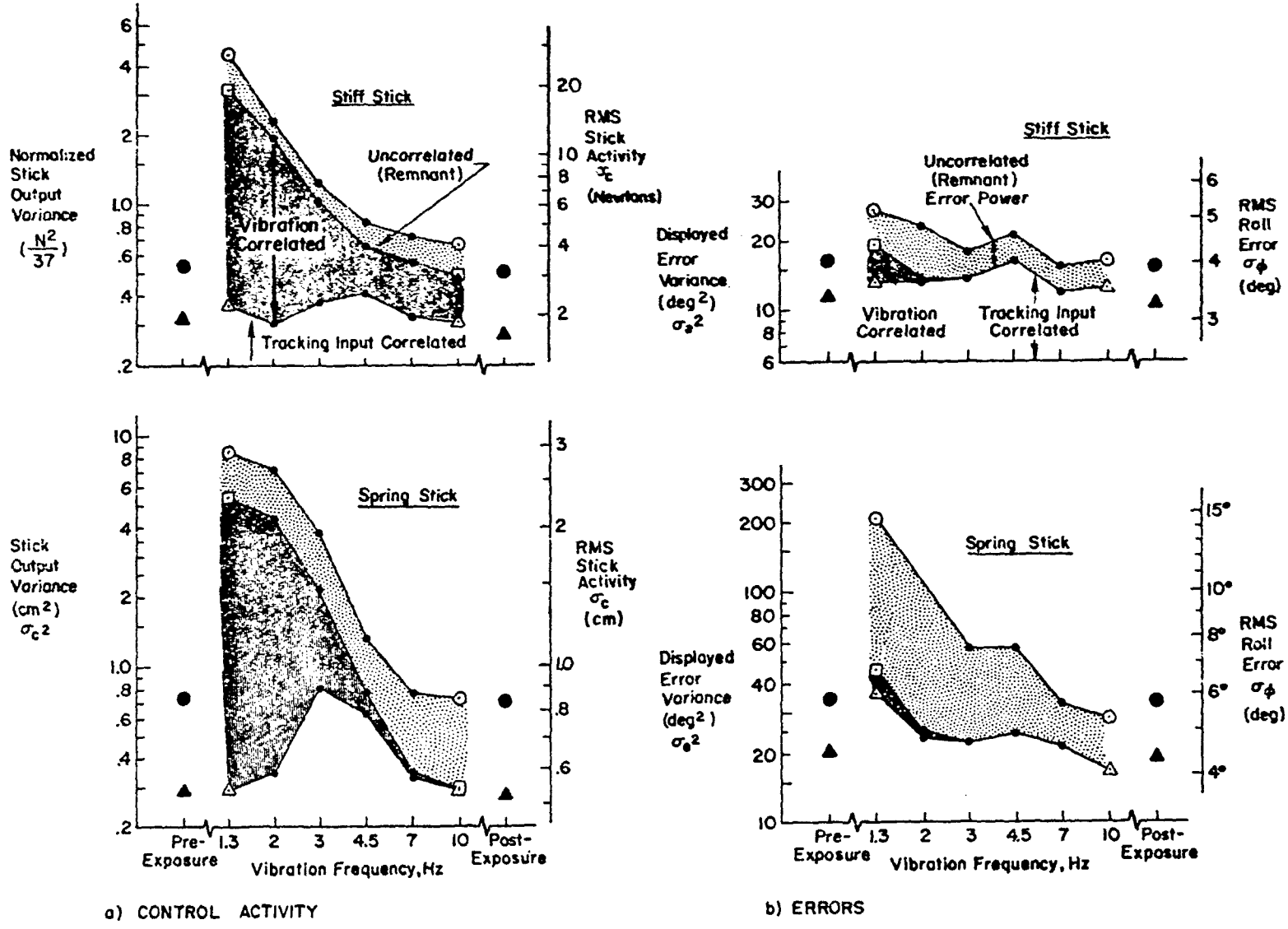

Figure 7. Control Stick and Error Variance Components
Averaged over 4 Subjects for ±0.4 G_y Sinusoidal Vibration

The control activity for either control stick is dominated by vibration feedthrough power under low frequency vibration, and the remnant portion is generally larger for the spring stick. In general, the trends for each control variance component are similar between the two sticks. This is definitely not the case for error variance, however. The stiff stick yielded a relative constant proportion of remnant across the vibration conditions, while uncorrelated errors increased severalfold under 3-5 Hz vibration with the spring stick.

Considering the dynamics of the control loop as analyzed previously (Eqs. 1 and 2) it is felt that the large remnant errors induced by lateral vibration are due to an increase in the low-frequency portion of the operator's remnant spectrum, which has only a small effect on the net control variance but is considerably amplified by the free integrator in the controlled element dynamics. Subjects' comments during the tests indicate that the proprioceptive feedback of spring stick control position was masked by the large body and stick motion under low frequency lateral vibration, and this is probably the effect that precipitated the increased low frequency remnant. Because the remnant is such a large proportion of the error increase under lateral vibration, its detailed investigation deserves high priority in further research.

For a more detailed picture of the dynamic response variations under vertical and lateral vibration, complete operator describing function plots for all of the above conditions are given in Ref. 30. Simplified biodynamic models which explain the large control feedthrough and its attenuation at mid frequency are also given therein.

CONCLUSIONS AND RECOMMENDATIONS

The modern manual control measurement techniques employed here have allowed a comprehensive battery of dynamic response and performance data to be efficiently and reliably collected under adverse experimental stress conditions. The measurements allowed the analysis of the effects of vibration on the components of system performance and the dynamic response properties of the human operator. For the first time, the different causes of performance degradation under vertical (G_z) and lateral (G_y) sinusoidal vibration have been revealed.

Error performance generally degraded mainly from remnant increases. Under vertical vibration this occurred at high frequency motion and may correlate with visual blurring. For lateral vibration the performance decreased because remnant increased under low frequency vibration. It was worst for the low-spring-gradient stick, possibly due to large body and control motions swamping out proprioceptive stick position cues. The influence of vibration on the human operator's dynamic response (describing function) behavior was small compared to the remnant and feedthrough effects. There was a general tendency for the operator to increase the stability margins of the tracking loop dynamics under vibration.

To complete the investigation of sinusoidal vibration, work on axial (G_x) vibration is continuing, with emphasis on detailed feedthrough and remnant measurements. The present research has just begun to really explain the processes by which manual control performance is influenced by vibration, so that predictive models suitable for analyzing new situations can be developed. The present results should be extended to the random vibration regime and include multi-axis vibration situations. Tasks which demand more of the operator's attention should be considered, including two axis tracking situations and subsidiary loading tasks. Finally, considering the major influence of control feedthrough on lateral vibration effects, research should be conducted on more operational control configurations, including wheel-columns and side mounted hand controllers which are under consideration for future fly-by-wire systems.

REFERENCES

1. Buckhout, Robert, A Working Bibliography on the Effects of Motion on Human Performance, MRL-TDR-62-77, July 1962.

2. Linder, Gerald S., "Mechanical Vibration Effects on Human Beings," Aerospace Medicine, Vol. 33, No. 8, Aug. 1962, pp. 939-950.

3. Chiles, W. Dean and Carolyn L. Custer, Summaries of Research on the Human Performance Effects of Vibration, AMRL TR 77-172, Nov. 1963.

4. Guignard, J. C., "Vibration," A Textbook of Aviation Physiology, J. A. Gillies, ed., Pergamon Press, New York, 1965, pp. 813-894.

5. von Gierke, H. E., "Response of the Body to Mechanical Forces — An Overview," paper presented at the Conference on Prevention of and Protection against Accidental Explosion of Munitions, Fuels and Other Hazardous Mixtures, New York Academy of Sciences, New York, 10-13 Oct. 1966.

6. Roth, Emanuel M., ed., Compendium of Human Responses to the Aerospace Environment, Vol. II, Sections 7-9, NASA CR-1205(II), Nov. 1968.

7. Beaupeurt, J. E., F. W. Snyder, S. H. Brumaghim, et al, Ten Years of Human Vibration Research, Boeing Co. Wichita Div. Rept. No. D3-7888, Aug. 1969.

8. Rustenburg, John W., Development of Tracking Error Frequency Response Functions and Aircraft Ride Quality Design Criteria for Vertical and Lateral Vibration, ASD-TR-70-18, Jan. 1971.

9. Grether, Walter F., "Vibration and Human Performance," Human Factors, Vol. 13, No. 3, June 1971. pp. 203-216.

10. Shoenberger, Richard W., "Human Response to Whole-Body Vibration," Perceptual and Motor Skills, Monograph Supplement 1-V34, 1972, pp. 127-160.

11. Weis, Edmund B., Neville P. Clarke, James W. Brinkley, et al, "Mechanical Impedance as a Tool on Human Response to Acceleration," Aerospace Medicine, Vol. 35, No. 10, Oct. 1964, pp. 945-950.

12. Lee, Richard A. and Fred Pradko, Analytical Analysis of Human Vibration, SAE Paper No. 680091, Jan. 1968.

13. Magid, Edward B., Rolf R. Coermann and Gerd H. Ziegenruecker, "Human Tolerance to Whole Body Sinusoidal Vibration Short-Time, One-Minute and Three-Minute Studies," Aerospace Medicine, Vol. 31, No. 11, Nov. 1960, pp. 915-924.

14. Mandel, Morris J. and Richard D. Lowry, One-Minute Tolerance in Man to Vertical Sinusoidal Vibration in the Sitting Position, AMRL-TDR-62-121, Oct. 1962.

15. Aspinall, D. T. and R. J. Oliver, Vehicle Riding Comfort—The Correlation Between Subjective Assessments of Vehicle Ride and Physical Measurements of Vehicle Motion, Motor Industry Research Assn. Rept. No. 1964/10, Feb. 1964.

16. Bryce, W. D., A Review and Assessment of Criteria for Human Comfort Derived from Subjective Responses to Vibration, National Gas Turbine Establishment Rept. No. R. 286, Dec. 1966.

17. Van Deusen, Bruce D., Human Response to Vehicle Vibration, SAE Paper No. 680090, Jan. 1968.

18. McRuer, Duane, Dunstan Graham, Ezra Krendel and William Reisener, Jr., Human Pilot Dynamics in Compensatory Systems — Theory, Models, and Experiments with Controlled Element and Forcing Function Variations, AFFDL-TR-65-15, July 1965.

19. McRuer, D. T., L. G. Hofmann, H. R. Jex, et al, New Approaches to Human-Pilot/Vehicle Dynamic Analysis, AFFDL-TR-67-150, Feb. 1968.

20a. Jex, Henry R., "Interfacing Man-Machine Control Performance in a Biodynamic Environment," Symposium on Biodynamic Models and Their Applications, 26-28 October 1970, AMRL-TR-71-29, Dec. 1971, pp. 769-790.

b. Jex, Henry R., "Modeling Man-Machine Control Behavior in Biodynamic Environments," 1971 IEEE Systems, Man and Cybernetics Group Annual Symposium Record, Anaheim, Calif., Oct. 25-27, 1971, pp. 91-96.

21. Jex, H. R. and R. W. Allen, "Research on a New Human Dynamic Response Test Battery," Proceedings of the Sixth Annual Conference on Manual Control, Wright-Patterson AFB, Ohio, April 1970, pp. 743-777.

22a. Allen, R. Wade and Henry R. Jex, "A Simple Fourier Analysis Technique for Measuring the Dynamic Response of Manual Control Systems," IEEE Trans., Vol. SMC- (publication pending).

b. Magdaleno, R. E., "Serial Segments Method for Measuring Remnant," IEEE Trans., Vol. SMC- (publication pending).

23a. Levison, W. H., S. Baron and D. L. Kleinman, "A Model for Human Controller Remnant," IEEE Trans., Vol. MMS-10, No. 4, Dec. 1969, pp. 101-107.

b. Jex, H. R. and R. E. Magdaleno, "Corroborative Data on Normalization of Human Operator Remnant," IEEE Trans., Vol. MMS-10, No. 4, Dec. 1969, pp. 137-139..

24. Jex, Henry R., R. Wade Allen, and Raymond E. Magdaleno, Display Format Effects on Precision Tracking Performance, Describing Functions, and Remnant, USAF Aerospace Medical Div. AMRL TR-71-63, Aug. 1971.

25. Allen, R. W. and Henry R. Jex, Visual-Motor Response of Crewmen During a Simulated 90-Day Space Mission as Measured by the Critical Task Battery, NASA CR- , (forthcoming (published in part previously in NASA SP-261, pp. 421-435).

26. Magdaleno, Raymond, E., R. Wade Allen, and Henry R. Jex, Biomechanical Models for Describing Vibration-Induced Control Responses in Manual Control Tasks, Paper to be presented at Univ. of Michigan-NASA Conference on Manual Control, May 17-19, 1972.

27. Shoenberger, Richard W., Investigation of the Effects of Vibration on Dial Reading Performance with a NASA Prototype Apollo Helmet, AMRL-TR-67-205, Feb. 1968.

28. Hornick, Richard J., Charles A. Boettcher and Allison K. Simons, The Effect of Low Frequency, High Amplitude, Whole Body, Longitudinal and Transverse Vibration upon Human Performance, Bostrom Research Labs., July 1961.

29. Coermann, Rolf R., The Mechanical Impedance of the Human Body in Sitting and Standing Position at Low Frequencies, ASD TR-61-492, Sept. 1961.

30. Allen, R. Wade, Henry R. Jex, and Raymond E. Magdaleno, Manual Control Performance and Dynamic Response During Vibration: Vol. I - Effects of Vertical and Lateral Vibration, STI TR-1013-1, March 1972 (forthcoming AMRL TR-).

CLINICAL APPLICATIONS OF TRACKING

Repa, B. S.*, Albers, J. W., Pew, R. W., and
Tourtellotte, W. W.**

The Bioengineering Program and the Departments
of Neurology and Psychology
The University of Michigan
Ann Arbor, Michigan

This study was supported in part by the E.I. DuPont de Nemours Company, The University of Michigan Institute of Science and Technology and Bioengineering Program, NASA Contract No. NSr 23-005-364, and NIH Training Grant No. 5 to 1 GM 01289-07, 1970-1971.

*Present address: General Motors Engineering Staff, General Motors Technical Center, Warren, Michigan 48090.
**Present address: Neurology Service, Wadsworth VA Hospital, Los Angeles, California 90073.

ABSTRACT

The objective evaluation of motor disabilities has received increased attention during the last few years. The intent of this paper is to demonstrate how two widely used systems analysis techniques, phase plane diagrams and power spectral density functions, can be used for describing the tracking behavior of patients with neurological disorders. Tracking performances for normal subjects and for patients with previous diagnoses of parkinsonism, multiple sclerosis, and cerebral palsy are considered. Both analysis techniques provide a compact way of describing tracking performance while still characterizing important features of the movement patterns. The phase plane method offers considerable promise for objectively evaluating intention tremor, while error power spectra reveal particular frequency distributions which can be used to characterize different groups of patients.

INTRODUCTION

The development of highly successful therapeutic methods for the treatment of neurological disorders and the expansion of experimental investigation in neurology and neuropharmacology have led to increasing use of objective methods in such research. Clinical investigators are becoming more exacting in their attempts to detect small changes in neurological function, and it is important that new methodologies for measuring human performance be thoroughly investigated. While considerable reliance is still placed on subjective clinical evidence, more and more attention is being devoted to the development of standardized quantitative performance indices.

The purpose of this paper is to consider the application of two frequently used systems engineering techniques, phase plane diagrams and power spectral density functions,for describing the tracking behavior of patients with neurological disorders. Samples from the tracking records of 35 normal subjects, ages 18 to 74 years, and 35 patients demonstrating movement disorders with previous neurological diagnoses of multiple sclerosis, Parkinson's disease, and cerebral palsy were examined using these techniques. Representative time records and phase plane diagrams for a step tracking task and power spectra of the tracking error for a random tracking task are presented. In that the sample size is small and the application of these techniques is new, most of the discussion will be devoted to qualitative inferences.

SUBJECTS

Parkinsonian patients: The parkinsonian patients were participating in a drug study designed to compare the efficacy of L-DOPA and amantadine to that of L-DOPA and placebo in the treatment of Parkinson's disease. The 28 parkinsonian patients evaluated during the study were recruited from 42 patients participating in a previous study designed to evaluate the efficacy of amantadine alone in the treatment of Parkinson's disease (Walker et al, 1972). Patients having concurrent medical problems, questionable diagnoses, physical disabilities making it impossible for them to commute, or previous stereotactic surgery were not considered. The 28 patients consisted of 12 women and 16 men having an average age of 65.6 years and an average disease duration of 9.3 years. Unless stated otherwise, performance records presented are for the L-DOPA and placebo trial. A summary description of Parkinson's disease is shown in Table 1.

Multiple sclerosis patients: The 6 female patients were previously diagnosed by the University of Michigan Neurology Staff as having multiple sclerosis. All patients were ambulatory and had varying degrees of upper extremity ataxia ranging from slight to moderate-severe. Sensory deficit and motor weakness were minimal. The patients had an average age of 30.6 years and an average disease duration of 6 years. Table 1 gives a summary description of multiple sclerosis.

Cerebral palsy patient: Heterogeneous groups like cerebral palsy are usually not selected for group studies. In the present experiments, however, the evaluation techniques are of most importance; and documenting the performance of the adult male patient with a previous diagnosis of congenital cerebral palsy provided a further demonstration of the effectiveness of the tracking techniques. The patient demonstrated minimal resting tremor, mild upper and lower extremity spasticity, and no weakness or sensory dificit.

Young adult normal subjects: 10 right-handed male and 10 right-handed female undergraduates from the University of Michigan served as paid subjects in the present experiments. Responding to a newspaper advertisement, the students were required to answer a telephone questionnaire, designed to screen out non-normal subjects. In addition, all subjects passed an abbreviated neurological examination immediately prior to performing in the experiments. The students ranged in age from 18 to 21 years.

Older adult normal subjects: 15 subjects age-matched to the parkinsonian patients were also studied. Requirements for selection were that the subjects be neurologically and physically normal and right-handed. The subjects were predominantly the husbands and wives of the patients and consisted of 9 women and 6 men with an average age of 62.3 years.

METHODS

Figure 1 shows a picture of the display screen and control stick employed in the study. The display screen was positioned 80 cm from the subject. Two large vertical lines of 13 cm and 6 cm were used for the target and follower, respectively, to help reduce the effects of any patient visual problems. A large position stick with negligible dynamics was used for the control stick to keep response limitations imposed by the equipment to a minimum (see Herzog, 1967). The tasks were as follows:

Step Tracking: In this task the subject was required to execute a quick adjustive movement that transferred his upper limb from one position to another. A pursuit display was used with the target line occupying one of two positions, 14 cm to the right or left of center. The task of the subject was to maintain alignment of the target and follower. Interstep intervals ranged from 3.5 to 6.0 seconds and control stick movements of $\pm 20^{0}$ were required for alignment. Thirty trials were used.

Random tracking: In this task, using a compensatory display, the subject was required to follow a random appearing input signal. The difference between the subject's output and the desired output was displayed. The random input had a 0.3 radian/second cutoff frequency, and was generated by passing pseudo-random binary noise through a second order filter. Five 75 second trials were used, the score for each trial being the integral of the subject's absolute position error during the middle 45 second portion of the run.

Phase plane diagrams were used for describing step tracking behavior. A phase plane trajectory is simply a plot of velocity versus position with time appearing as a parameter. In engineering applications the chief value of the phase plane approach lies in the fact that the trajectories, which represent the transient behavior of a system, can often be determined even though the exact relationship between position and time is unknown. In this paper, phase plane trajectories were obtained by plotting known values of velocity against known values of position.

Even when the time behavior is already known there is still merit to examining performance in the phase plane. This is especially true when families of trajectories are examined. Motor performance testing is normally subject to considerable variability even when performance for the same individual is concerned, and this is even more true for patients with neurological disorders. Plotting several phase plane trajectories on the same graph provides a compact way of displaying the variability in step responses at the same time that it clearly illustrates characteristic movement patterns.

Power spectral density functions were used for describing random tracking behavior. Power density spectra basically describe the statistical behavior of random functions in terms of the frequency domain. Error patterns were selected for analysis because they are concerned with the relations between the desired response and the actual response, and skilled motor behavior is more concerned with this relation than with the response pattern itself. Spectral densities were used because the

traditional measure, integrated absolute error (IAE), fails to account for the actual movement patterns present in the error signal. Two subjects may have identical IAE scores but completely different error patterns. In addition, power spectral densities are less sensitive to transient and infrequent lapses in tracking accuracy which are often the cause of large variability in IAE scores for the same subject.

The power spectral density functions were obtained by first computing an autocorrelation function and then Fourier transforming this to obtain the desired spectral representations. While the absolute levels of the spectra shown are arbitrary, the power spectra are not normalized, thus allowing comparisons between the power in db for any given subject and the power at the same frequency for any other subject.

RESULTS

While quantitative indices of tracking performance are useful in evaluating the effects of different types of therapy (e.g., Repa et al, 1971 and Walker et al, 1972), spatial-temporal response records and frequency distributions provide a more complete source of information on tracking performance. Such representations preserve the interesting movement characteristics and often provide a basis for hypotheses which further the understanding of motor performance. Furthermore, inspection of graphic records often provides the rationale for choosing among different possible quantitative indicants.

Phase Plane Diagrams: Figure 2 illustrates typical step response patterns for four subjects with widely varying neurological conditions. The initial starting point of the phase plane trajectory is at a position of 40 degrees and the desired end point is at 0 degrees. Each response pattern will be considered individually.

1. Young adult normal: The step response is rapid and precise and exhibits a single small overshoot.
2. Multiple sclerosis patient with moderate to severe intention tremor: Classical intention tremor which appears only during active movements is clearly demonstrated here. No tremor is present at rest or during the early part of the movement; but as the target is approached, oscillations appear and then persist for several seconds after the target region has been reached. The step response is somewhat violent, the tremor is coarse, and the patient has considerable difficulty in settling on the exact target position.
3. Parkinsonian patient with severe resting tremor: A classical form of resting tremor is shown in this response. The tremor becomes manifest at rest and ceases during voluntary movement. There is a characteristic delay of several seconds between the completion of the movement and the reappearance of tremor. The tremor begins with small amplitude oscillations and reaches its accustomed level within a few cycles.
4. Adult cerebral palsy patient with mild intention tremor and slight resting tremor: The step response is rapid and precise except for mild oscillations at the end of the movement. These oscillations settle down to a low amplitude tremor which remains at rest.

Figure 3 shows families of trajectories for four normal young adult subjects. These trajectories are for both right to left and left to right movements. The starting point for the right to left movement is +40 deg. and the target point is 0 deg., while for the left to right movement they are just the opposite. While there is considerable variability in peak velocities between subjects, intra-subject variability is low. A single, small overshoot is characteristic of most of the responses.

Families of trajectories for six multiple sclerosis patients are shown in Figure 4. The patients are listed according to a physician's subjective evaluation of their intention tremor, from slight to moderate-severe. It is important to note that this evaluation was made prior to the time the patients were tested with the tracking battery. The movement patterns vary from those that are only slightly different from normal to patterns that show coarse and violent oscillations about the target point.

The information contained in these plots can be transformed into quantitative measures. For example, in the parkinsonian study described in Repa et al, 1971, a movement time measure was used which was based on the time between the first large move away from zero in the velocity record and the return to zero. While movement time is a meaningful measure of step tracking performance for normals and parkinsonian patients, inspection of the phase plane diagrams for multiple sclerosis patients suggests that additional

measures are required to effectively describe this performance. The neurologist's evaluation of intention tremor is based on a subjective weighing of different aspects of the speed and accuracy of a movement toward a target, as in the classic finger-to-nose test. Movement time, decomposition, overshoots, and oscillations about the target all enter into his evaluation. Control engineers use a number of precise performance measures for judging the step responses of physical systems which are equally appropriate for quantifying movement disorders in a step tracking task. Time delay and rise time are two measures that are closely related to reaction time and movement time. More important measures, as far as intention tremor is concerned, are peak overshoot and settling time. Peak overshoot is the largest error between input and output during the transient state. On the phase plane diagram for the moderate-severe multiple sclerosis patient this corresponds to 19 degrees for a left to right movement and 15 degrees for a right to left movement. A typical female normal, Figure 3 (b), has a left to right peak overshoot of 2 degrees and a right to left peak overshoot of 8 degrees. Settling time is the time required for the response to decrease and stay within a specified percentage of its final value, typically 5%. For the multiple sclerosis patient shown in Figure 2, the settling time is 3.8 seconds while for the normal young adult in the same figure it is only 0.28 seconds. Inspection of the phase plane trajectories for multiple sclerosis patients strongly suggests that the neurologist is also influenced by these performance measures in making his rating and that these measures can provide a meaningful and objective characterization of patient performance.

Power Spectral Densities: Figure 5 shows error power spectra for four normal control subjects. Based on previously obtained IAE scores, these control subjects span the range of performance found for the normal groups. The shapes of the spectra are basically similar with no sharp peaks. The fact that the two older control subjects have the highest and lowest low frequency power levels is worth noting. The variability in performance for the group of 15 older normals was much greater than for the 20 young normals.

Figure 6 shows the error power spectra obtained from the same older normal on two separate occasions three weeks apart. There is good agreement between the two sets of measurements especially at higher frequencies. The group of older normals tended to improve their performance when retested, i.e., they reduced their power density levels, but the trends were not statistically significant based on IAE scores (see Repa et al, 1971).

The error power spectra for three patients with widely varying neurological disorders are shown in Figure 7. The multiple sclerosis patient had a slow, coarse intention tremor which did not result in any sharp peaks in the error spectrum. The slowly moving random target signal did not require limb movements sufficiently rapid to always suppress resting tremor in the parkinsonian patients. As a result, the power spectrum for the parkinsonian patient has a rather broad peak in the 3 to 4 hz range indicating that his resting

tremor appeared only intermittently during the tracking task. In contrast, the cerebral palsy patient had a very regular, small amplitude tremor throughout the random tracking trials. This resulted in a very decided peak at about 3.5 hz.

Figure 8 compares the power spectra for 2 multiple sclerosis patients with that of a normal young adult. The differences in the power density levels at the low frequency end of the spectra is striking. The patient with the previously diagnosed intention tremor of mild to moderate does show a slight peak at around 2 hz.

Figure 9 shows the power spectra for a parkinsonian patient taking part in a drug trial designed to compare the efficacy of L-DOPA + amantadine to that of L-DOPA + placebo. This particular patient had severe hypokinesia and a severe resting tremor which did not cease during the tracking task and which was not affected differentially by the two treatments. There is a slight overall improvement with the L-DOPA + amantadine treatment combination, however. This improvement is not caused by learning as amantadine was administered first. Of course, some measure of variability would be required to assess the significance of this difference.

Figure 10 compares two parkinsonian patients with an age-matched control subject. The patient with severe hypokinesia has a very rapid fall-off in error power density with frequency and very high power

density at the low end of the spectrum. This type of characteristic indicates that the patient made predominantly slow, smooth motions and very few quick, corrective movements. The other parkinsonian patient had a severe resting tremor which appeared intermittently during voluntary movement, thus producing small peaks around 2.5 and 3.5 hz.

Although only a small sample of all the patients and control subjects tested have been analyzed using power density spectra, there do appear to be particular spectral patterns which characterize different groups of individuals. Normal subjects have a flatter spectrum than the other groups indicating they used a combination of slow, smooth movements and quick, corrective ones. Parkinsonian patients with severe hypokinesia showed much less power at higher frequencies relative to lower frequencies than did the normal subjects. Patients with tremulous movements can be identified by the presence of peaks at discrete frequencies in the spectral records.

CONCLUSIONS

Phase plane diagrams and power spectral density functions provide a useful means of characterizing the tracking performance of patients with movement disorders. Both techniques offer a compact way of describing tracking behavior while still retaining the important features of the actual movement patterns involved. The phase plane method, in particular, appears to offer much promise for objectively evaluating intention tremor.

Comparisons of phase plane diagrams and the neurologist's ratings of 6 multiple sclerosis patients with varying degrees of intention tremor demonstrated that the phase plane characteristics are in close agreement with what the neurologist can see.

There are many opportunities for collaboration between systems engineers and medical investigators, but the barrier between engineers and physicians is a formidable one. Perhaps the main challenge is for the engineer to demonstrate the value of his techniques for use in medical research and actual medical practice. Medical investigators have learned that it is useful to study those parts of the brain that deal with movement as a complete system rather than as isolated components. There is a growing awareness that the functions that feedback control systems are designed to perform are in many respects analogous to those required by humans in many of their everyday tasks. The tracking apparatus serves as a useful framework for studying and describing man's sensory-motor abilities in terms of systems engineering concepts.

The state of the art in data analysis and display technology is such that phase plane diagrams and power spectral densities can be made available very quickly with a small digital computer interfaced with the tracking apparatus. The same digital computer could be interfaced with other basic sensory-motor tests and thus serve as the control center for an automated quantitative neurological examination. A provision for automatically recording patient histories could also be included. Such

a system would not replace the clinical neurologist by any means but only serve to free him from a large part of the routine aspects of the examination and supply him with more objective information on the patient's neurological condition. It is hoped that this paper will help to stimulate more widespread application of systems engineering advances to problems in the evaluation of neurological disorders.

REFERENCES

1. Herzog, J. H. (1968), Manual Control Using the Matched Manipulator Control Technique, Doctoral Dissertation, The University of Michigan, Ann Arbor, Michigan.

2. Potvin, A. R. (1971) The Effects of Age, Motivation, and Learning on Performance in the Quantitative Examination of Neurological Function, Doctoral Dissertation, The University of Michigan, Ann Arbor, Michigan.

3. Repa, B. S., Albers, J. W., Potvin, A. R., and Tourtellotte, W. W. (1971), "The use of a Battery of Tracking Tasks in the Quantitative Evaluation of Neurological Function," 7th Annual NASA-University Conference on Manual Control, Los Angeles, California.

4. Walker, J. E., Potvin, A. R., Tourtellotte, W. W., Albers, J., Repa, B., Henderson W., and Snyder, D. (1972), "Amantadine and L-DOPA in the Treatment of Parkinson's Disease", Clinical Pharmacology and Therapeutics, Jan-Feb.

A SUMMARY DESCRIPTION OF MULTIPLE SCLEROSIS AND PARKINSON'S DISEASE CHARACTERISTICS

Descriptor	Multiple Sclerosis	Parkinson's Disease
Symptons and Physical Signs	Euphoria, scotoma, nystagmus, paresis, slowness, spasms, intention tremor, dysproprioception, and disorders of gait, equilibrium, speech, and bladder	Easily confused, masking, bradykinesia, resting tremor, rigidity, cogwheeling, hypokinesia, and disorders of gait, equilibrium, and speech
Cause	Unknown - may be viral or auto-immune	Unknown
Lesions	Degeneration of myelin on nerve fibers scattered throughout the central nervous system	Decrease of dopamine, and degeneration of cells and myelin in the basal ganglia
Disease Onset	15 - 30 years old	35 - 60 years old
Disease Course	Varied and unpredictable with relapses and remissions and/or chronic disease progression	Slow disease progression
Life Expectancy	Almost normal	Normal
Treatments	Drugs (ACTH), surgical intervention, e.g., thalamotomy for relief of intention tremor, and physical therapy	Drugs (L-DOPA, Amantadine, anti-cholinergics, antihistamines), surgical intervention, e.g., thalamotomy for relief of resting remor, and physical therapy

(Modified from Potvin, 1971)

Table 1

This page is reproduced at the back of the report by a different reproduction method to provide better detail.

Figure 1. Tracking Apparatus Utilizing Large Position Control Stick and Over-Sized Display Screen

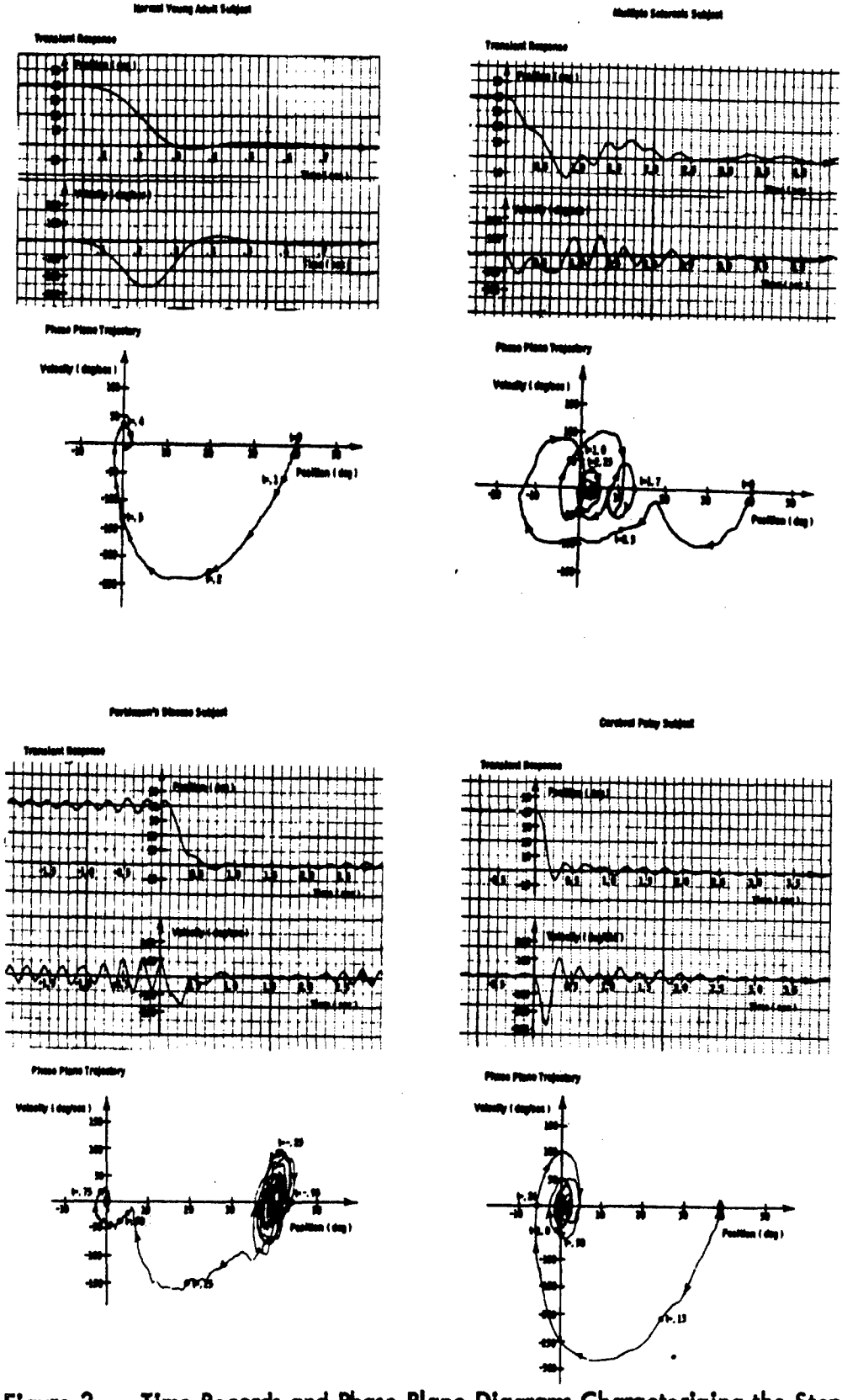

Figure 2. Time Records and Phase Plane Diagrams Characterizing the Step Tracking Performance of Representative Subjects

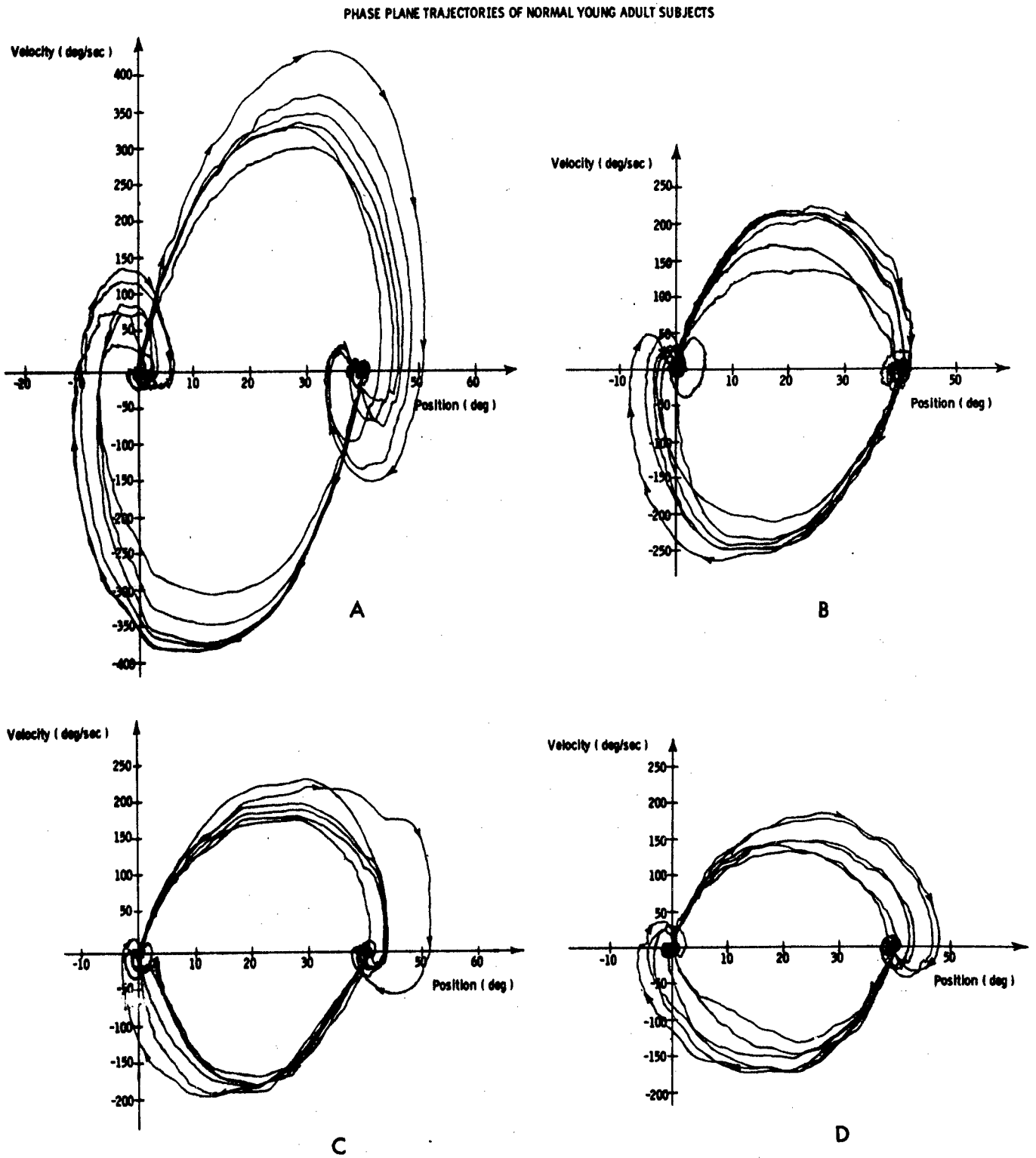

Figure 3. Phase Plane Trajectories of Normal Young Adults

PHASE PLANE TRAJECTORIES OF PATIENTS WITH MULTIPLE SCLEROSIS

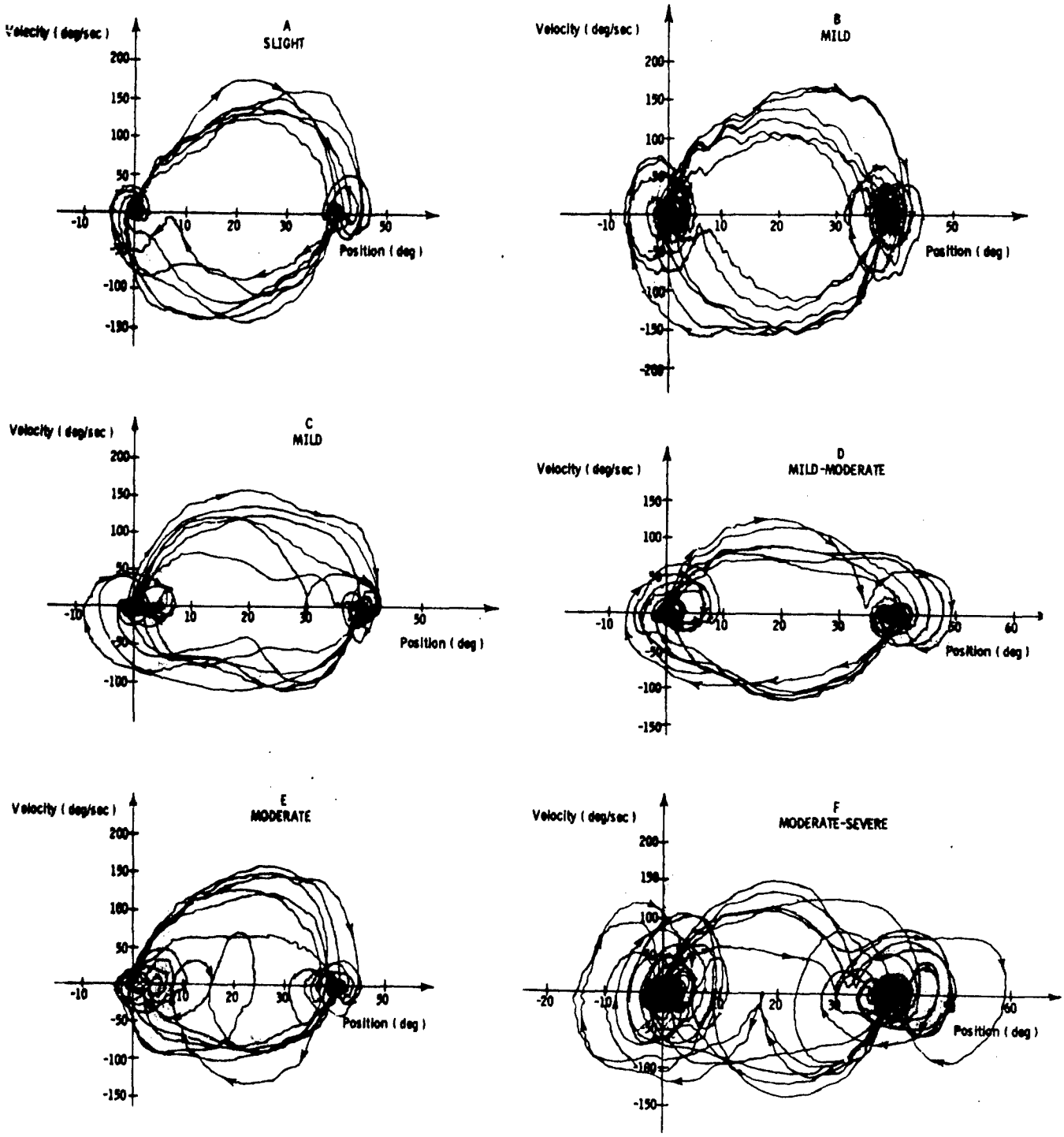

Figure 4. Phase Plane Trajectories of Multiple Sclerosis Patients

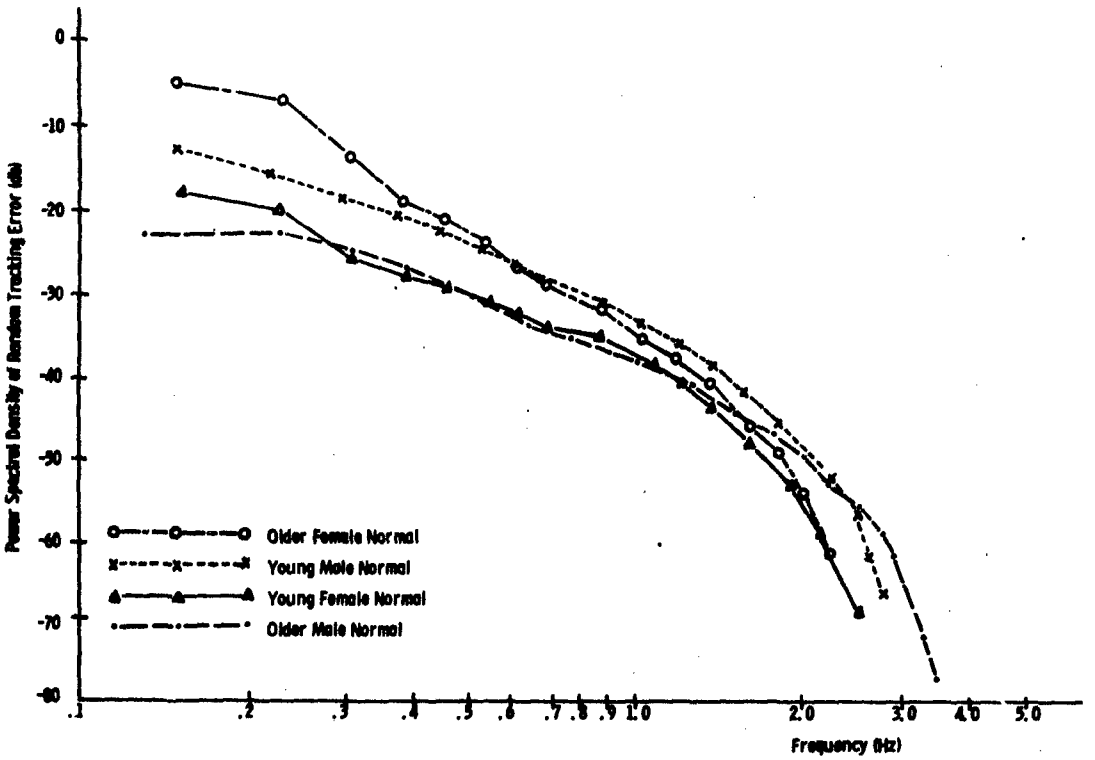

Figure 5. Error Power Spectra for Representative Normal Subjects

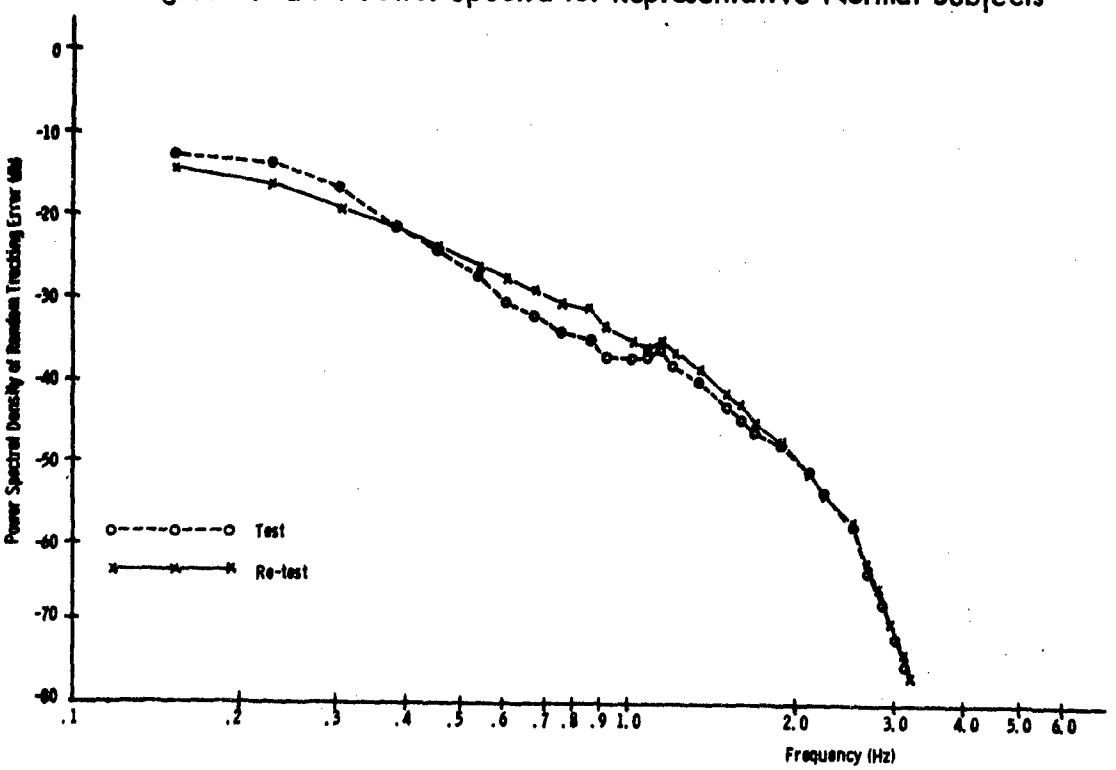

Figure 6. Error Power Spectra for a Normal Subject in a Test-Retest Study

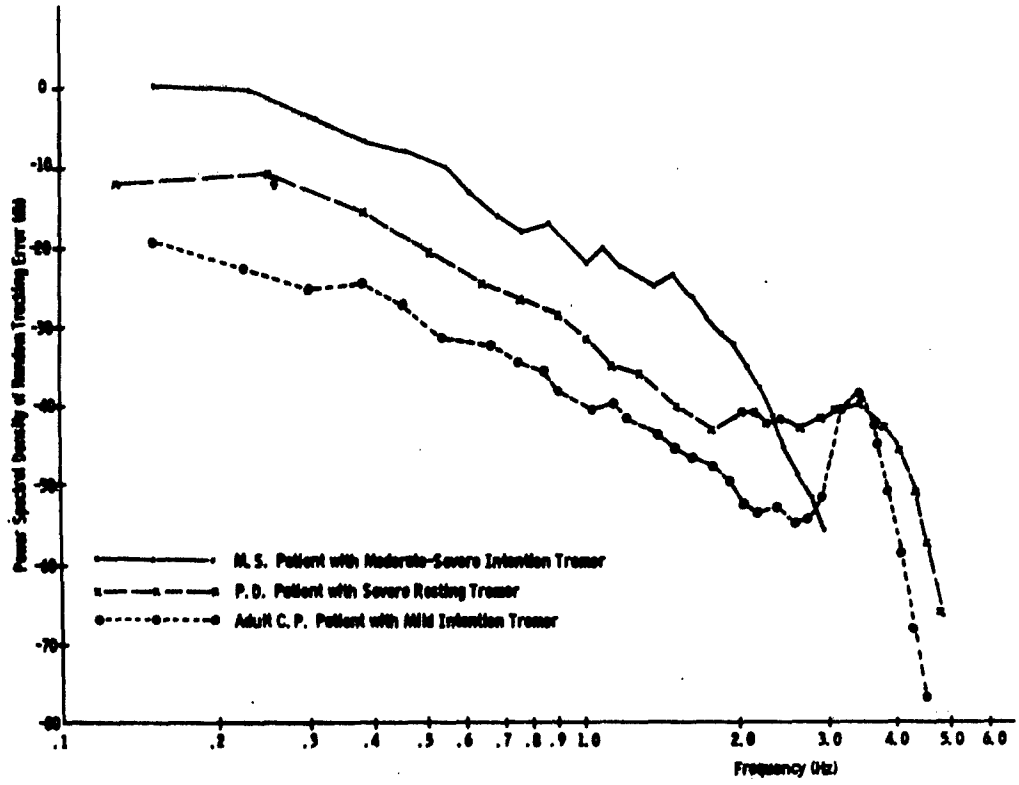

Figure 7. Error Power Spectra for Patients with Different Neurological Disorders

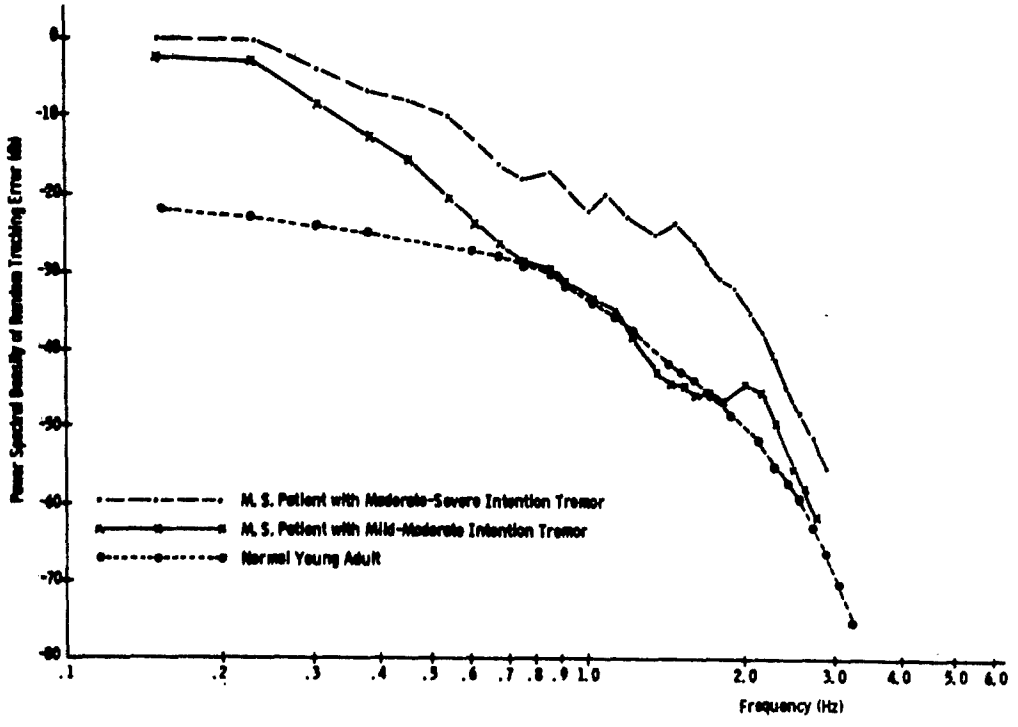

Figure 8. Error Power Spectra for 2 Multiple Sclerosis Patients Compared With a Normal Subject

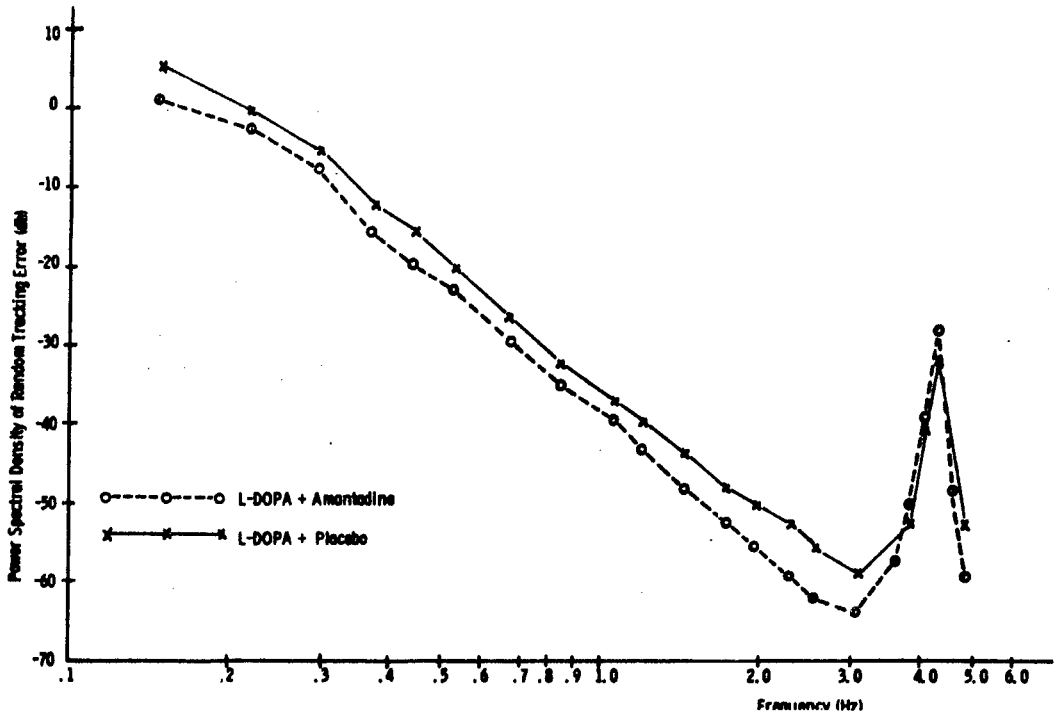

Figure 9. Error Power Spectra for a Parkinsonian Patient Participating in a Drug Trial

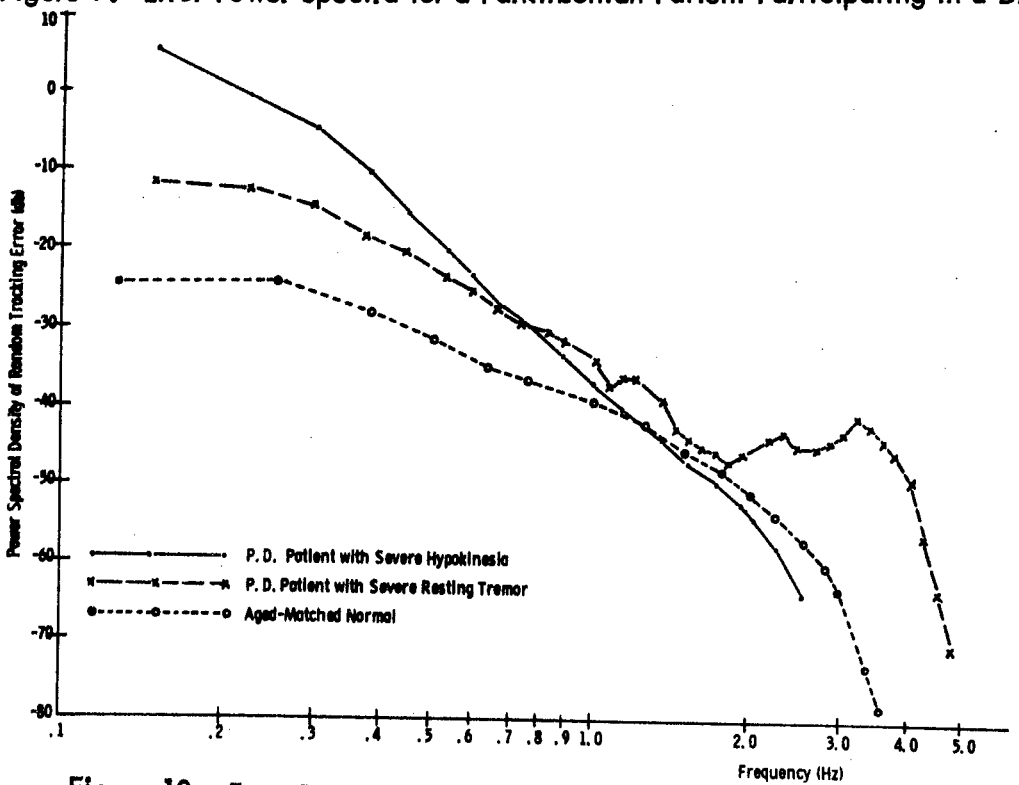

Figure 10. Error Power Spectra for 2 Parkinsonian Patients Compared With an Age-Matched Normal Subject

Abstract

Effects of d-Amphetamine on Quantitative Measures of Motor Performance*

J.W. Albers, Ph.D., B.S. Repa, Ph.D., E.F. Domino, M.D., A.R. Potvin, Ph.D., and W.W. Tourtellotte, M.D.,Ph.D.

It is well known that d-amphetamine in proper dosage and circumstance improves human performance on certain behavioral tasks[1,2], although there still is need for precise measures of the effects on motor performance. In this study, the effects of a standard oral dose of d-amphetamine and a placebo were determined using quantitative measures of motor performance in order to stimulate widespread use of such tests in assessing amphetamine-like drugs. It was hypothesized that such quantitative measures of motor performance would be an accurate means of determining the effects of small doses of d-amphetamine in normal subjects. The medication was administered to 6 volunteers in a random, double-blind crossover trial on 2 occasions 1 week apart. Each subject received 10 mg. of d-amphetamine one week and a placebo of similar appearance the other. Subjects were told that they might receive either active or inactive medication on one or both occasions. Each week the subjects completed the test battery to provide control data, received the medication, and 1 1/2 hours later repeated the test battery. The performance measures were an extension of the Clinical Quantitative Neurological Examination[3,4]. Included were measures of: Tremor, resting and sustention; Precision Hole Steadiness, static and dynamic; and Compensatory Tracking, constant force (supported and unsupported), random, and critical. Only 2 of 6 subjects reported an effect following the d-amphetamine trial and no effect following the placebo trial. The remaining subjects were unable to distinguish active drug from placebo. Paired t-tests were performed on the mean differences between placebo and d-amphetamine scores as well as on the mean differences between changes in scores following medication administistration. No significant differences were found between the effects of medications on resting tremor, sustention tremor, or precision hole steadiness. However, the constant force (unsupported) and critical tracking tasks were improved significantly with d-amphetamine. The constant force (supported) and random tracking tasks demonstrated trends favoring d-amphetamine, although the results were not significant. It appears that a 10 mg. dose of d-amphetamine does not significantly affect tremor or motor performance in tasks of short duration and minimal motor output. However, such a dose appears to significantly improve performance in more complex motor tasks requiring sustained subject attention. It is clear that d-amphetamine produces behavioral effects in relatively small dosage in normal nonfatigued subjects, and the use of sensitive, quantitative measures for recording the small changes in motor performance is justified. It should be noted that the urinary pH of all subjects was between 6 and 7 at the end of the experimental sessions, suggesting that the subject to subject variability in excretion due to differences in urinary pH was small.

Preceding page blank

1. Adler, H.F., Burckhardt, W.L., Ivy, A.C., and Atkinson, A.J.: Effect of various drugs on psychomotor performance at ground level and simulated altitudes of 18,000 feet in a low pressure chamber, Aviation Med. 21:221-236, 1950.
2. Weiss, B., and Laties V.G.: Enhancement of human performance by caffeine and the amphetamines, Pharmacol. Rev. 14: 1-36, 1962.
3. Tourtellotte, W.W., Haerer, A.F., Simpson, J.F., Kuzma, J. W., and Sikorski, J.: Quantitative clinical neurological testing. I. A study of a battery of tests designed to evaluate in part the neurological functions of patients with multiple sclerosis and its use in a therapeutic trial, Ann. N.Y. Acad. Sci. 122:480-505, 1965.
4. Repa, B.S., Albers, J.W., Potvin, A.R., and Tourtellotte, W.W.: The use of a battery of tracking tests in the quantitative evaluation of neurological function. Seventh Ann. NASA-University Conference on Manual Control, The Univ. of Southern Calif., Los Angeles, Calif., June 2 to 4, 1971.

*from the Michigan Neuropsychopharmacology Research Program, The Departments of Pharmacology and Neurology, and the Bioengineering Program, University of Michigan. For the complete report, see: Domino, E.F. et al., Clinical Pharmacology and Therapeutics, 13(2):251-257, 1972.

SESSION VIII

Improving and Evaluating Aircraft Handling qualities

PRELIMINARY SHORT PERIOD DESIGN CRITERIA THROUGH THE APPLICATION OF PILOT MODELING TECHNIQUE

By

E. P. Salmon
and
D. F. Kesler

Research and Technology Department
Northrop Corporation
Aircraft Division
Hawthorne, California

ABSTRACT

This paper discusses the development of short period handling quality criteria through pilot-in-the-loop analysis. An S plane map of performance and pilot compensation in a pitch attitude control task is presented. Open loop airplane and stability augmentation system design criteria are presented for short period characteristics in turbulence.

DISCUSSION OF THE PROBLEM

The ability of a pilot to control the pitch attitude of his aircraft is a fundamental consideration in longitudinal handling qualities criteria. The short period characteristics dominate pitch attitude response in conventional aircraft, and various criteria have evolved for acceptable short period frequency and damping. These criteria were evolved through detailed analysis of experimental data and are represented by the MIL 8785B boundaries and the CAL "thumbprint," Reference 9. However, the application of modern pilot modeling techniques can give greater insight into the use of short period design criteria for preliminary design.

Two distinct cases need to be considered for application of the pilot modeling technique: still air and turbulence. A review of the experimental results of References 1 and 2 will show that acceptable flying qualities in still air do not guarantee acceptability in turbulence. The aircraft described on page 28 of Reference 1 as BB2.3 is a classic example of this phenomenon, being very difficult in turbulence but receiving a pilot rating of 2 in still air. Hence, the pilot-models must be applied to pitch attitude control tasks representative of both still air and turbulence.

Evaluating the desirability of a particular set of short period dynamics requires relating the system to pilot acceptability. In this work, the authors have chosen to

Preceding page blank

present measures of best rms performance and required pilot compensation for this best performance. This allows for the broadest data base. The interested reader may wish to apply analytical pilot rating formulas of the type suggested in Reference 4. However, as will be shown, pilot rating information does not appear necessary for preliminary design consideration.

The problem under investigation can be readily summarized. Modern pilot modeling techniques are to be used to evaluate the acceptability of various short period characteristics in both still air and turbulence. Acceptability of various combinations of short period frequency and damping is to be related to pitch attitude performance of the pilot-vehicle system and the required pilot-model compensation.

PROBLEM MODEL

In order to reduce the problem to its simplest form, the pitch attitude response of the aircraft is assumed to be given by the conventional short period approximation, Reference 3. Hence, the analysis cannot exceed the limitations of this approximation.

The pilot-model form chosen for this study is representative of those used by Onstott, Anderson, Dillow and others, References 1, 2, 4, and 7. The model form is given by

$$K\,(T_L\,S+1)\,e^{-\tau S}$$

The selected time delay of .4 seconds and the allowable leads, $T_L \leq .45$ sec., are those found to be representative by Onstott.

The method of determining the required pilot compensation is again after that demonstrated by Onstott in his extensive experimental and analytical work. The pilot-model gain and lead were adjusted to minimize the rms error of the pilot-vehicle pitch attitude response. This method has been shown to give accurate predictions of rms performance, Reference 2. The lead compensation required in the model was taken to be a degrading term in evaluating the acceptability of the associated short period dynamics. However, unlike Anderson, Reference 4, no attempt was made to directly relate the lead to pilot workload. Higher values of lead were simply assumed to be associated with diminished acceptability.

The short period transfer function and pilot model were appropriately combined to give the required transfer functions: $\theta_e/\theta_{command}$ and θ/w_{gust}. These transfer functions were then premultiplied by appropriate filters so that a white noise input

would give the desired forcing function, i.e., tracking command or turbulence. This allowed use of the Phillips integral to calculate the rms θ response of the system and thus evaluate various short period characteristics.

STILL AIR ANALYSIS

The ability of the pilot-vehicle system to follow a random pitch attitude command in still air is described in the following paragraphs.

A block diagram of the tracking task without gusts is represented below:

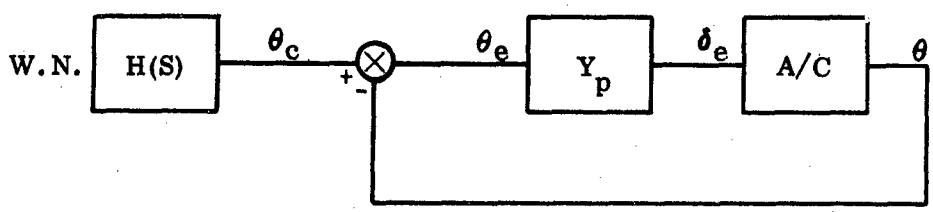

The θ/δ_e transfer function was represented by the two-degree-of-freedom short period approximation given below:

$$\frac{\theta}{\delta_e} = \frac{M_{\delta_e}(S - Z_w)}{S\left[S^2 - (U_o M_{\dot{w}} + Z_w + M_q)S + (M_q Z_w - U_o M_w)\right]}$$

It may be assumed that the poles of the transfer function can be located at will through use of an appropriate feedback control system. Hence, the θ/δ_e transfer function may be written in the general form below:

$$\frac{\theta}{\delta_e} = \frac{K(S - Z_w)}{S(S^2 + AS + B)}$$

The control system is not allowed to affect the zero, i.e., change the value of the effective Z_w. The Z_w selected for this study was $Z_w = -1.678$ which corresponds to the example aircraft of Reference 3.

The short period eigenvalues can then be specified by appropriate selection of the parameters A and B.

The pilot-model was the familiar gain-delay-lead, with the delay of .4 seconds

approximated by a second order Padé, as shown below:

$$K_p (T_L S + 1) \frac{.16S^2 - 2.45S + 12}{.16S^2 + 2.45S + 12}$$

Values of T_L of 0, .15, .3, and .45 were investigated. No restrictions were placed on K_p.

The tracking task was to follow a pseudo random band limited signal.

The filter used to specify a pitch command in still air in this study has been used in the past by other researchers, Reference 8. Its form is:

$$\frac{S^2}{S^4 + 1.772S^3 + .9422S^2 + .1393S + .006178}$$

Ideally, the filter would be adjusted to give an output with a power spectral density representative of the task to be studied whether it be air-to-air gun firing, dive bombing, landing approach, etc. Unfortunately, this kind of adjustment is not currently within the state-of-the-art. However, this preliminary work is intended to give only trends to aid in design. Hence, a filter with a relatively wide bandwidth was chosen. The interested reader may elect to do a systematic study of the effects of the filter break points on the outcome. However, the correlation of tracking command filter characteristics with a specific flying task is difficult and conclusions may be speculative. For these reasons, it is left for the reader to design a special purpose tracking filter if he feels one is necessary.

A computer program was written to select values of the augmented aircraft short period poles and compute rms tracking θ_e error. The pilot-model was optimized by varying K_p and T_L until the minimum tracking error was found.

The results are normalized and plotted on the S plane in Figures 1 and 2. Smaller numbers represent less error.

Figure 1 can be utilized as an aid in designing stability augmentation systems for the short period dynamics. Starting with the unaugmented dynamics, Figure 1 indicates that performance is likely to improve if damping is increased while the undamped short period natural frequency is held constant. Similarly, pilot compensation may be lessened by increasing the undamped natural frequency at constant damping. The area indicated as having acceptable short period characteristics is arbitrarily suggested as that region where "relatively large" changes in short period

dynamics produce a "relatively small" payoff in terms of improved performance or decreased pilot compensation. Hence, the suggested diminishing return boundary should not be taken as absolute, but rather as an aid in selecting compensation for a short period stability augmentation system.

Comparisons of the suggested boundary (the diminishing return boundary) developed by this study with the "CAL thumbprint" and MIL 8785B are given in Figure 2. Note that the suggested diminishing return boundary weighs the rate of change of performance explicitly while the others do not.

The limitations of the pilot-model are evidenced by the fact that higher aircraft ω_n's will give lower tracking error without bound. Thus care should be taken when very high aircraft natural frequencies are allowed.

TURBULENCE ANALYSIS

The development of short period criteria in the presence of turbulence is complicated by the fact that both the unaugmented and augmented airframe parameters affect the aircraft's response in gusts. This phenomenon can be seen by studying the open loop transfer function below. (The derivation of the transfer function is detailed in Reference 5.)

$$\frac{\theta}{w_g} = \frac{-M_w}{S^2 - (U_o M_{\dot{w}} + Z_w + M_q)S + (M_q Z_w - U_o M_w)}$$

If the short period frequency is changed through variation of M_w of the aircraft, the numerator of the transfer function will be affected as well as the denominator. All other parameters being held constant, a larger value of M_w will result in a greater pitching moment from any given gust. However, a device such as a common pitch rate damper will affect only the denominator. Thus, the gust response of two aircraft with the same short period characteristics will be vastly different if one utilized an augmentor and the other aerodynamic means to achieve the short period poles. Hence, the two cases of aerodynamic variation of short period characteristics and stability augmentation system variation must be discussed separately.

As in the still air case, the format of the θ/w_g transfer function can be represented by:

$$\frac{\theta}{w_g} = \frac{-M_w}{S^2 + AS + B}$$

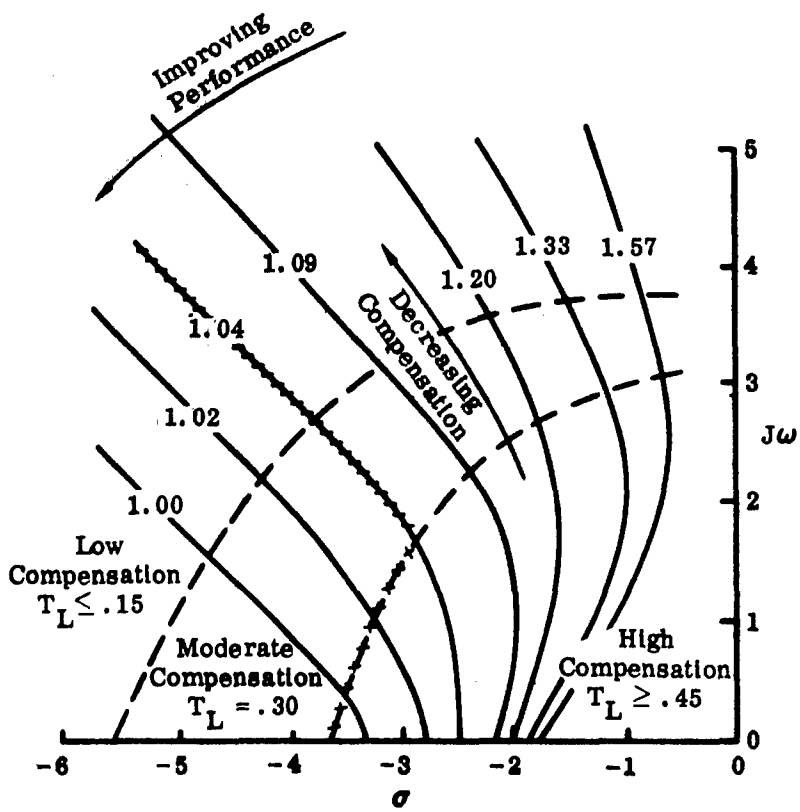

Figure 1. Normalized Tracking Performance and Pilot Comparison for Short Period Pole Locations

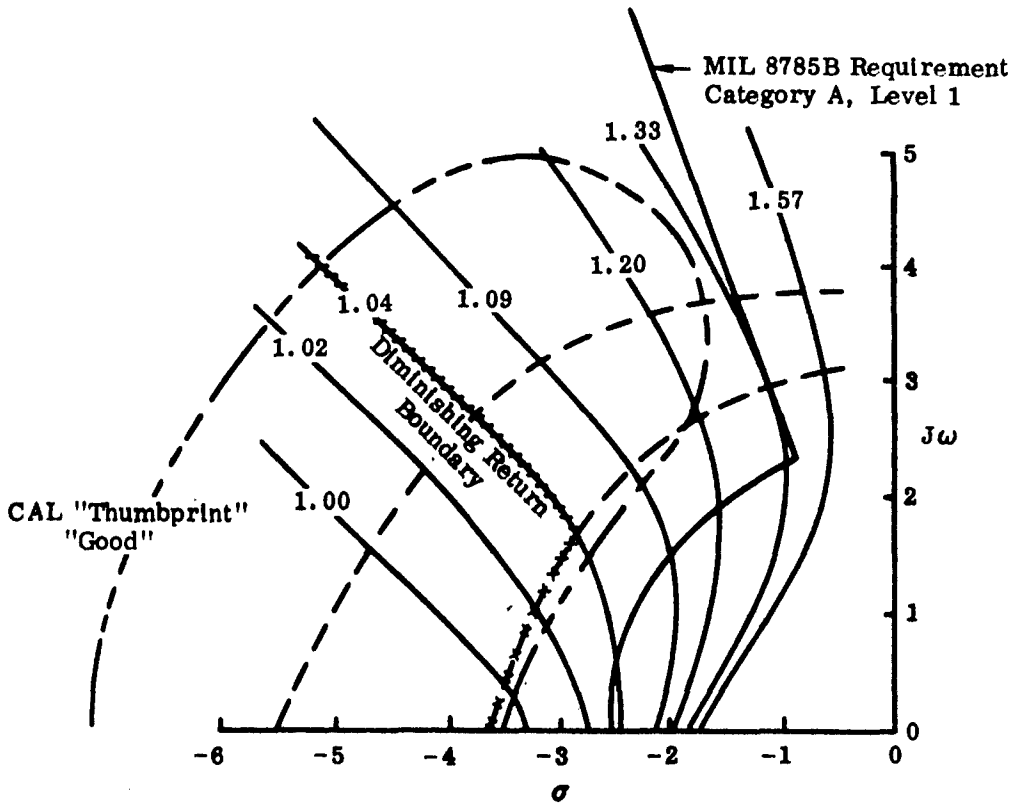

Figure 2. Comparative Boundaries

This allows A and B to be chosen arbitrarily to give the desired short period characteristics.

The gust sensitivity of the basic aircraft, i.e., with no pilot closure, can be obtained from the system description below:

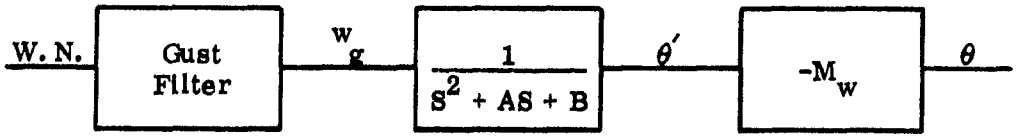

The pilot-model can be added to the above system through simple manipulation of the system blocks.

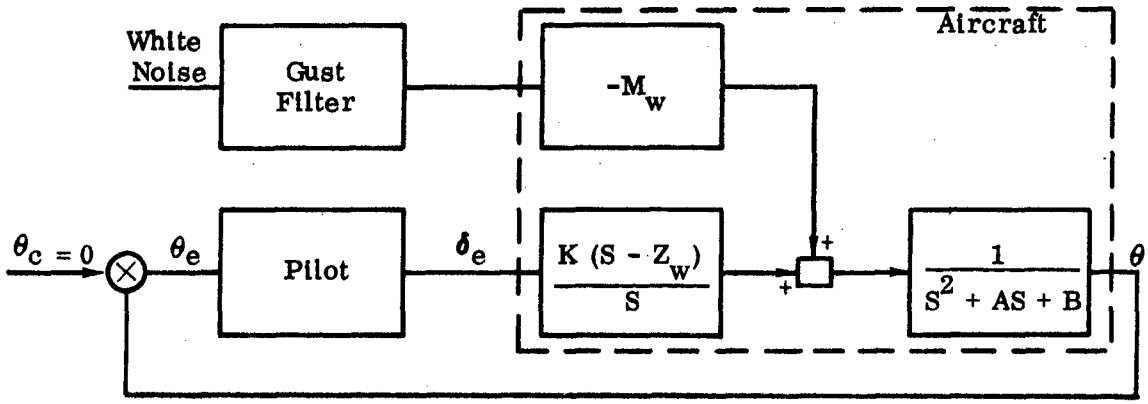

The turbulence filter chosen for this work is the Dryden form described in Reference 6. Since this filter is dependent upon aircraft speed and altitude, the generality of this analysis is constrained by the choice of a particular velocity and altitude. The specific filter used is given below:

$$\frac{w_g}{W.N.} = K \frac{6.518S + 1}{14.16S^2 + 7.526S + 1}$$

The generality of the analysis is further limited by the required selection of Z_w for the case of the pilot closure. The value used was $Z_w = -1.678$, which corresponds to the example aircraft of Reference 3.

A normalized theta error (θ^*) was computed as a function of short period pole location for both an optimized pilot and no pilot. The data were plotted on the S plane and lines of constant θ^* were drawn.

Use of the results of the analysis is straightforward. θ error for any airplane is obtained as follows:[1]

1. find the short period pole locations of the airplane,
2. find θ^* corresponding to the SP pole locations from Figures 3 and 4,
3. multiply θ^* by M_w and rms W gust,
4. the θ rms computed from Figure 3 is the airplane's response without a pilot and,
5. the θ rms computed from Figure 4 is the response with a pilot.

It should be noted that Figures 3 and 4 do not lend themselves to the ready development of design criteria such as the still air case. For the unpiloted airplane, reducing M_w to zero aerodynamically will result in no pitching moment due to turbulence, an obvious result. However, if the frequency of the aircraft is reduced through use of a control system, the same result cannot be obtained. Thus, to determine the performance change for a given change in short period characteristics, not only the poles must be considered, but also the method of obtaining them, i.e., aerodynamically or through feedback control. This difficulty is illustrated in the design example following.

EXAMPLE

Given a basic airplane, the goal is to achieve superior tracking performance in still air and in gusts. The task is to design a control system and specify the C. G. location to best satisfy the goal.

First consider the basic airplane at various C. G. 's. Compute the roots for the C. G. 's at the nominal flight conditions and find the tracking and gust performance.

Assume:

$M_w = +.00245$	$S = -1 \pm J1$	aft C. G.
$M_w = -.0147$	$S = -1 \pm J3$	mid C. G.
$M_w = -.0492$	$S = -1 \pm J5$	fwd C. G.

[1] To be very precise, the open loop (no pilot) results do not depend on Z_w and can represent any airplane. With the pilot closure, the results do depend on Z_w because the pilot closure is around the θ transfer function as shown in the block diagram. Since the range of values of Z_w is small and M_w is so dominant other airplanes cannot differ greatly from the trend.

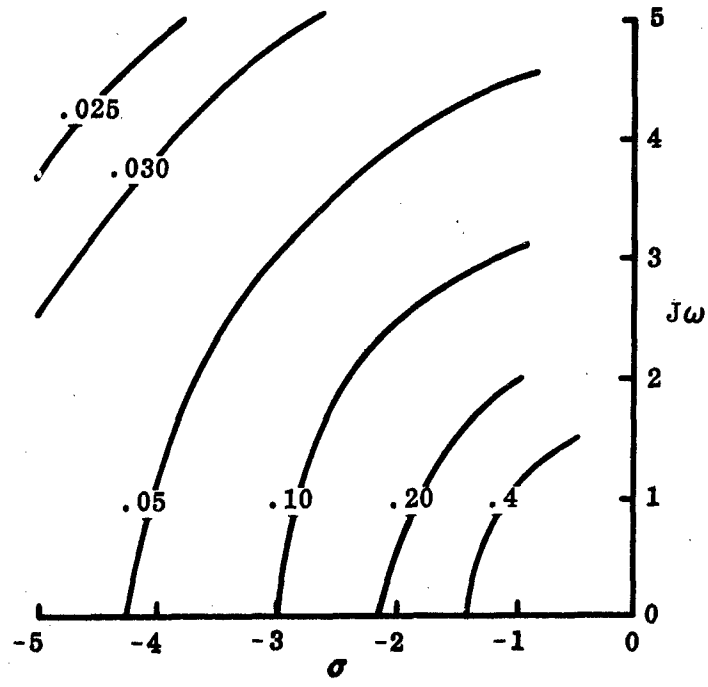

Figure 3. Normalized Theta Error (θ^*) Without Pilot

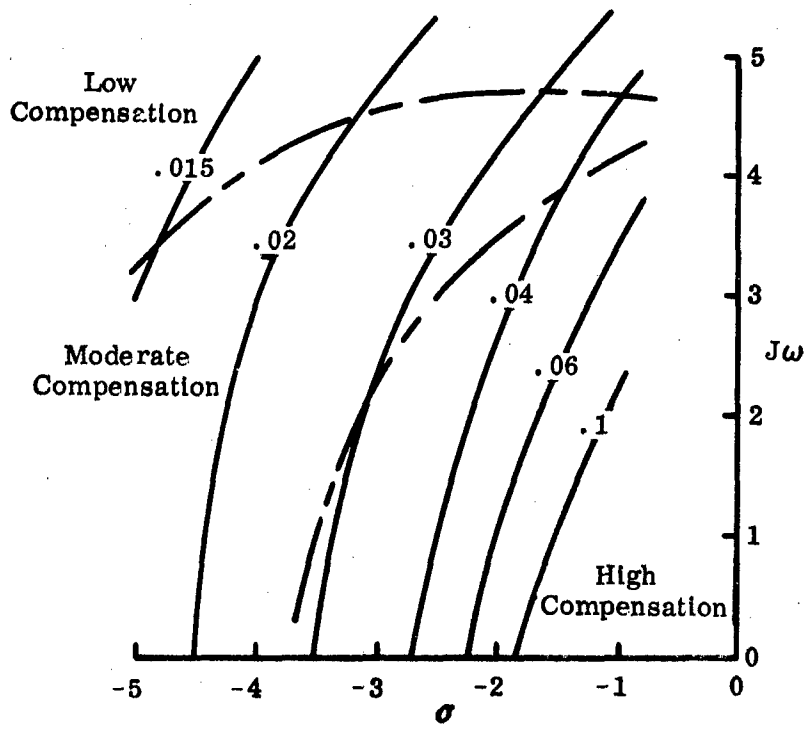

Figure 4. Normalized Theta Error (θ^*) with Pilot

From the tracking graph, the aft C.G. has a relative tracking performance of 1.57 and a high compensation. In a gust environment, θ^* without a pilot is .450 and with a pilot $\theta^* = .185$. θrms is obtained by multiplying θ^* by M_w.

$$\underset{\text{no pilot}}{\theta \text{rms}}/\text{f/s} = .450\ (.00245) = .0011 \text{ rad/f/s}$$

$$\underset{\text{pilot}}{\theta \text{rms}}/\text{f/s} = .185\ (.00245) = .000453 \text{ rad/f/s}$$

A table for all values is shown below:

	$\underset{\text{no pilot}}{\theta \text{rms}}/\text{f/s}$	$\underset{\text{pilot}}{\theta \text{rms}}/\text{f/s}$	Compensation	Normalized Tracking Error	Compensation
Fwd	.00203	.00181	L	1.6	L
Mid	.00155	.00112	H	1.34	M-H
Aft	.0011	.00045	H	1.57	H

Since the best performances occur at high compensation and the areas of low compensation have poor performance, a rate damper will be tried. A rate feedback is applied to the system and the roots are calculated. θ^* is found from the table and multiplied by M_w to find θrms/fps. Figure 5 gives the θrms/fps for the airplane with damper without a pilot and Figure 6 is the corresponding system with a pilot. Relative compensation is also shown. The performance numbers of these plots will vary slightly with various airplane designs because of the $M_q Z_w$ and $K_{\dot{\theta}} M_{\delta_e} Z_w$ contribution to the natural frequency. The compensation required will not vary, however.

Increasing the damping improves the performance, both the open loop and with the pilot. Tracking without gusts is improved greatly by damping. Required compensation is lessened by increases in ω.

We have reached a dilemma by requiring a high ω and damping for tracking performance and requiring a low ω and high damping for gust performance. A best compromise between tracking and gust performance and pilot workload might be to set the poles at $S = -4 \pm J1$.

If we were not satisfied with this performance we could use θ feedback to make the airplane "stiffer." The form of the transfer function now differs from the one

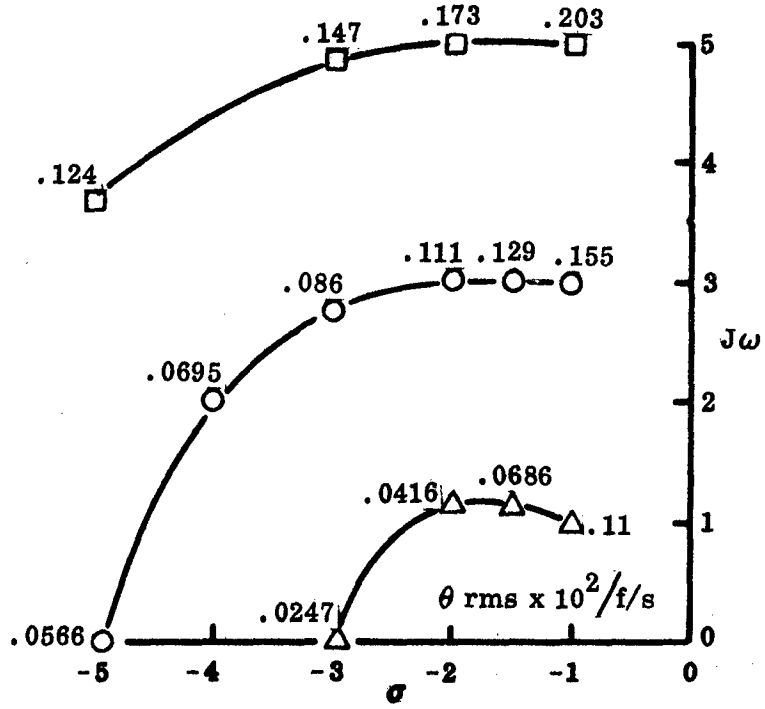

Figure 5. Example Airplane Rate Feedback Variations - No Pilot

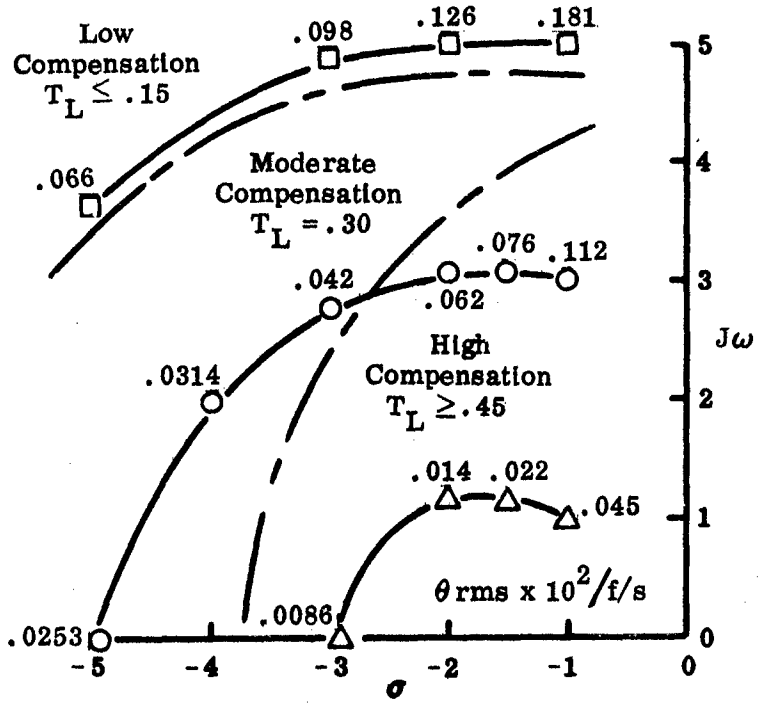

Figure 6. Example Airplane Rate Feedback Variations - with Pilot

used to develop Figures 1 through 4, and the validity must be checked.

The new gust sensitivity transfer function with rate and θ feedback becomes:

$$\frac{\theta}{\omega_{gust}} = \frac{M_w S}{S^3 + A_1 S^2 + B_1 S + C_1}$$

when factored and partitioned:

$$\frac{\theta}{\omega_{gust}} = \left[\frac{M_w}{S^2 + AS + B}\right]\left[\frac{S}{S + C}\right]$$

Thus, the performance figures will be in error by the effect of the lead lag.

The actual rms will be less than the figures predict by the amount the S/(S + C) filters the gust spectrum. Figures 1 through 4 give a conservative estimate of the performance with θ feedback. The applicability of the figures to other feedback compensations can be verified by checking the resultant transfer function with the one from which these results were computed.

If θ and $\dot{\theta}$ feedback is applied to the middle C. G. aircraft to give roots at S = -5 ± J2, the performance will be better than the values calculated below:

$$\theta_{\substack{\text{rms} \\ \text{no pilot}}}/\text{f/s} \leq .0147\ (.03272) = .000481$$

$$\theta_{\substack{\text{rms} \\ \text{pilot}}}/\text{f/s} \leq .0147\ (.01558) = .000229$$

If the same pole locations were achieved through rate damping and C. G. location, the rms error would have been approximately twice as much.

It is shown that various feedbacks are applicable to the method of determining the rms errors. Also, care must be taken to be sure that the transfer function form applies. Most feedbacks can be handled by an adjustment in the D. C. gain. For example $\dot{\theta}$ feedback results in a transfer function of the form

$$\frac{\theta}{W_g} \frac{M_w}{(1 + K_{\dot{\theta}} \cdot M_{\delta_e})S^2 + AS + B}$$

To obtain the proper form, the coefficient of the S^2 term must equal 1.

$$\frac{\theta}{W_g} = \frac{M_w}{S^2 + \frac{A}{1 + K_\theta \cdot M_{\delta_e}} + \frac{B}{1 + K_\theta \cdot M_{\delta_e}}} \left(\frac{1}{1 + K_\theta \cdot M_{\delta_e}} \right)$$

Thus the performance numbers in the figures must be multiplied by $\frac{1}{1 + K_\theta \cdot M_{\delta_e}}$.

SUMMARY

The application of simple pilot modeling techniques to the determination of acceptable short period characteristics can give great insight into preliminary design considerations. Correlation of still air trends with MIL 8785B requirements and the CAL "thumbprint" is excellent and the method also allows consideration of tradeoffs between performance and required pilot compensation. Use of the methodology in turbulence clearly shows the requirement for considering control system and aerodynamic variation of short period characteristics as separate entities. The simple analysis described in this paper can be expected to have a good payoff when used as a preliminary design tool.

REFERENCES

1. Onstott, E. D. and Salmon, E. P., "Airplane Flying Characteristics in Turbulence," AFFDL-TR-70-143, February 1971.
2. Onstott, E. D., Salmon, E. P., and McCormick, R. L., "Prediction and Evaluation of Flying Qualities in Turbulence," AFFDL-TR-71-162, February 1972.
3. "Dynamics of the Airframe," AE-61-4 II, September 1952.
4. Anderson, R.O., "A New Approach to the Specification and Evaluation of Flying Qualities," AFFDL-TR-69-120, June 1970.
5. Ashkenas, I. L. and McRuer, D. T., "Approximate Airframe Transfer Functions and Applications to Single Sensor Control Systems," WADC TR 58-62, June 1958.
6. "Military Specification - Flying Qualities of Piloted Airplanes," MIL-F-8785B (ASG), 7 August 1969.
7. Dillow, J. D., "The 'Paper Pilot' - A Digital Computer Program to Predict

Pilot Rating for the Hover Task," AFFDL-TR-70-40, March 1971.

8. Neal, T. P. and Smith, R. E., "An In-Flight Investigation to Develop Control System Design Criteria for Fighter Airplanes," AFFDL-TR-70-74, December 1970.

9. Chalk, C. R., "Additional Flight Evaluation of Various Longitudinal Handling Qualities in a Variable-Stability Jet Fighter," WADC TR 57-719, January 1958.

PILOT/VEHICLE CONTROL OPTIMIZATION USING AVERAGED OPERATIONAL MODE AND SUBSYSTEM RELATIVE PERFORMANCE INDEX SENSITIVITIES

by Gary G. Leininger,* Bruce Lehtinen,† and John P. Riehl‡

ABSTRACT

A method is presented for designing optimal feedback controllers for systems having subsystem sensitivity constraints. Such constraints reflect the presence of subsystem performance indices which are in conflict with the performance index of the overall system. The key to the approach is the use of relative performance index sensitivity (a measure of the deviation of a performance index from its optimum value). The weighted sum of subsystem and/or operational mode relative performance index sensitivies is defined as an overall performance index. A method is developed to handle linear systems with quadratic performance indices and either full or partial state feedback. The usefulness of this method is demonstrated by applying it to the design of a stability augmentation system (SAS) for a VTOL aircraft. A desirable VTOL SAS design is one that produces good VTOL transient response both with and without active pilot control. The system designed using the method introduced in this paper is shown to effect a satisfactory compromise solution to this problem.

---

*Assistant Professor, Department of Electrical Engineering, University of Toledo, Toledo, Ohio.

†Aerospace Engineer, Spacecraft Technology Division, NASA Lewis Research Center, Cleveland, Ohio.

‡Mathematician, Instrument and Computing Division, NASA Lewis Research Center, Cleveland, Ohio.

1.0 INTRODUCTION

The study of complex systems often involves an investigation into the interconnection of many subsystems and the influence each subsystem has in achieving a prespecified design objective. The optimization of the composite system with respect to a set of adjustable parameters relies upon a knowledge and understanding of the interconnecting structure. Individual subsystem optimization without concern for its cause and effect relation to the composite system may yield an overall system response which deviates substantially from the design specifications. Conversely, a composite system design satisfying the required design objectives might dictate a need for increasingly sophisticated and expensive subsystems. It is, therefore, in the interests of the system designer to have the practical and analytical flexibility to properly aline the priorities of competitive subsystems with composite system objectives. A system typifying this design analysis is a pilot/vehicle system.

In the process of designing and evaluating the suitability of a pilot/vehicle system, it is necessary to solicit the pilot's comments and opinion of the handling qualities as one facet of the design. This subjective opinion forms an integral part of the ultimate evaluation of the vehicle and is therefore considered seriously and continuously throughout the design. Optimal performance of the aircraft including the pilot may be in direct conflict with the optimal performance and efficiency of the aircraft when the aircraft is treated as a separate entity. In this respect many studies have been conducted with the objective of mathematically modeling pilot-control characteristics (refs. 1 to 3) and from a practical engineering viewpoint, the development of the quasi-linear model for human pilot dynamics have been one of the beneficial results of these studies (ref. 1). These pilot models can then be used in conjunction with airframe dynamic models in the design of aircraft control systems.

Composite system design can best be achieved when the design criterion includes the evaluations, requirements, and limitations of each individual subsystem. To accomplish this, a generalized theory and design technique is presented. The theory evolves from the concepts and conditions imposed by optimal control theory supplemented by subsystem sensitivity characteristics.

The objective of optimal control theory is to determine the control signals that will cause a process to satisfy the physical constraints and at the same time minimize some performance criterion. In the case of feedback control, the parameters to be optimized are the feedback gains. Once the optimization has been completed, it is natural to inquire into the relative effect of the system response and/or the performance measure to a deviation of the feedback gains from their optimal values. This area of concern is often referred to as "sensitivity."

The design and evaluation of dynamic control systems through the utilization of sensitivity functions has been the subject of intensive research during the past decade. Many different definitions of sensitivity have evolved and system stability, controllability, and other system characteristics have been directly related to these sensitivity functions.

Many analysis, synthesis and optimization techniques used in control theory utilize the sensitivity functions of the state of the system with respect to the system parameters (refs. 4 and 5). These parameter sensitivity functions are often generated by sensitivity models of the system. However, the use of presently available techniques for generating sensitivity functions for linear system containing many parameters results in the simulation of high order dynamic systems. Similarly, control sensitivity (ref. 6), trajectory sensitivity (refs. 4 and 7), eigenvalue sensitivity (ref. 8) and output sensitivity with respect to pole location (ref. 9) all require a simultaneous solution of high order dynamic sensitivity expressions. These sensitivity methods, however, are only intended to account for very small perturbations

from some nominal (or optimal) position. For this reason, most of the above sensitivity functions are not compatible with on-line design, but are primarily used to evaluate the final design. Papers by Cadzow (ref. 10), Dougherty, et al. (ref. 11) and others have applied performance index sensitivity methods to the problem of determining feedback control laws when system parameters are subject to small variations. For larger variations, authors such as Whitbeck (ref. 12), Zadicario and Sivan (ref. 13), and Tuel (ref. 14) have discussed methods for designing controllers which minimize the expected value of the cost functional. All of these techniques are addressed to the plant parameter variation problem as well as a single scalar performance measure.

The emphasis in this paper is directed toward developing a method for designing a practical feedback controller for multivariable linear systems which may be stabilized by output feedback over the entire range of feedback parameters. The distinguishing feature of the proposed technique is the generation of a constant feedback control law subject to the minimization of the performance index sensitivity functions of the composite system and the individual subsystems. This is accomplished by defining a performance index consisting of the sum of relative sensitivity terms of each subsystem multiplied by scalar weighting factors.

Relative sensitivity is a measure of the deviation between the actual value of the performance index and that which would be obtained if the control were optimal, i. e.,

$$S^R(K) = \frac{J(K) - J(K^O)}{J(K^O)} \tag{1.1}$$

where K^O is the optimal set of feedback parameters

$$J(K^O) = \min_{K^O} J(K) \tag{1.2}$$

Note that the relative sensitivity is always positive, and thus system performance is always compared with an attainable value.

The performance index of concern here is chosen to be of the form

$$\tilde{J}(K) = \sum_{i=1}^{N} \lambda_i S_i^R(K) \tag{1.3}$$

$$\sum_{i=1}^{N} \lambda_i = 1 \tag{1.4}$$

where N is the number of subsystems, $S_i^R(K)$ is the relative sensitivity of the i^{th} system, and λ_i is a weighting factor (or probability factor) associated with the i^{th} subsystem. The performance index of equation (1.3) reflects the interest and concerns of the individual subsystems in the overall decision process. Clearly, small relative sensitivity assures a design close to the optimum and, hence, a smaller influence in the final optimization procedure. Furthermore, the performance measure $J_i(K)$ associated with subsystem i ($i = 1, 2, \ldots, N$) need not be of the same form, i.e., quadratic, absolute value, uniform, etc. This, therefore, greatly enhances the design capabilities for large scale systems with subsystem design limitations.

The merit of the performance index of equations (1.3) and (1.4) in the design of practical engineering systems is considered in the next section. Here we restrict the discussion to linear systems with quadratic performance criteria. This restriction enables the designer to utilize the well-developed theory of the optimal linear regulator in establishing the sensitivity terms needed in equation (1.3). The section is then concluded with an example demonstrating the effectiveness of the technique as a useful design tool.

2.0 SENSITIVITY DESIGN FOR OPTIMAL LINEAR REGULATORS

This investigation is concerned with the design of a feedback control law for a time invariant linear system subject to the minimization of a prespecified scalar performance index. The performance index is chosen in such a manner as to include sensitivity terms associated with subsystems comprising the composite system. Initial consideration is given to the optimization of an individual subsystem with respect to a selected array of feedback parameters. The method is then extended to include several subsystems in the overall optimization procedure using sensitivity concepts derived for the individual subsystem.

Subsystem Optimization

Consider a subsystem whose dynamic performance is characterized by a set of n first order linear time invariant differential equations.

$$\dot{x}(t) = Ax(t) + Bu(t) \tag{2.1}$$

where $x(t)$ is the n dimensional state vector, $u(t)$ is a vector consisting of m control inputs, and A and B are nxn and nxm constant matrices describing the system dynamics. The feedback control law

$$u(t) = -Lx(t) \tag{2.2}$$

will be optimal if the feedback gain matrix L is chosen so as to minimize a performance index which is quadratic in the state and control variables

$$J(x, u) = \frac{1}{2}\int_0^\infty \left\{x^T(t)Qx(t) + u^T(t)Ru(t)\right\} dt \qquad (2.3)$$

where weighting matrix Q is positive semidefinite and weighting matrix R is positive definite. The minimization of equation (2.3) will yield a set of constant feedback gains of the form

$$L^* = R^{-1}B^TP^* \qquad (2.4)$$

where P^* is a positive definite matrix which is the solution of the steady-state Riccati equation

$$0 = A^TP^* + P^*A + Q - P^*BR^{-1}B^TP^* \qquad (2.5)$$

Combining equations (2.4) and (2.5), one obtains

$$0 = (A - BL^*)^TP^* + P^*(A - BL^*) + Q + L^{*T}RL^* \qquad (2.6)$$

which is the well-known Lyapunov equation. The resulting value of the performance index when the feedback gain matrix equation (2.4) is substituted into equation (2.2) is

$$J^* = \frac{1}{2}x_o^TP^*x_o \qquad (2.7)$$

The evaluation of P^* from equation (2.5) requires the solution of $n(n + 1)/2$ nonlinear simultaneous equations. Alternatively, one could use equations (2.6) and (2.7) in conjunction with a gradient minimization algorithm. For a nonoptimal set of feedback gains L, equation (2.6) becomes

$$0 = (A - BL)^TP + P(A - BL) + Q + L^TRL \qquad (2.8)$$

Here A, B, Q, R, and L are known and the nxn symmetric matrix P can be easily obtained using any of the well-known Lyapunov solving algorithms (refs. 16 and 19). The performance index is evaluated using

$$J = \frac{1}{2} x_o^T P x_o \tag{2.9}$$

and can be minimized by adjusting the elements of the gain matrix using a gradient minimization algorithm yielding L^* and P^*.

In most practical situations, the initial state of the system is unknown and must be treated as a random vector. Taking the expected value of equation (2.9) yields

$$E\{J\} = \hat{J} = \sum_{i=1}^{n} \gamma_{ii} p_{ii} \tag{2.10}$$

where p_{ii} are the diagonal elements of the P matrix and γ_{ii} is the covariance of the i^{th} component of the initial state vector with the additional assumption that

$$\gamma_{ij} = E\{x_i(0) x_j(0)\} = 0 \tag{2.11}$$

Note that the minimization of equation (2.10) subject to equation (2.8) will yield an "averaged" set of feedback gains independent of the statistics of the initial state random vector.

The above analysis assumes that the feedback control law u(t) is a linear combination of all the elements of the state vector. In the event that only a select number of the state variables will comprise the feedback control law, equation (2.8) must be modified. Let the p dimensional vector

$$y(t) = Cx(t) \tag{2.12}$$

represent the state variables to be fed back. For a control law of the form

$$u(t) = -Ky(t) = -KCx(t) \tag{2.13}$$

equation (2.8) becomes

$$0 = (A - BKC)^T P + P(A - BKC) + Q + C^T K^T RKC \tag{2.14}$$

The minimization of equation (2.10) subject to equation (2.14) proceeds as above with the additional restriction that the closed loop system (A - BKC) be stable. This latter restriction is, of course, in effect in the full state feedback system; however, it is well known that the optimal linear state regulator is always stable independent of the open loop dynamics. Clearly, this is not true, in general, for the partial state feedback system and thus one must be cognizant of the location of the closed loop poles, since any solution to equation (2.4) yielding an unstable closed loop system is meaningless.

Relations similar to those of equations (2.8) and (2.14) have been obtained by Kleinman (ref. 17) and Levine (ref. 18), respectively. However, their results are predicated upon the existence of the first partial derivative of equation (2.10) with respect to the unknown feedback gain matrix. Setting this derivative to zero provides the relations upon which their derivation and subsequent results ultimately rely. Consequently, if the feedback gains are constrained in any manner, then $\partial\hat{J}/\partial L \neq 0$ or $\partial\hat{J}/\partial K \neq 0$ at the optimum and the results of (ref. 17) and (ref. 18) no longer apply. However, the constraint boundaries can be incorporated into the gradient algorithm described above and thus minimization of equation (2.10) with respect to the constrained gains can be achieved. The stabilization of (A - BL) for full state feedback and (A - BKC) for partial state feedback is an additional restriction placed upon the feedback gains.

Up to this point a technique has been presented for the optimization of a single subsystem with respect to a set of feedback gains comprising a feedback control law. The method was shown applicable to systems with full state feedback, partial state feedback and both full and partial state feedback with gain constraints. The method will now be extended to include several subsystems with conflicting objectives.

Consider a composite system $\mathcal{S}_0$ which contains a definable subsystem of interest $\mathcal{S}_2$. Two quadratic performance indices, $\hat{J}_0$ and $\hat{J}_2$, are defined for $\mathcal{S}_0$ and $\mathcal{S}_2$, respectively. Each index has been suitably averaged over the initial conditions (as was done in eq. (2.10)). For ease of discussion, assume the system is structured as follows (see figs. 1 and 2).

System $\mathcal{S}_0$

$$\left.\begin{aligned}
\dot{x} = \begin{pmatrix} \dot{x}_1 \\ \dot{x}_2 \end{pmatrix} &= \left[\begin{array}{c|c} A_{11} & A_{12} \\ \hline 0 & A_{22} \end{array}\right] \begin{pmatrix} x_1 \\ x_2 \end{pmatrix} + \left[\begin{array}{c|c} 0 & 0 \\ \hline B_1 & B_2 \end{array}\right] \begin{pmatrix} u_1 \\ u_2 \end{pmatrix} \\
\begin{pmatrix} y_1 \\ y_2 \end{pmatrix} &= \left[\begin{array}{c|c} C_1 & 0 \\ \hline 0 & C_2 \end{array}\right] \begin{pmatrix} x_1 \\ x_2 \end{pmatrix} \\
\begin{pmatrix} u_1 \\ u_2 \end{pmatrix} &= \left[\begin{array}{c|c} -K_1 & 0 \\ \hline 0 & -K_2 \end{array}\right] \begin{pmatrix} y_1 \\ y_2 \end{pmatrix} \\
&\min_{K_1, K_2} \hat{J}_0(x_2, u_1, u_2) \triangleq \hat{J}_0^*
\end{aligned}\right\} \quad (2.15)$$

Subsystem $\mathcal{S}_2$ (System $\mathcal{S}_0$ with $C_1 = 0$)

$$\left.\begin{aligned} \dot{x}_2 &= A_{22}x_2 + B_2u_2 \\ y_2 &= C_2x_2 \\ u_2 &= -K_2y_2 \\ \min_{K_2} \hat{J}_2(x_2, u_2) &\triangleq \hat{J}_2^* \end{aligned}\right\} \qquad (2.16)$$

Note that both $\hat{J}_0$ and $\hat{J}_2$ are functions of subsystem states (x_2) only. Let K_1^0 and K_2^0 be the values of K_1 and K_2 that minimize $\hat{J}_0$, and let K_2^2 be the value of K_2 that minimizes $\hat{J}_2$. In most physical situations $K_2^0 \neq K_2^2$. This fact reflects a degradation in the performance of subsystem $\mathcal{S}_2$ when the gains K_2^0 that optimize system $\mathcal{S}_0$ are used. This degradation can be measured using relative sensitivity, i. e.,

$$S_2^R(K) = \frac{\hat{J}_2 - \hat{J}_2^*}{\hat{J}_2^*} \qquad (2.17)$$

where $\hat{J}_2^*$ is the value of the performance index for subsystem $\mathcal{S}_2$ when the feedback gains K_2^2 are employed. A similar expression for the relative sensitivity of $\hat{J}_0$ is

$$S_0^R(K) = \frac{\hat{J}_0 - \hat{J}_0^*}{\hat{J}_0^*} \qquad (2.18)$$

where $\hat{J}_0^*$ is the value of $\hat{J}_0$ at K_1^0, K_2^0. Clearly, $S_2^R = 0$ if $K_2 = K_2^2$, and $S_0^R = 0$ if $K_1 = K_1^0$ and $K_2 = K_2^0$. Consequently, a composite performance index can be defined which incorporates equations (2. 17) and (2. 18).

$$\hat{J}_3 = \lambda S_2^R(K) + (1 - \lambda) S_0^R(K) \tag{2.19}$$

where λ is a weighting (or probability) factor $0 \leq \lambda \leq 1$. For $\lambda = 0$, the minimization of equation (2. 18) will yield the gains K_1^0 and K_2^0, while for $\lambda = 1$ the gains K_2^2 will result and K_1 will have no effect in the minimization. Thus, for λ in the range of zero to one the minimization of equation (2. 18) will result in a tradeoff between the design objectives of subsystem $\mathcal{S}_2$ and system $\mathcal{S}_0$. The appropriate value of λ will depend entirely upon the physical, as well as design, requirements of both the individual subsystem and the composite system.

To generalize the above technique, consider a composite system $\mathcal{S}_0$, and N definable subsystems $\mathcal{S}_i$, i = 1, 2, . . ., N, which may be coupled either through state or through control. For each subsystem, define a relative sensitivity of the form

$$S_i^R(K) = \frac{\hat{J}_i - \hat{J}_i^*}{\hat{J}_i^*} \tag{2.20}$$

where $\hat{J}_i^*$ is the value of the performance index when (sub)system i is optimized independent of the rest of the system. The relative performance index can then be formulated as a linear combination of the subsystem sensitivity functions

$$\hat{J} = \sum_{i=0}^{N} \lambda_i S_i^R(K) \tag{2.21}$$

$$\sum_{i=0}^{N} \lambda_i = 1 \qquad (2.22)$$

where λ_i is the weighting factor associated with the i^{th} (sub)system. The minimization of equation (2.21) will yield a set of feedback gains for the composite system which will provide satisfactory overall performance, while maintaining subsystem response within the design (and economic) specifications. To demonstrate the effectiveness of the proposed technique as a suitable design tool, as well as to illustrate the approach, an example is now presented.

3.0 EXAMPLE

Consider the problem of designing the stability augmentation system (SAS) for a turbojet/lift fan powered VTOL aircraft. Figure 3 is the block diagram for a linearized pitch axis model of a typical VTOL being controlled by a pilot in the hover mode. The states considered in the VTOL model are pitch angle, pitch rate, and acceleration produced by the moment generated by the lift fans. To be designed are SAS gains K_θ, $K_{\dot{\theta}}$, and $K_{\ddot{\theta}}$ such that pitch angle θ is kept close to zero using reasonable amounts of control, u. The complete system is similar in form to the one depicted in figure 2, where the VTOL pitch dynamics comprise the primary subsystem of interest. In this example, C_1 reflects the fact that only one pilot state (δ) is measurable; and for simplicity, the gain K_δ associated with this state was fixed.

Pilot dynamics are described by the third order model shown in the diagram (ref. 20). Pilot parameters are pilot gain K_p, lead time constant τ_L, muscle lag τ_M, sensor lag τ_S, and pilot dead time τ_D (as a Pade approximation). Aircraft handling qualitites studies have shown that if the parameters the pilot adaptively adjusts (K_p and τ_L) are not too large, the pilot will give the aircraft a high rating. For

this example, K_p was fixed at 13.5 cm/rad and τ_L was fixed at 0.5 sec. These are relatively low values; hence the resulting design should get a good pilot rating. Fixed pilot parameters were assumed to be $\tau_S = 0.062$ sec, $\tau_M = 0.36$ sec, and $\tau_D = 0.35$ sec. As indicated previously, stick sensitivity K_δ was not optimized, but was chosen to be 0.6 rad/sec^2/in., based on typical pilot preferences.

The VTOL dynamic model includes parameter τ_1 which represents the lag between stick deflection and pitching moment produced by the engine/lift fan combination. τ_1 was assumed to be 0.3 second in this study, since experience has shown that pilot may have difficulty in controlling the system is the actuation lag is greater than this amount. Conversely, it is desirable, as far as lift fan/engine design is concerned, to have τ_1 as large as possible.

The VTOL can be operated in either of three modes: (1) pilot-in-the-loop (PIL) where both pilot and SAS contribute to stabilization ($K_p \neq 0$), and (2) pilot-out-of-the-loop (POL) where $K_p = 0$ and all stabilization derives from the SAS, and (3) SAS-failed mode, where the pilot provides all stabilization. Because of these three modes of possible operation, a conflict arises in designing the SAS and stick sensitivity K_δ. It was decided that K_δ would not be optimized in this study, hence, the SAS-failed mode has been ignored. For the PIL and POL modes, SAS optimized for the POL mode may produce a system too insensitive to the pilot's control during PIL mode operation. On the other hand, a SAS which is designed to be optimal when the pilot is in the loop may not sufficiently stabilize the aircraft in the fixed-stick (POL) mode. For this example, the problem of conflicting performance objectives was solved by using a composite performance index

$$\hat{J}_3 = \lambda\left(\frac{\hat{J}_2 - \hat{J}_2^*}{\hat{J}_2^*}\right) + (1 - \lambda)\left(\frac{\hat{J}_0 - \hat{J}_0^*}{\hat{J}_0^*}\right) \qquad (3.1)$$

Here, $\hat{J}_2$ is an index of performance for POL operation, $\hat{J}_0$ corresponds to PIL operation, and λ is a weighting factor. Lambda could

be, for example, the probability of the aircraft being flown in the POL mode. The starred $\hat{J}$ values are those that are obtained when optimizing for PIL or POL mode operation separately.

The form of the performance index chosen to be minimized in each mode of operation is

$$\hat{J} = E\{J\} = E\left[\int_0^\infty \left(\theta^2 + k_\delta \delta^2 + k_u u_{SAS}^2\right) dt\right] \tag{3.2}$$

where k_δ and k_u are scalar weighting constants and $\hat{J}$ is to be averaged over the initial states. The three terms in this performance index were selected in accordance with the following considerations: (1) θ should be driven to zero as rapidly as possible, (2) required pilot stick deflection should not be excessive, (3) a control moment command, u_{SAS}, generated by the SAS should not cause the lift fans to exceed their rated thrust. For POL operation, the aircraft performance index can be written in the form of equation (2.10) as

$$\hat{J}_2 = \sum_{i=1}^{3} \lambda_{ii} p_{ii} \tag{3.3}$$

where the P matrix for the aircraft subsystem is obtained by solving a third order equation of the form of equation (2.14). Similarly, for the pilot-in-the-loop,

$$\hat{J}_0 = \sum_{i=1}^{6} \gamma_{ii} p_{ii} \tag{3.4}$$

Here P is the solution of equation (2.14) for the complete sixth order system with the stipulation that $\gamma_{ii} = 0$ for the three pilot states (initial pilot states are assumed to have zero mean and variance). For

both modes, initial states are assumed to be uncorrelated ($\gamma_{ij} = 0$, $i \neq j$).

Solutions were obtained (optimal SAS gains) for various values of λ. Powell's method (ref. 21) of function minimization was used along with the Lyapunov equation solution technique of reference 16 for evaluation $\hat{J}$. Covariances γ_{11}, γ_{22}, and γ_{33} were all assumed to be 1.0, and weighting factors k_δ and k_u were chosen as 0.0015 and 0.15, respectively. Figure 4 graphically presents the results of the optimization of the composite performance index, $\hat{J}_3$, as a function of SAS pitch gain K_θ for a selection of λ values. Each curve is a section through the performance surface with $K_{\dot{\theta}}$ and $K_{\ddot{\theta}}$ held constant at the optimum values obtained for that particular λ value. Optimal K_θ's (which occur at the minima) range from 2.19 to 3.69; however, their magnitudes are quite similar for the extreme cases ($\lambda = 0$ and 1). The design trade-off is evidenced by the fact that $\hat{J}_3$ increases as λ moves away from 0 or 1, up to a maximum of about 0.04 for the $\lambda = 0.6$ curve.

To further demonstrate the influence of λ on control system behavior, typical transient responses for fixed initial conditions were computed. Figures 5(a) and (b) show, respectively, PIL and POL responses of pitch angle θ, moment command due to the pilot u_p, moment command due to the SAS u_{SAS}, and the resulting VTOL pitch acceleration $\ddot{\theta}$. Transients are displayed for four λ values (0, 0.2, 0.8, and 1.0) for zero pilot initial conditions and VTOL initial conditions of 0.1, 0.1, and 0.1.

Comparing the pitch angle transients, it can be seen that for PIL operation (fig. 5(a)), the best transient occurs for the system optimized for $\lambda = 0$. Conversely, the best POL transient (fastest response) occurs in figure 5(a) for the system optimized for $\lambda = 1$. As an example, consider the case when the VTOL is in the POL mode 80 percent of the time, i.e., $\lambda = 0.8$. The θ curve for $\lambda = 0.8$ in figure 5(a) shows performance is somewhat degraded (higher overshoot, poorer damping) over the $\lambda = 0$ case, but is not nearly so poor as the highly underdamped $\lambda = 1$ case. In figure 5(b) it can be seen that the $\lambda = 0.8$

design is very nearly as fast responding as the $\lambda = 1$ design, and much faster than the system designed for PIL operation ($\lambda = 0$).

Similar comparisons can be made for u_p, u_{SAS}, and $\ddot{\theta}$ transients. For instance, pilot control excursion is high in figure 5(a) for the $\lambda = 1$ case, (PIL operation with POL feedback gains). However, using these same gains in POL operation gives the best transient performance. Note that u_p is zero in figure 5(b), since the pilot is not exercising control. Pitch acceleration histories are included to demonstrate that all of the optimal controllers give rise to VTOL accelerations which are "reasonable" in magnitude. The rather anomalous behavior of u_p in PIL operation (fig. 5(a)) at $t = 0$ is due to the fact that in the analysis and transient calculation, pilot dead time has been approximated by a first order Pade approximation. What appears to be the pilot initially attempting to increase the error in θ is actually due to the inaccuracy in modeling his dead time with a Pade.

In the preceeding example, no constraints were imposed on the SAS gains. One obvious constraint that could be considered is one on $K_{\ddot{\theta}}$. As $K_{\ddot{\theta}}$ becomes large, the lift fan/engine eigenvalue increases, such that eventually saturation will certainly occur. Thus, for a reasonable solution, $K_{\ddot{\theta}}$ must be bounded. Another problem, mentioned in Section 2, is system stability. The system in this example was open loop stable such that even though not all states were fed back, a set of (optimal) gains were found which produced a stable system. This will not be the case, in general, so that periodic stability checks must be made during the optimization to insure each set of (sub-optimal) gains corresponds to a stable system.

4.0 CONCLUSIONS

An approach has been formulated to the problem of designing a control for a system with conflicting subsystem performance indices. Use was made of relative sensitivity by introducing it into the system's performance index. A method was developed for handling linear systems

with quadratic subsystem performance indices, for either full or partial state feedback. The approach was demonstrated by using it to design the pitch axis SAS for a piloted VTOL, where the main subsystem of interest was the VTOL aircraft. A design was obtained, consisting of a fixed set of SAS gains, which gave acceptable performance both with and without pilot control. The methods developed could be extended to include nonlinear plants, state variable constraints, and nonquadratic performance indices. They could also be applied to designing the complete three axis SAS for a VTOL, capable of operating throughout the hover, transition and cruise modes.

REFERENCES

1. McRuer, Duane T.; Graham, Dunstan; Krendel, Ezra; and Reisener, William, Jr.: Human Pilot Dynamics in Compensatory Systems. Theory, Models, and Experiments with Controlled Element and Forcing Function Variations. Systems Technology, Inc. (AFFDL-TR-65-15, AD-470337), July 1965.

2. McRuer, Duane T.; and Jex, Henry R.: A Review of Quasi-Linear Pilot Models. IEEE Trans. on Human Factors in Electronics, vol. HFE-8, no. 3, Sept. 1967, pp. 231-249.

3. McRuer, D. T.; and Magdaleno, R. E.: Human Pilot Dynamics with Various Manipulators. Rep. STI-TR-134-3, Systems Technology, Inc. (AFFDL-TR-66-138, AD-645289), Dec. 1966.

4. Sundararajan, N.; and Cruz, J. B., Jr.: Trajectory Insensitivity of Optimal Feedback Systems. IEEE Trans. on Automatic Control, vol. AC-15, no. 6, Dec. 1970, pp. 663-665.

5. Kreindler, Eliezer: Closed-Loop Sensitivity Reduction of Linear Optimal Control Systems. IEEE Trans. on Automatic Control, vol. AC-13, no. 3, June 1968, pp. 254-262.

6. Belanger, Pierre R.: Some Aspects of Control Tolerances and First-Order Sensitivity in Optimal Control Systems. IEEE Trans. on Automatic Control, vol. AC-11, no. 1, Jan. 1966, pp. 77-83.

7. Kreindler, Eliezer: Formulation of the Minimum Trajectory Sensitivity Problem. IEEE Trans. on Automatic Control, vol. AC-14, no. 2, Apr. 1969, pp. 206-207.

8. Mantey, Patrick E.: Eigenvalue Sensitivity and State-Variable Selection. IEEE Trans. on Automatic Control, vol. AC-13, no. 3, June 1968, pp. 263-269.

9. Divieti, L. D.; Rossi, C. M.; and Schmid, R. M.: Output Sensitivity to Real and Imaginary Parts of Complex Poles. IEEE Trans. on Automatic Control, vol. AC-13, no. 2, Apr. 1968, pp. 213-214.

10. Cadzow, James A.: Optimal Control of a System Subject to Parameter Variation. Joint Automatic Control Conference, 1966, pp. 807-810.

11. Dougherty, Hugh J.; Lee, Imsong; and DeRusso, Paul M.: Synthesis of Optimal Feedback Control Systems Subject to Parameter Variations. Joint Automatic Control Conference, 1967, pp. 125-134.

12. Whitbeck, Richard F.: A Suboptimal Approach to the Control of Systems Containing Uncertain Parameters. J. Spacecraft Rockets, vol. 4, no. 11, Nov. 1967, pp. 1431-1437.

13. Zadicario, J.; and Sivan, R.: The Optimal Control of Linear Systems with Unknown Parameters. IEEE Trans. on Automatic Control, vol. AC-11, no. 3, July 1966, pp. 423-426.

14. Tuel, William G., Jr.: Optimal Control of Unknown Systems. Ph.D. Thesis, Rensselaer Polytechnic Inst., 1965.

15. Fath, A. F.: Computational Aspects of the Linear Optimal Regulator Problem. Joint Automatic Control Conference, 1969, pp. 44-49.

16. Chen, C. F.; and Shieh, L. S.: A Note on Expanding $PA + A^TP = Q$. IEEE Trans. on Automatic Control, vol. AC-13, no. 1, Feb. 1968, pp. 122-123.

17. Kleinman, David L.; Fortmann, Thomas; and Athans, Michael: On the Design of Linear Systems with Piecewise-Constant Feedback Gains. IEEE Trans. on Automatic Control, vol. AC-13, no. 4, Aug. 1968, pp. 354-361.

18. Levine, William S.; and Athans, Michael: On the Design of Optimal Linear Systems Using Only Output-Variable Feedback. Sixth Annual Allerton Conference on Circuit and System Theory. T. N. Tuck and R. T. Chien, eds., IEEE, 1968, pp. 661-670.

19. Smith, P. G.: Numerical Solution of the Matrix Equation $AX + XA^T + B = 0$. IEEE Trans. on Automatic Control, vol. AC-16, no. 3, June 1971, pp. 278-279.

20. Reid, L. D.: An Investigation into Pursuit Tracking in the Presence of a Disturbance Signal. Fifth Annual NASA-University Conference on Manual Control. NASA SP-215, 1970, pp. 129-169.

21. Powell, M. J. D.: An Efficient Method for Finding the Minimum of a Function of Several Variables without Calculating Derivatives. Computer J., vol. 7, no. 2, July 1964, pp. 155-162.

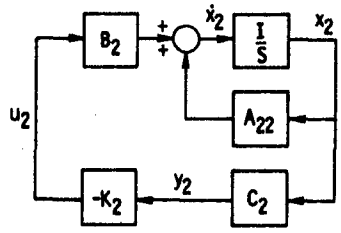

Figure 1. - Subsystem $\mathcal{S}_2$ isolated from composite system $\mathcal{S}_0$.

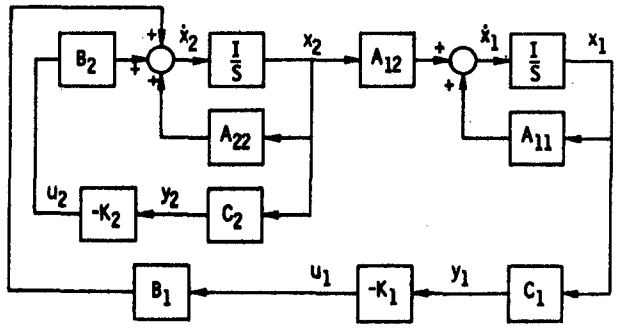

Figure 2. - Composite system $\mathcal{S}_0$.

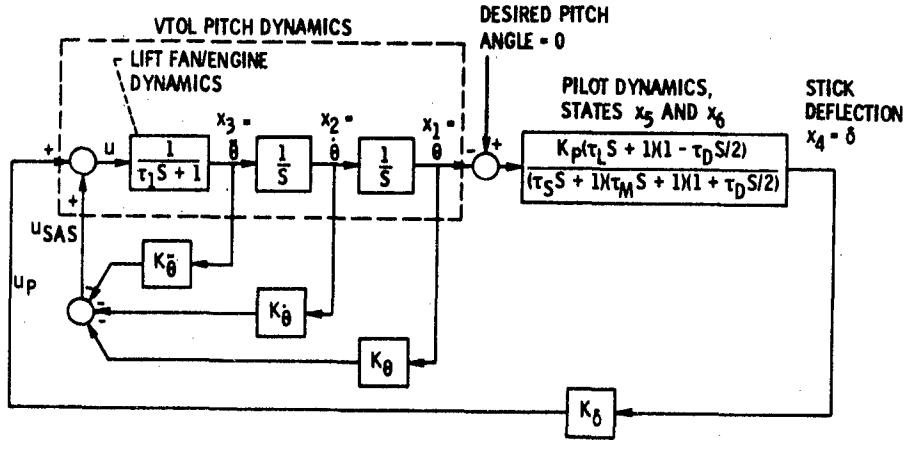

Figure 3. - Block diagram of VTOL aircraft controlled by pilot in hover mode.

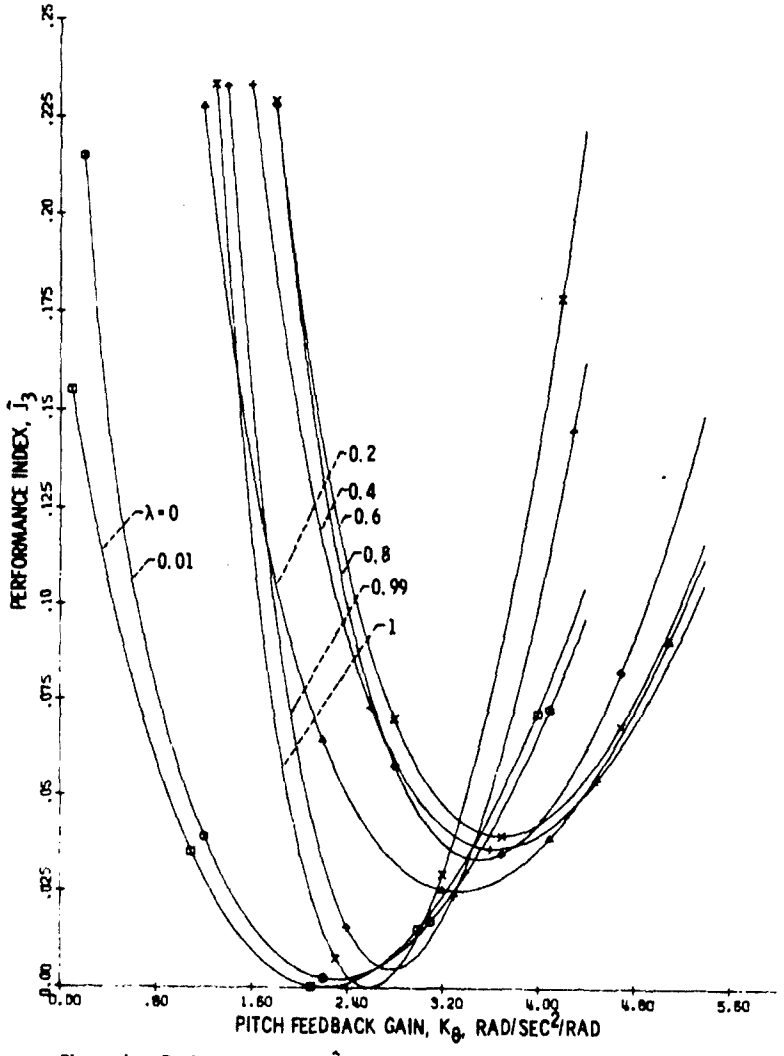

Figure 4. - Performance Index $\hat{J}_3$ as a function of K_θ for $K_{\dot{\theta}}$ and $K_{\ddot{\theta}}$ kept at optimum values; weighting factor $\hat{\lambda}$ as a parameter.

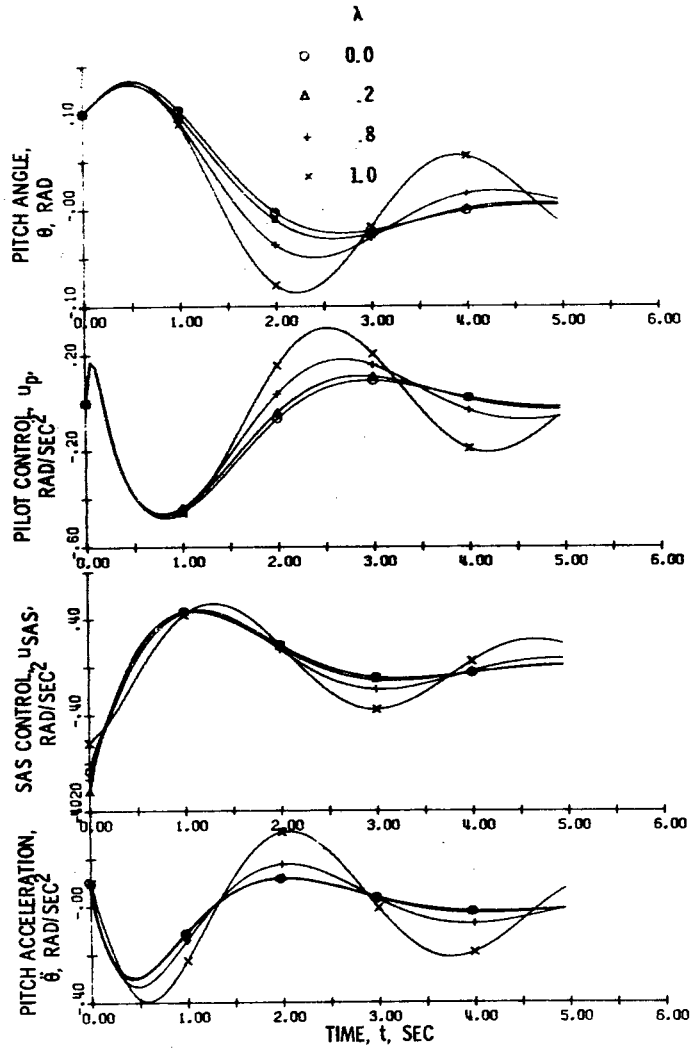

(a) RESPONSES WITH PILOT IN THE LOOP (PIL).

Figure 5. - Transient responses for VTOL and pilot for different sets of optimal gains; initial pilot states equal zero, $\theta(0) = \dot{\theta}(0) = \ddot{\theta}(0) = 0.1$.

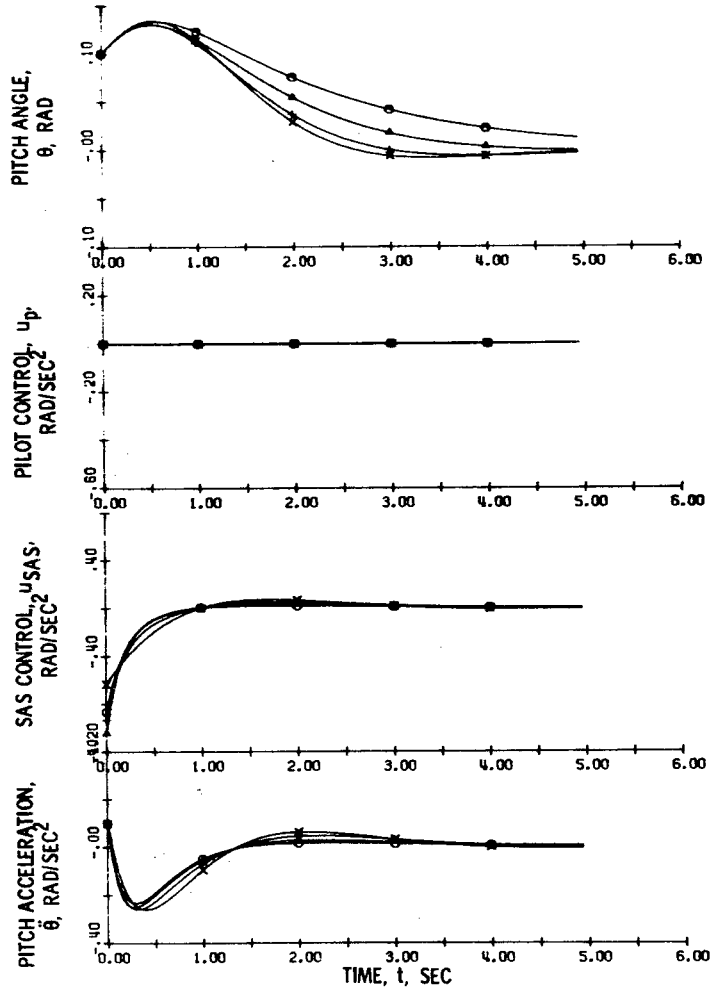

(b) RESPONSES WITH PILOT OUT OF THE LOOP (POL).

Figure 5. - Concluded.

The Use of Nonadjectival Rating Scales in Human Response Experiments

Ronald A. Hess and Donald M. Layton
Department of Aeronautics
U. S. Naval Postgraduate School
Monterey, California

ABSTRACT

Three human response experiments are described in which the participants were asked to rate the task difficulty via a linear, nonadjectival, nonordinal rating scale. The first experiment involved the solution of a simple puzzle. Upon the successful solution of the puzzle or at the expiration of an allotted time, whichever occurred first, the subject was asked to rate his impressions of the difficulty he encountered in working the puzzle on the nonadjectival scale. A high correlation coefficient was found between ratings and performance. The second experiment involved a new set of subjects and the "subcritical-critical" tracking tasks. After completing a number of critical runs, the subject performed five subcritical tasks with different instability levels. After each of these subcritical runs, he was asked to rate the task difficulty on the nonadjectival scale. Finally, another group of subjects was utilized in an experiment in which an "optimum" manipulator sensitivity was chosen for a subcritical system using the nonadjectival scale. This rating concept shows potential for discerning relatively minor changes in system acceptability. It is particularly useful in cases where adjectival scales are either inappropriate or difficult to design in a linear fashion.

Preceding page blank

THE SENSUOUS SAS BY PAPER PILOT

Teddy L. Hollis*, Russell A. Hannen, James D. Dillow
Air Force Institute of Technology, Wright-Patterson AFB, Ohio

ABSTRACT

A new procedure for designing pitch stability augmentation was investigated. The technique involves minimizing the "Pitch Paper Pilot" rating subject to rms constraints on the stability augmentation system (SAS) authority. The technique was applied to T-33 aircraft dynamics for six flight conditions. Optimal gains were determined for two possible SAS configurations. A simple gain scheduling law resulted which provides excellent handling qualities for all the flight conditions considered.

INTRODUCTION

In the last twenty years, much research has been devoted to the study of pilot-vehicle systems. Most of the work was directed towards the development of a satisfactory model for the pilot. Finding such a model was not easy, since the human being is probably the most sophisticated and complicated feedback control system in existence. The models which evolved, therefore, contained terms such as pure time delays, neuromuscular leads and lags, etc. A good account of some of the presently existing quasi-linear pilot models is given by McRuer, et al (Ref. 1). These models made it possible to predict, to a certain degree, the dynamic behavior of pilot-vehicle systems.

Parallel to the development of the pilot model, equally important efforts were directed towards the development of the pilot rating concept as a means to measure pilot opinion. Noteable work in this area was done by Cooper (Ref. 2) and subsequently Harper (Ref. 3). They established rating scales ranging from a pilot rating of 1, representing excellent flying qualities, to a pilot rating of 10, representing unflyable conditions. The Cooper scale is shown in Table I. With a scale for measuring an aircraft's handling qualities, investigations were made to determine how aircraft dynamics affected pilot parameters and pilot opinion for compensatory tasks (Ref. 4). Most of this work, however, was concentrated toward examing trends and amassing data.

In 1969 the first fully automated method, for mathematically relating the pilot-vehicle system to pilot opinion, was developed. It was at this time, Anderson (Ref. 5) presented a method whereby the pilot opinion could

*Currently assigned to Aeronautical Systems Division, Air Force Systems Command, Wright-Patterson AFB, Ohio.

Preceding page blank

Table I

Cooper Pilot Rating System (Ref. 8)

Operating Conditions	Adjective Rating	Numerical Rating	Description	Primary Mission Accomplished	Can Be Landed
Normal Operation	Satisfactory	1	Excellent, includes optimum	Yes	Yes
		2	Good, Pleasant to fly	Yes	Yes
		3	Satisfactory, but with some mildly unpleasant characteristics	Yes	Yes
Emergency Operation	Unsatisfactory	4	Acceptable, but with unpleasant characteristics	Yes	Yes
		5	Unacceptable for normal operation	Doubtful	Yes
		6	Acceptable for emergency condition only[1]	Doubtful	Yes
No Operation	Unacceptable	7	Unacceptable even for emergency condition[1]	No	Doubtful
		8	Unacceptable - dangerous	No	No
		9	Unacceptable - uncontrollable	No	No
	Catastrophic	10	Motions possibly violent enough to prevent pilot escape	No	No

[1]Failure of a stability augmenter.

be predicted for the hover task of vertical-takeoff-landing (VSTOL) aircraft. The method was dubbed "Paper Pilot" since a digital computer program was used to implement the prediction scheme (Ref. 6). A year later this work was extended to handle the pitch tracking task of conventional aircraft (Ref. 7).

There are a couple of ways that the handling qualities of an aircraft can be improved. One way is to "build them in" structurally, i.e., by proper design of the structure, wing size, tail placement, aircraft weight, etc. However, the degree to which handling qualities can be built in is limited, due to factors which stem from the operational requirements of the aircraft. For example, if the aircraft is to be flown at a wide range of altitudes and Mach numbers, it is difficult if not impossible to "build in" handling qualities which will be the same for all flight conditions. Additional limitations are due to tolerances in airframe configuration changes.

Handling qualities can also be improved by employing a stability augmentation system (SAS). Not only can a SAS reduce the aircraft's sensitivity to flight condition and airframe configuration changes, but also reduce its sensitivity to wind gusts.

Until now SAS design has been constrained to using those systems which have historically shown merit in terms of simplicity of design, reliability, responses to unwanted inputs, sensitivity to changes in airframe configuration, etc. Criteria, for practical SAS design, have been related to handling qualities by specifying the requirements in terms of a broad range of damping ratios and short period natural frequencies. These requirements have been shown, from past experience, to result in handling qualities for which the pilot has no strong disagreements with. Hence, the pilot's opinion was considered only in a subjective sense in SAS design.

As a result of the paper pilot concept, the pilot opinion can now be used directly as a SAS design parameter. This is in fact the approach taken in this paper for developing a pitch axis SAS. The procedure is briefly described and the results obtained for T-33 aircraft dynamics are presented in this paper.

SAS OPTIMIZATION PROCEDURE

The first consideration in the design procedure is the pilot rating. In order to determine the pilot rating, the pitch paper pilot rating method described in Ref. 7 is used. This method provides a means for analytically computing pilot rating of an aircraft in a pitch tracking task.

The pitch paper pilot rating method is based on the pilot-vehicle model shown in Fig. 1. The principle elements of the model are:

1. The commanded input, θc. This is taken to be the output of a first order filter driven by Gaussian white noise. The bandwidth of the filter is 1.0 rad/sec. This input provides the disturbance to the aircraft via the pilot tracking.

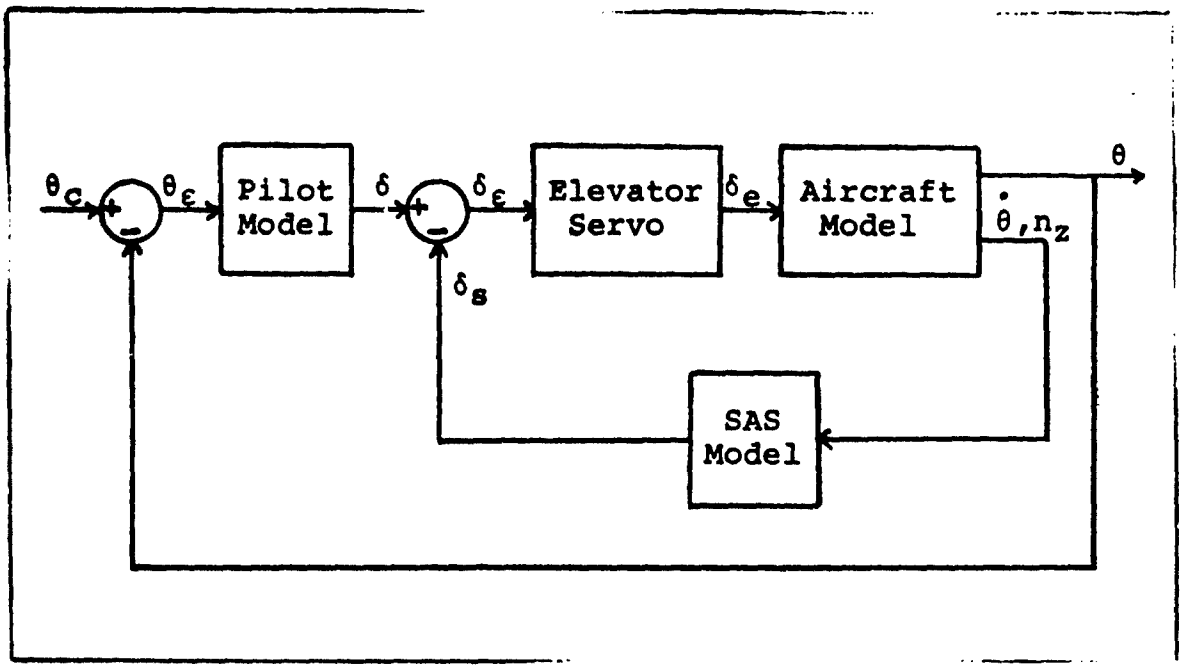

Fig. 1 Pilot-Vehicle Model

2. The pilot model. The pilot model is taken to be a first order lead of the form $K_p(T_L s + 1)$ followed by a pure reaction time delay. See Fig. 2.

3. The aircraft pitch dynamics (as well as the elevator servo dynamics).

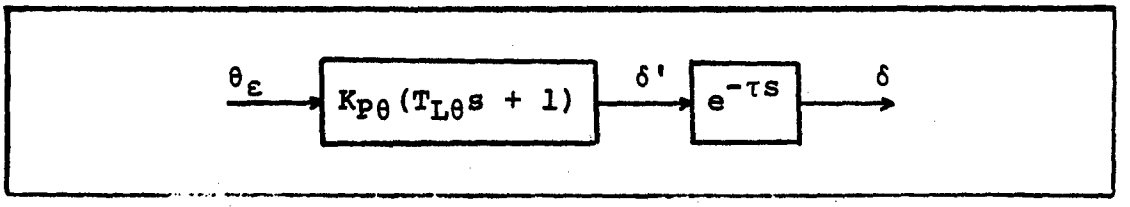

Fig. 2. Pilot Model

4. The stability augmentation system (SAS). The pitch paper pilot rating scheme doesn't require a particular form for the SAS since the method conceptually applies to any augmented aircraft dynamics. For the example developed in this paper, feedbacks of pitch rate and normal acceleration were considered. See Fig. 3.

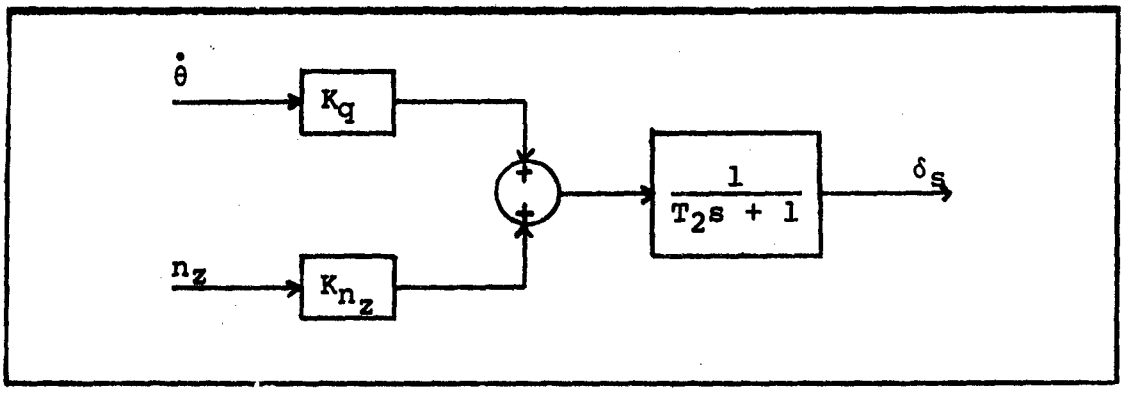

Fig. 3. SAS Model

For a given aircraft - SAS configuration (including the values of the SAS gains), the pilot rating is determined by finding the pilot gain and lead, K_p and T_L, that minimize a given function of tracking performance and pilot lead (Ref. 7). As a side benefit, the pilot model parameters and closed-loop pilot-vehicle performance (in terms of rms values of the aircraft state variables) are also derived. The main point is, however, that this method provides an analytic procedure for determining pilot rating.

A second consideration in the design procedure is the automatic control authority. Even with complex augmentation, the vehicle's effective dynamics cannot be completely changed at the designer's will. One reason for this is that control authority limits must be met. That is, only a certain control surface rate can be tolerated without undue control power requirements,

and actual surface deflections are limited by aerodynamic or physical constraints. In addition, the control authority allotted to the SAS may well also be restricted for safety reasons, depending upon the attendant reliability of the SAS. These restrictions or authority limits are imposed on the SAS output in order to insure that the pilot has sufficient authority to override "hard over" failures of the SAS. At any rate the design procedure must account for these limitations in order to arrive at a "reasonable" design with respect to automatic control limits.

With these considerations in mind, the SAS design procedure is conceptually quite simple:

1. Select the SAS configuration based upon the feedbacks available (i.e., based upon the outputs of the onboard sensors).

2. Select a rms value of the commanded input which will provide a moderate to severe disturbance to the aircraft.

3. Determine the control limitations either based upon the physical limitations of the control surfaces and the associated actuators or based upon the SAS authority limits.

4. Determine the SAS gains which minimize the pilot rating subject to 3 sigma constraints on the control activity.

In practice the fourth step of the procedure was dealt with by finding the SAS gains which minimize a cost functional of the form

$$J = PR + S_1\sigma^2_{\delta_s} + S_2\,\sigma^2_{\dot{\delta}_s}$$

where

PR = Pilot rating (as determined from the pitch paper pilot method; low numerical values are "best")

$\sigma^2_{\delta_s}$ = augmentation system control deflection variance

$\sigma^2_{\dot{\delta}_s}$ = augmentation system control deflection rate variance

S_1 and S_2 = constants

The values of S_1 and S_2 were then determined which minimized the pilot rating and still satisfy the 3 sigma constraints on the augmentation system control activity. This results in an "optimal" SAS in that, for the given authority limits, the feedback gains provide the best pilot acceptance possible. Or in other words, this results in a SENSUOUS SAS.

The details of the optimization procedure are given in Ref. 9. The attractive features of the procedure are (1) The SAS design is directly based upon pilot acceptance or the pilot's evaluation of the handling qualities of the augmented aircraft, (2) The control authority limits are

accounted for, and (3) The procedure can be completely automated via the digital computer.

RESULTS

The procedure described above was analyzed for aircraft dynamics representing the USAF/CAL variable stability T-33 Jet Trainer (Ref. 10). This particular aircraft has been extensively modified so that it can be used to simulate the handling qualities of and presently existing, future, or hypothetical aircraft.

Two different SAS configurations were considered; one using only pitch rate feedback and the other using pitch rate and normal acceleration feedbacks. Each of these systems were examined over six different flight conditions. The flight conditions and the corresponding pitch paper pilot ratings for the aircraft without SAS are listed in Table II. These ratings agree with those given in the military specifications (Ref. 11), i.e., when the ω_{sp} is near the lower boundry of the spec limits, the actual pilot ratings are on the average around 3.5. Flight condition 3 has a higher pilot rating (PR = 4.68) because of low damping (ζ_{sp} = .381). (For a listing of ω_{sp} and ζ_{sp} for the basic aircraft and how they compare with the specs, see Table V.)

SAS deflection and SAS rate limits are not specified for this aircraft. Therefore, for the purpose of example, it was assumed that the SAS deflection limit is ±6deg and the SAS rate limit is 26 deg/sec. In order to statistically represent these constraints, the values of ±6 deg and 26 deg/sec were used as 3σ constraints. Then, in terms of standard deviations, these limits become 0.036 rad and 0.15 rad/sec respectively.

Table II

Flight Conditions Used in the Analysis

Flight Condition	Mach Number	Altitude (ft)	Pilot Rating Without SAS (Predicted)
1	.5	0	3.40
2	.5	15000	3.71
3	.5	35000	4.68
4	.7	0	2.90
5	.7	15000	3.02
6	.7	35000	3.48

A 3.33 deg rms commanded input was used. This level for the commanded input was selected as a "reasonable" value, and resulted in unaugmented vehicle pilot rating predictions that match well with the supporting data used to develop Ref. 11. The detailed results are described in Ref. 9. The pertinent results are described herein.

Pitch Rate Feedback

For a SAS using only pitch rate feedback the following cost function was used:

$$J = PR + S_2\sigma_{\dot{\delta}_s} \tag{1}$$

The minimum of J, with respect to K_q was determined for several different values of S_2.

A plot of PR versus $\sigma_{\dot{\delta}_s}$ for three of the extreme flight conditions is shown in Fig. 4. Notice that the most significant improvement in pilot rating occurs for values of $\sigma_{\dot{\delta}_s}$ between 0 and 0.1 rad/sec.

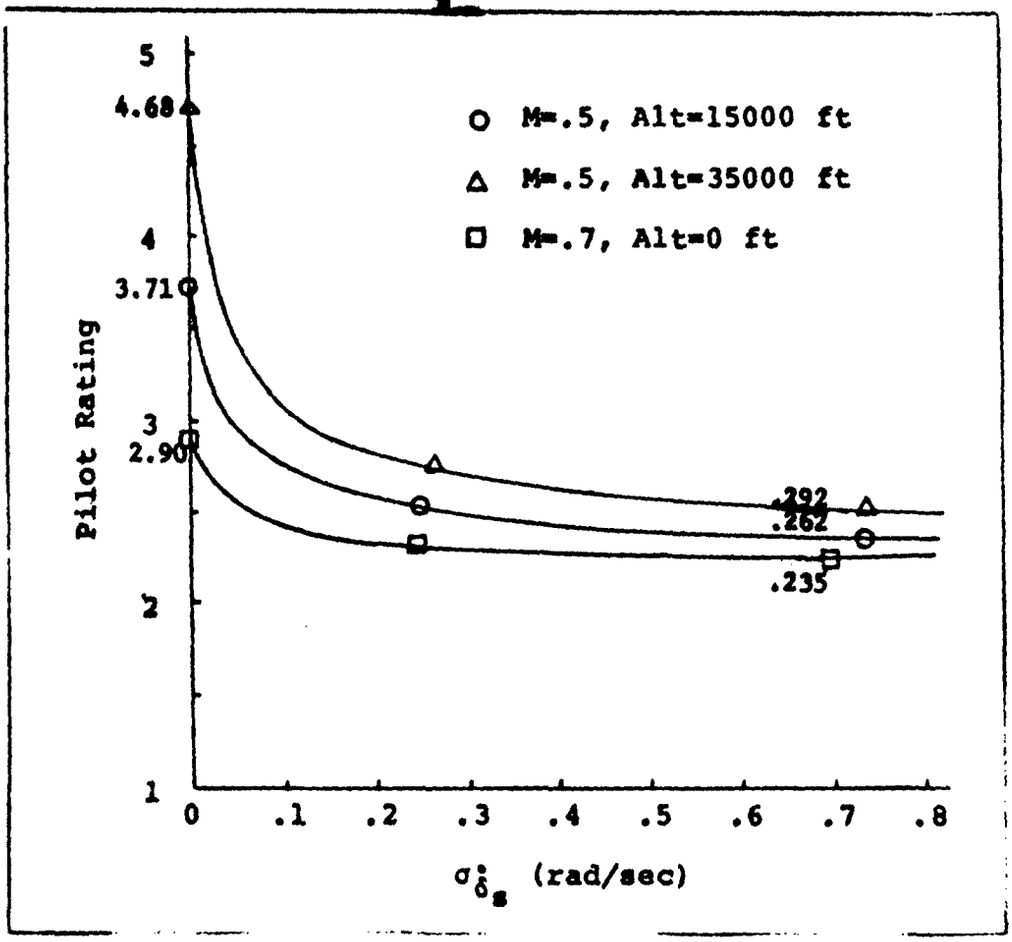

Fig. 4. Pilot Rating versus SAS Rate for a $\dot{\theta}$ SAS

In Table III the pilot ratings for the aircraft with a pitch rate SAS are compared with the basic aircraft without SAS. The improvement in pilot rating for the aircraft with a SAS is 0.5 to 1.5 ratings. To realize these improvements, however, K_q must be scheduled. One way that this could be accomplished is by implementing a gain changer which is a function of the dynamic pressure.

Table III

Comparison of Pilot Ratings for $\dot{\theta}$ SAS

Flight Condition	Basic A/C	A/C With $\dot{\theta}$ SAS			
	PR	PR	K_q (sec)	$\sigma_{\dot{\delta}_s}$ (rad/sec)	σ_{δ_s} (rad)
1	3.40	2.52	-.270	.151	.0220
2	3.71	2.62	-.365	.151	.0273
3	4.68	2.92	-.550	.151	.0337
4	2.90	2.35	-.195	.151	.0182
5	3.02	2.40	-.252	.151	.0220
6	3.48	2.53	-.400	.151	.0280

In Fig. 5, K_q is plotted as a function of $\left(\frac{1}{2}\rho V^2\right)^{-1}$ for each of the six flight conditions. Notice that the relationship is nearly linear. Hence, it is feasible that K_q could be scheduled this way.

It might be specified that, for all flight conditions, K_q is a fixed value. If this were the case, K_q could be no larger than -0.195. Using a value larger than this would result in the SAS rate limit being exceeded for flight condition 4. Table IV lists the pilot ratings corresponding to this value of gain. It is questionable however, if using a fixed gain is really worth the effort since the pilot rating for flight condition 3 is still quite high (i.e., PR = 3.70).

Pitch Rate and Normal Acceleration Feedback

To find the optimal SAS parameters, K_q and K_{n_z} the cost function given by eq. (1) was used. For flight condition 3, however, it was found that the SAS deflection limit was exceeded before reaching the SAS rate

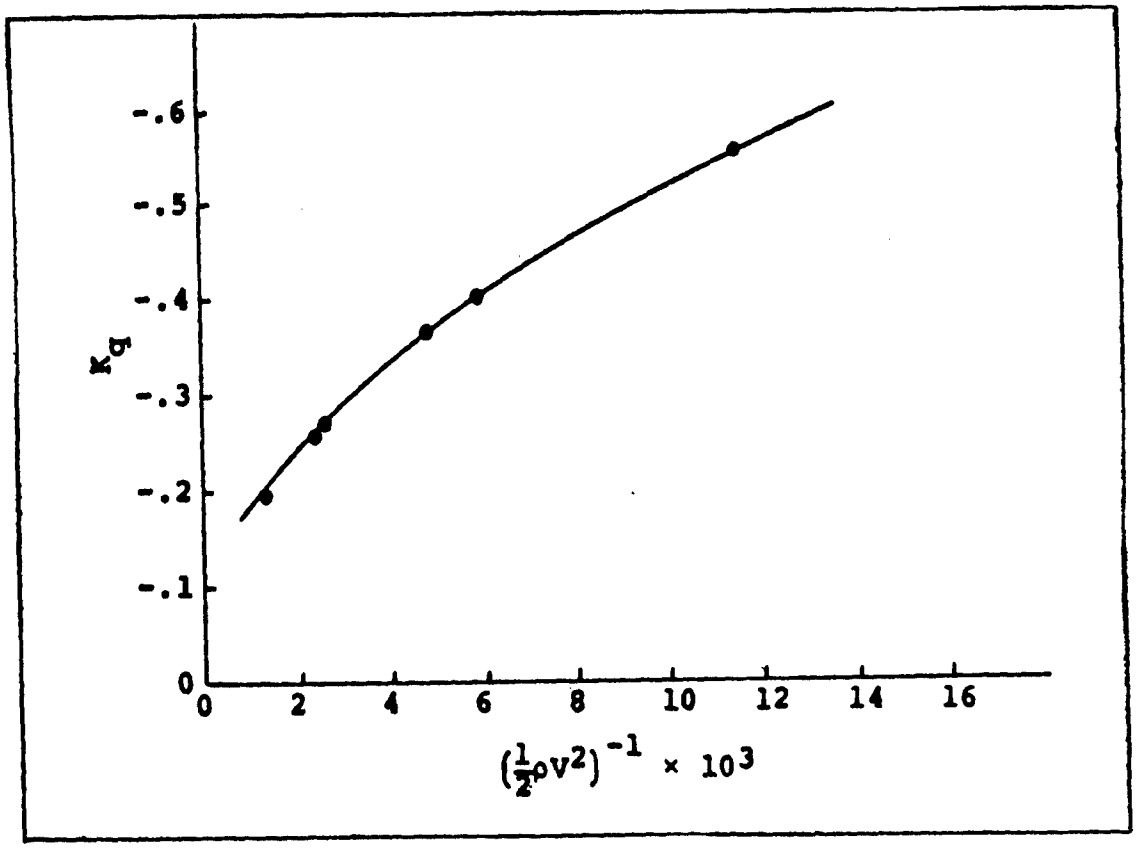

Fig. 5. K_q versus $\left(\frac{1}{2}\rho V^2\right)^{-1}$ for θ SAS

Table IV

A Comparison of the Pilot Ratings for a Fixed Pitch Rate Gain in the $\dot{\theta}$ SAS

Flt. Cond	1	2	3	4	5	6
PR	2.63	2.73	3.70	2.90	2.48	2.75
K_q (sec)	-.195	-.195	-.195	-.195	-.195	-.195
σ_{δ_e} (rad)	.0095	.0100	.0105	.0182	.0157	.0140
$\sigma_{\dot{\delta}_e}$ (rad/sec)...	.082	.060	.025	.151	.100	.060

limit. Therefore, for flight condition 3, the following cost function was used:

$$J = PR + S_1\sigma_{\delta_s}$$

J was minimized with respect to K_q and K_{n_z} for several different values of S_1.

In Fig. 6, the pilot rating versus the SAS rate is shown for three of the six flights conditions. Notice that the pilot ratings decreases as the SAS rate increases, as in the case where only pitch rate feedback was used. Again, the most significant improvement occurs for SAS rates between 0.0 and 0.1 rad/sec. A comparison between pilot ratings for the basic aircraft and the aircraft with a SAS pitch rate and normal acceleration as feedbacks is given in Table V.

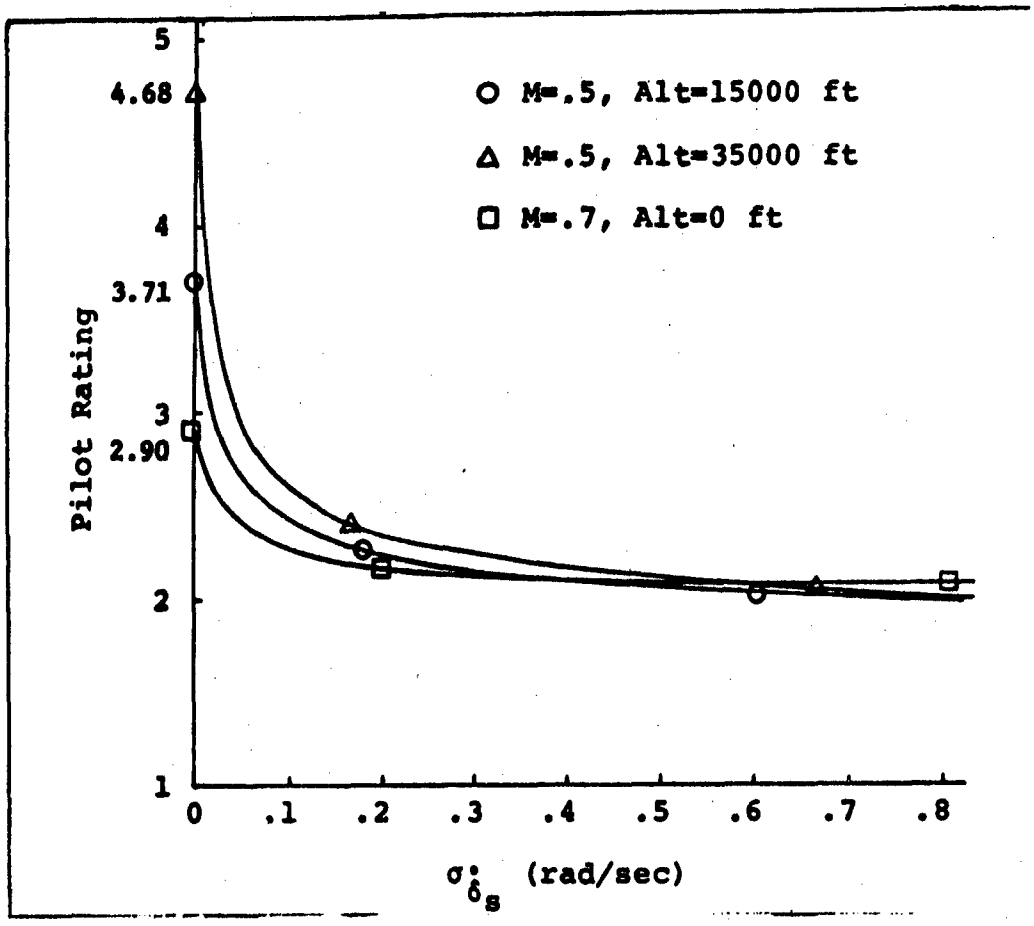

Fig. 6. Pilot Rating versus SAS Rate for a $\dot{\theta} + n_z$ SAS

Table V

Comparison of Pilot Ratings for $\dot{\theta}$ + n_z SAS

Flight Condition	Basic A/C PR	With $\dot{\theta}$ SAS PR	With θ + n_z SAS				
			PR	K_q (sec)	K_{n_z}	σ_{δ_s} (rad)	$\sigma_{\dot{\delta}_s}$ (rad/sec)
1	3.40	2.52	2.25	-.235	.0195	.0275	.151
2	3.71	2.62	2.30	-.330	.0310	.0340	.151
3	4.68	2.92	2.45	-.500	.0770	.0360	.125
4	2.90	2.35	2.18	-.160	.0080	.0230	.151
5	3.02	2.40	2.20	-.225	.0113	.0225	.151
6	3.48	2.53	2.25	-.375	.0245	.0350	.151

There is quite an improvement in the pilot rating for all flight conditions, (0.72 - 2.23 ratings). The best improvement occurs at flight condition 3. It should be noted that for this flight condition, the minimum pilot rating is constrained by the allowable σ_{δ_s}. For the other flight conditions, the minimum pilot rating is constrained by the allowable $\sigma_{\dot{\delta}_s}$.

The pitch rate feedback gains can be scheduled much in the same way as done for the pitch rate feedback case, as can be seen in Fig. 7. Note that there is nearly a linear relationship between K_q and $\left(\frac{1}{2}\rho V^2\right)^{-1}$

The normal acceleration gains, on the other hand, can not be scheduled in this manner. Although there is a linear relationship with $\left(\frac{1}{2}\rho V^2\right)^{-1}$, the linearity exists only for gains with the same Mach number. In Fig. 8, $K_{n_z} \times M$ is shown as a function of $\left(\frac{1}{2}\rho V^2\right)^{-1}$. This relationship appears to be nearly linear. Therefore, it may be possible to schedule K_{n_z} in this way.

Comparisons with Military Specifications

A comparison of the results with the current military specifications (Ref. 11), are shown in Table VI. These values were computed by using the short period approximation. Notice that the short period natural frequency for the basic aircraft is low for all flight conditions and that flight condition 3 has low damping ($\zeta_{sp} = .381$). As was mentioned earlier, the lower limit for ω_{sp} in the military specifications corresponds to a pilot rating of 3.5. As ω_{sp} or ζ_{sp} decrease the pilot rating starts increasing rapidly. A pilot rating corresponding to the upper limit on ω_{sp} has not yet been established, therefore, it is hard to ascertain if high natural frequencies are necessarily undesirable.

When the basic aircraft is augmented with pitch rate SAS, using the optimal values for K_q given in Table III, there appears to be a significant increase in the damping. For all flight conditions the damping has increased to approximately 1.1. In addition the short period natural frequencies for all flight conditions have been increased, the most noticeable increase being for flight condition 4. The most important fact to note, however, is that ω_{sp} is now within the spec limits for all flight conditions.

With a pitch rate plus normal acceleration SAS, ω_{sp} is greater than that of the basic aircraft and the basic A/C with a pitch rate SAS. It appears that ω_{sp} is near the middle of the spec limits for all but one flight condition (flight condition 4). For flight condition 4, ω_{sp} is on the high side of the spec limits, but as was noted before, this does not

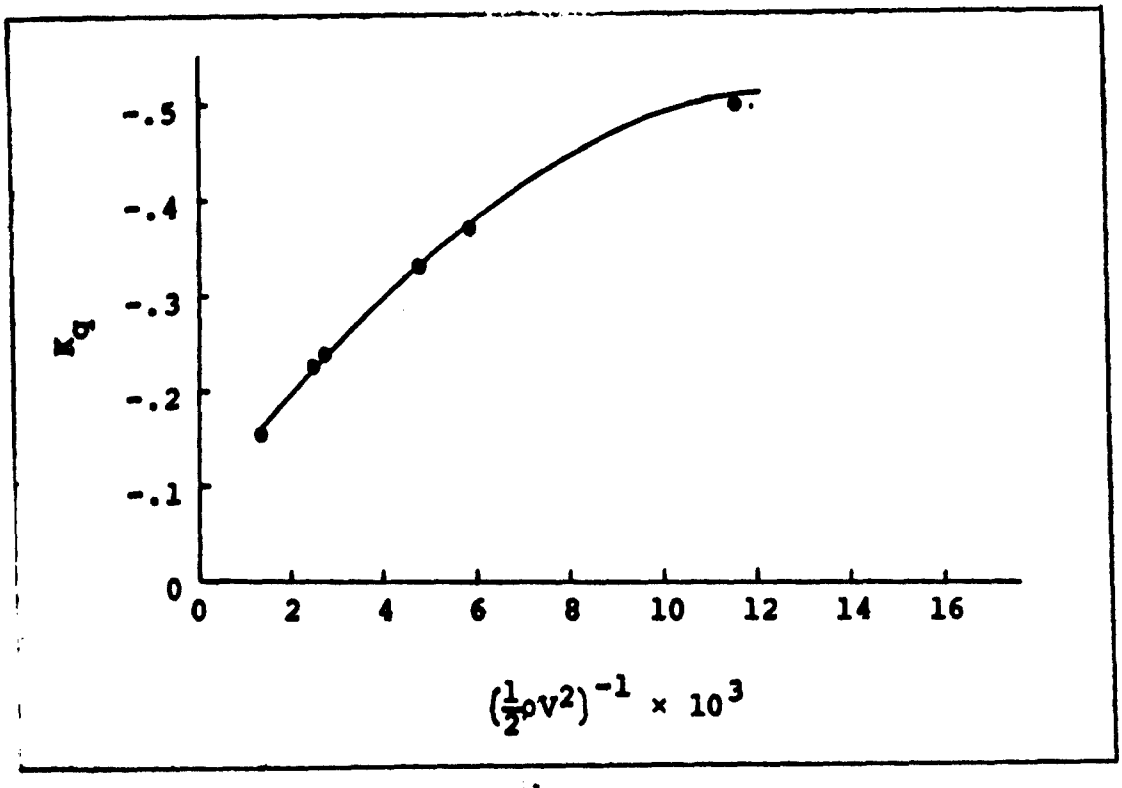

Fig. 7. K_q versus $\left(\frac{1}{2}\ \rho V^2\right)^{-1}$ for $\dot{\theta} + n_z$ SAS

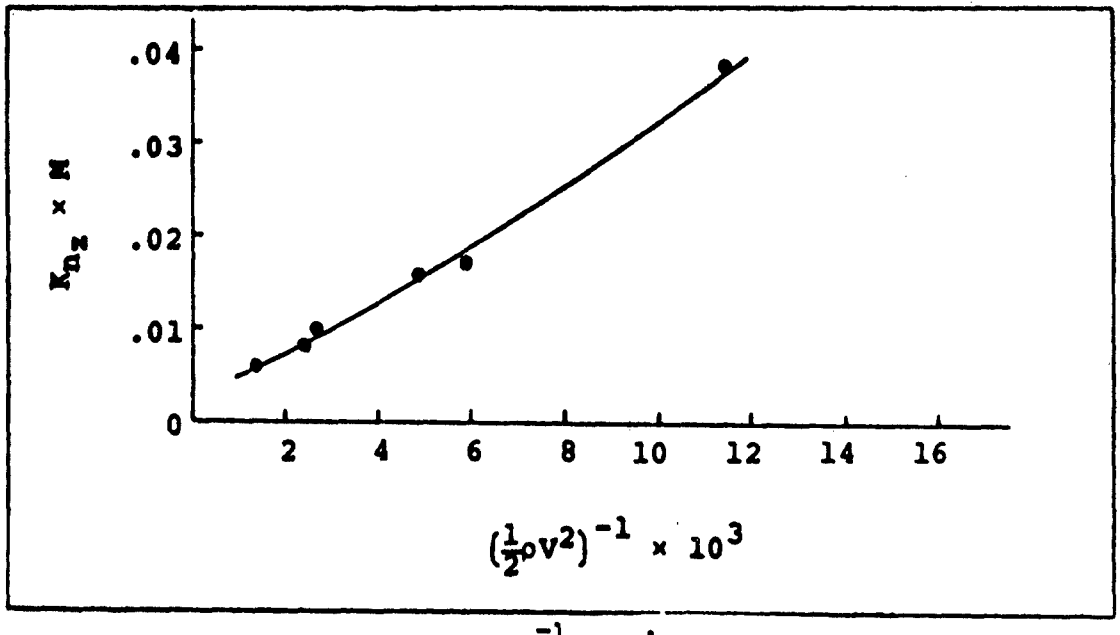

Fig. 8. K_{n_z} x M versus $\left(\frac{1}{2}\ \rho V^2\right)^{-1}$ for $\dot{\theta} + n_z$ SAS

Table VI

Comparison of Optimal Results with Military Specifications

Flt. Cond.		A/C Without SAS	A/C With $\dot{\theta}$ SAS	A/C With $\dot{\theta} + n_z$ SAS	Military Specifications[1]
1	ω_{sp} (rad/sec)	3.31	4.99	6.71	3.5 – 11.0
	ζ_{sp}	.644	1.11	.787	.35 – 1.30
2	ω_{sp} (rad/sec)	2.42	3.42	4.69	2.5 – 9.25
	ζ_{sp}	.531	1.13	.799	.35 – 1.30
3	ω_{sp} (rad/sec)	1.55	1.93	2.87	1.5 – 5.6
	ζ_{sp}	.381	1.15	.748	.35 – 1.30
4	ω_{sp} (rad/sec)	4.85	7.94	9.93	5.1 – 10.8
	ζ_{sp}	.674	1.07	.788	.35 – 1.30
5	ω_{sp} (rad/sec)	3.50	5.39	6.78	4.0 – 10.3
	ζ_{sp}	.560	1.07	.812	.35 – 1.30
6	ω_{sp} (rad/sec)	2.21	3.10	4.03	2.5 – 9.0
	ζ_{sp}	.406	1.10	.826	.35 – 1.30

[1]Ref. 3 requirements, Category A, Level 1

necessarily indicate that an undesirable situation exists. The damping is also near the center of the specs for all flight conditions. Notice that ζ_{sp} is less than the $\dot{\theta}$ SAS case but more than that of the basic aircraft.

These results are very encouraging and indicate that the design procedure described for finding the optimal SAS gains does indeed give very good results.

SUMMARY AND CONCLUSIONS

The presented method of selecting stability augmentation parameters for excellent pilot acceptances seems to produce very "good" systems designs. Furthermore, the method is fully automated, relying on modern parameter optimization techniques, and can be easily applied to higher order aircraft dynamics.

What is most important, however, is the fact that this procedure uses a very realistic performance measure for piloted aircraft augmentation system design. Such a "universal" performance index, suitable for modern control theory use, has indeed been elusive in the past.

The secondary benefits of this approach are also of importance. For example, the fact that pilot acceptance predictions are available early in the design stage is extremely important, and the predicted performance measures (root-mean-square-errors in tracking) can be used directly to evaluate overall man-machine performance and, therefore, system effectiveness.

YOU DID GOOD PAPER PILOT. Keep up the good work.

References

1. McRuer, D. J., et al. New Approaches to Human Pilot/Vehicle Dynamic Analysis. AFFDL-TR-67-150, February 1968

2. Cooper, G. E. "Understanding and Interpreting Pilot Opinion." Aeronautical Engineering Review. 16(3):47-52 (March 1957)

3. Harper, Robert P., Jr. In-Flight Simulation of the Lateral-Directional Handling Qualities of Entry Vehicles. WADD-TR-147, November 1961.

4. Hall, I. A. M. Effects of Controlled Element on the Human Pilot. WADC-TR-57-509, August 1958.

5. Anderson, R. O. A New Approach to the Specification and Evaluation of Flying Qualities. AFFDL-TR-69-120, December 1969.

6. Dillow, James D. The Paper Pilot--A Digital Computer Program to Predict Pilot Rating for the Hover Task. AFFDL-TR-70-40, March 1971.

7. Anderson, R. O., Connors, A. J., and Dillow, J. D. Paper Pilot Ponders Pitch. AFFDL/FGC-TM-70-1, November 1970

8. Miller, David P. and Vinje, Edward W. Fixed-Base Simulator Studies of VTOL Aircraft Handling Qualities in Hovering and Low-Speed Flight. AFFDL-TR-67-152, January 1968.

9. Hollis, T. L., "Optimal Selection of Stability Augmentation System Parameters to Reduce the Pilot Rating for the Pitch Tracking Task", CGC/EE/71-10, AF Institute of Technology Thesis, June 1971.

10. Hall, Warren G. and Huber, Ronald W. System Description and Performance Data for the USAF/CAL Variable Stability T-33 Airplane. AFFDL-TR-70-71, August 1970.

11. Chalk, C. R., Neal, T. P., Harris, T. M., Pritchard, F. E. Background Information and User Guide for MIL-F-8785B (ASG), "Military Specification-Flying Qualities of Piloted Airplanes." AFFDL-TR-69-72, August 1969.

SESSION IX

Manual Control Analysis of Aircraft: Control and Handling Qualities

Preceding page blank

NASA - Langley

AN ANALYTICAL STUDY OF AIRCRAFT LATERAL-DIRECTIONAL HANDLING QUALITIES USING PILOT MODELS

By James J. Adams

Abstract of Paper for
8th Annual NASA - University Conference on Manual Control
University of Michigan, Ann Arbor, Michigan
May 17-19, 1972

An analytical study has been made of the system response of the pilot lateral-directional aircraft system. The aircraft were represented by conventional, linear, three-degree-of-freedom differential equations. The pilot was represented by a linear transfer function model. Two levels of pilot response were described by the pilot model. The first level contained a static gain and a second order lag function with a lag time constant of 0.2 seconds. The second level added a 1 second lead time constant.

The analyses demonstrates the correlation that exists between the pilot model levels, the pilot-aircraft system response, and the experimentally determined pilot ratings for 66 aircraft configurations. It is shown that if a stable bank angle system response with characteristic frequencies larger than 1.9 radians per second, and a stable heading system response with characteristic frequencies greater than 1.7 radians per second can be achieved with the first level pilot model, the aircraft is rated satisfactory (pilot rating of 1 to 3). If the second level pilot model is required to achieve this system response, the aircraft is rated tolerable (pilot rating of 3 to 6). If further compensation on the part

Preceding page blank

of the pilot is required, the aircraft is rated controllable only (pilot rating of 6 to 9). It is necessary to notice if pole zero cancellation occurs in the system response, and if adding lead to the pilot response does improve the system response for both roll and heading control, in order to correctly evaluate all configurations. These additions to the rules for determining pilot ratings are necessary because in some cases the lowest system frequency was less than 1.9 radians per second, but this lowest frequency was cancelled by a zero. Since this mode of motion would not therefore appear in the system response, it can be ignored when determining the pilot rating. In other cases the computed roll response was satisfactory; however, further examination of the heading response revealed that the system could not meet the heading response requirements, and that adding lead to the pilot's response did not improve the system response. Therefore, it was the heading response of the system that determined the pilot rating.

PREDICTION AND EVALUATION OF FLYING QUALITIES IN TURBULENCE*

Edward D. Onstott
Aerodynamics and Propulsion
Research and Technology

Northrop Corporation
Aircraft Division
Hawthorne, California

ABSTRACT

A fixed form pilot model technique for predicting the attitude hold tracking performance of piloted airplanes in turbulence has been validated through an extensive moving base simulation of 49 fighter class airplane configurations. Both lateral and longitudinal dynamics are considered and the accuracy of the prediction method is assessed.

INTRODUCTION

Although there has been a great deal of research into the role of atmospheric turbulence as a cause of structural deterioration in airplanes, little has been learned until recently about the dynamics of piloted flight in gusty air. Except for the problem of stability in heavy turbulence penetration, not much concern for handling qualities effects has been shown beyond a few general guidelines aimed at reducing the aircraft's rotational moments in gusts.

It is generally presumed that if a pilot can control the airplane easily in still air he can adequately reduce the attitude displacements encountered during any cruise or military mission in rougher air. This has been more or less successful for two reasons, 1) light turbulence is not a threat to the pilot or the system, and 2) the additional accuracy to be possibly gained by optimizing the airplane design around an expected gust level has not been required. Now, however, it is often the case that a large percentage of an airplane's cost is for additional design and equipment to improve the weapons delivery or mission accuracy by a small percentage. Thus, system improvements that can be obtained by considering the realistic atmosphere of an actual operating environment represents not only improved design, but also an amount of the production cost worth considering.

*This research was largely carried out under contracts F33615-71-C-1076 and F33615-70-C-1156 for the Air Force Flight Dynamics Laboratory.

With this in mind, two years of research into this subject were sponsored by the Air Force Flight Dynamics Laboratory. Since accuracy of a weapons platform requires the pilot to control attitude excursions, attitude hold tasks in turbulence were selected for both analytical and experimental studies. Gaussian turbulence models (Dryden spectra) were employed for the zero mean tasks and the resulting distribution of the system tracking errors is described by the variance, or the root mean square (rms) average.

Reference 1. contains the mathematical details of the derivation of the pilot-vehicle transfer functions and how they are used to calculate the rms tracking errors. Bank angle hold tasks were the most important studied, and this discussion will be confined mostly to this wings level task.

BANK ANGLE CONTROL IN TURBULENCE

If the pilot is asked to hold wings level with no regard for heading angle, the lateral dynamical system which represents this is as shown in Figure 1.

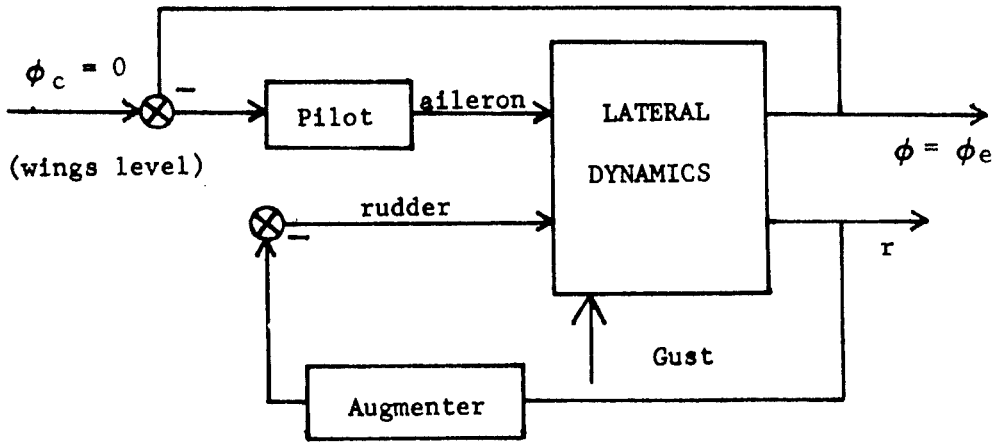

Figure 1. Wings level task in turbulence.

If the linear lateral dynamics and the gust representations are held fixed, the rms tracking error ϕ_e is a function of the pilot model only. In order to select a model that would lead to a practical method of analyzing and predicting flying qualities in turbulence, the following conditions had to be met:

1) The same model and standard prediction procedure must work for diverse airplanes of a given class, i.e. fighters, bombers, etc.

2) The assumption that the pilot minimizes the tracking errors in an rms sense must be used to obtain the predicted tracking error.

3) The number of free parameters must be kept minimal.

4) The predicted tracking errors must agree well with a moving base simulation of airplanes having generally satisfactory handling qualities in still air.

5) The method should indicate dynamical problems that would deteriorate pilot ratings.

In view of these requirements, it was natural to try very simple pilot models. Modeling the precise pilot aileron inputs was not a concern, nor was pilot injected noise (remnant) that is largely filtered out by the system.

The model Y_p that was used consisted of a gain K_p, a lead T_L, and a lumped transport lag time delay τ approximated by first or second order Padé formulas:

$$Y_p(s) = K_p(T_L\, s + 1)\, e_i^{-\tau s},\ i = 1,2...$$

This model works well with the following values:

K_p = optimum

T_L = .5 seconds

τ = .3 seconds

where these values apply only for the bank angle wings level task.

THE PREDICTION METHOD

With K_p as the only free parameter, the prediction method works in the following way. For convenience, the lateral v gust is standardized to 10 ft/sec rms and then the rms tracking error ϕ_e is computed for pilot model gains throughout the range of stability. Typically, this results in functions whose graphs resemble Figure 2a, and the interior minimum of the function

$$\phi_e = \phi_e(K_p)$$

serves as the predicted tracking error. If there is no interior minimum, the open loop ($K_p = 0$) tracking error is used. As a check on the appropriateness of the assumed .5 second lead, ϕ_e is recomputed with the optimum gain as a function of leads varying from zero to one second. In almost all cases the .5 second lead was verified as being near optimum as shown in Figure 2b.

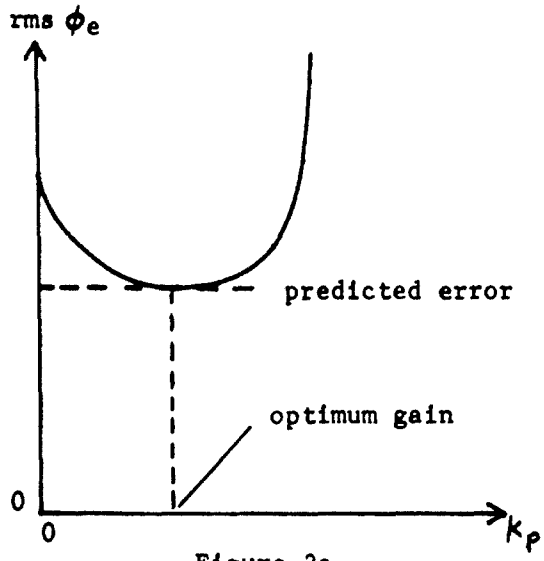

Figure 2a.

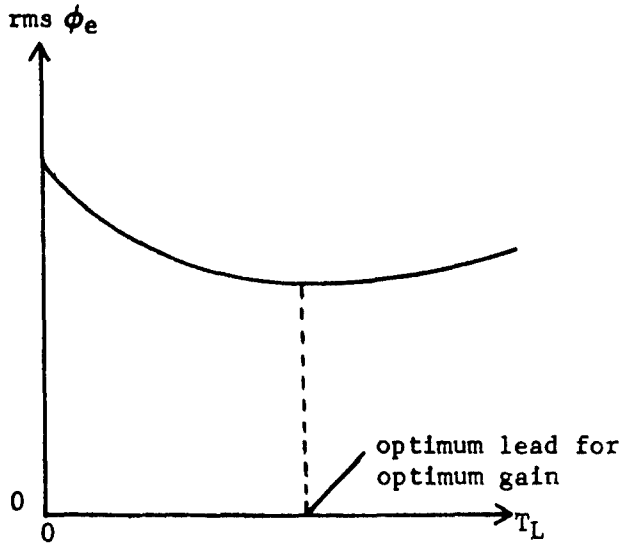

Figure 2b.

The case from which Figure 2 is drawn is reported in Reference 1, and turns out to be one of the most instructive that was encountered in the entire program. This airplane has exceptionally good general flying qualities, being rated 2 in the Cornell simulation. A former Navy test pilot flew it during the first turbulence simulation on the Northrop Large Amplitude Flight Simulator and found that the airplane was very pleasant to fly in still air. However, in turbulence of only 5 ft/sec rms the same pilot objected to the control response, and even expressed doubt that the airplane dynamics were the same.

There were two problems. First of all, the tracking error was exceptionally large, and in fact agreed closely with the predicted value shown in the above Figure 2. In the second place the steep slope of the rms ϕ_e versus K_p graph indicates a noticeable and objectionable sensitivity to changes in pilot gain. This was borne out when the test pilot was questioned about his complaints. He reported that the slightest bit of relaxation on his part led to an alarming increase of bank angle excursions. The simulation of this airplane also included flights at higher turbulence levels, but it was found experimentally that it was dangerous or unflyable in levels exceeding 10 ft/sec rms, a moderate turbulence intensity at most.

In order to have a wide range of airplane dynamics, eight of the variable stability T-33 configurations flown by Cornell were studied along with the F-5 airplane. Many interesting examples presented themselves, such as the one discussed above (which is the third in the BB-2 series) in a search of over sixty of the configurations. These were studied analytically by the above methods and the selected eight were simulated on the Northrop Large Amplitude Flight Simulator. Three pilots were used, including the test pilot mentioned above, in turbulence levels from light to heavy.

The agreement of the predicted tracking errors, which were submitted to the Air Force project engineer before the simulation, with the simula-

tion results is shown in Figure 3. Each point represents a configuration, and the simulator value was obtained by normalizing the tracking errors to 10 ft/sec rms and then averaging. All simulator data were used; no simulation flight data were excluded for any reason other than equipment failure.

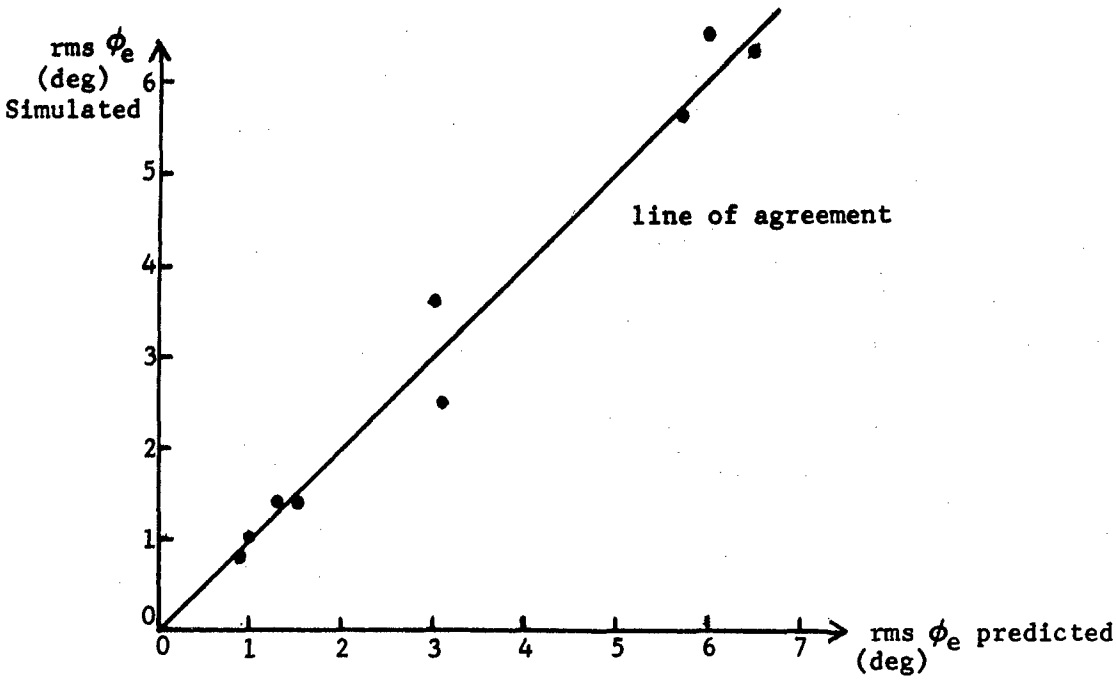

Figure 3. Agreement of predictions and simulation.

As an indication of the repeatability of the experimental tracking errors, individual simulator flights are shown in Figure 4. The rms errors were obtained over a 100 second period. The predicted error at 10 ft/sec rms turbulence extends by linearity to the lines through the origin.

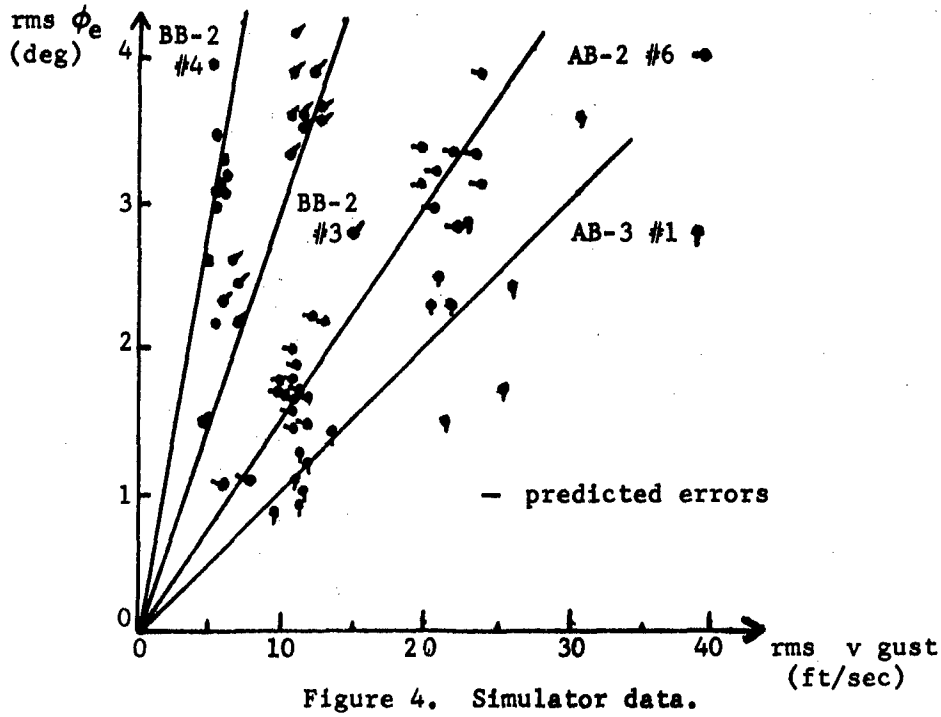

Figure 4. Simulator data.

VALIDATION OF THE METHOD

The results shown in the previous sections were striking enough that a decision was made to continue the program of turbulence research to achieve a validation of the method. During the resulting program, reported in Reference 2, longitudinal dynamics were also studied and the validation simulation was based on four F-5 and four A-7 flight conditions. These airplanes were simulated as realistically as possible with respect to both the airframe and the control systems; additional variations were produced by failing parts of the control and augmentation systems. A total of 1326 simulator flights were made that included bank, heading, and pitch angle tasks. The former Navy test pilot used in the above program was again available along with a former Air Force test pilot and a retired Air Force Colonel. A prefilter was used on the digital noise generator to reduce the low frequency components that may bias the first moment of the gust distribution. This was successful, and the simulator data obtained are characterized by very tight clustering.

Reference 2 contains tables of the raw simulator data for all recorded flights. These data include the measured turbulence level, the rms tracking error, and pilot ratings for all lateral and longitudinal tasks. If the bank angle results are plotted as in Figure 3, the resulting Figure 5 shows that the prediction method works well for all the normal (no control failure) mode airplanes.

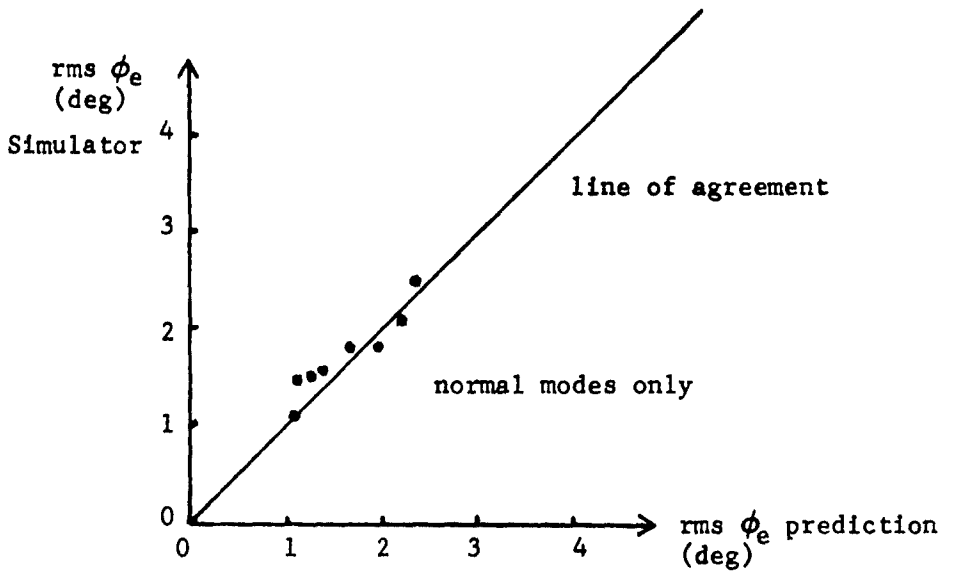

Figure 5. F-5 and A-7 bank angle prediction and simulation data.

If all configurations are considered, including the many cases of control and augmentation failures, the agreement is as shown in Figure 6.

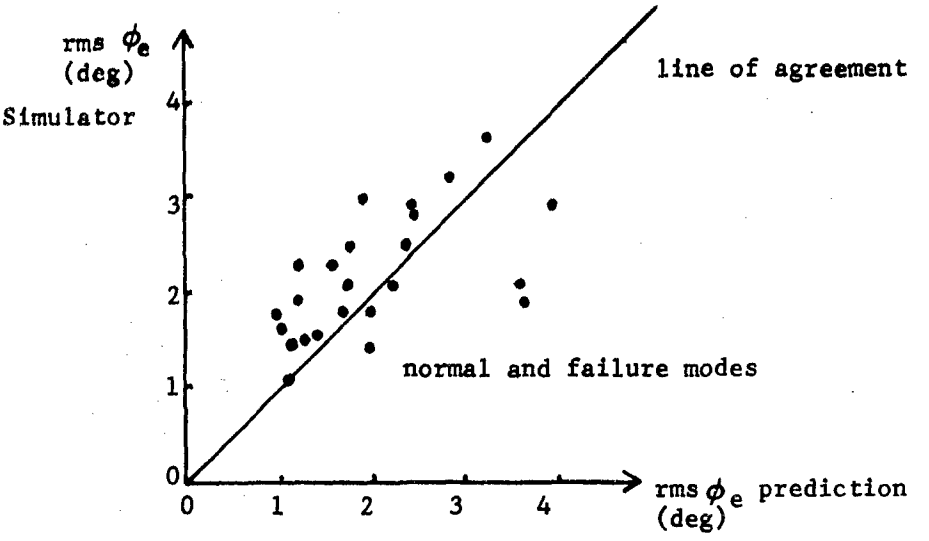

Figure 6. F-5 and A-7 bank angle prediction and simulation data.

The pitch angle task in turbulence is analogous to the bank angle task described above, and the averages of the simulator data compared to the predictions are shown in Figure 7 for normal mode airplanes, and in Figure 8 for all configurations.

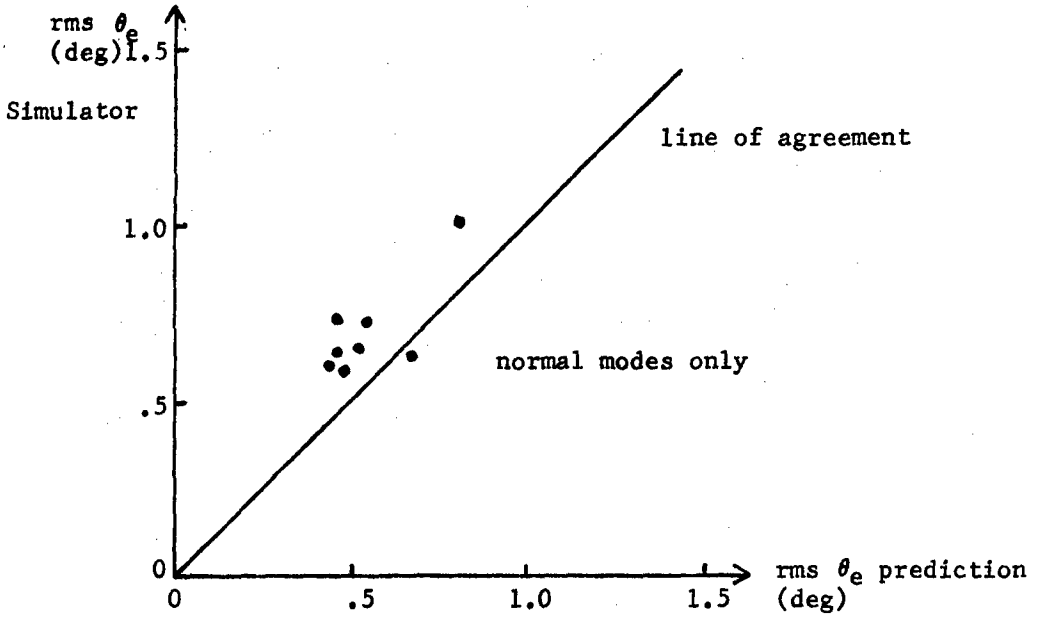

Figure 7. F-5 and A-7 pitch angle prediction and simulation data.

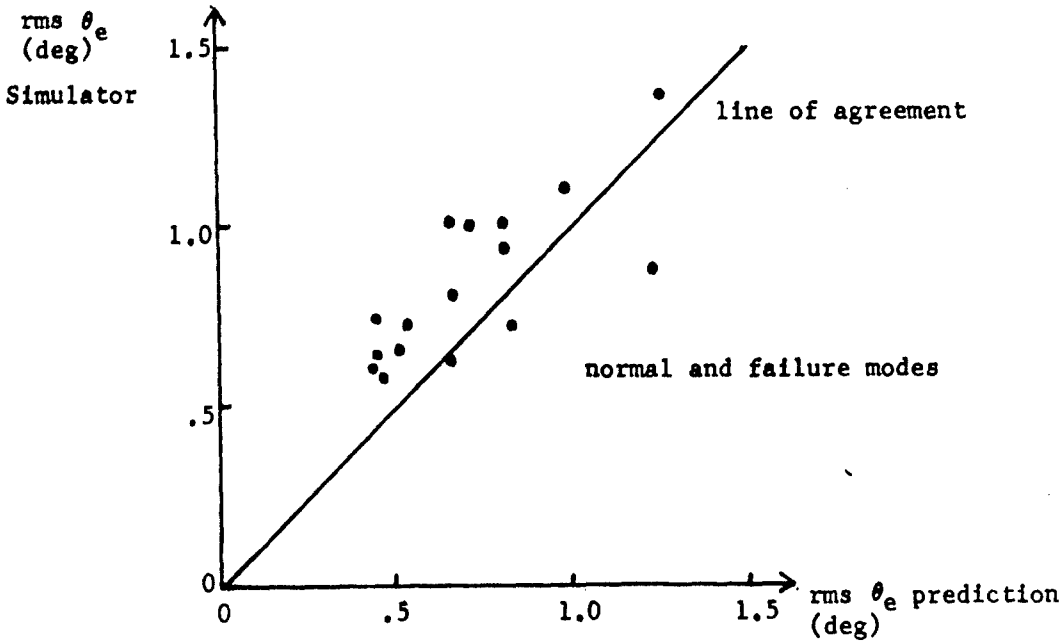

Figure 8. F-5 and A-7 pitch angle prediction and simulation data.

A statistical analysis of these data is given in Reference 2 which indicates that for the bank angle task the average percent error of the predictions is 13.35 for the normal mode airplanes over a range in the predicted tracking errors of 205 percent.

PILOT RATINGS IN TURBULENCE

As indicated above, pilot ratings were taken during the validation simulation. The earlier study of the T-33 configuration in the BB-2 series suggested that acceptability to pilots of airplanes in turbulence is largely independent of acceptability in still air. Since what was desired was a way of evaluating the pilot workload, the ratings were obtained in the following way.

Pilot ratings were requested after repeated flights at approximately the same gust level. The pilots were given a simplified rating sheet and asked to rate the difficulty of the task, but not to rate the roughness of the ride or to compensate the rating for the turbulence level. The pilots felt some uncertainty about the meaning of such ratings in turbulence, but they were able to assign numbers without difficulty. The consistency of the pilot ratings for the two test pilots is shown in Figure 9. Here the ratings for the entire bank angle simulation are cross plotted for the two pilots. A count shows that 83 percent of the ratings are within one rating unit of agreement.

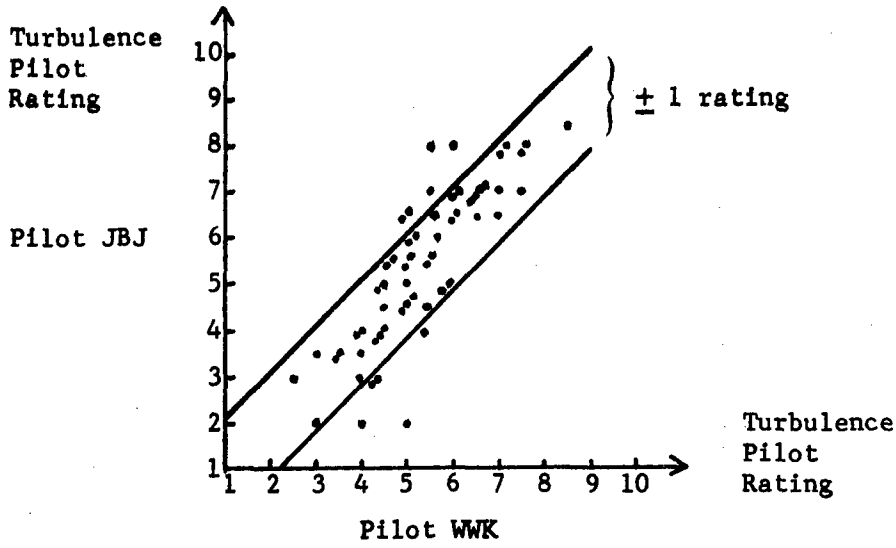

Figure 9. Agreement between pilot ratings for the two test pilots in the bank angle simulation.

It should be carefully noted that the pilot ratings obtained in the above manner may not correspond to familiar Cooper or Cooper Harper rating scales since these scales reflect the global merit of the airplane in still air tasks or in turbulence. If given accurately, the Cooper or Cooper Harper ratings in turbulence may be only weakly related to turbulence intensity since the pilot might compensate the rating for the turbulence level. In other words, the pilot might reason, after a particular flight in rough air, that the flight was difficult but the gusts were very strong and, therefore, the airplane must be given a good rating since it was controllable in the presumed heavy turbulence. On the other hand, the pilot might have been flying a configuration that was very susceptible to atmospheric disturbance under conditions of only light to moderate turbulence. Since the pilot can in no way sense the turbulence level, he is not able to estimate how good an airplane is with respect to the gust intensity. Thus, by asking for the actual workload, a more precise measure of airplane controllability can be obtained. Since the pilots agree in their ratings, this method appears to open up a promising area of pilot evaluation.

These turbulence ratings, according to the method announced above, increase numerically with the turbulence level. Figure 10 shows an example from the validation simulation where individual flights are indicated by the points, the predictions by the solid lines, and the ratings by the attached numbers.

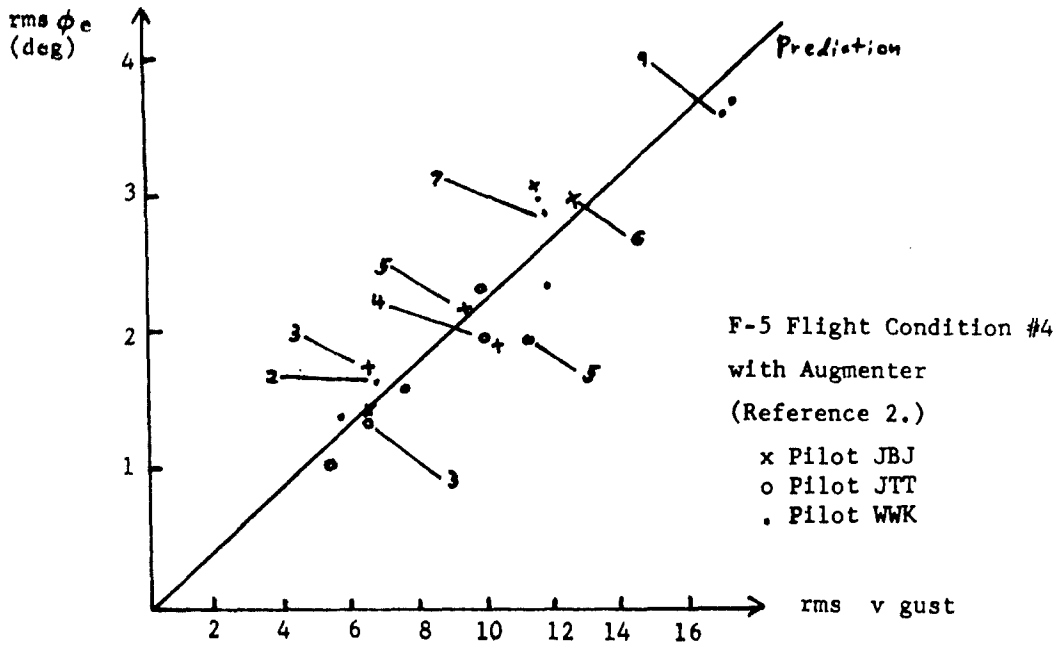

Figure 10. Pilot ratings at differing gust intensity for the bank angle task in turbulence.

The relative independence of the still air and the turbulence flying qualities is not unexpected if the nature of the system disturbance inputs is considered. First of all, any still air inputs enter the dynamics through the pilot and hence the airplane controls; turbulence enters directly into the airframe dynamics through arbitrarily different transfer functions. Since the spectral content of these two kinds of inputs also differs markedly, it is not meaningful to attempt to evaluate either of these control situations in terms of the other. A word of caution; as pointed out above, it is imprudent to regard good still air handling qualities as an indication of good characteristics in turbulence. Furthermore, it is just as risky to base any flying qualities analysis procedure whose objective is global still air rating on analysis or flight testing of the turbulence task. Flying qualities in turbulence and in still air are two different quantities and must not be confused.

An examination of the data also reveals that the turbulence pilot ratings do not correlate well with tracking error. Figure 11 shows a cross plot of these quantities for the bank angle task for the normal F-5 and A-7 airplanes at all turbulence levels.

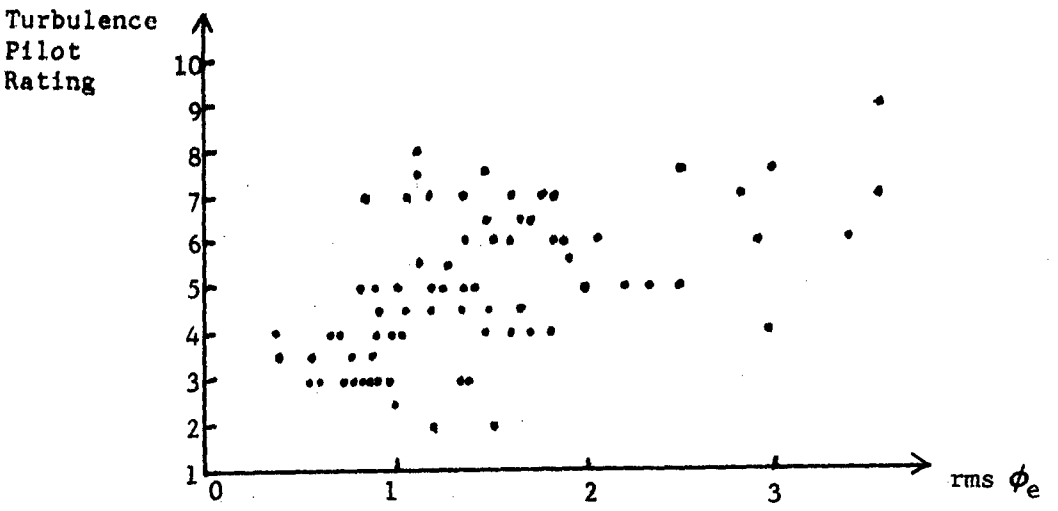

Figure 11. Bank angle errors versus turbulence pilot ratings for normal F-5 and A-7 airplanes

This lack of correlation between turbulence pilot rating and tracking error is not to be regarded as a defect in the rating method, but as an important feature of the nature of flying qualities in turbulence. Many of the airplanes studied were easy to fly in turbulence, yet had higher tracking errors than some very touchy airplanes that had lower tracking errors. Since the turbulence pilot ratings were defined as essentially a pilot workload level, this simply says that pilot workload is determined by many factors such as sensitivity to stick amplitude - analogous to pilot model gain - together with the more expected parameters of pilot lead, tracking error, and gust level. One area of further research is to identify these factors and their relative importance from the 500 pilot ratings reported in Reference 2.

FINAL REMARKS

It is clear at this point that the five conditions for a useful prediction and evaluation method for flying qualities in turbulence have been easily met. The method employs a standard model for the pilot-airplane system that has only one adjustable parameter. All other quantities are fixed and yet the agreement between the predictions and the simulator flight test data show useful accuracy over a large range of gust susceptibility. Furthermore, the graph of tracking error versus this one free parameter reveals much about the difficulty of the pilot's task.

These methods have been in use at Northrop and elsewhere for several years now, and some interesting applications have been made. One case that illustrates the usefulness of these techniques arose during the design of an augmentation system. It turned out that the optimum system for still air was not very good in low level turbulence and that another near optimum augmenter in still air noticeably improved the weapons delivery performance

in the expected turbulence of the primary mission. The ease of application of the method is enhanced by the availability of a digital computer program that was prepared during the course of the above program. It will accept arbitrary equations of motion, up to sixteen, and automatically generates the multiloop transfer functions for arbitrary pilots models in both lateral and longitudinal tasks. This is available upon request from the Flight Dynamics Laboratory Wright-Patterson Air Force Base.

REFERENCES

1. Onstott, E. D., and Salmon, E. P., Airplane Flying Qualities in Turbulence, AFFDL-TR-70-143 Air Force Flight Dynamics Laboratory, Wright-Patterson Air Force Base, Ohio Feb. 1971

2. Onstott, E. D. et al, Prediction and Evaluation of Flying Qualities in Turbulence, AFFDL-TR-71-162 Air Force Flight Dynamics Laboratory, Wright-Patterson Air Force Base, Ohio Feb. 1972

SESSION X

Manual Control of Non-Flying Vehicles

SIMULATION INVESTIGATION OF DRIVER/VEHICLE PERFORMANCE IN A HIGHWAY GUST ENVIRONMENT

D. H. Weir, R. K. Heffley, and R. F. Ringland
Systems Technology, Inc.
Hawthorne, California

ABSTRACT

Procedures for investigating the effect of aerodynamic disturbances on a dynamic system consisting of driver and vehicle in highway operation are developed and illustrated. The disturbing forces and moments are determined from model scale experiments in a wind tunnel. The lateral-directional dynamic response of the vehicle is characterized by differential equations of motion, and multiloop describing functions are used to model the driver's steering control response to perceptual cues. The resulting driver/vehicle system is subjected to the measured aerodynamic disturbances using a digital simulation, and the path performance is obtained for a range of situational variables and driver/vehicle control characteristics. Corresponding full scale field investigations serve to confirm the simulation results. The resulting performance estimates are useful in assessing the effects of varying vehicle design, highway geometry, and operational constraints.

INTRODUCTION

Increasing attention is being paid to car/driver handling and performance problems. Highway gusts can provide one source of disturbance input to the vehicle which can lead to safety performance difficulties under certain conditions. Analytical and experimental techniques have been developed to investigate response and performance in gust disturbance situations, and they are described in this paper.* The resulting techniques are useful in vehicle design and highway planning and design activities.

The approach presented involves an empirically based, combined analysis procedure, for estimating safety performance in a given gust disturbance situation. The empirical bases consist of data and models for driver behavior and vehicle response, wind tunnel or full scale data to quantify the disturbing forces and moments, and supplementary full scale tests to confirm the analytical results.

The paper begins by describing the car/driver analysis procedure. Then a car-truck aerodynamic disturbance example illustrates the application and provides for comparison with real-world results. A list of symbols is included in the Appendix.

DRIVER/VEHICLE ANALYSES

The typically skilled driver adjusts his steering response properties to suit the vehicle's handling dynamics, thereby achieving some acceptable or required level of directional performance in path following and disturbance regulation tasks[1-3]. Variations in driver control characteristics with attention, skill, fatigue, and degradation of visual cues cause changes in path following (lane keeping) performance in the presence of an aerodynamic disturbance input.

Driver Describing Function and Perceptual Structure

Operation in a highway gust environment results in a significant aerodynamic disturbance only under certain environmental and operational conditions. Thus, the driver can not necessarily expect a large input, and he must compensate for path errors as they develop. Precognitive operation involving execution of a learned, internally programmed, discrete steering response is not generally appropriate. The driver's compensatory closed-loop steering control with gust disturbances can be quantified by a quasi-linear describing function[1-3] which contains the following driver parameters:†

- Gain, which expresses the amount of steering correction for a perceived level of error.
- Time delay, which accounts for latencies due to perception, interpretation, and neuromuscular actuation.
- Equalization, which tailors the form of the driver's response to suit a given vehicle's handling qualities.

*The results reported here derive in part from research accomplished for the Federal Highway Administration, Office of Research, under Contract FH-11-7570. They reflect the opinions of the authors and not of the Federal Highway Administration.

†Remnant effects can be added to the quasi-linear behavior to account for control inputs not linearly correlated with the disturbance. Such effects generally cause a small added random variation in driver steering response and in the vehicle path.

Preceding page blank

These parameters, together with the vehicle handling dynamics determine the car/driver system performance.

The structure of the car/driver system used in the analyses is given in Fig. 1. The driver is assumed to respond to perceptual feedbacks of car heading angle (ψ) and lateral deviation (y_I) to produce a net steering wheel correction (δ_{sw}). While not unique, these heading and path feedbacks satisfy the system's guidance and control requirements, as well as driver centered requirements relating to ease of control and good subjective opinion of his ability to accomplish the driving task[1]. As later shown, the resulting computed car/driver performance compares well with that observed in full-scale. The feedbacks may change as the situation varies.

Car Dynamics

Estimating car/driver system steering response and performance requires numerical definition of the car's lateral-directional dynamic response properties, Y_c. A three-degree-of-freedom (heading, lateral velocity, and roll) vehicle model was used. These equations for car motion response to driver steering wheel and aerodynamic inputs were initially based on design data from the vehicle manufacturer, as modified for a standard experimental loading condition (driver, experimenter and 350 lbs of instrumentation). These initial estimates were then refined using measured dynamic responses (from full-scale tests) to obtain more precise results. A comparison of the measured (full-scale) and analytically computed (model) vehicle responses to a test steering wheel input (δ_{sw}) is given in Fig. 2. The heading angle rate (r), roll angle rate (p), and lateral acceleration (a_y') all show excellent agreement between the analyses and full-scale tests. The complete equations and additional details are given in the Appendix.

The steering response transfer functions resulting from the equations are:

Heading angle, ψ:

$$\frac{\psi}{\delta_{sw}} = \frac{0.67(s+3.8)[s^2+2(0.28)(8.5)s+(8.5)^2]}{s[s^2+2(0.61)(4.5)s+(4.5)^2]} \qquad [s^2+2(0.35)(9.2)s+(9.2)^2] \qquad (1)$$

Lateral deviation, y_I:

$$\frac{y_I}{\delta_{sw}} = \frac{3.1[s^2+2(0.08)(7.7)s+(7.7)^2]}{s^2[s^2+2(0.61)(4.5)s+(4.5)^2]} \qquad [s^2+2(0.26)(7.3)s+(7.3)^2] \qquad [s^2+2(0.35)(9.2)s+(9.2)^2] \qquad (2)$$

The moderately damped, high frequency quadratic pair in the numerator and denominator of each transfer function is realted to the roll mode, and it tends to cancel out.

For purposes of estimating driver dynamic behavior, a simpler set of two-degree-of-freedom (heading and sideslip) equations is used. The corresponding simplified steering wheel transfer functions at 60 mph are:

Heading angle, ψ:

$$\frac{\psi}{\delta_{sw}} = \frac{0.49(s+3.5)}{(s)[s^2+2(0.63)(4.04)s+(4.04)^2]} \qquad (3)$$

Lateral deviation, y_I:

$$\frac{y_I}{\delta_{sw}} = \frac{2.82[s^2+2(0.17)(7.3)s+(7.3)^2]}{s^2[s^2+2(0.63)(4.04)s+(4.04)^2]} \qquad (4)$$

The roll mode effects are included implicitly in these expressions, and they are used in the car/driver closed-loop analyses presented below.

Nominal Car/Driver Response Properties

Based on the car/driver loop structures and vehicle response properties, driver dynamic response can be estimated using the previously developed describing function models[1-3]. The assumed feedbacks and computed vehicle dynamics indicated that an appropriate form for the driver describing function blocks in Fig. 1 is, for this example vehicle:

Heading response:

$$Y_{p_\psi} = K_{p_\psi} e^{-\tau_e j\omega} \qquad (5)$$

Lateral deviation (path) response:

$$Y_{p_y} = K_{p_y} \qquad (6)$$

Equation 5 shows that the driver's heading response is nominally a gain (K_{p_ψ}) plus a time delay (τ_e). The path response in Eq. 6 is a simple gain (K_{p_y}).

Combining the driver characteristic Y_{p_ψ} with the car heading transfer function of Eq. 3 gives the car/driver heading response properties of Fig. 3. The open-loop frequency response on the right of Fig. 3 shows a heading crossover frequency (bandwidth) of about 2.3 rad/sec, which is based on established driver modeling rules, and (in part) values observed in recent describing function measurements[2,3] for a range of drivers in simulated steering control tasks with crosswind gust inputs. The resulting closed-loop heading response dynamics are shown on the root locus, on the left side of Fig. 3, as solid rectangles. These inner-loop results (roots) become the outer-loop starting point (roots) for estimating the lateral deviation response in Fig. 4. The frequency response in Fig. 4 shows an outer-loop lateral deviation crossover frequency (path bandwidth) of about 0.4 rad/sec.

The car/driver system described by Figs. 3 and 4 is designated as car/driver combination A in the subsequent example, and it is the nominal case.

To obtain the desired performance estimates for the various situations, the resulting car/driver response models are subjected to aerodynamic force and moments inputs, derived from wind tunnel measurements (as described below). For a given situation, an aerodynamic disturbance causes side forces, yawing moments, and rolling moments on the car which change with time as the car proceeds at some relative speed. Operationally, with the car/driver model, the effect is treated in the time domain using digital computation. The closed-loop equations of motion for the car/driver system are integrated in the presence of a given aerodynamic input to obtain the time history of driver steering control actions and vehicle motion response.

TABLE I

DRIVER DESCRIBING FUNCTION PARAMETERS†

DRIVER MODEL	CROSSOVER FREQUENCY		GAIN		REMARKS
	ω_{c_ψ} (RAD/SEC)	ω_{c_y} (RAD/SEC)	K_{p_ψ}	K_{p_y}	
A	2.3	0.4	0.56	0.25	60 mph nominal
D	1.5	0.2	0.42	0.13	60 mph degraded
E	2.3	0.9	0.56	0.57	60 mph optimum

†The driver's effective delay, τ_e, is a nominal 0.40 sec in all cases.

Variations in Car/Driver Response Properties

The car/driver response properties shown in Figs. 3 and 4 represent a nominal case. Degrading or improving the car/driver dynamic characteristics produces corresponding changes in path performance. This can result from changes in the driver, the car, or both. The levels of driver behavior are determined by the describing function parameters (gain, time delay, and equalization). Changes in the car handling dynamics can occur by varying the load, tire properties, etc, or by using a different disturbed vehicle. The general result is to change the system bandwidth and other response properties, which in turn modify the path performance.

Changes in driver gain provide an appropriate way to demonstrate such variations. For the standard car, the effects on path performance of changes in driver gain (response amplitude and alertness) are presented in Fig. 5 for the example gust disturbance discussed subsequently. The three car/driver combinations are summarized in Table I. The performance in Fig. 5 is given in terms of both peak deviation (y_I) and integral absolute deviation $\overline{|y_I|}$, where

$$\overline{|y_I|} = \frac{1}{T}\int_0^T |y_I| dt \qquad (7)$$

This approximates the standard deviation under some conditions, and provides an estimate of path variability. Peak deviation ($\hat{y}_I$) is more convenient to use, and the trends are similar in the region at and below the optimum. The main difference in the measures is seen in Fig. 5, where $\hat{y}_I$ continues to decrease even though the steering response becomes very oscillatory. This undesirable (and unrepresentative) oscillation is reflected in larger values of $\overline{|y_I|}$ above $K_{p_\psi}K_{p_y} = 0.4$. Hence $\overline{|y_I|}$ provides a better measure of overall performance and stability, as described below.

While "optimum" performance as measured by $\overline{|y_I|}$ occurs for $K_{p_\psi}K_{p_y}$ values* between 0.38 and 0.44, such values are separated from the stability limit by gain margins of only 35 percent to 20 percent. These do not allow for inherent car/driver response variability, and the driver will normally adopt somewhat lower levels of activity. The response qualities are further demonstrated in Fig. 6 which compares selected lateral deviation and steer angle responses to a discrete disturbance for these two gain values with those for an overall gain of 0.32 (car/driver E). The comparison clearly shows that the highest value is close to a sustained car/driver oscillation, and the midvalue is still more oscillatory than is consistent with observed driver behavior. Furthermore, any decrease in driver time delay will make the response more oscillatory.† Hence, faster driver reactions or an increased level of effort will serve to worsen performance. In view of these considerations, car/driver E represents about the best that can reasonably be expected of an alerted experienced driver with this vehicle.

Car/driver A (Table I) has about half of the car/driver E lateral deviation gain and a nominal gain margin of 6 dB (Fig. 4), which is representative of normal operation. Figure 5 shows it to be on the conservative edge of the good performance minimum, and well suited as a nominal, typical case. As a representative degraded case, car/driver D reflects not only a further reduction in outer-loop (lateral deviation) gain, but also a departure from the inner-loop characteristics shown in Fig. 3. As already mentioned, this combination has a dual character in that it can be either a standard car and a degraded driver, or a degraded car and a nominal driver.

COMPUTATIONAL PROCEDURE

The overall flow chart of the computation process is shown in Fig. 7. The wind tunnel force and moment coefficient data, properly scaled, act as forcing functions for the equations of the car/driver system. These equations are integrated digitally and plotted for ease in assessing the safety performance measures.

*The value of K_{p_ψ} used here is referred to the steer angle, δ_w.

†These gain levels, which are roughly three times more than for car/driver A, shift the amplitude crossover line on the frequency response plot of Fig. 4 down about 10 dB; the gain line would then pass below the amplitude ratio peak at about 3 rad/sec. The phase angle at this frequency is roughly −260 deg, so the system, corresponding to these higher gain levels, is phase rather than gain stabilized. This means that any reduction in phase lag will tend to decrease rather than increase the closed-loop damping.

The basic wind tunnel data provide normalized side force (C_y), yawing moment (C_n), and rolling moment (C_ℓ) coefficients, as functions of the crosswind direction and the longitudinal car location in the disturbance. The basic moment coefficients are referenced to the ground plane at the midpoint of the wheelbase, and these are translated to the car center of mass for purposes of analysis. Examples of these data are shown below.

The computer program used to integrate the car/driver equations uses linear interpolation between the basic data points of the forcing functions to achieve an integration interval of 0.05 sec. The integration method is second-order Runge-Kutta. The output plots include lateral acceleration (a_y), lateral deviation (y_I), heading rate (r), heading angle (ψ), roll rate (p), and front wheel steer angle (δ_w).

TRUCK-INDUCED AERODYNAMIC DISTURBANCE EXAMPLE

A typical disturbance example is given by the aerodynamic forces and moments on a car due to air flow caused by a large adjacent vehicle such as a truck[4]. These forces and moments can pull the car toward the truck or push it away, depending on the conditions. One disturbance component occurs in still air due to displacement of the air around the front of the truck. Another component results with an ambient crosswind, when the car is on the downwind side moving in and out of the wake behind the truck. The emphasis is on steering control. A convenient single performance measure is the "peak lateral deviation" of the driver/vehicle system during a truck disturbance.

The example situation consists of a full-sized station wagon passing a tractor/semitrailer truck on a two-lane roadway. Variations in performance with crosswind and car-truck lateral separation are shown. Other situational variables which have been investigated include truck size and shape, car type, and relative speed.

Wind Tunnel Data

Wind tunnel experiments were used to obtain aerodynamic force, moment, and flow data. These data provided the needed inputs to the analyses, and the flow measures helped to correlate the analytical and model scale results with the full-scale measures.

The basic tests were run in the Northrop Aircraft 7×10 ft subsonic wind tunnel using 1/10 scale models. The metric model was a 1970 full-size station wagon. It contained a six-component strain gauge balance, connected to the yaw table in the tunnel floor by a balance block and strut. A probe was mounted ahead of the car (on its centerline) to measure the angularity and magnitude of the local horizontal flow component. The truck model was a 86 in. cab over engine tractor (186 in. wheelbase) towing a 40 ft two-axle dry freight van. Line drawings of the models are shown in Fig. 8. The models were mounted on a 10 ft diameter yaw table set in the tunnel floor. Special floor plates were fabricated to permit movement of the interfering truck model relative to the metric car model. Most of the tests were run at a dynamic pressure, q, of 140 psf, corresponding to a tunnel airspeed of 343 ft/sec. At each location the entire assembly was tested at zero deg and yawed ±5, ±10, ±20, and ±30 deg to simulate the effect of various crosswinds. The resultant force and moment data for the car were then cross plotted to give variations with position for a given crosswind flow angle.

Example force and moment data on the car are given in Figs. 9 and 10. The zero crosswind plot of Fig. 9 shows the measured yawing moment coefficient (C_n) and side force coefficient (C_y) for the car as functions of relative car position (x_r) for various lateral separations. The data show the large disturbance of the car due to the bow wave adjacent to and in front of the tractor which characterizes the axial flow (zero crosswind) situation.

Crosswind results for three truck configurations are given in Fig. 10 for a flow angle of −20 deg, with the car downwind of the truck at various points in the wake. The large disturbances due to crosswind flow through and under the standard truck are apparent by comparison with the data for a rectangular block and for the trailer with a van underbody.

Car/Driver Response and Performance Estimates

Example results are given in Fig. 11 for car/driver A at 60 mph, passing the truck at 50 mph in an 18 mph ambient crosswind (−20 deg crosswind towards the car). The figure shows lateral acceleration (a_y), lateral deviation (y_I), heading rate (r), and driver steer angle* (δ_w) as a function of the car center of mass location relative to the front of the truck. Note that the car mass center is a few inches ahead of the mid-wheelbase. In Fig. 11 the peak lateral deviation ($\hat{y}_I$) is about 2.6 ft toward the truck, occurring at a point alongside the front of the trailer. The steer angle trace shows that the driver makes several steering corrections in an effort to stay in the center of his lane. These steering corrections are reflected in the high frequency heading rate and lateral accelerations of the car, along with the car/driver response to the external forces and moments.

Repeating the calculations of Fig. 11 for a variety of crosswind angles and magnitudes, and taking the peak lateral deviation ($\hat{y}_I$) in each case, leads to the type of performance cross plot shown in Fig. 12. Here car/driver system A is going 60 mph, passing the truck which is proceeding at 50 mph. The respective vehicle centerlines are 12 ft apart. The car's peak lateral deviations are measured from the lane centerline for the corresponding conditions. Positive values of $\hat{y}_I$ are toward the truck. The Fig. 12 curves represent the extreme deviation in a given encounter; all other deviation amplitudes during the maneuvers fall within the curves. This region of response levels is shown shaded in Fig. 12, and labeled a performance corridor.

*Steer angle (δ_w) is measured at the front wheel, while δ_{sw} in Fig. 2 is measured at the steering wheel. The steering system gain under dynamic conditions is about 32 to 1.

Figure 12 shows that the severity of the disturbance depends on the magnitude and direction of the ambient wind. For zero crosswind ($\psi_W = 0$) the main effect of the truck disturbance is to push the car away from the truck a small amount. For positive crosswinds, the truck wake is blown away from the car. The bow wave disturbance persists, and the performance is roughly unchanged from the zero crosswind case, as shown in Fig. 12. For negative crosswinds, however, where the truck wake is blown towards the car, there is a significant decrement in performance for flow angles beyond about −15 deg. The disturbance now pulls the car toward the truck, with increasingly larger excursions as the relative crosswind increases in magnitude, and the peak displacement can exceed the boundary of a 12 ft lane.

Ambient headwind components can have a significant added influence because the magnitude of the force and moment inputs to the car is proportional to the product of car and truck airspeeds. This is illustrated by the dashed boundaries in Fig. 12.

In summary, the example simulation results of Fig. 12 divide the car-passing-truck problem into two basic situations. The first is the zero crosswind case, where the truck interference effect pushes the car away, sometimes to distances approaching the lane boundary. This is also representative of car passing upwind of truck in a crosswind. The other is the leeward pass (car downwind) in a relatively strong crosswind where the truck interference effect pulls the car towards the side of the truck. Headwinds increase, and tailwinds diminish, these consequences.

Full-Scale Tests

Full-scale tests with instrumented vehicles were accomplished for car-truck distrubance situations to verify the analytical results and to measure driver psychophysiological response. The station wagon was instrumented with rate gyros, accelerometers, speed tachometer generator, steering wheel potentiometer, and relative wind vector vane. A vector vane was also fitted to the truck.

The full-scale tests were run on two-lane perimeter roads at the STI Mojave Airport Test Site. This permitted a wide range of relative wind angles and road conditions, and provided realistic situations for close proximity passing of car and truck. The perimeter roads had a paved surface about 24 ft wide with soft shoulders. There was very little crown or grade, and the tangent test sections were approximately one mile long.

Full-scale and model-scale flow properties were measured using the car model prove and the corresponding forward mounted full-scale vector vane. An example comparison is given in Fig. 13. The car at 60 mph is passing on the downwind side of the truck which is going 45 mph. The free stream crosswind relative to the truck was approximately −4 deg, while the ambient crosswind was about 10 ft/sec at −40 deg. The basic time traces are the full-scale vector vane angle ($\measuredangle WV_1$) and velocity ($|WV_1|$). Overlaid, in the region of the truck, are the wind tunnel flow probe measurements. The comparison is seen to be very good. This serves to confirm the basic applicability of the wind tunnel results to the full-scale conditions because if the flow field around the truck and car are the same in model and full-scale, then the forces and moments will correspond.

Car/Driver Dynamic Response Comparison

A typical data comparison is shown in Fig. 14 where the full-scale data correspond to the car at 62 mph passing a 45 mph truck. The car is downwind and the flow angle is about −11 deg relative to the truck. The driver was skilled and alerted. The full-scale lateral deviation (y_T) measure was obtained by double integrating lateral acceleration. It shows variations about the car's lane centerline. The truck was proceeding in the center of its lane.

The nominally comparable analytical results are shown in Fig. 14 for car 60 mph, truck 50 mph, a crosswind relative to the truck of −15 deg, and (the good) car/driver E. The full-scale y_T data show a drift toward the truck of about 2 ft in the wake region, followed by a 1 to 2 ft push away from the truck due to the bow wave. The full-scale and analytical bow wave disturbances match well, but the full-scale wake response begins further aft of the truck due to variability in the real wind and/or initial car/driver misalignment in the lane. The somewhat larger amplitude of the full-scale responses is due in part to the full-scale ambient head wind component of about 13 ft/sec. The lateral acceleration, heeding rate, and steering wheel response traces, full-scale and analysis, show similar dominant features in the vicinity of the truck, bearing in mind that the two plots are mirror images. The dominant period (peak-to-peak interval) in the lateral acceleration response alongside the truck is about 50 to 60 ft relative distance in both cases. The additional, lower amplitude random response which persists throughout the full-scale data is due, of course, to added random disturbances and variability in the real world. It results from such things as turbulence in the ambient wind, roadway irregularities, and additional driver steering response (modeled as remnant in an operational description of the driver).

Taken together, these and other full-scale results demonstrate the applicability of the empirically based analysis and simulation to estimating car/driver response and performance in highway gust disturbance situations. The results of this type of investigation are useful in vehicle and highway design and in defining criteria for rules and limits in traffic operations.

REFERENCES

1. Weir, David H., and D. T. McRuer, "A Theory for Driver Steering Control of Motor Vehicles," Road User Characteristics, Highway Research Record No. 247, 1968, pp. 7-28.

2. Weir, D. H., and Charles K. Wojcik, "Simulator Studies of the Driver's Dynamic Response in Steering Control Tasks," Driving Simulation, Highway Research Record No. 364, 1971, pp 1-15.

3. Weir, David H., and Duane T. McRuer, "Measurement and Interpretation of Driver-Vehicle System Dynamic Response," paper presented at Symp. on Psychol. Aspects of Driver Behavior, Noordwijkerhout, Netherlands, Aug. 1971.

4. Weir, David H., Robert F. Ringland, Robert K. Heffley, et al, An Experimental and Analytical Investigation of the Effect of Truck-Induced Aerodynamic Disturbances on Passenger Car Control and Performance, Systems Technology, Inc., Tech. Rept. 1001-1, Oct. 1971.

5. Weir, D. H., C. P. Shortwell, and W. A. Johnson, Dynamics of the Automobile Related to Driver Control, Systems Technology, Inc., Tech. Rept. No. 157-1, July 1966 (also SAE Paper No. 680194).

APPENDIX. CAR/DRIVER EQUATIONS AND CONFIGURATION

The car/driver equations of motion used in the analysis are listed in Table II. Equations 8 through 16, descriptive of the vehicle dynamics, are adapted from Ref. 5, with some simplifying approximations. The notation of Ref. 5 is used. Table III lists the vehicle data used. These are largely vehicle design data obtained from the manufacturer with certain parameters modified to match measured vehicle time responses as noted in the main text.

The appendix concludes with a list of symbols, Table IV.

TABLE II

CAR/DRIVER EQUATIONS OF MOTION

Lateral Acceleration

$$a_y = \frac{2}{57.3m}\left(\frac{\partial Y}{\partial \alpha_1}\alpha_1' + \frac{\partial Y}{\partial \alpha_2}\alpha_2'\right) - \frac{m_s e}{57.3m}\dot{p} + \frac{qA}{m}C_y(x_T) \tag{8}$$

Lateral Velocity

$$\dot{v} = a_y - \frac{U_c}{57.3}r \tag{9}$$

Heading Acceleration

$$\dot{r} = \frac{2}{I_{zz}}\left(a'\frac{\partial Y}{\partial \alpha_1}\alpha_1' - b'\frac{\partial Y}{\partial \alpha_2}\alpha_2'\right) - \frac{I_{pz}}{I_{zz}}\dot{p} + \frac{57.3qA}{I_{zz}}\left[\ell C_n(x_T) + \frac{a-b}{2}C_y(x_T)\right] \tag{10}$$

Heading Rate

$$\dot{\psi} = r \tag{11}$$

Roll Acceleration

$$\dot{p} = -L_p - L_\varphi\varphi - \frac{57.3m_s e}{I_\varphi}a_y - \frac{I_{pz}}{I_\varphi}\dot{r} + \frac{57.3qA}{I_\varphi}\left[tC_\ell(x_T) + \ell\lambda C_n(x_T) - (h_f + \frac{t}{2}\lambda)C_y(x_T)\right] \tag{12}$$

Roll Rate

$$\dot{\varphi} = p \tag{13}$$

Effective Front Tire Slip Angle

$$\alpha_1' = \delta_w - \frac{57.3}{U_c}v - \frac{a}{U_c}r + \epsilon_1'\varphi \tag{14}$$

Effective Rear Tire Slip Angle

$$\alpha_2' = -\frac{57.3}{U_c}v + \frac{b}{U_c}r + \epsilon_2'\varphi \tag{15}$$

Lateral Deviation

$$\ddot{y}_I = a_y \tag{16}$$

Driver Steer Angle Response

$$\delta_w = K_{p_\psi}[-\psi(t-\tau_e) - K_{p_y}y_I(t-\tau_e)] \tag{17}$$

Dynamic Pressure

$$q = \frac{1}{2}\rho U_T U_c \frac{\sqrt{1+\left(\frac{U_T}{U_c}\right)^2\tan^2\psi_I}}{\cos\psi_I} \tag{18}$$

Rate of Change of Relative Distances

$$\dot{x}_T = U_T - U_c \tag{19}$$

Subsidiary Relations

$$a' = a + \frac{\partial AT/\partial\alpha_1}{\partial Y/\partial\alpha_1} \qquad \epsilon_1' = \epsilon_1 + \frac{\partial \ell}{\partial\varphi_1}\frac{\partial Y/\partial\ell_1}{\partial Y/\partial\alpha_1}$$

$$b' = b - \frac{\partial AT/\partial\alpha_2}{\partial Y/\partial\alpha_2} \qquad \epsilon_2' = \epsilon_2 + \frac{\partial \ell}{\partial\varphi_2}\frac{\partial Y/\partial\ell_2}{\partial Y/\partial\alpha_2} \tag{20}$$

TABLE III

VEHICLE DESIGN PARAMETERS*

SYMBOL	UNITS	VALUE	SYMBOL	UNITS	VALUE
m	slugs	165.5	ρ	slugs/ft^3	0.002377
I_{zz}	slug-ft^2	4858.3	$m_s e/m$	ft	1.32
ℓ	ft	9.92	$m_s e/I_\varphi$	ft	0.2939
a	ft	5.86	$I_{\varphi z}/I_\varphi$	—	0.360
a'	ft	5.788	$I_{\varphi z}/I_{zz}$	—	0.0636
b	ft	4.06	$\partial Y/\partial\alpha_1$	lb/rad	7415.
b'	ft	4.182	$\partial Y/\partial\alpha_2$	lb/rad	13470.
t	ft	5.28	ϵ_1'	—	0.160
h_f	ft	-0.01	ϵ_2'	—	-0.100
λ	rad	0.096	L_p	sec^{-1}	-2.935
A	ft^2	23.9	L_φ	sec^{-2}	-62.5

*Test station wagon with instrumentation, driver and passenger.

TABLE IV. SYMBOLS

a	Distance from mass center to front axle
a_y	Car lateral acceleration (mass center)
a_y'	Car lateral acceleration at accelerometer
A	Vehicle frontal area
b	Distance from mass center to rear axle
C_ℓ	Rolling moment coefficient
C_n	Yawing (heading) moment coefficient
C_y	Side (lateral) force coefficient
e	Distance from center of sprung mass to roll axis
h_f	Roll axis height at front wheels
I	Moment of inertia
$K_{p\psi}$	Driver heading loop gain
K_{py}	Driver lateral deviation loop gain
ℓ	Wheelbase
L	Roll moment
m	Vehicle total mass
m_s	Vehicle sprung mass
p	Car roll angle rate
q	Dynamic pressure for force and moment scaling
r	Car heading angle rate
s	Laplace transform variable
t	Time; track
U_o	Car forward velocity (relative to ground)
U_T	Truck forward velocity (relative to ground)
v	Lateral velocity
x_T	Car mass center longitudinal position relative to truck front
y_I	Car lateral deviation (side-to-side position of car center of mass)
$\hat{y}_I$	Car peak lateral deviation from lane centerline
y_T	Lateral separation of car and truck centerlines
Y	Side (lateral) force
Y_c	Controlled element (vehicle) dynamics
Y_{py}	Driver describing function for lateral deviation control
$Y_{p\psi}$	Driver describing function for heading control
α	Tire slip angle
δ_{sw}	Car steering wheel angle
δ_w	Car front wheel steer angle (average of left and right)
ϵ	Roll steer coefficient
λ	Roll axis tilt angle
ξ	Camber angle
ρ	Air density
τ_e	Driver time delay
φ	Roll angle
ψ	Car heading (yaw) angle relative to roadway centerline
ψ_I	Ambient wind angle relative to roadway centerline (ground)
ψ_W	Crosswind angle relative to moving truck
ω_{c_y}	Crossover frequency for lateral deviation
ω_{c_ψ}	Crossover frequency for heading control

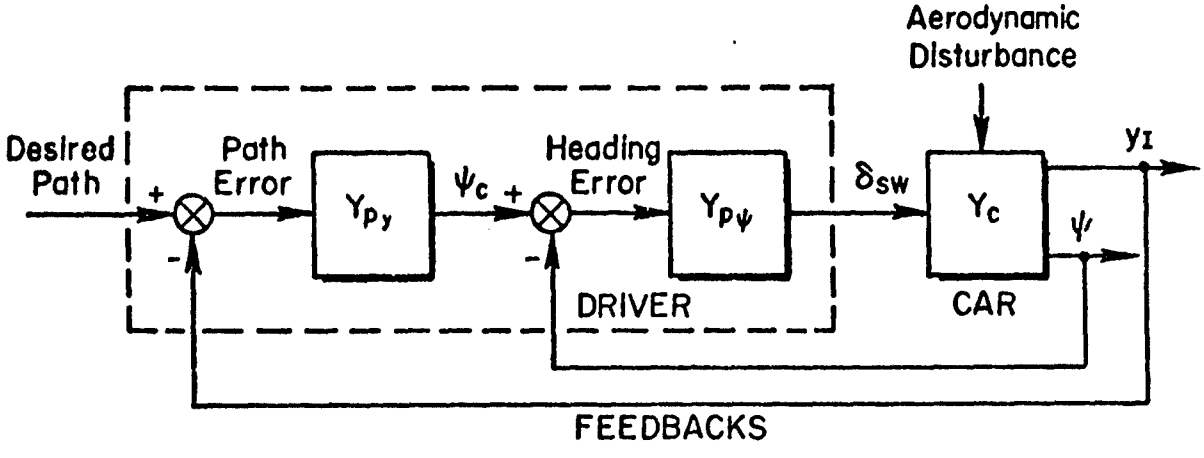

Figure 1. Driver/Vehicle System Structure for Analyses

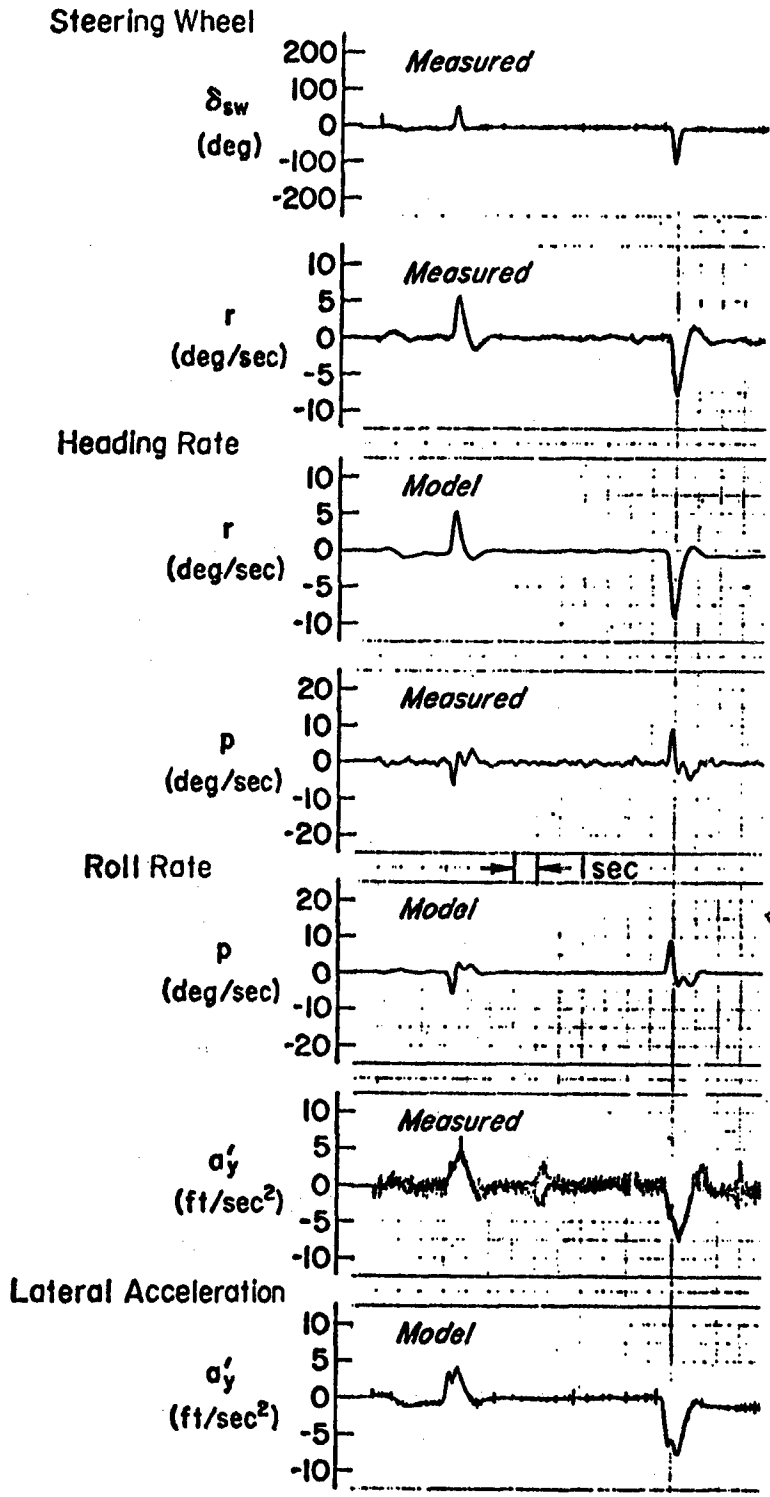

Reproduced from best available copy.

Figure 2. Comparison of Measured and Computed Car Dynamic Response at 60 mph

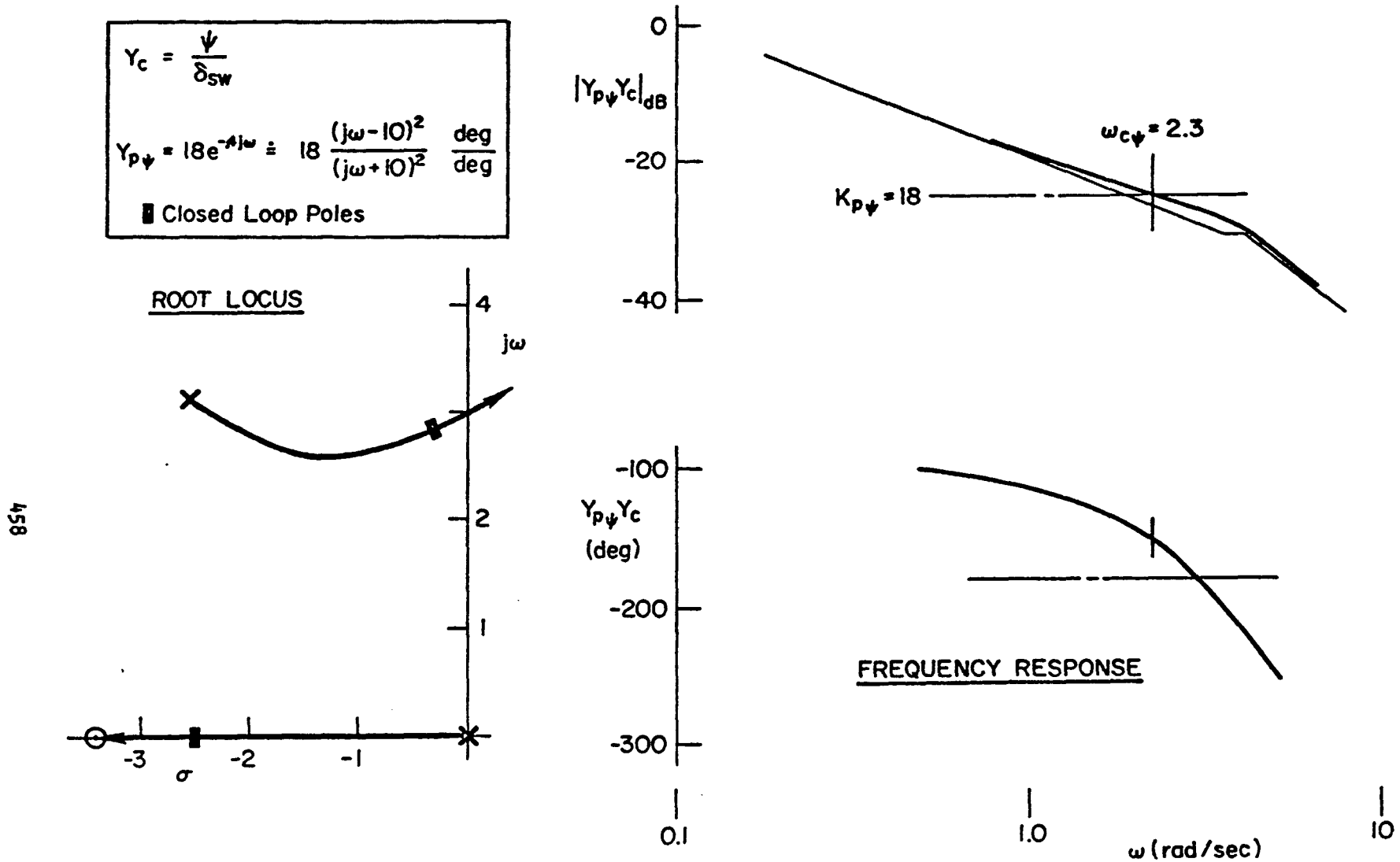

Figure 3. Car/Driver Response with Heading Angle Feedback

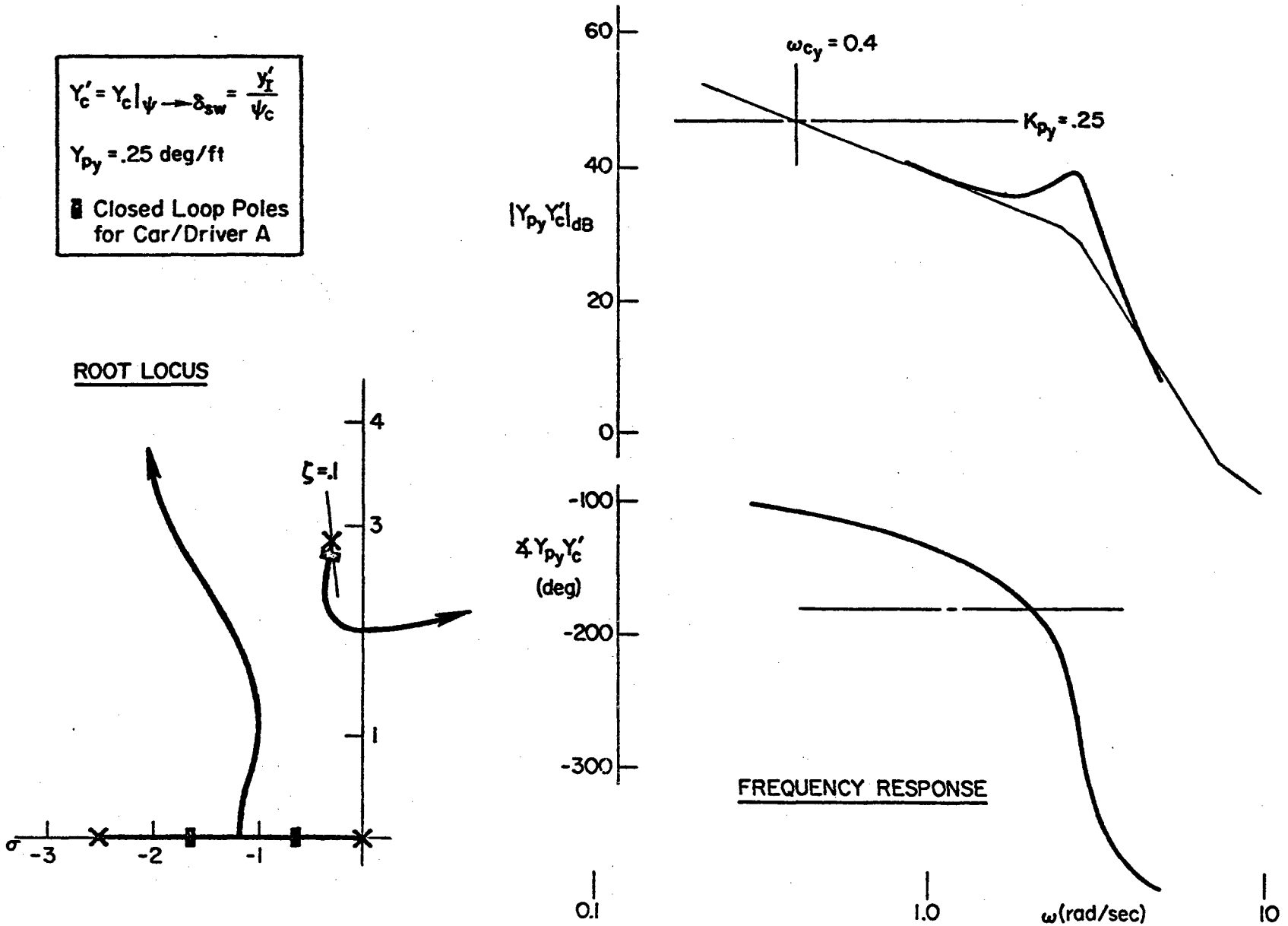

Figure 4. Car/Driver Response with Heading Angle and Lateral Deviation Feedbacks

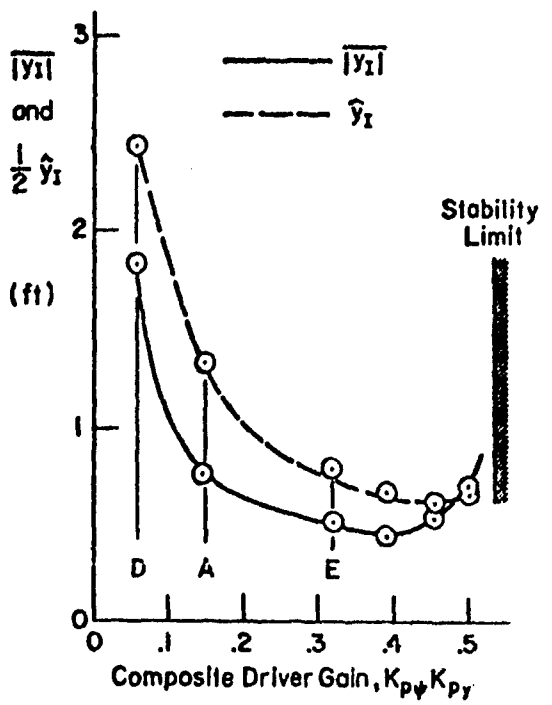

Figure 5. Effect of Driver Response on Performance: 12 Ft $\mathbb{Q}$ Separation, ψ_W = −20 Deg, Car 60, Truck 50

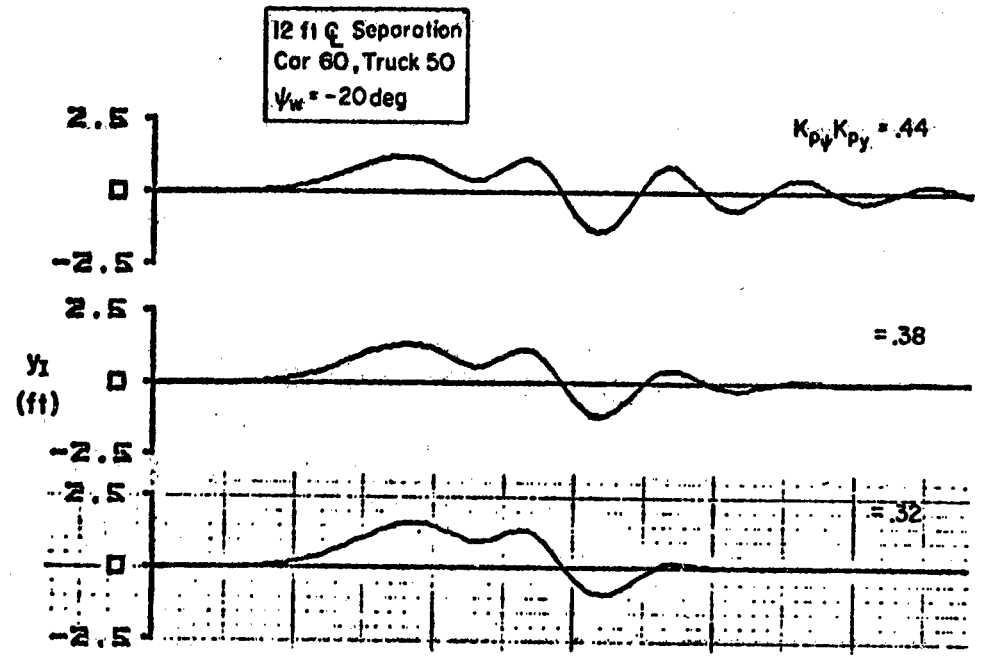

a) Lateral Deviation Responses

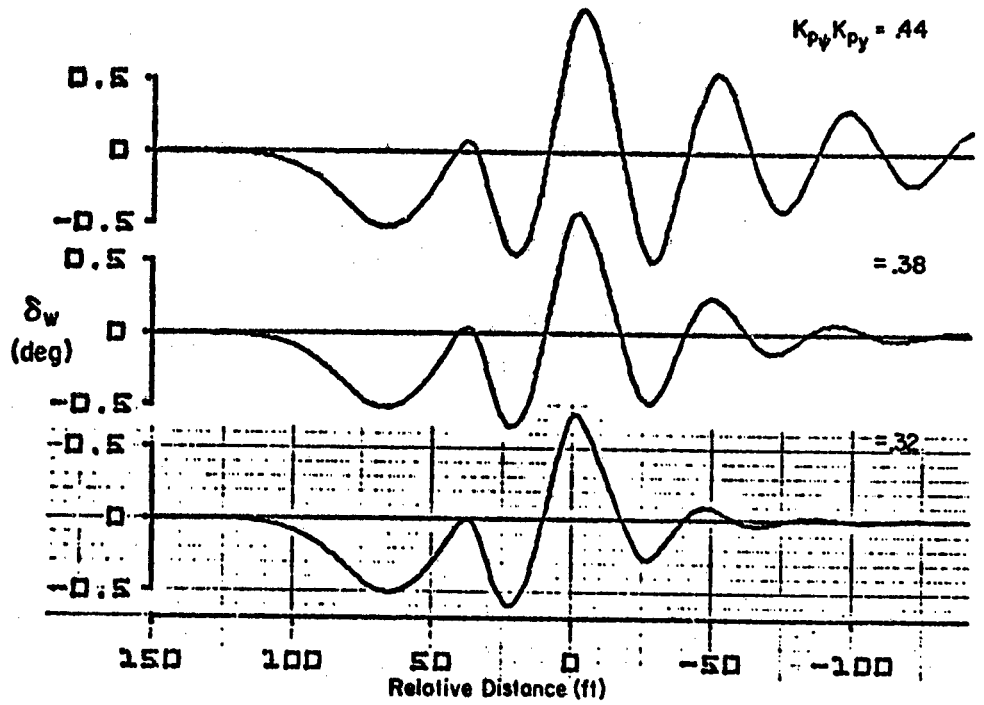

b) Steer Angle Responses

Figure 6. Computed Effects of Driver Gain Variation on Car/Driver Performance

Reproduced from best available copy.

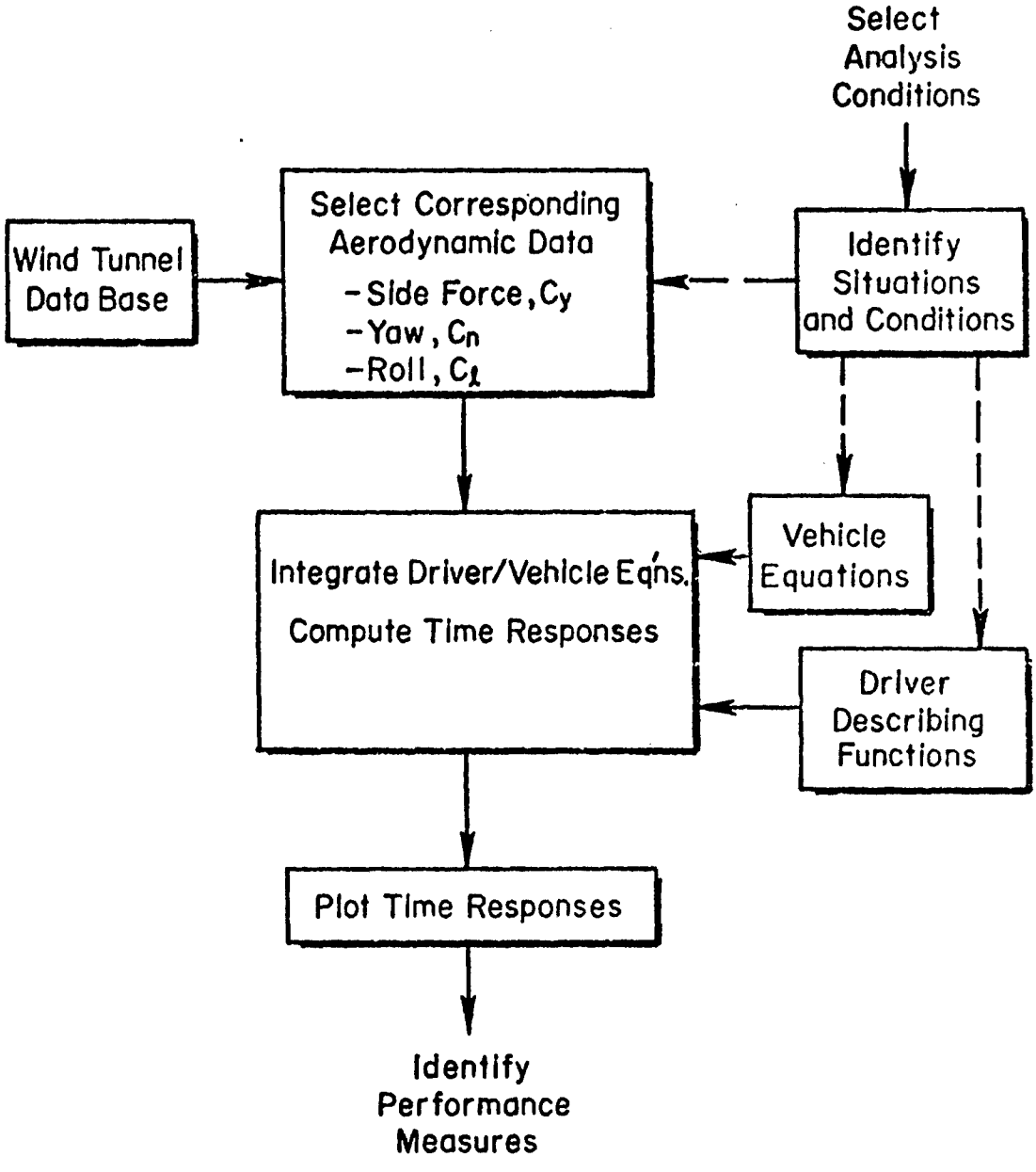

Figure 7. Combined Analysis Flow Chart

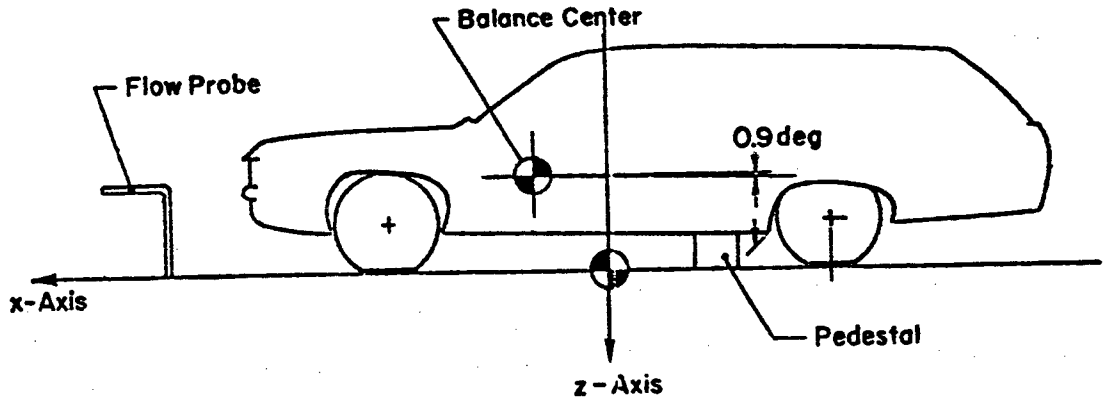

a) Station Wagon Model

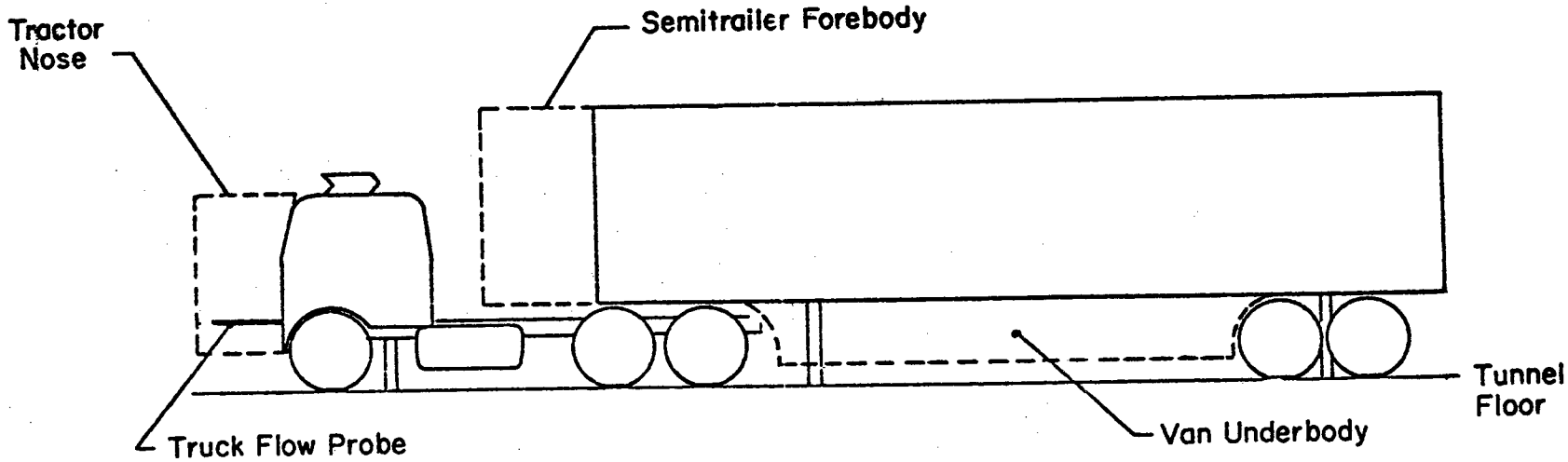

b) Tractor/Semitrailer Truck Model

Figure 8. Wind Tunnel Models

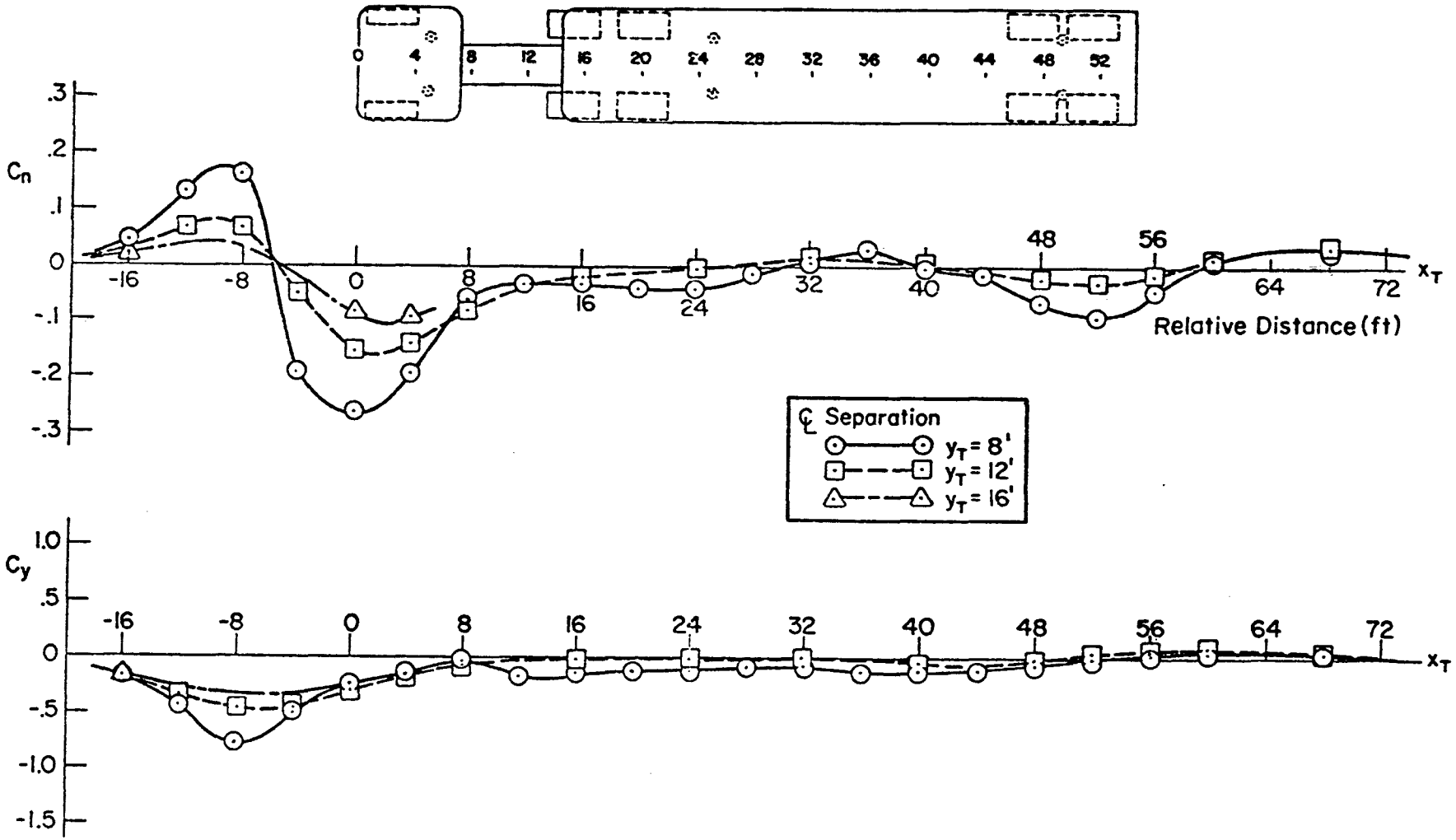

Figure 9. Typical Axial Flow Wind Tunnel Data

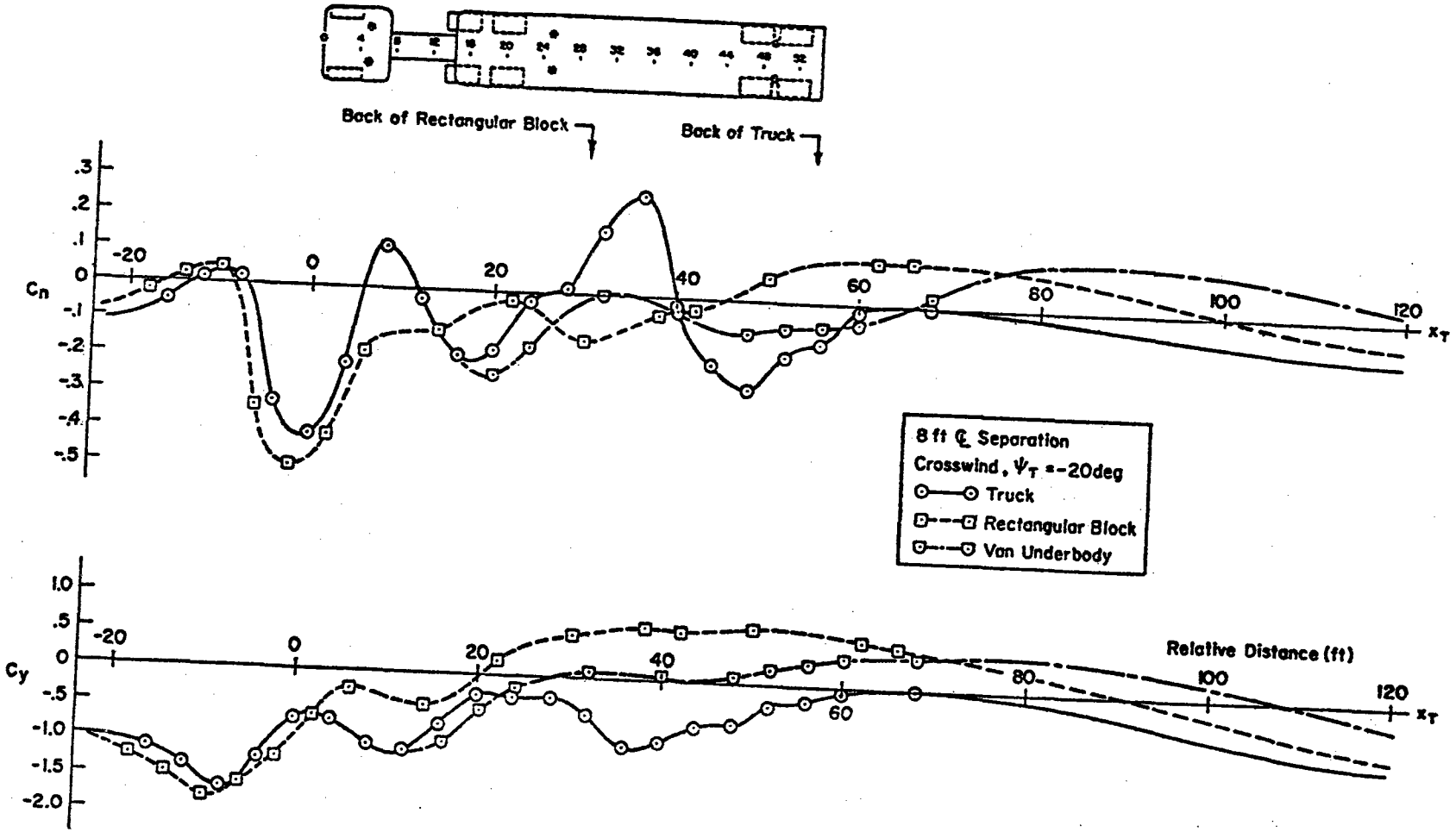

Figure 10. Typical Crossflow Wind Tunnel Data

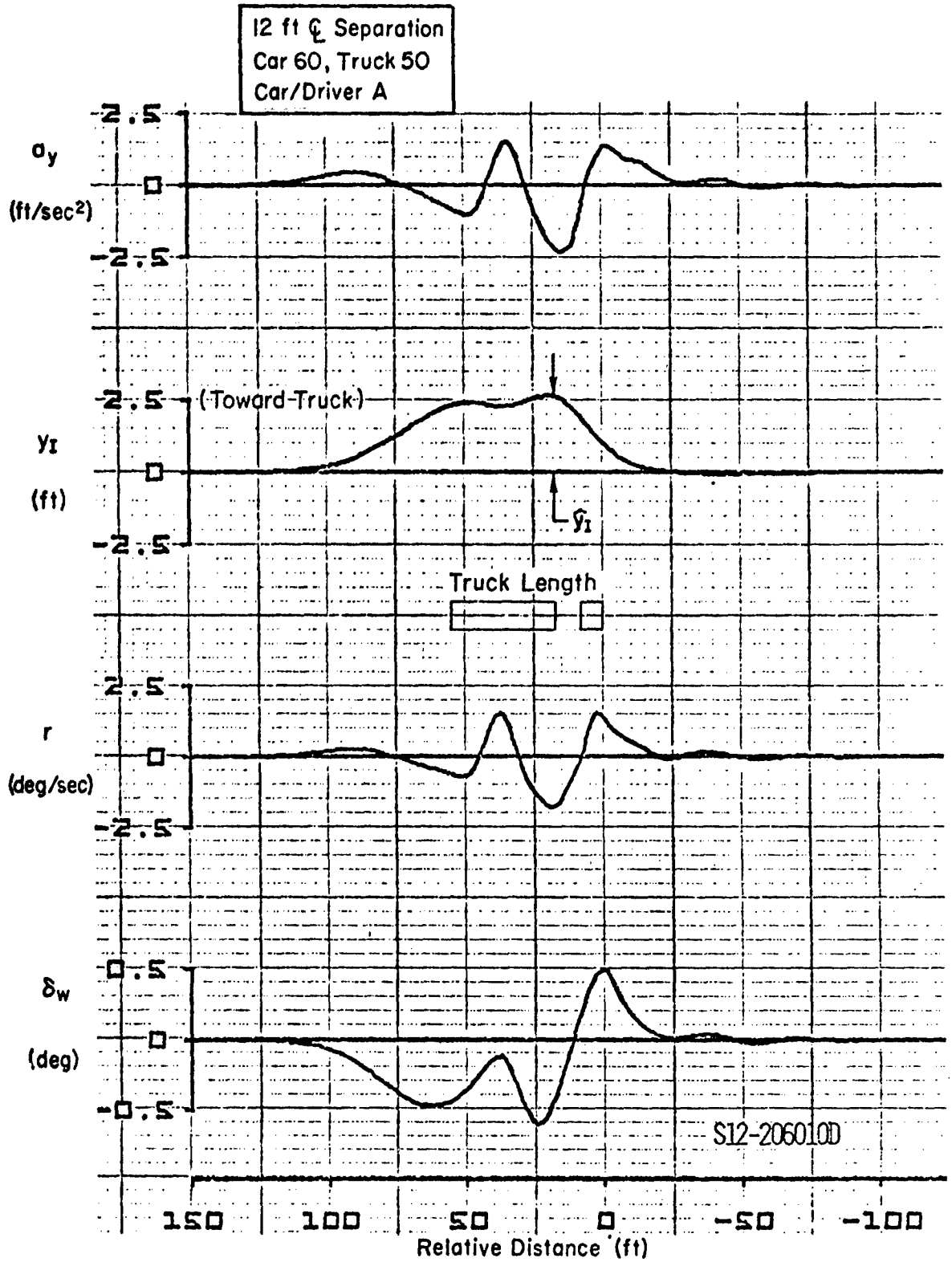

Figure 11. Computed Car/Driver Responses: Car Passes Truck, Crosswind = 18.2 mph (ψ_W = -20 deg)

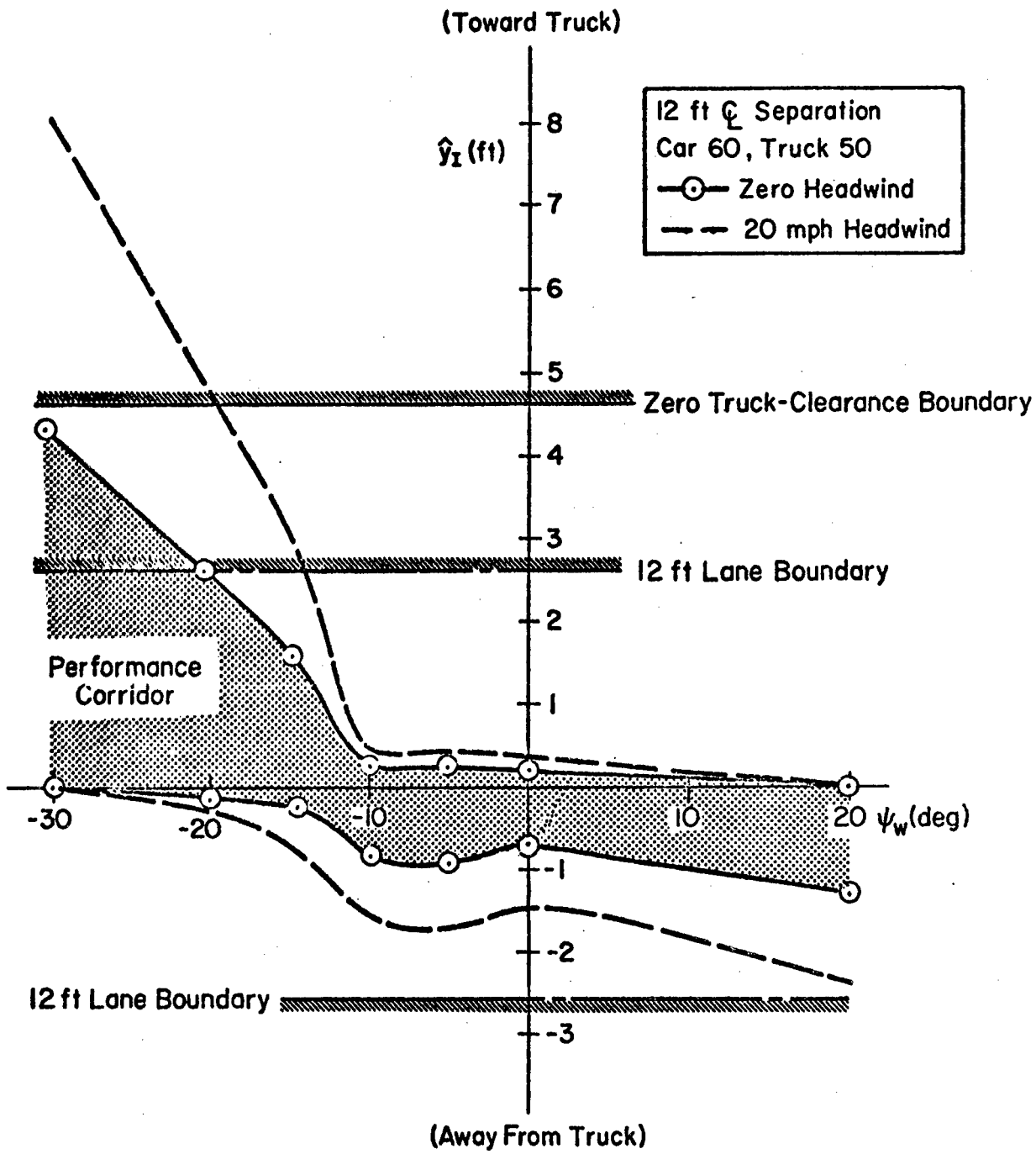

Figure 12. Effect of Relative Wind on Car Performance: Car/Driver A

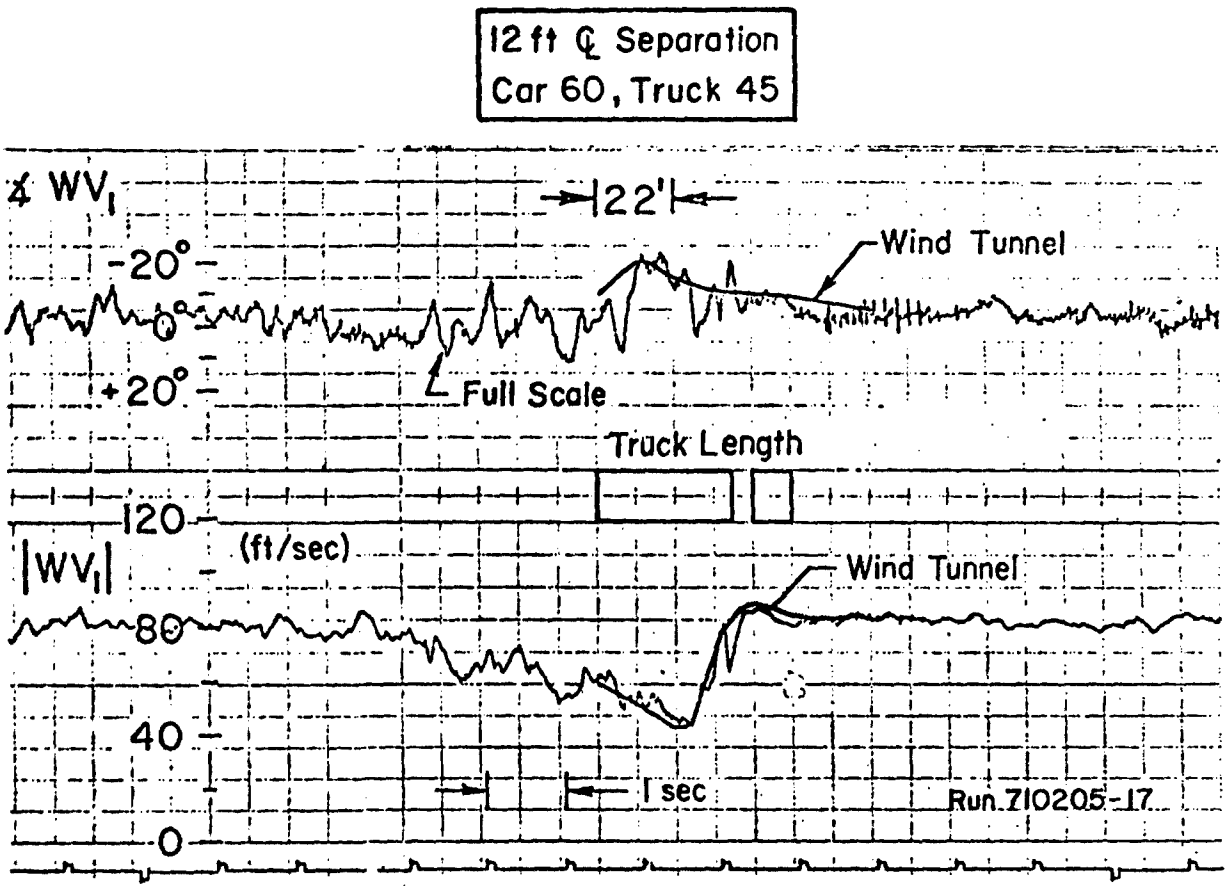

Figure 13. Full Scale and Wind Tunnel Flow Data Comparison; −4 Deg Crosswind Angle

Reproduced from best available copy.

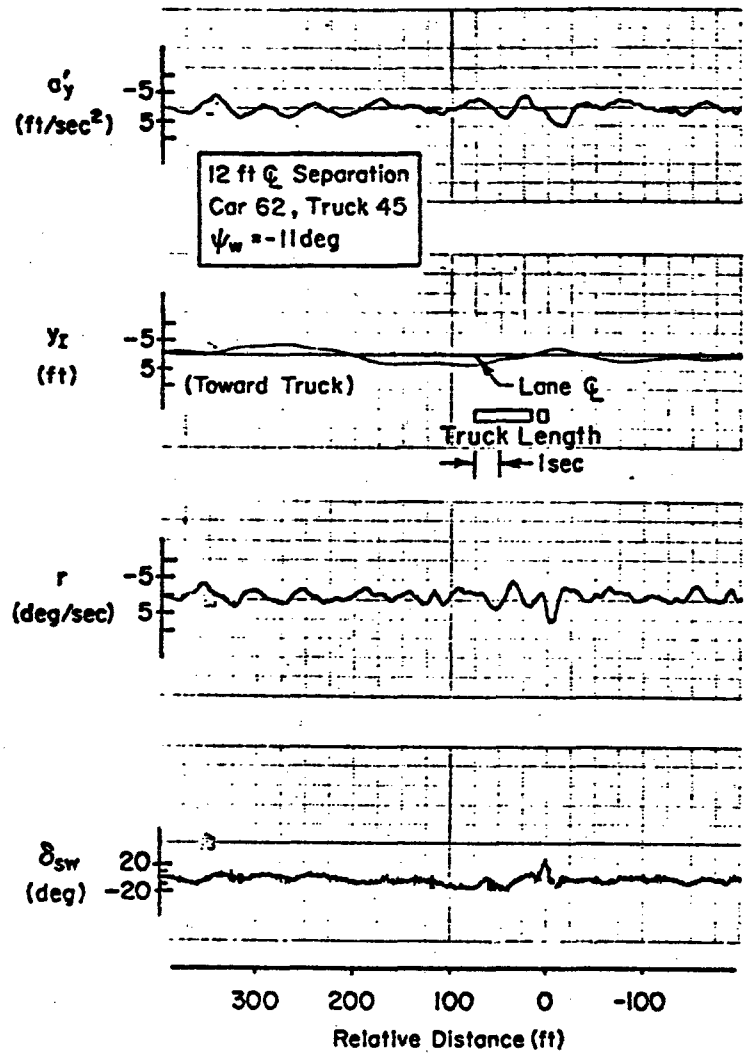

a) Full Scale Results

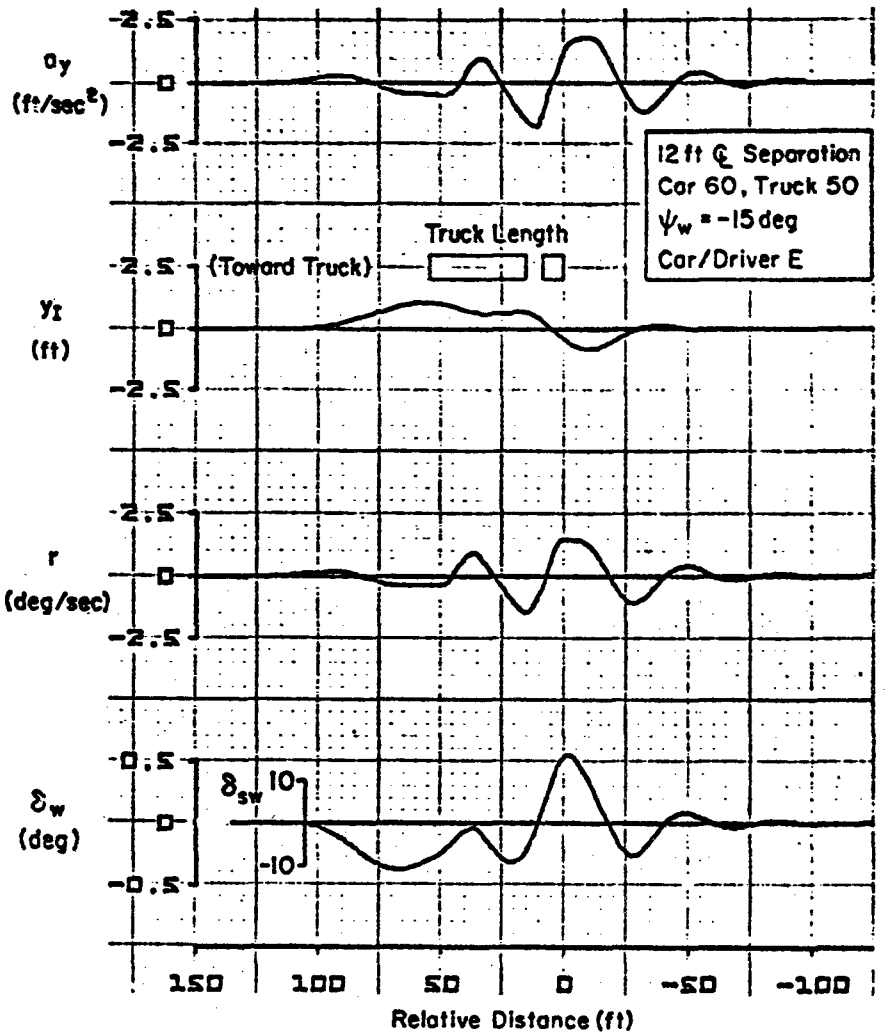

b) Analytical Results

Figure 14. Comparison of Full Scale and Analytically Computed Results

THE EFFECTS OF VEHICLE DYNAMICS ON ASYMPTOTIC STABILITY IN CAR FOLLOWING

Gerald O. Burnham
Department of Electrical Engineering
University of Southern California
Los Angeles, California

and

George A. Bekey
Department of Electrical Engineering
University of Southern California
Los Angeles, California

ABSTRACT

The results of an early paper by Herman et al on stability in car following are presented. Based on the theory used in that paper, the asymptotic stability of a string of cars was computed for various dynamic models of the vehicle. The results are compared and the limitations of the theory are discussed.

Preceding page blank

I. INTRODUCTION

In a 1958 paper by Chandler, Herman and Montroll [2] a theoretical investigation was made of several models of car following. A subsequent paper by Herman, Montroll, Potts and Rothery [4] presented a computer simulation based on one of the proposed models and the results for the propagation of a velocity disturbance. These early models of car following utilized a point mass model of the automobile dynamics and were concerned primarily with a macroscopic view of car following theory. This paper shows how changes in the basic assumptions about the automobile dynamics radically alter the results obtained in earlier papers.

Before proceding with the analysis, a few basic concepts of car following theory will be presented.

II. CAR FOLLOWING THEORY

Car following theory pertains to single lane dense traffic with no passing and is based on the assumption that each driver reacts in some specific fashion to a stimulus from the car or cars ahead and/or behind him. This stimulus could be the inter-vehicular distance or velocity or other sensory inputs such as auditory and possibly even tactile information. The basic differential-difference equation of car following theory expresses the idea that each driver of a vehicle responds to a given stimulus such that

response = Sensitivity x Stimulus

The stimulus is a functional of the position of a number of cars and their time derivatives. The response is the acceleration or forcing function applied to the vehicle by a driver through a pedal to carburetor throttle linkage.

One of the simplest models assumes proportional control, as given by the differential difference equation [2]

$$M \frac{d U_n}{d t} = \lambda (U_{n-1} - U_n) \qquad (1)$$

where M is the mass of each vehicle, U_n and U_{n-1} are their perturbation Velocities, (that is, the deviations from the desired velocity), and the subscripts refer to the n-th car and the car directly ahead of it.

The model utilized by Herman, et al [4] differs from the model of eq. (1) by the introduction of a time delay to represent the driver's

reaction time. The differential difference equation is of the form

$$M \frac{d U_{n-1}}{dt} (t) = \lambda \left[U_{n-1} (t-\Delta) - U_n (t-\Delta) \right] \quad (2)$$

where Δ is the time delay. Making a change of variables $t = \tau \Delta$

$$\frac{d U_n}{d\tau} = C \left[U_n(\tau - 1) - U_{n-1}(\tau - 1) \right] \quad (3)$$

$$\text{where } C = \frac{\lambda \Delta}{M}$$

It was shown experimentally that $\Delta \cong 1.5$ Sec and that $\lambda/M \cong .37$ Sec^{-1} for normal traffic flow. Conditions for local stability are shown in Table 1.

III. A MORE GENERAL MODEL

A block diagram of a more general model, as used in this paper is shown in figure 1.

Notice that if the constants $A=B=0$ the automobile is represented by a point mass and the model reduces to eq. (2). If $B \neq 0$ and $A=0$ the automobile is represented by a first order lag. Bender and Fenton [7] used a first order lag as a car model. If $A \neq 0$, a nonlinear term (proportional to the square of the velocity) is used to represent air resistance. The nonlinear model will be further discussed below.

It should be noted that the desired or reference velocity term V_o must be added to maintain a constant velocity when the dynamics are assumed to be nonlinear, or a first order lag. V_o need not be explicitly included in a linearized point mass model.

A car following simulation with a human operator model and non-linear automobile dynamics such as figure 1 was used to generate results for comparing effects of the various dynamic configurations.

The human operator represented was a pure delay so that results could be compared directly with earlier models.

Early Computer Results

The results of Herman's et al [4], using an analog computer and an IBM 704 at General Motors Research Laboratories, are shown in figures 2, 3, 4 and 5.

Figure 2 shows the velocity perturbation of the lead car and the resulting velocity and distance perturbation of the first car following for $\Delta = 1.5$ and $C = .368$.

Figure 3 shows the deviation from constant spacing of two cars for different values of C.

Figure 4 shows separation distances of a line of cars under the influence of velocity control.

Car following stability is concerned with the manner in which fluctuations in the lead car velocity are propagated down a line of cars. Figure 5 shows the results of a simulation of this phenomenon. Note that a collision occurs between the 7th and 8th car at $t \cong 24$ sec.

IV. NEW COMPUTER RESULTS

The model shown in figure 1 was used to obtain results for comparison with those of Herman [4].

The simulation was programmed at the University of Southern California on an IBM 360-44 using MOBSSL, a block structured simulation language. A Padé approximation was used for the time delay.

The lead car velocity was essentially the same as figure 2, that is a constant velocity for 2 seconds, a constant deceleration of -6 ft/sec^2 for 2 seconds followed by a constant acceleration for 2 seconds at 6 ft/sec^2, after which the velocity remained constant for the remainder of the run.

(a) Point Mass Vehicle

The perturbations in intercar spacing for the point mass model are shown in figure 6, note the collision between the 7th and 8th car at approximately 27 seconds. This is close to the Herman model [4], in which collision occured at 24 seconds. This difference could be attributed to differences in the computer implementation of eq. (2).

(b) First Order Lag Vehicle

Figures 7 and 8 show the response when the automobile is represented by a first order lag with $\tau = 4$ and $t=20$ respectively. In figure 7 the perturbation is damped out. However in figure 8, with $\tau = 20$, the perturbation is transmitted virtually intact after the third automobile. These results indicate that $\tau = 20$ is close to the maximum value for asymptotic stability.

(c) Nonlinear Vehicle Dynamics

Figure 9 shows the results obtained with nonlinear automobile dynamics. Although a collision did not occur in the 30 second time limit, the minimum distance between cars decreased along the line. Extrapolating the results, one would expect a collision between the 13th and 14th car at approximately 45 seconds. The actual equations used to represent the n-th car in this simulation were:

$$M \frac{d V_n(t)}{d t} = \lambda \left[V_{n-1}(t-\Delta) - V_n(t-\Delta) \right] - B V_n(t) - A V_n^2(t) + f(V_0)$$

where $V_n(t)$ and $V_{n-1}(t)$ are velocities
$M = 178$ Slugs
$V_0 = 60$ fps
$f(V_0) = B V_0 + A V_0^2 = .88$ Slug ft/sec^2
$A = .04$ Slug/ft
$B = .255$ Slug/sec
$\lambda = 75$ Slug/sec
$\Delta = 2$ sec

The results given in figures 6 through 9 show how the choice of automobile dynamics alter the behavior of a Simulation. These results indicate that the stability conclusions obtained from early car-following models must be interpreted carefully before applying them to any specific situation.

V. THE PROBLEMS OF BRAKING

The earlier models of car-following did not include braking as a means of longitudinal control. Braking as a separate process may be eliminated in macroscopic car-following theory but it must be included and dealt with separately in microscopic concepts of car-following theory.

Braking has two problems of no small magnitude associated with it: (1) when is the brake to be applied? (2) how much force is used to brake? These problems are further complicated by the fact that the brake is a non-linear, saturating control which can exert decelerating forces much greater than the decelerating (resistive) forces associated with tire friction and aerodynamic properties or the accelerating force applied by an accelerator. The minimum braking deceleration recommended by the California State Highway Patrol is .61g (approximately 20 ft/sec^2). The stopping distance versus velocity for an automobile with .61g deceleration (braking), with and without reaction time (.75 seconds) is shown in figure 10. The distances are representative of a panic stop (maximum de celeration without skidding). The reaction time is the time to transfer control from the accelerator to the brake.

While the results in this paper were obtained using positive and negative acceleration, without the use of a separate braking control to obtain comparisons with the Herman paper [4], it is evident that braking must be included in a more accurate vehicle model.

VI. INTERPRETATION OF RESULTS

Although Chandler [2] stated that the point mass model gives a fairly accurate macroscopic description of the dynamics of a string of cars, it is interesting that the model is not physically realizable. The

lead car acceleration was limited to accelerations of ± 6 ft/sec^2. A point mass with an acceleration of 6 ft/sec^2 would reach a velocity of 60 mph (88 ft/sec) in 14.66 secs. This is reasonable performance for a standard automobile. The accelerations of cars 6 through 8 exceeded 6 ft/sec^2. In fact at the time the collision took place between the 7th car and the 8th car, the 7th car was accelerating with a value of 8 ft/sec^2 and the 8th car was decelerating at -2.8 ft/sec^2. An acceleration of 8 ft/sec^2 represents quite an improvement in car performance. A point mass with an acceleration of 8 ft/sec would reach a velocity of 60 mph in 11 seconds. Not many standard automobiles are capable of this performance. Another example of unsatisfactory performance of the model can be seen by looking at the deceleration of the 8th car at the time of collision. The car was decelerating at only -2.8 ft/sec^2 when it had at least -20 ft/sec^2 deceleration available.

The results indicate that there should be limits associated with the model to keep it from exceeding the limitations of the physical plant. Also a realistic model must include braking according to some criteria.

The Best Microscopic Model

Another problem associated with the point mass model is its inability to exhibit resistive forces known to exist in the automobile. As previously stated for macroscopic applications the restrictions of a point mass model may not be prohibitive but when investigating the microscopic case it does not adequately describe the situation.

The representation of the vehicle dynamics as a first order lag is a more adequate description when dealing with the concept of local stability. However, the asymptotic behavior of the model varies considerably as the time constant of the system varies. As the time constant increases the system tends to be unstable. It can also be shown that for the first order lag the value of the time constant is dependent on the vehicle velocity and remains relatively constant over a small range of velocities. Therefore the first order lag model becomes invalid if velocity perturbations get too large.

The non-linear model for vehicle dynamics, shown in figure 1, is probably the most intuitively satisfying one in that it includes resistive forces of friction and the aerodynamic term relating to crossection area. The constants A and B in figure 1 are independent of the vehicle's velocity and depends only on the cars parameters (i.e. weight, type of tires, crossection, etc.). This model will be used in future investigations of car-following.

Conclusion

It has been shown that the results of a car-following simulation can be varied substantially by changing the dynamic representation of the automobile. It was also shown that the point mass and the non-

linear models were asymptotically unstable but the first order lag model was asymptotically stable depending on the value of the time constant.

REFERENCES

1. Pipes, L.A., "A Operational Analysis of Traffic Dynamics", Journal of Applied Physics, Vol. 24 (1953), pp. 271-281.

2. Chandler, R.E., Herman, R., and Montroll, E.W., "Traffic Dynamics: Studies in Car Following", Operations Research, Vol. 6 (1958), pp.165-184.

3. Fenton, R.E., and Montano, W.B., "An Intervehicular Spacing Display for Improved Car Following Performance", IEEE Transactions on Man-Machine Systems, Vol. MMS-9 (1968), pp. 29-35.

4. Herman, R., Montroll, E.W., Potts, R.B., and Rothery, R.W., "Traffic Dynamics: Analysis of Stability in Car Following", Operations Research, Vol 7. (1959), pp. 86-106

5. Edie, L.C., "Car Following and Steady-State Theory for Non-Congested Traffic", Operations Research, Vol 9 (1961), pp.66-76.

6. Steeds, W., Mechanics of Road Vehicles, Iliffe, (1960).

7. Bender, J.G., Fenton, R.E., "On Vehicle Longitudinal Dynamics", Paper presented at the 5th International Symposium on the Theory of Traffic Flow and Transportation, University of California, Berkeley, California (June 16-18, 1971).

Table 1

Conditions for Local Stability

c	Response (acceleration)
$c > \frac{1}{2}\pi$	Oscillatory with increasing amplitude
$c < \frac{1}{2}\pi$	Oscillatory undamped amplitude
$\frac{1}{e} < c \leq \frac{1}{2}\pi$	Oscillatory damped amplitude
$c \leq \frac{1}{e}$	Nonoscillatory and damped

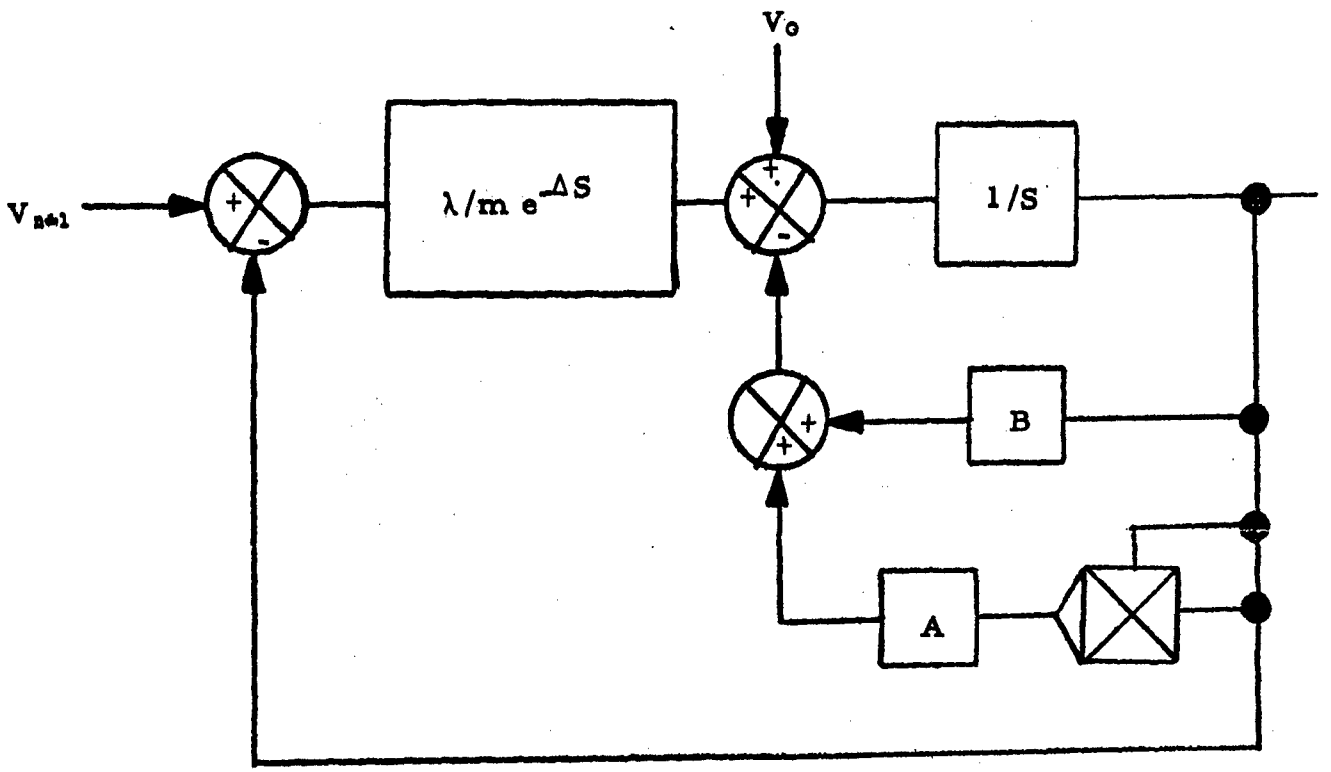

$A = K x_4 \text{Frontal Area}_4$
$5 \times 10^{-4} < K < 30 \times 10^{-4}$
$B = \beta \times W$
W = weight in tons
$.1 < \beta < 3.5$

FIGURE 1

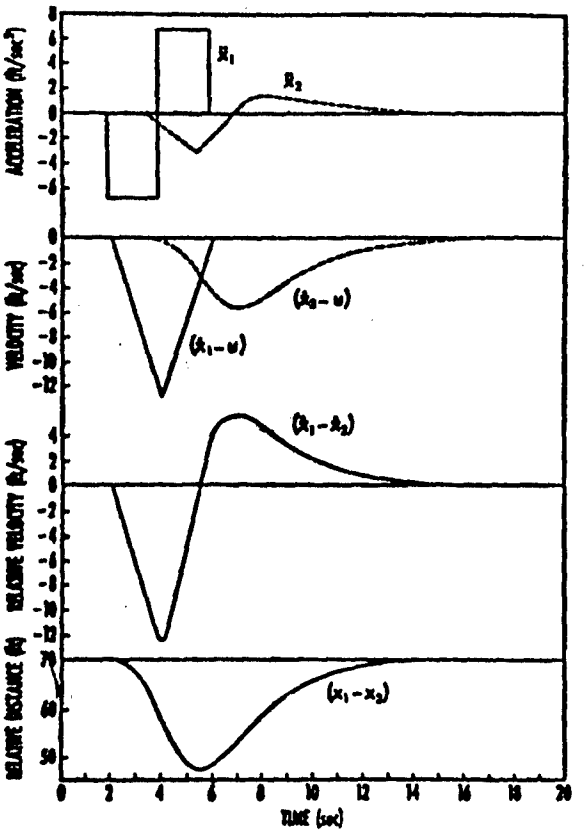

Fig. 2 Detailed motion of two cars showing the effect of a fluctuation in the acceleration of the lead car. The second car follows the first with velocity control with time lag $\Delta = 1.5$ seconds and $C = c^{-1} = 0.368$, the limiting value for local stability. The initial velocity of each car is u.

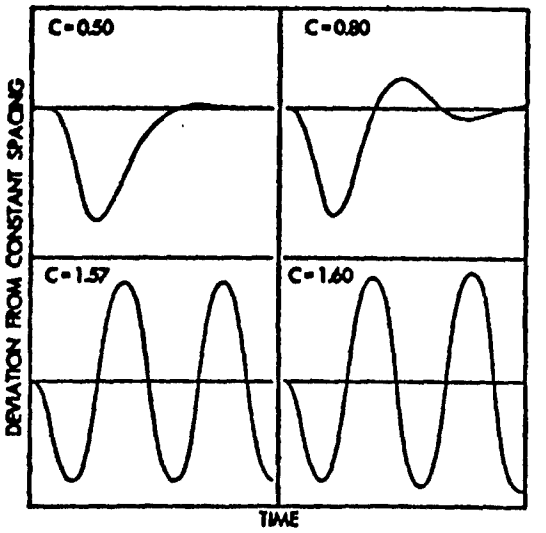

Fig. 3. Deviation from constant spacing of two cars for different values of C; the acceleration of the lead car is the same as that shown in Fig. 2.

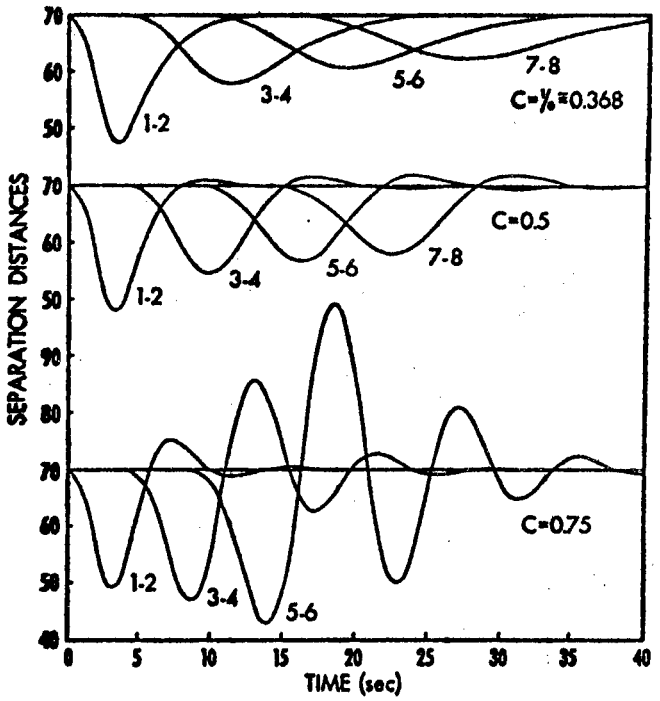

Fig. 4. Separation distances of a line of cars under the influence of velocity control for different values of C. The fluctuation in acceleration of the lead car is of the same form as that shown in Fig. 2. For $t \leq 0$ the cars are separated by a distance of 70 feet.

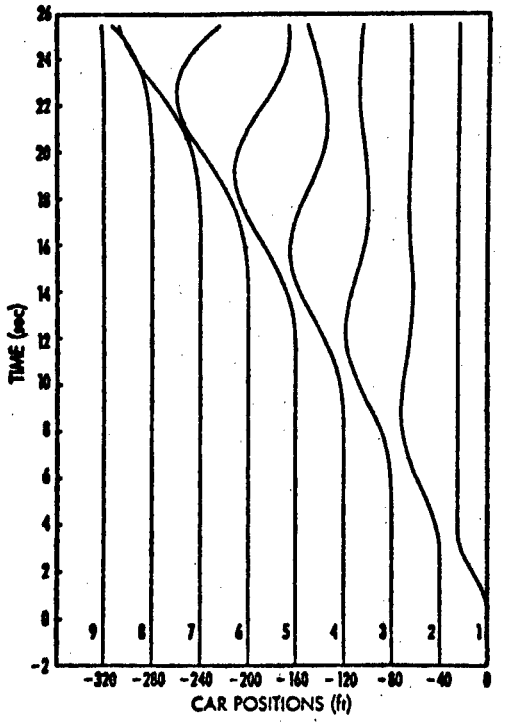

Fig. 5. Asymptotic instability of a line of nine cars under the influence of velocity control, $C=0.8$ and $\Delta=2$ seconds. For $t \leq 0$, the cars move with a velocity u and are separated by a distance of 40 feet. The positions relative to a coordinate system moving with a velocity u have been plotted as a function of time. The collision between the 7th and 8th cars results from a fluctuation in acceleration of the lead car.

FIGURE 7

PROPAGATION OF A VELOCITY DISTURBANCE

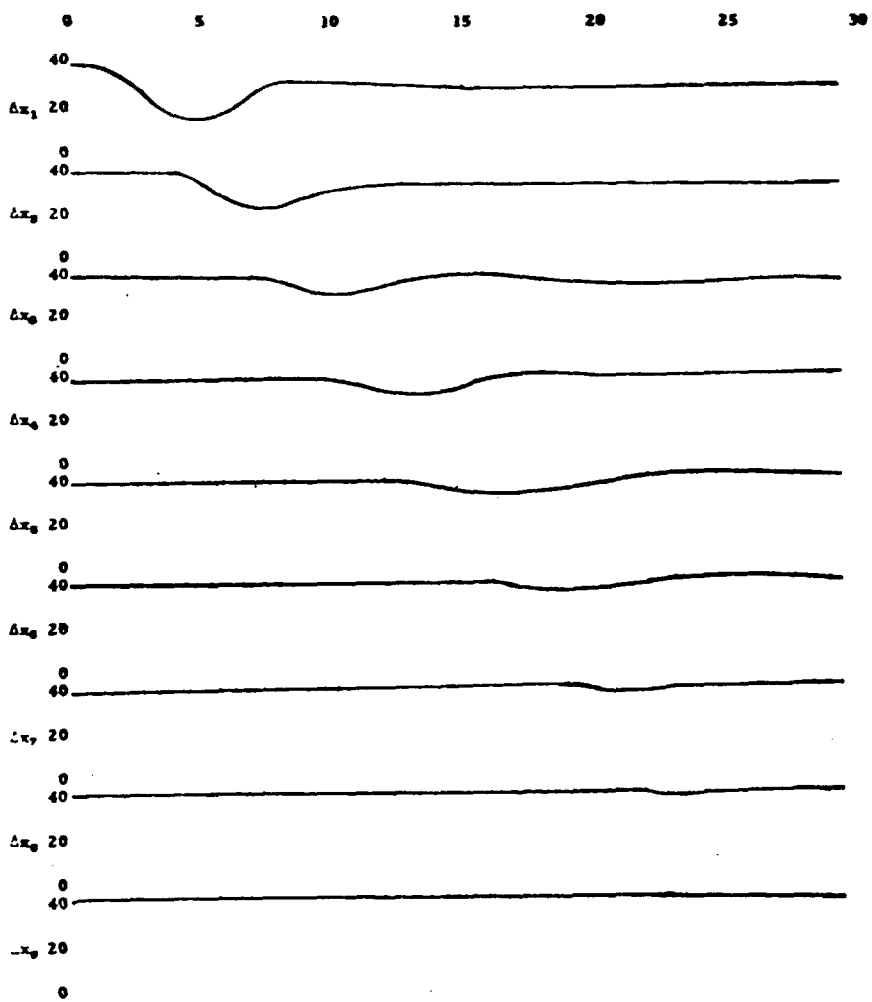

Car Dynamics
First Order Lag $\tau = 4$
(Linear Control)

FIGURE 6

PROPAGATION OF A VELOCITY DISTURBANCE

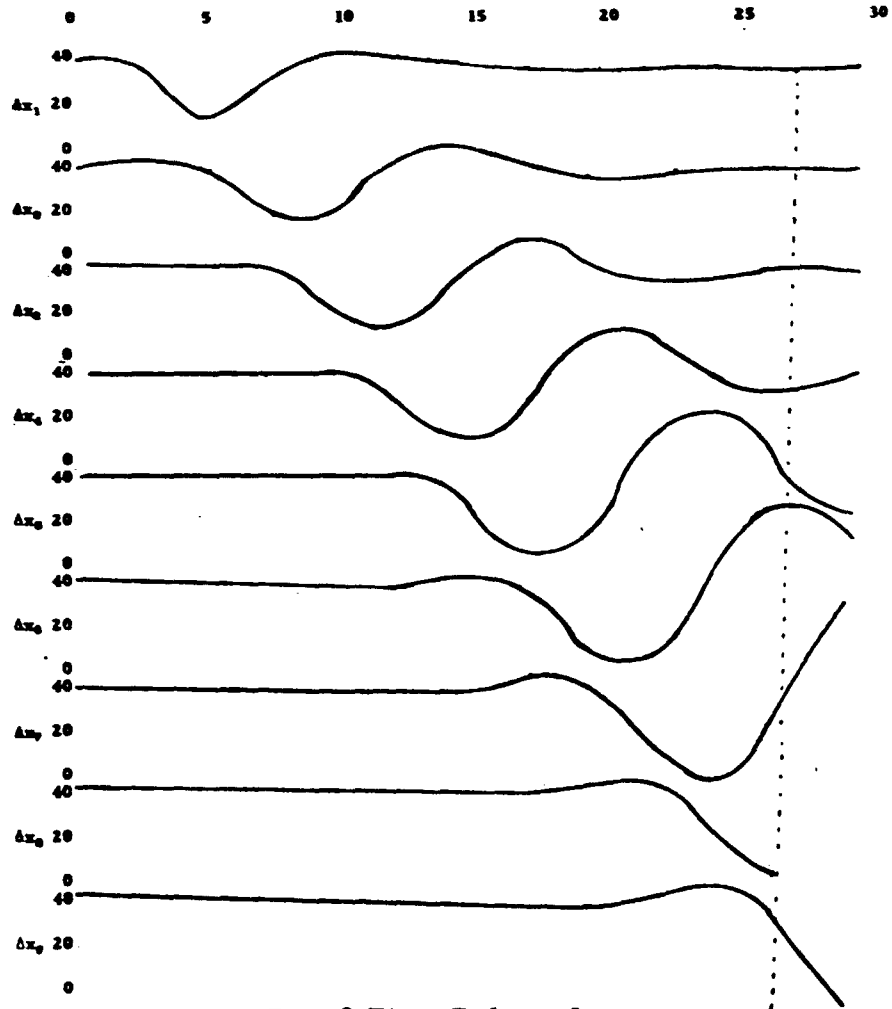

C = .8 Time Delay = 2.
Collision between 7th and 8th car at ≈ 27 seconds
(Linear Control)

FIGURE 9

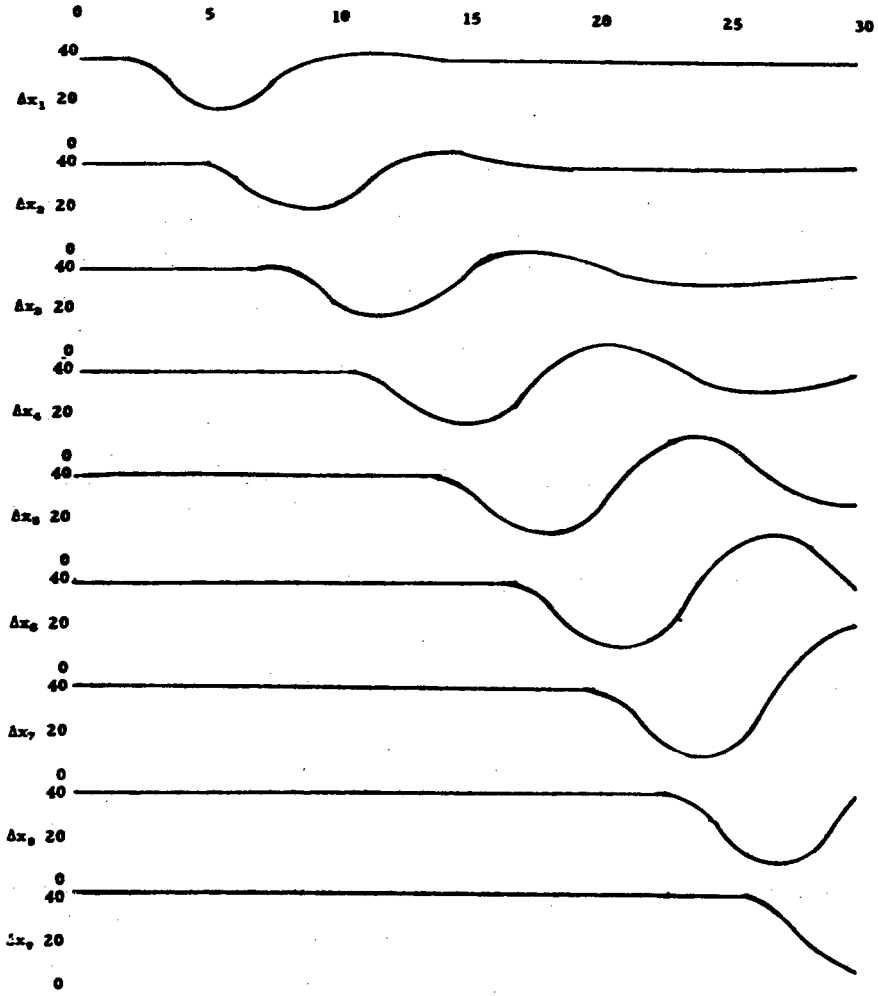

A = .04, B = .255
W = 5700 lbs
V = 60 fps
Car Dynamics
Non Linear
Linear Control

FIGURE 8

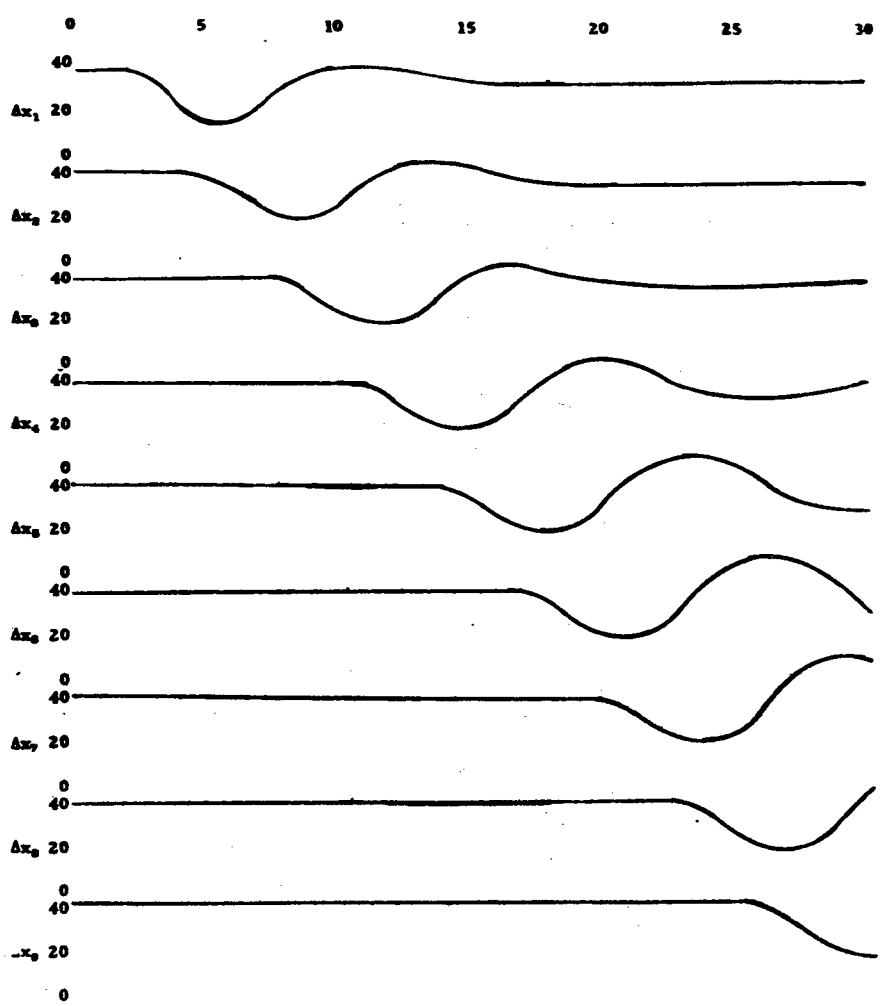

Car Dynamics
First Order Lag $\tau = 20.$
(Linear Control)

STOPPING DISTANCE VS. VELOCITY
Bracket shows distance traveled for .75 sec reaction time
(Taken from California Driver's Handbook)

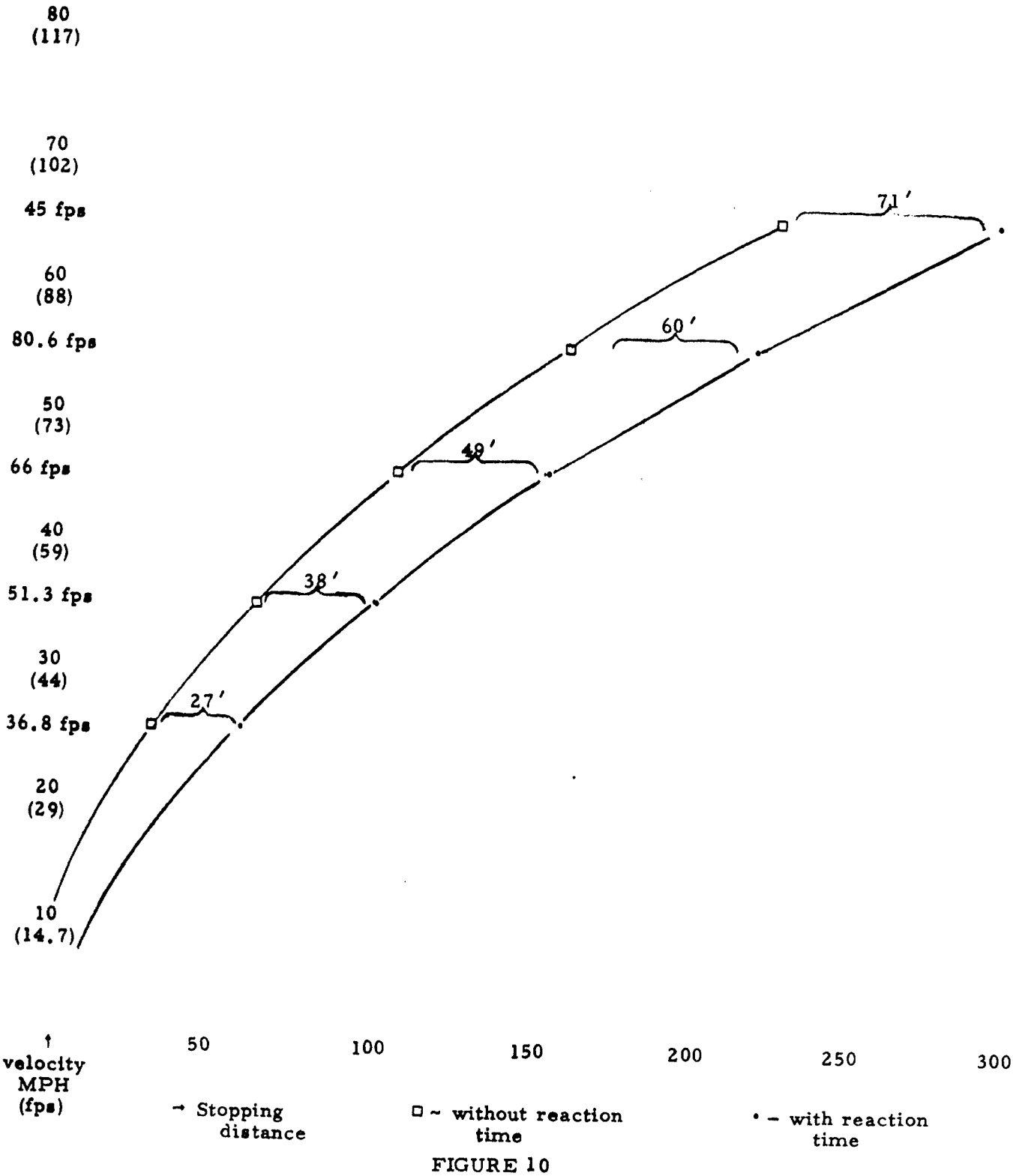

FIGURE 10

MODELLING THE HELMSMAN OF A SUPERTANKER: SOME PRELIMINARY EXPERIMENTS.

by

W. Veldhuyzen; A. van Lunteren and H.G. Stassen.

Man-Machine Systems Group,
Laboratory for Measurement and Control,
Department of Mechanical Engineering,
Delft University of Technology,
The Netherlands.

0. Abstract

A fully loaded supertanker is a nonlinear system which responds very slowly to changes in the rudder position. Moreover, in general it is unstable, i.e. it has a tendency to start turning either to the left or to the right. These properties make a supertanker very hard to handle. The Institute T.N.O. for Mechanical Constructions at Delft built a simulator in order to study the maneuverability of ships. Using this simulator some attempts have been made to model the behavior of a helmsman during course keeping.

1. Introduction

Most of the investigations concerned with the behavior of the human operator as a controller have been executed with reference to the pilot of an aircraft or spacecraft. Some work in this field has been done on the control of submarines. The human operator as a controller of surface ships, however, did not get very much attention until recently.

In the Netherlands about two years ago the Institute TNO for Mechanical Constructions (TNO-IWECO) at Delft built a ship maneuvering simulator [1] in order:

- to study ship maneuverability
- to obtain data for ship and harbor design
- to establish criteria for ships and harbors
- to execute traffic control studies
- to study nautical instrument design and automatic control
- to train officers and pilots.

The simulator design was based on data and experiences obtained with a previously built experimental simulator, designed by TNO-IWECO in cooperation with the TNO Institute for Perception (TNO-IZF) at Soesterberg; another partner in the simulator project was the Shipbuilding Laboratory of the Delft University of Technology.

Earlier Stuurman [2] executed a number of trials on the experimental simulator in which he showed that for small ships the control behavior of the helmsman could very well be approximated by means of a describing function model. He also found evidence that for larger ships a nonlinear model probably would give a more realistic description of the helmsman's behavior.

In consult with TNO-IWECO it was decided to continue the work of Stuurman as a joint activity of the Shipbuilding Laboratory and the Man-Machine Systems Group. Special emphasis was to be laid on modelling the helmsman of a supertanker with the following goals in mind:

a) To provide a data base on which the maneuvers of this type of ship under human control can be predicted in a number of situations.
b) To enable an evaluation of the employment of a human pilot versus the use of an autopilot.
c) To investigate in more detail the advantages of predictive displays in supertanker control.

Some introductory experiments have been executed using the simulator as a supertanker moving at constant speed on an almost straight course. A first attempt has been made to describe the behavior of the helmsman by means of a nonlinear model using five trainees of the School of Navigation at Rotterdam as subjects.

2. Ship dynamics

The dynamics of a ship depend not only on the properties of the ship itself like shape, dimensions, mass and engine power, but also on the topology of the surrounding water. The motions of a ship in the horizontal plane can be described by a set of nonlinear differential equations. These equations describe the translations of the ship in a direction corresponding to the longitudinal axis of the ship and in a direction perpendicular to this axis as well as the rotation about a vertical axis through the center of gravity.
Fig. 1 gives an indication of the variables concerned.

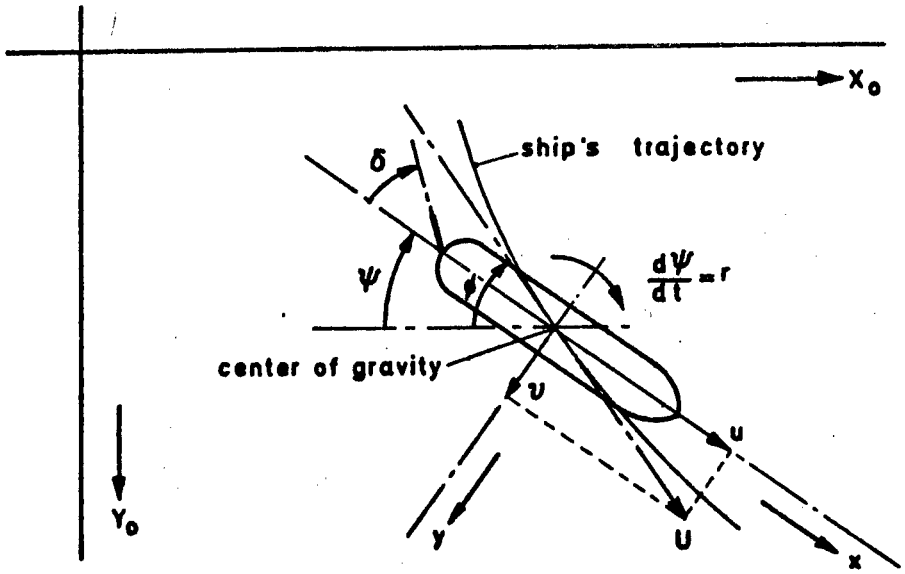

Figure 1: The quantities involved in the description of the ship's maneuvers.

In 1957, Nomoto [3] showed that if it is assumed that the ship is sailing at a constant speed, then the relation between the rudder angle δ and the rate of turn r can be described by means of a second order linear differential equation. For most of the smaller ships this equation gives an adequate description of the ship's behavior in a number of standard maneuvers. For a supertanker, however, it was found that the behavior was essentially nonlinear. Based on full scale trials Bech [4] proposed to extend Nomoto's equation with a nonlinear term. This leads to the following relation:

$$T_1T_2\,\ddot{r}(t)+(T_1+T_2)\dot{r}(t)+a_1r(t)+a_2\left[r(t)\right]^3=K\left[T_3\dot{\delta}(t)+\delta(t)\right]. \quad (1)$$

where, $r(t) = d\psi(t)/dt$ is the rate of turn, $\psi(t)$ is the heading angle, $\delta(t)$ is the rudder angle, and where the quantities a_1, a_2, T_1, T_2, T_3 and K are constants.

Here, it should be noted that all constants in this equation are dependent on the hydrodynamic behavior of the ship, which is related to, among other things, its speed, its load condition and to possible restrictions in the surrounding water.

In this study a particular ship viz a 220 000 tons dead weight tanker in loaded condition has been chosen. Table I shows the principal data of the ship.

Table I: Principal data of the 220 000 ton dead weight tanker in fully loaded condition.

Length	310.00 m
Breadth	47.16 m
Depth	24.50 m
Draft	18.90 m
Displacement	238 000 m3
Speed	7.72 m/sec
Froude number	0.14

The constants in Eq. (1) for this ship have been determined by Glansdorp [5,6] in a series of full scale trials; they are given in Table II.

Table II: Constants in the equation describing the relation between the rudder angle and the rate of turn for the supertanker considered.

constant	dimension	numerical value
a_1		-1
a_2	sec^2/rad^2	80 000
T_1	sec	250
T_2	sec	10
T_3	sec	20
K	sec^{-1}	-0,0434

If a stationary situation is considered, that is, $\ddot{r}(t) = 0$, $\dot{r}(t) = 0$, $\dot{\delta}(t) = 0$, then Eq. (1) changes into:

$$a_1 r + a_2 r^3 = K\delta. \qquad (2)$$

Fig. 2 represents Eq. (2); this static characteristic is given for the ship in fully loaded condition, and shows that the ship is course unstable, i.e. the ship has a natural tendency to deviate from the straight course and start turning either in one direction or in the other.

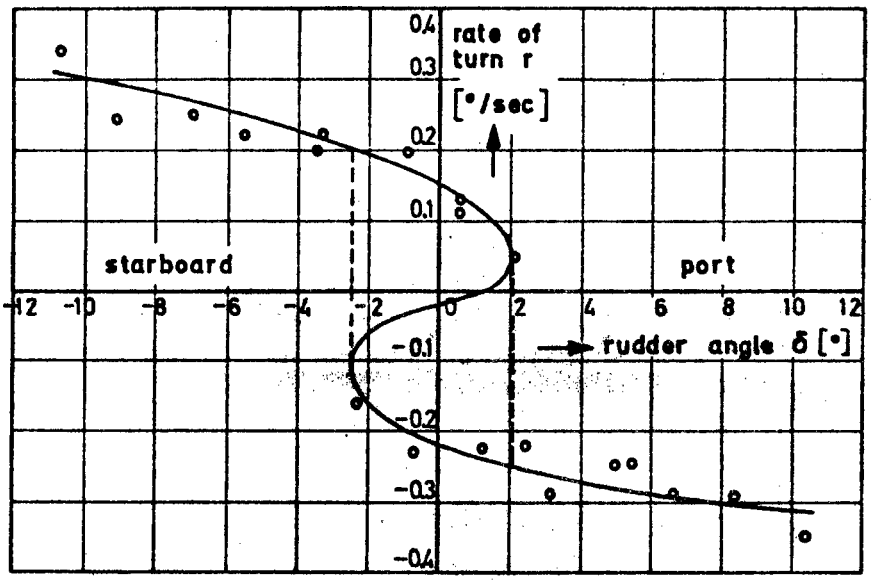

Figure 2: Relation between the rudder angle δ and the rate of turn r in the stationary state for the ship considered in this investigation, as found by Glansdorp [5].

3. The maneuvering simulator

The simulator consists of a wheelhouse which has the same appearance as that of a real sea-going vessel. The fore-part of the ship, the sea and a coastline are displayed on a screen in front of the wheelhouse. The angle of vision of the helmsman is 120°. The image of the fore-part of the ship is static; it is produced by two slide projectors which have a fixed position. The coast-line is generated by means of a point light source and a movable model with 3 degrees of freedom viz. two translations and one rotation in the horizontal plane. Fig. 3 shows the simulator during a simulated approach of a harbor.

This page is reproduced at the back of the report by a different reproduction method to provide better detail.

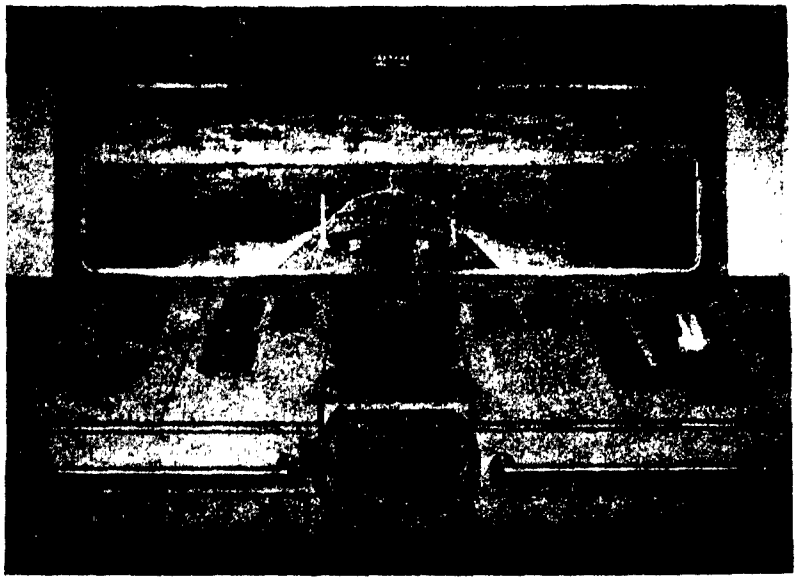

Figure 3: The Ship Research and Maneuvering Simulator of the Institute TNO for Mechanical Constructions at Delft.

A block diagram of the system, including the helmsman, is given in Fig. 4.

On an analog computer the dynamics of the ship to be simulated, including the characteristics of thrust engine and rudder engine, can be programmed. The computer yields the signals which control the environmental display system and also the instruments such as compass, rudder position indicator, log, etc. The helmsman has the same controls at his disposal for maneuvering as on a real ship viz. the wheel, which gives the input to the rudder engine, and the telegraph to the engine, which governs the speed of the propeller. External disturbances simulating the effects of wind, waves and currents can also be introduced into the model on the analog computer; the same applies for the information on the desired state which is of importance for the settings of the instruments in the wheelhouse.

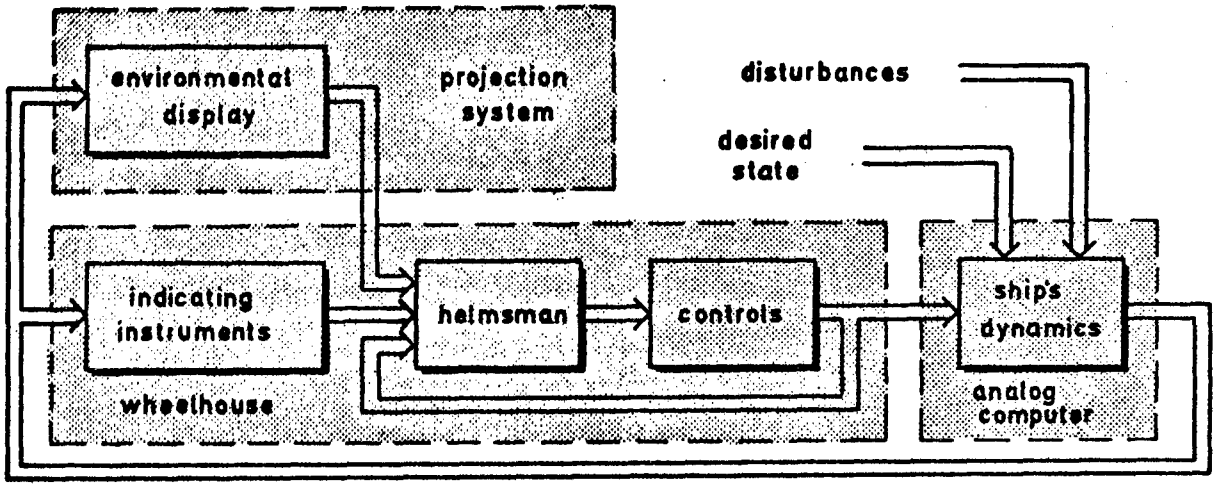

Figure 4: Blockdiagram of the TNO simulator.

4. The experiments

In the experiments described here, the simulator has been used as a supertanker at full sea, moving at a constant speed on an almost straight course. The wheelhouse was equipped with a compass and a rate of turn indicator. The analog computer was programmed according to Eq. (1) based on the constants given by Glansdorp as indicated in Table II. The rudder engine was also included in the simulation. Its dynamics have been chosen according to the Eqs. (3) en (4).

$$T_4 \dot{\delta}(t) + \delta(t) = w(t); \tag{3}$$

$$|\dot{\delta}(t)| \leq M, \tag{4}$$

where $w(t)$ is the position of the steering wheel or the desired rudder angle, and where T_4 is a time constant of 1 sec and the quantity M is the maximal value of the rotation speed of the rudder (0.045 rad/sec).

The subjects were five trainees of the School of Navigation at Rotterdam. They were studying for the rank of first or second mate after having been at sea for several years. Only one subject, hereafter indicated as subject A, had sailed on a ship larger than 50 000 tons.

Their task consisted of keeping the tanker on a straight course for about half an hour. During these experiments the compass as well as the rate of turn indicator were used. No external disturbances simulating wind, waves and currents were introduced. The purpose of these tests was to get some data on which to make a choice for one or more helmsman models to be tested in a further series of experiments. During the tests the position of the wheel $w(t)$, the rate of turn $r(t)$ and the heading angle $\psi(t)$ were recorded on paper.

5. Modelling the helmsman

When choosing a model for the human operator controlling a given system, one has to bear in mind the requirement that the model should enable the investigator to make reliable predictions, preferably for a number of different tasks. On the one hand, the number of parameters should be large enough to describe the significant characteristics of the human operator behavior observed. On the other hand, the number of parameters should be small enough to yield consistent results when the parameters are estimated in different trials with a similar task.

It may be true that a describing function based on the cross-over model [7] leads to a good description of the helmsman's behavior for a number of situations. However registrations of the input and output of a trained helmsman suggest that there may be a better way to describe his behavior. The Figs. 8 through 11 give some examples. The figures selected represent different types of behavior observed in the trials. The records show in all cases that the helmsman generates an output consisting of discrete steps. This suggests that the helmsman bases his decision on when to move and how much to move the wheel, on some criterion which, for instance, is a function of the heading angle $\psi(t)$ and the rate of turn $r(t)$. As a first attempt to describe the human operator output in the four cases just-mentioned a model is proposed which is based on the following assumptions (See Fig. 5):

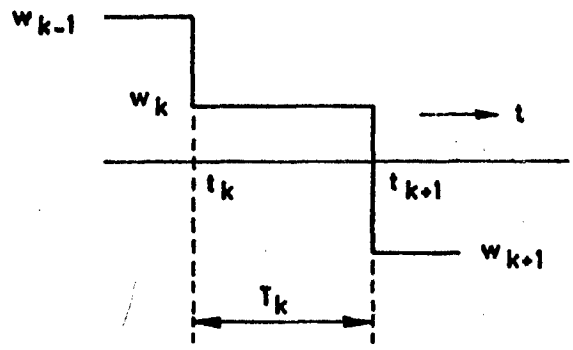

Figure 5: Some of the quantities involved in the proposed model for the helmsman.

- The duration of the k^{th} period $T_k = t_{k+1} - t_k$, over which the wheel position w(t) is kept constant at a value $w_k = w(t_k)$, can be predicted only from the values of the previous wheel position w_{k-1}, the heading angle $\psi_k = \psi(t_k)$ and the rate of turn $r_k = r(t_k)$ at the time t_k, where the time t_k means the starting point of the k^{th} period. The simplest equation to describe this relation is a linear one:

$$T_k^* = a_o + a_1 w_{k-1} + a_2 r_k + a_3 \psi_k, \qquad (5)$$

where T_k^* is the value of T_k as predicted by the model, and where the quantities a_o, a_1, a_2 and a_3 are constants.

- The magnitude of the desired rudder angle w_k at the time t_k will only depend on the values of w_{k-1}, r_k and ψ_k. Again a simple linear relation is chosen for the value w_k to be generated by the model, viz:

$$w_k^* = b_o + b_1 w_{k-1} + b_2 r_k + b_3 \psi_k, \qquad (6)$$

where w_k^* is the predicted value of w_k and b_o, b_1, b_2 and b_3 are constants.

6. Parameter Estimation

The parameters a_o, a_1, a_2, a_3, b_o, b_1, b_2 and b_3 can be estimated by minimizing a quantity E defined as:

$$E = \frac{1}{T} \int_o^T [\varepsilon(t)]^2 dt, \qquad (7)$$

where the signal $\varepsilon(t)$ represents the difference between the human operator output $w(t)$ and the model output $w^*(t)$. The minimal value of the quantity E can be found by partial differentiation of this quantity with respect to each of the unknown parameters and by setting the result equal to zero. This yields as many equations as there are unknown parameters. Fig. 6 shows an example of how a possible realization of the signals $w(t)$, $w^*(t)$ and $\varepsilon(t) = w(t)-w^*(t)$ might look for a chosen set of parameters a_i and b_i where i=0(1)3. As both the signals $w(t)$ and $w^*(t)$ occur in discrete steps, Eq. (7) can be replaced by Eq. (8), which consists of a summation over a number of terms:

$$E = \frac{1}{T} \sum_{j=0}^{m} (w_j - w_j^*)^2 (t_{j+1} - t_j). \qquad (8)$$

Here, it should be observed that the index j refers to the steps in the signal $\varepsilon(t)$, while the index k belongs to the steps in the signal $w(t)$ and the index k^* indicates the steps in the model output for which the Eqs. (5) and (6) were proposed. This means that it is not possible to insert Eqs. (5) and (6) into Eq. (8) in a simple way (See Fig. 6).

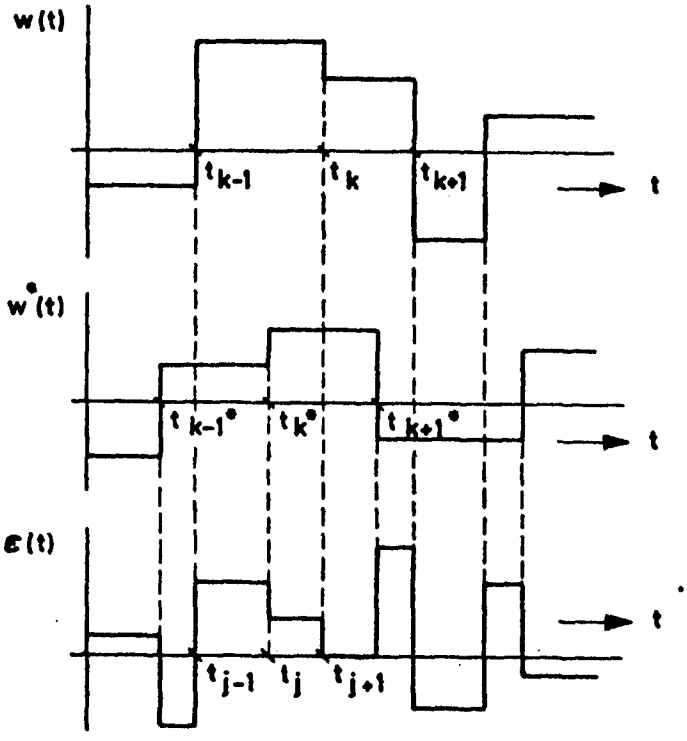

Figure 6: Possible time history of a helmsman's output $w(t)$, the output of a helmsman's model $w^*(t)$ and the difference between these two signals $\varepsilon(t)=w(t)-w^*(t)$.

Furthermore, it should be noted that if a model with given parameters should be inserted into the control loop instead of the helmsman, this would lead to another time history for the quantities w(t), ψ(t) and r(t). So, in order to get an unbiased estimate of the parameters in the human operator model, a comparison should be made between the output of the helmsman and the output of the model, where this model is also part of the closed loop system with the ship model (See Fig. 7).

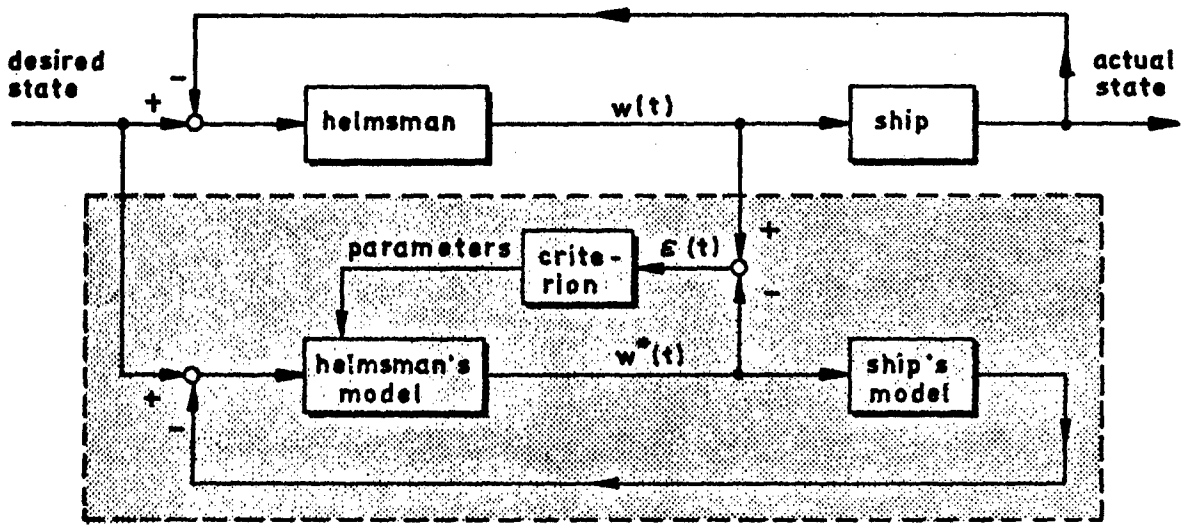

Figure 7: Application of an error criterion in such a way that unbiased parameters can be obtained for a model of a system in a closed loop.

In view of the problems just-mentioned, it may be assumed that the estimation of the parameters in the model of the helmsman will not be a simple straightforward matter.

As a possible procedure it is proposed to obtain an initial estimate based on a very simple method, which, however, yields biased results. These estimates are then inserted into the helmsman's model of Fig. 7. Next, the error signal $\varepsilon(t)$, which follows from a comparison of the actual output w(t) and the model output w*(t), is used to compute corrections on the initial estimates. From the values of the parameters obtained in this way a new output w*(t) of the model is computed and the procedure is repeated until the quantity E does not decrease any more. As a way to obtain the initial estimates the following method is proposed:
Consider Eq. (6) and assume that the time intervals T_k^* of the model have the same values as those which result from the real system, i.e. as far as Eq. (6) is concerned it is assumed

that $T_k^* = T_k$. Now minimize the quantity:

$$E_1 = \frac{1}{T} \int_0^T \left[w(t)-w^*(t)\right]^2 dt,$$

which can be rewritten as:

$$E_1 = \frac{1}{T} \sum_{k=1}^{n} (w_k-w_k^*)^2 T_k. \qquad (9)$$

By defining the quantities: $u_{ok}=1$; $u_{1k}=w_{k-1}$; $u_{2k}=r_k$ and $u_{3k}=\psi_k$, Eq. (6) can be transformed into Eq. (10).

$$w_k^* = \sum_{i=0}^{3} b_i u_{ik}. \qquad (10)$$

By inserting Eq. (10) into Eq. (9) and by minimizing this result with respect to the parameters b_i, a set of linear equations arises from which the quantities b_i for i=0(1)3 can be calculated.
In a similar way Eq. (5) can be considered. Here, an initial estimate for the parameters a_i for i=0(1)3 can be calculated by minimizing the quantity $E_2 = \sum_{k=1}^{n} (T_k-T_k^*)^2$ with respect to the parameters a_i.

7. Results

In the Figs. 9, 10, 11 and 12 some examples are given of the time history of the desired rudder angle w(t), the rate of turn r(t) and the heading angle $\psi(t)$ during a course keeping task. As mentioned already, the examples have been chosen in such a way that the different types of characteristic behavior are represented. Fig. 8, for instance, shows the performance of subject A, who had some experience with large ships. The recording was made after a one hour training period on the simulator. Fig. 9 shows the results of subject B, also after a one hour training period. Here, it should be mentioned that subject B had been watching subject A during the execution of his task and obviously had learned A's strategy.
Fig. 10 shows the performance of subject C during his first run on the simulator. The record shows that he moved his rudder almost every 10 seconds as distinct from the subjects A and B, where these intervals were approximately 40 seconds. After this run subject C was instructed to use longer intervals.

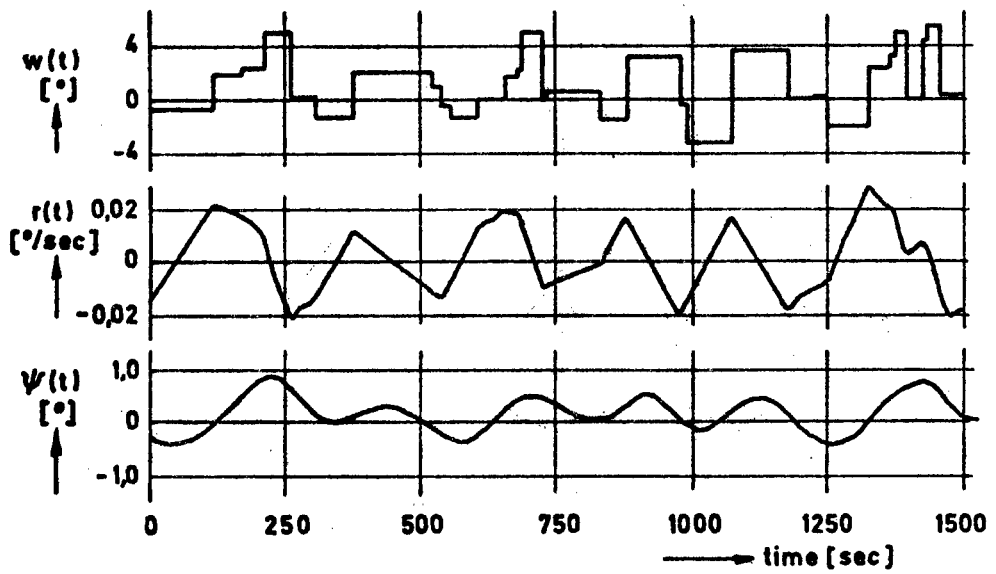

Figure 8. Time history of the wheel position (on desired rudder angle) w(t), the rate of turn r(t) and the heading angle ψ(t) for subject A during course keeping for half an hour.

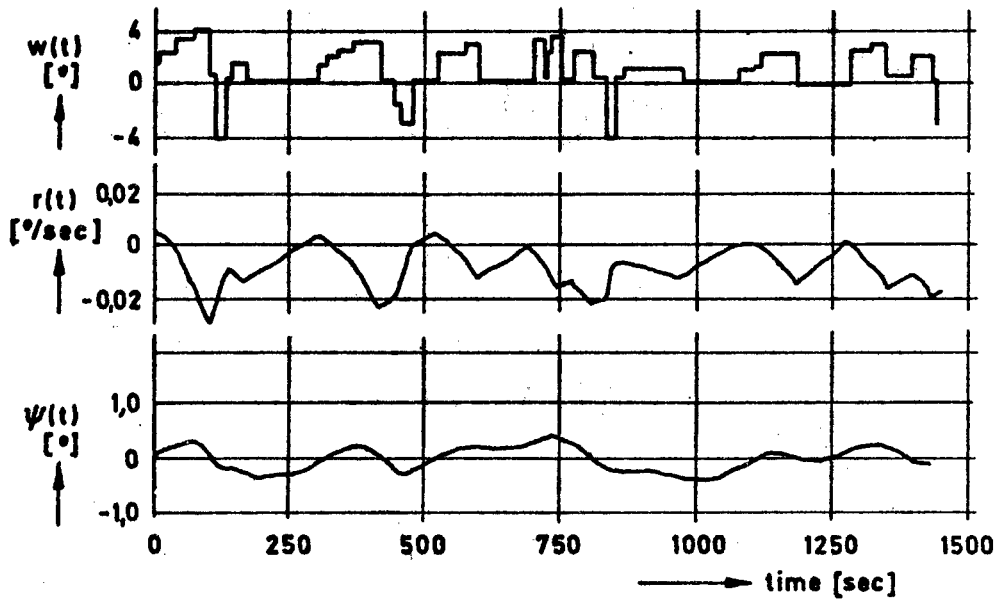

Figure 9. Time history of the signals w(t), r(t) and ψ(t) for subject B during course keeping for half an hour.

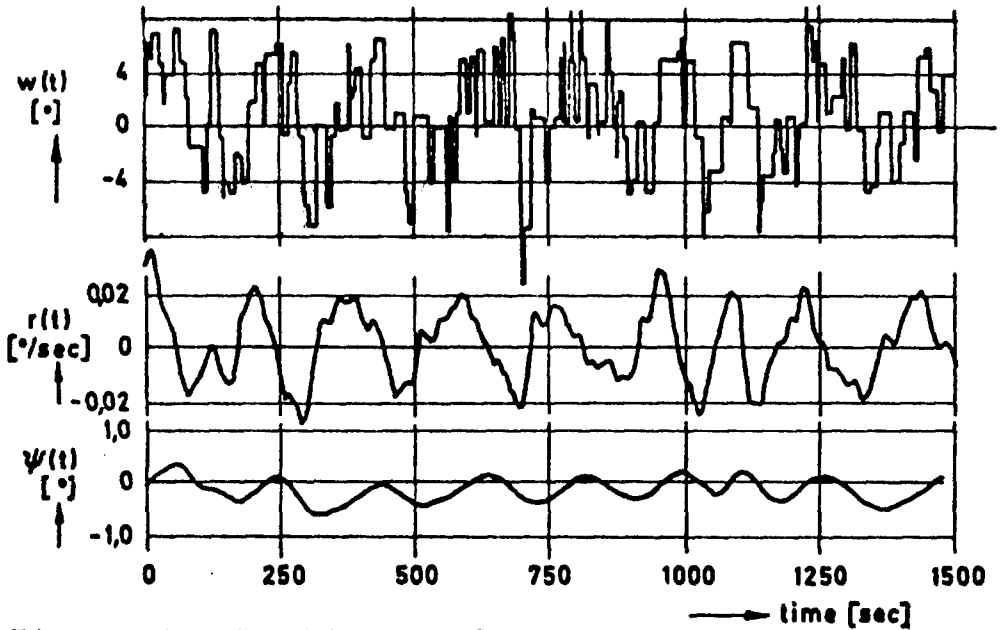

Figure 10. Time history of the signals w(t), r(t) and ψ(t) for subject C during a first trial in a course keeping test.

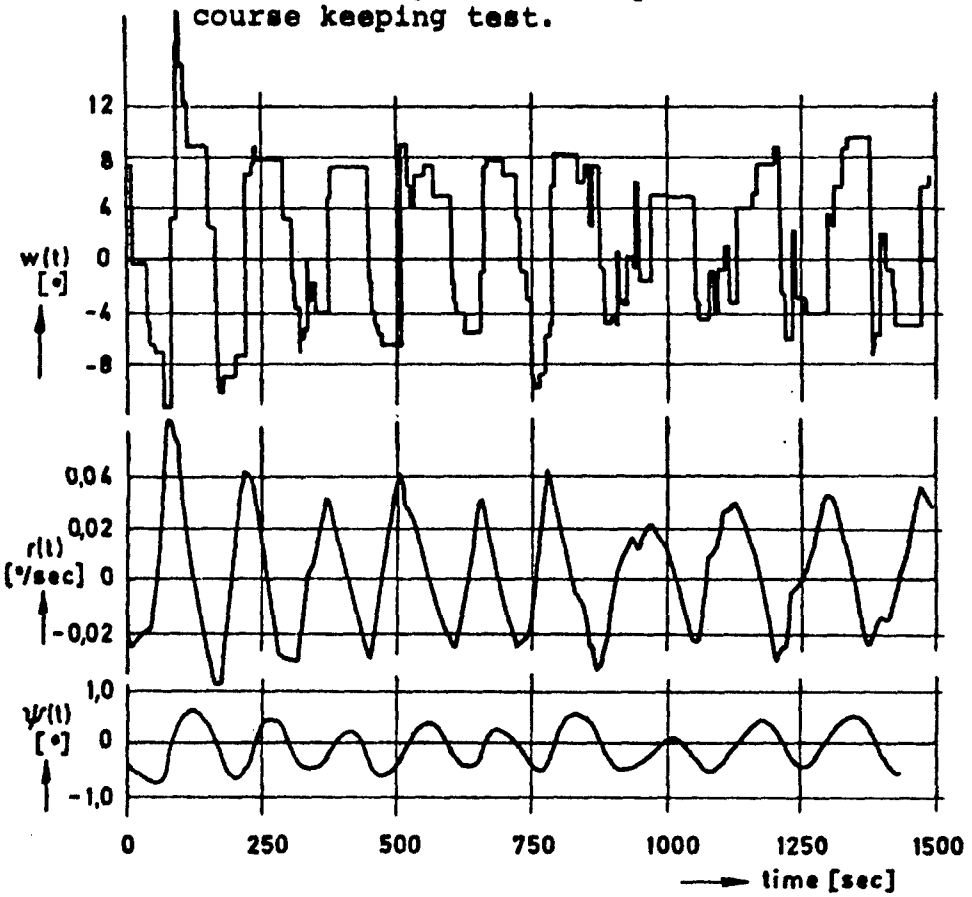

Figure 11. Time history of the signals w(t), r(t) and ψ(t) for subject C during his third trial in a course keeping task.

Fig. 11 shows the results of subject C during his third run, so also after one hour of practice. The results of the other experiments, the results from which lay somewhere in between the two extremes just shown, are not given here.

As a first step towards modelling the helmsman the records shown in the Figs. 8, 9, 10 and 11 have been sampled at the moments where the helmsman changed the rudder angle. From these data the initial estimates of the parameters have been calculated according to the method mentioned before. Although these values are biased, they are listed in Table III in order to give a first idea about the usefulness of this type of model.

Table III: The constants a_i and b_i for i=0(1)3 and the quantities E_1 and E_2 as an initial estimate for the parameters in the model described by:

$$T_k^* = a_o + a_1 w_{k-1} + a_2 r_k + a_3 \psi_k;$$

$$w_k^* = b_o + b_1 w_{k-1} + b_2 r_k + b_3 \psi_k.$$

subject	trial	a_o	a_1	a_2	a_3	E_1	b_o	b_1	b_2	b_3	E_2
A	3	60	-14	-1190	33	0.20	0.37	0.01	92	3.3	0.22
B	3	30	9	650	-87	0.31	0.75	0.18	129	2.7	0.31
C	1	12	-4	-31	0	0.21	1.95	0.09	120	8.5	0.55
C	3	19	0	84	7	0.35	3.06	0.00	54	14.6	0.22

8. Conclusions and further research

In Table III it can be seen that the numerical values of the parameters vary over a wide range; this is clearly illustrated by the values for the parameters a_2 and a_3. This result is not surprising since the number of parameters is rather large in relation to the data records length and because very different types of behavior are considered. Besides, it has to be taken into account that these values are biased estimates.

Therefore, in the near future the following steps will be executed:

a. The development of a computer program to generate unbiased estimates.

b. A further investigation of possible structures for the model; special emphasis will be directed at a sensible reduction of the number of parameters.
c. A comparison between the model obtained and a describing function model, especially with respect to the validity of both the models in a number of different situations.
d. Estimation of the mean value and the variance of the model parameters for one subject as well as for a group of subjects in a number of different tasks.

9. Acknowledgements

The authors gratefully acknowledge the contribution of C.C. Glansdorp of the Shipbuilding Laboratory of the Delft University of Technology.
They are also greatly indebted to TNO-IWECO for providing the facilities to do the experiments. Our special thanks go to the staff of the TNO-IWECO simulator group for their contributions in the preparation as well as in the execution of the trials. Finally, we would like to express our gratitude to the subjects from the School of Navigation at Rotterdam for their wholehearted cooperation.

10. References

1. Brummer, G.M.A. and van Wijk, W.R.: "The Ship Manoeuvring and Research Simulator of the Institute TNO for Mechanical Constructions", Delft, Inst. TNO for Mech. Constr., Report Nr. 8133/1, September 1970.
2. Stuurman, A.M.: "Modelling the helmsman: A study to define a mathematical model describing the behaviour of a helmsman steering a ship along a straight course", Delft, Inst. TNO for Mech. Constr., Report Nr. 4701, May 1969.
3. Nomoto, K; Taguchi, T; Honda, K. and Hirano, S.: "On the steering qualities of ships", International Shipbuilding Progress, Vol. 4, Nr. 35, July 1957, pp. 354 - 370.
4. Bech, M. and Wagner Smitt, L.: "Analogue Simulation of Ship Manoeuvres", Lyngby (Denmark), Hy A Report Hy 14, September 1969.
5. Glansdorp, C.C. and Buitenhek, M.: "Manoeuvring Trials with a 200 000 tons Tanker", Delft, Shipbuilding Laboratory of the Delft University of Technology, Report Nr. 248, August 1969.

6. Glansdorp, C.C.: "Simulation of Full Scale Results of Manoeuvring Trials with a 200 000 tons Tanker with a simple Mathematical Model", Delft, Shipbuilding Laboratory of the Delft University of Technology, Report Nr. 301, March 1971.

7. Mc Ruer, D.T. and Jex, H.R.: "A Review of Quasi Linear Pilot Models", IEEE Trans. on Human Factors in Electronics, Vol. HFE-8, No. 3, September 1967, pp. 231 - 249.

SESSION XI

Eye Movements, Eye Tracking, and the Distribution of Attention

Preceding page blank

A MODEL FOR THE STEP-LIKE COMBINED EYE-HEAD MOVEMENT.

By Gerhard Vossius, Karlsruhe

In the research on the control of voluntary movement mostly the characteristics of single systems, as handtracking, were considered. The eye movement was performed under the artifical condition of having the head in a fixed position. The next step was to study the integration of two such systems as a functional unit within the CNS, because a new organisational level in the hierarchy of the motor control system can possibly be reached in this manner.

If a step-type horizontally moving command signal is displayed to a subject with full freedom of head motion, the pursuit movement for small amplitudes will only be performed by the eye in the manner described above. In the case of command steps, whose amplitudes are greater than 10°-20°, the head also turns. The pursuit movement is started by an eye movement, which is performed initially in the direction of the target as a fast saccade.

With the initiation of head movement, the motion direction of the eye is reversed, so that the eye and the head perform movements of identical velocity in opposite directions. The direction of the visual axis, which is the sum of the eye and the head position, thus remains constant. If the initiating saccade of the eye has already reached the target, the visual object is fixed and cannot be lost again during the subsequent tracking movement of the head. The fixation occurs within an optimum by short time. The slower tracking movement of the head, caused by its greater mass, is balanced by the time-coordinated reset motion of the eye (fig.1). If the visual axis in the final position of the eye and the head does not reach the target line of sight, the reverse eye movement is interrupted by a motion towards the target by one or more saccades (fig.2). If the initial saccade of the eye movement is too large, the reset motion of the eye will occur in a direction opposit that of the head. The dynamics of the eyes motion are identical to those of the head but with a gain factor larger then one (fig.3). Likewise the second, usually retrograde phase of the eye movement, can sometimes be reversed into a parallel movement, if the initial saccade is too small. If the reset movement occurs too fast, this retrograde movement is interrupted just at the moment when the eye has reached a position which yields, together with the final head position, the target amplitude. Subsequently the head movement is completed (fig.4).

The eye and the head movement thus cooperate in a functional unit with the head movements as the dominant part. The head movement is fed as a negative command signal to the eye. Besides, the eye movement is able to compensate directly for errors. The eye movement, however, is not only a negative copy of the head movement, but both of these movements are controlled by a higher coordinating center. This follows from the results of the experiments described above: First, the feedback of the eye is performed at the ratio >1, if the final position of the visual axis otherwise shows a deviation. Secondly, corrective saccades appear

Preceding page blank

when the initial eye movement is too small even before completion of the slow phase of the eye and head movement.Thirdly, the eye movement is interrupted too soon in the case where a reset motion is performed too fast. Forthly, the eye movement can reverse before the head movement starts (fig.5), therefore its reversal cannot be a consequence of head motion.

As a result the eye and head movements are initiated by a common higher coordinating center and monitored in their progress. In order to be able to control properly the velocity of the reversal of the eye movement, a model of the head dynamics is required in this center. Like the necessary additional corrective saccades, the magnitude of the scale factor can be calculated by comparing the command step function amplitude with the jump motion amplitude of the eye and the head initiated by the CNS. Fig.6 shows a model which accounts for all of the step responced dynamics so far observed.

From the model we guessed, that for to large a step response of the head the second phase of the eye motion should not be reversed. Looking carefully on our records we discovered an example, where the eye movement, after to fast initial motion components, shows this pattern.

Thus the step transfer characteristics of eye-head movement can be explained through the use of a very clear and relatively simple model. This should not conceal, however, the fact that the CNS performs a very effective controlling function on the dynamics of the total motion, which includes such complex components as a model describing the dynamics of the head. Thus from a control theory point of view the brain needs no further implementation beyond that described for its function in this area. All possibilities of error occurence, including estimation errors, which occure during the determination of the eye and head movement amplitudes, can be corrected for during the process of the movement.

This work was partly conducted with D. FLEMING.

References: Vossius, G.:
Higher coordinative functions of the vestibular and oculo-motor systems,
in: Vestibular and Oculomotor Problems;
Tokyo 1965, p. 183.

Vossius, G.:
The functional organisation of object directed human intended-movement and the forming of a mathematical model,
in: Displays and Controls, Ed. R.K.Bernotat and K.-P.Gärtner;
Amsterdam 1972, p. 389.

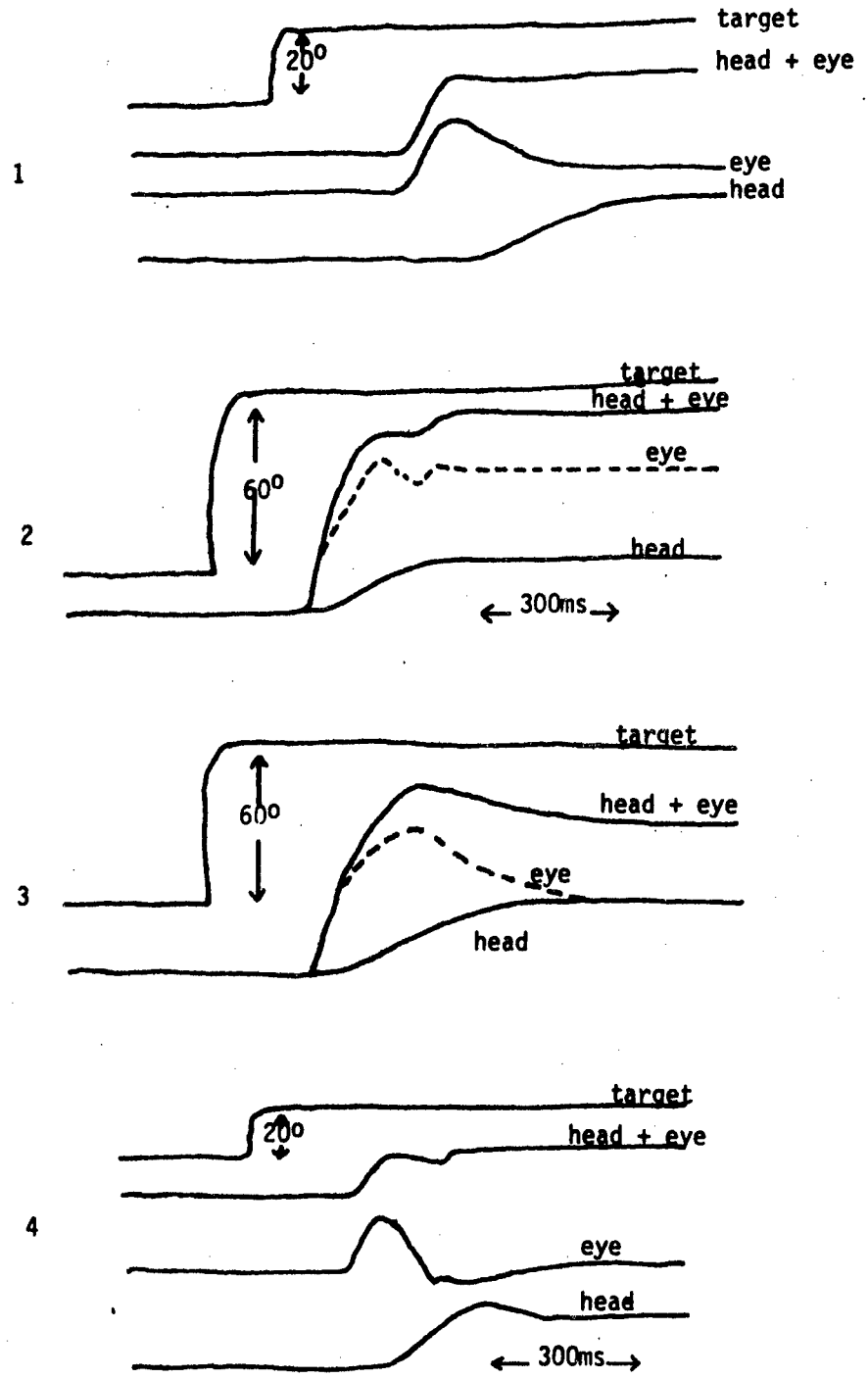

Fig. 1 - 4 : Step response of eye - head movements.

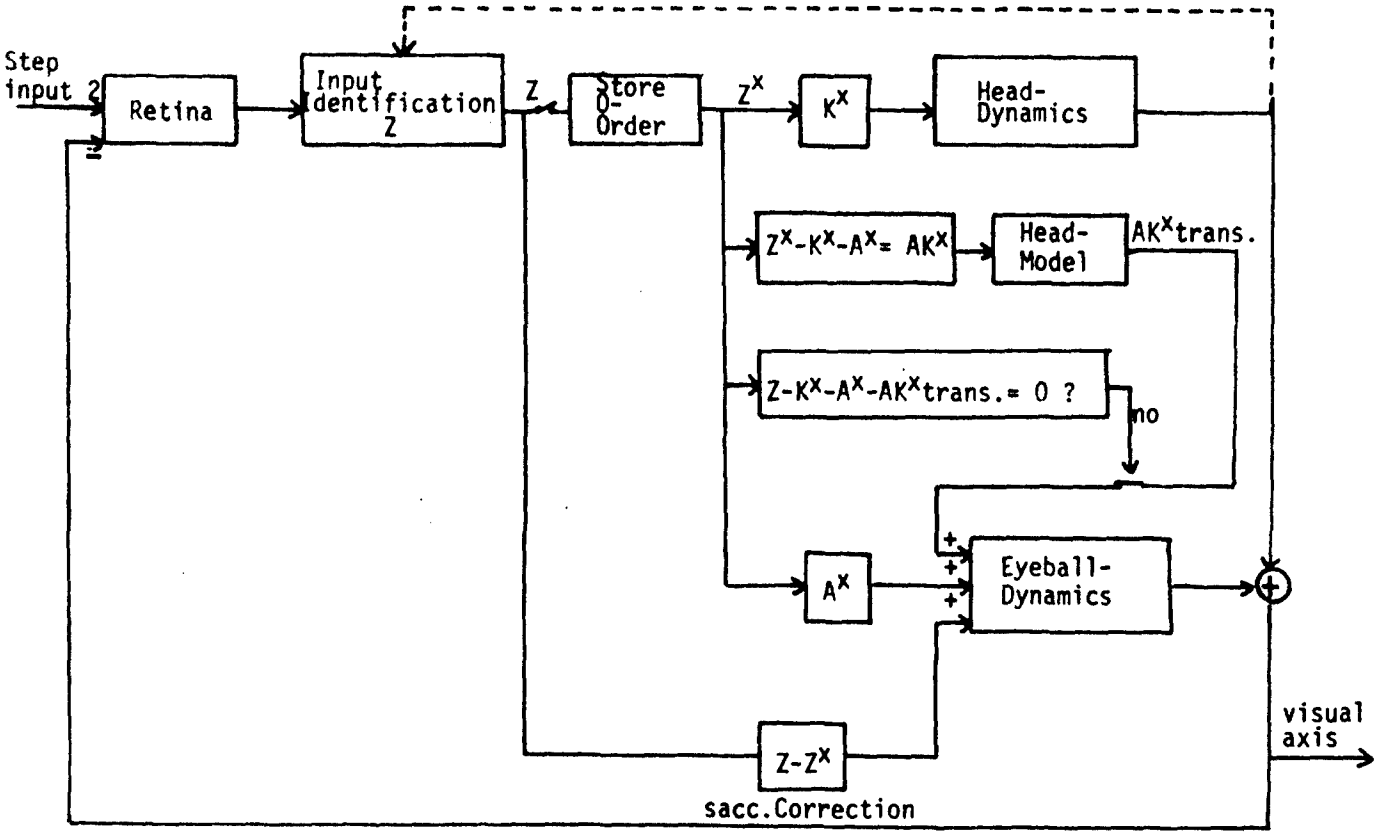

Fig. 5 : Schema of the calculation of the combined step-type eye-head movement.

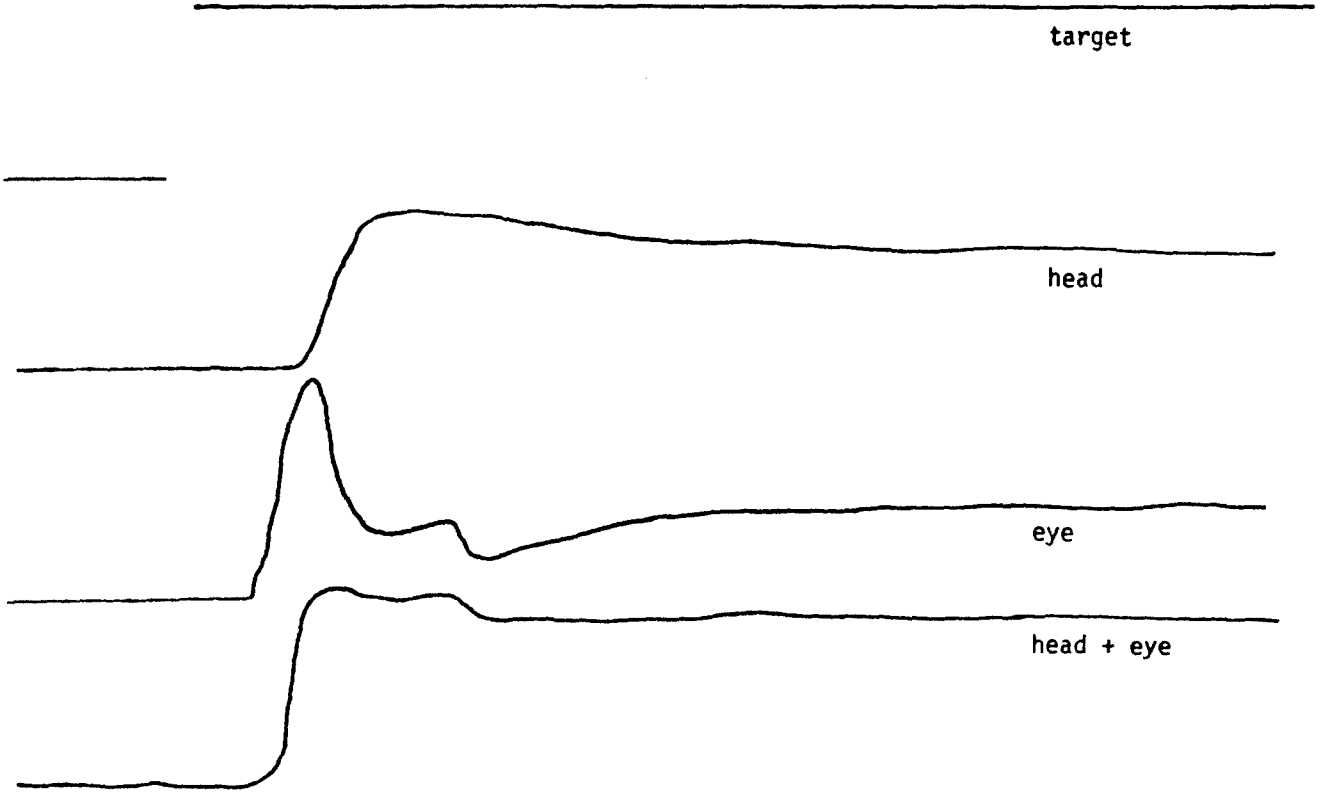

Fig. 6 : Step response of an eye-head movement, where the head movement is to large.

A SINGLE-CHANNEL MODEL OF ATTENTION SHARING IN A DYNAMIC DUAL-TASK ENVIRONMENT

Robert C. Cliff
Department of Industrial Engineering and Operations Research
University of California
Berkeley, California

Abstract

Based on experimental findings reported previously, a deterministic, single-channel model of human attention sharing was developed, and implemented in the form of an on-line hybrid computer simulation. The model structure is discussed and the results are compared with human operator data. Design and research implications of the model are also discussed.

Introduction

At the onset of the present investigation into dual-task performance, two objectives were set out. First and primarily, the aim was to conduct an experimental investigation which would provide basic data on dual-task performance, and which would point to the major mechanisms accounting for the decrement in performance when a second task was added to the task environment. The second objective was to develop a preliminary model of dual-task performance. The model was to be based on observations made during the experimental phase, and would supply a method for testing the validity of the hypotheses formulated during this phase.

In response to the first objective, results from an experimental investigation of dual-task performance, utilizing a compensatory tracking task and a concurrent shadowing task, have been previously reported [1, 2]. Before offering a model which may account for these results, a brief summary will be provided of the experimental procedures used in this investigation and of the results obtained.

An experiment was conducted in which subjects were seated in a soundproofed room approximately two feet in front of an oscilloscope displaying a point of light which could move along the 4.5 inch horizontal diameter. In the center was a vertical arrow which represented the zero error condition for a compensatory tracking task. Control was accomplished through a zero order control knob which had left-right compatibility with the display. S.T.I. type forcing functions (ten summed sinusoids) were used as input to the tracking task.

The subject was also equipped with headphones through which a shadowing input was received. Volume on the headphones was adjusted for comfortable listening for each subject. The shadowing task required the subject to repeat aloud random number pairs which were received through the headphones.

For each tracking forcing function used, subjects were required to track once without shadowing and once while simultaneously shadowing. The following is a summary of the principal experimental findings.

(1) When "slow" shadowing (about one random number pair per second) was performed simultaneously with a zero order compensatory tracking task, there was no evidence of a performance decrement on either the tracking or shadowing task attributable to their concurrent performance.

(2) When "fast" shadowing (about one and a half random number pairs per second) was performed simultaneously with a zero order compensatory tracking task, there was a consistent performance decrement on both the tracking and shadowing tasks attributable to their concurrent performance.

(3) The tracking decrement, as measured by normalized rms error, increased with forcing function bandwidth.

(4) There was no evidence to support the view that the dual-task decrement could be accounted for by a simple information channel capacity model.

(5) A major source of the dual-task decrement on both tasks seemed to stem from holds or cessation of response output for brief periods of time.

(6) It was not possible to account for the holds on either task in terms of a fatigue phenomenon.

(7) A contingency analysis of the shadowing and tracking holds revealed that for three of the five subjects analyzed there were slightly more simultaneous shadowing and tracking holds than would be expected if the two types of holds had been generated independently.

(8) A close analysis of the onsets and offsets of the tracking holds indicated that there was a high probability that the tracking error state was quite low at the onset of a hold, and that the subjects seemed to wait for the error magnitude to begin decreasing before resuming control.

(9) Closed loop frequency plots of the tracking response indicated less loop gain and greater phase lag when the shadowing task was added to the task environment.

(10) Cross-correlation analysis of the tracking records revealed that the open loop tracking lags increased from 0.05 seconds to 0.10 seconds with the addition of the shadowing task.

The above findings do not in themselves specify a unique model for dual-task performance; however, they do appear to be suggestive of an underlying single-channel process. This conclusion is drawn both from the empirical findings mentioned above and from a consideration of the vast amount of evidence for a single-channel mechanism in the resolution of temporal and spatial uncertainty with respect to response selection in discrete tasks [2, 3]. The facts that tracking and shadowing holds were found

not to be completely independent, and that there seemed to be a definite relationship between the tracking error state and the probability of a tracking hold certainly suggested an interrelationship between the current task demands and the other task. Furthermore, an examination of the human operator's tracking transfer characteristics showed an increase in the transport lag term with the addition of the shadowing task. If there were no attention sharing, and the dual-task decrement were solely due to the quality of control devoted to each task simultaneously, one would expect a lower tracking gain and probably a longer time constant; however, one would not necessarily expect an increased transport lag. On the other hand, it is easy to account for the increased transport lag in an attention sharing model as an increased average time away from the tracking task.

Before presenting the model developed here, it should be pointed out that there have been other attempts to develop multi-task control models [4, 5, 6, 7]. While these models do show value in predicting the correct distribution of visual attention between two visual-manual tasks, they have not been concerned with attention sharing between tasks with independent input-output modes, where task interference is limited to the human central processes. The attempt here was to start the development of a micro-information processing model which would closely resemble the human strategy in monitoring and controlling a variety of continuous independent tasks.

The Model Assumptions and Hypotheses

Based on the experimental results from the study summarized above, and published results from other fundamental human performance studies, a set of assumptions for a model of dual-task control were constructed. The following five assumptions formed the basis for the model to be presented in this paper. (Pertinent references which help to substantiate each assumption are given in brackets).

(1) The human operator is inherently a single-channel attention mechanism which can process only one stimulus-response transfer at a time when the resolution of uncertainty is required [1, 2, 3].

(2) There is a buffer storage capability for limited amounts of past input data inherent in the senses and the early signal processing neural networks [8, 9, 10].

(3) There is an inherent internal human operator "cycle time" of about 50 msec, (perhaps a slightly variable period corresponding to α-rhythm zero crossings) which governs the input, output, and switching of attention in stimulus-response tasks [11, 12].

(4) Stimulus-response decision making, attention switching, and other mental tasks will require exactly one or more "cycle time" units depending on the task difficulty as measured by the resolution of uncertainty required by the response [11].

(5) The operator allocates his attention between the two tasks in response to the current state of each task [1].

Assumptions one and two seem reasonable in light of the referenced literature and the results from the first phase of the work. Assumptions three, four, and five, however, are on more tenuous ground. Although there is evidence to suggest that input and output of information is a discrete process [1, 3], Kristofferson's [11, 12] is the only work suggesting a 50 msec "cycle time". Others have suggested about 100 msec [13]; however, this may be an aggregate of the 50 msec unit as suggested in assumption four and by Kristofferson [8]. Finally, the results presented by Cliff [1, 2] dealing with the tracking error state and its relationship to the probability of the occurrence of a tracking hold, empirically support assumption five.

Within the framework of the above assumptions, a specific micro-information processing model for dual-task shadowing and tracking performance was constructed based on the following set of specific hypotheses:

1. The displayed tracking error is sampled discretely and a response decision made, a process which takes two "cycle times" (100 msec)

2. Based on the sampled tracking error state the following response is made:

   (a) If the error state is low (i.e. sampled $|$ error $|$ is $\leq e_L$), a step command is sent to the neuro-muscular system of the hand to null out the sampled error, and attention is then switched to the shadowing task.

   (b) If the error state is medium (i.e. $e_L \leq$ sampled $|$error$| \leq e_M$), a step command is sent to the neuro - muscular system of the hand to null out the sampled error, and attention is continued on the tracking task.

   (c) If the error state is high (i.e. sampled $|$error$| \geq e_M$), the sampled value is stored and another sample is taken during the next two 50 msec periods. Subsequent action is then dependent on the rate of changes of the error magnitude:

      (i) If the magnitude of the error is increasing, no control is exerted on the tracking task and attention is switched to the shadowing task.

      (ii) If the error magnitude is decreasing, a step command is sent to the hand to null out the error and the tracking is again sampled.

3. The switching of attention from shadowing input to tracking input and vice versa takes one "cycle time" (50 msec).

4. While attention is focused on the tracking task, shadowing input can be temporarily stored in a buffer storage system which can store N_B shadowing input number pairs.

5. The shadowing buffer is filled from the bottom up, so that the last number pair into the buffer is the last out.

6. Shadowing number pairs are read out of the buffer one at a time, each number pair taking two "cycle times" for processing. After one number pair is processed for response, attention is switched back to the tracking task.

7. If attention is switched to the shadowing, and there is not an input in the buffer, attention is redirected to the tracking task during the next 50 msec interval.

The above hypotheses have been embodied in a state space diagram of the task, Figure 1. In the figure the selected states are indicated by circles, and the arcs connecting the states diagram the model structure outlined above. Dashed arcs represent state transitions dependent on the properties of the tracking forcing function at that point. Numbers on the arcs represent the number of "cycle times" (50 msec units) taken to make the transition between states.

Again, the proposed structure is not a unique outcome from the present and cited research. In fact, several modifications of this structure were investigated, and it was evolutionary process which led to the current model. However, there are several important parts of the structure which are substantiated by the experimental data and did not change. Most important is the dependence of tracking response on the sampled error state. This type of structure was suggested by the error hold analysis presented by Cliff [1]. It is clear from that analysis that the probability of a hold is function of the preceding error state and that tracking holds, in general, are terminated only when the tracking error starts to decrease. The shadowing function of the model is also fundamental and merely samples the shadowing input buffer and processes the appropriate verbal response during a 100 msec period if there is input to be processed.

The shadowing task clearly plays a secondary role in this model. While there was evidence for a causal relationship implying that a tracking hold causes a shadowing hold (items 7 and 8 in the summary at the beginning of the paper), there was little evidence to suggest that a shadowing hold might cause a tracking hold. These findings have been reflected in this model structure.

Given the above model algorithm, there were three adjustment parameters which could be used to obtain a fit of the model results to the actual subject generated experimental results. The adjustment parameters were:

(1) N_B, the shadowing input buffer length;
(2) e_L, the lower error threshold value; and
(3) e_M, the upper error threshold value.

FIGURE 1: STATE SPACE MODEL FOR TRACKING-SHADOWING TASK

(See Text for Explanation)

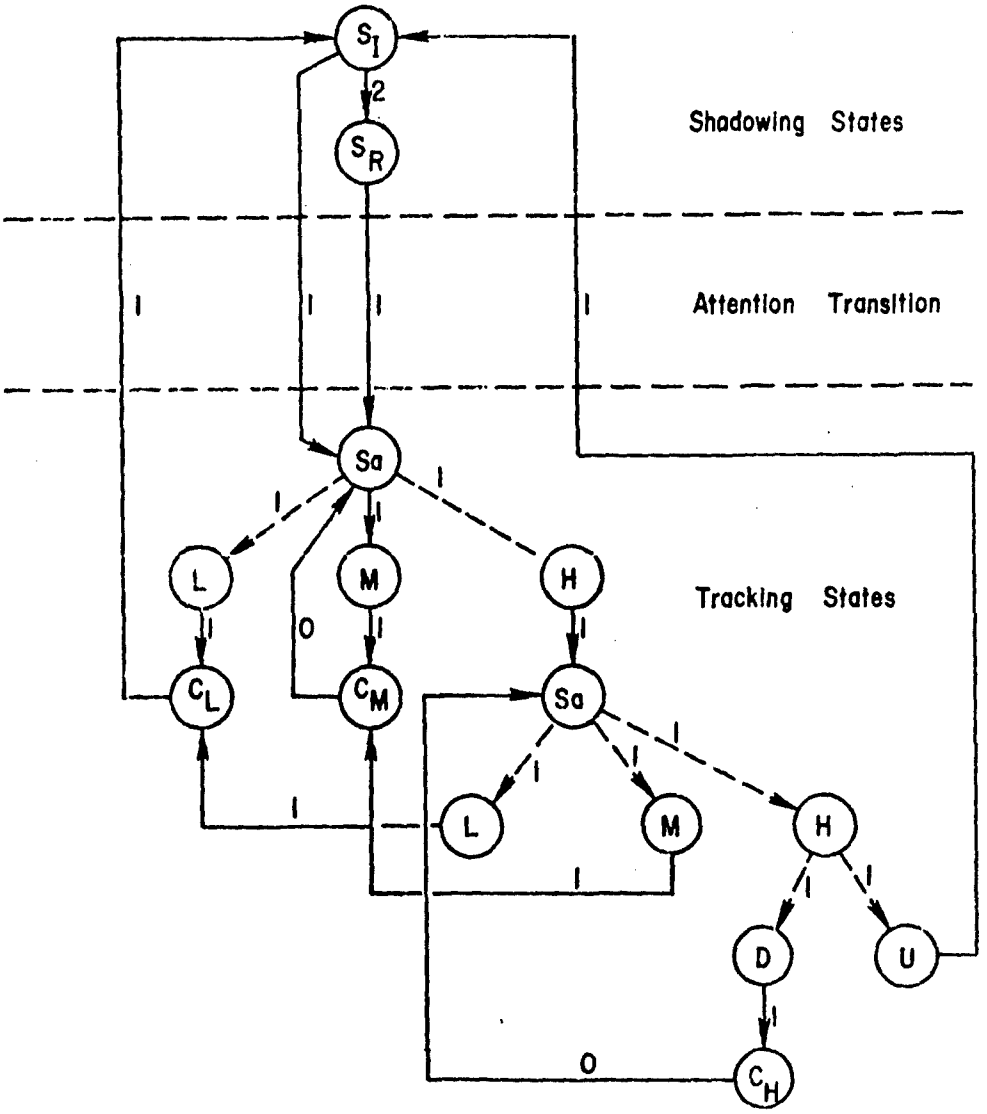

STATE SYMBOLS

S_I = begin sample of the next input from shadowing buffer

S_R = finished "programming" shadowing response

Sa = begin sampling tracking error
L = error state perceived as low
M = error state perceived as medium
H = error state perceived as high
C = tracking control response processed and sent to hand
U = error magnitude perceived as increasing
D = error magnitude perceived as decreasing

Numbers on arcs represent number of 50 msec time units for the transition

The Model Simulation

The model was implemented by way of a hybrid computer simulation. The state space decision portion of the model shown in Figure 1 was implemented on a PDP-8 digital computer, while the output commands were sent as voltages to an analog simulation of the neuro-muscular dynamics of the hand-arm system. At the present stage, a second order lag:

$$\frac{1}{s^2 + 11.77s + 96.00}$$

was used to simulate the hand dynamics. This transfer function was obtained by averaging step tracking responses (with the transport lag term omitted) for three subjects using the same apparatus that subjects used in the previously summarized study [1]. Figure 2 gives a schematic diagram of the complete system. The digital program also included a routine for online computation of the rms tracking error, and a real time chart recording was made of the pertinent model input and output states.

The tracking input to the model was the S.T.I.-type forcing function C used in the previous study [1], and is summarized in Table I. This input was selected because it produced the greatest increase in actual subject tracking error when shadowing was added and because the results obtained from this input have been extensively analyzed [1]. A fast shadowing input of two random number pairs per second was simulated internally in the digital program. It was also possible to vary the shadowing input rate or to eliminate it entirely, thus simulating the case of tracking without shadowing.

TABLE 1: FORCING FUNCTION C

Frequency		Normalized
Hz	RPS	Amplitude
2.200	13.800	0.1
1.210	7.570	0.1
0.642	4.030	1.0
0.404	2.540	1.0
0.237	1.490	1.0
0.154	0.969	1.0
0.096	0.602	1.0
0.063	0.393	1.0
0.042	0.262	1.0
0.025	0.157	1.0

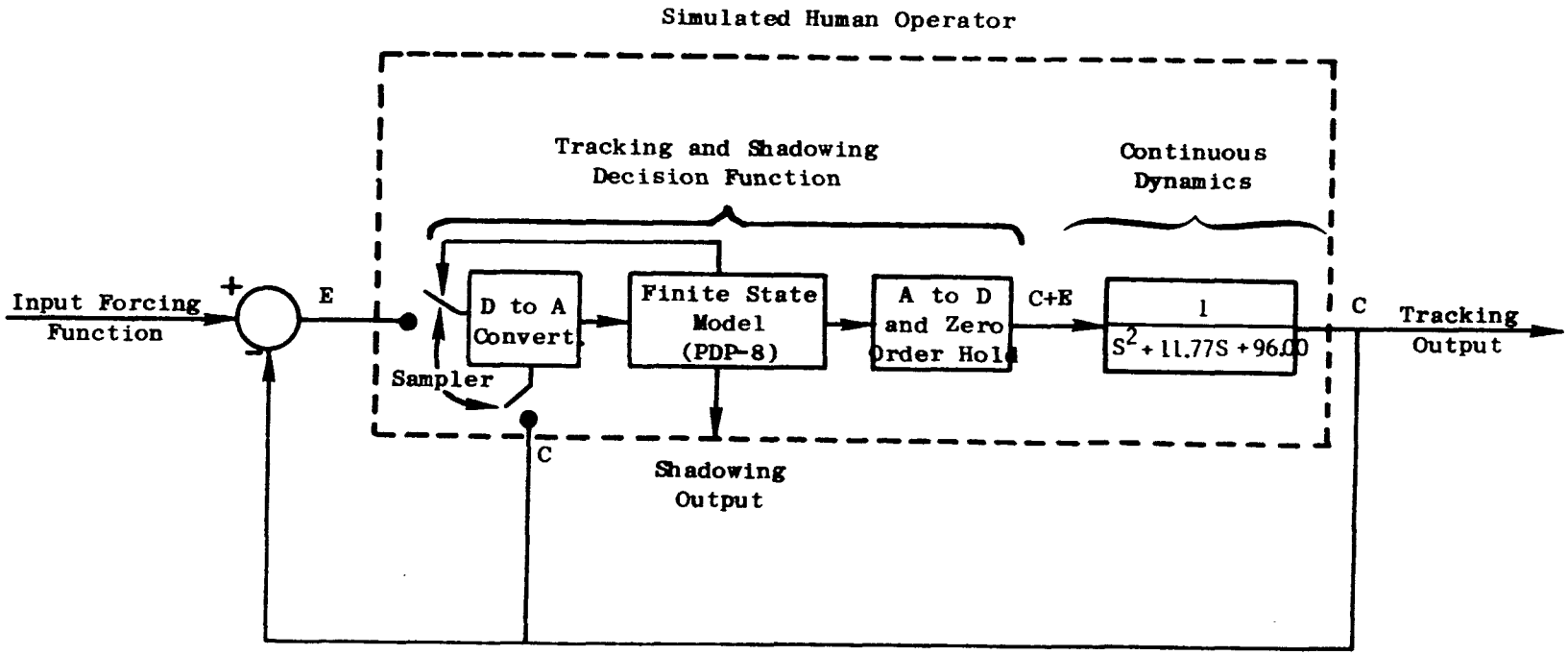

FIGURE 2: BLOCK DIAGRAM OF DUAL-TASK HUMAN OPERATOR MODEL IMPLEMENTATION

As a test case, an attempt was made to match the model's performance to the performance of subject number 10 from the previous study [1]. The three model parameters were adjusted in order to obtain an acceptable fit of model output to the records of the subject's responses. Two criteria were used in adjusting the model parameters. First, for the tracking while shadowing condition, it was desired that the normalized rms tracking error and the percent shadowing not missed should be about 68% and 79% respectively, and actual values for subject 10. Secondly, for tracking without shadowing it was desired that the model generate about a 43% normalized rms tracking error, again the value for subject 10.

The e_L e_M and N_B parameter space was searched and an acceptable fit was established based on the criteria above. The only acceptable value for N_B, the shadowing input buffer, was one. Upon re-examination of the original shadowing response recordings, it was found that this seemed also to fit with the observed data from the subjects. Subjects did not seem to lag behind the current shadowing input by more than one past input. With respect to the error thresholds, the best fitting values for e_L and e_M were respectively 0.25 and 0.54 standard deviations of the total error distribution. Since the error amplitude distribution was approximately normal, the resultant probability of a low error state ($|error| \leq .25$) was 20% of a medium error state ($.25 \leq |error| \leq .54$) was 21% and of a high error state ($.54 \leq |error|$) was 59%.

Results

The model was able to account for the actual human performance data fairly well. A sample of the model's tracking record is shown in Figure 3, and can be visually compared to the tracking record for subject 10 in Figure 4. With respect to the parameter adjustment measures used, the model was able to replicate subject 10's gross performance. In the dual-task mode, the model generated a 68% normalized rms tracking error with 77% of the random numbers successfully shadowed, which closely matched the 68% tracking error and 79% shadowing success for subject 10. Without shadowing, the normalized rms tracking error generated by the model was 42% compared with 43% for subject 10.

As a further test, the model was given the "slow" shadowing input of one random number pair per second along with the simultaneous tracking task. Although subject 10 was not required to track and shadow with the "slow" shadowing input, subjects 1 through 5 did receive this shadowing input. For these subjects the shadowing did not cause a tracking decrement (see item 1 in the summary of results at the beginning of this paper). This situation was closely duplicated by the model. Normalized tracking error with the "slow" shadowing was 44% compared with 42% error for tracking without shadowing. This result was obtained by leaving e_L as indicated above and eliminating e_M and the high error state. Under this condition all of the shadowing input was successfully processed, as was the case for subjects 1 through 5.

A more detailed examination of the model output also indicated fairly close agreement with results from subject 10. The model generated hold distributions on both the tasks which, like those generated by the subjects,

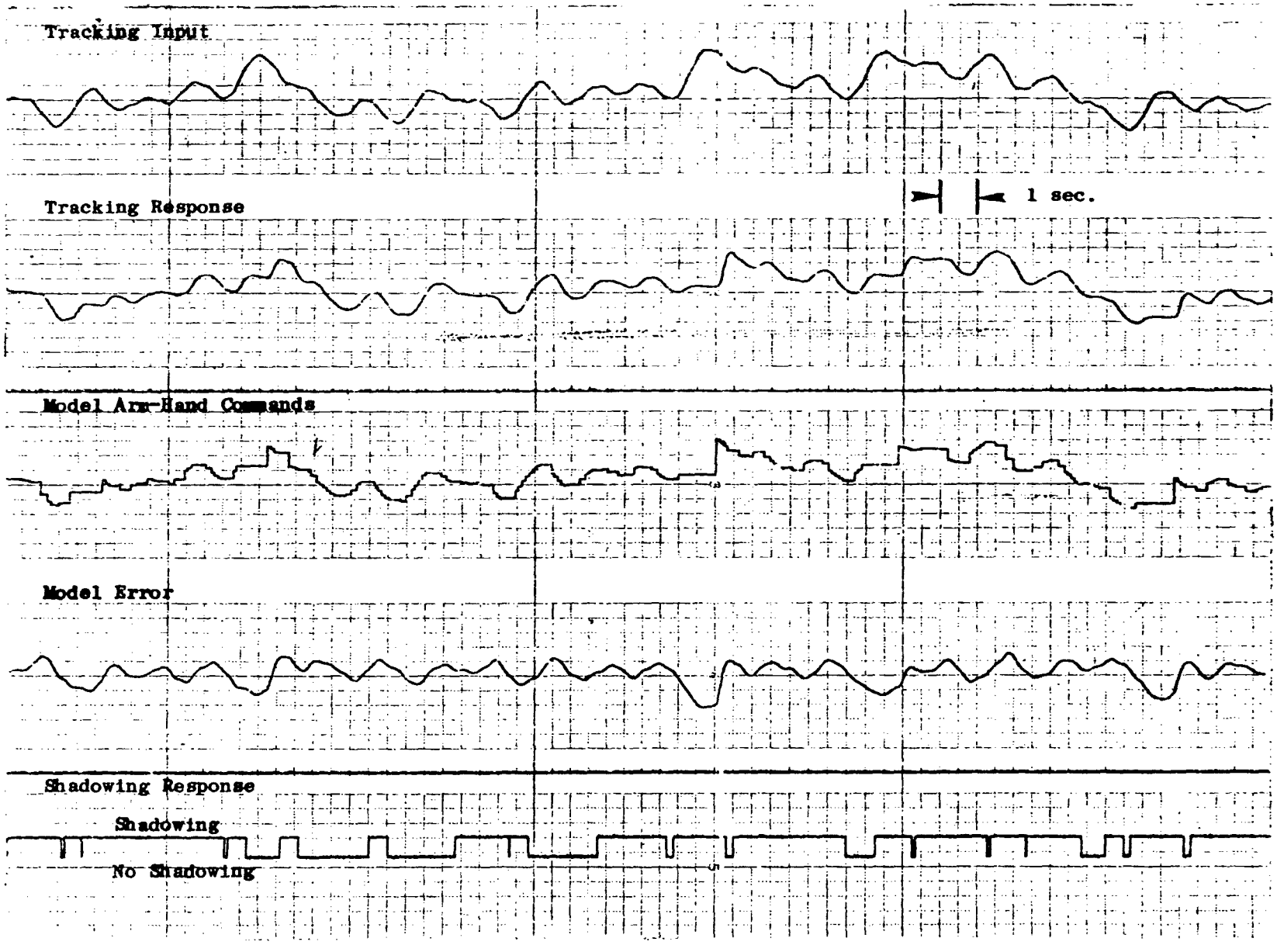

FIGURE 3: TYPICAL TRACKING AND SHADOWING RECORDS FOR THE MODEL, FORCING FUNCTION C AND FAST SHADOWING INPUT

Reproduced from best available copy.

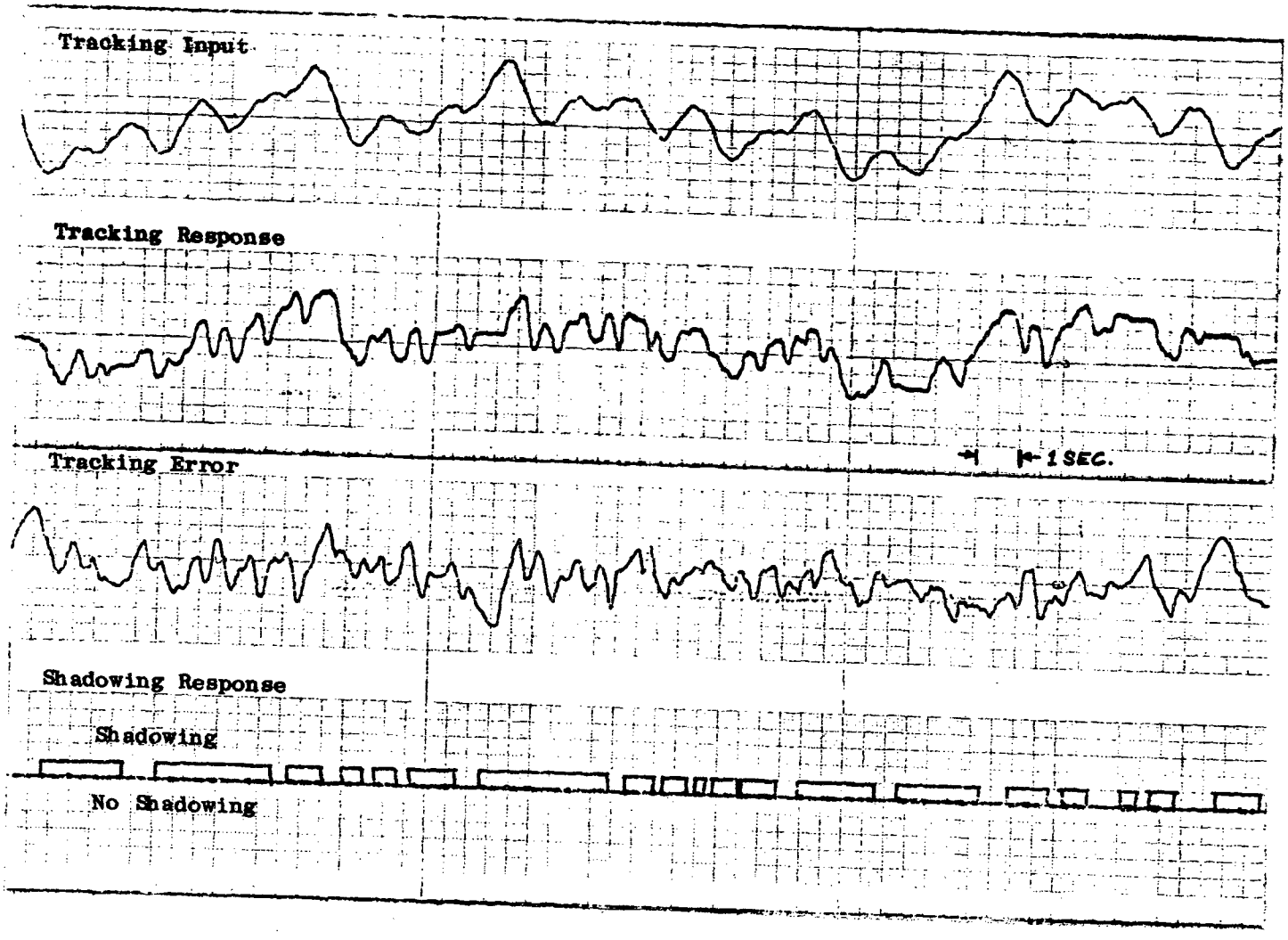

FIGURE 4: TYPICAL TRACKING AND SHADOWING RECORDS FOR SUBJECT 9, FORCING FUNCTION C AND FAST SHADOWING INPUT

had a decreasing frequency of occurrence with increased hold length. The hold distributions on both the tracking and shadowing tasks are given in Tables II and III for both subject 10 and the model. Here a hold has been defined as a cessation of tracking or shadowing activity for 0.3 sec. or longer. For the tracking hold distributions a Chi-squared test accepts the hypothesis that the two distributions are equivalent. The shadowing hold distribution did not match so well however. The model tended to generate shadowing holds which were on the average longer than those generated by the subject. Subject 10's mean shadowing hold time was 0.61 sec., while the model's was 1.00 sec. With respect to the interaction between the holds, the number of overlapping or simultaneous tracking and shadowing holds was only slightly more than would be expected if they had been generated independently. This was in agreement with results from subject 10. In fact, this was the case for most of the subjects [1].

Figures 5 and 6 are estimates of the closed loop tracking transfer Bode Plots for the model and for subject 10 respectively. Each Bode Plot includes estimates obtained from no shadowing and with shadowing tracking runs. There is more phase lag in the model transfer under both conditions at the higher frequencies; however, the general effect of the shadowing is strikingly similar in both cases.

Referring again to Figures 3 and 4 it can be seen that there is a considerably larger remnant term in the actual human operator output. This accounted for a sizable part of the operator's tracking error. Thus, by adjusting the model parameters to produce the same tracking and shadowing error scores as the operator, we have had to make the arm-hand response slower than it might actually be, and have set error thresholds so that they will account for the remaining tracking error, including the error due to remnant. This could explain why the model's phase lag is greater than the subject's. By injecting the operator's remnant spectrum into the model tracking output and then readjusting the error thresholds, a more accurate representation of the operator's response functions could be obtained. This, however, would not alter the underlying structure and logic proposed in the present model.

TABLE II: TRACKING HOLD DISTRIBUTIONS

Hold Duration (seconds)	Subject 10 Percent Occurrence	Model Percent Occurrence
0.3	23	23
0.4	20	18
0.5	18	15
0.6	12	17
0.7	11	13
0.8	6	8
0.9	6	3
1.0	4	3

TABLE III: SHADOWING HOLD DISTRIBUTIONS

Hold Duration (seconds)	Subject 10 Percent Occurrence	Model Percent Occurrence
0.3	17	8
0.4	16	3
0.5	10	0
0.6	13	15
0.7	12	15
0.8	14	3
0.9	3	10
1.0	3	10
1.1	2	8
1.2	2	5
1.3	3	0
1.4	0	0
1.5	0	0
1.6	2	7
1.7	1	3
1.8	2	3
1.9	0	7
2.0	0	3

FIGURE 5 MODEL CLOSED LOOP BODE PLOT – FORCING FUNCTION C

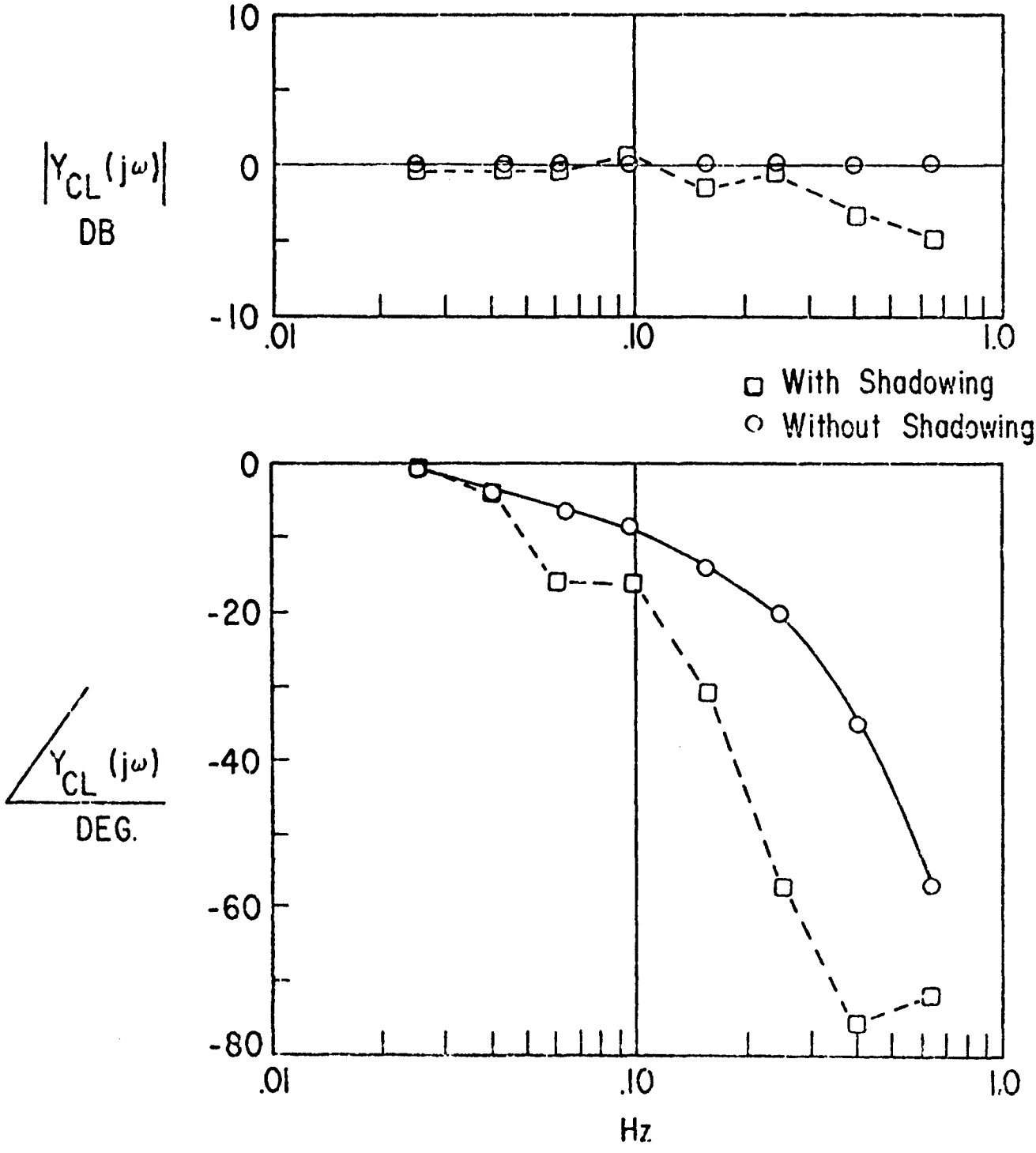

FIGURE 6: Subject 10 Closed Loop Bode Plot- Forcing Function C

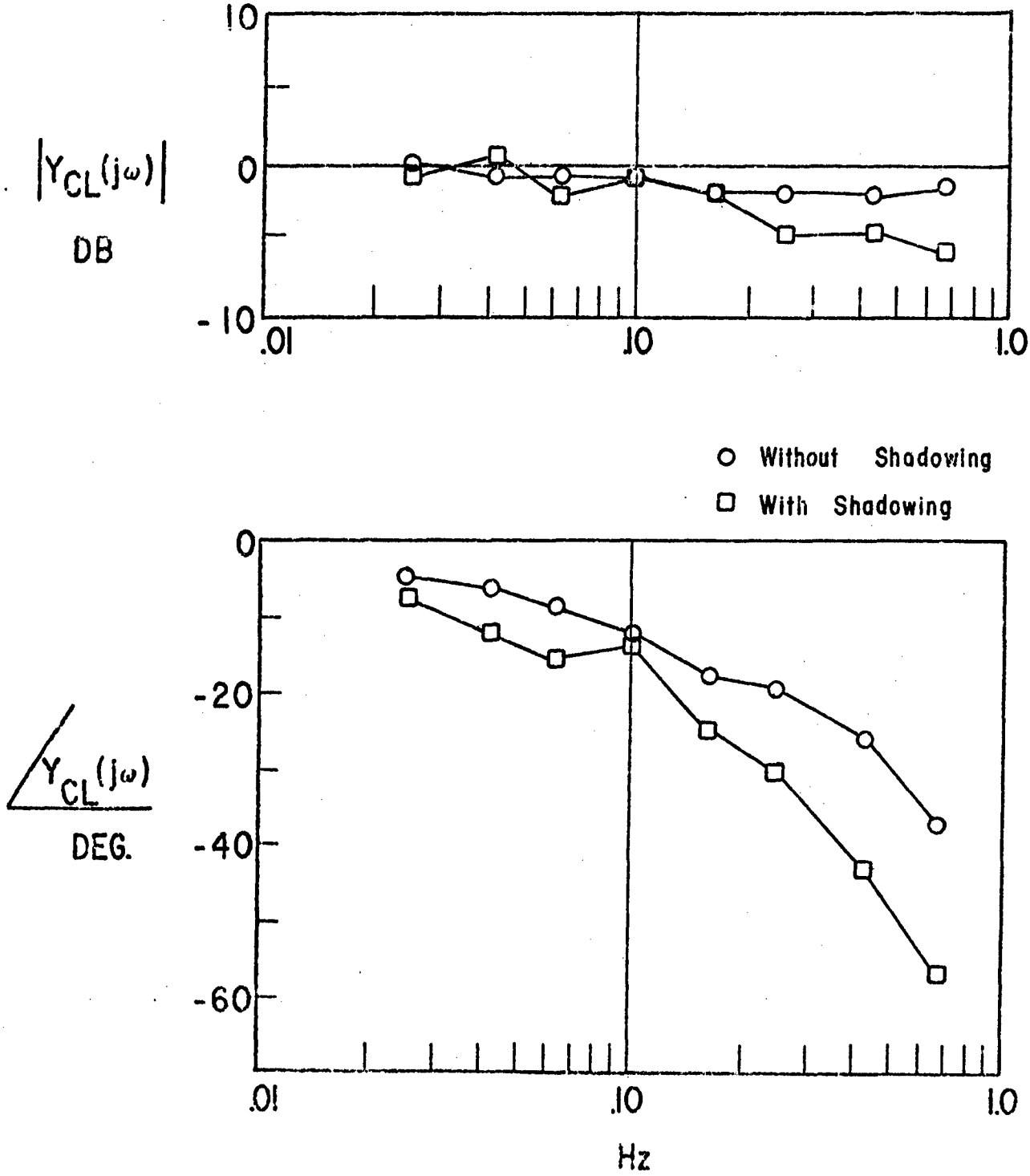

Conclusions and Discussion

The results discussed above demonstrate that the basic assumptions and hypotheses outlined at the beginning of this paper can account for much of the human performance data. By readjusting both the decision parameters, e_L and e_M, and the second order muscle dynamics, similar model matches have been obtained for other subjects.

At this stage in the present research the intent of the modeling effort is two-fold: (1) to illustrate the feasibility of the model hypotheses to account for the underlying mechanisms of simultaneous tracking and shadowing control; and (2) to help point the direction for future research whereby the present model may be refined and elaborated. The simulation has demonstrated the ability of this type of hybrid discrete decision model to account for the major properties of the dual-task performance, particularly the holds. It now seems that some of the important underlying hypotheses have been made sufficiently explicit so that fruitful directions for future work are fairly clear.

Simultaneous tracking and shadowing was chosen as the dual-task situation in order to achieve true task independence with respect to task input / output modes. However, now that task interference has been demonstrated for this case, and a single-channel mechanism has been shown to be the most likely mechanism to account for the decrement, it may be more appropriate to use non-independent tasks for future work.

Experiments could and should be conducted in order to more directly examine the hypothesized causality associated with the holds on each task. This might best be accomplished by using two mutually exclusive visual-manual tasks and thereby directly observing the attention function by eye fixation records.

Another important hypothesis contained in the model which needs direct verification relates to the attention requirements during a tracking hold. The model hypotheses imply that more attention is required during a tracking hold than is required during ongoing tracking. This correlated with results from the subjects which showed an increased probability of a shadowing hold during the termination phase of a tracking hold. This again might best be tested by using two visual-manual tasks and directly observing the attention pattern from eye movement records.

Through experimental investigations like those suggested above, the present model can be modified as necessary and finally validated. Immediate applications would include predictions of diving or aircraft piloting performance under various information processing load conditions. Also, stresses such as sleep deprivation, alcohol, or other drugs, may have their major effect on the ability to appropriately allocate and switch attention. A detailed understanding of normal human performance would serve as a valuable base line for understanding results obtained under these and other stress conditions.

References

1. Cliff, R.C. "The Effects of Attention Sharing in a Dynamic Dual-Task Environment", Proceedings of the Seventh Annual NASA-University Conference on Manual Control, 1971.

2. Cliff, R.C. "Attention Sharing in a Dynamic Multi-Task Environment", Ph.D. Dissertation, Department of Industrial Engineering and Operations Research, University of California, Berkeley, 1971.

3. Welford, A.T. Fundamentals of Skill, Methuen & Co., Ltd., London, 1968.

4. Senders, J.W. "The Human Operator as a Monitor and Controller of Multidegree of Freedom Systems", IEEE Transactions on Human Factors In Electronics, Vol. HFE-5, pp. 2-5, September 1964.

5. Carbonell, J.R. "A Queuing Model of Many-Instrument Visual Sampling" IEEE Transactions on Human Factors in Electronics, Vol. HFE-7, pp. 157-164, no. 4, 1966.

6. Carbonell, S.R., J.L. Ward and J.W. Senders, "A Queuing Model of Visual Sampling Experimental Validation", IEEE Transactions on Man-Machine Systems, Vol. MMS-9, No. 3, September 1968, pp. 82-87.

7. Merritt, M.J. "The Application of Discrete Modeling Elements to the Synthesis and Identification of a Deterministic Model for the Visual Scanning Behavior of Human Operators", NASA SP-192, 1968, pp. 289-311.

8. Sperling, G. "The Information Available in Brief Visual Presentation" Psychological Monographs, 74, Whole No. 498, 1960.

9. Broadbent, D. Perception and Communication, Pergamon Press, London, 1958.

10. Cherry, Colin On Human Communication, M.I.T. Press, Cambridge, Mass., 1966.

11. Kristofferson, A.B. "Successiveness Discrimination as a Two-State Quantal Process", Science, Vol. 158, December 8, 1967, pp. 1337-1339.

12. Kristofferson, A.B. "Attention and Psychophysical Time", Acta Psychologica, 27, 1967, pp. 93-100.

13. Crossman, E.R.F.W. and P. Goodeve, "Feedback Control of Hand Movement and Fitt's Law", HFT Report 64-16, Revised April 1972, Human Factors in Technology Research Group, Department of Industrial Engineering and Operations Research, University of California, Berkeley, 1964.

SESSION XII

Theory and Application of the "Critical Tracking Task"

Preceding page blank

DEVELOPMENT OF THE DUAL-AXIS AND CROSS-COUPLED CRITICAL TASKS

H. R. Jex, W. F. Jewell, and R. W. Allen
Systems Technology, Inc., Hawthorne, California

ABSTRACT

Multiaxis offspring of the well-established single-axis Critical Instability Task are described. The Dual-Axis Critical Task requires the operator to simultaneously stabilize two identical, increasingly unstable, controlled elements (one in each axis), using identical control and display gains. The dual-axis score, λ_D, is the level of instability at which control is lost in either axis. Pilot experiments show that λ_D is a sensitive indicator of display format and control stick effects.

The Cross-Coupled-Instability Task involves any arbitrary primary control task (which may itself be multiloop), with a "subcritical" secondary task whose unstability level is adaptively cross-coupled to the primary task performance index. The cross-coupled score, λ_X, is the asymptotic level of secondary task instability, which is shown to be sensitively related to the attentional workload margin of the primary task. Subtle initializing and adaptive logic was evolved to permit a single mechanization to handle a wide variety of primary tasks and individual skill levels. Some early applications of these tasks are reviewed.

INTRODUCTION

For several years, Systems Technology, Inc., under sponsorship of NASA and the Air Force has been developing a series of "critical-instability" task measures and apparatus to provide more efficient tests of some key man-machine dynamic control parameters (Refs. 1-3). The state-of-the-art in single-loop critical task testing is now mature. Critical tasks requiring any degree of operator equalization can be prescribed with near-certain a priori confidence that the desired equalization will be elicited; furthermore, a well-validated background of applications and statistical data exists on which to base rational and efficient experimental designs and data processing (e.g., Refs. 3-6).

*This work was sponsored under Contract NAS2-6409 from the NASA Ames Research Center's Man-Machine Integration Branch, where the technical monitors were Messrs. M. Sadoff and N. McFadden.

Preceding page blank

The main goal of the work summarized here was to provide analogous multiloop critical tasks, suitable for more realistic tests of controls, displays, and operator workload. Based on research using a fixed subcritical instability task to change the scanning workload of a primary task (Refs. 7 and 8), a prototype "Cross-Coupled" critical task, using experimenter-adjusted parameters, had been used by McDonnell to establish a quantitative measure of excess control capacity and to correlate this with Cooper-Harper Scale handling quality ratings (Ref. 9). The success of this research led to one of our main objectives: to establish a standard set of cross-coupling algorithms and parameters suitable for widespread application, with sufficient built-in versatility to permit the scheme to be used with a variety of displays, controls and situations.

Other objectives were to evolve a set of test parameters which: a) would be suitable at any level of operator training, and b) could be mechanized on analog or digital computers or even manually controlled in frugal situations. Our general approach (based on successful results with single-loop critical tasks) was to find the task parameters, control type and display format giving the best score, and having the least number of control and display parameters to specify (i.e., no detents, limits, friction, display lags, or quanta, etc.). Then any other display or control investigated should yield a decrement in score from this lab standard. Pilot experiments with a few subjects were performed to optimize the parameters and yield some procedural and data norms.

The basic principle of critical-instability tasks is that: closed-loop human operator control of a first-order divergent controlled element (analogous to steering a caster wheel backwards) is dominated by the operator's effective control delay, τ_e (primarily the sum of delays from visual perception, signal processing, and neural transport, plus neuromuscular lags, in the single-loop configurations). "Autopacing" algorithms have been developed to take each subject towards his "critical" (loss-of-control) limit, rapidly at first while control is easy, then more slowly as incipient instability of the man-machine system is approached. Extensions to second- and third-order controlled elements (requiring rate and acceleration signal equalization, respectively) have been made and validated by concurrent operator describing function measurements (Ref. 3).

First, we will review the simpler Dual-Axis critical task which is a simple multiaxis extension of the single-loop critical-instability task.

DUAL-AXIS CRITICAL INSTABILITY (λ_D)

Mechanization

The Dual-Axis Critical Instability Task is similar to the conventional single-axis case. Both horizontal and vertical axes have identical unstable controlled elements and gains, with the subject's remnant as the only forcing function. An autopacer simultaneously increases the instability in both axes to the "critical" limit, as defined by loss of control in either axis. This limit is designated the "Dual-Axis Critical Instability," λ_D. A block diagram of the Dual-Axis Critical Instability Task is shown in Fig. 1.

It must be emphasized that the critical-instability runs have no fixed length, nor is λ_D simply proportional to time. Since the controlled element varies continuously, the error statistics vary, and average error performance measures are not appropriate for critical instability tasks.

Display Format

The two-axis display symbol format was optimized experimentally in a brief investigation involving two well-trained subjects. Our experiments showed that, if a combined two-axis display and single-hand two-axis control stick are used, the autopacing parameters of the single-axis task may be retained for the dual-axis task. The corresponding dual-axis scores only suffer by 10-20 percent from the single-axis case, because this configuration provides a sort of "vector" display and control problem. A typical time trace of a dual-axis critical task run is shown in Fig. 2. Notice the shift of $\dot{\lambda}$ from its high initial rate to the asymptotic creeping rate.

The symbol formats under consideration were: "Dot" (3 mm dia.), "Greek Cross" (with equal 1 mm thick arms increasing from 1 to 2 cm in length as λ_D increases), "Crosspointer" (separate vertical and horizontal bars spanning the display), and a "Pitch-Roll" format simulating a gyro horizon line. A two-axis pressure control (MSI 435 isometric controller) was used for most tests. There was a surprisingly large and consistent effect of display format on λ_D, as shown in Fig. 3.

Figure 1.

MECHANIZATION OF DUAL AXIS CRITICAL INSTABILITY TASK

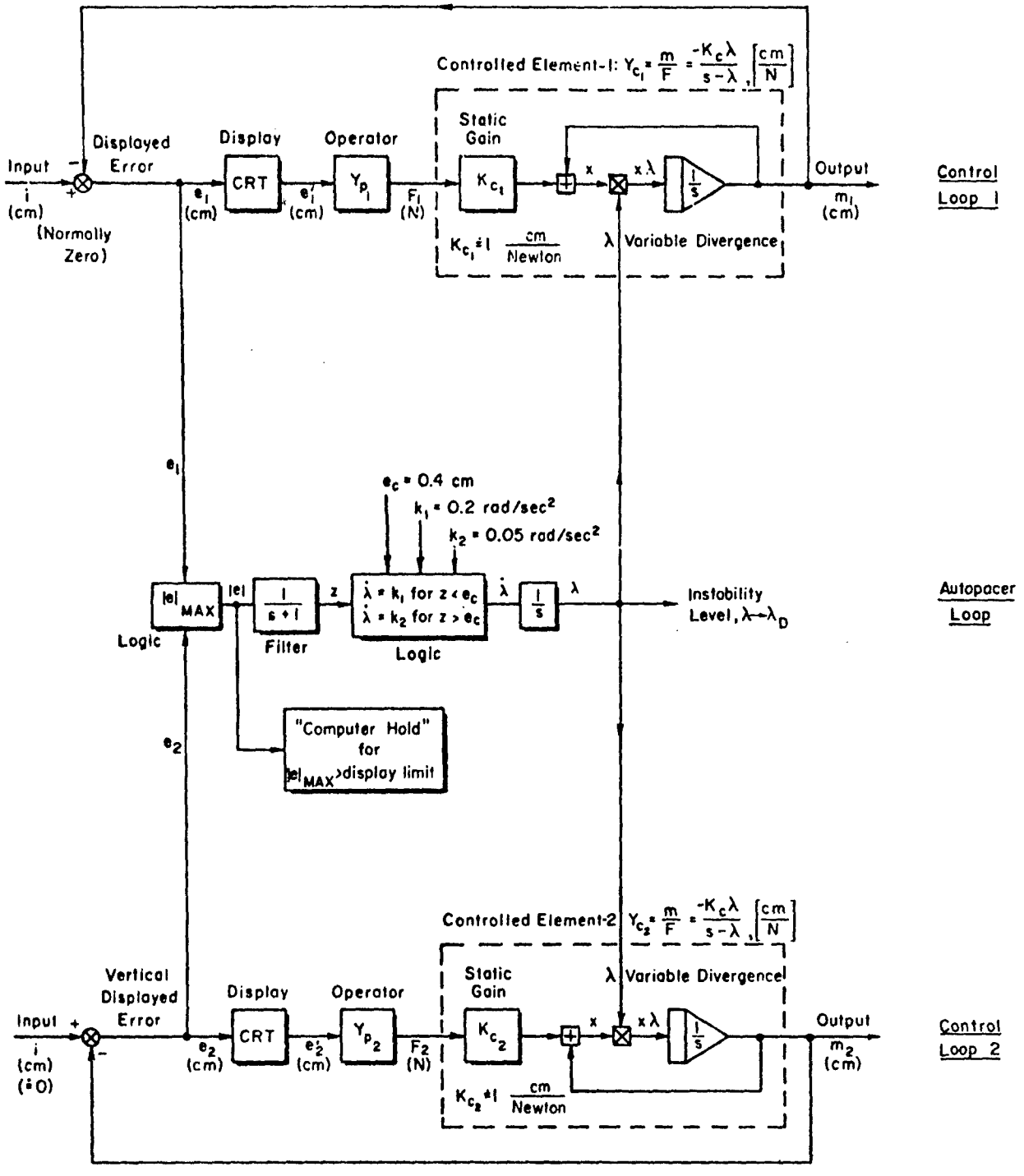

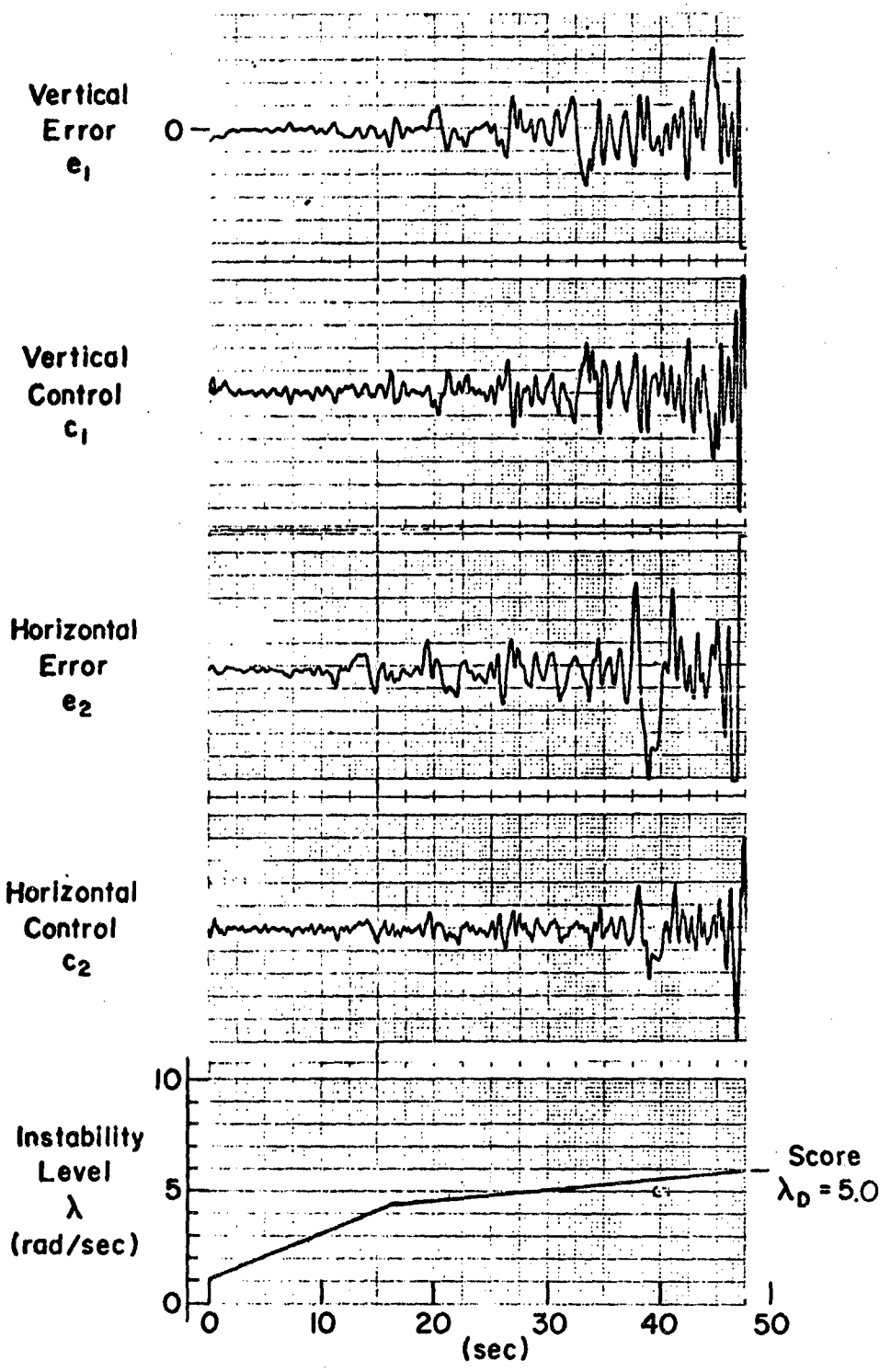

Figure 2. Time History of a Dual-Axis Critical Task Run

Reproduced from best available copy.

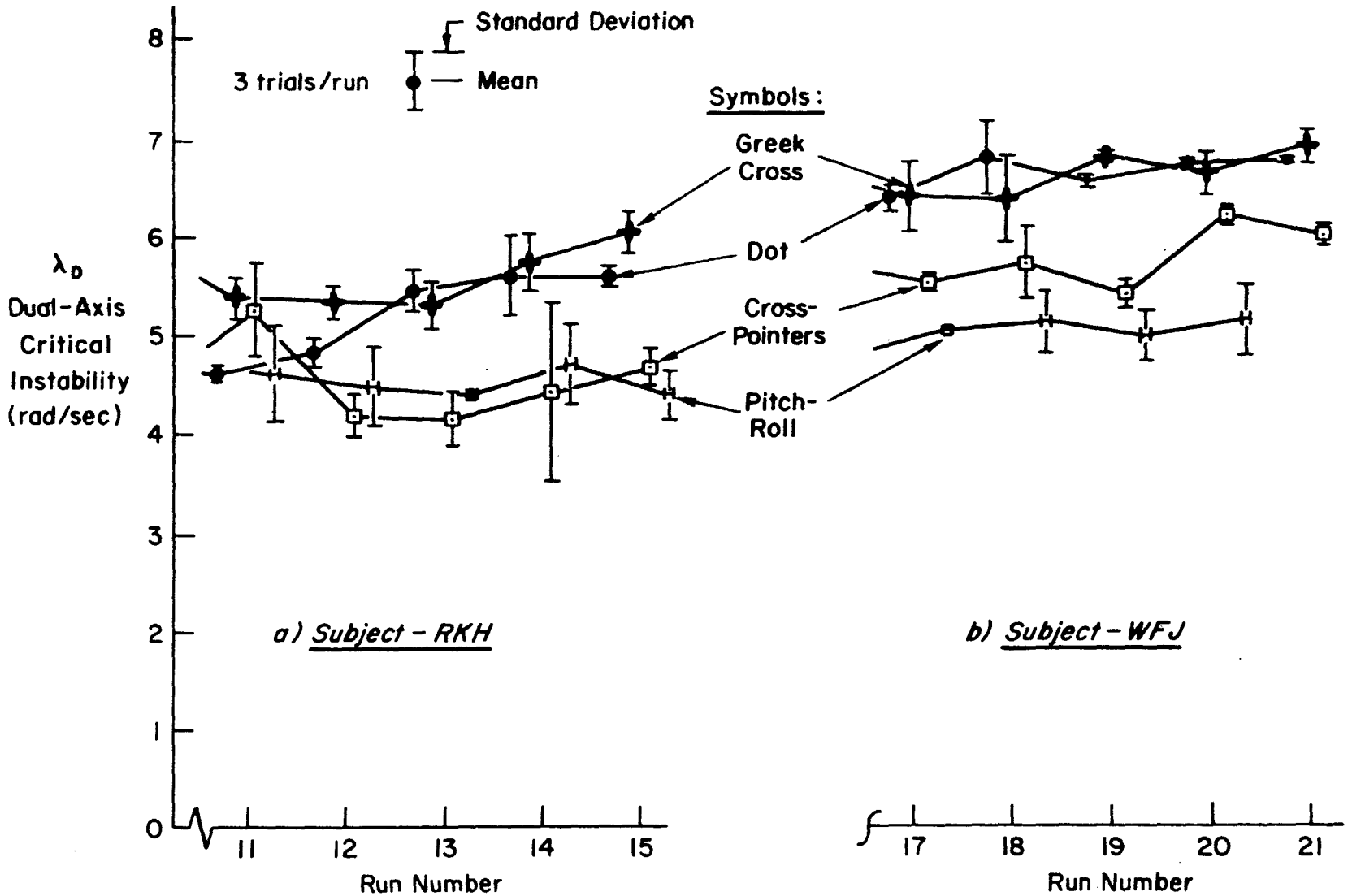

Figure 3. Dual-Axis Critical Instability Scores for Various Display Symbols (Isometric Stick)

Some conclusions drawn from the experiments performed to date are as follows:

1. The "Greek Cross" format is optimum for the Dual-Axis Critical Instability Task, which has identical controlled elements and is performed as an error vector correction. The Greek Cross yields the highest λ_D scores. A simple dot gives nearly the same results, but is less preferred by the subjects.

2. The "Crosspointer" format is recommended for other tasks in which different controlled elements (requiring different equalization) exist on each axis. The cross-pointers permit easier subjective separability of the two axes but do not seem to allow the "vector" integration of the two display axes as found with the dot and Greek Cross formats. Probably because of this, the λ_D scores with crosspointers are consistently about 1 rad/sec lower than the Greek Cross cases.

3. The "Pitch Roll" format was most difficult to learn, yet gave the greatest degree of subjective display axis separability. Performance often reached the Crosspointer's level of λ_D, however.

4. Preference ratings for the displays were ranked as follows (decreasing preference): a) Greek Cross, b) Dot, c) Crosspointer, d) Pitch/Roll.

5. The Dual-Axis Instability Task is a sensitive and efficient means to explore multiaxis display formats.

Control Stick

Using the two recommended display formats (Greek Cross and Crosspointer), a comparison was made between the recommended force-stick and a softly-sprung finger control stick with preloaded nulls (modified from a radio-controlled model aircraft finger stick). These results are given in Fig. 4, which shows that the two-axis force stick gives consistently better scores, by $\Delta\lambda_D$ = 0.5 to 1.0 rad/sec. This difference is very significant, statistically, again illustrating the sensitivity of λ_D to two-axis display/control variables. Because an isometric stick has fewer parameters to specify and gives highest scores, it is recommended as standard for both the single-axis and dual-axis Critical Tasks.

Applications

Because of its high test power (ratio of mean/standard deviation), the Dual-Axis Critical Task is well suited as an efficient measure for manual

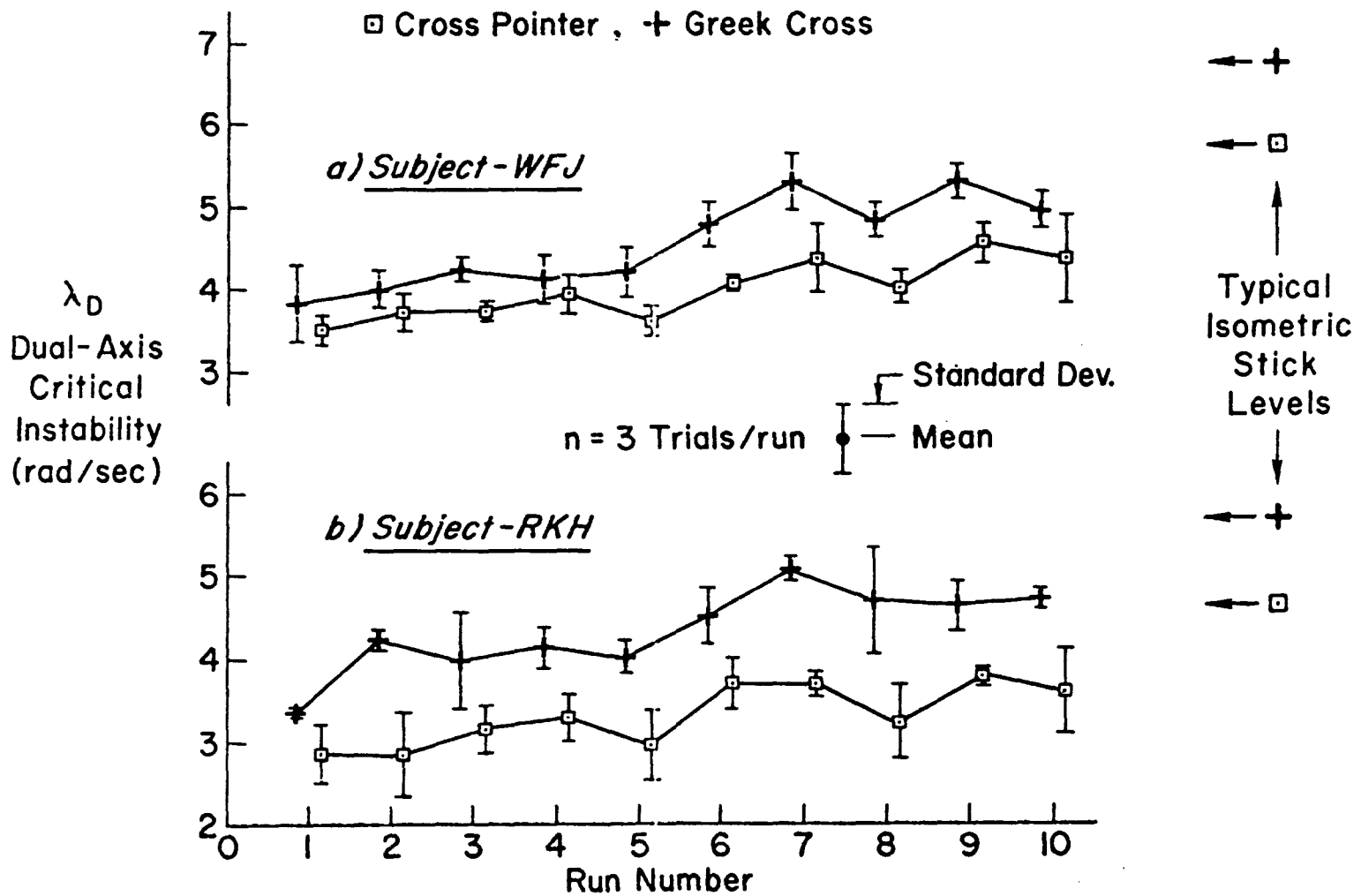

Figure 4. λ_D Data for Small Spring Stick with Detents and Comparison with Typical Isometric Stick Data

control situations where the required operator equalization in each axis is the same. Some problems for which λ_D should be a sensitive measure are:

Displays

- Symbol format (e.g., as discussed above), contrast, color, size, etc.
- Separated versus unitary symbols for flight directors.
- Scanning effects for separated instruments.
- Other display modalities or mixtures thereof (aural, tactile, digital, color).

Controls

- Separated versus combined controls.
- Stick properties (e.g., as discussed above).
- Orientation, grip design, and feel properties.
- Use of different muscle groups and limbs.

Operator Properties

- Scanning of separated displays.
- Multiloop tracking with lead equalization in each (using second-order dual-axis task).
- Neuromuscular "crosstalk" for combined and separate controls.
- Fingers versus hands versus feet or combinations for multiloop controls.

Miscellaneous Problems

- Fly-by-wire control optimization.
- Display symbol optimization.
- Training for more complex multiaxis tasks.

CROSS-COUPLED INSTABILITY

Principles

Adaptive loading tasks have been receiving much emphasis, recently (see Ref. 10 for a good review). The basic concept of the STI Cross-Coupled Instability Task is to load up the attentional workload margin of a primary control task (Y_1) by a particular type of secondary tracking task (Y_2), namely a subcritical first-order task of adjustable instability level. The level of secondary task instability allowed, before significant deterioration of the primary task performance occurs, is a measure of the "workload margin" of the primary task (Ref. 9, p. 52). Figure 5 illustrates the principle.

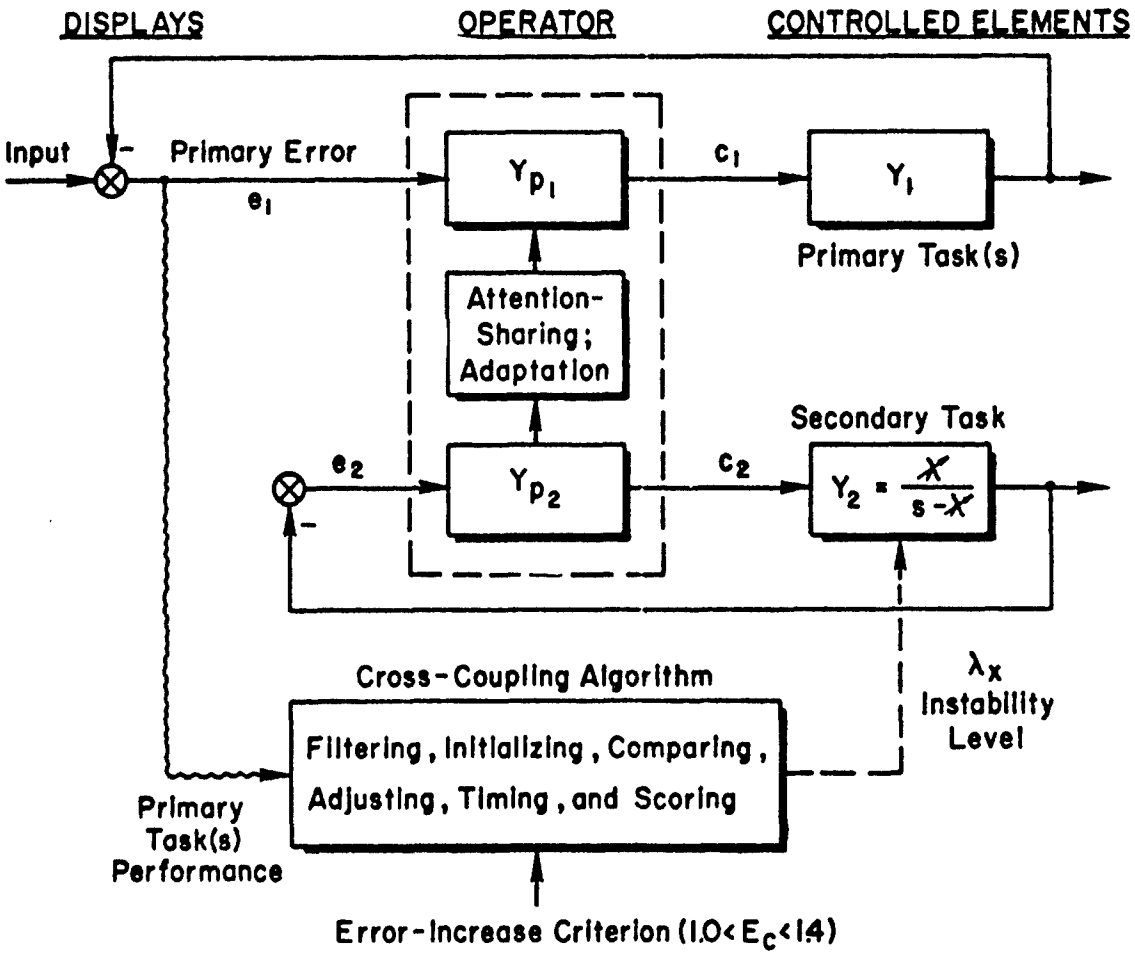

Figure 5. Principle of Cross-Coupled Instability

In developing the present task configuration there are several implicit assumptions and criteria which we attempted to meet:

1. The operator's basic behavior on the primary task should not be drastically altered by the secondary task (i.e., Y_2 should not require him to appreciably change his equalization or performance criteria on Y_1, although it may increase his delays, remnant, etc.).

2. Increasing the difficulty of Y_2 must, eventually, cause some manifestation of incipient workload saturation on Y_1. If average error performance of Y_1 is used to measure this, the percentage increase must be small enough to represent "insignificant deterioration" of the primary task performance, yet large enough to represent a rapidly measurable indicator of overload.

3. The variations of the operator's attention-sharing between Y_1 and Y_2 are fast compared with the cross-adaptive adjustments, and are comparatively small. Otherwise, no meaningful measurement can be defined.

4. Differences in individual operator levels of performance, due to practice, intrinsic ability limits, and different primary task variables (e.g., input level) must be handled by the cross-coupling algorithm, with a minimum of the experimenter's judgment or participation.

5. The cross-coupling algorithm should be usable with other operational-type primary displays and controls, to permit wide application to practical problems.

We encountered considerable difficulty in meeting these criteria, yet all except No. 3 (time variations) have finally been accommodated. The biggest obstacle is scaling the "loaded" error with respect to the error-increase criterion, E_c (for a given run), since σ_{e_1} depends on: Y_1, the rms input, the subject's practice, and his skill level. This was accomplished by having the subject track the primary task for 10-30 sec without significant secondary task instability (a nominal instability is present to preclude a different attention-sharing strategy). A low frequency lead-lag circuit decides when stable "unloaded" performance is reached, sets an error scaling multiplier to unity at this level, and allows cross-coupled adaptation to start. The secondary instability is then increased or decreased at a slow rate proportional to the difference between E_c (E_c = 1.1-1.3) and the (now rescaled) level of the rectified, smoothed primary task error. As the secondary task instability increases, the primary task error increases slightly to E_c, as the excess control capacity is used up. The smoothed level of this Cross-Coupled Instability, $\tilde{\lambda}_X$, is scored. A measure of the "tracking accuracy" is $A = \sigma_i/e_1^*$ where e_1^* is the smoothed absolute value of the washed-out primary task error as noted in Fig. 6. A composite "performance" score, P, can be compiled from a weighted function of A and $\tilde{\lambda}_X$, such as $P = A^j\lambda_X^k$ or $P = qA + r\tilde{\lambda}_X$.

Figure 6 shows the functional mechanization of the Cross-Coupled Instability Task. It has been mechanized on both analog equipment at STI and on the Ames Research Center's EAI 8400 hybrid digital-analog computer.

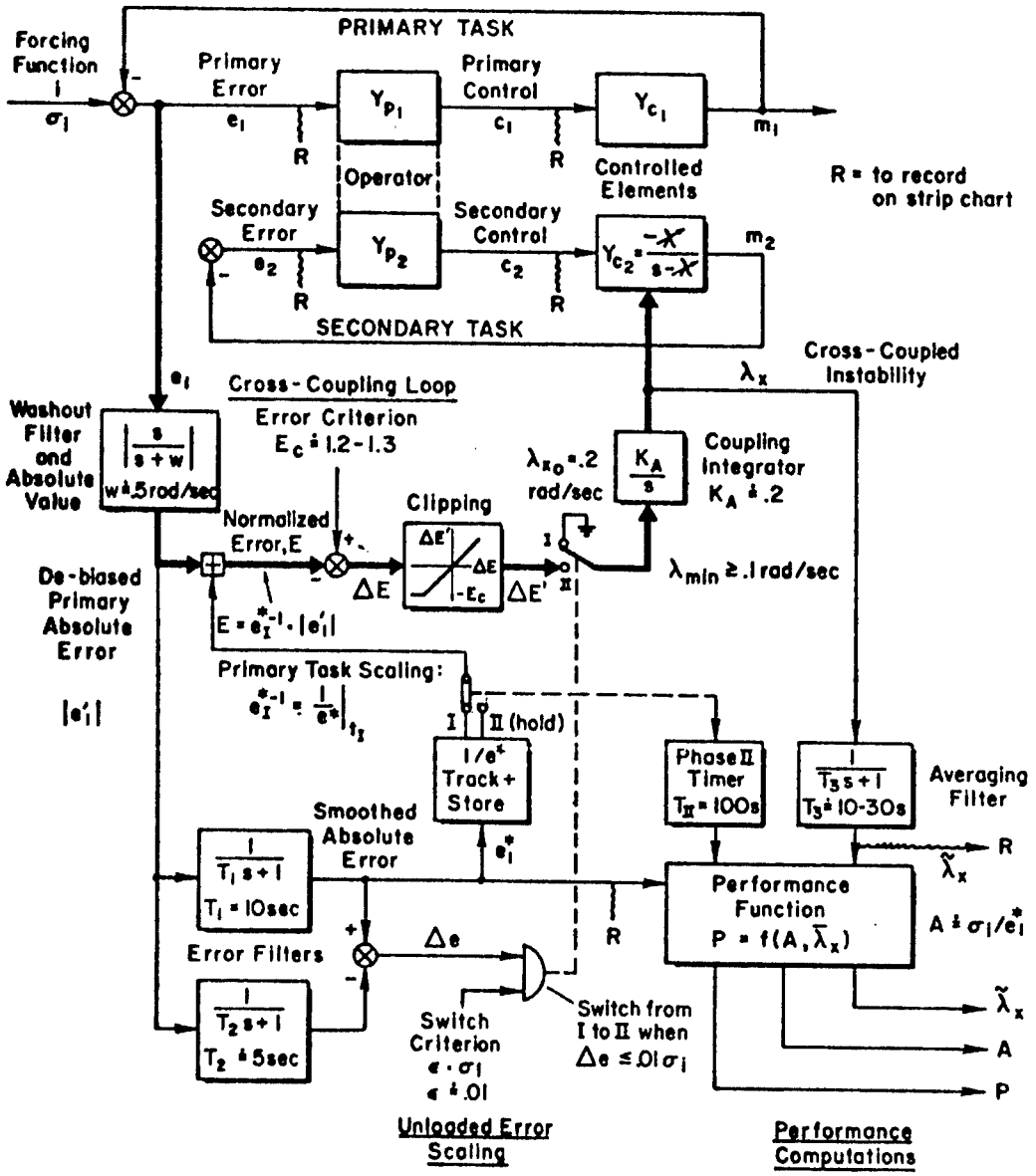

Operation:

Phase I (unloaded) — λ_X held at λ_{X_O} = 0.1 rad/sec; $\Delta e^* < 0.01\sigma_i$ detects when subject has reached a stable primary task performance level, e^*, i.e., 1 is normalized to average unity by $1/e_I^*$.

Phase II (cross-coupling) — λ_X allowed to integrate $\Delta E'$. $\Delta E'$ is difference between Error Criterion and normalized primary error magnitude. $|e_1'|$ is scaled by the fixed value of $1/e_I^*$, the inverse averaged error at the end of Phase I.

Final scores comprise the cross-coupled instability λ_X, the unloaded accuracy $A = \sigma_i/e_1^*$, and a composite Performance Index $P = f(\lambda_X, A)$.

Figure 6. Functional Mechanization of Cross-Coupled Instability Task and Scoring

Under spartan lab conditions it is even possible for the experimenter to do most of the cross-coupling functions (by manually increasing λ_X while monitoring the smoothed primary task error with respect to a criterion level) but the process is tedious and test reliability may be poor.

The adaptive initializing scheme for scaling the error primary task is the key to having a single cross-coupled algorithm to handle the problems of a range of operator skill levels during learning, and use with other display and control setups, and with various inputs and primary controlled elements.

Specifying the cross-coupling error criterion, E_c (ratio of loaded/unloaded average absolute error), was another complex compromise. A large error criterion is desired to accommodate the natural waxing and waning of error during a run and to provide a more solid indication of imminent overload. However, our definition of primary task overload allows only a small increase in primary errors. Too small a value for E_c does not provide sufficient performance margin to cope with ordinary time variations in error, while a too large E_c induces the operator into spending too much attention to the secondary task, thereby making it the primary task and violating the basic assumptions. The latter behavior results in wildly gyrating λ_X and occasional aborts. A ratio of loaded/unloaded average error of E_c = 1.20 to 1.30 was found to be satisfactory. This range is compatible with the effective value of 1.2 used in Ref. 9 and 1.25 in Ref. 14.

Referring to the functional diagram of Fig. 6, the basic operation is as follows:

a. During the "unloaded" first phase of the run, the side task is present at a constant, minimal level. The subject tracks the primary task as well as he can with "typical" attention. As soon as the low frequency rate circuit indicates a stable running average error, the second phase (cross-coupled) begins. This switching time is arbitrary to preclude "end spurt" effects by the operator.

b. Meanwhile, another circuit computes a smoothed normalized accuracy index, $1/e_1^*$. The value of this at the end of Phase I is used as an error normalizing factor throughout the (cross-coupled) second phase of the run. The ongoing value of $A \equiv \sigma_i/e_1^*$ is computed as a measure of tracking accuracy.

c. The cross-coupled Phase II of the run begins with no apparent sign to the operator. The de-biased absolute tracking error is normalized by the previously described e_1^{*-1} factor and subtracted from the constant error criterion, E_c. This difference is clipped (to prevent excessive negative $\dot{\lambda}$), scaled by an integrating constant, K_A, and integrated to provide the level of instability in the side task. Consequently, the side task demands more attention and the (normalized) main task error magnitude grows towards E_c. (E_c is normally 1.2.) The cross-coupled circuit seeks the level of λ_X which will permit E_c times the unloaded error. The normal run length is 2-3 minutes, and the level of smoothed λ_X after 100-150 sec of Phase II is scored as the "Cross-Coupled Instability."

d. A composite Tracking Performance index, P, is computed as $P = f(A, \tilde{\lambda}_X)$. (The specific function has not yet been optimized.)

Results

A typical cross-coupled run is shown in Fig. 7. The primary task was tracking a 1.5 cm rms input with a K/s element, and the error criterion was $E_c = 1.25$. Typical observations, exemplified on Fig. 7, are as follows:

- The first phase results in a stable unloaded error estimate within 20-40 sec.
- The (cross-coupled) second phase seems to settle out in 60-150 sec, thus requiring 2 to 3 minutes for the entire run. The value of smoothed λ_X near T = 100 sec is usually representative of a subject's average capability. Longer runs tend to fatigue the operator.
- With this simple (K/s) element the instability integrand ($\dot{\lambda}$) remains well below the clipping level, resulting in relatively smooth action of $\lambda(t)$. For more complex primary tasks the normalized errors are larger, hence $\dot{\lambda}$ is larger and clipping is necessary to keep λ from excessive excursions. (From another point of view, limiting $\dot{\lambda}$ stabilizes the cross-coupled loop for large excursions of attention or primary error.) In special cases removing this lower limit on $\dot{\lambda}$ may be desirable to enable the operator to get out of trouble faster than he gets into it.

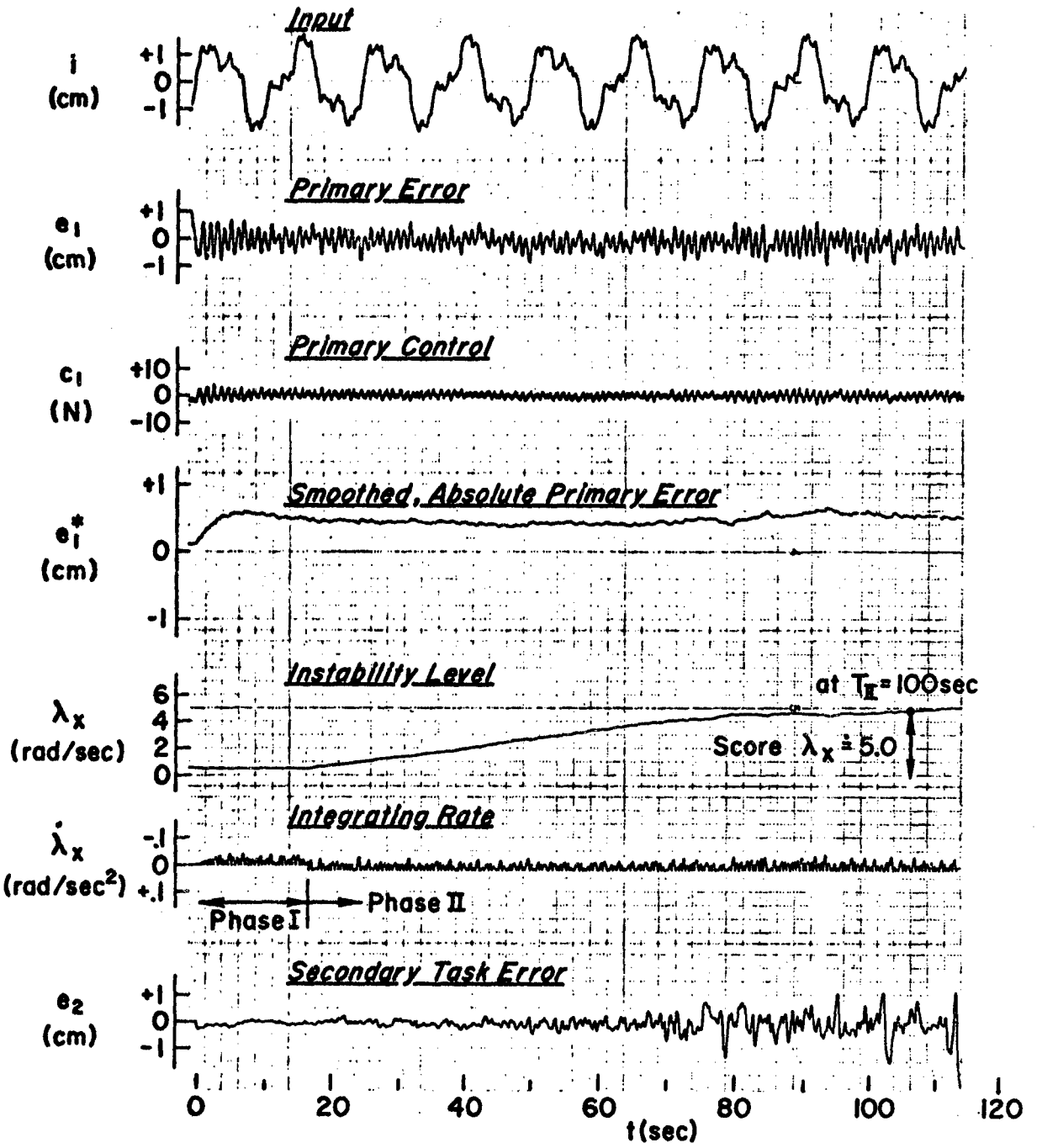

Figure 7. Time History of a Cross-Coupled Run

- Multiple plateaus of λ_X occur during some runs. Whether these represent learning or a natural waxing and waning of excess control capacity (or both) cannot be conclusively stated until more data are gathered. It does imply that λ_X scores are intrinsically less stable than λ_C scores, i.e., a sharp endpoint for control capacity apparently does not exist.

- Providing the subjects with a foveal clue as to the state of λ_X (e.g., by the lengthening arm of the Greek Cross symbol) is a big factor in helping him remain fully willing to expend maximal control capacity.

Coupling Parameters

A brief experiment was performed, using three pilot subjects, to optimize and validate the cross-coupled task parameters. A range of error-increase criteria from $E_C = 1.1$ to 1.3, and of adaptive integrating rates from $K_A = 0.10$ to 0.20, was tested. The results were not as clean as hoped, but the general trends showed that the higher integrating rate, $K_A = 0.2$, could be safely used because of the self-limiting action of the cross-coupled feedback signal, $E_C - E$. This acts to stabilize the adaptive loop under increasing workload conditions while allowing a rapid reduction in λ_X when sudden large errors indicate the operator is overloaded. As expected, the λ_X score increased roughly linearly over the range of $E_C = 1.1$ to 1.3, and no serious instability of λ_X resulted. In the light of these results, "standard" values of $E_C = 1.2$ and $K_A = 0.20$ are recommended for routine cross-coupled tasks. For special cases, these may be changed to provide more rapid or more stable adaptation, but bear in mind that the asymptotic λ_X score will then vary by 20-30 percent from the "standard" levels for a given primary task. In this respect the cross-coupled task parameters are not as "robust" as the earlier critical instability task, where variations of ±20 percent in the test parameters do not significantly alter the λ_C scores.

Scoring

One of the most difficult problems in developing this task has been that of the best scoring technique. The absolute-error signal driving $\dot{\lambda}_X$ fluctuates continuously over the short and long term as the input properties vary and as the operator's attentional commitment waxes and wanes. Consequently, only the

average λ_X over many seconds means anything. But if a several-second smoothing filter is put <u>in</u> the cross-coupling loop, it tends to destabilize the adaptation process and lengthens the time to reach asymptote. We finally solved this problem by placing the smoothing filter outside the cross-coupling loop (see Fig. 6) with T_f set between 10-30 seconds. Matching T_f to T_1 (the absolute-error smoothing filter) at 10 seconds each makes for convenient monitoring of smoothed $|e|$ and λ_X time functions during time-varying situations. For lab trials, where a single-average λ_X score is desired, the λ_X smoothing filter lag should be increased to about T_f = 20 seconds and the score recorded after 100 seconds of Phase II running.

Validation

The effect of secondary task loading on the primary task behavior was investigated by measuring pilot describing functions at both the unloaded and fully loaded conditions for a given subject and run. An on-line recycling feature of the STI Mk II Describing Function Analyzer (Ref. 11) made it possible to measure multiple short-term (25 sec) operator describing functions during a run. Figure 8 shows some typical DF data where the primary task was tracking with $Y_c = K/s(s + 3)$, which theoretically requires moderate lead of about $T_L = 0.33$ sec. Results are given for three subjects: 1) Ha — a well-trained pilot tested in many earlier experiments, 2) Ho — a light plane pilot instructor minimally trained for tracking, and 3) He — an occasional pilot moderately trained on this task. Data are shown for both the unloaded condition at the start of the cross-coupled run and under the high secondary task loading ($\lambda_X \doteq 3.5$) near the end of a run. Typically, under the adaptively cross-coupled secondary task load, the results show:

- Small increases in the delay time (more τ_e).
- Small decreases in the lead equalization (less T_L).
- Moderate increases in the remnant, shown by lower error coherence (less ρ_E^2).
- Small increases in the normalized error, as allowed by the rectified error criterion of 1.2 times the unloaded score (larger e^2/i^2).

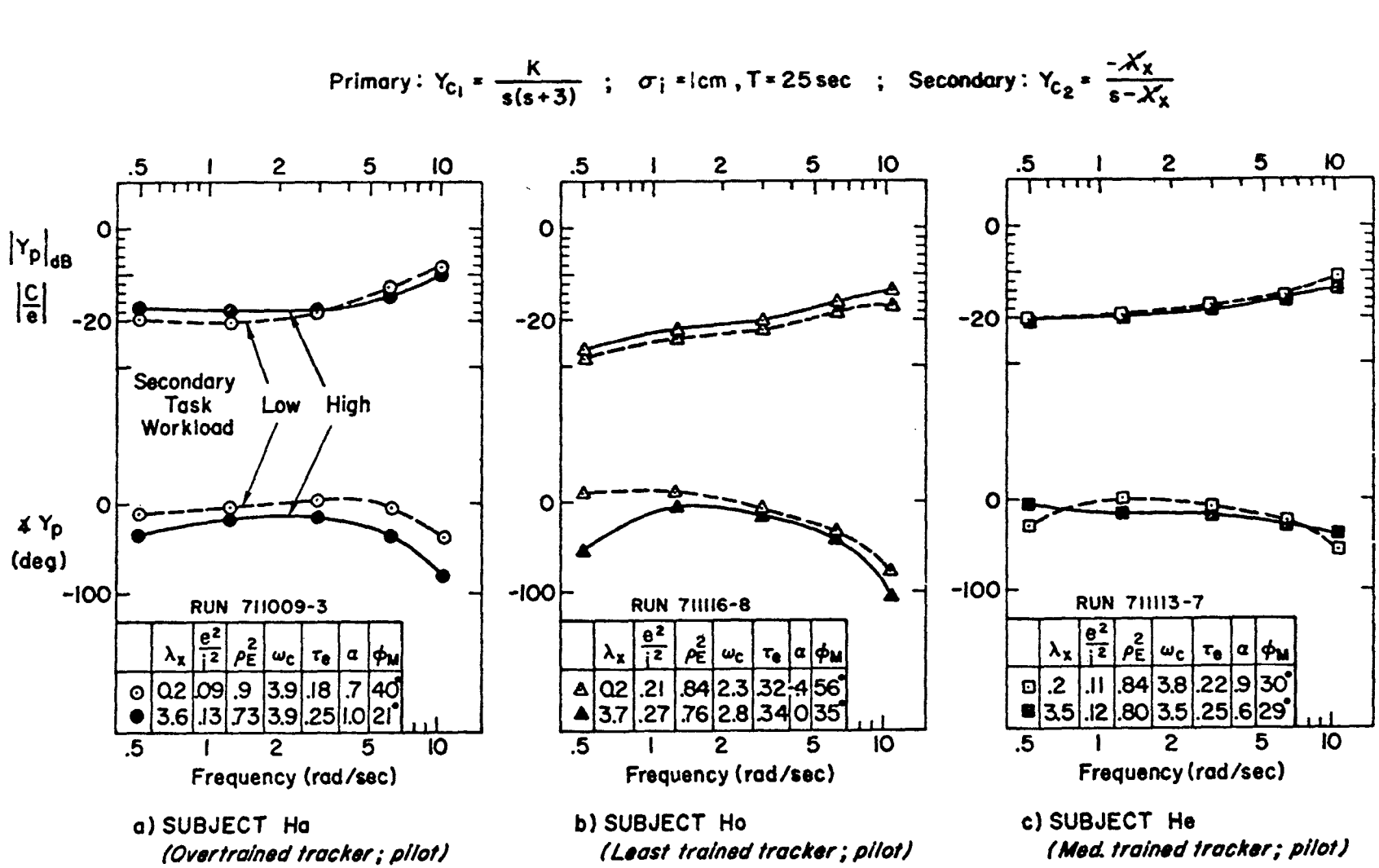

	λ_x	$\frac{e^2}{i^2}$	ρ_E^2	ω_c	τ_e	α	ϕ_M
⊙	0.2	.09	.9	3.9	.18	.7	40°
●	3.6	.13	.73	3.9	.25	1.0	21°

	λ_x	$\frac{e^2}{i^2}$	ρ_E^2	ω_c	τ_e	α	ϕ_M
△	0.2	.21	.84	2.3	.32	.4	56°
▲	3.7	.27	.76	2.8	.34	0	35°

	λ_x	$\frac{e^2}{i^2}$	ρ_E^2	ω_c	τ_e	α	ϕ_M
⊡	.2	.11	.84	3.8	.22	.9	30°
■	3.5	.12	.80	3.5	.25	.6	29°

Figure 8. Operator's Describing Functions and Performance Measures at Low and High Workloads

These results validate the assumption that the primary task behavior is not strongly changed in kind, and only slightly changed in degree, commensurate with the operator's working at full control capacity.

Controlled Element Effects

A limited number of runs were made with the same three subjects tracking three different controlled elements as the primary task: $Y_{c_1} = K/s$, $K/s(s + 3)$, and K/s^2; which require zero through full lead equalization, respectively. The input was a sum-of-five-sinusoids, with a varying amplitude inversely proportional to the log-spaced frequencies (see Ref. 4). To keep the displayed error signals about equal on the display, the inputs were reduced for the harder elements, being $\sigma_i = 1.5$, 1.0, and 0.7 on the CRT, respectively. The effective input bandwidth was about 2 rad/sec.

The cross-coupled scores are shown in Fig. 9 for each of the elements. There is reasonable concordance among the subjects, and no systematic effect of practice is apparent at this state of training (successive replications were on different days). Also shown on Fig. 9 as ✖ are the "best gain" values of λ_s from McDonnell's hand-adjusted cross-coupled data of Ref. 9. The tie-in with this early work is good, considering that the higher input level for our K/s case degrades the score compared to the constant-input ✖-data. (This effect is shown for other inputs in Ref. 9.)

We also noted that the standard deviations of the λ_X scores from successive tests for a given subject is "normal" and independent of λ_X, implying that raw λ_X scores are suitable for parametric statistical treatment (i.e., Analysis of Variance) without transformation.

Applications

The Cross-Coupled Critical Task is fairly new and has not been thoroughly refined or exploited yet. Nevertheless, some significant areas of application have been made.

One of the earliest applications of this task, already mentioned, is McDonnell's correlation of Pilot Handling Qualities Ratings with λ_X (then called λ_s, which was hand-adjusted with respect to subject's error level, scoring, etc.). See Ref. 9, pp. 52ff and 88ff for details.

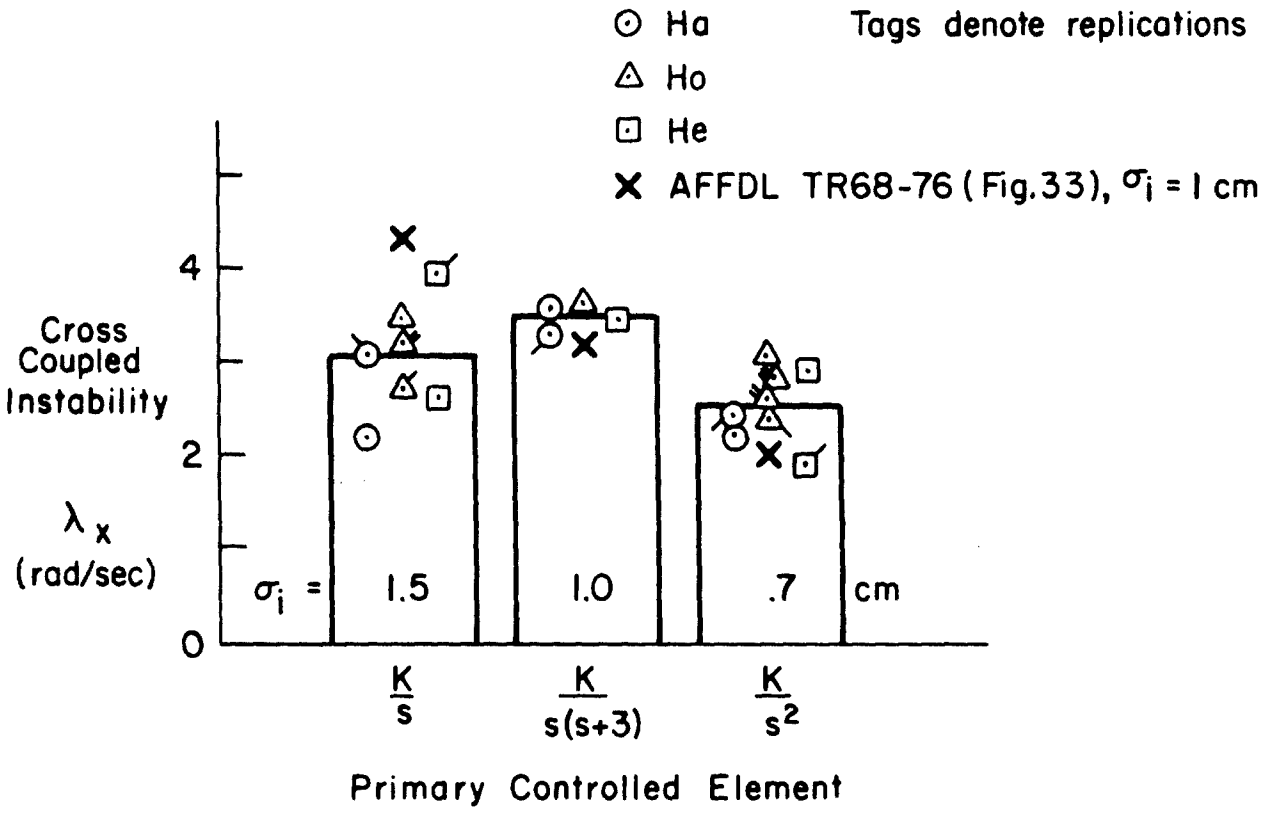

Figure 9. Cross-Coupled Instability Scores for Different Controlled Elements

Other applications take advantage of the fact that λ_X is a fairly direct measure of the operator's excess control capacity (sometimes termed control workload margin), because $T_\lambda = \lambda_X^{-1}$ is proportional to the time that can be spent away from the secondary task (as explained in Ref. 8, p. 68ff).

In Ref. 8, a fixed subcritical side task was used with separate displays to force scanning frequency and dwell time to vary. The cross-coupled task can be used in a similar manner to force natural, yet high workload, scanning between a main set of tasks and the secondary task. In this role it acts as a surrogate for other, perhaps more complex, real world tasks. For instance, a λ_X task can easily be substituted as the roll control task for pitch axis studies, or as a throttle loop during a car steering simulation.

Promising results have been obtained using our prototype λ_x task to measure excess control capacity for a series of integrated display formats (Refs. 12 and 13). Exemplary results are shown in Fig. 10.

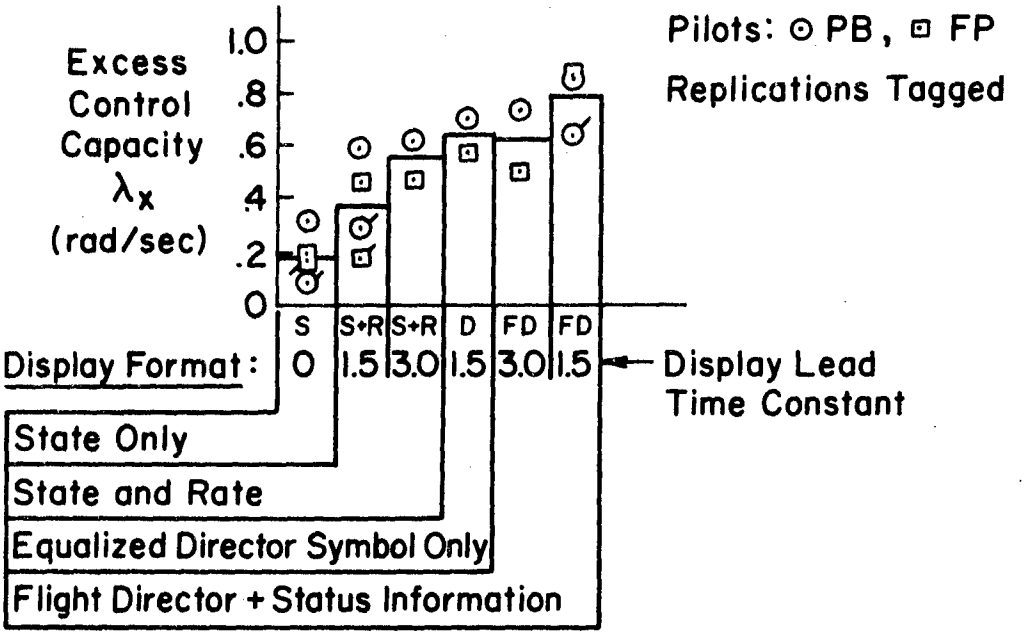

Figure 10. λ_x as a Measure of Excess Control Capacity for Various VTOL Integrated Displays (Adapted From Ref. 12)

Some other applications for which the cross-coupled instability is either in use or contemplated are: Category II and III landing studies with various degrees of pilot control; effects of long term acceleration; vibration or noise; effects of alcohol on car drivers; etc. We plan to continue its refinement and validation and hope that others will independently do so, too. Many basic problems remain which would make ideal thesis studies, such as the physical nature of the human operator's adaptation to secondary

tracking tasks (the mechanics by which a change in λ_X causes an error increase at e_1), sensitivity of λ_X scores to procedural and task variables, optimum training regimens, and so on.

CONCLUSIONS

Two promising multiloop critical tasks have been developed and some exploratory applications to control and display problems have been made.

Regarding the Dual-Axis Critical Instability Task, we conclude:

- The same autopacing principle and parameters as used for the earlier single-axis critical instability tasks can be used.
- For the best (combined) displays and controls the λ_D scores are only 10-20 percent less than single-axis scores on the same display.
- Changes in 2-axis symbology from Greek Cross to Cross-pointers or Roll/Pitch formats, or from an isometric stick control to a spring stick, produced surprisingly large decrements in λ_D (on the order of 10-20 percent). The apparent sensitivity of λ_D to such subtle displays should be verified and exploited.

The Cross-Coupled Critical Instability Task was considerably more difficult to develop to an automated status, because it must cope with a vast range of primary controlled elements (single- or multi-loop), inputs, displays, controls and operator skill levels. Nevertheless, the mechanization shown in Fig. 6 has proven very versatile and satisfactory in the limited number of experiments to date. Major conclusions from this work are as follows:

- A single cross-coupling algorithm will cope with a wide range of conditions and situations.
- The key to achieving a stable, meaningful λ_X score is to make the allowed error increase under workload to a small fraction of the unloaded error (i.e., set the error criterion near $E_C = 1.2$) and keep all filtering lags out of the cross-coupling loop. This assures that the primary task remains the primary attentional demand.

- The unloaded error level must be measured at the outset of <u>each</u> trial, because the small (20 percent) increase in error allowed under workload requires that the unloaded error be precisely known for that particular operator, situation and training level. The special circuit devised for automating this adjustment has worked very well in all cases tried.

- The excess control capacity score, λ_X, under maximal workload should be combined with a measure of tracking accuracy, $A = 1/e_1^*$, to provide an overall performance index, $P = f(\lambda_X, A)$. Work along these lines is in progress.

- Time variations in λ_X still remain due to: statistical variations in short-term properties in the primary task input (hence in primary error), as well as the waxing and waning of operator attention and reserve capacity. A better physical understanding of the psychophysiological processes involved is required before more meaningful measurements of excess control capcity can be made.

The authors invite communication from anyone who attempts to use these new critical tasks, in order to help interpret test functions, understand results, and refine the tests and protocols.

A FORTRAN IV digital program mechanizing these tests has just been developed for use on the EAI 8400 hybrid computer at the Ames Research Center, and could be adapted to other fast computers with a minimum of effort.

REFERENCES

1. Jex, H. R., J. D. McDonnell, and A. V. Phatak, "A 'Critical' Tracking Task for Manual Control Research," IEEE Trans. on Human Factors in Electronics, Vol. HFE-7, No. 4, Dec. 1966, pp. 138-145.

2a. Jex, H. R., J. D. McDonnell, and A. V. Phatak, A "Critical Tracking Task for Man-Machine Research Related to the Operator's Effective Delay Time. Part I: Theory and Experiments with a First-Order Divergent Controlled Element, NASA CR-616, Nov. 1966.

2b. McDonnell, J. D., and H. R. Jex, A "Critical" Tracking Task for Man-Machine Research Related to the Operator's Effective Delay Time. Part II: Experimental Effects if System Input Spectra, Control Stick Stiffness, and Controlled Element Order, NASA CR-674, Jan. 1967.

3. Jex, H. R., and R. W. Allen, "Research on a New Human Dynamic Response Test Battery. Part I: Test Development and Validation; Part II: Psychophysiological Correlates," 6th Annual NASA-Univ. Conf. on Manual Control, AFIT, Wright-Patterson AFB, Ohio, 7-9 Apr. 1970, pp. 743-777.

4. Allen, R. Wade, and Henry R. Jex, "Visual-Motor Response of Crewmen During a Simulated 90-Day Space Mission as Measured by the Critical Task Battery," 7th Annual NASA-Univ. Conf. on Manual Control, USC, 2-4 June 1971.

5. Jex, Henry R., R. Wade Allen, and Raymond E. Magdaleno, Display Format Effects on Precision Tracking Performance, Describing Functions, Remnant, AMRL-TR-71-63, Aug. 1971.

6. Pitkin, E. T., and E. W. Vinje, Evaluation of Human Operator Aural and Visual Delays with the Critical Tracking Task, paper presented at the Eighth Annual NASA-Univ. Conf. on Manual Control, U. of Mich, Ann Arbor, Mich., May 1972.

7. Jex, H. R., Two Applications of the Critical Instability Task to Secondary Work Load Research, Systems Technology, Inc., Paper No. 76, 21 Feb. 1967 (also AMRL-TR-67-94).

8. Allen, R. W., W. F. Clement, and H. R. Jex, Research on Display Scanning, Sampling, and Reconstruction Using Separate Main and Secondary Tracking Tasks, NASA CR-1569, July 1970.

9. McDonnell, John D., Pilot Rating Techniques for the Estimation and Evaluation of Handling Qualities, AFFDL-TR-68-76, Dec. 1968.

10. Kelley, Charles R., "The Measurement of Tracking Proficiency," Human Factors, Vol. 11, No. 1, Feb. 1969, pp. 43-64.

11. Allen, R. Wade, and Henry R. Jex, "A Simple Fourier Analysis Technique Measuring the Dynamic Response of Manual Control Systems," Sixth Annual NASA-Conf. on Manual Control, AFIT, Wright-Patterson AFB, Ohio, 7-9 Apr. 1970, pp. 785-801, (also IEEE Trans., Vol. SMC- , forthcoming).

12. Clement, Warren F., R. Wade Allen, and Dunstan Graham, Pilot Experiments for a Theory of Integrated Display Format, Systems Technology, Inc., Tech. Rept. 183-2 (JANAIR Rept. 711107), Oct. 1971.

13. Clement, W. F., D. T. McRuer, and R. H. Klein, Systematic Manual Control Display Design, Systems Technology, Inc., Paper No. 113, presented at the 13th AGARD Guidance and Control Panel Symposium on Guidance and Control Displays, Paris, France, Oct. 1971.

EVALUATION OF HUMAN OPERATOR AURAL AND VISUAL DELAYS WITH THE CRITICAL TRACKING TASK

E.T. Pitkin*
University of Connecticut
Storrs, Connecticut

E.W. Vinje†
United Aircraft Research Laboratories
East Hartford, Connecticut

ABSTRACT

The effects of aural, visual, and combined displays on human tracking performance were evaluated using the critical tracking task. Four visual displays and an aural display were used in this study. Values of $\bar{\lambda}_c$, the critical root, were developed for each display alone and also for the visual displays used in combination with the aural presentation. These experiments were motivated by the results of a previous study by the authors which indicated that combined displays might lead to improved performance.

Tracking performance, as measured by $\bar{\lambda}_c$, was consistently better for combined visual and aural presentations than for either type of display used alone. This trend was exhibited for each of the four visual displays and for both experienced and inexperienced trackers. These results suggest that combined displays supply the human's central processor with additional usable information. It appears that the operator relies primarily upon the aural display for rate information while using the visual display to monitor displacement.

I. Introduction

Recently the authors presented[1] comparative describing functions for subjects performing single loop compensatory tracking tasks using aural, visual and aural plus visual stimuli. The major goal of that work was to determine whether differences might exist in human response to aural and visual cues and also to obtain some indication of performance level for purely aural stimulation. The experiments were designed to be compatible with and therefore comparable to previous work by McRuer et al[4]. The pseudo random input disturbance was a sum-of-sine waves of various bandwidths and the controlled elements were K, K/s and K/s^2. It was concluded that there were no large differences between responses to aural and visual stimuli; however, indications of some more subtle differences were apparent. For instance, it was noted that there was a slight improvement in tracking performance with combined aural and visual displays of error, suggesting that the total information input might have been greater or that the central processing from two sources was more efficient.

---

*Professor of Aerospace and Mechanical Engineering

†Research Engineer

After some reflection upon the results of these studies, it was felt that the subtle differences between visual and aural displays might be further enhanced with the critical tracking task first proposed by Jex et al[2]. The critical tracking task consists of controlling a first order unstable controlled element, $\lambda/(s-\lambda)$, between the human operator and the output of the compensatory tracking loop as shown in Fig. 1. The value of λ is increased monotonically until control becomes impossible. The "critical" value, λ_c, at which this happens has been shown[2] to be closely related to the reciprocal of the operator's effective delay time, τ_e, when he is modeled as a simple gain plus time delay, $Y_p = K_p e^{-\tau_e s}$.

This study then consists of a systematic survey of λ_c for some of the displays and operators examined in Ref. 1. One additional but untrained operator was examined, and two visual displays not examined in Ref. 1 were also used. The additional displays were included to provide greater insight into the effect of visual display information content on operator effective delay time. This is necessary because it has been found that visual analogs which provide exactly the same information as aural displays are difficult to construct. For example, the visual display of a spot or line on a cathode ray tube usually gives more precise position information than the aural display because the subject easily retains a reference position - the edges of the CRT.

II. The Experiment

The experiment consisted of a single loop compensatory tracking task for which the simulated controlled element was $Y_c(s) = \lambda/(s-\lambda)$ as indicated in Fig. 1. Except for the unstable controlled element and the loop static gain, the hardware and loop parameters were identical in all respects to those described by the authors in Ref. 1. The same three subjects examined in Ref. 1 were used again and, in addition, one untrained subject, KEB, was tested in order to get some feeling for the effects of prior training.

The control stick was constrained to left-right movement with a force gradient of 1 lb/in. and had to be moved away from the error in order to reduce the error. Stick motion was converted to a d.c. voltage by means of a linear transducer and gain was set so that one inch of stick movement resulted in 35 volts output (.35 Machine Units). Forward loop static gain was set at K = 5 which represented the best feel to the experienced operators.

The error was displayed either aurally via earphones and/or visually via the left-right position of a line or spot on a CRT. The aural display was a single frequency of $330 + 64|e|$Hz (e measured in volts) presented to the left or right ear depending upon the sign of the error. As the error increased, the frequency increased in either ear.

Four visual displays were employed in this series of experiments and they are sketched in Fig. 2. The first, designated I, was a vertical line on the face of a 5 inch CRT grid which moved left or right according to the error voltage. Sensitivity was set at 5 V/cm. This display was also used in Ref. 1 and is comparable to displays employed by Jex et al. in Ref. 2.

The second display, designated II, consisted of a spot moving left or right according to the error voltage on the face of a 15 inch, gridless, CRT. In addition, there was a 10 cm vertical jump at zero error so that "right" errors were displayed above and to the right of "left" errors. This gave a sudden discontinuity at zero error, the same point at which a discontinuity is encountered through switching of ears in the aural display. The third visual display, III, consisted of a spot moving upward at 30° from the vertical to the left or right according to the error and with a 10 cm horizontal jump at zero error. The last visual display, IV, was nearly the same as III but the spot moved in a vertical path rather than at a 30° angle. In these last two displays continuity of direction of motion was lost when passing through the zero error point thus degrading velocity information. It is felt that this is somewhat more akin to what happens in the aural display as the zero error point is passed. In all the visual displays, the CRT sensitivity was set to give 1 cm of displacement for 5 volts (.05 Machine Units) of error voltage. Combined displays using visual plus aural input were also examined. These are designated I-A, II-A, etc.

In all experiments the value of λ was manually controlled via a potentiometer and was increased from λ=2 rad/sec, an easily controllable situation, to λ_c at a rate $\dot{\lambda} \approx .03$ rad/sec^2. As a result, the individual tests were approximately 1 to 2 minutes duration. (This is comparable to the slow rate recommended in Ref. 4.) There was no evidence that slight variations in $\dot{\lambda}$ due to manual control had any effect upon results.

In those tests in which the loop was disturbed by a pseudo-random input, the sum-of-sine waves functions of Ref. 1 were again used here. This input was essentially that described by Jex et al.[2] with input frequencies of ω = .14, .21, .35, .63, 1.05, 1.75, 2.62, 3.50, 5.24 and 10.47 rad/sec. Random phasing of these components gave a random appearing input signal. The bandwidths used were ω_i = 1.75, 2.62 and 3.50 rad/sec. Those components of the input greater than ω_i were reduced in amplitude by 14 dB. These input functions were previously recorded on tape so that they could be used repeatedly. In each individual case the tests were started from the same point on the tape so that the disturbance levels throughout the individual runs would be essentially the same.

III. Results

The first series of tests were performed with no input disturbance so that the noise content of the operator's output was the sole disturbing signal. Average values of the critical λ, designated $\bar{\lambda}_c$, and the standard deviation, σ, for five or more runs with a given subject and given display are reported in Table I. In some cases up to 20 runs were made with no significant change in either $\bar{\lambda}_c$ or σ as compared to 5 runs so it is felt that 5 runs were sufficient to obtain reasonably good values. Jex et al.[3] came to a similar conclusion and also reported data for 5 runs with standard deviations of the same magnitude as reported here. The displays are listed in order to difficulty as measured by $\bar{\lambda}_c$, the lowest value being for the most difficult task. This order also agrees generally with the operator's subjective evaluation. Columns are arranged by operator in the table, the first two being well

trained and the third a moderately trained operator. These three were previously tested with different simulated dynamics as reported in Ref. 1. The last operator, KEB, was a novice as is evidenced by his $\bar{\lambda}_c$ being 1 to 2 rad/sec below those of the well trained operators. It is interesting to note however that, according to the standard deviations, he appears to be as consistent as the well trained subjects. Indeed, it became evident during the test program that accumulated practice had no effect upon consistency although $\bar{\lambda}_c$ could be increased somewhat. Furthermore, it can be seen from the maximum $\Delta\bar{\lambda}_c$'s in the last column that the difference between the untrained and well trained operators narrows as the more difficult displays are encountered. This suggests that the more difficult displays have less information content that can be extracted and used upon additional training.

It is also seen upon inspection of Table I that the aural display gives $\bar{\lambda}_c$ scores very close to those obtained with visual displays III and IV. This tends to verify that these displays are acceptable visual analogs of the aural display and supports the choice of display IV as an analog in Ref. 1. It will also be noted that in every case the operator's performance improved when the visual display was augmented with the aural display. This effect was only faintly suggested by the describing function results reported in Ref. 1, but is quite pronounced here. The reason for this improvement may be that the two displays present complementary information to the operator who then selects error position from the visual display and velocity from the aural display. Although both e and $\dot{e}$ can be obtained from either display, it was readily apparent that the lack of a zero reference made it difficult to estimate e with the aural display. On the other hand, being very sensitive to pitch changes, the ear seemed to act as a better differentiator than the eye and yielded a better estimate of $\dot{e}$. The operators also expressed the feeling that they had "quicker knowledge of error divergence" when operating with the aural display. Whether this is due to smaller time delays in the aural channel or to a better estimate of $\dot{e}$ is not known at this point. It is interesting to note, however, that the run-to-run consistency did not seem to improve with the combined display as the average standard deviation for the visual displays, $\bar{\sigma}$ = .268 rad/sec is essentially the same as that for the combined display, $\bar{\sigma}$ = .263 rad/sec. This is contrary to what would be expected from the previous discussion and may be related to the test procedure, as will be discussed in more detail later. The apparent complementary effect of combined aural and visual displays of the same information might well be of some importance in the design of pilot displays for aircraft.

The values of $\bar{\lambda}_c$ in Table I most comparable with the results of Jex et al.[3] are those for display I. Their lowest value of $\bar{\lambda}_c$ = 6.6 ± 0.31 rad/sec for a given operator is .5 rad/sec greater than the highest value, 6.1 ± 0.33 rad/sec given here. This is probably due to the difference in control sticks. Jex used a force stick which is definitely faster in response than the spring restrained stick used here, as was shown by McRuer and Magdaleno[5]. With this difference in mind, these results appear to be compatible with those of Jex et al.

The effect of disturbance level can be seen in Fig. 3. In this series of experiments, the RMS value of the input, i, was varied from 0V to 13V, the level used in Ref. 1. The corresponding $\bar{\lambda}_c$'s of operator ETP with four

displays, I, IV, IV-A and A are plotted vs. i/i_{max}. The error bars here on the data for display I represent one standard deviation. They were not included for the other displays to avoid confusion, but were of approximately the same magnitude. Each run was initiated from the same position on a tape on which the disturbance was recorded with bandwidth $\omega_i = 2.6$ rad/sec. The time history of the disturbance for each run was then the same. A significant decrement in $\bar{\lambda}_c$ is noticeable in all cases as disturbance level increases. This effect was not evident in Jex et al.'s[3] results, probably because their maximum disturbance level was only 12 percent of the maximum used here. Again it is evident that displays IV and A result in considerably lower scores than display I while the dual display IV-A is superior to either of the corresponding aural or visual displays which themselves are quite comparable.

The slope of the decrement in $\bar{\lambda}_c$ with increasing disturbance level in Fig. 3 is decidedly steeper for the "easiest" display I than that for the more difficult displays. This is illustrated by the straight line fit of the data. However, the dashed line fit which defines two regions of about the same slope joined by a sudden transition may be more appropriate and might be explained by a change in control strategy. The operator learns very quickly that the speed of error divergence is highly amplitude dependent with this statically unstable controlled element and thus finds there is great motivation to keep the amplitude of the error small. This amplitude dependence is readily apparent from the differential equation for the error in the absence of disturbance, which is $\dot{e} = \lambda(e-c)$, where c is the control input of the operator. When e is kept small, the required control ($\approx e$) is small. With low control effort the noise and $\dot{e}$ will also be small, so the operator has more than adequate time to react before the system error diverges beyond controllable bounds. If there is little or no external disturbance and the display gives good position and velocity information, one soon finds that very little control effect is required and automatically limits inputs to "finger-only" motion. This tends to minimize operator estimation errors and the output is akin to that of a force stick. When λ gets very large during a test the amplitude of e at some point finally gets large enough to require hand and wrist motion and the attendant larger estimation errors. Suddenly $\dot{e}$ is so large that the system is almost immediately driven to a limit. The value of $\bar{\lambda}_c$ obtained this way will be larger than that which would obtain if larger amplitudes of e and hence larger stick inputs were required throughout the run as is the case with larger disturbance inputs and more difficult displays.

Some additional tests were run to examine this control strategy hypothesis and results are given in Fig. 4. Although the values of $\bar{\lambda}_c$ for low disturbance levels are slightly higher here, due most likely to considerable additional training of the operator, the same trend is apparent. Also note that with large input disturbance $\bar{\lambda}_c$ drops back to the level recorded before the additional training. This is consistent with the evidence in Table I that the difference in $\bar{\lambda}_c$ between well trained and untrained subjects decreases as the task becomes more difficult. Note again that the standard deviations in Figs. 3 and 4 remain fairly large and appear independent of the difficulty of the tracking task. This result again might be associated with the amplitude dependence effect, i.e., if there is a "true" λ_c for a

given run, the recorded λ_c will be somewhat larger and correspond to that value attained at the time of the random first appearance of a large error after the true λ_c has been passed. This effect could degrade the consistency of the reported values.

A final series of tests were run to determine the effect of disturbance bandwidth. Three bandwidths, ω_i = 1.7, 2.6 and 3.5 rad/sec were presented to operator ETP at 7.5V (1.5 cm) RMS on three displays; IV-A, IV and A. The results are summarized in Table II. Oddly enough, there seems to be no frequency dependence in the results in spite of the fact that the higher bandwidth inputs were definitely found more difficult to handle in the tests of Ref. 1. Again, it appears that the previously discussed amplitude effects may have masked out any frequency trends. Although tests were always started from the same point on each tape, the time history of the input disturbance on each tape is quite different due to the different bandwidth. The pseudo-random input function will have from time to time short periods of combined high amplitude and slope, i.e., high "activity". These periods naturally do not coincide as bandwidth is changed so the portions of the input that are most difficult to track occur at different times and therefore at different λ's, since λ is varied uniformly in time in this experiment. It would appear from the results in Table II that a period of high activity was encountered earlier with the ω_i = 2.6 rad/sec input than with the others, thus giving lower values of λ_c. It may be better then to modify the test procedure when working with external inputs to the critical tracking task to circumvent this difficulty. If λ_c were redefined to be the largest value at which the operator could consistently control an integral number of cycles of input, e.g., a full three minute tape in this case, it would insure that the relative positioning of quiescent and active periods would not bias the results.

IV. Conclusions

The value of the critical tracking parameter, $\bar{\lambda}_c$, increased when a given visual display was used in combination with the aural display for each case considered in this study. This was true for both experienced and naive trackers. Since $\bar{\lambda}_c$ is an indicator of operator effective time delay, τ_e, this would indicate that either the operator could supply more lead when the displays were combined or that his inherent processing delays were reduced. The mechanism by which $\bar{\lambda}_c$ increased may be that the aural display increased the amount of rate information available to the operator while the visual display provided displacement information lacking in the aural display. These results would also indicate that the operator's central processor was not saturated when the displays were used separately.

The $\bar{\lambda}_c$ measured for visual displays and with loop input disturbances indicates that the amplitude of the disturbances has a much greater effect than the frequency content. Changing the information content of the display does not alter this characteristic, except that the rate of decrease in $\bar{\lambda}_c$ with disturbance amplitude is greater for displays providing more information. The larger input amplitudes led to larger control stick movements and attendant larger estimation errors in control stick position. This is turn resulted in the smaller $\bar{\lambda}_c$.

References:

1. Vinje, E.W. and E.T. Pitkin, "Human Operator Dynamics for Aural Compensatory Tracking", IEEE Transactions on Systems, Man, and Cybernetics. (In Publication) (1972).

2. Jex, H.R., J.D. McDonnell, and A.V. Phatak, "A Critical Tracking Task for Manual Control Research", IEEE Transactions on Human Factors in Electronics, HFE-7, (1966), pp. 138-143.

3. Jex, H.R., J.D. McDonnell, and A.V. Phatak, "A Critical Tracking Task for Man-Machine Research Related to the Operator's Effective Delay Time", Part I, NASA CR 616 (Oct. 1966), Part II, NASA CR 674 (Jan. 1967), National Aeronautics & Space Administration, Washington, D.C.

4. Jex, H.R., and R.W. Allen, "Research on a New Human Dynamics Response Test Battery", Proc. 6th Annual Conf. on Manual Control, (April 1970), Wright Patterson AFB, Ohio, pp. 743-777.

5. McRuer, D.T., D. Graham, and E.S. Krendel, "Manual Control of Single Loop Systems", J. Franklin Inst., 283, pp. 1-29, Jan. 1967, pp. 145-168, Feb. 1967.

6. McRuer, D.T., and R.E. Magdaleno, "Human Pilot Dynamics with Various Manipulators", AFFDL-TR-66-138, Air Force Flight Dynamics Laboratory, Wright Patterson Air Force Base, Ohio (1966).

TABLE I

SUMMARY OF AVERAGE CRITICAL ROOT FOR LOOP
DISTURBED ONLY BY OPERATOR

($\bar{\lambda}_c$ and σ in rad/sec)

SUBJECT:	ETP		EWV		MHS		KEB		
DISPLAY	$\bar{\lambda}_c$	σ	$\bar{\lambda}_c$	σ	$\bar{\lambda}_c$	σ	$\bar{\lambda}_c$	σ	MAX$\Delta\bar{\lambda}_c$
I-A	6.6	.22	5.9	.36	5.5	.26	4.5	.35	2.1
I	6.1	.33	5.3	.28	4.5	.18	4.1	.32	2.0
II-A	6.0	.31	5.5	.12	5.0	.15	4.0	.19	2.0
II	5.5	.32	5.4	.30	4.4	.36	3.7	.24	1.8
III-A	5.5	.32	5.0	.34	4.5	.21	3.9	.19	1.6
III	5.1	.11	4.6	.22	4.1	.21	3.4	.13	1.7
IV-A	4.7	.34	4.6	.42	4.1	.22	3.6	.20	1.1
IV	4.2	.24	3.9	.33	3.5	.30	3.2	.42	1.0
A	4.5	.26	4.3	.17	4.1	.17	3.4	.22	1.1

TABLE II

EFFECT OF BANDWIDTH FOR
EXTERNALLY DISTURBED LOOP

($\bar{\lambda}_c$ and ω_i in rad/sec)

BANDWIDTH →	ω_i = 1.7		ω_i = 2.6		ω_i = 3.5	
DISPLAY	$\bar{\lambda}_c$	σ	$\bar{\lambda}_c$	σ	$\bar{\lambda}_c$	σ
IV-A	4.7	.31	4.2	.26	4.6	.37
IV	4.5	.18	3.9	.40	4.1	.23
A	4.1	.28	3.8	.30	4.3	.17

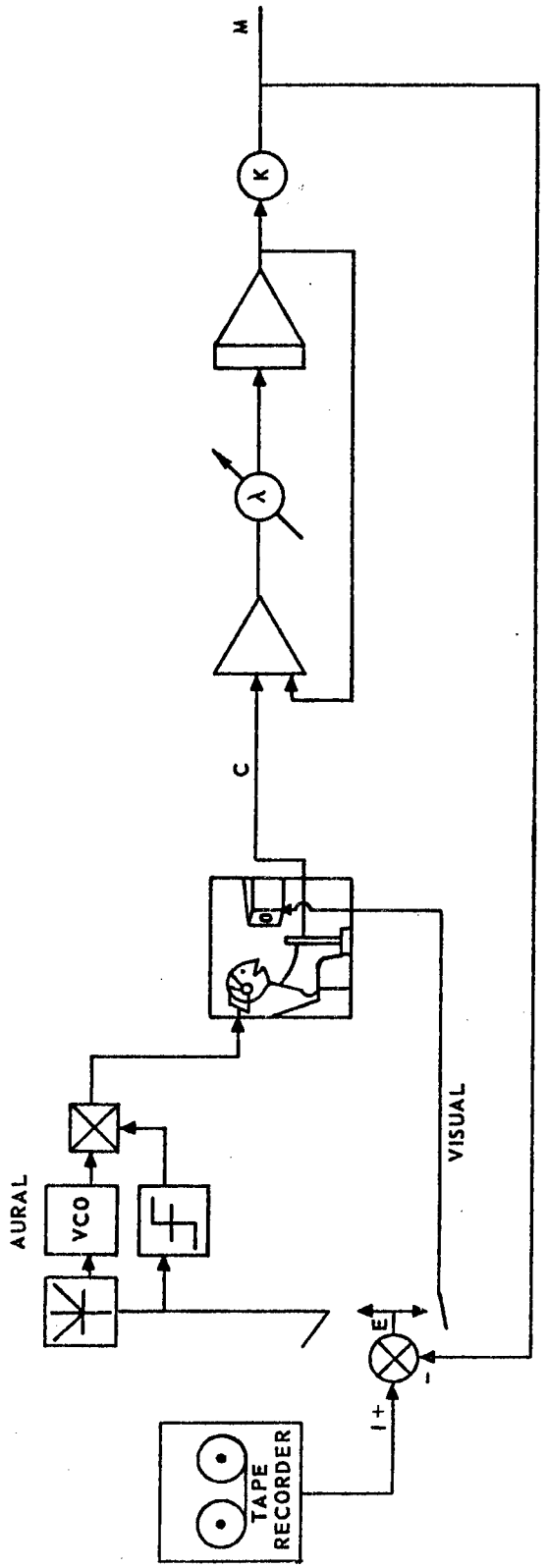

FIG. 1. CRITICAL TRACKING TASK FOR AURAL AND/OR VISUAL DISPLAYS

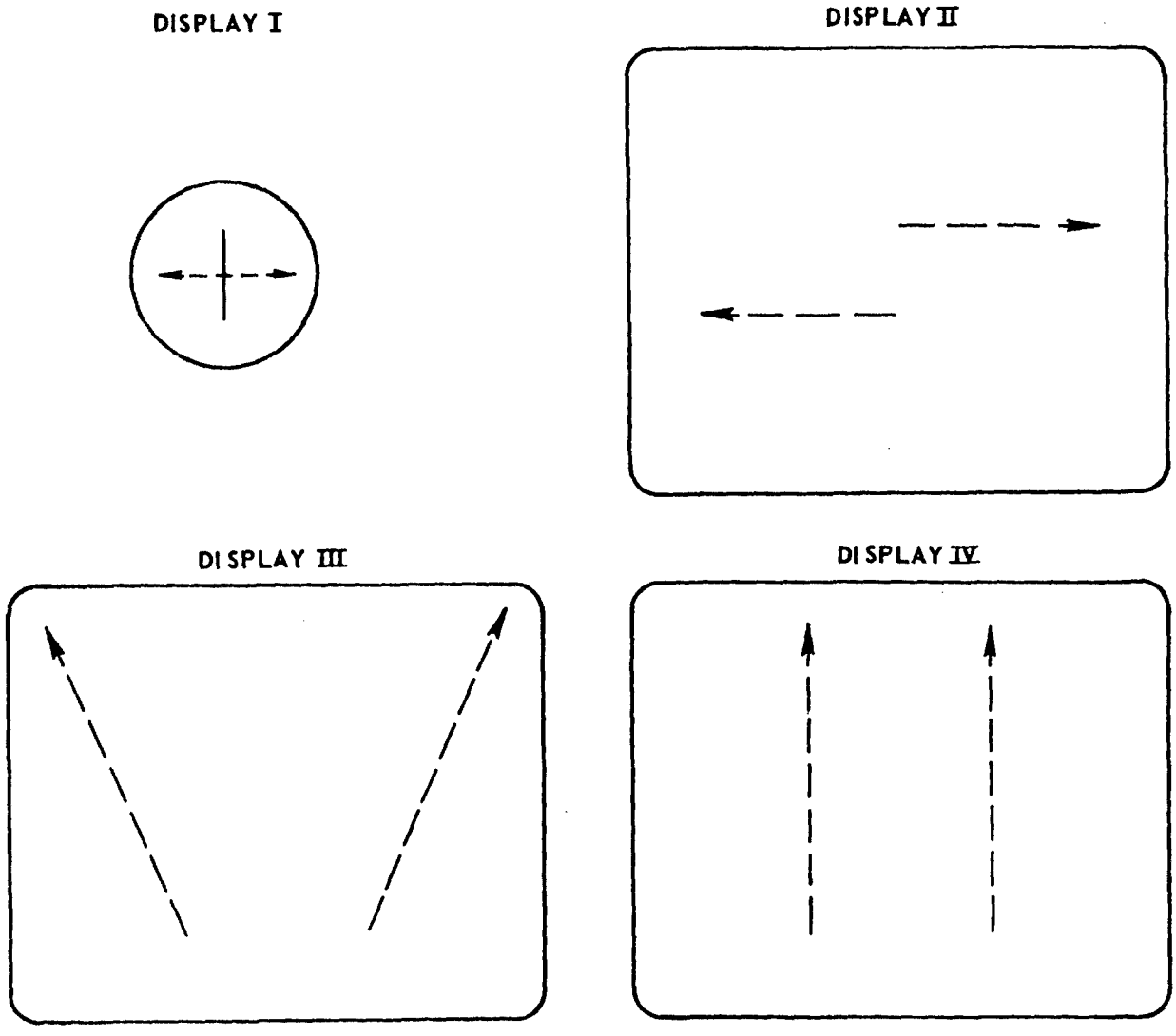

FIG. 2. VISUAL DISPLAYS USED FOR THE CRITICAL TRACKING TASK

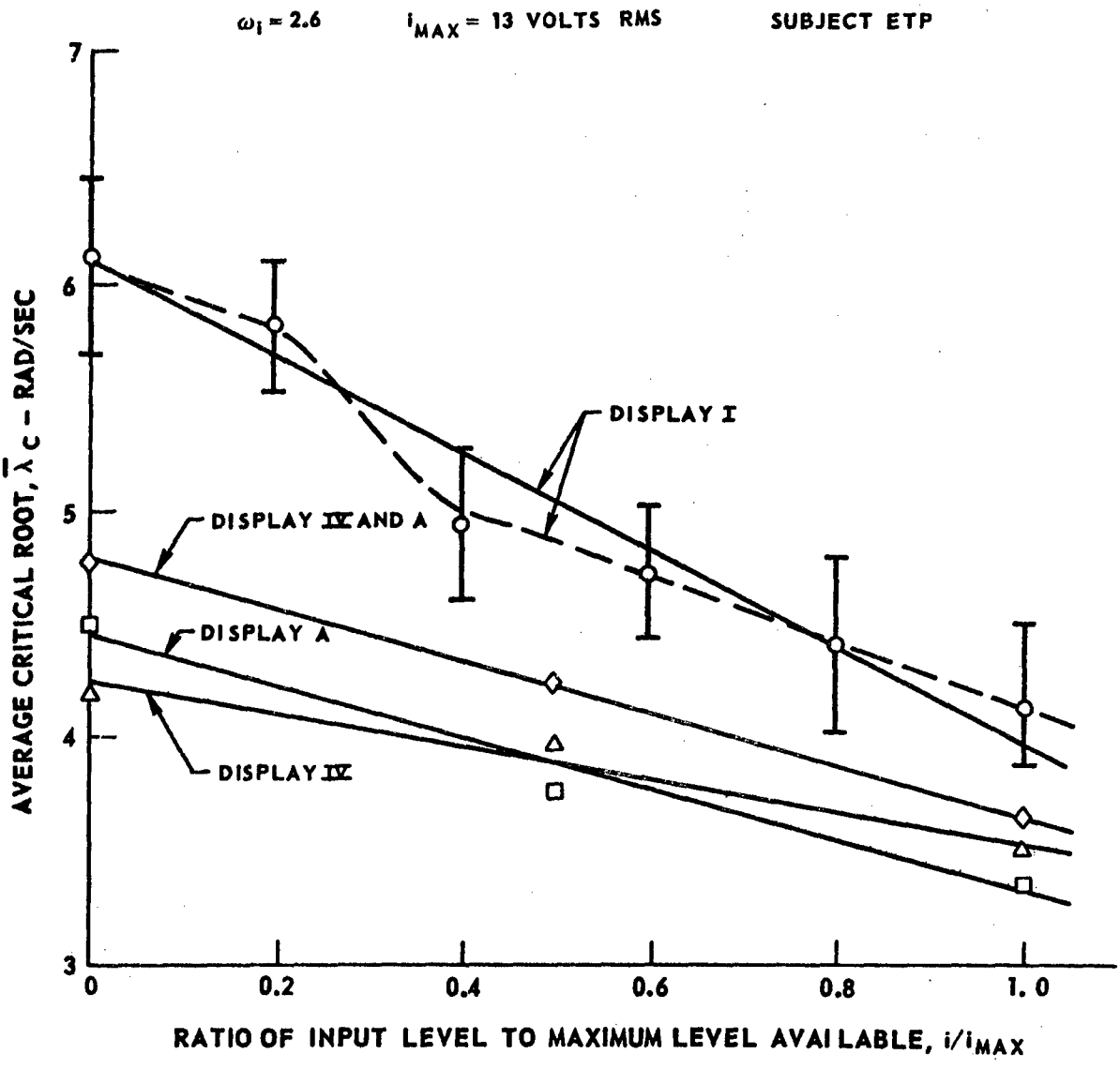

FIG. 3. EFFECT OF DISTURBANCE LEVEL ON $\bar{\lambda}_c$ FOR AURAL, VISUAL, AND COMBINED DISPLAYS

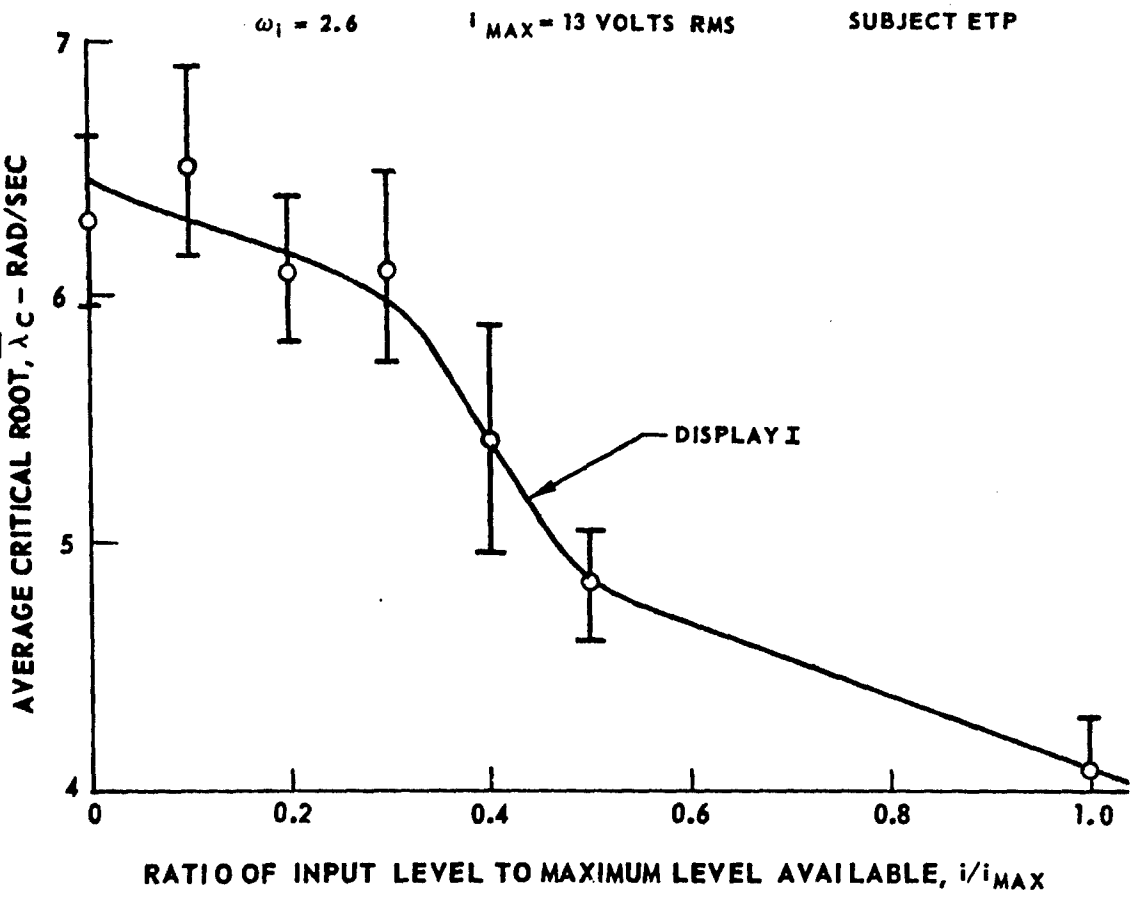

FIG. 4. EFFECT OF DISTURBANCE LEVEL ON $\bar{\lambda}_c$ FOR VISUAL DISPLAY I

HUMAN OPERATOR REMNANT IN A SUBCRITICAL TASK

by

J.N.M. de Jong and A. van Lunteren

Man-Machine Systems Group,
Laboratory for Measurement and Control,
Dept. of Mechanical Engineering,
Delft University of Technology
Netherlands

0 Abstract

Some experiments have been executed with a human operator controlling a system characterized by the transfer function $\lambda/(s-\lambda)$. For one subject the parameters of the transfer function of the human operator and the spectral density of his remnant have been determined as a function of the parameter λ and of the standard deviation σ_i of the forcing function i(t). The forcing function i(t) was a Gaussian noise having an almost flat spectrum in a frequency range of 0.02 to 2.5 Hz.

The results suggest that the spectral density of the remnant located at the human operator input is independent of the parameter λ, but does change as a function of the standard deviation of the forcing function, where the bandwidth of this forcing function is kept constant.

1 Introduction

In many situations where the behavior of the human operator is considered, a quasi linear model [1], also called describing function model, gives a good description of his input-output relation. The describing function model consists of two elements viz. a transfer function $H(\nu)$ and a remnant signal $N(\nu)$, where ν is the frequency in Hz. The remnant can be defined either as a signal $N_e(\nu)$ added to the input $E(\nu)$ of the human operator or as an additional signal $N_c(\nu)$ at the output $C(\nu)$ of the human operator (see Fig. 1). Since the late forties many investigations have been

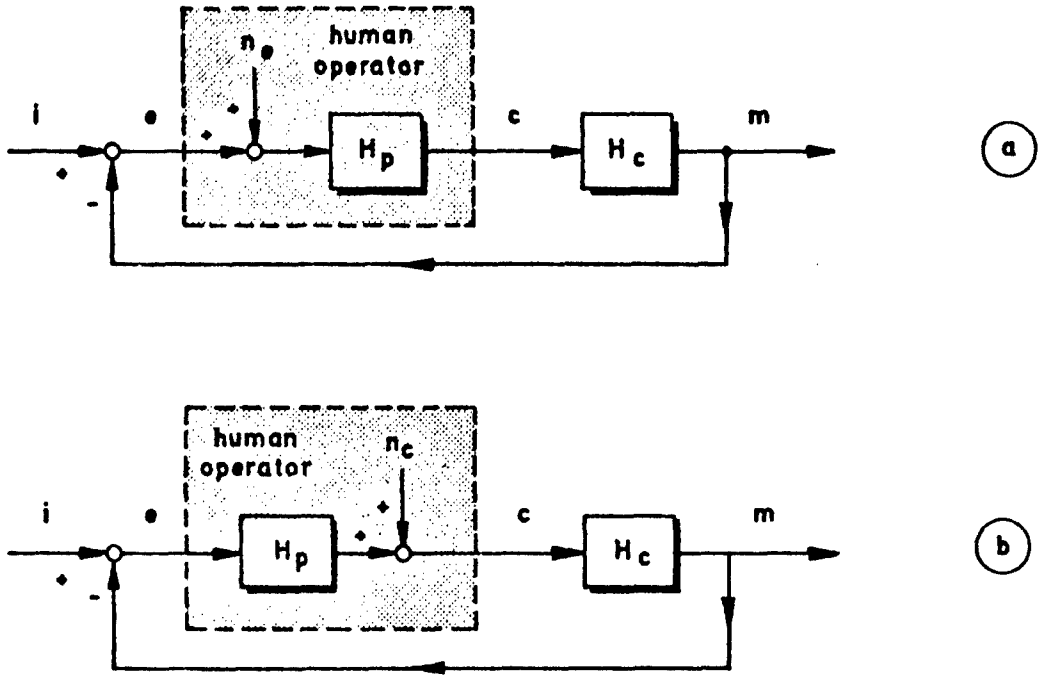

Figure 1. Two equivalent representations of the human operator executing a control task.

dedicated to the identification of the transfer function $H(\nu)$ of the human operator in a variety of control situations, resulting in McRuer's cross-over model [1]. Only recently more effort is being put into studies concerning the factors which influence the spectral density of the remnant [2, 3, 4]. As possible sources of the remnant the following causes have been mentioned by a number of investigators [5, 6, 7, 8, 9]:

- nonlinear behavior,
- non-stationary behavior,
- sampling behavior,
- sensory properties,
- scanning behavior if more than one input is presented,
- neuromuscular properties,
- introduction of a test signal by the human operator.

In general, it is not possible to isolate the effects of the different sources. Only in some cases, as for instance when the remnant results partly from nonlinear behavior [5, 10] or from periodic sampling [6], can this be achieved. Another case may be the deliberate introduction of a test-signal by the human operator.

In some earlier experiments within the Man-Machine Systems Group a tracking task was executed using a tactile display, which included a nonlinear element [11]. In these

experiments it was found that the human operator introduced a kind of test signal in the case that he did not get enough information about the state of the system to be controlled. The test signal just mentioned looked like a narrow band noise with a mean frequency of about 1 Hz.

Another indication concerning the generation of a test signal was found in early experiments with a bicycle simulator where the spectral densities of the input and output signals of the human operator were measured while no external forcing function was applied. In some of these experiments a peak could be detected in the spectral densities of all signals at a frequency of about 0.5 Hz [12]. This peak could not be explained as being caused by the natural frequency of the man-bicycle simulator system.

The experiments described here are meant as a first step in order to acquire more knowledge about the conditions which lead to the introduction of a test signal by the human operator. If it is assumed that the human operator introduces such a signal in those cases where his input is not adequate, then this investigation may yield information on how, in some cases, a better information exchange between man and machine may be achieved.

2 Determination of transfer function and spectral densities

For the system of Fig. 1 the transfer functions $H_p(\nu)$ and $H_c(\nu)$ can be determined according to:

$$H_p(\nu) = \frac{S_{ic}(\nu)}{S_{ie}(\nu)} \quad , \tag{1}$$

and

$$H_c(\nu) = \frac{S_{im}(\nu)}{S_{ic}(\nu)} \quad , \tag{2}$$

where the quantities $S_{ie}(\nu)$, $S_{ic}(\nu)$ and $S_{im}(\nu)$ indicate the cross-spectral densities of the forcing function i(t) and the signals e(t), c(t) and m(t) respectively. If the auto-spectral densities of the signals i(t) and c(t) are indicated as $S_{ii}(\nu)$ and $S_{cc}(\nu)$ respectively and if the coherency function $\Gamma_{ic}(\nu)$ is defined as:

$$\Gamma_{ic}(\nu) = \sqrt{\frac{|S_{ic}(\nu)|^2}{S_{ii}(\nu)S_{cc}(\nu)}} \quad , \tag{3}$$

then the spectral density $S_{nn_e}(\nu)$ of the remnant $n_e(t)$ located at the input (See Fig. 1a) can be computed from Eq. (4):

$$S_{nn_e}(\nu) = \left\{ \frac{1}{[\Gamma_{ic}(\nu)]^2} - 1 \right\} S_{ii}(\nu) \, . \tag{4}$$

An equivalent description of this remnant is given by the spectral density $S_{nn_c}(\nu)$ of the quantity $n_c(t)$ which represents the remnant located at the output of the human operator. Between the two a simple linear relation exists so that:

$$S_{nn_c}(\nu) = |H_p(\nu)|^2 S_{nn_e}(\nu) = \left|\frac{S_{ic}(\nu)}{S_{ie}(\nu)}\right|^2 \left\{\frac{1}{[\Gamma_{ic}(\nu)]^2} - 1\right\} S_{ii}(\nu) \quad (5)$$

The Eqs (1), (2), (4) and (5) can be derived by taking into account that the remnant is uncorrelated with the forcing function i(t).

The system of Fig. 1 can also be represented by the equivalent open loop system of Fig. 2. The spectral density

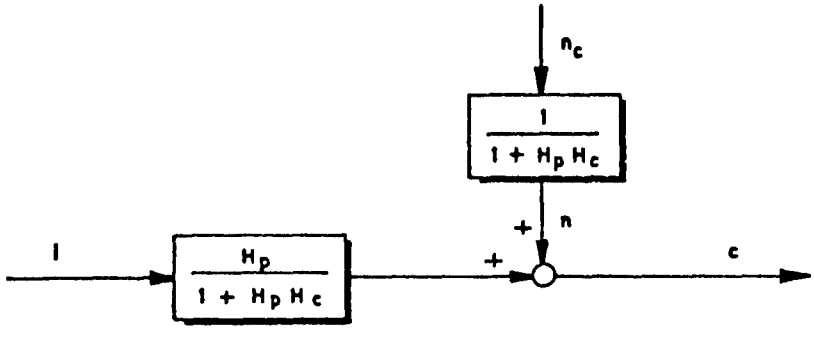

Figure 2. Open loop representation of the system given by Fig. 1.

$S_{nn}(\nu)$ of the signal n(t) which is defined by McRuer [1] as the closed loop remnant can be computed from Eq. (6)

$$S_{nn}(\nu) = \left\{1 - [\Gamma_{ic}(\nu)]^2\right\} S_{cc}(\nu) \quad (6)$$

In a similar way as in Fig. 1 a remnant might be defined located at the input of the open loop system. This idea has not been applied here, however.

3 The experiments

As a starting point for a closer study of remnant spectral densities a simple visual tracking system has been chosen with a controlled element described by $H_c(s) = \lambda/(s-\lambda)$. As this system in itself is unstable, the human operator always has to generate an output signal, even when no external forcing function is applied. Experiments with such

a system have been reported by Jex and Magdaleno [3], so that the initial results can be compared with known data.

The experimental set up is given in Fig. 3. The input signal is a Gaussian noise filtered by a 4th order band-pass

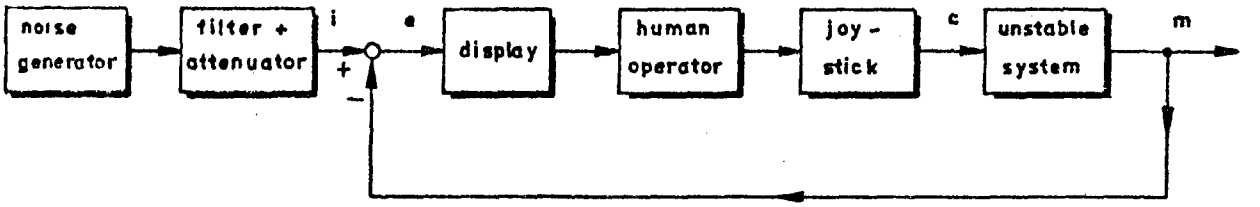

Figure 3. The experimental setup.

filter with cut off frequencies of 0.02 Hz and 2.5 Hz. By means of a potentiometer the variance of the signal i(t) could be changed. The display was a 10 cm x 8 cm (4" x 3¼") CRT placed at a distance of 74 cm (29") from the eyes of the subject and adjusted at a sensitivity of 0.5 V/cm. The manipulator was a vertically mounted aluminium rod with a diameter of 1.6 cm (5/8") and a length of 72 cm (28") which was fixed at its lower end. The stiffness for a horizontal displacement of the top end was 1.8 N/mm (10.3 lb/inch). Near the base this joystick had been provided with straingauges, which produced an electrical signal such that 1 mm stick displacement at the top was equivalent to 2 V. The output of the straingauge bridge was filtered by means of a first order filter, having a break frequency of 10.5 Hz, in order to eliminate high frequency noise. For frequencies lower than 3 Hz the dynamics of the straingauge bridge and this filter could be approximated by a time delay of 0.015 sec. The gainfactor of these components is not of interest here.

It was shown by Jex et al [13] that in this control task the human operator model could be described by:

$$H_p(\nu) = K_p e^{-j(2\pi\nu\tau_e + \alpha/2\pi\nu)}, \qquad (7)$$

in which τ_e is a measure for the high frequency phase lag due to the reaction time of the human operator and due to the dynamics of the neuromuscular system. This parameter will not become smaller than about 0.1 sec. The parameter α describes a low frequency phase lag, which is taken into account in McRuer's "extended cross-over model"[1]. For given values of τ_e and α it is possible to indicate the region of stability as function of the parameter λ and the gain factor K_p of the human operator [13].

A series of experiments has been carried out in which two quantities were varied viz. the standard deviation σ_i of

the forcing function i(t) and the system parameter λ which is a measure for the level of instability of the system to be controlled. The bandwidth of the forcing function i(t), however, was kept constant. The parameter λ was given the values 1.0, 1.5, 2.0, 2.5, 3.0, 3.5 and 4.0 For each of these values a testrun was executed with each of the following values of the standard deviation σ_i, expressed in cm displacement on the CRT: 0.52, 0.30, 0.16 and 0.00.

The experiments were executed with only one subject, age: 18, sex: female. Before the experiments started the subject passed through a training program of about 40 runs, each lasting about 5 minutes, in which all values of σ_i and λ to be used in the actual experiments were tried. The actual experiments were executed in the course of one week. Each experiment lasted somewhat more than 5 minutes. Between the experiments the subject had a rest period of at least 15 minutes.

4 Data processing

During the experiments the quantities i(t), e(t), c(t) and m(t) were measured and recorded on an analog taperecorder. Afterwards the signals were processed over an observation time of 5 minutes by means of the polarity coincidence correlation method [14, 15]. The correlation functions thus determined were transformed to spectral densities which, together with the standard deviations of the signals, were further processed in order to obtain the human operator transfer functions and the remnant spectra in the way indicated under 2. From the spectral densities the variances $\sigma_{n_e}^2$, $\sigma_{n_c}^2$ and σ_n^2 of the remnants $n_e(t)$, $n_c(t)$ and n(t) respectively have been calculated.

By using curve fitting techniques, based on minimization of the least square error, the parameters K_p, τ_e and α in Eq. (7) have been calculated from the frequency characteristics $H_p(\nu)$ of the human operator. It has to be taken into account that the value of τ_e, found in this way, is not yet the quantity τ_e of the pilot model but $\tau_e' = \tau_e + \tau_s$, where τ_s is a time delay of 0.015 sec due to the dynamics of the joystick. Fig. 4 shows the system with the transfer functions of its components. From the values of the parameters obtained, the stability margins with the related frequencies as indicated in Fig. 5 have been calculated. Moreover, also the lower boundary K_1 and the upper boundary K_2 for the pilot gain have been calculated from $K_1=K_p/A_1$ and $K_2=K_p/A_2$, where A_1 and A_2 are the quantities indicated in Fig. 5.

Finally, it should be mentioned that all these data are given only for those cases where $\sigma_i \neq 0$, because an unbiased estimate for the pilot transfer function $H_p(\nu)$ could

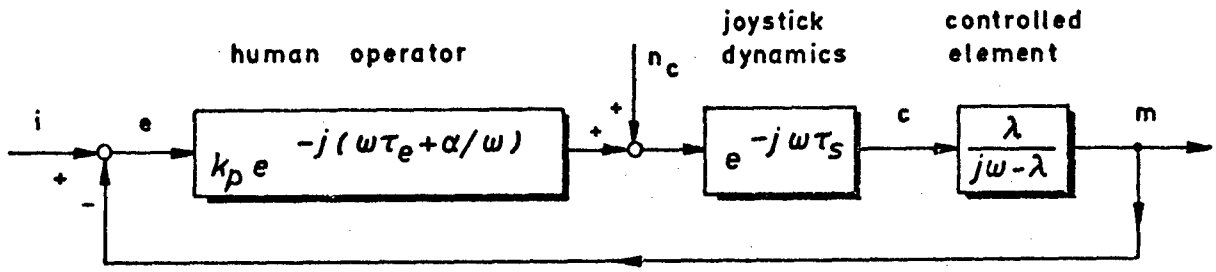

Figure 4. The man-machine system and its transfer functions.

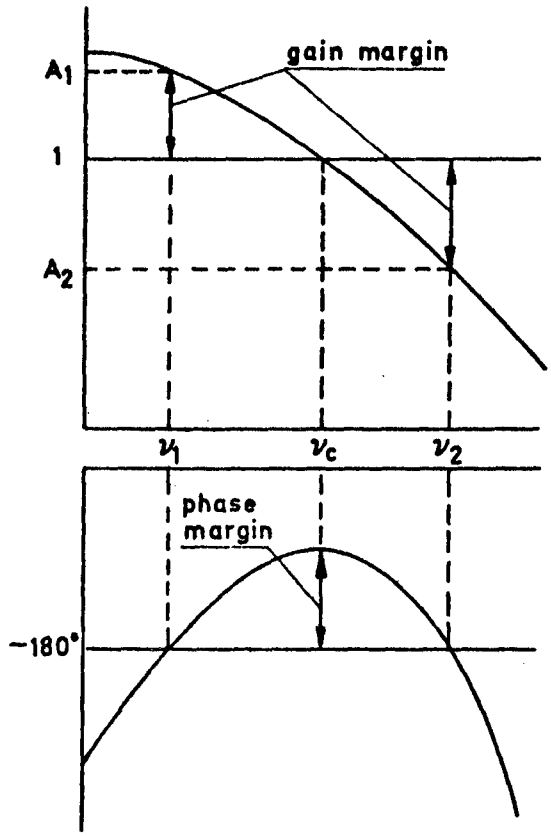

Figure 5.

Indication of the quantities which have been determined for the experiments executed with the system of Fig. 4.

only be determined from the relation $H_p(\nu) = S_{ic}(\nu)/S_{ie}(\nu)$. The estimation of the pilot transfer functions for those measurements, where the forcing function i(t) was zero, has

been executed according to some of the methods proposed by Wingrove and Edwards [16, 17, 18]. The results of these computations, however, will not be dealt with in this paper. Here, it should only be mentioned that the results are in accordance with the conclusions of Wingrove [18] viz. that a parameter estimation method gives the smallest bias in the estimated transfer functions. This bias becomes larger as the bandwidth of the remnant becomes smaller.

5 Results

Unfortunately, for 2 trials from all the data mentioned under 4 the results are missing viz. for the case $\lambda = 4.0$ and $\sigma_i = 0.52$, where the subject did not succeed in keeping up the task over a 5 minutes period, and for the case $\lambda = 3.0$ and $\sigma_i = 0.30$, where it turned out that the forcing function i(t) had not been recorded properly.

As an example the auto-spectral densities $S_{ii}(\nu)$ of the forcing function i(t), $S_{ee}(\nu)$ of the error signal e(t), $S_{cc}(\nu)$ of the control signal c(t) and $S_{mm}(\nu)$ of the system output m(t) are given in the Figs. 6 a, b, c and d for the case $\lambda = 2.5$ and $\sigma_i = 1.04$ V = 0.52 cm (displacement on the CRT). In the Figs 6 e and f the auto-spectral densities $S_{nn_e}(\nu)$ and $S_{nn_c}(\nu)$ of the remnant located at the human operator input and at the human operator output respectively are given for the same case. Also for this case the Figs 7 a, b and c give the data points of the transfer functions $H_p(\nu)$ of the human operator, $H_c(\nu)$ of the controlled element and the open loop transfer function $H_p(\nu)H_c(\nu)$ of the complete system. In the Figs 7 a and c the 75% confidence intervals for these data points have been indicated. They have been computed according to a method for closed loop systems, which was based on a method described by Jenkins and Watts [19] for a system in an open loop. A description of this method is given in the appendix. In Fig. 7 a also the lines have been drawn which belong to the human operator transfer function $H_p(\nu)$ according to Eq.7, with the parameters determined by curve fitting through the data points. In Fig. 7 b the lines of the known transfer function of the controlled element $H_c(\nu)$ have been drawn, while in Fig. 7 c the open loop transfer function based on the descriptions of $H_p(\nu)$ and $H_c(\nu)$ has been indicated.

The numerical data for all testruns have been summarized in Table I. These results can be distinguished in data on the human operator transfer function and remnant data. They will be discussed separately.

5.1 Transfer functions

The parameters of the human operator transfer function are

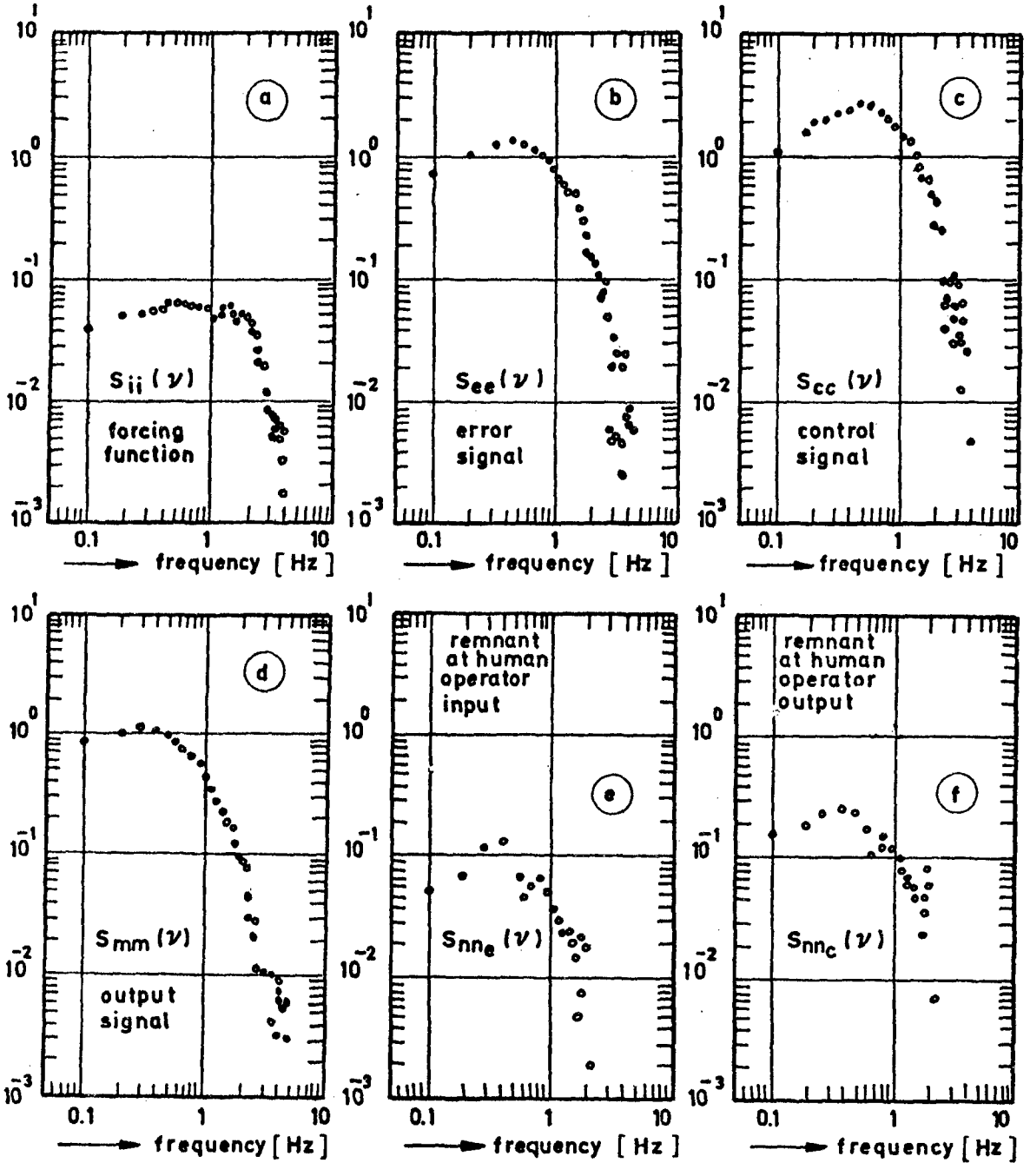

Figure 6. Auto-spectral densities in $cm^2 sec$, where the cm refer to a displacement on the CRT, for the forcing function i(t), the error signal e(t), the control signal c(t), the system output m(t), the remnants $n_e(t)$ and $n_c(t)$ for the case that the system parameter λ = 2.5 rad/sec and the standard deviation of the forcing function σ_i = 0.52 cm.

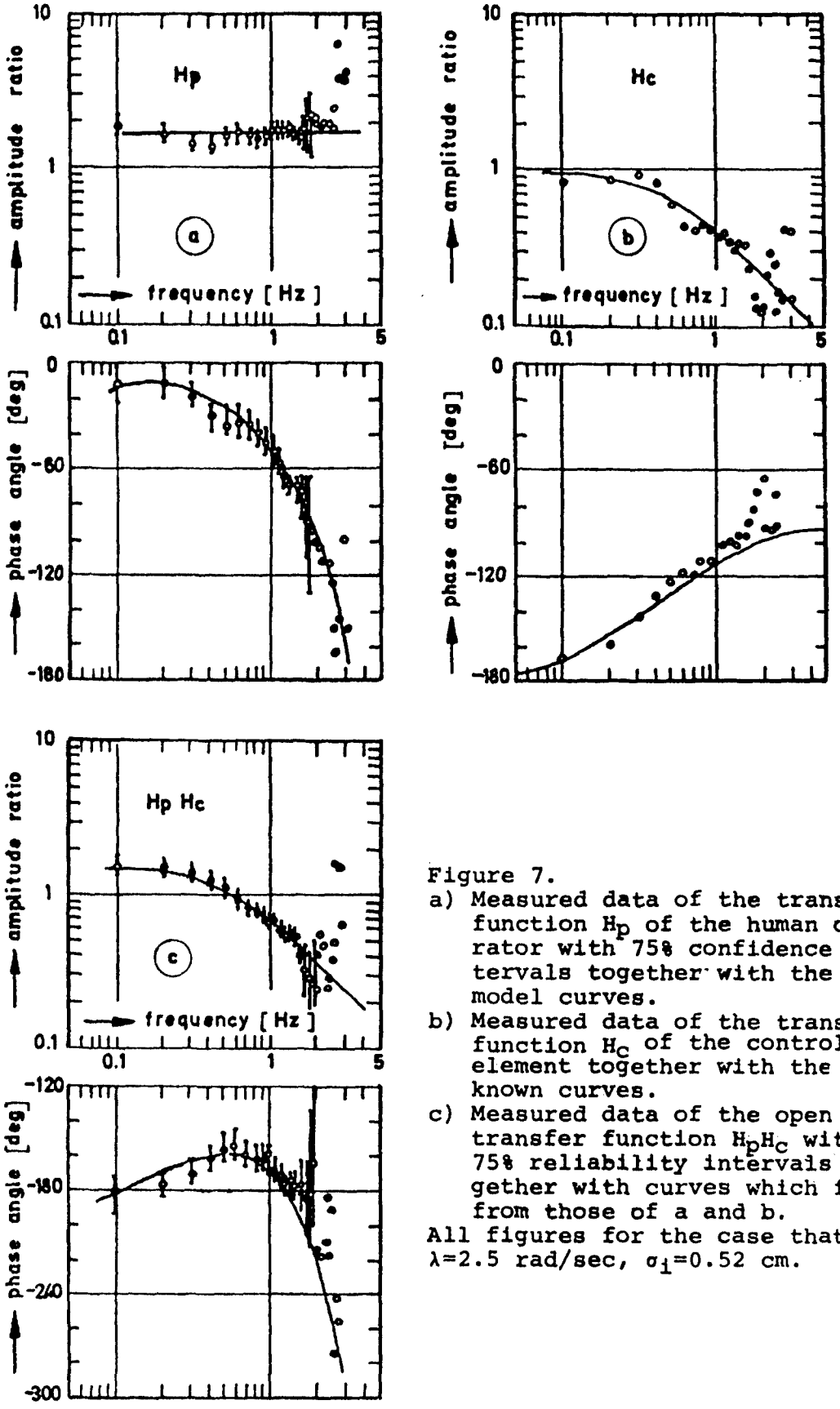

Figure 7.
a) Measured data of the transfer function H_p of the human operator with 75% confidence intervals together with the model curves.
b) Measured data of the transfer function H_c of the controlled element together with the known curves.
c) Measured data of the open loop transfer function H_pH_c with 75% reliability intervals together with curves which follow from those of a and b.
All figures for the case that λ=2.5 rad/sec, σ_i=0.52 cm.

given in Table I as a function of λ and σ_i. They are represented in the Figs 8 a, b and c. It seems that they do not depend very much on the standard deviation σ_i of the forcing function i(t) but change as a function of the parameter λ.

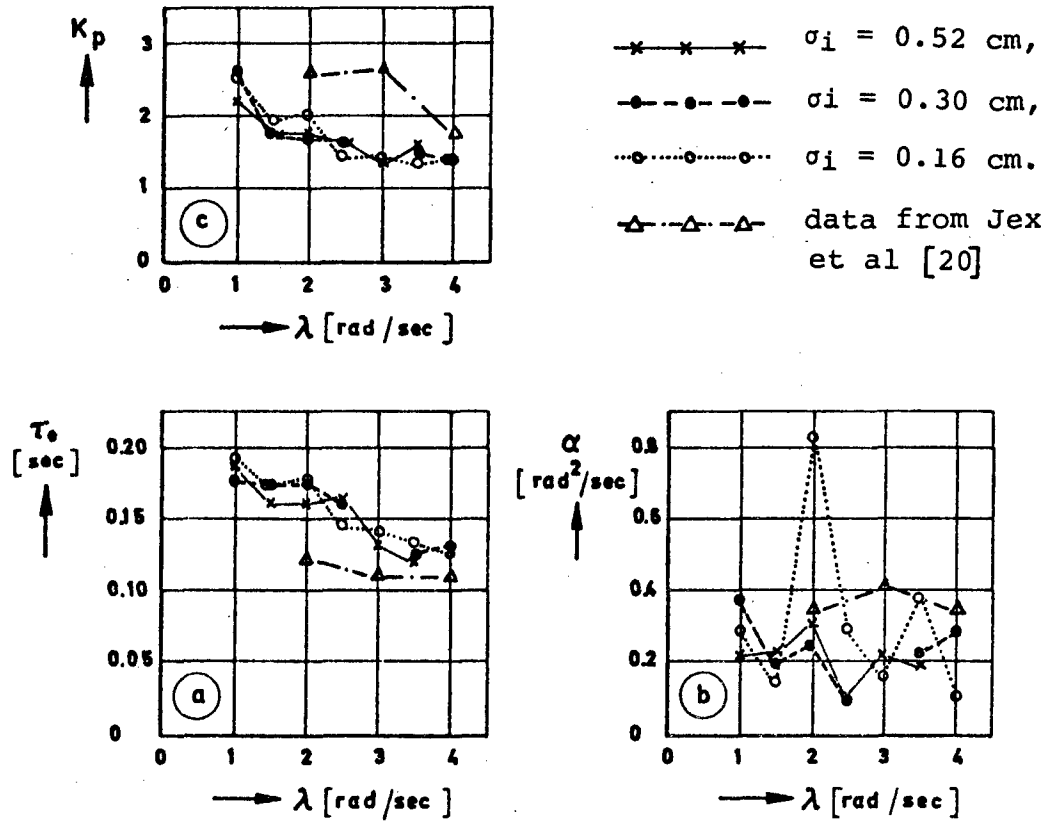

Figure 8. Pilot gain K_p, effective time delay τ_e and low frequency phase lag parameter α as a function of the system parameter λ for different values of the standard deviation σ_i of the forcing function in comparison with results found by Jex et al [20].

Also in these figures the results are given which were found by Jex et al [20] with a forcing function consisting of a sum of sinusoids having an equivalent bandwidth ω_i of 1.5 rad/sec and a standard deviation σ_i = 0.32 cm.

A closer inspection of the data of Table I showed an interesting phenomenon, which has also been found in [20], viz. that the ratio between the standard deviation σ_c of the human output and the standard deviation σ_e of the human input is very close to the human operator gain K_p. This is illustrated in Fig. 9

From the human operator parameters given in Table I a number of quantities related to the stability margins have

Table I: Remnant data and human operator model parameters as function of λ and σ_i.

system param.	RMS-values for signals				RMS-values for remnant						human operator model parameters		
λ [rad/sec]	σ_i [cm]	σ_e [cm]	σ_c [cm]	σ_m [cm]	σ_{n_e} [cm]	σ_{n_c} [cm]	σ_n [cm]	$\frac{\sigma_{n_e}}{\sigma_e}$	$\frac{\sigma_{n_c}}{\sigma_c}$	$\frac{\sigma_n}{\sigma_c}$	K_p	τ_e [sec]	α [rad^2/sec]
1.0	0.00	0.10	0.29	0.10									
	0.15	0.29	0.77	0.24	0.15	0.37	0.60	0.52	0.48	0.78	2.56	0.193	0.28
	0.30	0.55	1.48	0.43	0.27	0.48	0.86	0.49	0.32	0.58	2.59	0.177	0.37
	0.50	0.87	2.00	0.67	0.39	0.84	1.28	0.45	0.42	0.64	2.21	0.188	0.21
1.5	0.00	0.13	0.29	0.13									
	0.16	0.39	0.73	0.35	0.15	0.28	0.52	0.38	0.38	0.71	1.89	0.173	0.14
	0.30	0.58	1.04	0.52	0.22	0.39	0.68	0.38	0.38	0.65	1.77	0.173	0.19
	0.53	1.06	1.96	0.84	0.35	0.63	1.19	0.33	0.32	0.61	1.76	0.160	0.22
2.0	0.00	0.22	0.39	0.23									
	0.17	0.60	1.16	0.54	0.25	0.49	0.94	0.42	0.42	0.81	2.02	0.177	0.83
	0.31	0.94	1.63	0.84	0.27	0.46	1.27	0.29	0.28	0.78	1.69	0.174	0.24
	0.51	1.37	2.43	1.25	0.45	0.75	1.58	0.33	0.31	0.65	1.75	0.161	0.31
2.5	0.00	0.35	0.53	0.35									
	0.15	0.60	0.84	0.58	0.17	0.25	0.69	0.28	0.30	0.82	1.45	0.145	0.29
	0.30	1.08	1.72	1.03	0.28	0.46	1.25	0.26	0.27	0.73	1.62	0.158	0.09
	0.53	1.65	2.69	1.53	0.44	0.71	1.85	0.27	0.26	0.69	1.61	0.160	0.10
3.0	0.00	0.32	0.45	0.32									
	0.16	0.77	1.07	0.74	0.18	0.26	0.86	0.23	0.24	0.80	1.46	0.143	0.16
	0.52	1.81	2.48	1.72	0.49	0.70	1.72	0.27	0.28	0.69	1.41	0.131	0.22
3.5	0.00	0.53	0.70	0.53									
	0.16	0.92	1.22	0.90	0.25	0.42	1.01	0.27	0.34	0.83	1.34	0.133	0.38
	0.31	1.40	2.01	1.40	0.36	0.54	1.56	0.26	0.27	0.78	1.48	0.126	0.22
	0.52	2.03	3.12	2.15	0.51	0.79	2.26	0.25	0.25	0.72	1.61	0.122	0.19
4.0	0.00	0.70	0.85	0.70									
	0.16	1.12	1.47	1.12	0.22	0.30	1.21	0.20	0.20	0.82	1.38	0.126	0.10
	0.30	1.85	2.42	1.82	0.46	0.73	2.14	0.25	0.30	0.88	1.37	0.131	0.29

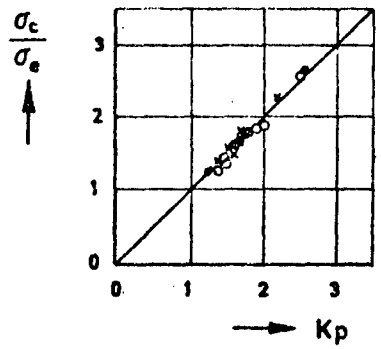

Figure 9.
Ratio between the standard deviations of human operator output and input versus his gain factor.

been derived. They are represented in Table II. Graphically these data are reproduced in the Figs 10 a, b, c and d. Also in these pictures the data from Jex et al [20] are given. The difference in bandwidth between the forcing function applied in ref. [20] and the one in this study (ω_i = 1.5 rad/sec versus ω_i = 15.7 rad/sec) accounts for the large differences, particularly in the values of the cross-over frequencies (about 1 Hz in ref. [20] as against about 0.5 Hz in the present study). This can be easily explained from the fact that the large bandwidth of 15.7 rad/sec (2.5 Hz) causes a crossover regression as has been pointed out by McRuer and Jex [1].

5.2 The remnant

The standard deviation of the remnant as given in Table I is shown in the Figs 11 a, b, c and d as a function of λ for different values of σ_i. The Figs 11 a and b indicate that the standard deviation of the nonnormalized remnant, whether located at the human operator input or at his output, hardly depends on λ. The figures also show, that the nonnormalized standard deviation of the remnant increases with increasing values of σ_i. When the standard deviations σ_{n_e} and σ_{n_c} are normalized with respect to the standard deviations σ_e and σ_c respectively (Fig. 11 c and d), they hardly change with σ_i, but decrease with increasing λ.

The spectral densities $S_{nn_e}(\nu)$ of the human operator located at the input are given in the Figs 12 a, b, c, d, e, f and g. These figures show that the spectral density is higher when the standard deviation of the forcing function is higher. Therefore, the same spectral densities have been drawn again in the Figs 13 a, b and c, but arranged in a different way, i.e. now all spectral densities for different values of λ are drawn in one picture for each of the three values of σ_i. These figures show that all lines in one picture vary about a common mean value. This is in agreement with the results of Jex and Magdaleno [3], viz. that the nonnormalized

Table II: Data on the stability margins of the system as function of λ and σ_i.

system param. λ [rad/sec]	RMS of input σ_i [cm]	cross-over frequency ω_c [rad/sec]	cross-over frequency ν_c [Hz]	phase margin m [degr.]	lower freq. for phase=-180° ω_1 [rad/sec]	lower freq. for phase=-180° ν_1 [Hz]	gain at A_1 [cm/cm]	gain margin at ω_1 [dB]	lower gain limit K_1	upper freq. for phase=-180° ω_2 [rad/sec]	upper freq. for phase=-180° ν_2 [Hz]	gain at A_2 [cm/cm]	gain margin at ω_2 [dB]	upper gain limit K_2
1.0	0.00													
	0.15	2.36	0.37	32	0.64	0.10	2.15	6.7	1.19	6.63	1.05	0.38	8.4	6.70
	0.30	2.39	0.38	32	0.74	0.12	2.08	6.4	1.25	7.19	1.14	0.36	9.0	7.26
	0.50	1.97	0.31	34	0.54	0.09	1.94	5.8	1.14	6.88	1.09	0.32	9.9	6.95
1.5	0.00													
	0.16	2.41	0.38	29	0.56	0.09	1.77	5.0	1.07	7.15	1.14	0.39	8.2	4.87
	0.30	2.19	0.35	27	0.66	0.11	1.62	4.2	1.09	7.11	1.13	0.37	8.7	4.84
	0.53	2.17	0.35	28	0.70	0.11	1.59	4.1	1.10	7.72	1.23	0.34	9.5	5.24
2.0	0.00													
	0.17	3.51	0.56	8	2.05	0.33	1.41	3.0	1.43	5.64	0.90	0.67	3.4	2.99
	0.31	2.72	0.43	19	0.93	0.15	1.53	3.7	1.10	6.55	1.04	0.49	6.1	3.42
	0.51	2.87	0.46	20	1.04	0.17	1.55	3.8	1.13	7.12	1.13	0.47	6.5	3.70
2.5	0.00													
	0.15	2.62	0.42	16	1.16	0.18	1.31	2.4	1.10	7.59	1.21	0.45	6.9	3.20
	0.30	3.19	0.51	19	0.64	0.10	1.57	3.9	1.03	7.03	1.12	0.54	5.3	2.98
	0.53	3.15	0.50	18	0.68	0.11	1.55	3.8	1.04	6.91	1.10	0.55	5.2	2.94
3.0	0.00													
	0.16	3.19	0.51	15	0.99	0.16	1.39	2.8	1.05	7.35	1.17	0.55	5.2	2.65
	0.52	2.98	0.47	16	1.13	0.18	1.32	2.4	1.07	8.16	1.30	0.49	6.3	2.90
3.5	0.00													
	0.16	3.12	0.50	8	1.81	0.29	1.19	1.5	1.13	7.20	1.15	0.59	4.6	2.29
	0.31	3.82	0.61	13	1.29	0.21	1.39	2.9	1.07	8.03	1.28	0.59	4.6	2.50
	0.52	4.42	0.70	14	1.17	0.19	1.53	3.7	1.06	8.43	1.34	0.62	4.2	2.61
4.0	0.00													
	0.16	3.80	0.61	11	0.98	0.16	1.34	2.5	1.03	7.62	1.21	0.64	3.9	2.15
	0.30	3.75	0.60	7	1.81	0.29	1.25	1.9	1.10	6.85	1.09	0.69	3.2	1.98

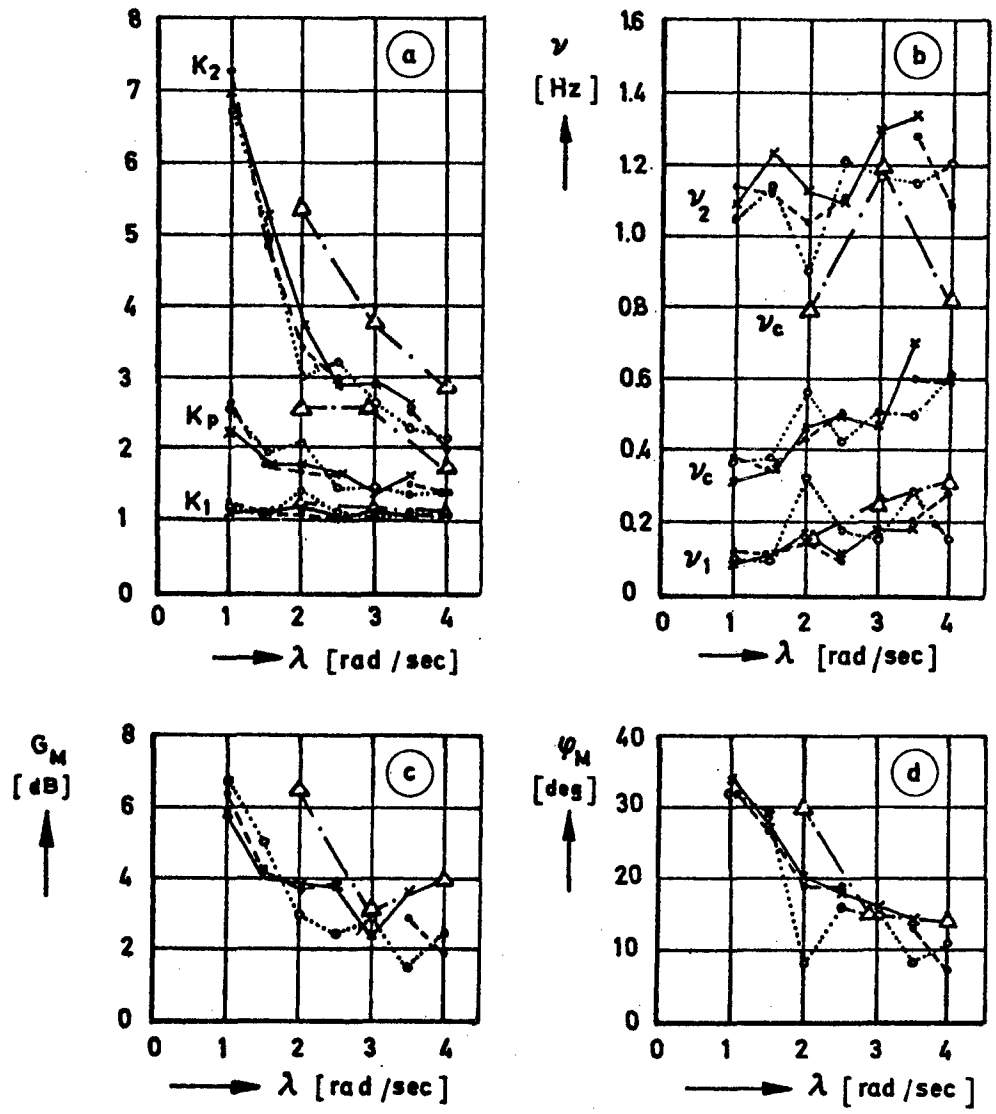

Figure 10. Data concerning the stability margins as a function of the system parameter λ for three values of the standard deviation σ_i of the forcing function, viz.

—×—×—×— σ_i = 0.52 cm,
-•-•-•- σi = 0.30 cm,
·····o····o····· σ_i = 0.16 cm,
–·–▲–·–▲–·– data from Jex et al [20].

Here, K_p is the human operator gain, K_1 and K_2 are the lower limit and upper limit for this gain; ν_c is the crossover frequency, ν_1 and ν_2 are the frequencies for the gain margins as indicated in Fig. 5; G_M is the gain margin at the frequency ν_1 and φ_M is the phase margin. In Fig. b the data from [20] for ν_2 are outside the range of the picture.

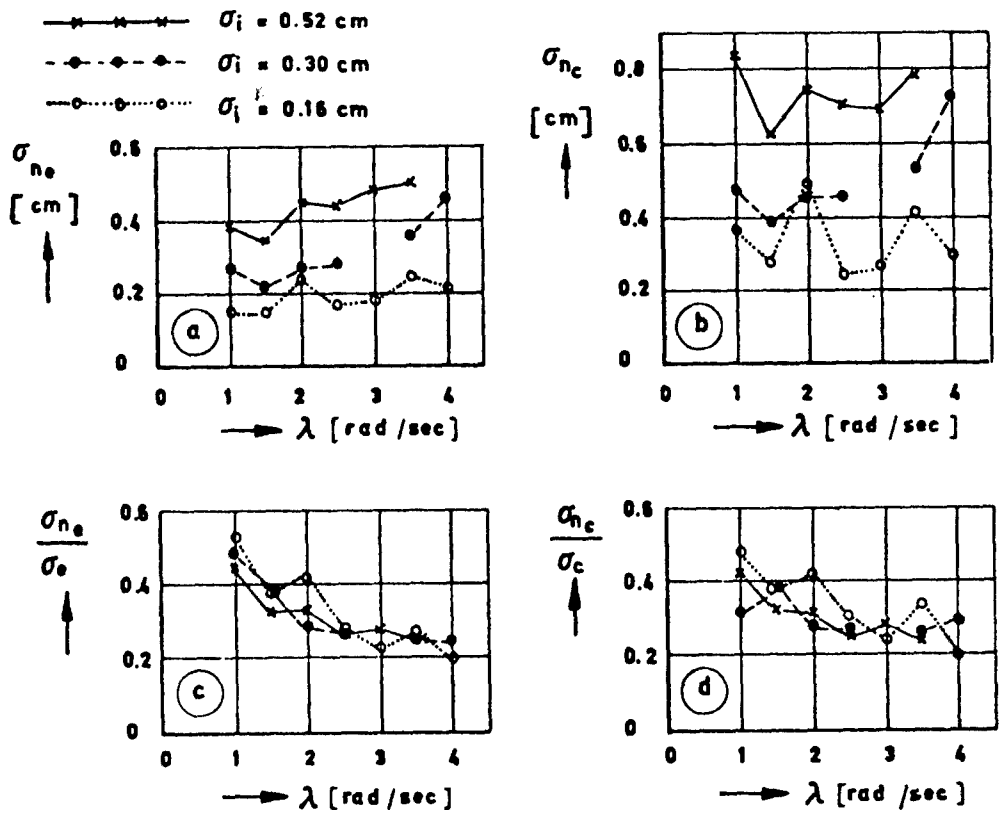

Figure 11. Standard deviations of the remnant σ_{n_e} located at the human operator input (a) and of the remnant σ_{n_c} located at the human operator output (b). The same data are given normalized with respect to the input signal e(t) and the output signal c(t) of the human operator respectively (c and d).

input remnant in a task with a first order unstable controlled element does not depend on the parameter λ. As a consequence, the spectral densities of the input remnant $S_{nn_e}(\nu)$ at a given value of σ_i have been averaged over the trials with different values of λ. The means and standard deviations are given in the Figs 14 a, b and c. In Fig. 15 these averaged spectral densities for the three values of σ_i are presented in one picture. An analytical description of these curves for the frequency range of $0.5 < \omega < 10$ rad/sec might be:

$$S_{nn_e}(\omega) = \frac{0.1}{1+0.5\omega} \ [cm^2 sec] \text{ with } \sigma_i = 0.52 \text{ cm};$$

$$S_{nn_e}(\omega) = \frac{0.06}{\omega} \ [cm^2 sec] \text{ with } \sigma_i = 0.30 \text{ cm};$$

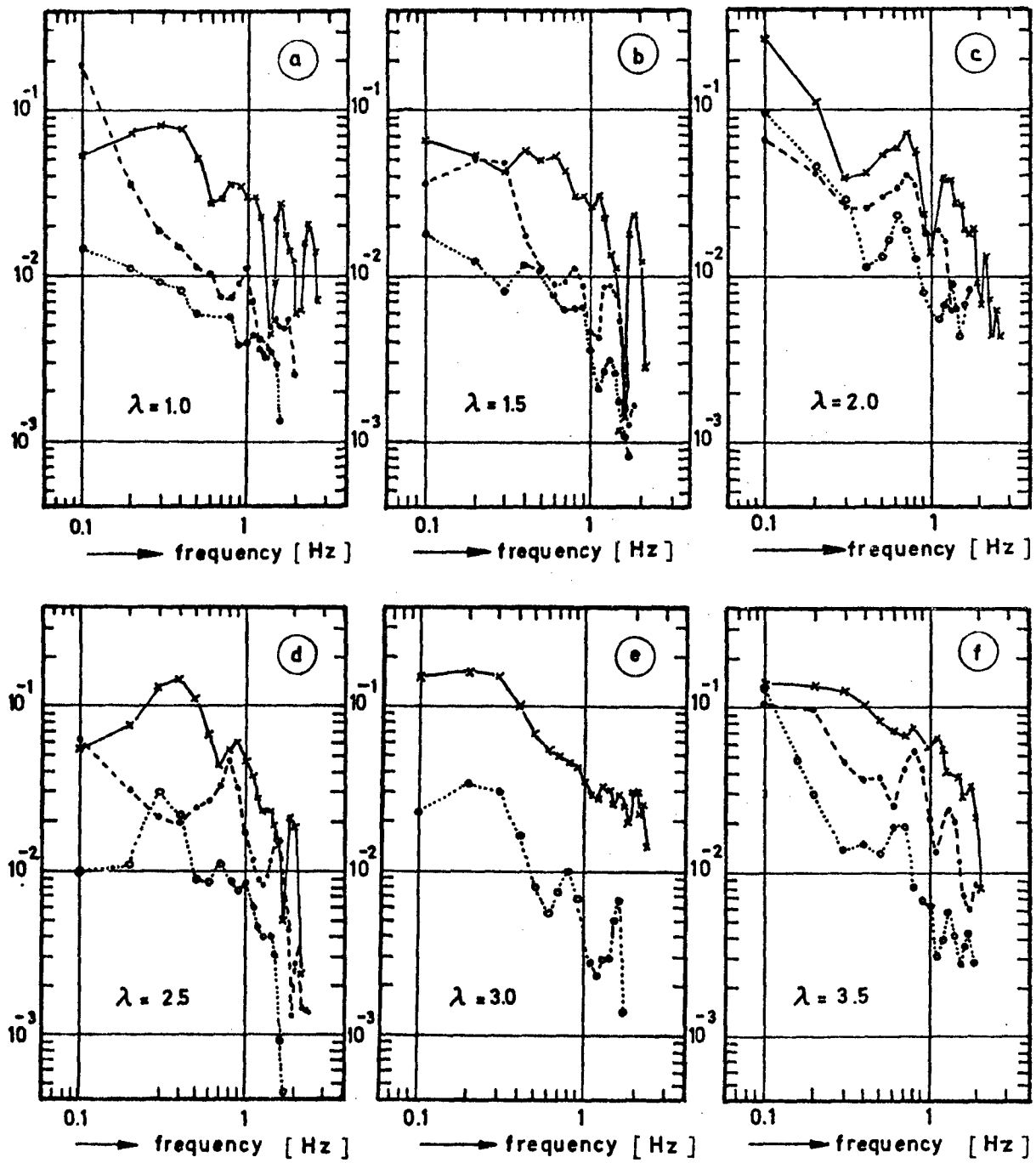

Figure 12. Spectral densities $S_{nn_\theta}(\nu)$ in $cm^2 sec$ of the remnant at the human operator input for 6 values of the system parameter λ and 3 values of the standard deviation σ_i of the forcing functions, viz.

—×—×—×— σ_i = 0.52 cm,

–·–·–·– σ_i = 0.30 cm,

·····o·····o····· σ_i = 0.16 cm.

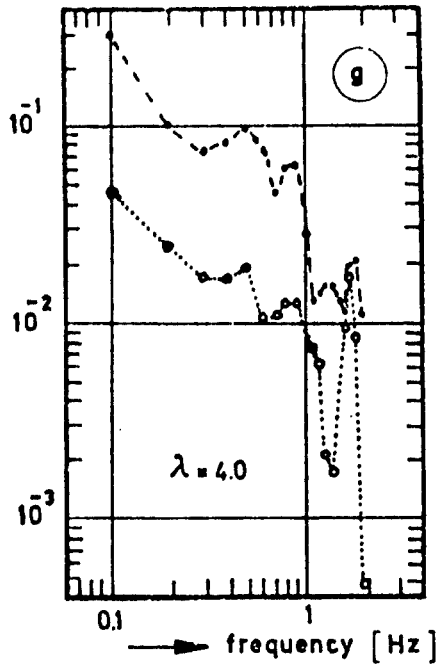

Figure 12 g.

Spectral densities $S_{nn_e}(\nu)$ in $cm^2 sec$ of the remnant at the human operator input, for the case where the system parameter $\lambda = 4.0$, with two different values of the standard deviation σ_i of the forcing function.

$\sigma_i = 0.30$ cm

$\sigma_i = 0.16$ cm

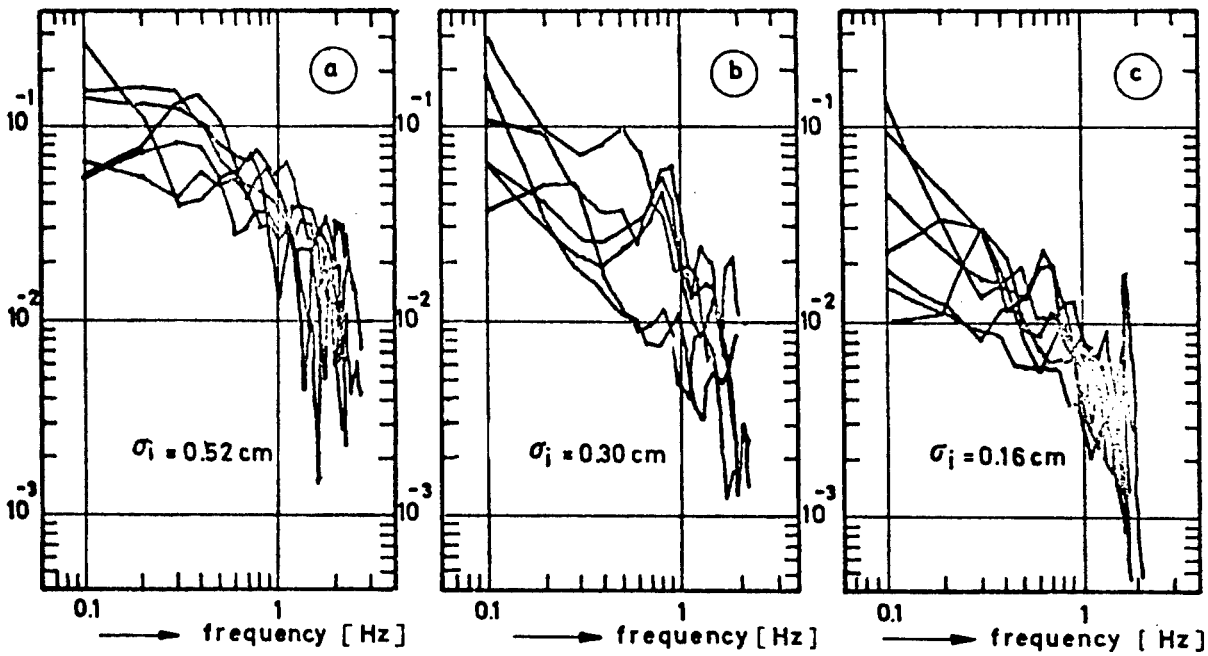

Figure 13. Spectral densities $S_{nn_e}(\nu)$ in $cm^2 sec$ of the input remnant for the different values of λ, each time with the same standard deviation σ_i of the input signal, for three values of σ_i.

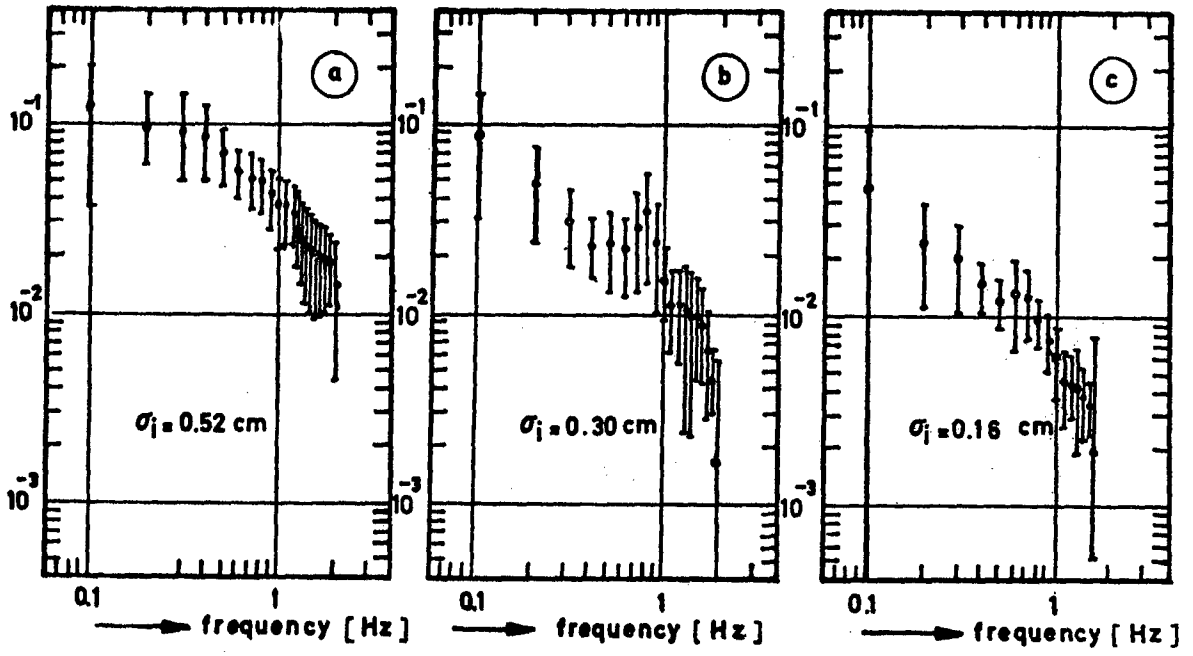

Figure 14. Mean values and standard deviations of the spectral density $S_{nn_e}(\nu)$ of the human operator input remnant for a constant value of σ_i. The results have been determined by averaging over the spectral densities obtained with 7 different values of the parameter λ.

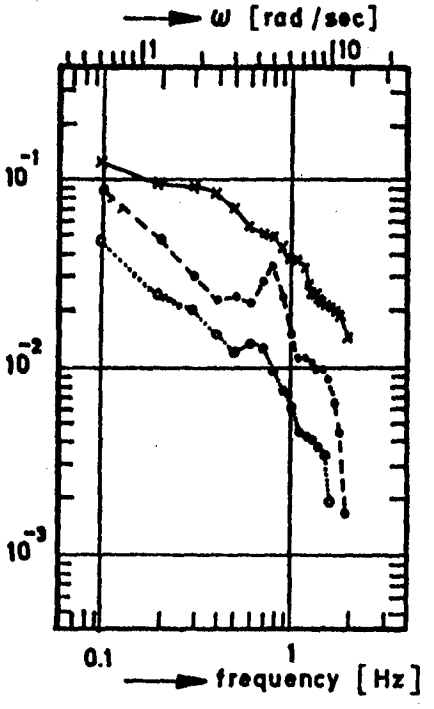

Figure 15.
Averaged spectral densities $S_{nn_e}(\nu)$ of the human operator input remnant for three different values of the standard deviation σ_i of the forcing function. In all cases the forcing function was Gaussian noise with a flat spectrum in the frequency range 0.02 - 2.5 Hz.

—×—×—×— σ_i = 0.52 cm
—•—•—•— σ_i = 0.30 cm
····o····o····o···· σ_i = 0.16 cm

$S_{nn_e}(\omega) = \frac{0.03}{\omega}$ [cm^{2}sec] with σ_i = 0.16 cm,

while a small peak occurs at ω = 4 rad/sec for σ_i = 0.16 cm and a somewhat larger peak at ω = 5 rad/sec for σ_i = 0.30 cm. Whether these peaks have any meaning, however, is an open question.

6 Conclusions

From the experiments with a first order unstable controlled element using a Gaussian forcing function which has a flat spectral density in the frequency range of 0.02 - 2.5 Hz and zero outside this range, the following conclusions can be drawn:

- The human operator transfer function found agrees with the one given by Jex et al [20].
- The large bandwidth of the forcing function causes a cross-over regression, which is also in accordance with the theory of the cross-over model [1]. Therefore, there is a difference in the numerical values of the parameters with regard to those in ref. [20].
- Just like in ref. [20], it was found, that the ratio between the standard deviations σ_c and σ_e of the output and input of the human operator was equal to the gain factor in the human operator transfer function in all experiments.
- The parameters of the human operator transfer function decrease when the system parameter λ increases, but do not depend on the magnitude of the forcing function.
- The spectral density $S_{nn_e}(\nu)$ of the remnant located at the human operator input is fairly independent of the system parameter λ, which affirms earlier results of Jex and Magdaleno [3].
- The spectral density $S_{nn_e}(\nu)$ does change with the magnitude of the forcing function. A normalization with respect to the standard deviation σ_e of the human operator input eliminates this dependency. The spectral density normalized in this way then becomes a function of the system parameter λ.
- The dispersion in the estimates of $S_{nn_e}(\nu)$ is rather large. After averaging over a number of spectral densities, the results suggest that an analytical description might be given by $K/(1+a\omega)$, where K and a depend on the magnitude of the forcing function. In some cases there is also a peak at about 0.6 to 0.8 Hz, whether these peaks are very significant is doubtful, however.

7 References

1. McRuer , D.T.; and Jex, H.R., A review of quasi linear pilot models, IEEE Trans. on Human Factors in Electronics, Vol HFE-8, No. 3, September 1967, pp 231-249.
2. Levison, W.H.,; Baron, S.; and Kleinman, D.L., A model for human controller remnant. IEEE Trans. on Man-Machine Systems, Vol MMS-10, No. 4, December 1969, pp 101-108.
3. Jex, H.R.; and Magdaleno, R.E., Corroborative data on normalization of human operator remnant, IEEE Trans. on Man-Machine Systems, Vol MMS-10, No 4, December 1969, pp 137-140.
4. Gordon-Smith, M., An investigation into certain aspects of the describing function of a human operator controlling a system of one degree of freedom. University of Toronto, Institute for Aerospace Studies, Report 149, February 1970, p 49 + 99.
5. McRuer , D.T.; Graham, D.; Krendel, E.S.; and Reisener, W.C., Human pilot dynamics in compensatory systems, AFFDL-TR-65-15, July 1965, pp 10-34, 188-189.
6. Bekey, G.A., The human operator as a sampled-data system, IRE Trans. on Human Factors in Electronics, Vol HFE-3, No. 2, September 1962, pp 43-51.
7. Bekey, G.A.; and Angel, E.S., Asynchronous finite state models of manual control systems, Proc. of the 2nd Annual Conference on Manual Control, NASA SP-128, 1966, pp 25-37.
8. Lange, G.W., Representation of the human operator as a sampled-data system, Proceedings of the IEE, Vol 115, No. 2, February 1968, pp 342-354.
9. Pew, R.W.; Duffendack, J.C.; and Fensch, L.K., Sine-wave tracking revisited, IEEE Trans. on Human Factors in Electronics, Vol HFE-8, No. 2, June 1967, pp 130-134.
10. Schweizer, G., Probleme und Methoden zur Untersuchung des Regelverhaltens des Menschen, in: Oppelt, W; und Vossius, G., Der Mensch als Regler, VEB Verlag Technik, Berlin, 1970, pp 159-238.
11. Stassen, H.G.; Meyer, A.W.A.; and Lunteren, A. van, On the possibilities of tactile information transmission for the use in arm prostheses.Proc. of the 6th Annual Conference on Manual Control, AFIT-AFFDL,Wright Patterson AFB, Ohio, 1970, pp 513-534.
12. Stassen, H.G., Research on information exchange in man-machine systems, Delft Univ. of Techn., Dept. of Mech. Engng, Lab. for Measurement and Control, Report No. N-32, November 1966, pp 3-4.
13. Jex, H.R.; McDonnell, J.D.; and Phatak, A.V., A "critical" tracking task for manual control research, IEEE Trans. on Human Factors in Electronics, Vol. HFE-7, No. 4, December 1966, pp 138-145.

14. Veltman, B.P.Th. and Kwakernaak, H., Theorie und Technik der Polaritäts Korrelation für die dynamische Analyse niederfrequenter Signalen und Systemen, Regelungstechnik, Vol 9, Nr. 9, 1961, pp 357-364.
15. Stassen, H.G., The polarity coincidence correlation technique - A useful tool in the analysis of human-operator dynamics, IEEE Trans. on Man-Machine Systems, Vol MMS-10, Nr. 1, March 1969, pp 34-39.
16. Wingrove, R.C. and Edwards, F.G., Measurement of Pilot Describing Functions From Flight Test Data With an Example From Gemini X., Proc. of the 4th Annual Conf. on Manual Control, NASA SP-192, 1968, pp 119-134.
17. Wingrove, R.C. and Edwards, F.G., A technique for identifying pilot describing functions from routine flight-test records., NASA TN D-5127, 1969.
18. Wingrove, R.C., Comparison of methods for identifying pilot describing functions from closed-loop operating records, NASA TN D-6235, March 1971.
19. Jenkins, G.M. and Watts, D.G., Spectral analysis and its applications, Holden Day, San Francisco, 1968, pp 429-436.
20. Jex, H.R., McDonnell, J.D., and Phatak, A.V., A "critical" tracking task for man-machine research related to the operator's effective delay time - Part I, NASA CR-616, November 1966, pp 47-52.

APPENDIX A

Confidence limits in the estimate of a transfer function in a closed loop.

For a system in an open loop disturbed by noise (Fig. A1), Jenkins and Watts [19] give a method to determine the confidence intervals of the estimate of a transfer function, obtained from estimated spectral densities according to the

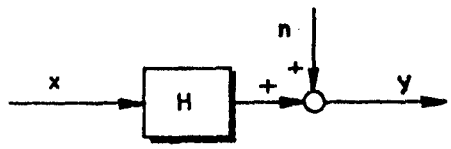

Fig. A1.
Open loop system to be identified.

wellknown relation:

$$H(\nu) = \frac{S_{xy}(\nu)}{S_{xx}(\nu)} \qquad (A.1)$$

When the estimated coherency function between x and y is indicated as $\hat{\Gamma}_{xy}(\nu)$ and when the quantity $Q(\nu;\alpha)$ is defined as:

$$Q(\nu;\alpha) = \frac{2}{\kappa-2} f_{2,\kappa-2}(1-\alpha) \frac{1-\left|\hat{\Gamma}_{xy}(\nu)\right|^2}{\left|\hat{\Gamma}_{xy}(\nu)\right|^2}, \qquad (A.2)$$

where $f_{2,\kappa-2}(1-\alpha)$ refers to Fisher's F distribution with 2 and $\kappa-2$ degrees of freedom and a $1-\alpha$ probability point, then it is possible to indicate the reliability intervals for the estimated gain $\hat{G}(\nu)$ and the estimated phase $\hat{F}(\nu)$. For the gain the $100(1-\alpha)$% limits are given by:

$$\text{gain conf. limit} = \hat{G}(\nu)\{1 \pm \sqrt{Q(\nu;\alpha)}\}. \qquad (A.3)$$

The $100(1-\alpha)$% confidence limits for the phase follow from:

$$\text{phase conf. limit} = \hat{F}(\nu) \pm \arcsin\{\sqrt{Q(\nu;\alpha)}\}. \qquad (A.4)$$

The overall system considered in this paper can be described by an unknown system with transfer function $H_1(\nu)$ and a known system with transfer function $H_2(\nu)$ linked up in a closed loop as indicated in Fig. A2. In order to calculate

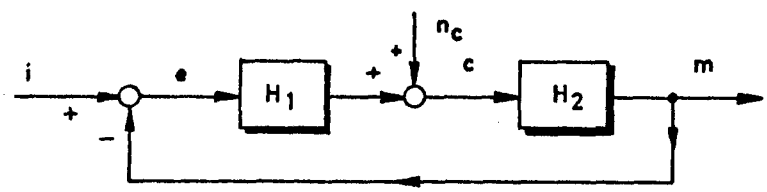

Figure A2. Closed loop system with unknown transfer function H_1.

the confidence limits for the estimate $\hat{H}_1(\nu)$ of the transfer function $H_1(\nu)$, the closed loop system is transformed into

the equivalent open loop system of Fig. A3. For the closed loop transfer function:

$$H_{cl}(\nu) = \frac{H_1(\nu)H_2(\nu)}{1+H_1(\nu)H_2(\nu)} \quad , \tag{A.5}$$

the confidence limits can be determined according to the method given by Jenkins and Watts, as this quantity is comparable to the quantity H in Fig. A1.

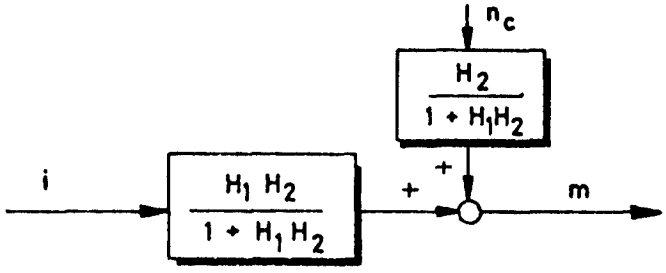

Figure A3. Open loop system which is equivalent to the closed loop system of Fig. A2.

The open loop transfer function $H_{ol}(\nu) = H_1(\nu)H_2(\nu)$ follows from:

$$H_{ol}(\nu) = \frac{H_{cl}(\nu)}{1-H_{cl}(\nu)} \tag{A.6}$$

From the known confidence limits of $H_{cl}(\nu)$ the confidence limits of $H_{ol}(\nu)$ can be calculated by using Eq. (A.6), and because the transfer function $H_2(\nu)$ is known, the confidence limits of the estimated transfer function $H_1(\nu)$ are easily found.

The results obtained in this way are valid for an estimate $\hat{H}_1(\nu)$, calculated according to the method just-mentioned, which is given in Eq. (A.7).

$$\hat{H}'_1(\nu) = \frac{1}{H_2(\nu)} \cdot \frac{H_{cl}(\nu)}{1-H_{cl}(\nu)} = \frac{1}{H_2(\nu)} \cdot \frac{\frac{S_{im}(\nu)}{S_{ii}(\nu)}}{1-\frac{S_{im}(\nu)}{S_{ii}(\nu)}} \quad ;$$

$$\hat{H}'_1(\nu) = \frac{1}{H_2(\nu)} \cdot \frac{S_{im}(\nu)}{S_{ii}(\nu) - S_{im}(\nu)} \; . \tag{A.7}$$

In fact the transfer function $H_1(\nu)$ has been calculated according to the well-known relation:

$$\hat{H}_1(\nu) = \frac{S_{ic}(\nu)}{S_{ie}(\nu)} \quad . \tag{A.8}$$

However, as $S_{im}(\nu) = H_2(\nu)S_{ic}(\nu)$ and $e(t)=i(t)-m(t)$, so that $S_{ie}(\nu) = S_{ii}(\nu) - S_{im}(\nu)$, it may be expected that both these methods will give the same results and also the confidence limits should be the same.

THE EFFECT OF INTERMITTENT ERROR DISPLAYS ON THE OPERATOR CRITICAL COMPENSATORY TRACKING PERFORMANCE

Richard J. Bethke, Ph.D.
George M. Swisher, Ph.D.
Michael J. Cook, B.S.

Wright State University
Dayton, Ohio

ABSTRACT

A critical compensatory task (similar to the zero order Jex task) was used with an intermittent error display to evaluate the effects of various display and blanking time combinations. The performance measures used were integrated and average absolute error, integrated and average absolute operator output, and total tracking time. The surfaces formed by display and blanking times, and performance measures were described via contour mapping. Results indicated marked non-linear relationships between display and blanking times and the performance measures, as well as highly variable interactive effects between the display and blanking times.

INTRODUCTION

This work investigates operator performance in a critical compensatory tracking task as a function of error display. Error information was restricted by intermittent presentation of the

display. Time of presentation and time between presentations were independently varied, and the effect on tracking error, operator output and tracking time were studied.

This present research does not attempt to break the performance results into the amount due to the actual information presented,perceived or needed and psychomotor ability, but instead lumps the system using display and blanking times as inputs and the discussed performance measures as outputs.

METHOD

Subjects

Three male subjects were employed. All subjects reported 20/20 (un) corrected vision and freedom from psychomotor deficiencies. Subject age ranged from 24 to 29 years of age. All subjects were trained for 8 hours on the blanked tracking task. Subject C had previously been used on unblanked experiments. Subject B was a light aircraft pilot, and Subject G had no previous related experience. They were tested in a 4' x 4' x 8' insulated test chamber.

Tracking Task

The compensatory tracking task used was a plant with unstable first order time varying dynamics. The task was similar to the Jex Task (1-3) except that the autopaced rate switching was not employed. The Laplace transform of the task was:

$$G_p(s) = \frac{\lambda}{s-\lambda} \qquad (1)$$

where

$G_p(s)$ $\triangleq$ transfer function of the task

λ $\triangleq$ divergence frequency in radians per second

s $\triangleq$ Laplace operator in seconds^{-1}

t $\triangleq$ time in seconds

The λ was increased with the relationship:

$$\lambda = 1.5 + 0.05t \qquad (2)$$

When the operator's limit is reached (control is lost), the frequency λ_c is recorded. The criterion for loss of control is that the error exceeds the scale of the display. The 0.05 rate corresponds to the slow rate of the Jex task. This was done because preliminary results indicated that

operators could not effectively follow the high rate Jex Task with an intermittent display.

Figure #1 shows the analog mechanization of the tracking task, the display blanking equipment, and the performance measuring circuits using two Electronic Associates Inc. TR-20 $\pm$ 10 volt analog computers in a slaved configuration. The scope used for the compensatory display was a Hewlitt Packard 122A set at 0.366 cm/volt sensitivity. The control stick was a USAF Type Number C-1 Formation Stick with $\pm$ 10.0 volt output. The force calibration of the stick and a 0.58 series potentiometer resulted in a sensitivity of 2.42 volts/Newton. The intermittent display was generated with a pulse generator controlling the high frequency input to the scope sweep trigger thru use of one of the relay comparators on the analog computer. Independent control of the on and off times was then possible by adjusting the pulse generator.

The tracking performance measures recorded for each tracking run were T, (time measured from the onset of a tracking trial until the subject lost control and the system went into the hold position), e, (the average absolute error):

$$e \triangleq \frac{1}{T} \int_0^T |\text{error}|\,dt \qquad (3)$$

and, U (the average absolute operator output).

$$U \triangleq \frac{1}{T} \int_0^T |\text{operator output}|\,dt \qquad (4)$$

Because integrated absolute error and operator output increase at a variable rate with time, the conventional practice of averaging these quantities with respect to time is of debatable value. For this reason both integrated absolute error and operator output (stick motion), and the time averages of these quantities are discussed herein.

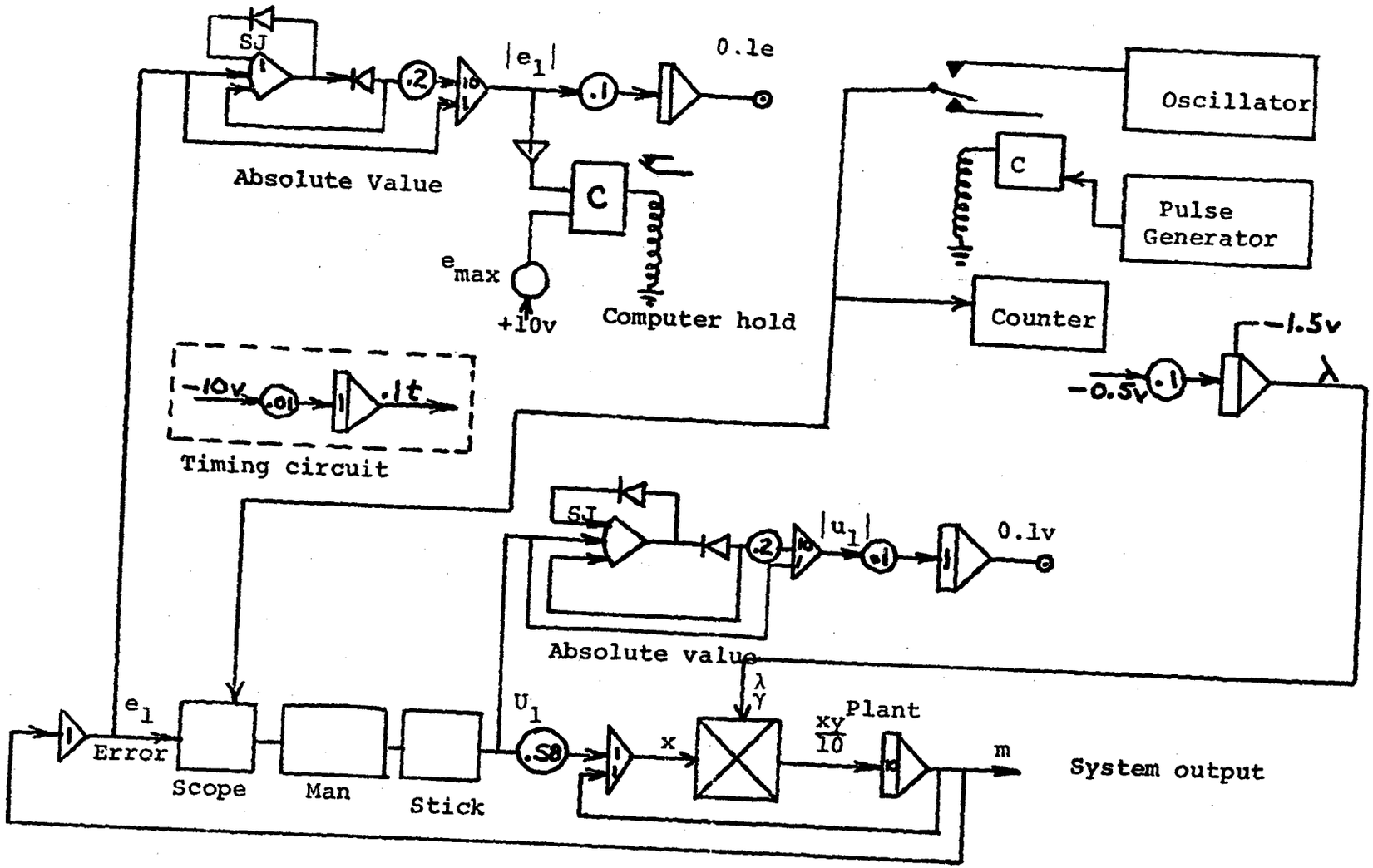

Figure 1. Analog Mechanization of the Tracking Task

Experimental Technique

Twenty-five test conditions forming a five by five matrix of the two independent variables were used. The display times were equispaced between 0.015 and 0.295 seconds; blanking times were equispaced between 0.05 and 0.61 seconds. The run order of test conditions was chosen at random for each subject. A subject ran five trials for each test condition at one sitting. Depending on the length of the tasks, as few as one and as many as three test conditions were included in the same sitting. Between sittings, rest periods of 20 to 30 minutes were provided. Light levels in the rest area were kept at those of the test chamber (1.5 foot candles) to eliminate visual adaptation problems. Subjects were never allowed to run if they had any perception of fatigue, and they were allowed warm-up trials at several test conditions at the start of a day's testing and after long breaks.

Analysis Technique

For each subject the above test configuration yielded 5 outcomes for each of the three dependent test variables at each of the 25 test conditions. For each of the dependent variables, the five outcomes were averaged and plotted versus the two independent variables. Contours were then drawn over this grid for various dependent variable levels using the IBM subroutine CONTR (4). These plots were made for each dependent variable for each subject, as well as for the average of a dependent variable between the subjects.

Results

Figure 2 is the subject average contour plot of integrated absolute error vs. display on and off times. Contours of equal error are shown. The highest integrated error values lie in the upper left corner of the plot in the easiest tracking region of high on times and low off times. The highest error values here are approximately equivalent to those run with no blanking. The lowest integrated errors

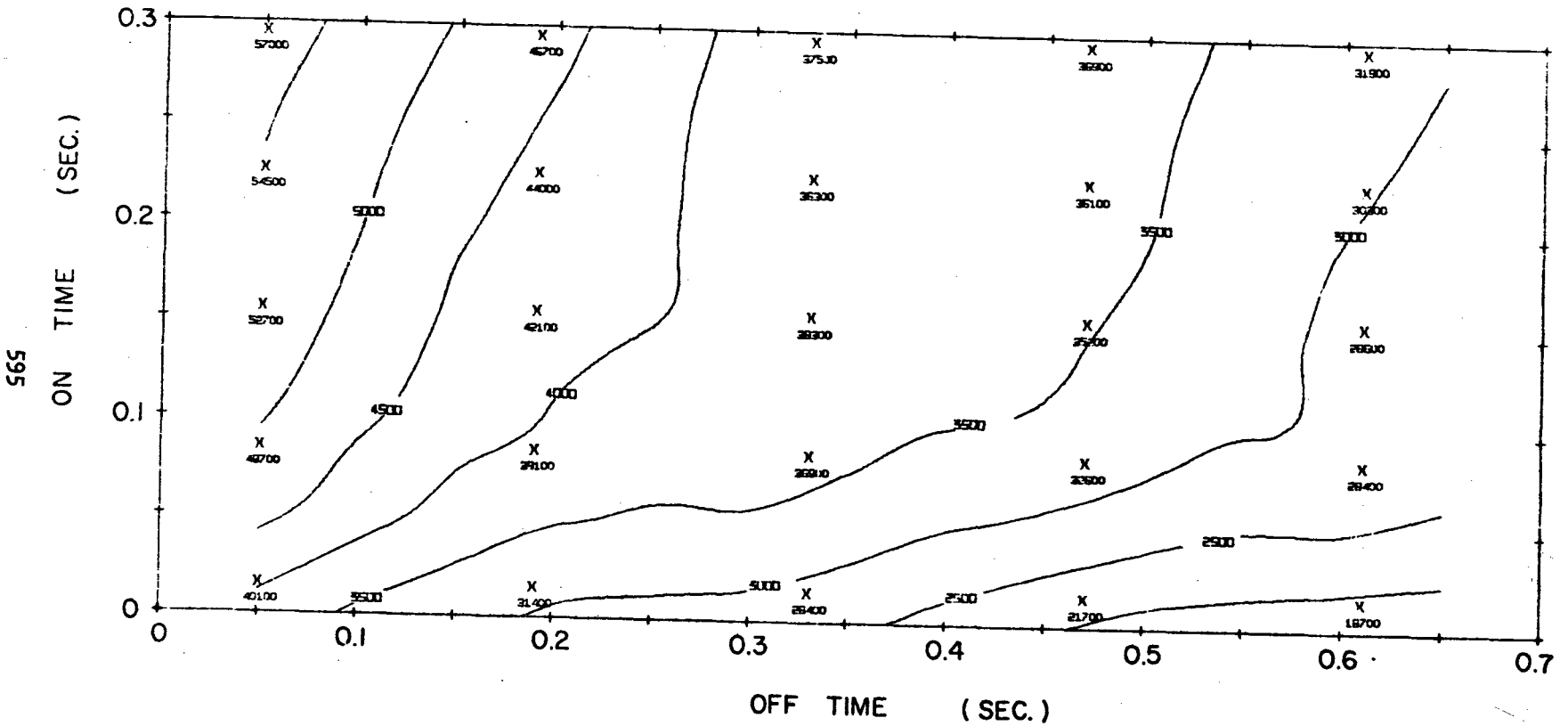

FIGURE 2 INTEGRATED ABSOLUTE ERROR SUBJECT AVERAGE

appear in the lower right corner in the most difficult tracking region of short on times and long off times. These lowest values were approximately 3 times smaller than the highest values.

Examination of the contours shows that for short on times the error is far more sensitive to on time than to off time, that is the equal error contours are relatively horizontal. For short off times the error is far more sensitive to off time than to on time, that is the contours are fairly vertical. In both the short on time and short off time regions, the contours are closely spaced, showing steep surface slope and high sensitivity to the variables as discussed above. The plot also shows that the error is more sensitive to off time than to on time. That is, for equal on and off times, the contours are more vertical than horizontal. This is also seen in the upper right section of the plot.

For short on times and long off times, the test subjects remarked that while they could get position information from the very short error display, their ability to extract velocity and higher order derivatives was markedly reduced. These effects are indicated in the relatively horizontal contour lines in this region, where small increases in on time gave relatively large increases in integrated error, indicating longer tracking times, perhaps made possible by acquisition of higher derivative error information by the subjects.

For short on times and short off times, while any one display did not give higher derivative error signal information, subjects felt the relatively short time between displays allowed this information to be gained from consecutive displays. This, along with more position information, may explain the higher contour slope in this region.

For high on times, the subjects received all the information from the error display when it was presented. Increases or decreases in the on time did not substantially affect the information transmitted. Off time, however, did show a marked relative influence on the integrated error, the most sensitive region being for short off times.

Figure 2a shows the subject average of the normalized integrated absolute error, that is, the values in Figure 2 divided by the respective average run times. The contour shapes in these two figures are similar except for the large fairly constant region in the upper left corner of Figure 2a. In this region of long on times and short off times, tracking is easy and tracking times are long. During these long runs the integrated absolute error increases at a reasonably constant rate for long periods until near the end of the run when it increases more rapidly. The time average is then insensitive to changes in run time produced by on and off time changes.

Figure 2b shows the normalized and nonnormalized integrated absolute errors plotted versus run time. For low run times, corresponding to the difficult tracking conditions in the lower right corner of Figures 2 and 2a, the normalized error is large while the nonnormalized error is small. As run time increases, corresponding to going from lower right to upper left corners of Figures 2 and 2a, the normalized error falls at a decreasing rate while the nonnormalized error climbs irregularly to a fairly constant rate of increase.

Figures 3 and 3a show the integrated absolute stick motion in nonnormalized and normalized form respectively. These figures show great similarity to their error counterparts in Figures 2 and 2a, indicating error and stick motion to be

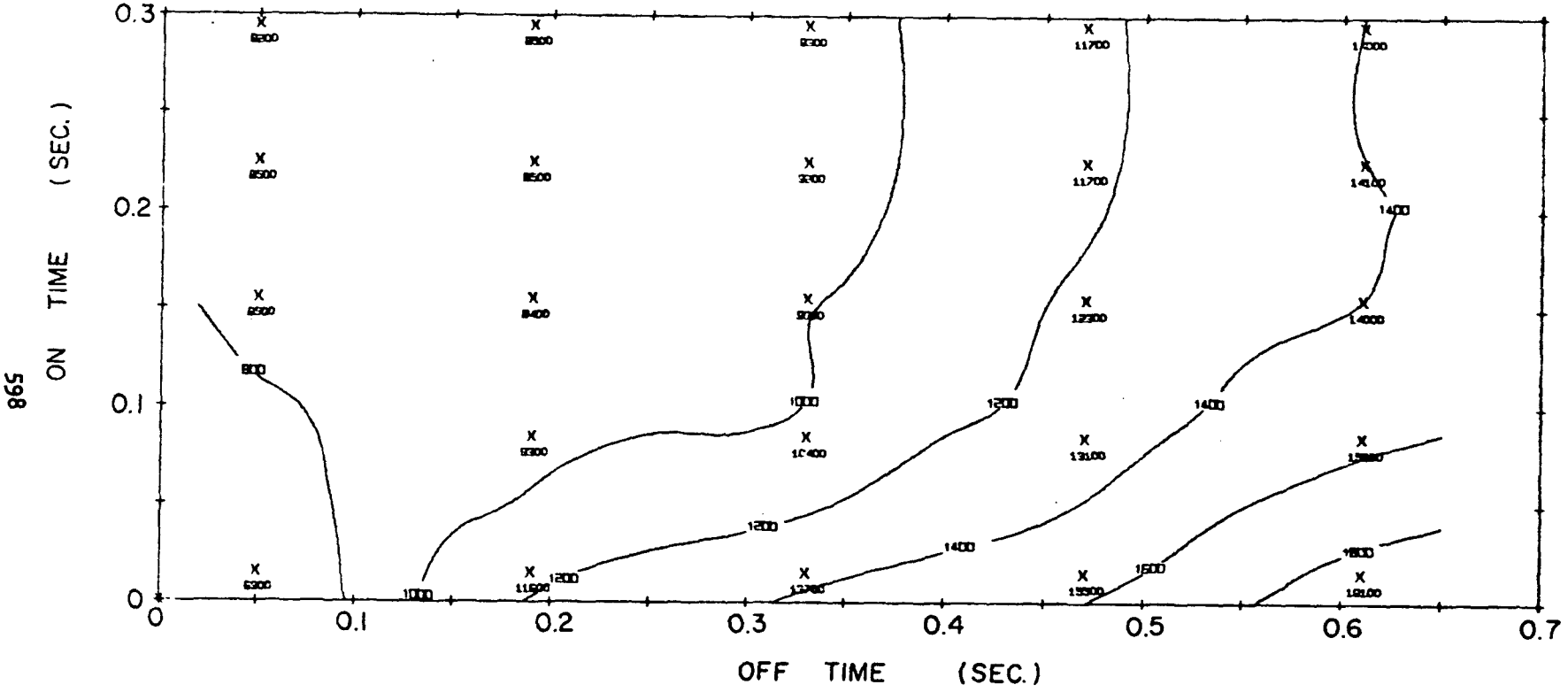

FIGURE 2a NORMALIZED INTEGRATED ABSOLUTE ERROR SUBJECT AVERAGE

FIGURE 2b ABSOLUTE ERROR COMPARISON

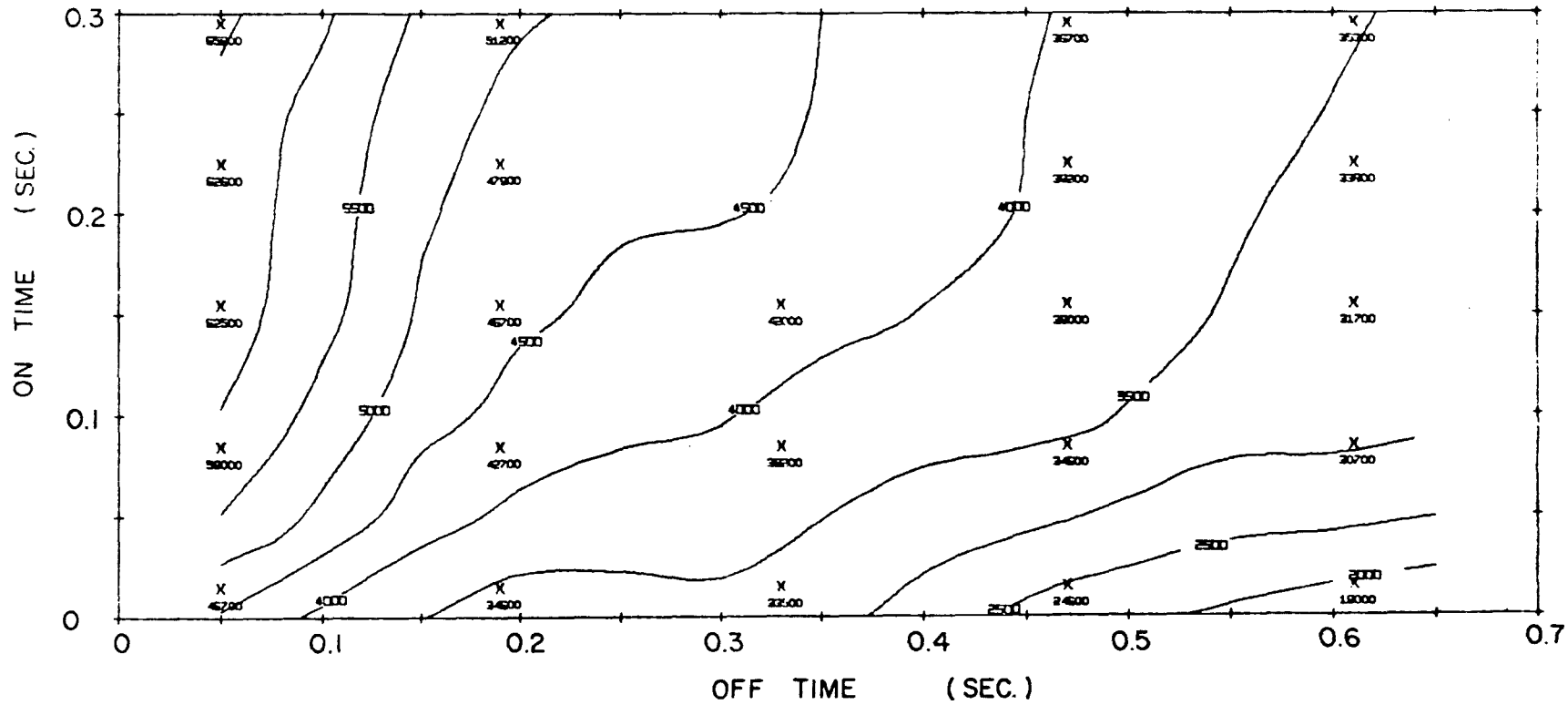

FIGURE 3 INTEGRATED ABSOLUTE STICK MOTION SUBJECT AVERAGE

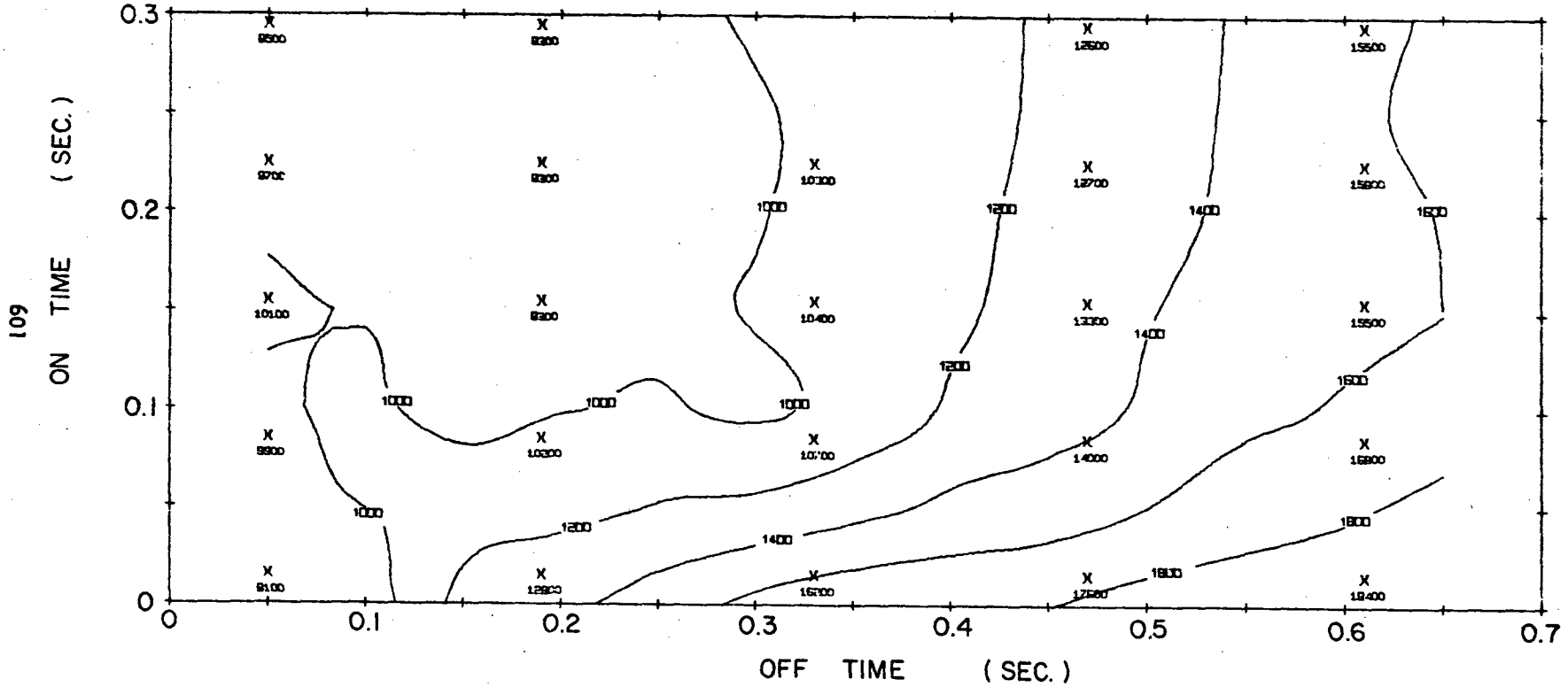

FIGURE 3a NORMALIZED INTEGRATED ABSOLUTE STICK MOTION SUBJECT AVERAGE

similar functions of display and blanking time. Normalized and nonnormalized integrated absolute stick motion viewed as functions of run time are very similar to Figure 2b and are omitted here for brevity.

Figure 4 shows the average tracking time of the subjects. In general this figure shows the same trends discussed for Figures 2 and 3. It does, however, exhibit unique behavior in the short off/short on time region. In this region, the contours are much more vertical than in the other figures discussed. These fairly vertical, closely spaced contours indicate tracking time is not very sensitive to on time, but is highly sensitive to off time.

The cause of the vertical turn in the tracking time contours is not known. When viewed in light of the equipment used, such as the p-31 oscilloscope phosphor (7 msec time constant), no probable cause could be found for this behavior. In addition, since the time contours turn toward the vertical, but the error and stick motion contours do not, it would seem that the cause is due to the subject and not the equipment.

Figure 5 is an overlay of Figures 2, 3 and 4. The similar shapes of the error, stick motion and time curves can be seen. As noted in the short on time, short off time region, the tracking time contours are seen to be more vertical than those of error and stick motion. For a given tracking time in this region, the error and stick motion were variable and dependent mainly on the on time. That is, the contours of constant tracking time were fairly vertical and cut across the error and stick motion contours. Lower error and stick motion for a given tracking time indicates a better tracking performance. In the short on/short off time region, it appears this tracking performance improves with shorter on times.

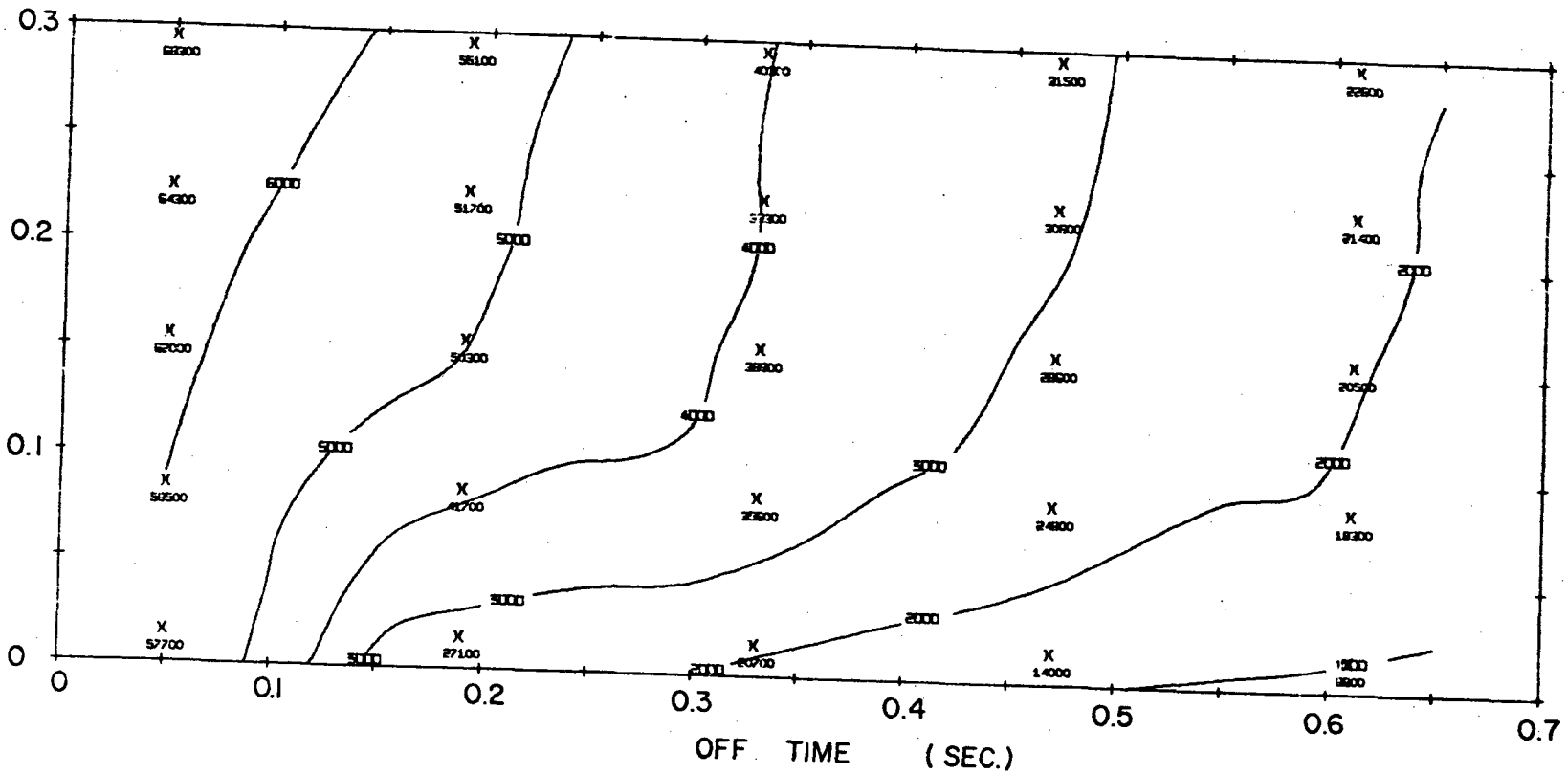

FIGURE 4 TRACKING TIME SUBJECT AVERAGE

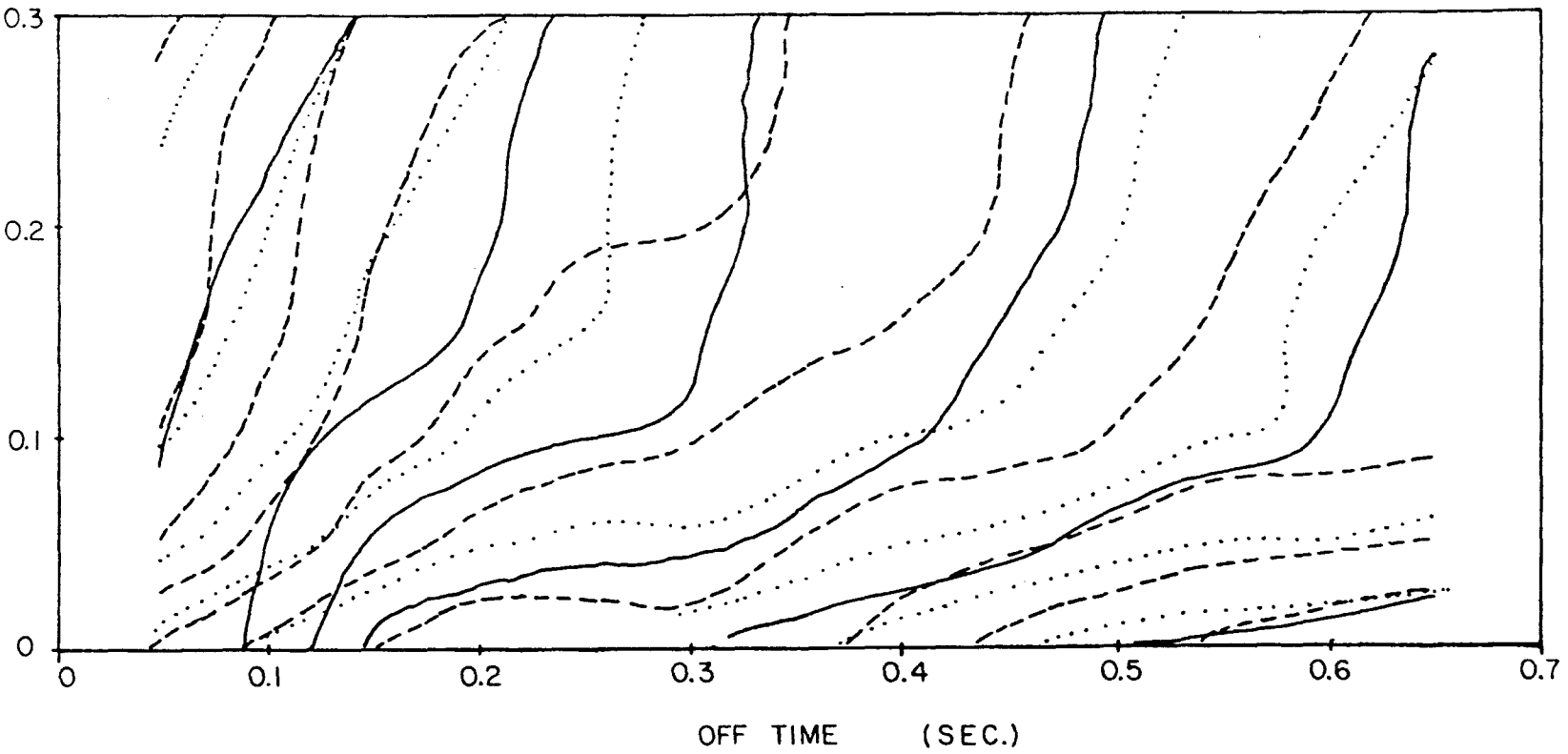

FIGURE 5 ERROR, STICK MOTION, TIME OVERLAY SUBJECT AVERAGE

The individual plots of all subjects are found in the appendix. All subjects had similar plots and exhibited the traits discussed above.

REFERENCES

1) Jex H.R., McDonnell, J.D., and Phatek, A.V. "A Critical Tracking Task for Manual Control Research" IEEE Trans. HFE-7 (4) December 1966, 138-154.

2) Jex H.R. and Allen, R.W., "Research on a New Human Dynamic Response Test Battery." 6th Annual Conference on Manual Control, April 1970.

3) Jex H.R., Two Applications of a Critical Instability Task to Secondary Work Load Research, Hawthorne California: Systems Technology Inc. TR#155-1 February 1967.

4) IBM 1130 Numerical Surface Techniques and Contour Map Plotting (1130-CX-11X) Programmer's Manual.

APPENDIX

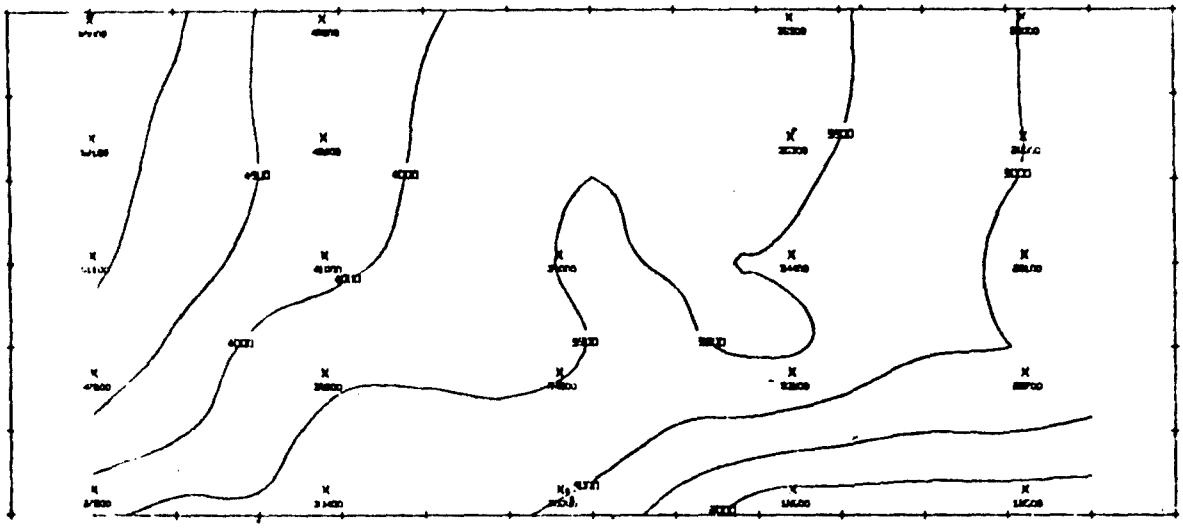

SUBJECT B INTEGRATED ABSOLUTE ERROR

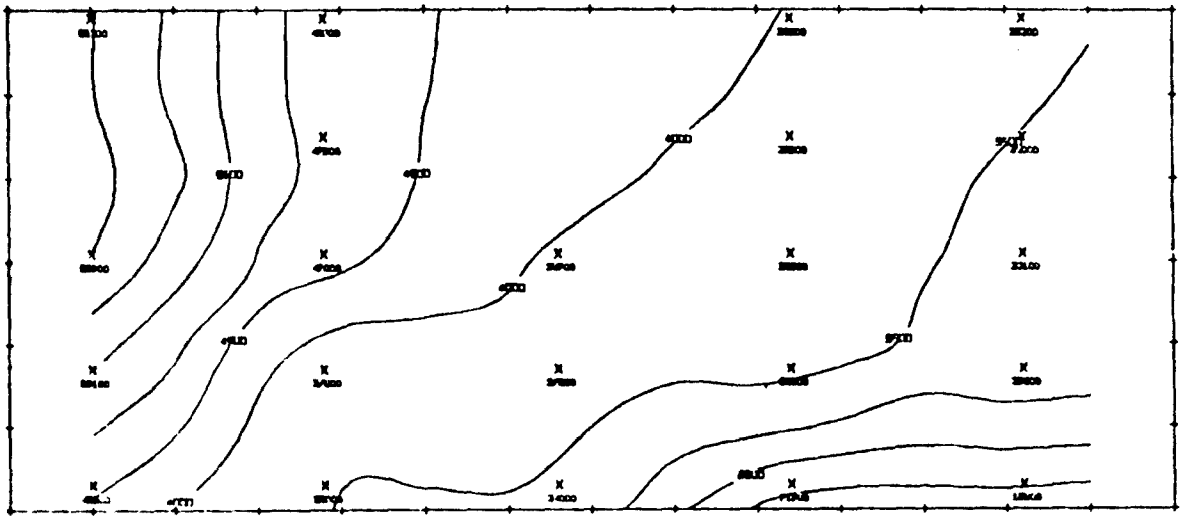

SUBJECT B INTEGRATED ABSOLUTE STICK MOTION

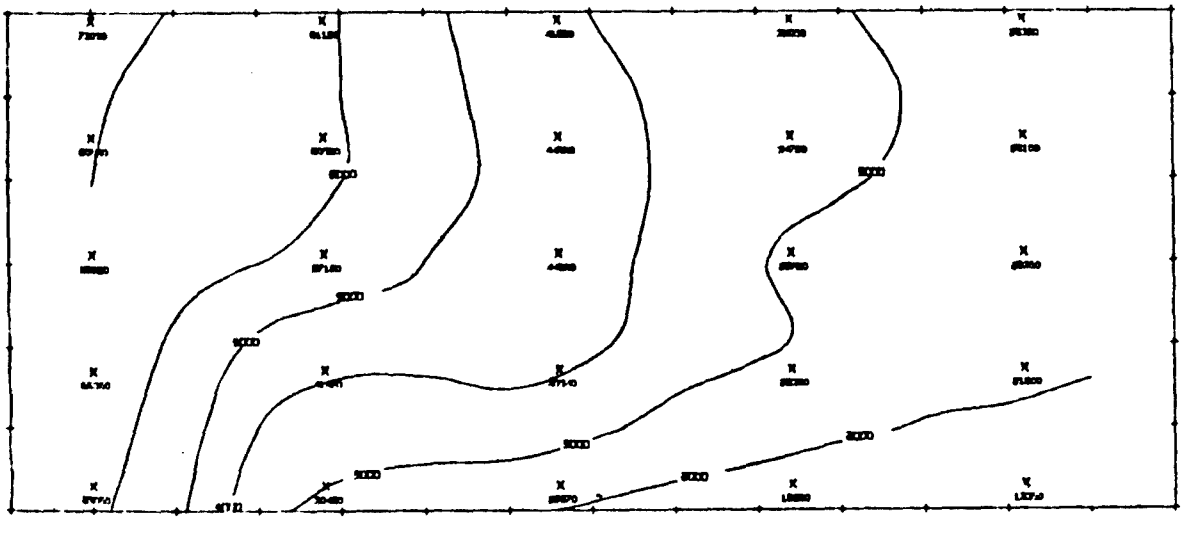

SUBJECT B TIME

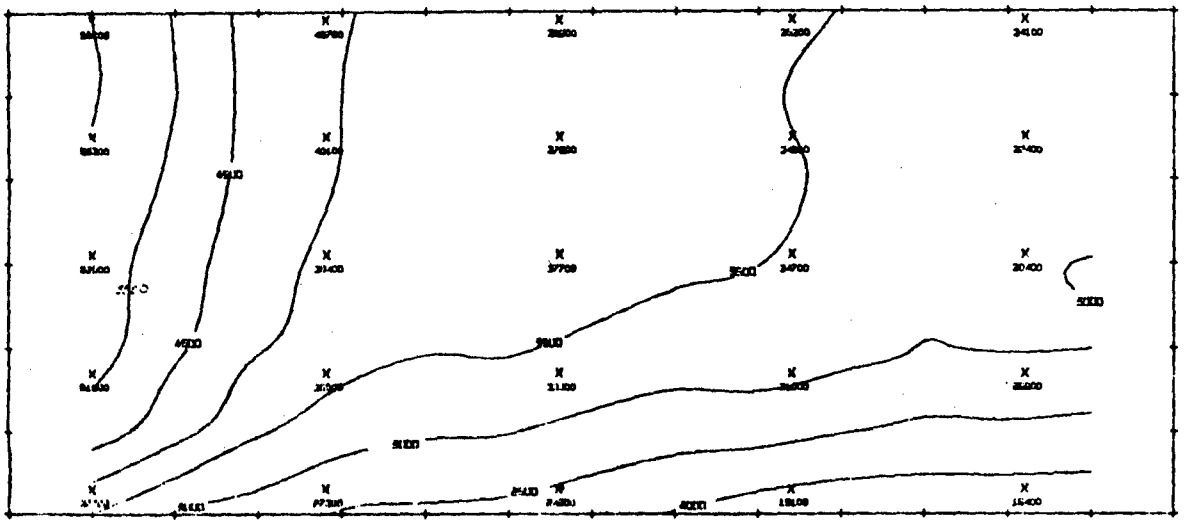

SUBJECT C INTEGRATED ABSOLUTE ERROR

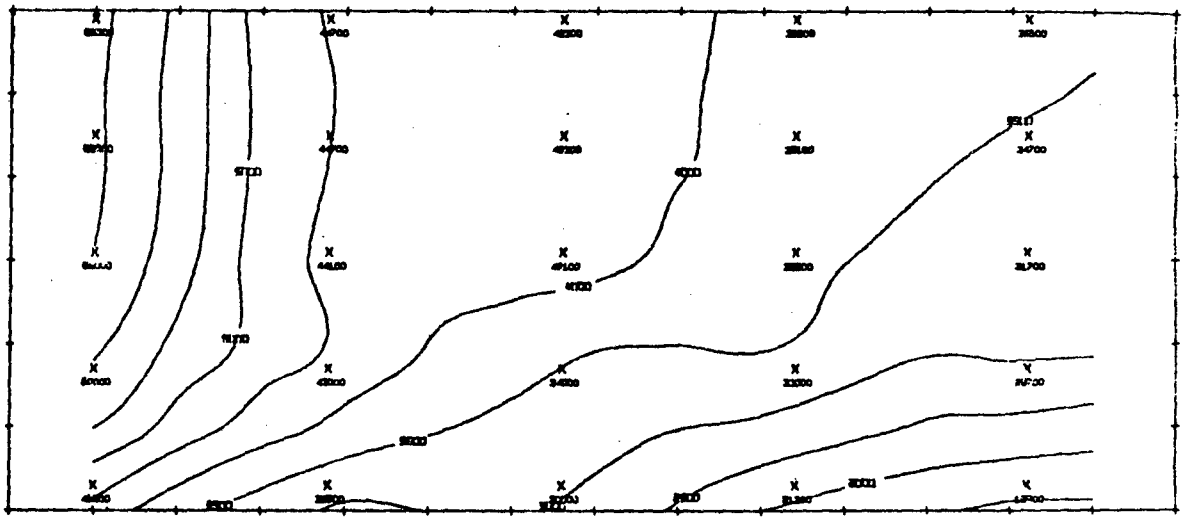

SUBJECT C INTEGRATED ABSOLUTE STICK MOTION

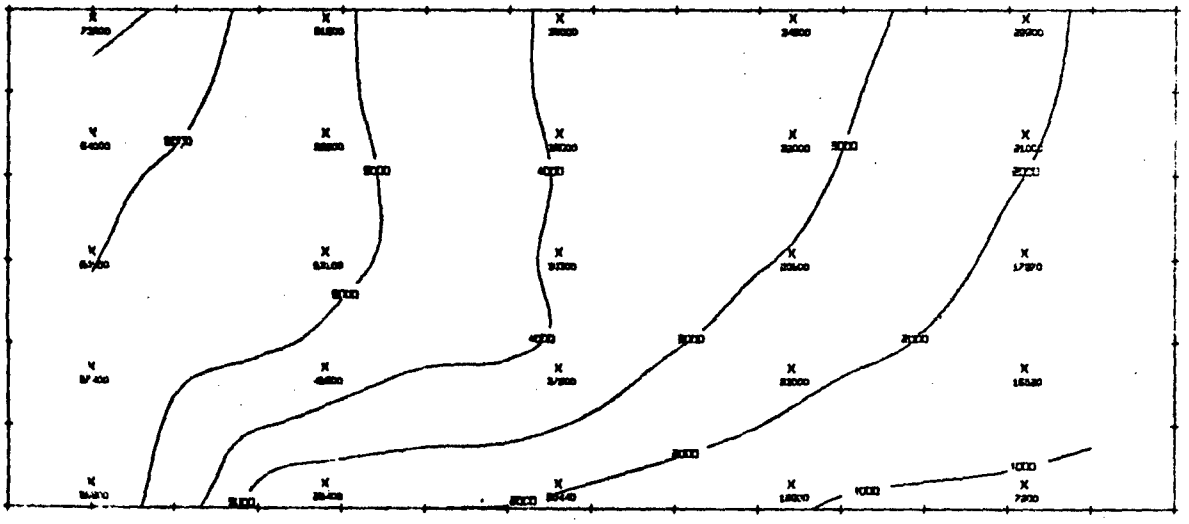

SUBJECT C TIME

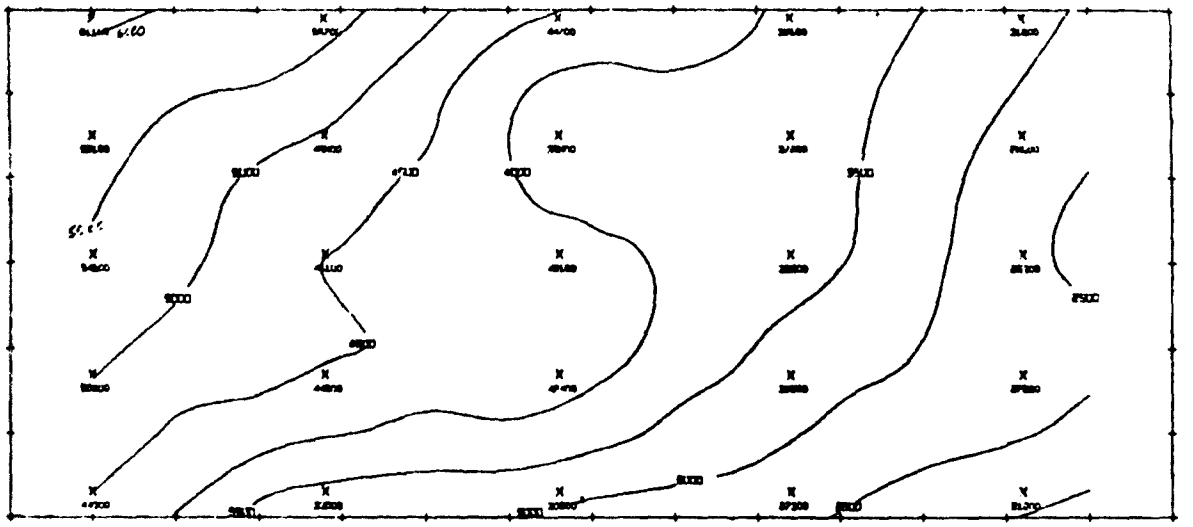

SUBJECT G INTEGRATED ABSOLUTE ERROR

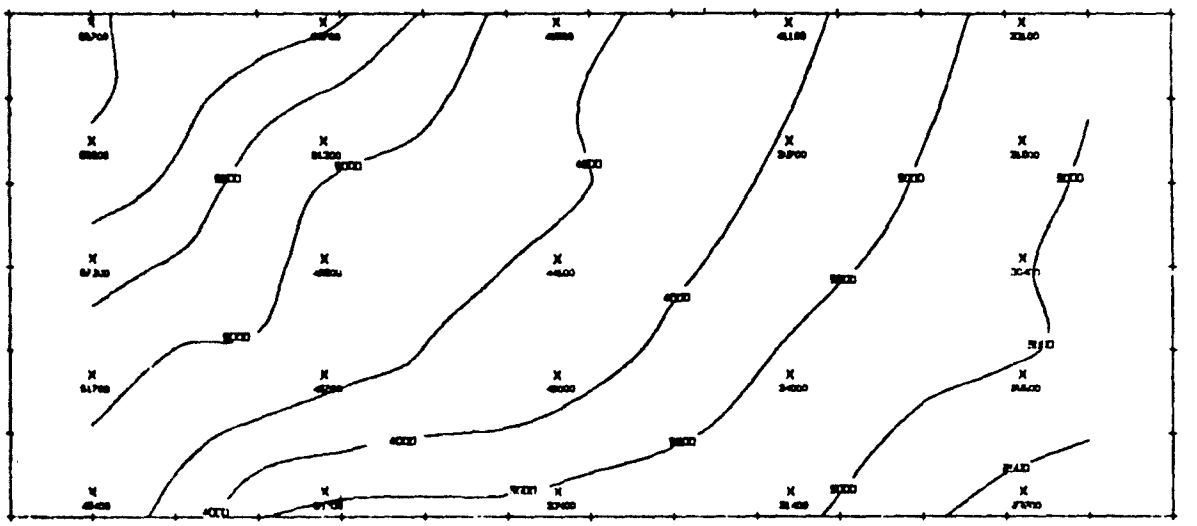

SUBJECT G INTEGRATED ABSOLUTE STICK MOTION

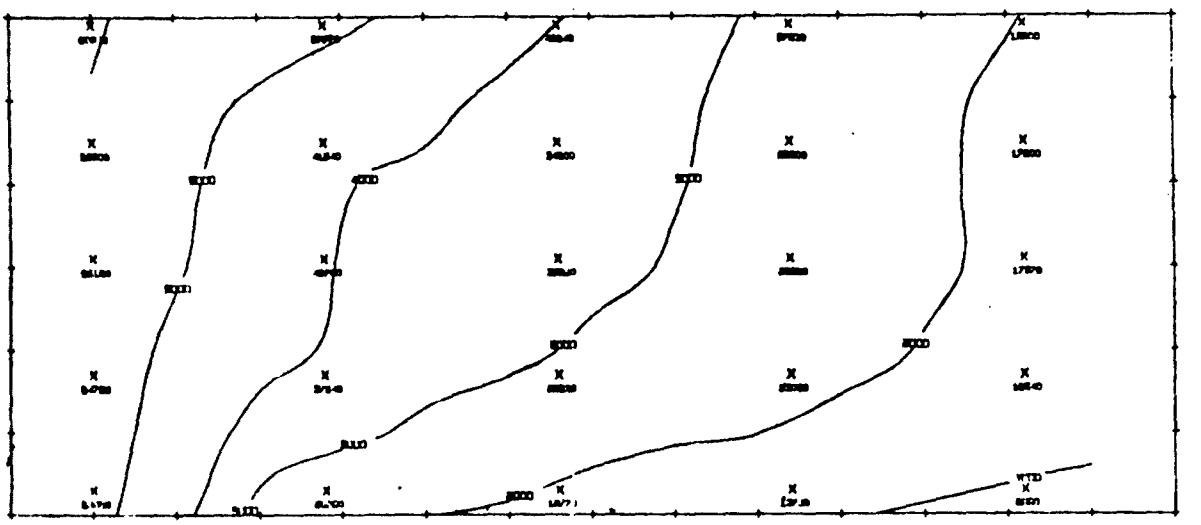

SUBJECT G TIME

SESSION XIII

Non-Visual Modes of Information Display

TRACKING WITH KINAESTHETIC AND AUDITORY FEEDBACK

Leslie Buck
Control Systems Laboratory
National Research Council of Canada

INTRODUCTION

All representations of a human operator as an information processing system show feedback loops. When it comes to specifying the form and content of the feedback a number of possibilities arise: the subject may see, hear or feel changes in the controlled element, the controlling element, or his limb position, and perhaps there are other possibilities as well.

The importance of feedback is recognised not only by being included in the system representation, but also in that recommendations are made concerning, for example, the design of displays and the feel of the controlling element. Generally speaking however, these are only acknowledgements of a problem rather than its solution. Precise definition of the form and content of feedback still remains to be done.

EXPERIMENTAL TASK

One means of studying feedback is the transfer of training method. The subject is trained on a certain regime which is then changed in such a way that the hypothesized feedback is either held constant or varied, and appropriate performance changes are predicted.

In the experiment described here we trained subjects on a tone tracking task. The subject held a control wheel (Figure 1) and on a given auditory signal (onset of a tone) he rotated it either left or right in order to bring the tone to either a minimum or maximum pitch (Figure 2). The task is comparable to that of tuning a radio precisely to the station.

We used an auditory task because it offered better chances of controlling the feedback available to the subject. With a visual task it is very difficult for the experimenter to restrict the subject's head and eye movements, and thus he is less able to determine precisely what feedback the subject receives, let alone specify and control it. This problem appears to be less acute with auditory feedback.

Preceding page blank

In this particular auditory task the subject had no standard tone available and no target presented, except insofar as they were present in memory, and no error information was displayed. In all these respects the task differed from the usual visual target acquisition task. It did mean however, that the auditory feedback had the same constraints as one finds with kinaesthetic feedback, that is to say, present feedback could be compared only with the memory of previous feedback.

To find a target in the first place, the subject had to search for changes in the direction of the change in tone. Subsequently he could find the target again either by reproducing the learnt tone or by reproducing the learnt movement. The question was which, if either, was the favoured method. We attempted to answer the question by compelling the subject to change his method in one or other of the two respects, leaving the other possibility still available.

EXPERIMENTAL PROCEDURE

The subject did not know in advance which way to rotate the controller. If he went the wrong way the tone remained constant in pitch. If it varied on rotating left it went down in pitch and he knew he was searching for a minimum; if it varied on rotating right it went up and he was searching for a maximum. In each set of twelve presentations the target appeared equally frequently left and right in random order.

When the subject had held the target for 2 s the tone stopped and he returned the wheel to centre position, which was indicated by a lamp coming on. After 2 s the lamp went out and the tone came on again. Apart from this, the task was performed in complete darkness.

The target, which was constant for any given experimental condition (constant, that is, except for the left/low : right/high variation), could be defined in terms of either angular position of the controlling element or pitch of the displayed tone, and these two were related in the display-control gain (Hz per degree).

EXPERIMENTAL DESIGN

In our first experiment we used four experimental conditions which involved two control positions, two displayed tones, and two display-control gains (Figure 3). We assigned subjects at random, 18 to a group, to the four conditions and measured their movement times. These were the intervals between initiations of movement and initiations of the 2 s residence at target required for alignment. The set of 12 presentations was repeated 12 times with pauses for rest during which the subject was told his total time for the trial. (This did not include time taken to return from the target to centre position.)

Movement times were averaged for each trial and these means were averaged over 18 subjects. Performance was clearly dependent on display-control gain (Figures 4 and 5).

Twelve subjects from each group returned for a second experiment some time after the first. On this occasion they were given three trials under the conditions of the first experiment, and then nine further trials under a new condition which was the same for all subjects.

The effect of the new condition was to change either the angular position of the controlling element required for target acquisition keeping displayed pitch constant, or to change the displayed pitch keeping angular position constant (Figure 3).

RESULTS

We predicted that subjects experiencing an increase in display-control gain (conditions 1 and 3) would improve their performance, while those experiencing a decrease in gain (conditions 2 and 4) would worsen. This prediction was confirmed (Figures 6 and 7).

We also predicted that subjects searching for the same controller position (conditions 3 and 4) would perform better than those searching for the same displayed pitch. This prediction is based on the hypothesis that kinaesthetic feedback plays the major role in movement control.

The results show that our predictions were only partly confirmed. Condition 4 subjects performed better than condition 2 subjects but condition 3 subjects did not perform better than condition 1 subjects. The reason for this is not clear at present.

The observed effect of display-control gain is the opposite to that found by, for example, Rotbauer, Kruger and Kruse (1972) and Gibbs (1962), who with zero time lag systems found lower movement times with lower gains. However, they used visual tasks with target and error information displayed. The present finding agrees better with the hypothesis that subjects were searching for changes in the direction of change of tone. Such changes were greater with higher gains.

The lower gain made it a much more difficult task, especially in the case of condition 3 where the target was marked by a small change in direction of change and where it was located close to the initial starting position. We found in fact considerable difficulty in the case of these latter subjects, in persuading them to return for the second part of the experiment, and some of the original eighteen categorically refused to do so. This may have some bearing on our failure to confirm our hypothesis in this case.

REFERENCES

C.B. GIBBS Controller design: interactions of controlling limbs, time-lags and gains in positional and velocity systems. Ergonomics, 1962, 5, 385-402

ROTBAUER, G., KRUGER, W., and KRUSE, W.
A fingerstick with binary selectable control gain. Proceedings of Eighth Annual Conference on Manual Control, 1972

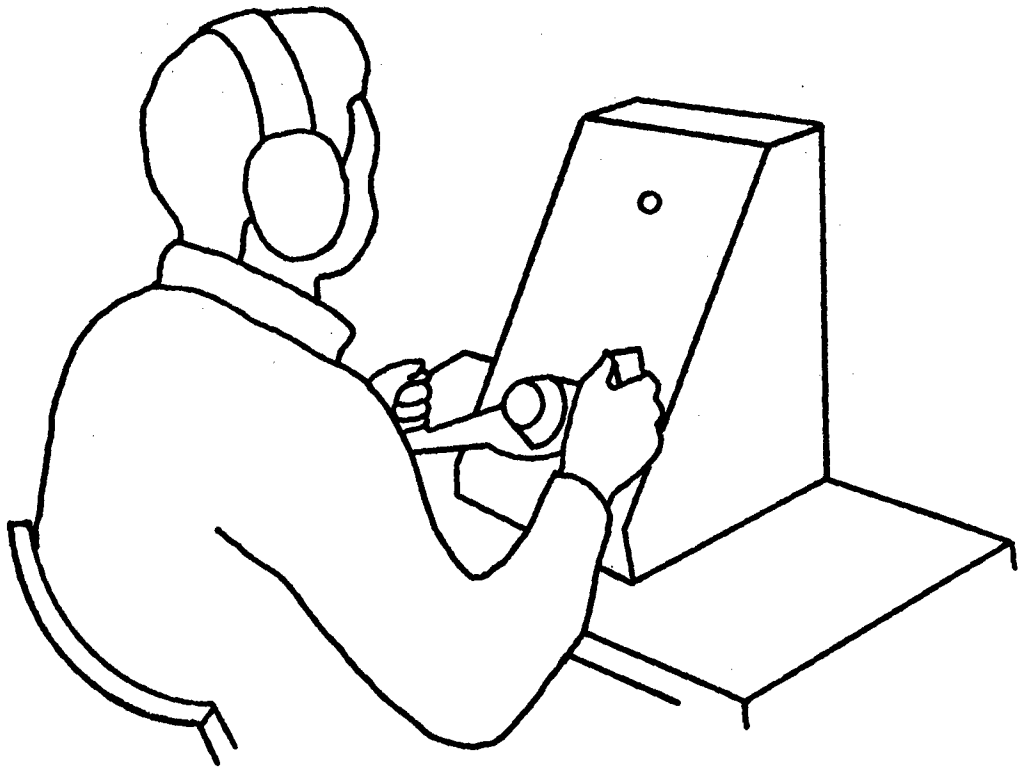

Figure 1. Subject seated at the apparatus

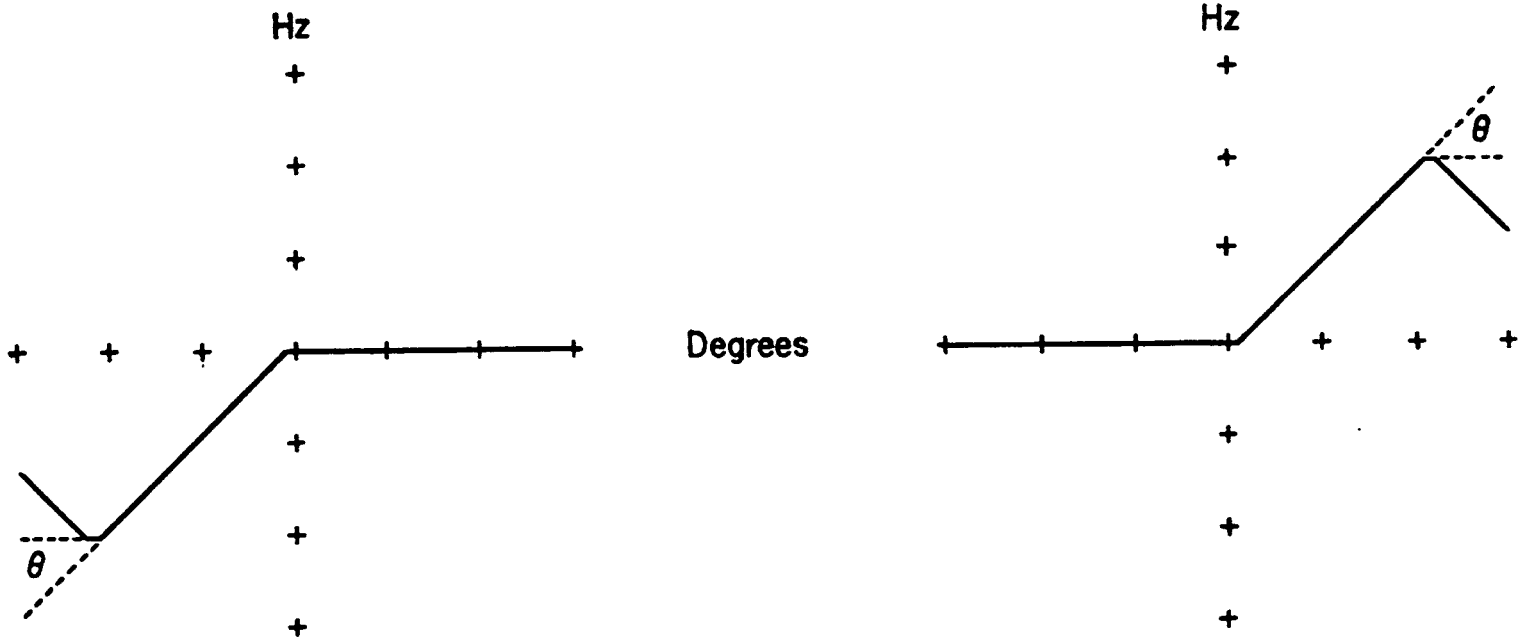

Figure 2 Relation between angle of rotation of controller and pitch of displayed tone for targets lying to left and right of centre position

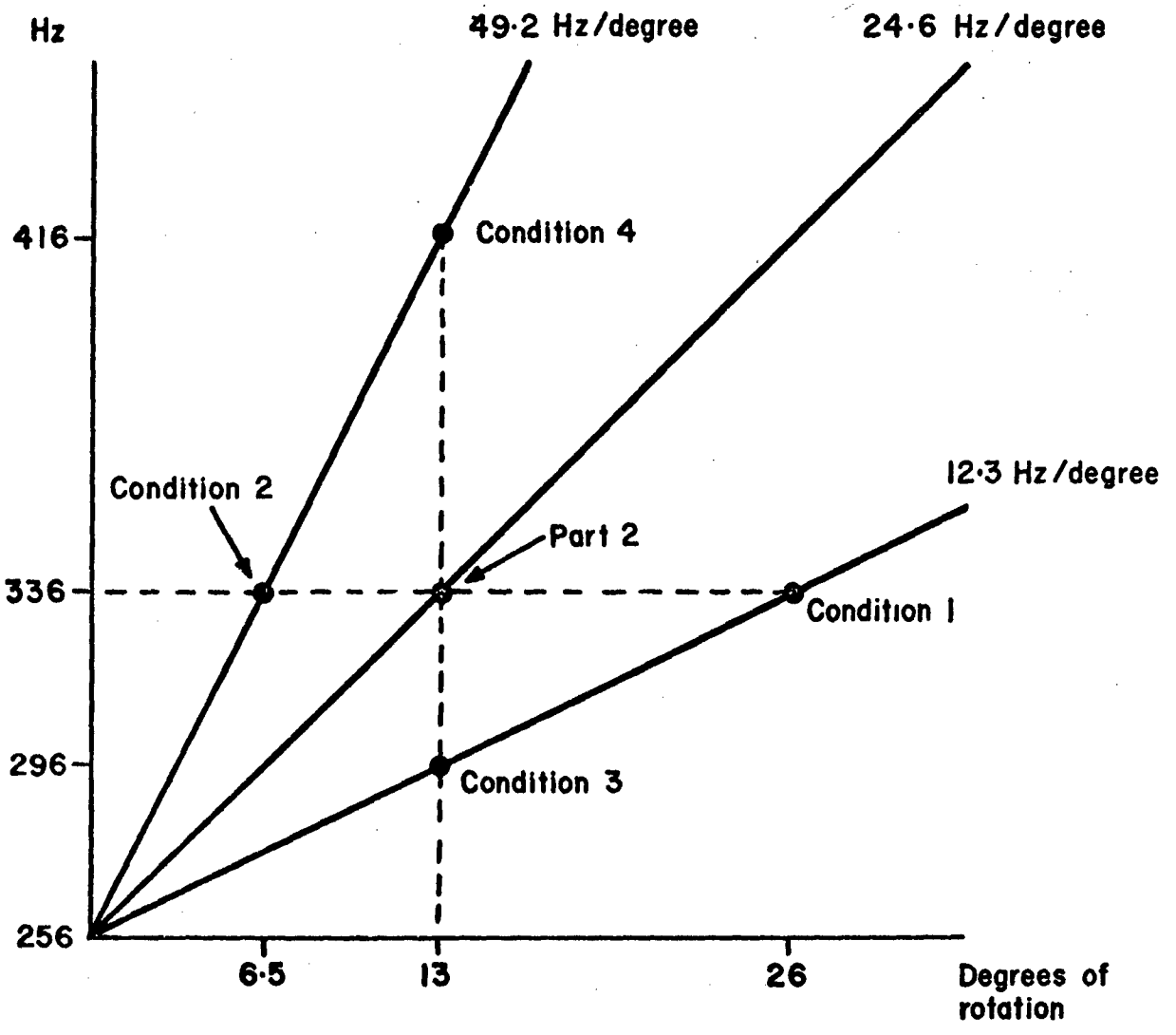

Figure 3. Experimental conditions for part 1 (conditions 1, 2, 3, and 4) and part 2 (all conditions).

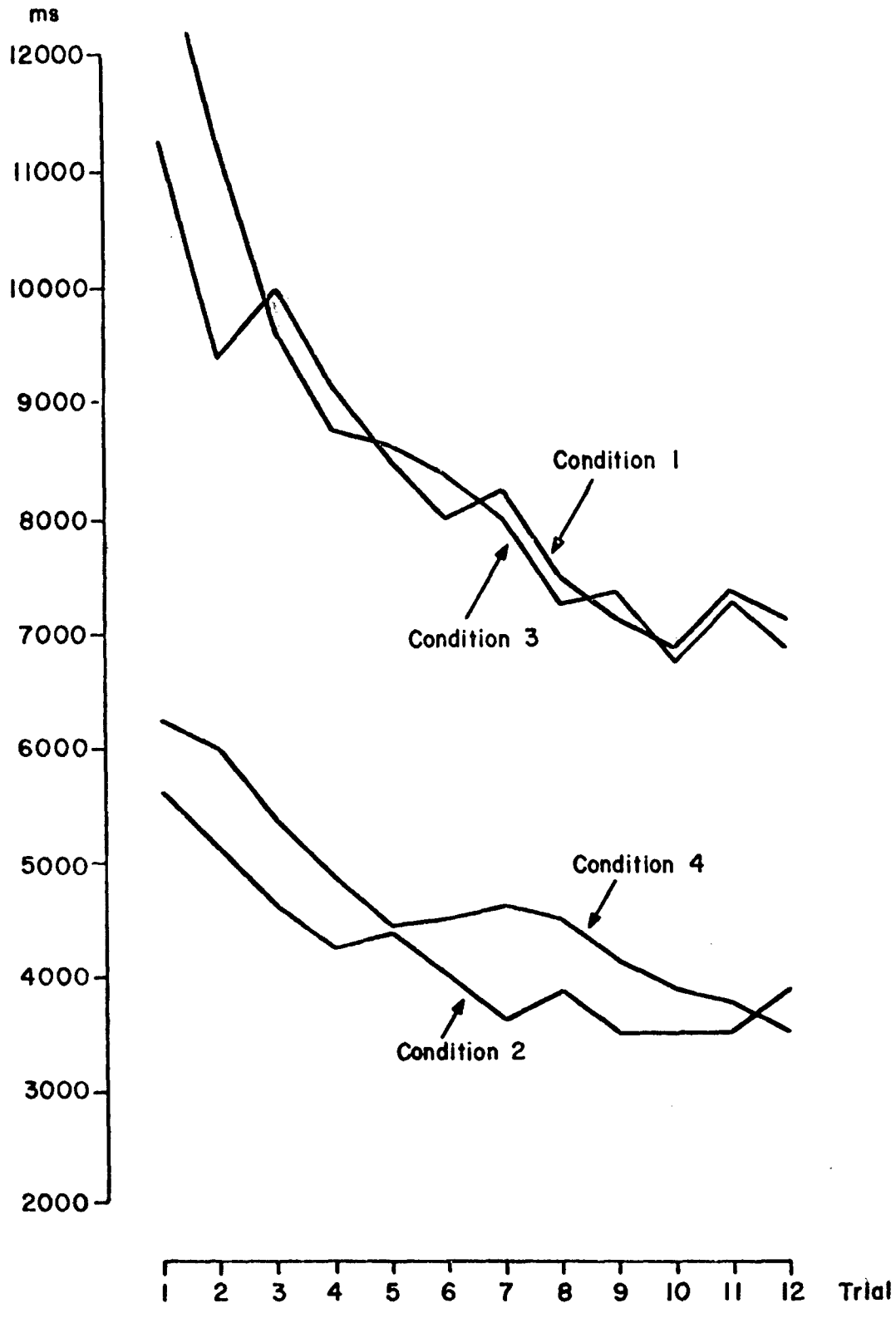

Figure 4 Movement times Part I n = 18

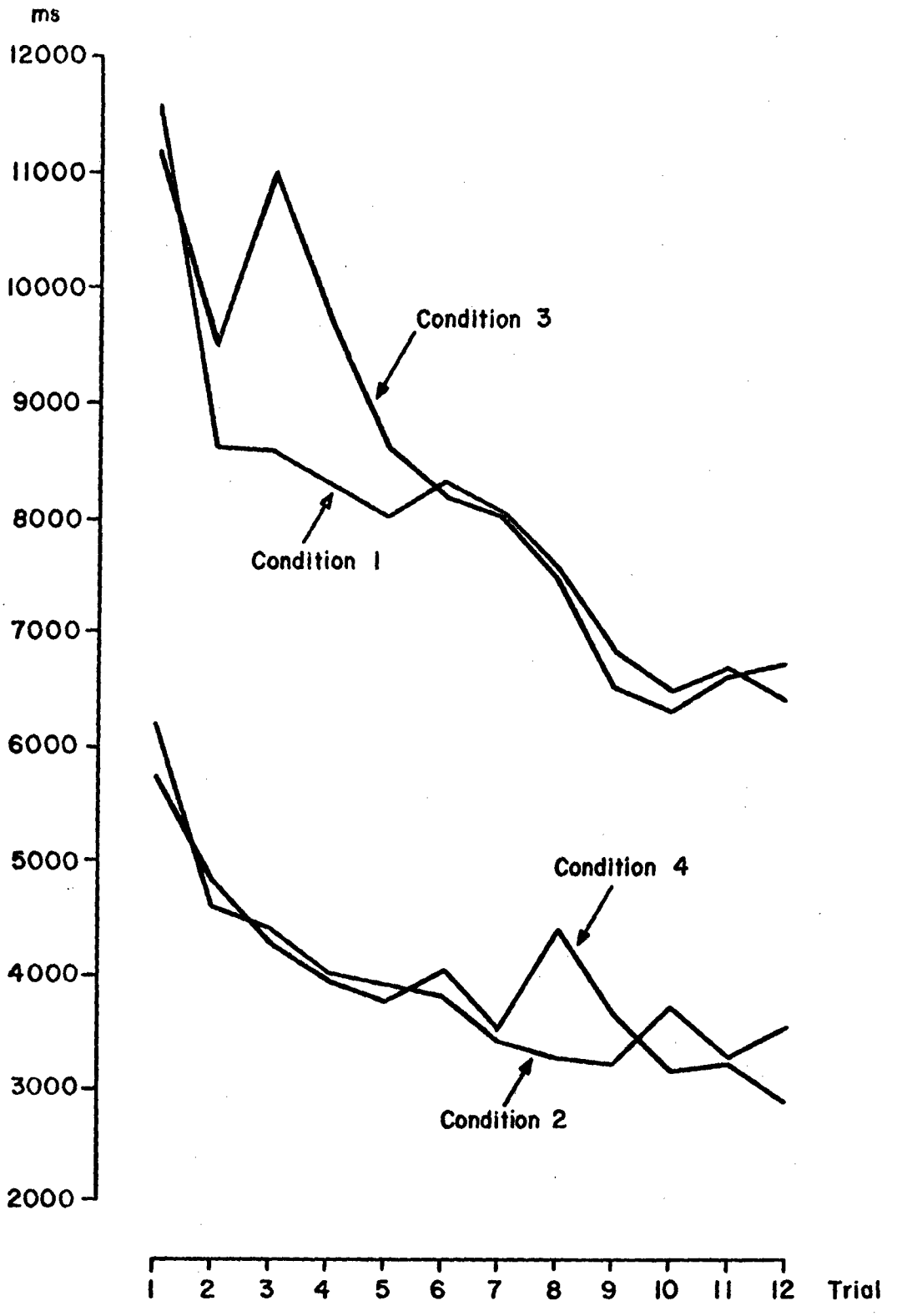

Figure 5 Movement times Part I n = 12

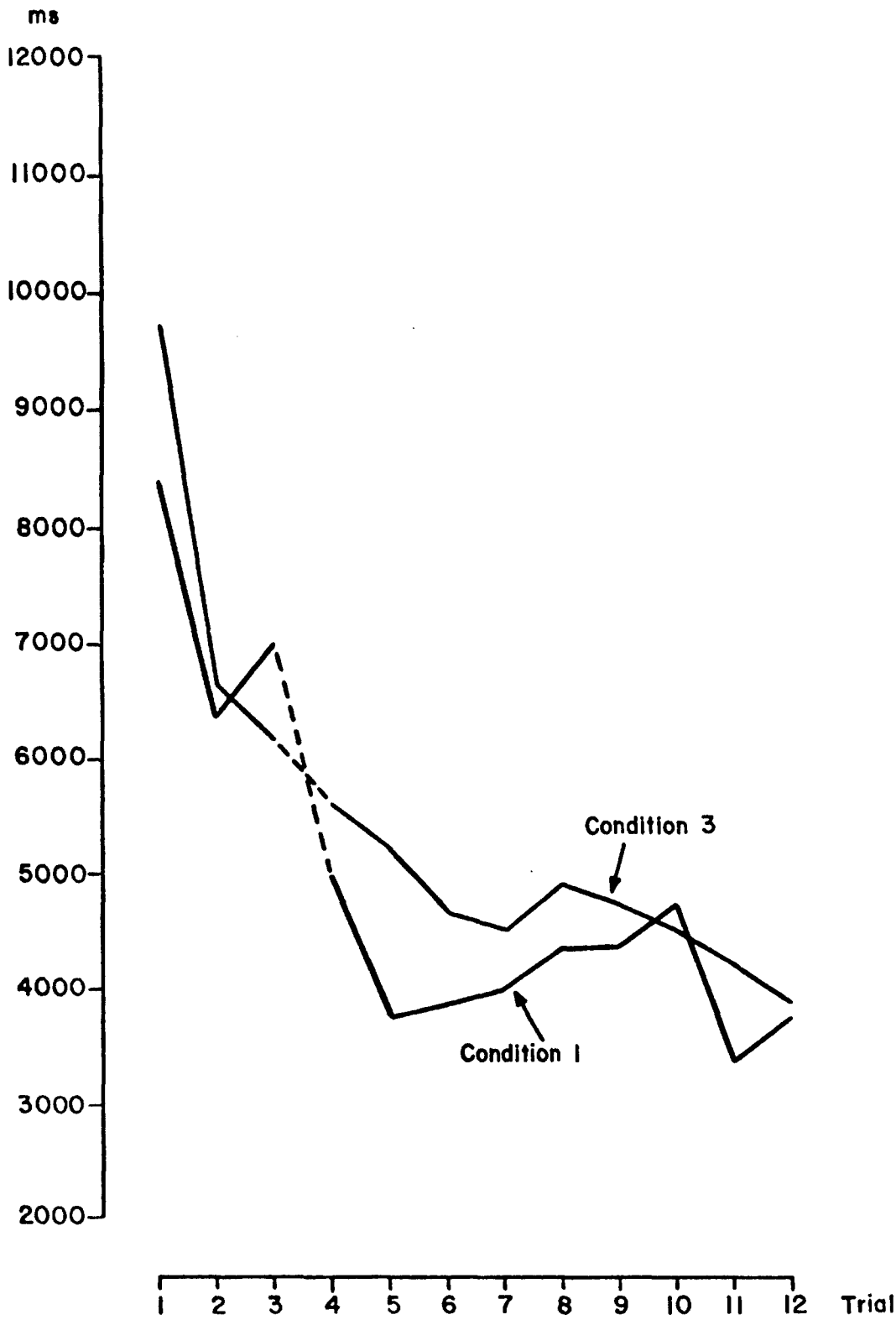

Figure 6 Movement times Part 2 n = 12

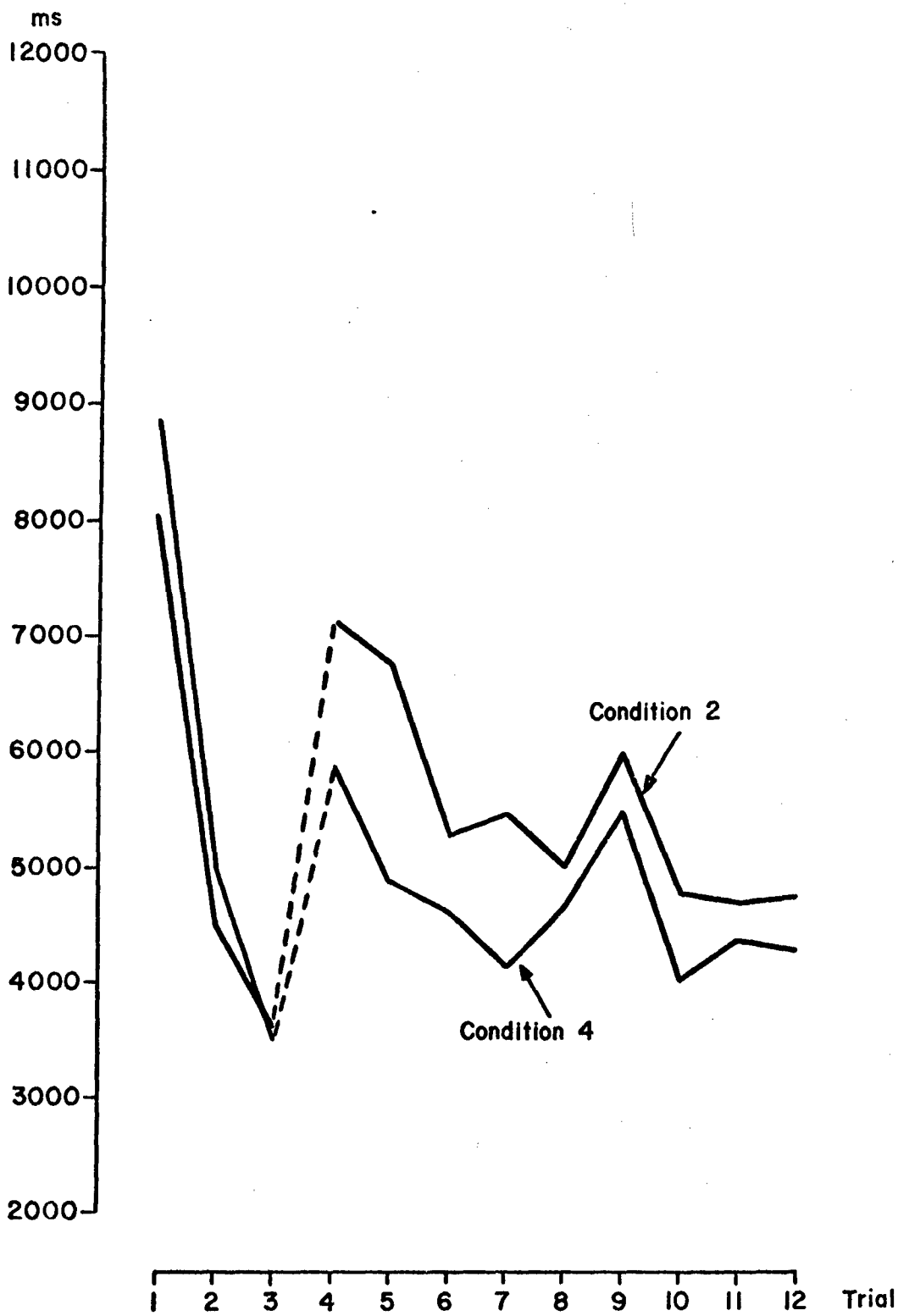

Figure 7 Movement times Part 2 n = 12

FLIGHT SIMULATOR EVALUATION OF AUDIO DISPLAYS FOR IFR HOVER CONTROL

E. Wayne Vinje
United Aircraft Research Laboratories
East Hartford, Connecticut

ABSTRACT

An exploratory study was conducted using the United Aircraft Flight Simulator to evaluate the effects of audio displays on pilot performance and workload for a simulated Instrument Flight Rules (IFR) V/STOL hover task. Single-degree-of-freedom audio displays for the longitudinal control command, heading and height were each evaluated in conjunction with the visual display system. For some of the experiments, the visual display of the corresponding function was replaced with an audio display; for others, the audio display supplemented the visual display.

Results showed that pilots could control an aurally displayed function and another visually displayed function better than if the two functions were both presented visually on separate displays. It appears, therefore, that the pilot was either controlling the aural and visual functions in parallel, or that his switching rate between the aural and visual displays was higher than his switching rate between the two visual displays. Pilots also commented that the workload for the hover task was reduced when the audio displays were used.

An audio display was most effective when it presented a signal which was important to the pilot, e.g., a nonredundant signal which changed rapidly and which was directly related to a controlled variable. The effectiveness of the audio display was further enhanced if its use led to the elimination of a visual display from the pilot's scan pattern.

INTRODUCTION

In many aircraft control tasks excessive demands are made on the pilot's ability to obtain control information from visual displays. Among these tasks are terrain following, delivery of certain weapons, and V/STOL aircraft IFR approach to landing and hover. There are data available which indicate that the human's auditory sense might be used as an effective supplement to vision in such complex control tasks.

Preceding page blank

The human operator's ability to perform a compensatory tracking task using only an audio presentation of tracking error was examined in detail in an earlier study (Ref. 1). Operator describing function and remnant data indicate that the human operator can control as well aurally as visually for this task. Multi-axis audio control was also evaluated in a study conducted during the latter part of World War II (Ref. 2). The audio display, designated "Flybar", was designed to enable pilots to control aircraft heading, roll, and airspeed (or pitch attitude) without visual references. Results indicated that, with training, subjects could perform this task as well with the audio display as with standard aircraft IFR visual displays. The use for over twenty years of low-frequency radio ranges for aircraft navigation is another example of using audio information for control (Ref. 3).

There are two fundamental questions which must be investigated further before it can be concluded that audio control information would be an effective supplement to a visual display system. The first question is whether a pilot can use both types of control information simultaneously. There is some evidence that humans can control in parallel with multiple inputs (Refs. 4 and 5). The second major question which needs investigating is whether control of the system is improved and/or pilot workload diminished when audio displays are provided. A recent study (Ref. 6) has provided some results which showed that an audio display was a useful supplement to vision in a two-degree-of-freedom control task.

The present study was undertaken to provide additional information on (1) the degree to which human operators can control simultaneously with audio and visual information, and (2) the changes in performance and workload which result for multi-degree-of-freedom control when audio displays are used.

DESCRIPTION OF THE EXPERIMENT

Control Task and Aircraft Simulation

The task performed in this study was six-degree-of-freedom (dof) hover control of a V/STOL aircraft in turbulence. The United Aircraft Flight Simulator was used in the fixed-base mode to simulate the task. A schematic diagram of the task, emphasizing the flow of information to and from the pilot, is shown in Fig. 1. The pilots tried to minimize the rms values of longitudinal, lateral and vertical hovering position error (σ_x, σ_y, and σ_h, respectively) and also the rms error in heading (σ_ψ). The major components of the simulated turbulence were input so that the aircraft was disturbed primarily along the longitudinal axis and about its directional axis. A smaller component of lateral turbulence was also present. Both large and small values of heading disturbances were considered ($N_v \cdot \sigma_{v_g}$ = 0.62 and 0.025 rad/sec^2). The longitudinal and lateral turbulence components were held constant at σ_{u_g} = 5.1 ft/sec^2 and σ_{v_g} = 1.3 ft/sec^2. Test pilots have described this combination of longitudinal and lateral turbulence as being characteristic of a moderately turbulent day (Ref. 7).

The large directional disturbances associated with $N_v \cdot \sigma_{v_g} = 0.62$ rad/sec^2, combined with other disturbances due to longitudinal and lateral turbulence, made the control task quite difficult to perform.

As indicated in Fig. 1, the control task was performed using visual IFR displays which were supplemented with single-degree-of-freedom audio displays. These audio displays were substituted for, or used in conjunction with, selected visual displays during different parts of the experiment. The visual and audio display systems will be described in more detail in the next two sections.

The simulated V/STOL aircraft controlled for the hover task was represented by a system of linear equations (Ref. 8). The stability derivatives for the aircraft simulation were as follows:

Longitudinal	Lateral	Directional	Height
$M_{ug} = 0.67$	$L_{vg} = -0.1$	$N_v = 0.002, 0.05$	$Z_w = -1$
$X_u = -0.1$	$Y_v = -0.1$	$N_r = -1$	$Z_{\delta_c} = 3.2$
$M_q = -3$	$L_p = -3$	$N_{\delta_r} = 0.4$	
$M_\theta = -5$	$L_\phi = -5$		
$M_{\delta_e} = 0.500$	$L_{\delta_a} = 0.500$		

The levels of longitudinal and lateral rate and attitude stabilization used in the simulation provided an attitude command response to control inputs for these axes. A rate command response resulted for directional and height control inputs. These control system characteristics are similar to those used in a V/STOL IFR approach and hover study conducted at the NASA Langley Research Center (Ref. 9). In that study it was determined that an attitude command system for longitudinal and lateral control was required as a minimum level of augmentation.

Visual Display System

The visual display system is shown schematically in Figs. 1 and 2. The general locations of the different displays can be seen in Fig. 1. In Fig. 2 the displays are diagrammed in more detail. Both flight director and situation displays were used. The flight director display indicated the direction in which the longitudinal, lateral, and height controls should be moved to decrease errors in longitudinal hover position, lateral hover position and height, respectively. The situation displays indicated the aircraft's attitude and position relative to the reference hover attitude and position. This visual display system is similar to that used in the NASA study mentioned previously (Ref. 9). The flight director and situation displays are described in more detail in the following paragraphs.

As shown in Fig. 2, the movable parts of the flight director display consisted of a horizontal bar, a vertical bar and a pointer. Vertical motion of the horizontal bar indicated longitudinal control commands, horizontal motion of the vertical bar indicated lateral control commands and vertical motion of the pointer indicated height (collective) control commands. The convention relating flight director commands to control motion required that the controls be moved so as to "push" the indicators back to their null positions to correct for hovering position error. For example, if the horizontal bar was above the null (center) position, the control stick had to be moved forward to reduce longitudinal hovering position error.

The signals which positioned the flight director indicators were functions of aircraft position error, error rate, and control position. That is, the analog computer was used to perform gain and lead operations for the pilot and also to translate these operations into control commands. For the lateral and longitudinal axes the control commands were equivalent to attitude commands because of the attitude command control system. The equation used to relate aircraft position error, error rate, and control motion to flight director indicator position was

$$\text{Indicator Position} = \pm\left[K_1(\tau(d(\ )/dt) + 1)\right] e(t) - K_2\delta(t) \qquad (1)$$

where

K_1, K_2 = gain constants
τ = lead time constant
e = position error
δ = control position

The values of the constants used for the different axes which were controlled were:

Longitudinal	Lateral	Vertical
$K_1 = 3$	$K_1 = 3$	$K_1 = 1$
$\tau = 5$	$\tau = 5$	$\tau = 4$
$K_2 = 15$	$K_2 = 15$	$K_2 = 45$

These values enabled the pilot to achieve good hovering performance with an acceptable amount of effort.

The visual situation display used in the experiment (Fig. 2) consisted of an artificial horizon, altimeter, direction indicator and the contact analog. The pilots could observe information on pitch and roll attitude, height error, heading error and longitudinal and lateral position, respectively, from these instruments.

Audio Displays

Audio displays for the longitudinal control command, height and heading were evaluated during this study. Two basic types of display formats were used. One format was used to represent the longitudinal control command and then later to display height. The other basic format was used to present heading. For both of these display types, the function being displayed was represented by a single tone whose frequency was related to the magnitude of the function.

The relationship between tone frequency and the function being presented is shown in Fig. 3. For the longitudinal control command or height display (Fig. 3(a)), a zero value of the input corresponded to a center frequency, f_o, of 2200 Hz. For positive input (control command signal) the frequency of the tone increased linearly with the input magnitude. For negative input the frequency decreased linearly from f_o. The scaling between the input and frequency was such that the maximum expected frequency of the tone was f_{max} = 4200 Hz and the minimum was f_{min} = 200 Hz. Also, if the input magnitude was less than some acceptably small value, the tone was interrupted (dashed) to indicate that corrective control action was not necessary (see Fig. 3(a)). The tone could be continuously presented to both ears or switched between ears as the input polarity changed.

For the heading display, the magnitude of the input was also linearly converted to a frequency. However, for this display, zero input corresponded to a low bias tone of f_{min} = 330 Hz and the frequency always increased with the magnitude of the input, regardless of its polarity. The sign of the input was indicated by switching the tone between ears as a function of input polarity. As for the other display type, the tone was dashed if the input magnitude was smaller than some predetermined value.

Test Cases and Subjects

Details of the specific test cases for which data were obtained are outlined in Table I. The specific characteristics of the audio displays used are outlined in Table II. The general structure of the audio display formats was described in the preceding section of this report. In Table I it is also noted that the phrase "A Only", for example, means that the displayed function being considered was presented aurally only. The visual representation of this function was eliminated, but all the other visual displays were operative.

The test cases were generally evaluated with only pilot A who was well trained in the use of audio displays. For the evaluation of audio directional control, however, two pilots were used. Pilot B had no previous experience with audio displays, but only a short training period was necessary to bring him to a reasonable proficiency level. The learning curves for pilot B are shown in Fig. 4. Curves of rms performance versus training run are shown for pilot B for all four of the pertinent degrees-of-freedom controlled (σ_x, σ_y, σ_h and σ_ψ). However, only heading was displayed aurally during his training and there was no visual heading display. The curves for both rms height and heading error (σ_h and σ_ψ) show learning effects through only the first seven or eight practice runs. After that, the performance scores obtained were relatively stable. It should be pointed out, however, that after this training period pilot B was still not as proficient at controlling with the aural heading display as was pilot A (see Table III and Fig. 4).

The data obtained for each of the test cases evaluated consisted of both rms hovering performance measurements and pilot comments. The rms hovering performance results presented in Table III and Figs. 5 through 9 are averages from 10 runs, each of 100-sec duration.

DISCUSSION OF RESULTS

Audio Longitudinal Control Command

Two audio displays (A and B) were considered for the evaluation of audio longitudinal control command. Each audio display was evaluated as a substitute for the visual longitudinal control command (LCC) presentation. The longitudinal control command signal was well suited for the evaluation of audio displays. The pilots relied very heavily on it when performing the hover task and could not control longitudinal position accurately without it. Also, this signal changed rapidly with time and required a great deal of attention if it was to be tracked accurately. Display A (see Table II) was considered first. Data were measured when this audio display was substituted for the visual LCC display (the visual lateral and vertical control command indicators were still operative), when both the audio and visual LCC displays were operating and when only the visual LCC display was used. It should be noted again that all the other visual displays were operating. Also, the large ψ disturbances were included in all of these cases.

The measured hovering performance data, σ_x, σ_y, σ_h and σ_ψ for this part of the study are presented in Table III and Fig. 5. Hover performance was best when both the audio and visual LCC displays were used. Hover performance with only the audio LCC display was next best, and the poorest performance resulted when only the visual LCC display was used. The audio LCC display permitted the pilot to spend less time on the visual flight director, while still receiving the high-

frequency command information he needed to control longitudinal position. This enabled him to spend more time on the other visual displays, e.g., the altimeter and the heading display. These audio display effects resulted in improved hover performance in all the axes controlled.

Display A was deficient, however, in that it did not give a very definite indication of changes in polarity of the longitudinal control command. As a result, the pilot sometimes made erroneous or inaccurate control inputs using the audio display, and this led to errors in hover position. This deficiency in display A would seem to be the reason that hover performance improved somewhat when the visual LCC display was used in conjunction with display A.

Display B (see description in Table II) was considered to be an improved version of display A. Display B was different in that the tone switched ears when the longitudinal control command changed sign. The tone was also dashed for display B when the magnitude of the LCC was smaller than a predetermined value. The measured hovering performance for the evaluation of display B is shown in Fig. 6. These results show that performance was generally better when display B was used to present the longitudinal control command (with no visual LCC display) than for the visual LCC display. Also, comparing the values of σ_x, σ_y and σ_h obtained using display B only with those for display A only (Table III) shows that the pilot was able to control hover position better with display B. Note, however, that the ψ disturbance level was smaller for the evaluation of display B and this could also have affected the measured values of σ_x, σ_y and σ_h. It very definitely affected the measured value of σ_ψ (Table III), i.e., σ_ψ was much smaller for the display B evaluation.

The results discussed previously show that the pilot can perform the parallel audio-visual control task well enough to significantly improve performance over that obtained with visual displays alone. This conclusion is based on results obtained for an audio display of an important, rapidly changing signal which required a considerable amount of pilot vigilance in order to be tracked accurately. Pilot comments also indicate that with the audio display the pilot felt that the overall task workload was reduced.

It is possible, however, that single-degree-of-freedom audio displays can be more effective when substituted for a different type of visual display. The pilot benefited from the audio LCC display because it permitted him to control more continuously an important, rapidly changing function. He also could reduce the amount of time spent looking at the flight director and spend more time on the other visual displays. However, he could not eliminate the flight director from his scan pattern since it provided necessary lateral and vertical control command data. If the audio display were substituted for a single-degree-of-freedom visual display the pilot could delete this display from his scan. This could conceivably lead to greater benefits from the use of audio displays. The evaluations of audio direction and height displays provide information related to this possibility.

Audio Directional Display

Hovering performance results from the evaluation of the audio heading display are shown in Fig. 7 and are also listed in Table III. The data plotted in Fig. 7 for pilot B are the results dated 1-26-71 in Table III. The "Visual Only" data for pilot A are those from 1-20-71. There was a definite improvement in hover performance for pilot A when the audio heading display (display C, Table II) was substituted for the corresponding visual display. However, for pilot B only heading control (σ_ψ) improved appreciably when display C was substituted for the visual heading display. As indicated previously, pilot B did not have as much experience with audio displays as pilot A and his performance with this display was not as good as that for pilot A. Note that pilot A's hover performance with "C Only" was also appreciably better than pilot B's "Visual Only" performance.

Both pilots commented that workload was reduced when the audio display was used because the heading display was eliminated from their visual scan pattern. It is interesting to note here also that pilot A's hover performance with the audio heading display ("C Only") was much better than his performance with the first audio longitudinal control command display ("A Only"). The "B Only" results are not comparable as the σ_ψ disturbance was smaller. This would tend to indicate that it was better to use the audio display in such a way that one of the visual displays could be completely eliminated from the scan pattern. This is apparently true for the situation in which the two alternative signals being considered are of nearly equal importance and have similar frequency content. As will be discussed in the succeeding paragraphs, eliminating one of the visual displays from the scan pattern is not as helpful when the displayed signal is of lesser importance.

Audio Height Display

Hover performance changed little when the audio height display was substituted for the corresponding visual presentation (Fig. 8). Also, the hover performance measured when both audio and visual height displays were used was very similar to the visual only or audio only data. The only notable difference among the data measured for the different display arrangements occurs in the height error results. The rms error in height was significantly smaller for the audio only and audio plus visual displays than for the visual only situation.

Substituting the audio height display for the visual display once more enabled the pilot to eliminate a display from his scan pattern. However, eliminating the height display from the pilot's scan did not reduce the visual workload greatly because the height display normally was not checked as frequently as the heading

or flight director visual displays. Also, a height control command was presented on the flight director which further decreased the importance of the height display. Because the visual height display was inherently not as important as, for example, the heading display, there was no dramatic improvement in hover performance when the audio height display was substituted for it. Height control was improved with the audio display, however, because the pilot had a continuous reference for height error.

Comparison of the Effects of the Different Audio Displays on Hover Performance

The rms hovering performance measured for three audio displays (longitudinal control command-display A, heading and height) when each was the only display used to present the given signal is shown in Fig. 9. The "Visual Only" results which are also shown in Fig. 9 are an average of the data measured on 1-20-71 and 1-26-71 (Table III). The data in Fig. 9 show that the rms height error was smallest when display D was substituted for the visual height display. The rms heading error was also smallest when display C was substituted for the visual heading display. Note, however, that the rms longitudinal position error was not smallest when audio display A was used. The reason may be that the continuous longitudinal control command information was not as beneficial to the pilot since, for the visual only case, he customarily spent the majority of his time monitoring the flight director. Consequently, the additional LCC information provided by the audio display was not as helpful as the audio directional and height information. It is also evident in Fig. 9 that the best overall hover performance was achieved with the audio heading display.

REFERENCES

1. Vinje, E. W.: Human Operator Dynamics for Audio Compensatory Tracking. Ph.D Thesis, Department of Aerospace Engineering, University of Connecticut; also presented at 7th Annual NASA-University Conference on Manual Control, University of Southern California, June 2-4, 1971.

2. Sinaiko, H. W., Ed.: Selected Papers on Human Factors in the Design and Use of Control Systems. Dover Publications, New York, 1961.

3. Chapanis, A., W. R. Garner, and C. T. Morgan: Applied Experimental Psychology - Human Factors in Engineering Design. John Wiley and Sons, Inc., New York, 1957.

4. Levison, W. H.: A Model for Task Interference. Proceedings of the Sixth Annual Conference on Manual Control, Wright-Patterson AFB, Ohio, April 1970.

5. Stapleford, R. L., R. A. Peters and F. R. Alex: Experiments and a Model for Pilot Dynamics with Visual and Motion Inputs. NASA CR-1325, May 1969.

REFERENCES (Continued)

6. Mirchandani, P. B.: Evaluation of a Supplementary Audio Display in a Dual Axis Compensatory Tracking Task. Man-Vehicle Laboratory, Massachusetts Institute of Technology, Cambridge, Massachusetts, Report MVT-71-3, September 1971.

7. Seckel, E., J. J. Traybar and G. E. Miller: Longitudinal Handling Qualities for Hovering. Princeton University Report No. 594, December 1961.

8. Miller, D. P. and E. W. Vinje: Fixed-Base Flight Simulator Studies of VTOL Aircraft Handling Qualities in Hovering and Low-Speed Flight. AFFDL-TR-67-152, January 1968.

9. Garren, J. F., J. R. Kelly and R. W. Sommer: VTOL Flight Investigation to Develop a Decelerating Instrument Approach Capability. SAE Paper No. 690693, October 1969.

LIST OF SYMBOLS

$\frac{d(\ )}{dt}$	First derivative of the quantity in parentheses, ( )/sec
e	General representation for longitudinal, lateral or vertical hover position error, ft
f	Frequency, Hz
f_{max}	Maximum frequency expected from audio display, Hz
f_{min}	Minimum frequency expected from audio display, Hz
f_o	Center frequency corresponding to zero tracking error for longitudinal control command audio display, Hz
g	Gravitational constant, 32.2 ft/sec^2
I_x, I_y, I_z	Moments of inertia in roll, pitch, and yaw, slug-ft^2
K_1	Gain constant relating hover position error to control command, in./ft
K_2	Gain constant relating control position to control command, in./in.
L_p	Rolling moment, divided by I_x, due to roll rate, 1/sec
L_v	Rolling moment, divided by I_x, due to lateral velocity, 1/ft-sec
L_{δ_a}	Rolling moment, divided by I_x, due to unit longitudinal control stick displacement, (rad/sec^2)/in.
L_ϕ	Rolling moment, divided by I_x, due to roll attitude, 1/sec^2
m	Mass of aircraft, slugs
M_q	Pitching moment, divided by I_y, due to pitch rate, 1/sec
M_u	Pitching moment, divided by I_y, due to longitudinal velocity, 1/(ft-sec)

M_{δ_e}	Pitching moment, divided by I_y, due to unit longitudinal control stick displacement, $(rad/sec^2)/in.$
M_θ	Pitching moment, divided by I_y, due to pitch attitude, $1/sec^2$
N_r	Yawing moment, divided by I_z, due to yaw rate, 1/sec
N_v	Yawing moment, divided by I_z, due to lateral velocity, 1/(ft-sec)
N_{δ_r}	Yawing moment, divided by I_z, due to unit directional control pedal displacement, $(rad/sec^2)/in.$
X_u	Longitudinal force, divided by m, due to longitudinal velocity, 1/sec
Y_v	Lateral force, divided by m, due to lateral velocity, 1/sec
Z_w	Vertical force, divided by m, due to vertical velocity, 1/sec
Z_{δ_c}	Vertical force, divided by m, due to unit collective control stick displacement, $(ft/sec^2)/in.$
δ	Control stick displacement, in.
σ_h	RMS vertical hovering position error, ft
$\bar{\sigma}_h$	Average rms vertical hovering position error, ft
σ_{u_g}	RMS longitudinal turbulence, ft/sec
σ_{v_g}	RMS lateral turbulence, ft/sec
σ_x	RMS longitudinal hovering position error, ft
$\bar{\sigma}_x$	Average rms longitudinal hovering position error, ft
σ_y	RMS lateral hovering position error, ft
$\bar{\sigma}_y$	Average rms lateral hovering position error, ft
$\sigma_{\sigma_h}, \sigma_{\sigma_x}, \sigma_{\sigma_y}$	Standard deviations of the rms hover position error measured along the vertical, longitudinal and lateral axes, respectively, ft

$\sigma_{\sigma_{\psi}}$	Standard deviation of the rms error in heading, rad
σ_{ψ}	RMS heading error, rad
σ_{ψ}	Average rms heading error, rad
τ	Gain constant relating the rate of change of hover position error to control command, (in.-sec)/ft
ψ	Yaw attitude angle, rad

TABLE I

TEST CASES FOR WHICH AUDIO
DISPLAYS WERE EVALUATED

Evaluation	Pilot	Date	ψ Disturbance		Display*
			Level	$N_V \cdot \sigma_{V_g}$ rad/sec^2	
Audio Longitudinal Control Command	A	1-20-71	Large	0.62	A Only ** A Plus Visual Visual Only
		1-22-71	Small	0.025	B Only Visual Only
Audio Directional Display	A	1-22-71	Large	0.62	C Only
	B	1-22-71	Large	0.62	C Only Visual Only
		1-26-71	Large	0.62	C Only Visual Only
Audio Height Display	A	1-26-71	Large	0.62	D Only D Plus Visual Visual Only

*See Table II for key to audio display designation.

**The designation "A Only", for example, means that the function was displayed aurally only. That is, the corresponding visual display for the function was eliminated, but all other visual instruments operated normally.

TABLE II

KEY TO LETTER DESIGNATION FOR AUDIO DISPLAYS

Display	Parameter Presented	Description of Display Characteristics
A*	Longitudinal Control Command	Longitudinal control command converted linearly to frequency, f (sensitivity = 600 Hz/in.) Zero error corresponds to f_o = 2200 Hz. Increase in f above f_o indicates stick forward command, decrease in f indicates rearward stick command. Tone is dashed when control command magnitude is less than $\pm$ 0.5 in.
B	Longitudinal Control Command	Similar to display A except tone also switches ears at zero control command. Tone is in left ear for $f > f_o$ and in right ear for $f < f_o$. Control command limit for dashed tone reduced to $\pm$ 0.25 in.
C	Direction Error	Direction error linearly converted to f. At zero error f_o = 330 Hz, sensitivity is 134 Hz/deg. Tone increases in left ear (no tone in right ear) for positive direction error; increases in right ear for negative error. Tone switches ears at zero error and is dashed when direction error magnitude is less than 3 deg.
D	Height Error	Similar to B. Height error linearly converted to f. At zero error f_o = 2200 Hz, sensitivity is 200 Hz/ft. Tone switches ears at zero error; higher tone in left ear indicates aircraft too high; lower tone in right ear indicates aircraft too low. Tone is dashed when height error magnitude is less than 2 ft.

* In the figures the designation "A ONLY", for example, means that the vertical input to the horizontal bar was removed and the pilot derived his longitudinal control information only from the audio signal. All other instruments operated normally.

TABLE III

SUMMARY OF RMS HOVERING PERFORMANCE DATA FROM AUDIO DISPLAY STUDY

Evaluation	Pilot	Date	Disturbance		Display	$\bar{\sigma}_x$ (ft) ($\sigma\sigma_x$)	$\bar{\sigma}_y$ (ft) ($\sigma\sigma_y$)	$\bar{\sigma}_h$ (ft) ($\sigma\sigma_h$)	$\bar{\sigma}_\psi$ (deg) ($\sigma\sigma_\psi$)
			Level	$N_v \cdot \sigma_{v_g}$ Rad/sec^2					
Audio Longitudinal Control Command	A	1-20-71	Large	0.62	A* Only	3.20(0.39)	1.80(0.32)	6.20(0.98)	5.53(0.92)
					A plus Visual	2.52(0.36)	1.56(0.28)	4.37(1.08)	5.34(0.90)
					Visual Only	3.82(0.50)	2.11(0.54)	7.09(2.14)	8.02(2.03)
		1-22-71	Small	0.025	B* Only	2.49(0.45)	1.49(0.28)	4.73(0.71)	2.37(0.32)
					Visual Only	3.50(0.80)	1.63(0.41)	6.86(2.42)	3.94(0.56)
Audio Directional Display	A	1-22-71	Large	0.62	C* Only	2.24(0.18)	1.28(0.12)	3.39(0.56)	2.92(0.42)
	B	1-22-71	Large	0.62	C Only	2.80(0.28)	1.52(0.22)	4.84(0.46)	5.85(1.66)
					Visual Only	3.14(0.54)	1.92(0.27)	4.97(1.82)	3.62(0.86)
		1-26-71	Large	0.62	C Only	2.40(0.40)	1.59(0.04)	4.34(0.47)	5.95(0.41)
					Visual Only	2.65(0.16)	1.60(0.04)	3.73(0.53)	7.07(0.59)
Audio Height Display	A	1-26-71	Large	0.62	D* Only	2.86(0.26)	1.47(0.02)	1.75(0.37)	6.26(0.42)
					D plus Visual	2.86(0.43)	1.40(0.06)	1.94(0.45)	6.64(0.78)
					Visual Only	2.52(0.41)	1.42(0.06)	3.23(0.93)	6.30(0.74)

* See Table I for key to audio display designation.

SIMULATED HOVER TASK

THE SWITCHES IN THE VISUAL DISPLAY CIRCUIT INDICATE THAT THESE DISPLAYS COULD BE TURNED OFF, IF DESIRED, WHEN THE DESIGNATED FUNCTION WAS BEING PRESENTED AURALLY. THE SWITCH PRIOR TO THE VOLTAGE-TO-FREQUENCY CONVERTER INDICATES THAT ANY ONE OF THE THREE DESIGNATED FUNCTIONS COULD BE CHOSEN FOR AUDIO PRESENTATION.

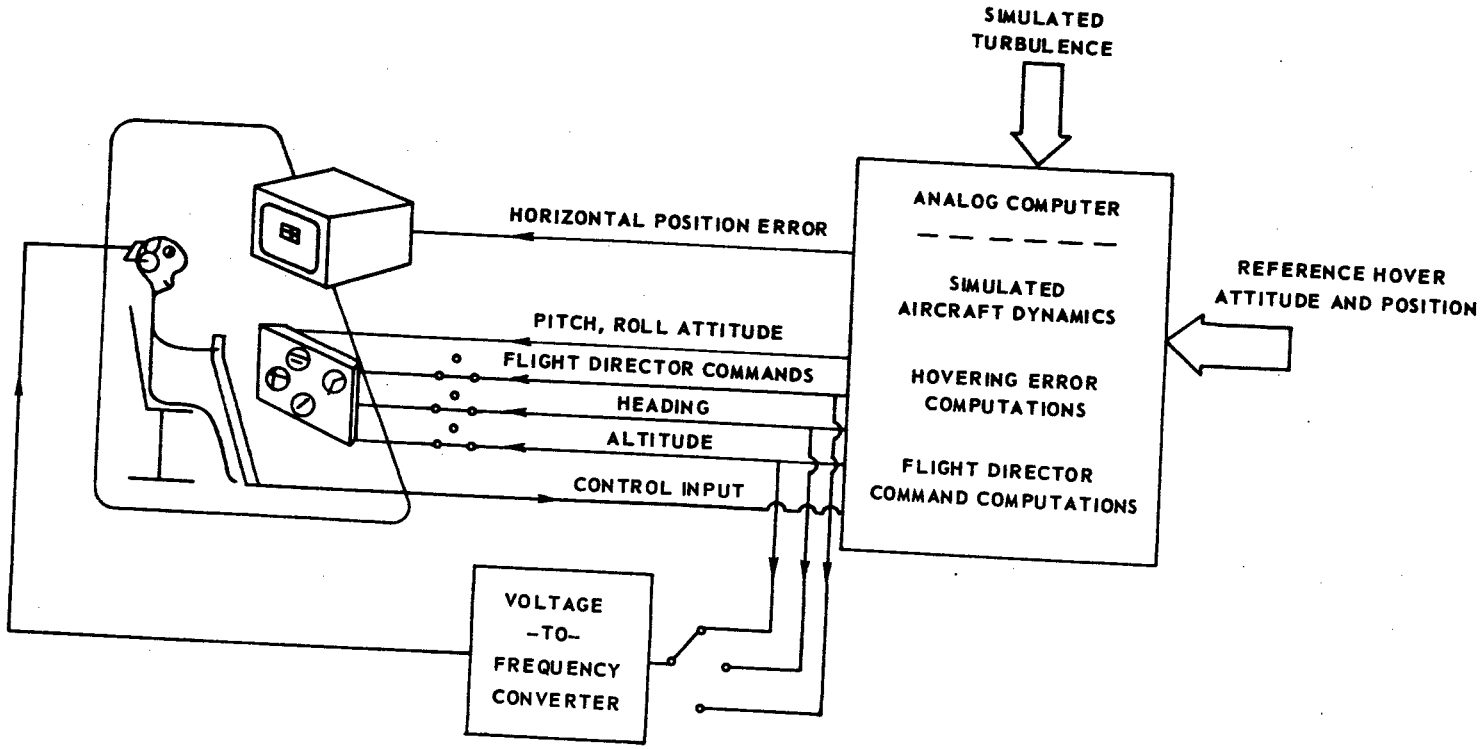

FIG. 1

VISUAL DISPLAY FOR THE SIMULATED HOVER TASK

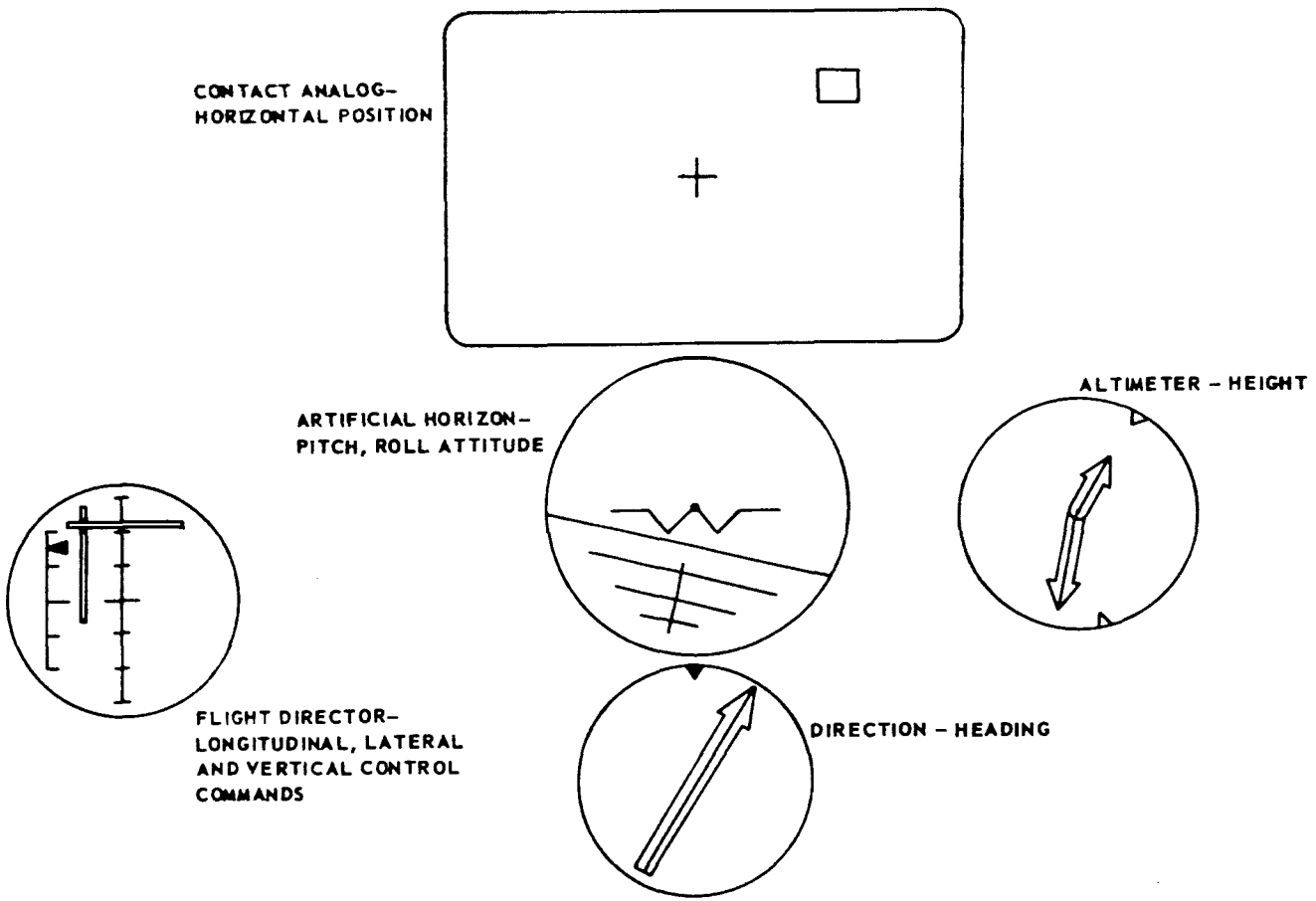

FIG. 2

FIG. 3

FREQUENCY VERSUS DISPLAYED PARAMETER CHARACTERISTICS FOR AUDIO DISPLAYS

SEE TABLE II FOR FURTHER DETAILS

(a) LONGITUDINAL CONTROL COMMAND OR HEIGHT DISPLAY

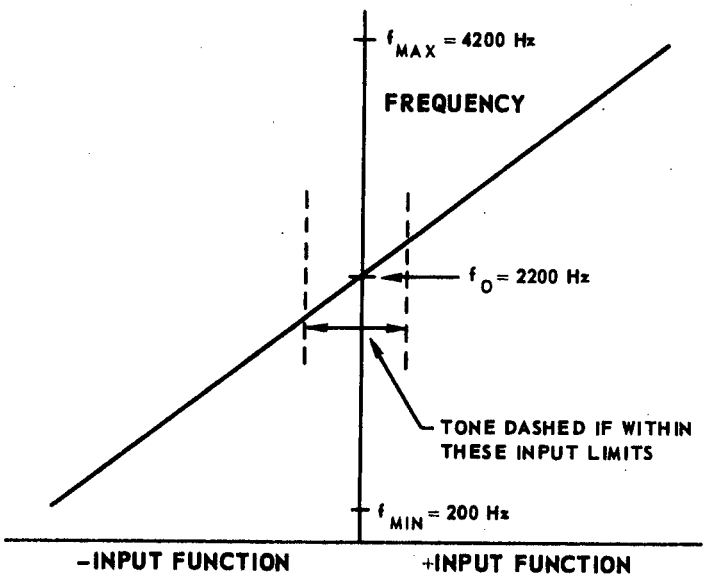

(b) HEADING DISPLAY

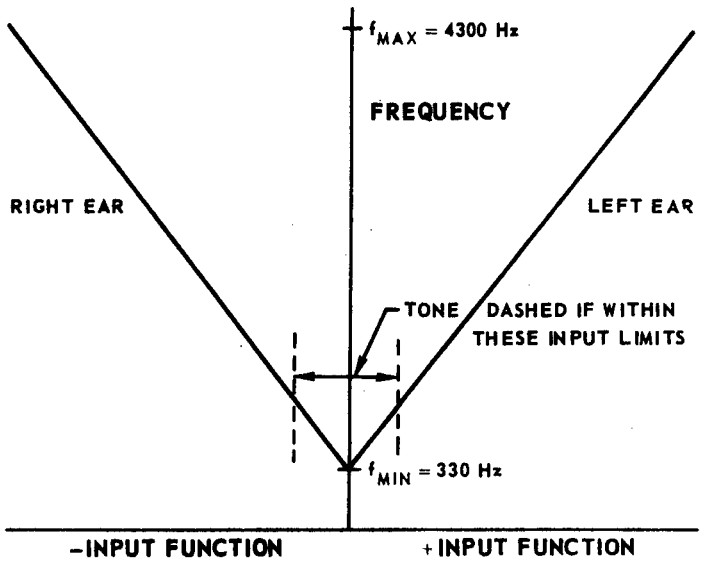

FIG. 4

EFFECT OF LEARNING ON RMS HOVERING PERFORMANCE WITH AUDIO DIRECTIONAL DISPLAY – DISPLAY C ONLY

LARGE ψ DISTURBANCES: $N_v \cdot \sigma_{v_g} = 0.62$ RAD/SEC^2 □ PILOT B

SEE TABLE II FOR DESCRIPTION OF AUDIO DISPLAY C

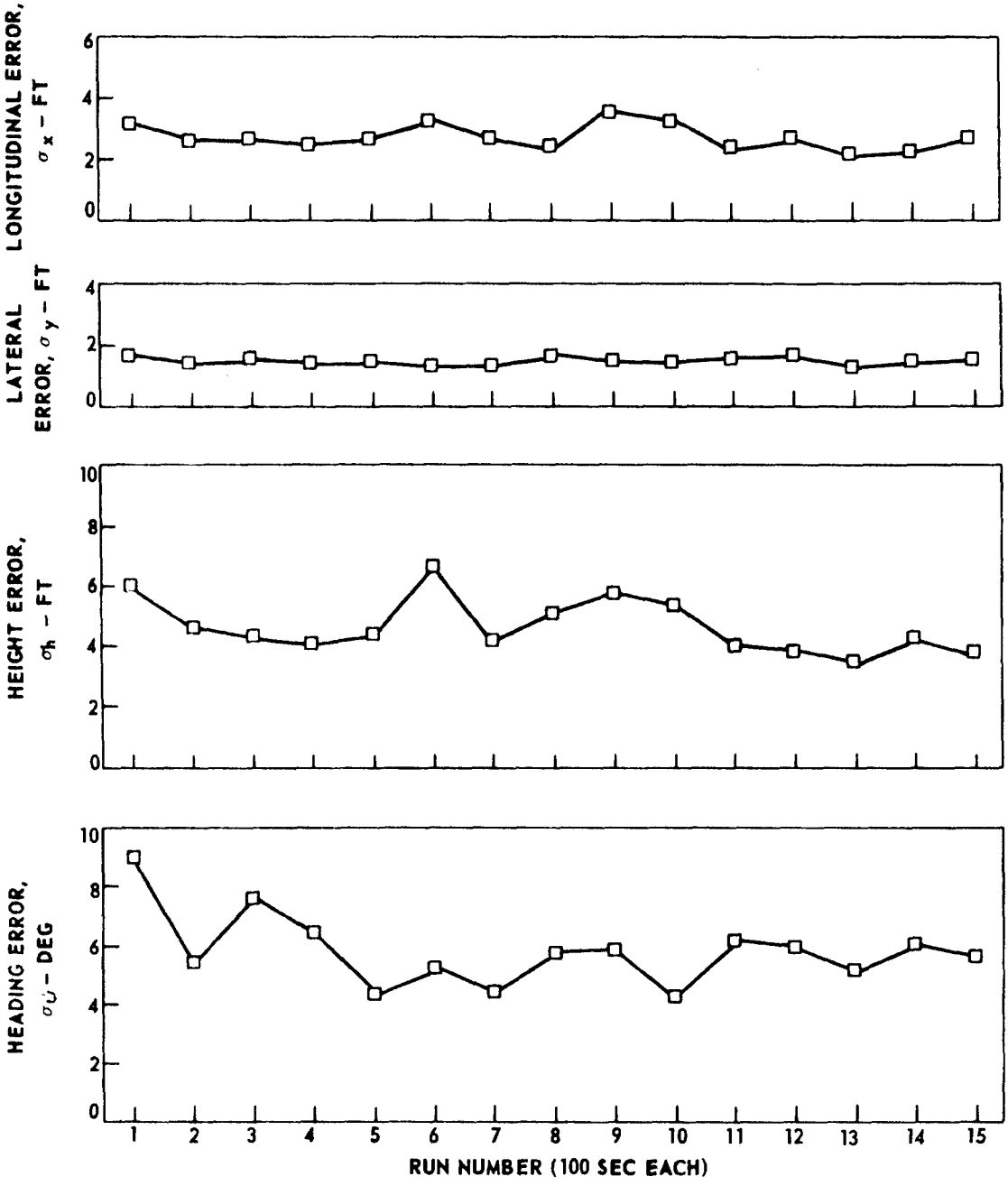

FIG. 5

RMS HOVERING PERFORMANCE WITH AUDIO DISPLAY FOR LONGITUDINAL CONTROL COMMAND – DISPLAY A

LARGE ψ DISTURBANCES: $N_v \cdot \sigma_{v_g} = 0.62$ RAD/SEC^2 ○ PILOT A

BARS DENOTE ± 1.0 STANDARD DEVIATION

SEE TABLE II FOR DESCRIPTION OF DISPLAY A

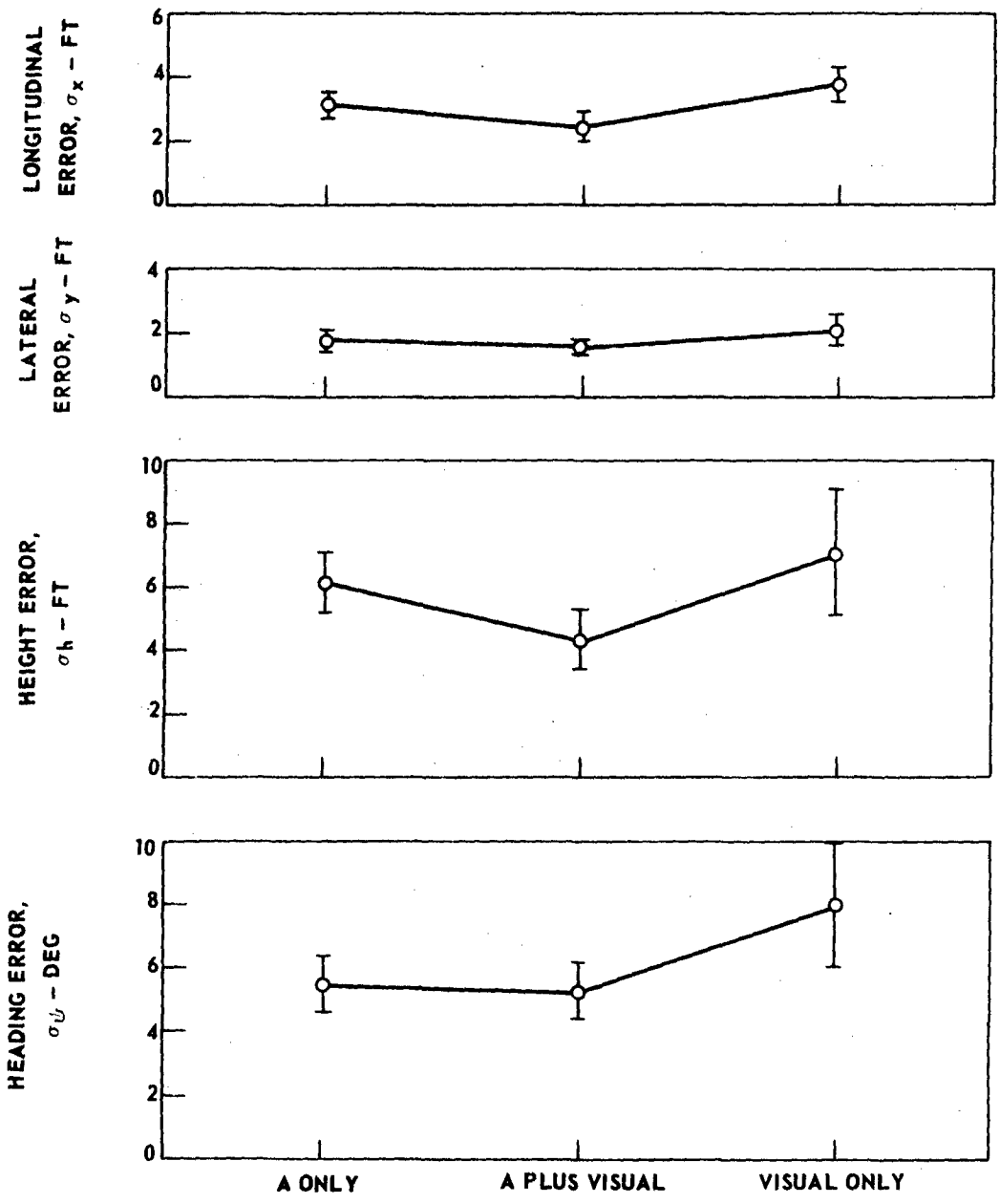

FIG. 6

RMS HOVERING PERFORMANCE WITH AUDIO DISPLAY FOR LONGITUDINAL CONTROL COMMAND – DISPLAY B

SMALL ψ DISTURBANCES: $N_v \cdot \sigma_{v_g} = 0.025$ RAD/SEC^2 ○ PILOT A

BARS DENOTE ± 1.0 STANDARD DEVIATION

SEE TABLE II FOR DESCRIPTION OF DISPLAY B

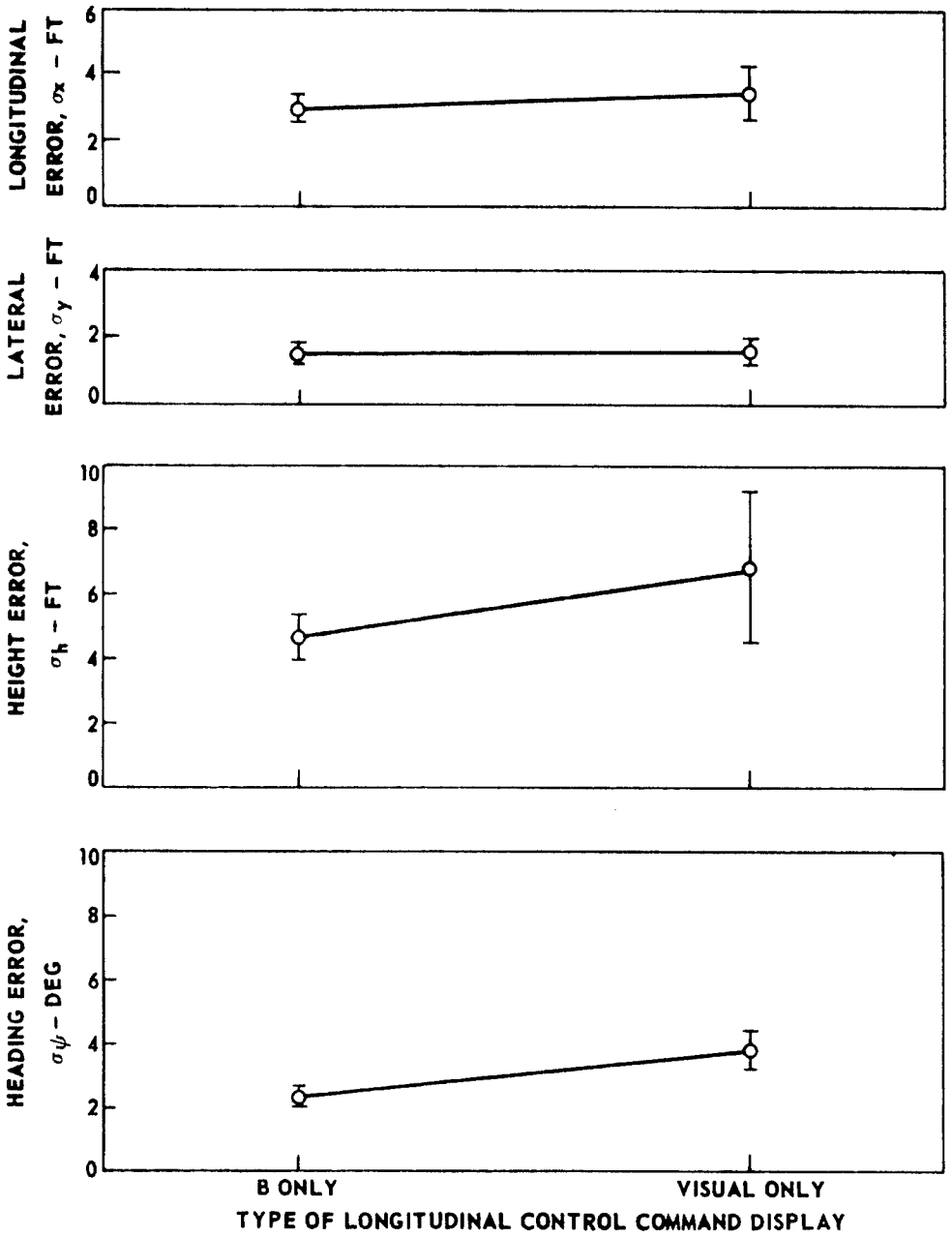

FIG. 7

RMS HOVERING PERFORMANCE WITH AUDIO DISPLAY FOR HEADING – DISPLAY C

LARGE ψ DISTURBANCES: $N_v \cdot \sigma_{v_g} = 0.62$ RAD/SEC^2 ○ PILOT A □ PILOT B

BARS DENOTE ± 1.0 STANDARD DEVIATION

SEE TABLE II FOR DESCRIPTION OF DISPLAY C

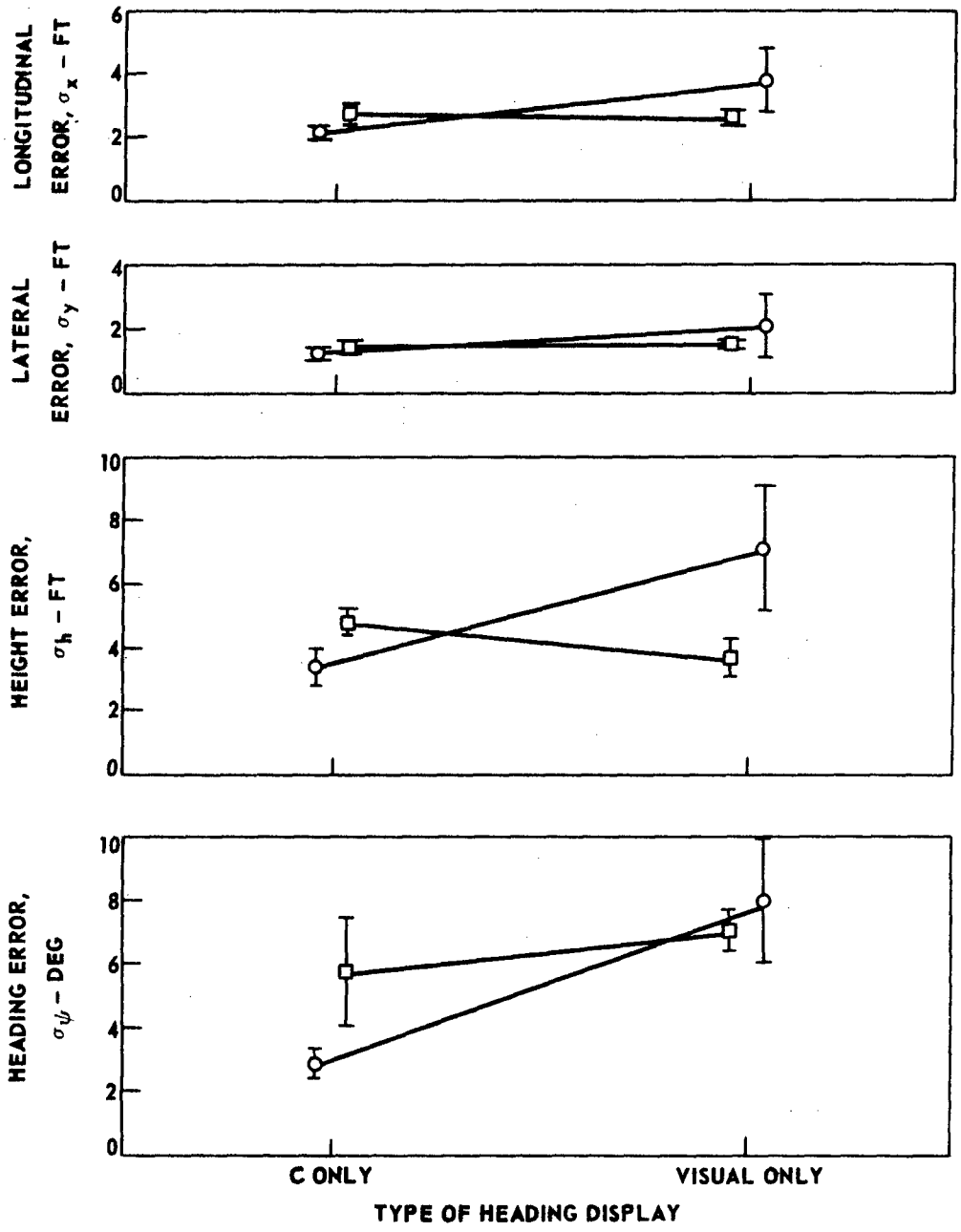

FIG. 8

RMS HOVERING PERFORMANCE WITH AUDIO DISPLAY FOR HEIGHT – DISPLAY D

LARGE ψ DISTURBANCES; $N_v \cdot \sigma_{v_g} = 0.62$ RAD/SEC ^{2} ○ PILOT A

BARS DENOTE ± 1.0 STANDARD DEVIATION

SEE TABLE II FOR DESCRIPTION OF DISPLAY D

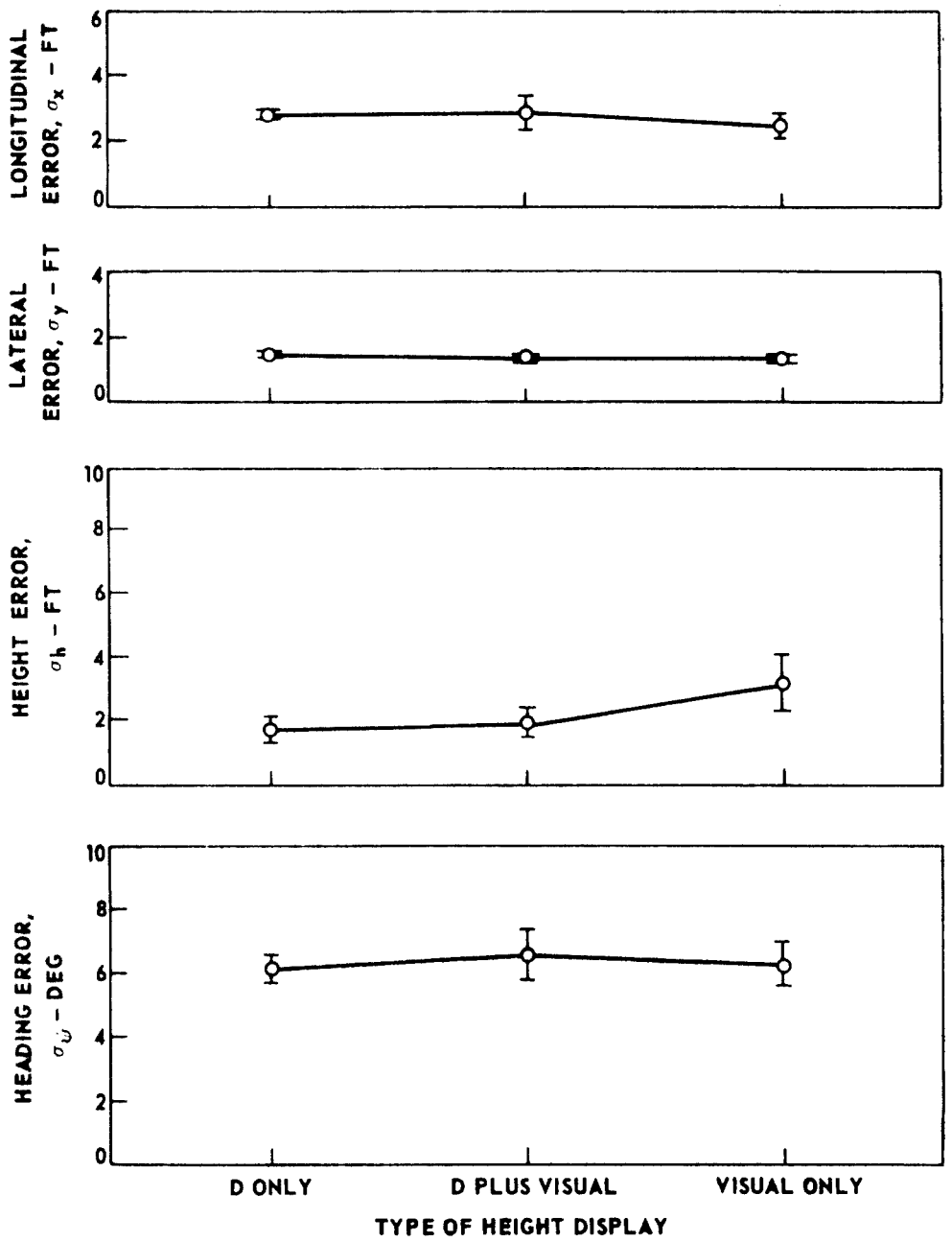

FIG. 9

COMPARISON OF RMS HOVERING PERFORMANCE WITH DIFFERENT AUDIO DISPLAYS

LARGE ψ DISTURBANCES: $N_v = \sigma_{v_g} = 0.62$ RAD/SEC^2 ○ PILOT A

BARS DENOTE ± 1.0 STANDARD DEVIATION

SEE TABLE II FOR DESCRIPTION OF AUDIO DISPLAYS

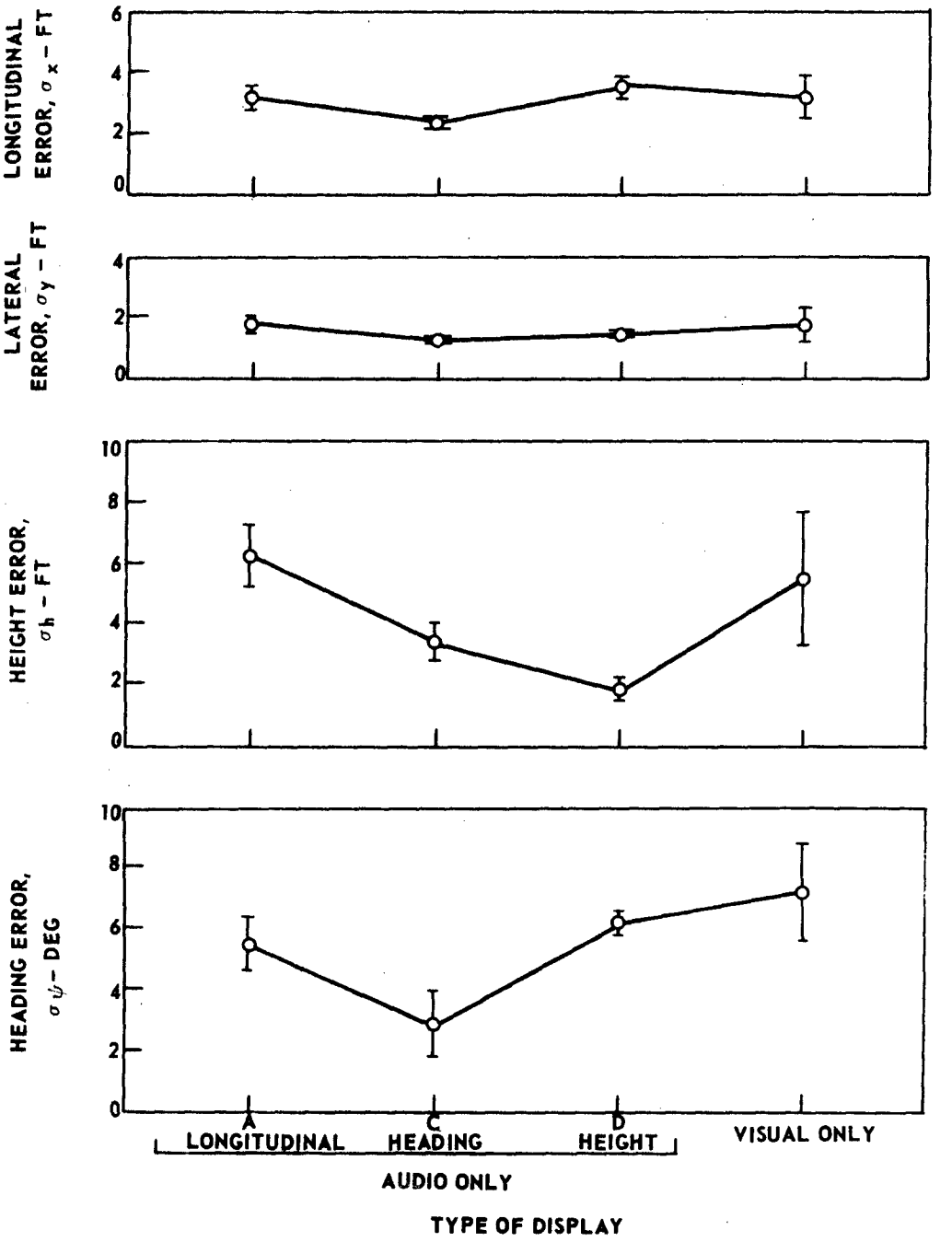

PILOT DESCRIBING FUNCTION MEASUREMENTS FOR COMBINED VISUAL AND LINEAR ACCELERATION CUES*

Robert F. Ringland and Robert L. Stapleford
Systems Technology, Inc., Hawthorne, Calif.

ABSTRACT

Pilot-vehicle describing functions and performance were measured in three (longitudinal, lateral, and vertical) single-axis tracking tasks [$Y_c = K_c/s^2(s + 1)$] with both visual and linear acceleration cues for two pilot subjects. The results show that subjects can improve tracking performance by increasing the crossover frequency when given the linear acceleration cues in addition to the visual cues.

INTRODUCTION

The role of linear acceleration sensing in discrete situations, for example, detection of simulated engine failures, is well known, but past simulation studies of continuous tasks, in particular, flight path regulation in the presence of disturbances, have failed to give any strong indication that a linear acceleration cue was being used. The results of one flight experiment (Ref. 1) suggest that subjects are unreliable in their sensation of vertical motion, which would imply that vertical acceleration cues may be unusable in a tracking task. On the other hand, manual control theory would suggest that such cues (linear accelerations), if sensible by the subject and useful in improving performance in a tracking task, will be used.

Presuming that the pilot can use these cues, there is question as to whether he is equally sensitive to vertical as opposed to horizontal accelerations. Physiological measurements (e.g., Ref. 2) would indicate no significant

*This research was sponsored by the Man/Machine Integration Branch, Biotechnology Division, Ames Research Center, National Aeronautics and Space Administration, under Contract No. NAS2-6433. The NASA Project Monitors were John D. Stewart and James Howard.

Preceding page blank

differences provided that the accelerations represent perturbations about a zero operating point. It might be argued that the effective threshold could be larger if the pilot is required to detect perturbations in the earth's gravitational field, i.e., with a vertical 1g bias.

To provide at least a partial answer to these questions, a brief (one-week duration) exploratory tracking experiment was conducted where the task dynamics were specifically contrived to render it sensitive (from the viewpoint of manual control theory) to the presence or absence of linear acceleration cues. The Six-Degrees-of-Freedom Motion Simulator (S.01) at the Ames Research Center of the National Aeronautics and Space Administration was used in the investigation. The experiment was "piggy-backed" on a more extensive experimental investigation, using time otherwise devoted to checkout of a real-time digital computer simulation of a STOL aircraft. Neither the time available nor the physical situation (STOL mockup in the simulator's cab) permitted optimization of the experimental design. Were the experiment to be repeated, there are several improvements which could be made. Nevertheless, the results obtained are felt to be significant—pilot subjects can use linear acceleration cues to significantly improve their tracking task performance.

EXPERIMENT DESCRIPTION

The block diagram of the experimental situation is shown in Fig. 1. The pilot's task is to control the displayed simulator cab's position along one axis (longitudinal, lateral, or vertical) at a time in the presence of disturbances. The figure shows a closed-loop system where the pilot affects control on a first-order lag element to which is added a disturbance provided by the describing function analyzer (DFA). The summed signals continue on into a double acceleration element from which they drive the display and (if moving-base) the motion simulator in one linear degree of freedom. The pilot responds to the displayed position error and (if moving-base) to the linear accelerations (simulator motions) experienced.

The controlled element dynamics are given by:

$$Y_c = \frac{K_c}{s^2(s+1)} \qquad (1)$$

This controlled element has considerable lag and can be expected to require considerable compensating pilot lead to control the system error. The lead can be generated either visually (as it must be, fixed-base) or using the linear acceleration cues to augment the visual cues when moving base.

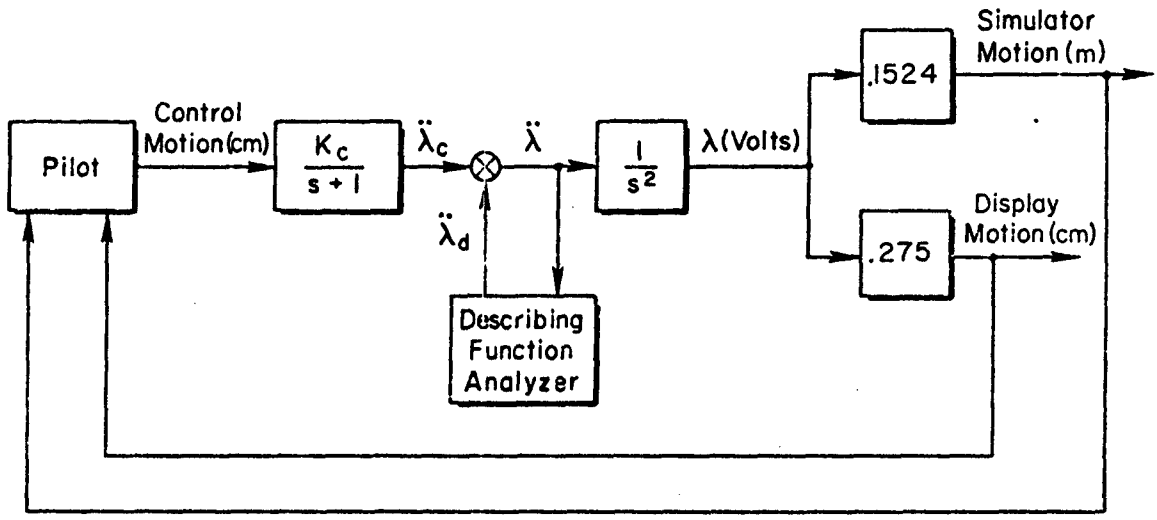

Figure 1. Block Diagram of Experiment

Displays, Controls, and Experimental Configurations

The cab's position was displayed to the pilot by means of either the glide slope (horizontal bar) or localizer (vertical bar) on an otherwise inactive attitude ball instrument located approximately 66 cm from the pilot's eyes. The bars were 5 cm long and could move through a range of 5 cm. The cab was closed; the pilot had no view of the external environment.

Either centerstick (for longitudinal or vertical) or pedals (for lateral) were used to affect control. The force and displacement characteristics of these two manipulators are listed in Table 1.

The five configurations for the experiment are given in Table 2. The table lists the symbols for each of the experimental configurations, the

manipulator and display bar that were used, and the motion simulator's activity (either fixed-base or moving in one of the three axes).

TABLE 1

MANIPULATOR CHARACTERISTICS

MANIPULATOR	FULL DEFLECTION		BREAKOUT	HYSTERESIS
	(cm)	(N)	(N)	(N)
Centerstick	±8.25	49.0	8.9	6.7
Pedals	±5.08	200.0	44.5	22.2

TABLE 2

EXPERIMENTAL CONFIGURATIONS

SYMBOL	MANIPULATOR	DISPLAY	SIMULATOR MOTION
S	Centerstick	Horizontal Bar	None
LON	"	" "	Longitudinal
VER	"	" "	Vertical
P	Pedals	Vertical Bar	None
LAT	"	" "	Lateral

Bobweight effects were unavoidably present for Congifuration LON because the arm-hand-centerstick combination could move back and forth relative to the cab when the cab accelerated. These effects were minimized for the VER and LAT configurations because the control motions were perpendicular to the direction of the accelerations. This was the reason the pedals were used for control in P and LAT — to avoid lateral bobweight effects which would be present if the centerstick were used for control. No attempt was made in this experiment to calibrate the LON configuration for the bobweight contribution. It was estimated to be relatively small.

The orientation of the controls and displays was such that the pilot "chased" the display; for example, if the horizontal bar moved up, he

would pull the stick back to "catch up" with the horizontal bar. When the stick was pulled back, the simulator cab moved either backwards or up, depending upon which axis was activated. The situation was similar with regard to the lateral task. If the needle moved to the right, the pilot would put in right rudder pedal to "chase" the needle, and the simulator cab moved toward the right. The pilot's objective was to maintain a centered position on the ILS display. This represented the desired cab position; needle position was directly proportional to cab position.

Motion Simulator and Display Compensation

Not shown in Fig. 1 is the lead compensation used to compensate for the inherent motion simulator lags. Measurement of the simulator dynamics failed to reveal any significant differences in response from earlier measurements, e.g., Ref. 3. Consequently, the simulator was compensated as in other programs using an equation of the form:

$$\lambda_c = \lambda + K_1\dot{\lambda} + K_2\ddot{\lambda} \qquad (2)$$

where λ_c is the simulator command and λ the computed value (within a constant gain factor). Table 3 lists the values of the compensatory coefficients, K_1 and K_2.

TABLE 3

MOTION SIMULATOR COMPENSATION

AXIS	K_1 (sec)	K_2 (sec^2)
Longitudinal	0.22	0.033
Lateral	0.21	0.028
Vertical	0.17	0.020

Similar compensation was used to overcome measured display lags of 0.06 to 0.08 sec. Consequently, there was, within the frequency range of interest, a close correspondence between the gain and phase of the desired and the actual accelerations and displayed positions. The acceleration

cues were contaminated, to some extent, with extraneous motion of the simulator associated with its vibration modes (principally in the lateral direction where twisting of the simulator tower is thought to contribute to the lateral acceleration sensed). However, for this experiment, there was no concern with how much "noise" there might be in addition to the "signal" in the cab's motions.

There was no motion washout used in this experiment — if the display bar headed off scale, the cab would hit its travel limit.

Performance Measurement

The describing function analyzer (DFA) was used to provide the disturbance (forcing function) and measure the system response. The DFA used was developed at Systems Technology, Inc., specifically for research into human performance. Its theory of operation is covered in Ref. 4. Briefly, it generates a random-appearing sum of five nonharmonically related sinusoids (given in Table 4) which is used as the forcing function. The closed-loop system's response is correlated with this disturbance by measuring the error-to-input describing function, in this experiment, given by:*

$$\frac{\ddot{\lambda}}{\ddot{\lambda}_d} = \frac{1}{1 + Y_p Y_c} \tag{3}$$

Off-line computer processing of the data yields the open-loop describing function of the system, $Y_p Y_c$, where Y_c is given by Eq. 1 and Y_p is the effective pilot describing function for visual or visual-plus-motion inputs.

An additional feature of the DFA permitted measurement of system performance in terms of the mean square error, σ^2_{λ}. Pilot commentary was noted as an auxiliary measure.

*An acceleration disturbance, $\ddot{\lambda}_d$, rather than a position disturbance, λ_d, was used because of the requirement for second-order simulator compensation.

TABLE 4

DISTURBANCE SPECTRUM*

FREQUENCY (rad/sec)	SIMULATOR ACCELERATION AMPLITUDE (m/sec^2)	DISPLAY AMPLITUDE (cm)
0.1886	0.0152	0.773
0.503	0.0366	0.261
1.257	0.229	0.261
3.016	0.229	0.047
6.283	0.110	0.005

*$\sigma_{SIM\ ACC} = 0.345\ m/sec^2$, $\sigma_{DISPL} = 0.858$ cm.

Subjects and Protocol

Two subjects, whose backgrounds are summarized in Table 5, were used in these experiments. The major difference between subjects is EF's helicopter experience, whereas JK's experience is entirely with fixed-wing aircraft.

TABLE 5

SUBJECT BACKGROUNDS

EF: Airline flight engineer, approximately 2500 hr in DC-8 and B-727. Former USMC pilot with 1550 hr as primary flight instructor; 2000 hr in heavy helicopters (H-34), 1500 hr as pilot-in-command. Age: 37.

JK: Airline reserve copilot/navigator, approximately 3000 hr in B-707. Former USN attack pilot with 1200 hr in A-4 jets. Has 300 hr in miscellaneous light planes. Age: 30.

There were approximately 40 runs for each subject during which data was recorded, preceded by about 30 exploratory (for best gains, disturbance amplitudes, etc.) and familiarization runs for both subjects

together. The protocol was to present the configurations to the subject in random order except that the centerstick tasks and pedal tasks were presented in a group — a convenience for the experimenter. There were typically ten runs (each configuration twice) in a session for each subject.

The controlled element gain was initially selected by EF in fixed-base trial runs where the lag time constant was 0.1 sec. This later proved sub-optimum when increased training on the part of both subjects plus increased lag (to 1.0 sec) resulted in using virtually full controller travel in each of the tasks.

In most cases, the data presented in this paper pertains only to the last two or three runs. (However, earlier data showed the same trends.) These were made for the express purpose of evaluating a 50 percent higher gain, K_c = 3.96 cm/sec^2(display)/cm(control deflection). Both pilots commented favorably on the gain increase. Even so, the gain was sub-optimum to judge by the subjects' control activity, particularly in the pedal tasks. The results obtained from these runs are felt to be closest to what well trained subjects can do in the experimental task.

RESULTS AND DISCUSSION

Pilot Commentary

Table 6 paraphrases the significant remarks by subject and configuration. With regard to the centerstick tasks, the commentary suggests that the pilots improve in their ability to track, that is, in holding the needle centered when they are in a moving-base condition. However, there is very little difference between having the simulator move back and forth as opposed to having it move up and down. There are also subject differences in the centerstick tasks. EF seems to benefit more from the presence of the motion cues, as opposed to JK.

In the pedal tasks, both pilots are somewhat disturbed by the lateral motion and, further, the task is regarded as less real, or more difficult, than the centerstick task. JK comments that the lateral motion causes his head to move and therefore reduces his ability to fixate on the vertical needle. There is relatively little difference, fixed-base to moving-base;

TABLE 6

PILOT COMMENTARY

	EF	JK
S LON VER	Lag is much more apparent in fixed-base condition. Prefer moving base, but cannot see much difference between LON and VER.	Task less difficult with motion; tend to disregard motion. VER seems more real; get a pitching sensation, perhaps because I strain forward.
P LAT	Side-to-side movement is disturbing. Pedal task is more difficult to learn than stick task.	Motion is better with centerstick tasks. Rocking of my head screws up my lateral control. Task may be tougher with motion.

and the reason apparently is that the lateral motion itself is more disturbing or inhibiting than it is beneficial.

In this connection, a single run with the simulator cab at the bottom of the tower in the LON and LAT configurations elicited remarks indicative of no change, LON, and smoother motion, LAT. EF noted, "less jerky," motion at the tower's bottom, while JK thought the acceleration response "delayed" in the LAT configuration. The implication is clear: there were extraneous accelerations in the LAT task which may have contributed to the task difficulty.

Tracking Performance

The two subjects' tracking performance is indicated in Fig. 2, together with the measured crossover frequency from the describing function measurements. The data show, for EF in the centerstick task, that motion improves performance, as signified by the reduction in σ_λ and the increase in ω_c. This improvement is significant at better than the 1 percent level (F test for equality of variance). There is a relatively small difference between the longitudinal and vertical motion cases which tends to confirm what the pilot had to say about the task. JK's performance was in general better than EF's, however, he showed a lesser degree of improvement (significant

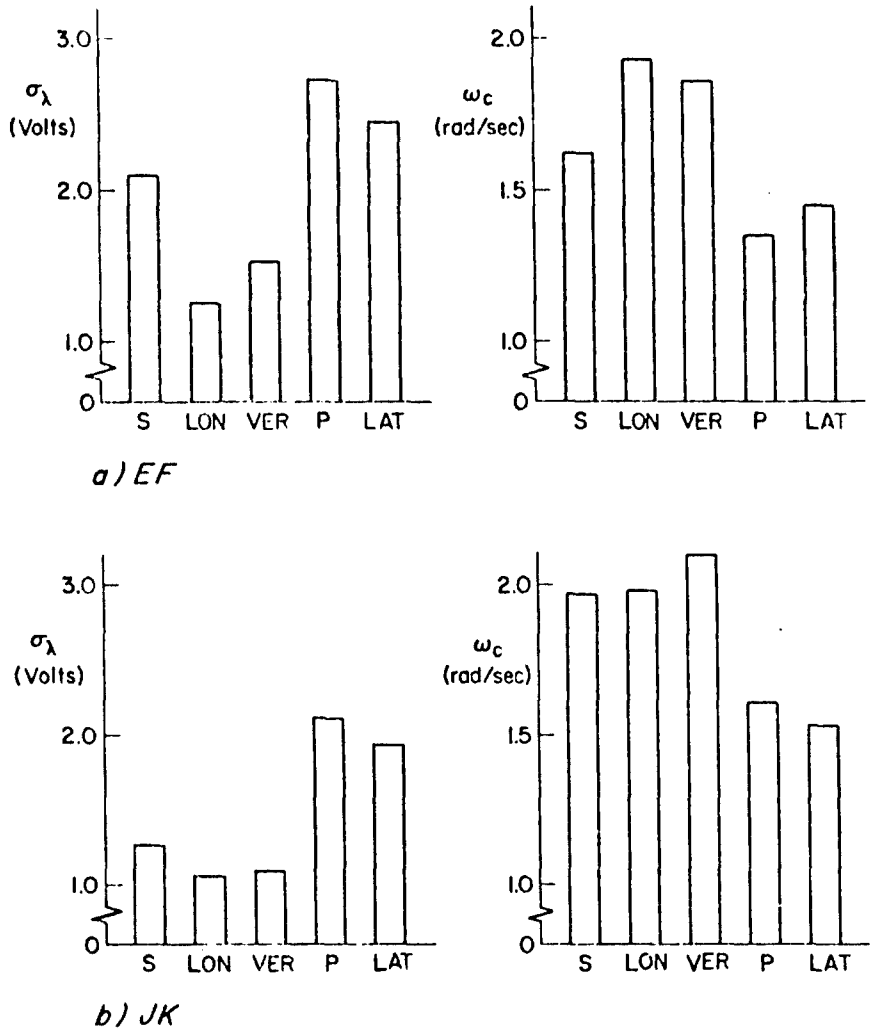

Figure 2. Averaged Performance and Crossover Frequency

only at the 10 percent level), going from fixed-base to moving-base, for the centerstick tasks.

Now, consider the lateral task performance exhibited in this figure. Although there is an improvement in performance on the part of both pilots, the improvement is relatively small and no significance can be established. The crossover frequencies change a relatively small amount, and for JK it goes down with motion, an apparent inconsistency since his performance improves. The explanation in this instance is that the coherence, as measured by the ratio between the correlated (with the disturbance, $\ddot{\lambda}_d$)

and total power in the λ signal, is increased in the LAT configuration by an amount more than sufficient to offset the decreased bandwidth as indicated by ω_c.

Describing Functions

Perhaps the most important data from this experiment are the describing function results. Figure 3 illustrates the open-loop describing functions for the centerstick tasks. The crossover model holds for these data as the gain characteristics show crossover at a slope of −20 dB per decade for both subjects. The task is difficult: gain margins vary between 2 and 6 dB; phase margins between 10 and 30 deg.

The most apparent differences between the fixed- and moving-base data are the reduction in high frequency (at 6.28 rad/sec) lag, moving-base (by about 120 deg, EF; 60 to 80 deg, JK), and the improved gain and phase

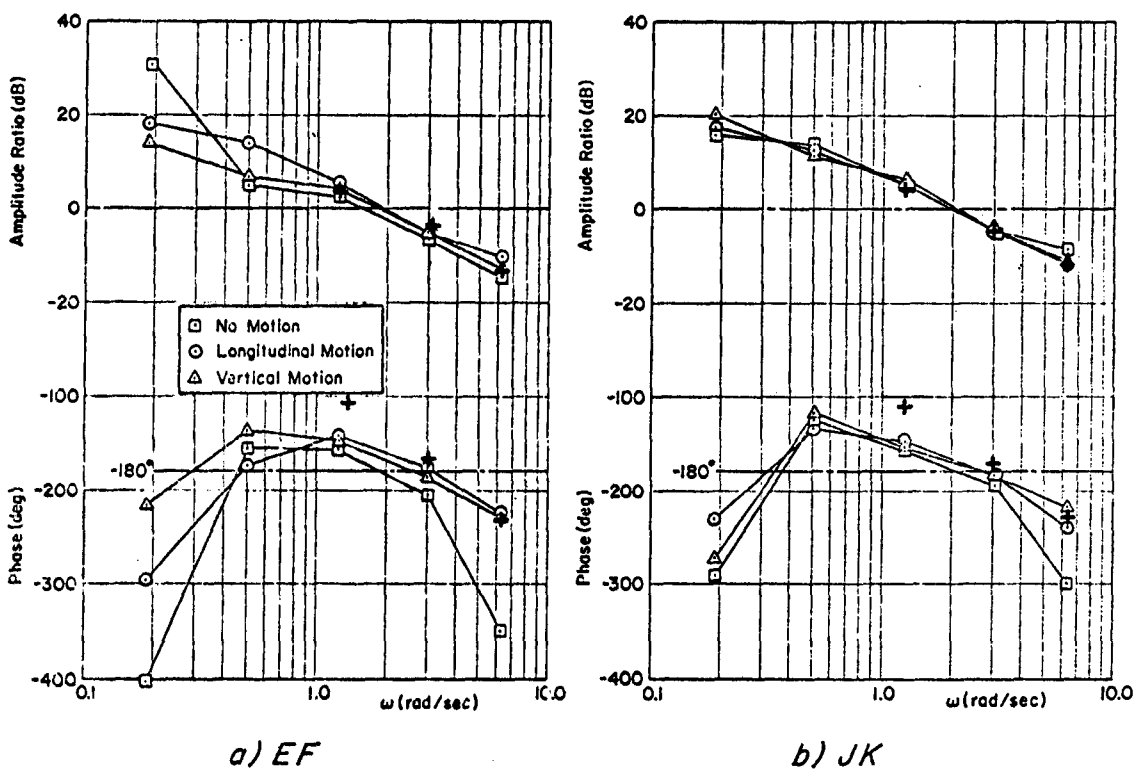

Figure 3. Describing Functions, Centerstick Tasks

margins, moving base (by about 2.5 dB and 8 deg). The pilot's effective time delay has been significantly reduced in the moving base cues, and for EF there is a substantial improvement in crossover frequency as already noted in Fig. 2. On the other hand, there are only slight differences between the two moving base conditions for either subject.

Comparing subjects, Fig. 3 shows that EF gets more benefit out of the linear motion than does JK. However both subjects show closely comparable data moving base — the major difference between the two subjects lies in their fixed base data.

No firm conclusions can be drawn from the low frequency data, i.e., the lowest two frequencies in Fig. 3. The measurements at these frequencies were quite noisy because of the very low signal levels. The data points shown at the two lowest frequencies represent a grand average of all the runs for a particular subject and configuration; while the highest three data points represent only the last two or three runs.

The data for the pedal tasks are shown in Fig. 4, and the same qualifying remarks concerning the two lowest frequencies apply. Here the fixed base versus moving base differences are substantially less than in Fig. 3. In particular, only the lag at the highest frequency shows a substantial improvement, moving base (by about 45 deg, JK; by almost 140 deg, EF!). Again, the intrasubject differences are small in the moving base case. The crossover frequencies for these tasks are less than for the centerstick tasks while the gain and phase margins are comparable. This bears out the earlier remarks concerning the inherent difficulty of the pedal tasks (Table 6).

The data of Figs. 3 and 4 are not incompatible with current models (in particular, that given in Ref. 5) of the dynamic response of the human otolith. Of course, other proprioceptive senses also contribute. The + symbols for the three highest frequencies in these figures represent a fit to a hypothesized model (valid only at high frequencies — visual

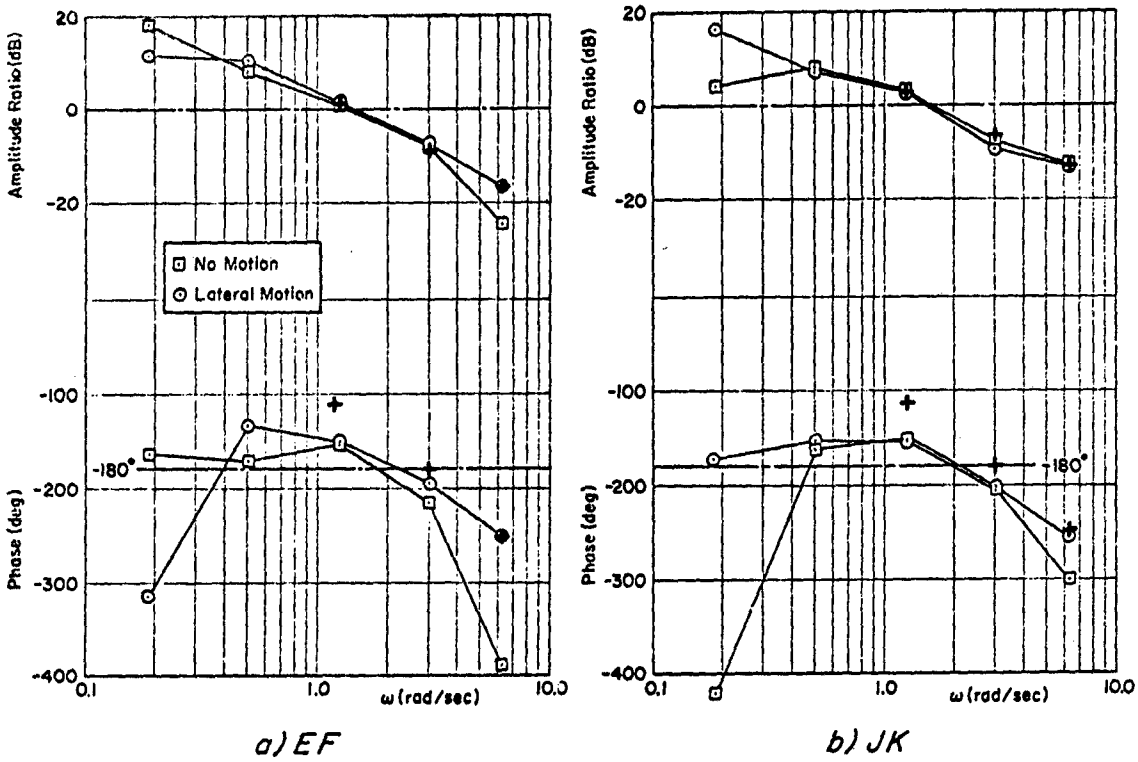

Figure 4. Describing Functions, Pedal Tasks

cues presumably dominate at lower frequencies) given by:*

$$Y_p Y_c|_{FIT} = \frac{K_p K_c}{s+1} Y_{OTOLITH}\, e^{-\tau s} \qquad (4)$$

For the centerstick tasks, τ = 0.2 sec; for the pedal tasks, τ = 0.25 sec — in both instances K_p is adjusted to fit the amplitude data. $Y_{OTOLITH}$ is based on Ref. 5 data which suggest a phase characteristic equivalent to a first-order lag with break frequency, 1/T = 1.5 rad/sec, and a gain characteristic which falls off at −6 dB per decade above 1 rad/sec.

*The s^2 term in the controlled element is eliminated because the otoliths sense acceleration.

Summary of Results

There are four major results contained in the foregoing material. The first of these relates to the dominance of motion effects. Pilot commentary, performance, and measured describing functions all show a substantial improvement, moving base, in the centerstick tasks; less so in the pedal tasks. The major effect is to reduce the pilot's effective time delay — in this respect the data resemble results obtained in attitude control tasks (c.f. Ref. 6) when going from fixed to moving base.

Secondly, subject differences are important. EF is a more relaxed flier while JK is more intent. JK comments, for example, that his head bobs up and down in the VFR configuration because he strains forward to see the display better. This difference in style is apparent in the better performance, increased crossover frequencies, and generally smaller gain and phase margins exhibited by JK relative to EF.

Thirdly, the data show that the effective acceleration thresholds in this task are relatively low. The root mean square acceleration ranges between 0.04 and 0.06 g. Since the pilots are using these signals effectively as indicated by the fixed base-moving base differences, the effective threshold lies near this level or lower. Physiological measurements of this threshold (c.f. Ref. 7) are around 0.01 g, vertically (in a 1 g field) and somewhat less when measured longitudinally or laterally. The result is therefore compatible with physiological measures.

Finally, the data indicate no substantial difference due to the direction of the acceleration in the pilot's ability to respond to this cue in a tracking task. Certainly no substantial vertical/longitudinal differences are indicated even though bobweight effects plus a presumed lower acceleration threshold, longitudinally, could contribute to improved performance in the LON configuration relative to VER. Such differences which do exist (see EF's data in Fig. 3) are substantially less than motion versus no motion differences.

No comparison can be made in the lateral direction. Substantial differences in the task (primarily in using pedals), the lack of lateral restraint, and (suggested by pilot commentary) extraneous lateral

accelerations may all contribute to the relatively small (and statistically insignificant) performance improvements, fixed- to moving-base.

CONCLUSIONS AND RECOMMENDATIONS

There are three major conclusions to be drawn from these data:

- Low level linear acceleration cues can be effectively used by pilots to improve performance in tracking tasks.
- Pilot sensitivity to these cues is approximately the same for the fore-and-aft and vertical directions.
- Performance improvements with linear motion cues are highly subject dependent.

The first of these is significant because in the past there have been doubts as to the utility of purely linear motion cues in continuous tracking tasks. The results here are unambiguous. The second conclusion is qualified by the magnitude of the linear accelerations used in this experiment — the rms levels are roughly five times as large as physiological measurements of linear acceleration threshold. The result is therefore not unexpected. At lower levels of acceleration, one would expect the overall benefits of motion to be lessened and the directional differences (if any) to be relatively increased. The final conclusion is to be expected on the basis of past experimentation with motion cues by a number of investigators.

At the outset of this paper it was noted that the experiment was exploratory in nature and of short duration. The major recommendation is that the experiment be repeated to refine the results. Clearly, more subjects at a higher level of training and with a more optimum controlled element gain are requirements for such an effort. Several improvements are possible in the experimental setup in the areas of manipulators (designed to minimize bobweight effects or calibrated to define what the bobweight contribution is), motion fidelity (extraneous simulator motions to be minimized), and measurement technique (to improve the signal to noise ratio in the measurement at low frequencies, perhaps simultaneous measurement of pilot visual and motion channel describing functions in the manner of, for example, Ref. 6). And finally, additional variables can be introduced,

for example, variations in controlled element, disturbances, and motion amplitudes relative to display motion amplitudes (the latter to determine effective acceleration thresholds).

REFERENCES

1. Malcolm, R., and G. M. Jones, Some Experiments on the Perception of Vertical Motion, enclosure in a letter written by R. Malcolm to G. R. Holden at ARC, Oct. 1970.

2. Walsh, E. G., "Role of the Vestibular Apparatus in the Perception Motion on a Parallel Swing," J. Physiol., Vol. 155, 1961, pp. 506-513.

3. Fry, Emmett B., Richard K. Greif, and Ronald M. Gerdes, Use of a Six-Degrees-of-Freedom Motion Simulator for VTOL Hovering Tasks, NASA TN D-5383, Aug. 1969.

4. Allen, R. W., and H. R. Jex, "A Simple Fourier Analysis Technique for Measuring the Dynamic Response of Manual Control Systems," paper presented at the Sixth Annual Conf. on Manual Control, Air Force Institute of Technology, Wright-Patterson AFB, Ohio, Apr. 7-9, 1970.

5. Young, L. R., "The Current Status of Vestibular System Models," Automatica, Vol. 5, 1969, pp. 369-383.

6. Stapleford, Robert L., Richard A. Peters, and Fred R. Alex, Experiments and a Model for Pilot Dynamics with Visual and Motion Inputs, NASA CR-1325, May 1969.

7. Peters, Richard A., Dynamics of the Vestibular System and Their Relation to Motion Perception, Spatial Disorientation, and Illusions, NASA CR-1309, Apr. 1969.

8. Ringland, R. F., R. L. Stapleford, and R. E. Magdaleno, Motion Effects on an IFR Hovering Task — Analytical Predictions and Experimental Results, NASA CR-1933, Nov. 1971.

9. Ringland, R. F., and R. L. Stapleford, Experimental Measurements of Motion Cue Effects on STOL Approach Task, Systems Technology, Inc., Tech. Rept. 1014-2, Apr. 1972.

THE FOLLOWING PAGES ARE DUPLICATES OF ILLUSTRATIONS APPEARING ELSEWHERE IN THIS REPORT. THEY HAVE BEEN REPRODUCED HERE BY A DIFFERENT METHOD TO PROVIDE BETTER DETAIL.

FIGURE 5. GAT-1 Panel with PWI Display and Tracking (VOR) Needle

FIGURE 4. View of GAT-1, Screen and Projection System

This page is reproduced at the back of the report by a different reproduction method to provide better detail.

This page is reproduced at the back of the report by a different reproduction method to provide better detail.

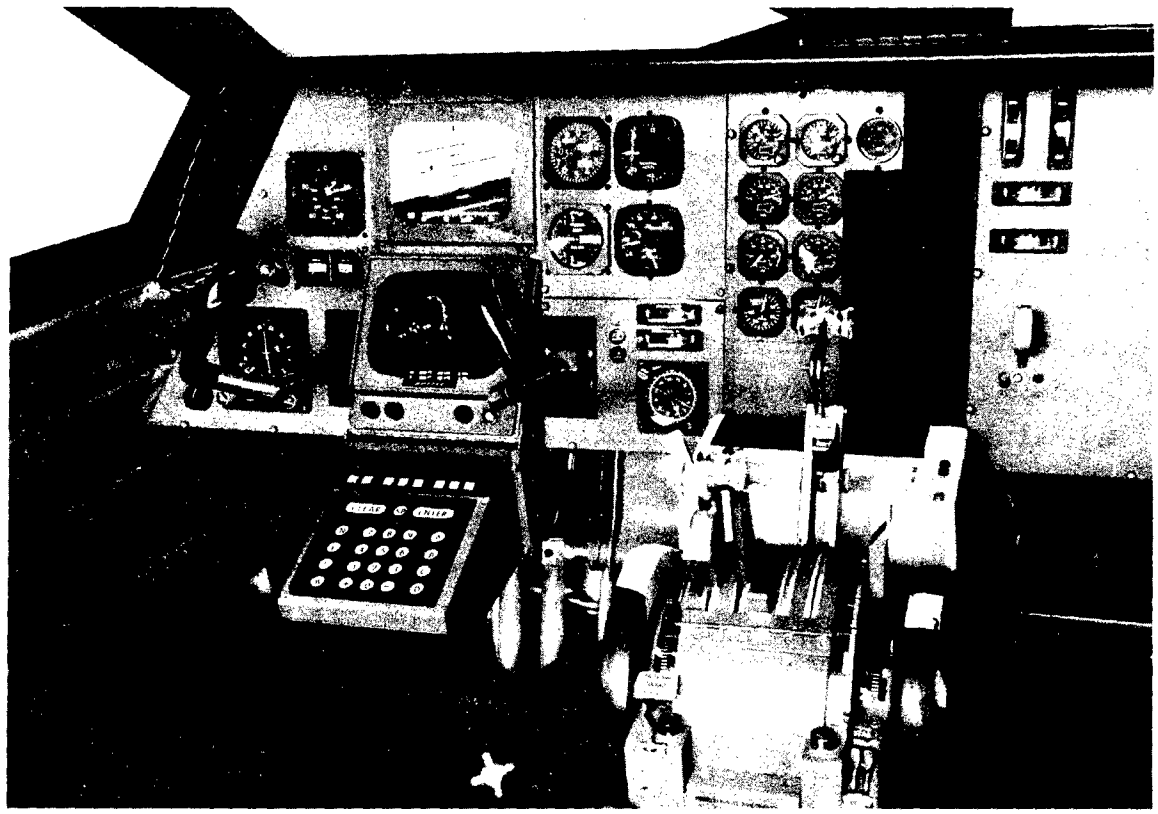

Figure 2. Integrated Display System in Simulator Cab

This page is reproduced at the back of the report by a different reproduction method to provide better detail.

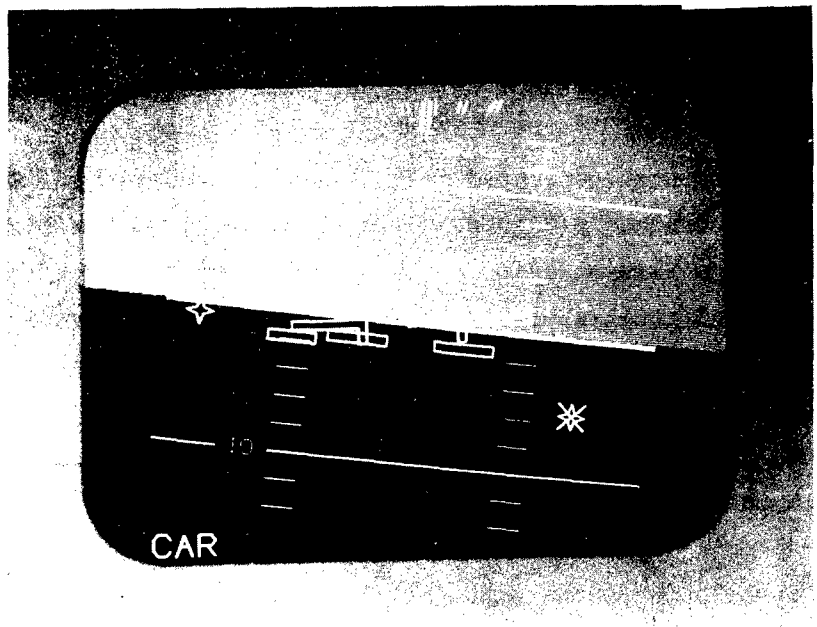

(a)

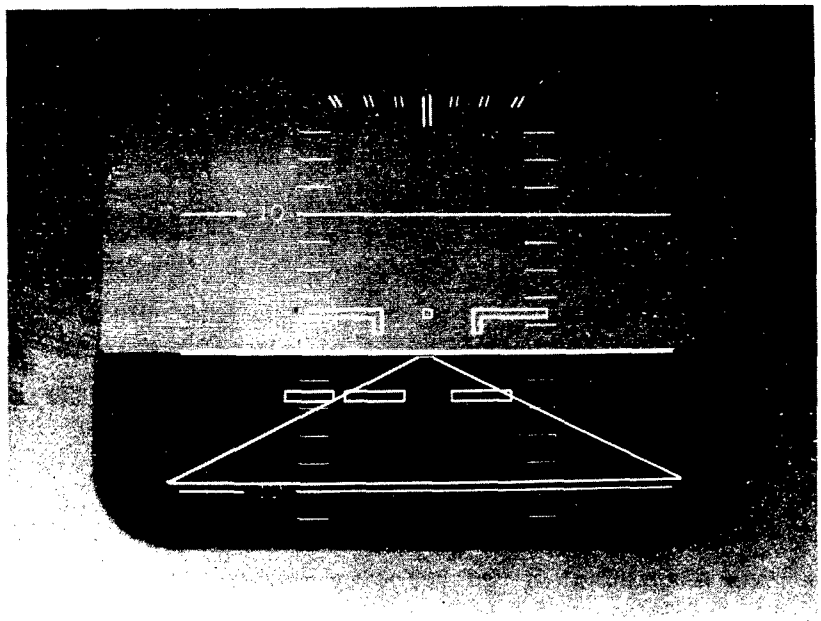

(b)

Figure 3. Electronic Attitude Indicator Formats

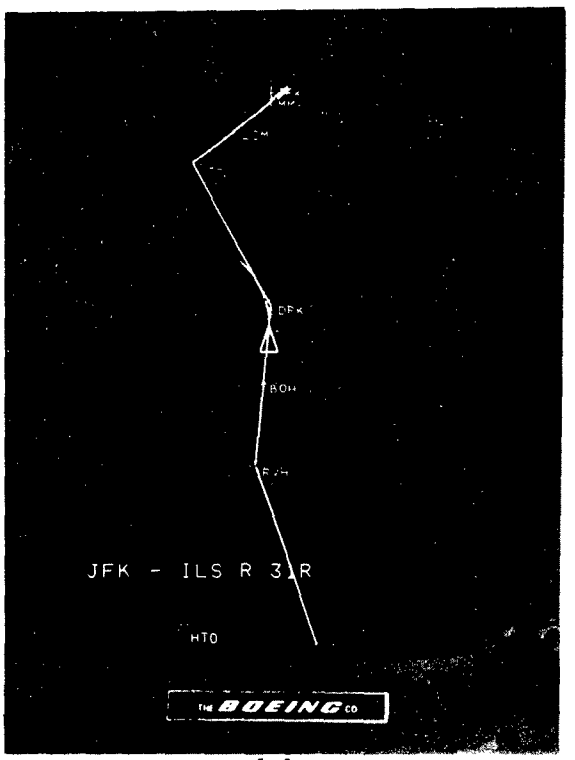

(a)

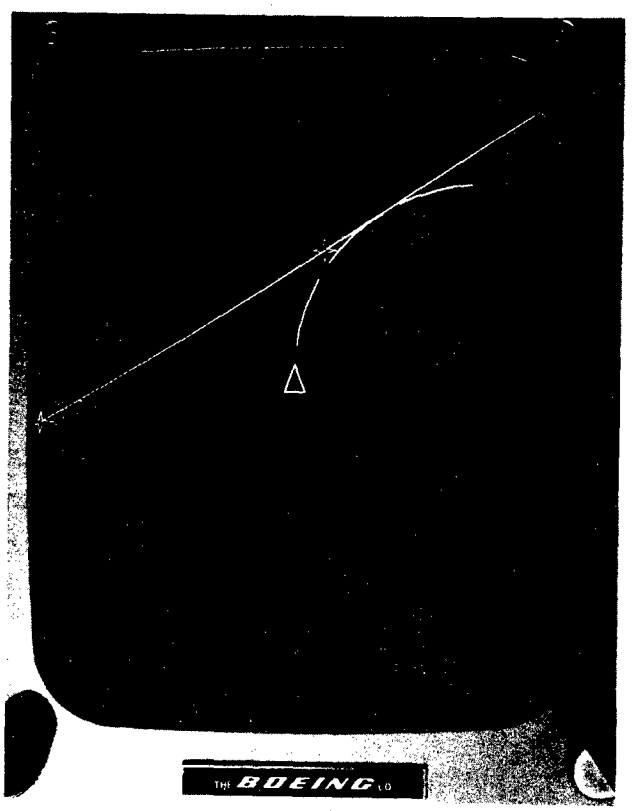

(b)

Figure 4. Horizontal Navigation Formats on the Multifunction Display

This page is reproduced at the back of the report by a different reproduction method to provide better detail.

This page is reproduced at the back of the report by a different reproduction method to provide better detail.

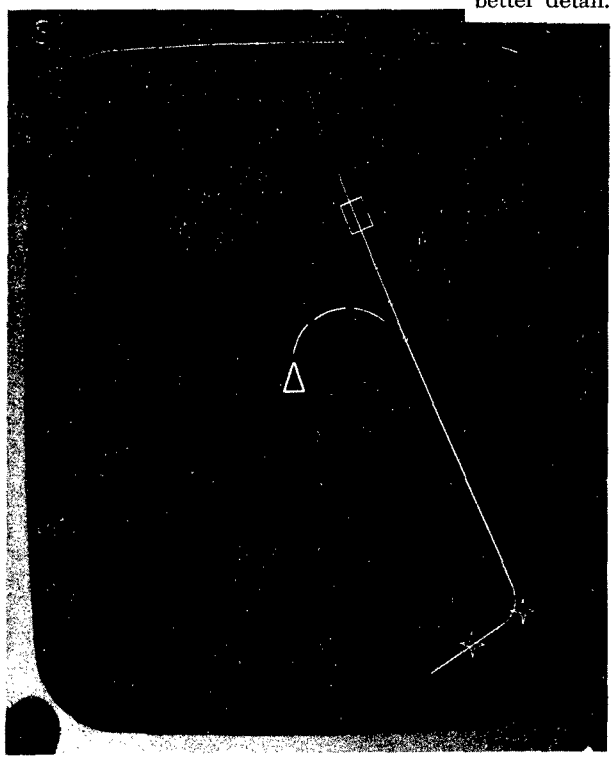

(a)

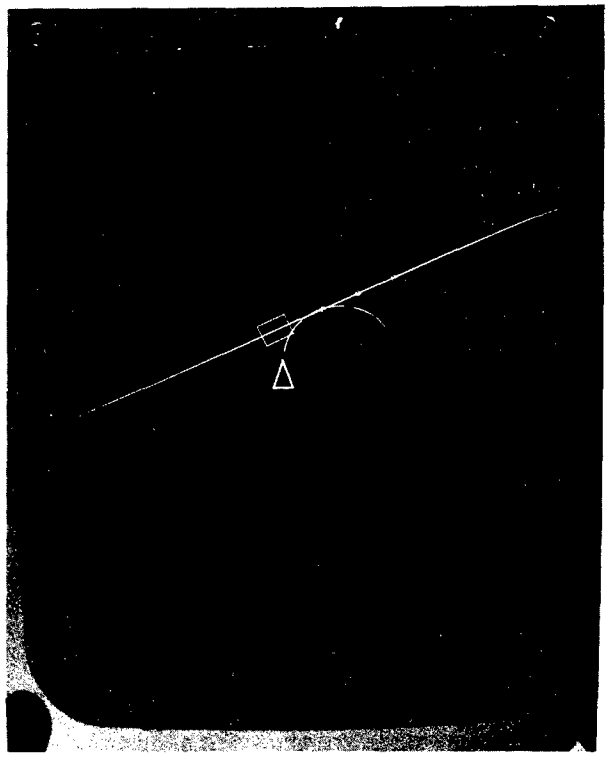

(b)

Figure 5. Moving Time-Slot Capture Using the Multifunction Display

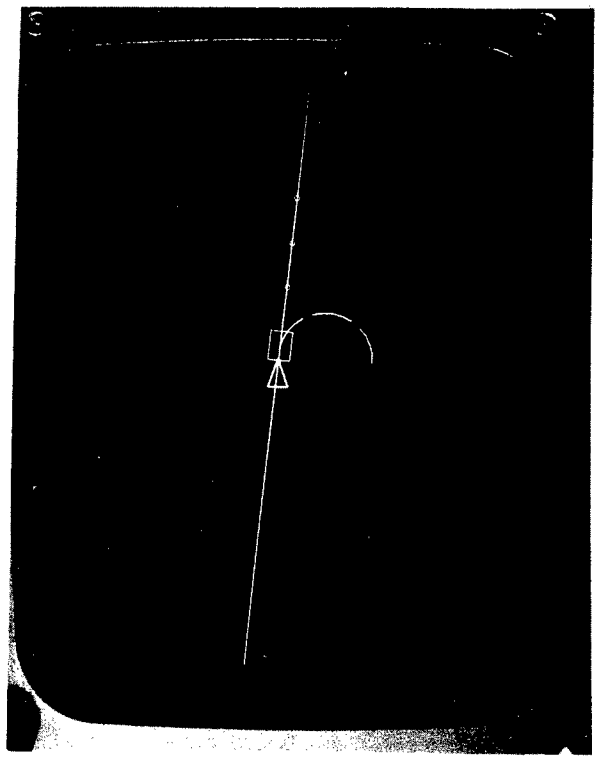

(c)

Figure 5. Moving Time-Slot Capture Using the Multifunction Display (Cont'd)

message is clear: electronic, computer-generated displays permit optimum forms of information presentation to the crew, making the most desired crew roles feasible.

This page is reproduced at the back of the report by a different reproduction method to provide better detail.

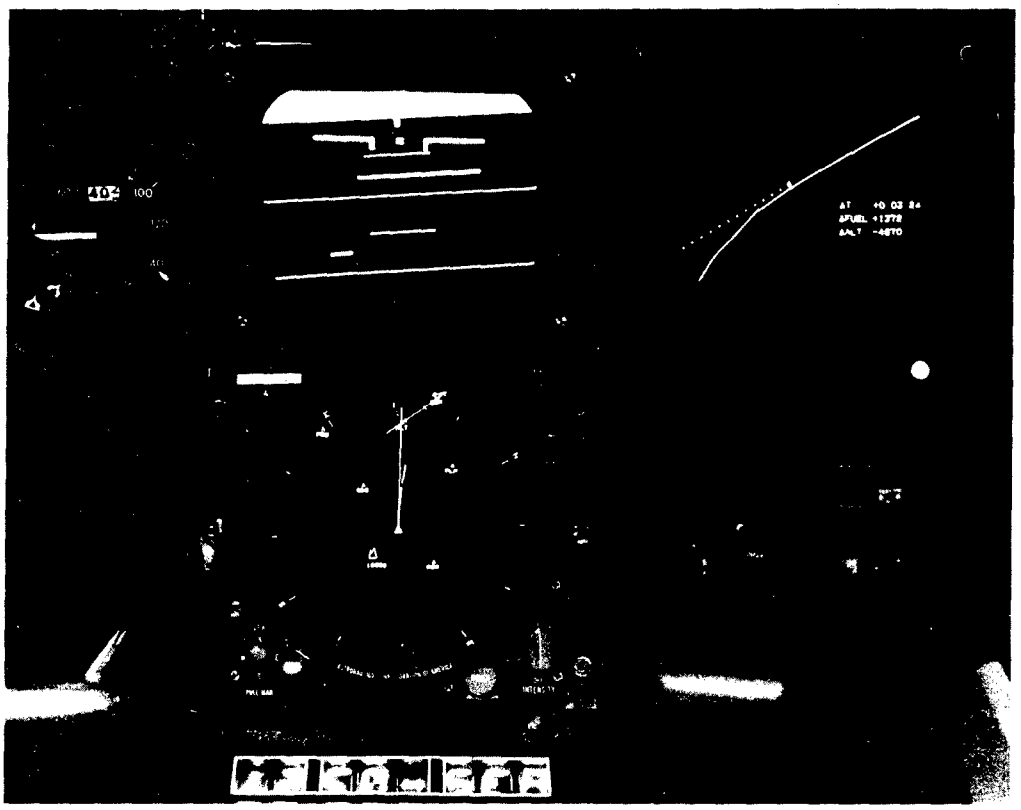

Figure 6. Simulator Cockpit with Second Multifunction Display

This page is reproduced at the back of the report by a different reproduction method to provide better detail.

This page is reproduced at the back of the report by a different reproduction method to provide better detail.

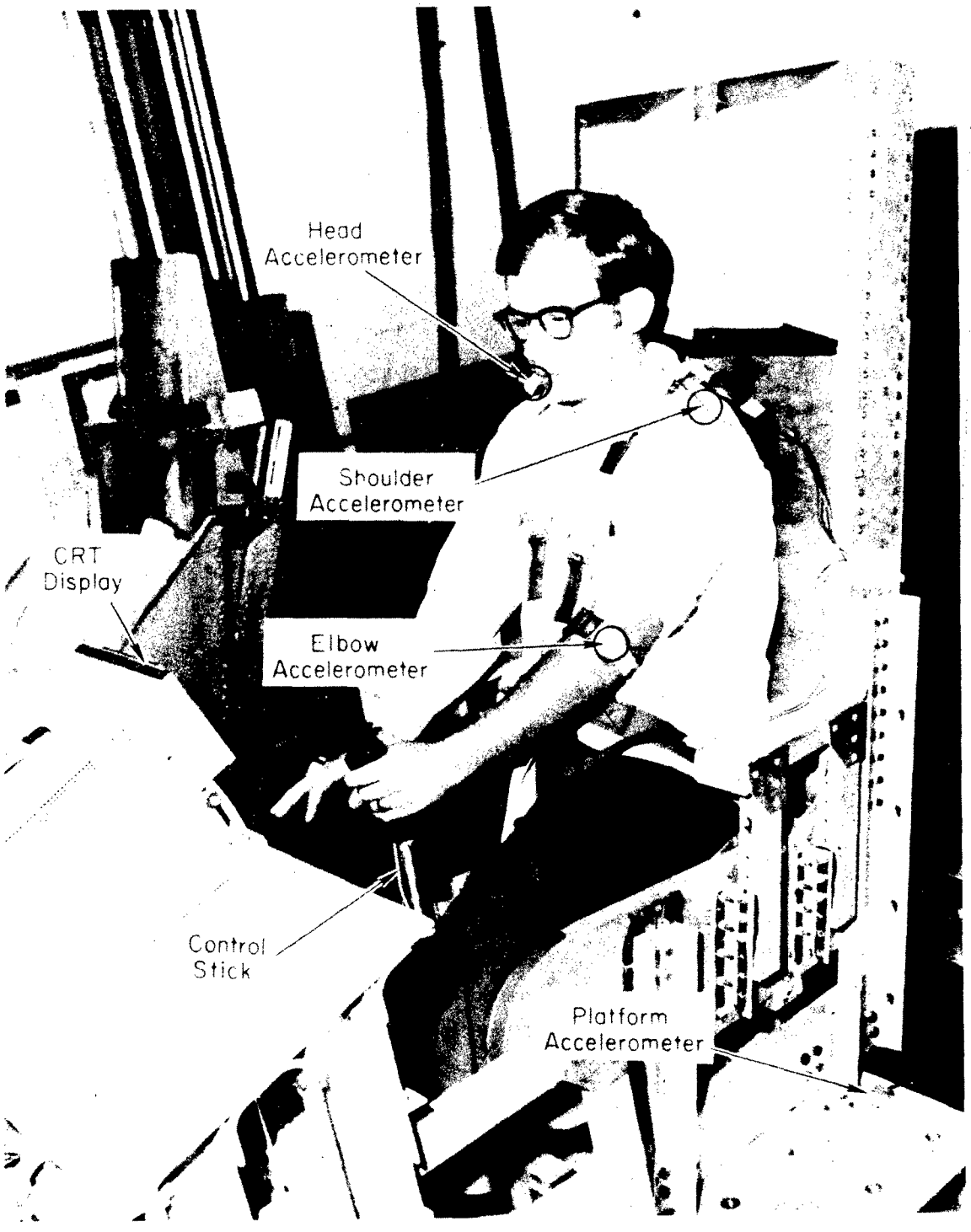

Figure 2. Instrumented Subject Performing Tracking Task Under Vibration

This page is reproduced at the back of the report by a different reproduction method to provide better detail.

Figure 1. Tracking Apparatus Utilizing Large Position Control Stick and Over-Sized Display Screen

This page is reproduced at the back of the report by a different reproduction method to provide better detail.

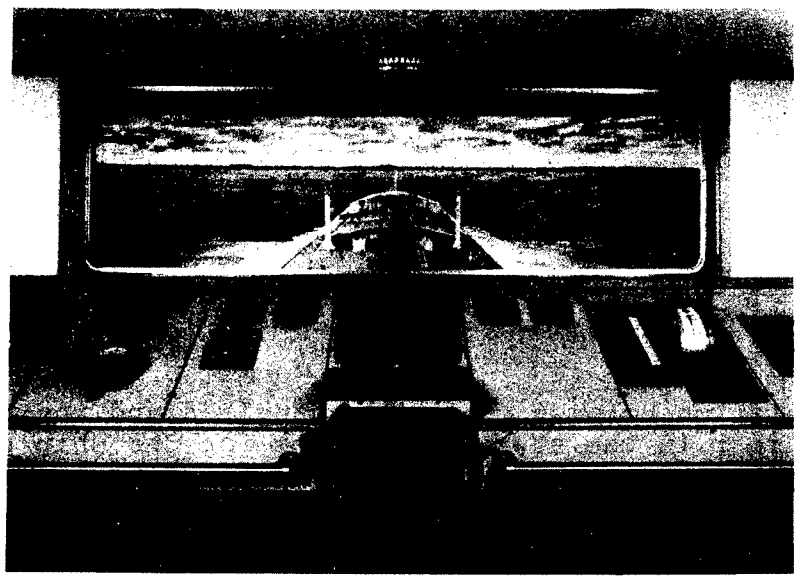

Figure 3: The Ship Research and Maneuvering Simulator of the Institute TNO for Mechanical Constructions at Delft.

A block diagram of the system, including the helmsman, is given in Fig. 4.

On an analog computer the dynamics of the ship to be simulated, including the characteristics of thrust engine and rudder engine, can be programmed. The computer yields the signals which control the environmental display system and also the instruments such as compass, rudder position indicator, log, etc. The helmsman has the same controls at his disposal for maneuvering as on a real ship viz. the wheel, which gives the input to the rudder engine, and the telegraph to the engine, which governs the speed of the propeller. External disturbances simulating the effects of wind, waves and currents can also be introduced into the model on the analog computer; the same applies for the information on the desired state which is of importance for the settings of the instruments in the wheelhouse.